

NASA Conference Publication 3162
Part 1

LDEF Materials Workshop '91

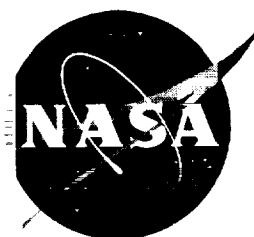


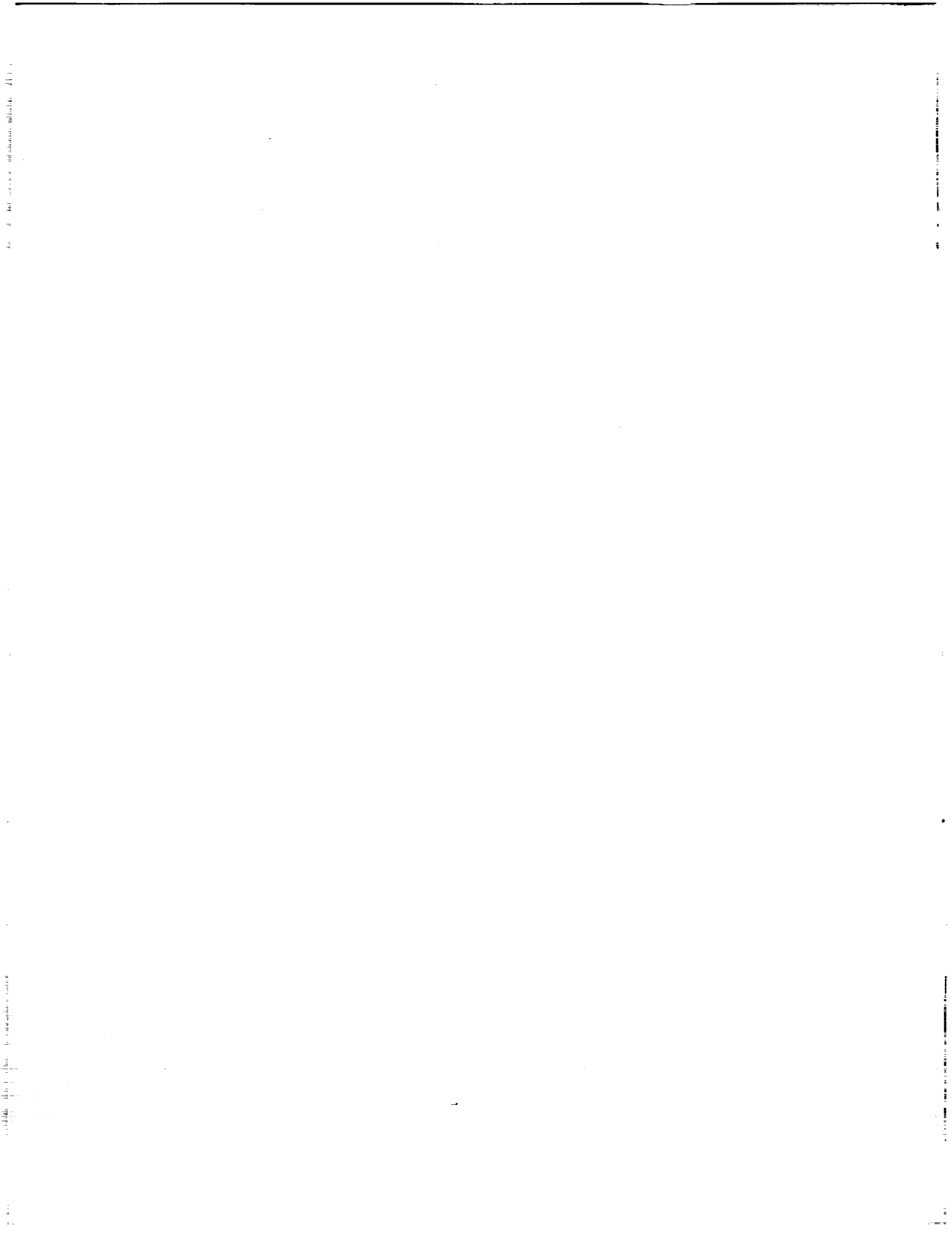
Proceedings of a workshop held at
H. J. E. Reid Conference Center
NASA Langley Research Center
November 19-22, 1991

(NASA-CP-3162-Pt-1) LDEF MATERIALS
WORKSHOP 1991, PART 1 (NASA)
461 p

N93-12769
--THRU--
N93-12789
Unclass

H1/27 0122380





LDEF Materials Workshop '91

Compiled by

Bland A. Stein and Philip R. Young

Langley Research Center

Hampton, Virginia

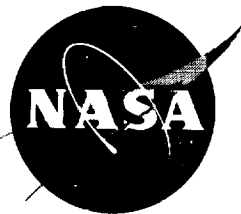
Proceedings of a workshop sponsored by

Langley Research Center and held at

H. J. E. Reid Conference Center

NASA Langley Research Center

November 19-22, 1991



National Aeronautics and
Space Administration

Office of Management

Scientific and Technical
Information Program

1992

COVER ILLUSTRATION

LDEF retrieval—the dawn of new and comprehensive understanding of space environmental effects on materials. Through analysis and modeling of materials exposed on LDEF, the enigmas of the combined effects of space environment parameters on spacecraft materials behavior in low-Earth orbit are being replaced by an emerging comprehension.

FOREWORD

The National Aeronautics and Space Administration Long Duration Exposure Facility (LDEF) was launched into low-Earth Orbit (LEO) from the payload bay of the Space Shuttle Orbiter Challenger in April 1984. It was retrieved from orbit by the Columbia in January 1990. The 57 LDEF experiments covered the disciplines of materials, coatings, and thermal systems; power and propulsion; space science; and electronics and optics. LDEF was designed to provide a large number of economical opportunities for science and technology experiments that require modest electrical power and data processing while in space and which benefit from post-flight laboratory investigations of the retrieved experiment hardware on Earth. Most of the materials experiments were completely passive; their data are being obtained in post-flight laboratory tests and analyses.

The 5.8-year flight of LDEF greatly enhanced the potential value of most LDEF materials, compared to that of the original 1-year flight plan. NASA recognized this potential by forming the LDEF Space Environmental Effects on Materials Special Investigation Group (MSIG) in early 1989. MSIG was chartered to investigate the effects of the long LEO exposure on structure and experiment materials which were not originally planned to be test specimens, and to integrate the results of this investigation with data generated by the Principal Investigators of the LDEF experiments into an LDEF Materials Data Base.

As a follow-on to the Materials Sessions at the First LDEF Post-Retrieval Symposium (in Kissimmee, Florida, June 1991), this workshop was envisioned as a series of technical sessions on LDEF materials themes, followed by theme panel meetings. The themes included Materials, Environmental Parameters, and Data Bases; LDEF Contamination; Thermal Control Coatings, Protective Coatings, and Surface Treatments; Polymers and Films; Polymer Matrix Composites; Metals, Ceramics, and Optical Materials; and Lubricants, Adhesives, Seals, Fasteners, Solar Cells, and Batteries. Each half-day technical session contained invited overview papers, with ample time for specific discussion after each paper and for general discussion on the technical session theme at the end of each session.

These technical sessions were followed by concurrent half-day meetings of each panel to produce theme reports and summary charts. These meetings addressed the following general questions plus a few specific questions developed by the panel chairmen concerning the panel theme discipline.

- How have initial LDEF results affected
 - potential space applications of this class of materials or understanding of environmental parameters?
 - materials development or environmental parameter definition needs?
 - ground simulation testing needs?
 - space environmental effects analytical modeling needs?

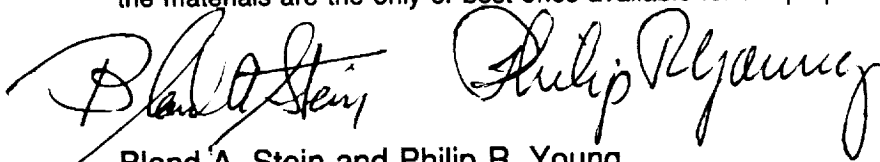
- What are the LDEF data-basing requirements for this discipline?
- What are the general needs for future flight experiments?

LDEF materials data has been eagerly awaited by the Space Environmental Effects on the Materials Technical Community for the better part of a decade. The most optimistic expectations of that community have been fulfilled. The remarkable attitude stability of LDEF during its entire flight permits evaluation of many well-defined combinations of space environment parameters on specimens of identical and/or similar materials located on experiment trays and on the spacecraft structure at various positions on the sides and ends of the satellite. As this workshop indicated, the LDEF data are, in general, remarkably consistent. Even at this interim point in the LDEF materials analyses, it is apparent that LDEF will provide a "benchmark" for materials design data bases for satellites in low-Earth orbit. Some materials were identified to be encouragingly resistant to LEO SEE for 5.8 years; other "space qualified" materials displayed significant environmental degradation. Molecular contamination was widespread; LDEF offers an unprecedented opportunity to provide a unified perspective of unmanned LEO spacecraft contamination mechanisms. New material development requirements for long-term LEO missions have been identified, and current ground simulation testing methods/data for new, durable materials concepts can be validated with LDEF results.

This is the report resulting from LDEF Materials Workshop 1991. It contains most of the papers presented at the technical sessions plus the panel theme reports. The approximately 200 persons who attended the Workshop were quite pleased with the information presented and with the technical interactions. The Workshop Chairmen wish to express thanks to the coordinator, Dr. Arlene Levine, to the staff at the NASA Langley H. J. E. Reid Activities Center, and to the session chairman recorders and authors who aided us in the planning of LDEF Materials Workshop 1991. We also wish to thank those who presented the papers and conducted the theme panel activities. We hope that this document satisfies the documentation requirements of the Workshop participants and other recipients.

The LDEF mission was a noteworthy success. It remains for us, the international space environmental effects technical community, to complete the analyses of the data, to generate new models for space environmental parameter interactions with materials from this data, and to devise more accurate ground simulation tests for space environmental effects on materials using the LDEF data for validation.

Certain materials are identified in this publication in order to specify procedures adequately. In no case does such identification imply recommendation or endorsement by the government, nor does it imply that the materials are the only or best ones available for the purpose.



Bland A. Stein and Philip R. Young
NASA Langley Research Center

CONTENTS

Foreword	iii
Part 1	
LDEF Materials: An Overview of the Interim Findings	1
Bland A. Stein	
LDEF Materials, Environmental Parameters, and Data Bases	
Co-Chairmen: Bruce Banks and Mike Meshishnek Recorder: Roger Bourassa	
LDEF Atomic Oxygen Fluence Update	59
Roger J. Bourassa and J. R. Gillis	
LDEF Yaw and Pitch Angle Estimates	71
Bruce A. Banks and Linda Gebauer	
LDEF Contamination	
Co-Chairmen: Wayne Stuckey and Steve Koontz Recorder: Russell Crutcher	
Materials SIG Quantification and Characterization of Surface Contaminants	95
Russ Crutcher	
Z306 Molecular Contamination Ad Hoc Committee Results	115
Johnny L. Golden	
Long Duration Exposure Facility (LDEF) Contamination Modeling	141
Tim Gordon and Ray Rantanen	
Surface Contamination on LDEF Exposed Materials	159
C. S. Hemminger	
Sources and Transport on Silicone NVR	175
Gale A. Harvey	
Thermal Control Coatings, Protective Coatings, and Surface Treatments	
Co-Chairmen: Ann Whitaker and Wayne Slemp Recorder: Johnny Golden	
Thermal Control Surfaces on the MSFC LDEF Experiments	187
Donald R. Wilkes, Ann Whitaker, James M. Zwiener, Roger C. Linton David Shular, Palmer Peters, and John Gregory	

Anodized Aluminum on LDEF: A Current Status of Measurements on Chromic Acid Anodized Aluminum	211
Johnny L. Golden	
Performance of Thermal Control Tape in the Protection of Composite Materials	223
Rachel R. Kamenetzky and Ann F. Whitaker	
Fluorescence of Thermal Control Coatings on S0069 and A0114	233
James M. Zwiener, Richard J. Mell, Palmer N. Peters, Donald R. Wilkes, Edgar R. Miller, and John C. Gregory	
Long Duration Exposure Facility M0003-5 Thermal Control Coatings on DoD Flight Experiment	245
Charles J. Hurley and William Lehn	
Element Material Exposure Experiment by EFFU	283
Yoshihiro Hashimoto, Masaaki Ito, and Masahiro Ishii	
Skylab DO24 Thermal Control Coatings and Polymeric Films Experiment	293
William L. Lehn and Charles J. Hurley	
Polymers and Films (Including Ag/FEP)	
Co-Chairmen: Phil Young and David Brinza	
Recorder: Gary Pippin	
Effects of the LDEF Environment on the Ag/FEP Thermal Blankets	311
Francois Levadou and Gary Pippin	
Recession of FEP Specimens from Trays D11 and B7	345
H. G. Pippin	
Characterization of Selected LDEF—Exposed Polymer Films and Resins	357
Philip R. Young and Wayne S. Slemp	
Effects of Orbital Exposure on Halar during the LDEF Mission	391
William E. Brower, Jr., Harish Holla, and Robert A. Bauer	
Long Duration Exposure Facility M0003-5 Recent Results on Polymeric Films	417
Charles J. Hurley and Michele Jones	
LDEF Materials Workshop '91 Agenda	449
Attendee List	455

Part 2*

Metals, Ceramics, and Optical Materials

Co-Chairmen: Roger Linton and John Gregory
Recorder: Gail Bohnhoff-Hlavacek

Selected Results for Metals from LDEF Experiment A0171	467
Ann F. Whitaker	
Some Results of the Oxidation Investigation of Copper and Silver Samples Flown on LDEF	479
A. de Rooij	
Changes in Oxidation State of Chromium during LDEF Exposure	491
Johnny L. Golden	
Effect of Space Exposure on Pyroelectric Infrared Detectors	501
James B. Robertson	
Long Duration Exposure Facility (LDEF) Optical Systems SIG Summary and Database	507
Gail Bohnhoff-Hlavacek	

Polymer Matrix Composites

Co-Chairmen: Gary Steckel and Rod Tennyson
Recorder: Pete George

Polymer Matrix Composites on LDEF Experiments M0003-9 and 10	515
Gary L. Steckel, Thomas Cookson, and Christopher Blair	
Space Environmental Effects on LDEF Low Earth Orbit Exposed Graphite Reinforced Polymer Matrix Composites	543
Pete George	
Additional Results on Space Environmental Effects on Polymer Matrix Composites—Experiment AO180	571
R. C. Tennyson	
Proposed Test Program and Data Base for LDEF Polymer Matrix Composites	593
R. C. Tennyson, P. George, G. Steckel, and D. G. Zimcik	

*Part 2 is presented under separate cover.

**Lubricants, Adhesives, Seals, Fasteners, Solar Cells,
and Batteries**

Co-Chairmen: James Mason and Joel Edelman
Recorder: Harry Dursch

Identification and Evaluation of Lubricants, Adhesives, and Seals Used on LDEF	603
Bruce Keough	
Results from the Testing and Analysis of LDEF Batteries	619
Steve Spear, Harry Dursch, and Chris Johnson	
Effects of Long-Term Exposure on LDEF Fastener Assemblies	633
Steve Spear and Harry Dursch	
Results from Testing and Analysis of Solar Cells Flown on LDEF	649
Harry Dursch	
System Related Testing and Analysis of FRECOPA	661
Christian Durin	
Panel Discussion Summary	
Theme Panel Discussion Topics	679
Bland A. Stein and Philip R. Young	
LDEF Materials, Environmental Parameters, and Data Bases	681
Bruce Banks, Mike Meshishnek and Roger Bourassa	
LDEF Contamination	689
Wayne Stuckey, Steve Koontz, and Russell Crutcher	
Thermal Control Coatings, Protective Coatings, and Surface Treatments	699
Ann Whitaker, Wayne Slemo, and Johnny Golden	
Polymers and Films (Including Ag/FEP)	707
Philip R. Young, David Brinza, and Gary Pippin	
Metals, Ceramics, and Optical Materials	719
Roger Linton, John Gregory, and Gail Bohnhoff-Hlavacek	
Polymer Matrix Composites	727
Gary Steckel, Rod Tennyson, and Pete George	
Lubricants, Adhesives, Seals, Fasteners, Solar Cells, and Batteries	737
James Mason, Joel Edelman, and Harry Dursch	
LDEF Materials Workshop 1991	747

LDEF Materials Workshop '91 Agenda	749
Attendee List	755



PART 1

LDEF MATERIALS: AN OVERVIEW OF THE INTERIM FINDINGS

Bland A. Stein

NASA - Langley Research Center
Hampton, VA 23665-5225
(804) 864-3492

SUMMARY

The flight and retrieval of the National Aeronautics and Space Administration's Long Duration Exposure Facility (LDEF) provided an opportunity for the study of the low-Earth orbit (LEO) environment and long-duration space environmental effects (SEE) on materials that is unparalleled in the history of the U.S. space program. The 5.8-year flight of LDEF greatly enhanced the potential value of materials data from LDEF to the international SEE community, compared to that of the original 1-year flight plan. The remarkable flight attitude stability of LDEF enables specific analyses of various individual and combined effects of LEO environmental parameters on identical materials on the same space vehicle. NASA recognized this potential by forming the LDEF Space Environmental Effects on Materials Special Investigation Group (MSIG) to address the greatly expanded materials and LEO space environment parameter analysis opportunities available in the LDEF structure, experiment trays, and corollary measurements, so that the combined value of all LDEF materials data to current and future space missions will be assessed and documented.

This paper provides an overview of the interim LDEF materials findings of the Principal Investigators and the Materials Special Investigation Group. These revelations are based on observations of LEO environmental effects on materials made in-space during LDEF retrieval and during LDEF tray deintegration at the Kennedy Space Center, and on findings of approximately 1.5 years of laboratory analyses of LDEF materials by the LDEF materials scientists. These findings were extensively reviewed and discussed at the MSIG-sponsored LDEF Materials Workshop '91. The results are presented in a format which categorizes the revelations as "clear findings" or "confusing/unexplained findings" and resultant needs for new space materials developments and ground simulation testing/analytical modeling in seven categories: Environmental Parameters and Data Bases; LDEF Contamination; Thermal Control Coatings and Protective Treatments; Polymers and Films; Polymer-Matrix Composites; Metals, Ceramics, and Optical Materials; and Systems-Related Materials. General outlines of findings of the other LDEF Special Investigation Groups (Ionizing Radiation, Meteoroid and Debris, and Systems) are also included. The utilization of LDEF materials data for future low-earth orbit missions is also discussed, concentrating on Space Station Freedom. Some directions for continuing studies of LDEF materials are outlined.

In general, the LDEF data is remarkably consistent; LDEF will provide a "benchmark" for materials design data bases for satellites in low-Earth orbit. Some materials were identified to be encouragingly resistant to LEO SEE for 5.8-years; other "space qualified" materials displayed significant environmental degradation. Molecular contamination was widespread; LDEF offers an unprecedented opportunity to provide a unified perspective of unmanned LEO spacecraft contamination mechanisms. New material development requirements for long-term LEO missions have been identified and current ground simulation testing methods/data for new, durable materials concepts can be validated with LDEF results. LDEF findings are already being integrated into the design of Space Station Freedom.

INTRODUCTION

The National Aeronautics and Space Administration / Strategic Defence Initiative Organization Space Environmental Effects on Materials Workshop, June 1988, identified and prioritized candidate materials spaceflight experiments needed to validate long-term performance of materials on future spacecraft (reference 1). The highest priority identified by all participants of that workshop was virtually unanimous: The return of the NASA Long Duration Exposure Facility (LDEF) safely to earth, followed by a detailed analysis of its materials to compare with data obtained in previous relatively short in-space exposures and to validate, or identify deficiencies in, ground testing and simulation facilities and materials durability analytical models. As the First LDEF Post-Retrieval Symposium proved (ref. 2), the expectations of the NASA/SDIO Workshop were well founded. The initial in-space and experiment deintegration observations of LDEF at the end of its remarkable flight provided to the LDEF investigators an unparalleled opportunity to define space environment parameters and their long-term individual and combined effects on critical properties of materials for spacecraft applications.

The National Aeronautics and Space Administration Long Duration Exposure Facility, ref. 3, was launched into low-Earth orbit (LEO) from the payload bay of the Space Shuttle Orbiter Challenger in April 1984 (figure 1). It was retrieved from orbit by the Columbia in January 1990 (fig. 2). The 57 LDEF experiments covered the fields of materials, coatings, and thermal systems; space science; power and propulsion; and electronics and optics. LDEF was designed to provide a large number of economical opportunities for science and technology experiments that require modest electrical power and data processing while in space and which benefit from post-flight laboratory investigations of the retrieved experiment hardware on Earth. It was also designed to maintain these experiments in a stable orbital attitude to enable determination of directional effects of the space environment parameters. Most of the materials experiments were completely passive; their data must be obtained in post-flight laboratory tests and analyses.

The 5.8-year flight of LDEF greatly enhanced the potential value of most LDEF materials, compared to that of the original 1-year flight plan. NASA recognized this potential by forming the LDEF Space Environmental Effects on Materials Special Investigation Group (MSIG) to address the expanded opportunities available in studies of the LDEF structure and experiment tray material which were not originally considered to be materials experiments, so that the value of all LDEF materials data to current and future space missions would be assessed and documented. Similar Special Investigation Groups were formed for the disciplines of Systems, Ionizing Radiation, and Meteoroids/Debris.

This paper provides an overview of the interim LDEF materials findings of the Principal Investigators and the Materials Special Investigation Group. These revelations are based on observations of LEO environmental effects on materials made in-space during LDEF retrieval and during LDEF tray deintegration at the Kennedy Space Center, and on findings of approximately 1.5 years of laboratory analyses of LDEF materials by the LDEF materials scientists. These findings were extensively reviewed and discussed at the MSIG-sponsored LDEF Materials Workshop '91 (ref. 4). The results are presented herein in a format which categorizes the revelations as "clear findings" or "confusing/unexplained findings" and resultant needs for new space materials developments and ground simulation testing/analytical modeling in seven categories: Environmental Parameters and Data Bases; LDEF Contamination; Thermal Control Coatings and Protective Treatments; Polymers and Films; Polymer-Matrix Composites; Metals, Ceramics, and Optical Materials; and Systems-Related Materials. General outlines of findings of the other LDEF Special Investigation Groups (Ionizing Radiation, Meteoroid and Debris, and Systems) are also included. The utilization of

LDEF materials data for future low-earth orbit missions is also discussed, concentrating on Space Station Freedom. Some directions for continuing studies of LDEF materials are outlined.

Although this overview paper was not presented at the Workshop, it is included in these proceedings for completeness.

THE LDEF MISSION, SCIENCE TEAM, AND MSIG

LDEF was a free-flying, 12-sided cylindrical structure, approximately 30-feet long and 14 - feet in diameter (ref. 3). It had the capability to accommodate 86 experiment trays, most of which were 50-inches long and 34-inches wide. LDEF had no central power or data systems and no capability to transmit data to Earth while in orbit. Thus, experiments which took data during the flight had power systems (batteries) and data recorders on the inside of their trays, designed for 1-year of operation. Despite the obvious constraints of such arrangements and the much longer flight than planned, these data systems worked exceedingly well in almost all cases. The in-flight data recovered from the data tapes was of high quality. The skeletal structure of LDEF weighed approximately 8000 lb; the combined structure and experiment weight launched into orbit was approximately 21,400 lb. The initial orbit was nearly circular, at 257 nautical miles, with a 32° inclination. General information concerning the flight period, experiments, and participants is shown in Table 1 and further detailed in refs. 2, 3, and 5.

The orientation of the spacecraft with respect to the Earth during the mission is shown in figure 3. Values of key parameters of the low-Earth orbit environment which LDEF encountered are listed in Table 2. This orientation was maintained throughout the flight, from release by the Shuttle Challenger Payload Bay Remote Manipulator System to retrieval by the Columbia Remote Manipulator by precision placement (release) into its orbit, plus a design which included gravity gradient stabilization, careful consideration of mass distribution, and a passive viscous magnetic damper system. The remarkable flight attitude stability of LDEF (within less than 1° of movement in yaw, pitch, or roll) enables specific analyses of various individual and combined effects of LEO environmental parameters on identical materials and systems on the same space vehicle. NASA recognized this potential by forming four LDEF Special Investigation Groups (SIGs) (Table 1) to address the greatly expanded materials and LEO space environment parameter analysis opportunities available in the LDEF structure, experiment trays, and corollary measurements.

The LDEF Science Team management structure is shown in figure 4. Overall responsibility rests with the NASA Office of Aeronautics and Space Technology. The LDEF Science Office is located in the Materials Division of the NASA Langley Research Center; it is responsible for coordination of all LDEF experiment data, supporting data, and data generated by the SIGs.

The LDEF Environmental Effects on Materials Special Investigation Group (MSIG) was chartered to investigate the effects of the long-term LEO exposure on structure and experiment materials which were not originally planned to be test specimens, and to integrate the results of these investigations with data generated by the Principal Investigators of the LDEF experiments into the LDEF Materials Data Base. The LDEF Materials Data Analysis Workshop (ref. 6) addressed the plans resulting from that charter. MSIG membership includes 25 technical experts in the fields of atomic oxygen, radiation, contamination and other space environment effects on materials. Researchers with experimental and analytical experience in chemical, mechanical and physical properties of spacecraft materials and data basing are included. Several members provide liaison with the other LDEF Special Investigation Groups. The members represent technical laboratories and organizations throughout the United States, and laboratories in Canada and Europe. A number of MSIG members are also Principal Investigators of LDEF experiments.

Initial considerations of MSIG related to significant issues concerning space environmental effects on materials and the data potentially available from LDEF analyses to address these issues, as outlined in fig. 5. The general plan for MSIG operations is as follows:

- Systematically examine identical materials in multiple locations around LDEF to establish directionality of atomic oxygen erosion, ultraviolet radiation degradation, contamination, etc.
- Analyze selected samples from LDEF "non-materials" experiments and samples contributed from LDEF materials experiments.
- Establish central materials analysis capability:
 - Standardized, non-contaminating procedures for sampling / shipping / archiving
 - Uniform test / analysis procedures and ground simulation tests
 - Basis for assessment of laboratory-to-laboratory variations in materials data
- Focal point for coordination of all LDEF materials analyses:
 - Sponsor LDEF materials workshops / symposia
 - Generate unified LDEF Materials Data Base, including data from principal investigators, supporting data groups, and special investigation groups

The Boeing Defense and Space Group Laboratories in Seattle and Kent, Washington were selected as the MSIG Central Analysis Laboratory by the MSIG shortly after its formation in 1989.

The LDEF Materials Workshop '91 (ref. 4) was scheduled to elucidate, compare, and assess the results of the initial 1.5 years of observations and laboratory analyses of LDEF materials by the LDEF materials scientists. Figure 6 outlines the Workshop objectives and the materials disciplines addressed. The results in each discipline were extensively discussed and reviewed by technical teams consisting of technologists from the International Space Materials Community, with various degrees of familiarity with LDEF. Their findings are detailed in ref. 4. The next section of this paper (LDEF Materials Findings) includes information presented to and generated during this workshop, plus information based on previous observations of LEO environmental effects on materials made in-space during LDEF retrieval and during LDEF tray deintegration at the Kennedy Space Center in 1990 (see, for example, ref. 2).

LDEF MATERIALS FINDINGS

Environments and Data Bases

In this section the LDEF materials results are presented in a format which categorizes them as "clear findings" or "confusing/unexplained findings." Table 3 is such a listing for the environments encountered by the materials on LDEF and the considerations for LDEF materials data basing. In subsequent sub-sections on polymers and polymer-matrix composites findings from LDEF specimens, the first two "clear findings" of Table 3 will be illustrated; LDEF clearly demonstrated in a long-term flight that LEO atomic oxygen will erode all polymeric materials that are flown, which includes all those commonly used on spacecraft for thermal and electrical insulation, as paint "vehicles," and as composite matrices. Rates of erosion vary in different

materials and appear to change with exposure time for some polymers. Thus, results of short-term LEO-exposure tests (e.g. - ref. 7) may not provide data which can readily be extrapolated to predict long-term erosion rates. Fortunately, this erosion was found to be completely preventable with even extremely thin coatings of metals such as aluminum and oxides such as silica; many such coatings also adhered well to the polymer or composite substrate specimen surfaces in spite of thermal cycling during each orbit. Further specimen examination, analysis, and ground simulation testing is required to define atomic oxygen erosion mechanisms and the synergism of the combined atomic oxygen / ultraviolet radiation (and other) parameters of the LEO environment, before these items can be removed from the "confusing/unexplained findings" category.

Extensive molecular and particulate contamination was found on LDEF during post-flight inspections; contamination is addressed in detail in the next sub-section of this paper. While some initial progress has been made in understanding the sources and mechanisms of this contamination, much remains to be done to exploit the immense amount of information that LDEF can contribute to unmanned LEO spacecraft contamination awareness.

MSIG had an important role in defining LDEF mission environments. Figures 7 and 8 summarize the results of calculations of atomic oxygen fluence and equivalent sun hours of UV radiation, respectively, at the end of the mission on each LDEF tray location. Examination of these figures reveals the many combinations of AO/UV exposure conditions available to the SEE analyst on LDEF, because of the remarkable attitude stability during the 5.8-year flight. Fig. 7 shows that the highest AO fluence was 8.81×10^{21} atoms/cm², on the LDEF leading edge, about 8.1° off row 9 (towards row 10). Experiment trays on the side rows experienced different AO fluences because of the 8° ram vector angle. The Earth and Space end AO fluences were more than one order of magnitude lower than the ram fluence. The lowest AO fluence on LDEF was 1.13×10^3 atoms/cm² between rows 3 and 4. During the LDEF flight, the total fluence for rows 2 through 4 was in the same order of magnitude as the lowest fluence listed in fig. 7. However, during the retrieval mission, after LDEF was safely clamped in the shuttle payload bay, an "anomaly" occurred, when LDEF rows 1 through 3 (which faced out of the bay) were inadvertently subjected to atomic oxygen at the retrieval altitude for approximately 15 minutes. That inadvertent exposure raised AO fluence from the 10^3 to the 10^{17} atoms/cm² order-of-magnitude for the experiment trays on those rows.

Fig. 8 shows vacuum ultraviolet radiation fluences on LDEF as a function of row position. The highest VUV fluences were 14500 equivalent sun hours (ESH) on LDEF space-end experiment trays, with intermediate values of 11100 ESH on leading and trailing edge trays and 6500 to 6900 ESH on side trays. The lowest VUV fluence was 4500 ESH, received by the Earth-end trays.

LDEF data presented later in this paper will illustrate another clear finding in Table 3: past atomic oxygen fluence models do not account for atomic oxygen impingement rates at "grazing" angles to the spacecraft. MSIG modified an AO fluence model to account for the thermal velocity distribution of the atomic oxygen atoms in LEO. As shown in fig. 9, this modification predicts orders-of-magnitude higher AO fluences than the previous model (with thermal molecular velocity excluded) at AO incidence angles to LDEF from 95° to 110°, which was verified by LDEF findings.

It has become clear that geometric details of the exposed surfaces in conjunction with their flight attitude are keys to understanding some of the space environmental effects that occurred differently on different parts of experiment trays. Such effects as atomic oxygen atoms which do not "stick" to a surface but deflect onto another surface and react with it, and partial shadowing of atomic oxygen and solar ultraviolet radiation on exposed surfaces will affect fluences of these

environmental factors. MSIG is developing analysis schemes to account for these "microenvironments."

MSIG is currently considering options and needs for data basing of the extensive LDEF materials data that has been generated to date and will be in the near future. The LDEF Materials Workshop '91 participants clearly indicated their expectations of two kinds of materials data bases: one for the spacecraft design community and another for the space environmental effects on materials research community. Initial MSIG data basing plans are indicated in figure 10.

LDEF Contamination

The basic contamination control requirement for LDEF was "visibly clean level II" (SN-C-0005) (ref. 8a). The provisions for contamination control are stated in the LDEF Experimenter's User Handbook (ref. 8b). General provisions included the following: "Control of contaminants represents a concern for the safe operation of the shuttle system. The shuttle requirements are defined in JSC Specifications SN-C-0005 and SP-R0022A. As applied to an LDEF experiment, these concerns become a requirement for control of particulate contamination, control of stray or trace quantity materials and control of outgassing-sublimation productions. Contamination control represents an element in the materials selection process...". Preflight cleaning procedures were those utilized for any shuttle payload to maintain the cleanliness of the payload bay. Even though these requirements were followed and all materials used on the spacecraft structure and experiments were nominally "space qualified," LDEF carried a significant amount of both particulate and molecular contaminants when it was placed in orbit. Fig. 11 is a general overview of the contamination history of LDEF.

A preliminary report on LDEF contamination is available, ref. 9, which documents initial observations made during the deintegration of LDEF experiments in the SAEF 2 Facility at NASA - KSC from February to April, 1990. Paraphrasing the conclusions of that report, silicones and hydrocarbons are significant contributors to the molecular films accumulated on the LDEF surfaces; the estimated total weight of outgassed material deposited was approximately one pound. The particle cleanliness of LDEF at launch exceeded a MIL STD 1246B level 1000 C. The Shuttle Orbiter Payload Bay is a source of contaminants. The orbital environment creates new particles and distributes particles, even for passive space platforms. Changes in motion of a spacecraft free many loose particles from the vehicle surfaces in orbit. A major redistribution of particles occurred during LDEF reentry, landing at Edwards AFB, California, and ferry flight to NASA - KSC, Florida. Although the cleanliness level of LDEF surfaces during deintegration still exceeded a MIL STD 1246B level 1000 C; an extensive variety of particle types was still present.

Table 4 is a listing of LDEF contamination findings, based on the LDEF experiment deintegration preliminary observations and subsequent studies. The scope of the contamination analyses is indicated in fig. 12 (see refs. 8a and 10). Fig. 13 is a photograph of the LDEF skeleton structure after experiment tray deintegration. The brownish-yellow or amber colored contamination film (which was once described to resemble a "nicotine stain") is clearly present on aluminum alloy structural element surfaces which were exposed directly to the space environment. The lighter regions of those structural elements were covered by experiment tray edges and clamps; thus, the molecular contamination film did not deposit on them. Also visible in this photograph of the aft end of LDEF is the magnetic viscous damper system which was a critical contributor to LDEF's remarkable attitude stability throughout its mission. The LDEF molecular contamination was extensive, apparently a result of multiple sources of organic hydrocarbons and silicones, both internal and external to LDEF (including cross-contamination from the Shuttle). The molecular contamination film detailed studies indicated a temperature dependence during the deposition process. A possible scenario for these observations is as follows: Outgassing products from a variety of silicones and organic materials formed a "contamination cloud" around LDEF during all

or most of the mission. Solar ultraviolet radiation and/or atomic oxygen polymerized some of the molecular components of that cloud, increasing molecular weight and, thus, increasing the temperature at which these materials will condense on adjacent surfaces. LDEF surfaces were alternately heated and cooled by the presence or absence of sunlight during the different portions of each 90-minute orbit. In the "mornings" of the orbits, when surfaces are coolest and the solar UV begins to polymerize the "cloud," deposition of a contamination film layer on LDEF surfaces is most probable. Observations of a number of LDEF surfaces indicated that the ubiquitous contamination "stain" had been deposited in numerous layers. In addition to this general contamination film, which was probably on the order of tens of nanometers in thickness, there were a number of localized areas of LDEF which had heavy molecular contamination deposits, such as areas adjacent to some electrical connectors.

There were apparently interactions of the space environment with the contamination films during the LDEF flight. Leading edge deposits were more transparent than those on the sides and trailing edges of LDEF. The effects of atomic oxygen, perhaps combined with the other parameters of the low-Earth orbit space environment, can be postulated to cause such an effect, by changing silicones to silicates, for instance. Some additional aspects of this general molecular contamination are discussed in refs. 9 through 14.

Particulate contamination (table 4) was deposited on and from LDEF surfaces throughout its pre-flight, on-orbit, and post-flight history. An example of a particle which came from a degraded LDEF specimen is shown in fig. 14; it is an orbit-modified carbon fiber composite particle which was found in the Shuttle Orbiter Columbia payload bay on the cradle from which the Syncom satellite was launched during the LDEF retrieval mission. Further information on LDEF particulate contamination is found in refs. 9, 10, 13, and 15.

The right side of table 4 lists the findings related to LDEF contamination that have yet to be explained or quantified, including sources of contaminants, quantitative degradation mechanisms, and the contributions, if any, of chemical derivatives of LDEF materials which resulted from AO interactions. Perhaps the most important of the findings to be definitized are the effects of the LDEF contamination on analyses of materials for other space environmental effects.

At the bottom of table 4 are self-explanatory comments on new materials development requirements for future spacecraft and ground simulation testing requirements which have resulted from the initial LDEF contamination studies.

LDEF provides a unique opportunity to provide a unified perspective on unmanned spacecraft contamination mechanisms in low-Earth orbit. It was the ultimate witness plate for the shuttle orbiter payload bay. It was a molecular film deposition experiment. It provided data for many potential studies of orbital effects on surface contaminants, both molecular and particulate. It provides data for validation of current and future contamination monitoring systems for spacecraft.

Thermal Control Coatings and Protective Treatments

Table 5 outlines the findings of LDEF materials studies on thermal control coatings and protective treatments. One of the most important (and reassuring) findings to spacecraft designers regards the excellent stability of chromic-acid anodized aluminum as a thermal control surface. Fig. 15 summarizes solar absorptance (α_s) and thermal emittance (ϵ) data, averaged for 228 tray clamps on all areas of the LDEF structure (ref. 16). A slight increase in average values of α_s/ϵ was noted after the 5.8-year low-Earth orbit exposure, as compared to both ground- and flight-control specimen data; this increase is insignificant from an engineering consideration. However, additional data of this type from other LDEF investigators indicates that this small increase is a real

effect which may require consideration for critical components on much longer flights than LDEF experienced.

Fig. 16 illustrates the second clear finding in table 5. The solar absorptance of white thermal control paints on a leading edge LDEF tray was measured before, during, and subsequent to the flight (refs. 17 and 18). The stable emittance behavior of the Z-93 coating is representative of only four of the many thermal control paints flown on LDEF. Many other "space qualified" white paints behaved like the A276 paint, increasing in solar absorptance as the flight progressed (as shown in fig. 16). Fig. 17 shows α_s/ϵ ratios of A276 paint disks located on many regions of the LDEF external surface. It is obvious that the white paint surfaces facing the front of LDEF (and thus the atomic oxygen fluence) retained the α_s/ϵ ratios of the control specimen, while those on the rear face of LDEF (where atomic oxygen fluence was low) showed a doubling of α_s , compared to that of the control specimen (ϵ values were not affected during the flight). Note that the α_s changes occurred at an incidence angle of approximately 100° to 105° , confirming the discussion presented previously in relation to fig. 9. The thermal control property stability of the Z-93 (and similar) thermal control paint coatings is attributed to its high purity potassium silicate binder; organic paint binders such as the polyurethane used in the A276 paint are affected by solar ultraviolet radiation, which darkens their surface (raising α_s). Large fluences of atomic oxygen erode this dark surface layer away, "cleaning" the white paint surface. It is postulated that the A276 ram-facing surfaces on LDEF may actually have darkened during the earlier part of the mission when atomic oxygen flux was relatively low, then were "cleaned up" during the last few weeks of the mission, when atomic oxygen flux was much higher.

As noted in the discussion of table 3, atomic oxygen erosion of FEP Teflon was higher than that predicted on the basis of short-time LEO exposures. Predicted erosion of FEP on leading edge LDEF trays was approximately eight times lower than that measured after the flight.

Fig. 18 illustrates microcracking which occurred in the silver/Inconel layer of silvered Teflon (Ag/FEP) second-surface mirror insulation blankets (ref. 18). Such microcracking has been shown to be preventable by modifying the adhesive-backed Ag/FEP application procedures. This microcracking resulted in bleed-through of adhesive to the base of the FEP during the LDEF flight; when the adhesive in the microcracked areas was affected by solar ultraviolet radiation, it darkened and the solar absorptance of the Ag/FEP substantially increased. Figure 19 illustrates another important finding of the LDEF experiments: clear silicone coatings on some substrates experienced extensive surface "crazing" (ref. 4), which could affect light transmittance for some critical applications.

Atomic oxygen "undercutting" of polymer substrates under protective coatings is a phenomenon that can be a particular concern for space applications of multilayer insulation (ref. 19). The phenomenon is illustrated in fig. 20. The low reaction probability with a polymer such as Kapton at the initial impact of monatomic oxygen causes the atom to scatter with a cosine distribution, so that even for coating defects (i.e.- holes or cracks) facing the atomic oxygen ram direction, the underlying Kapton substrate will be undercut. This effect was measured on LDEF multilayer insulations of aluminized Kapton; the results are shown in fig. 21. Undercut widths range from approximately eight times the defect crack width for small cracks ($\sim 0.1\mu\text{m}$ wide) to approximately three times for larger cracks ($\sim 0.6\mu\text{m}$ wide). Thus the LDEF data gives a good engineering perspective on this phenomenon.

The unexplained findings in table 5 included a fluorescence shift in surfaces of several LDEF coating specimens. Whereas the unexposed coatings fluoresced in the ultraviolet portion of

the spectrum when subjected to UV radiation, the exposed coatings fluoresced in the visible portion of the spectrum (ref. 18). Although this phenomenon has been noted previously (see, for instance, ref. 20), the details of the surface chemistry changes for the LDEF specimens have not yet been elucidated. Two important coatings, S-13GLO (ref. 21) and black chromium showed variabilities in their thermal control properties which have not yet been explained. The synergistic roles of UV, electron and proton radiation in the atomic oxygen erosion of certain polymeric materials such as FEP Teflon have not yet been quantitatively defined.

New materials development requirements in thermal control coatings and protective treatments for long-term LEO missions are listed in table 5. Included are thin, transparent silicate overcoats resistant to crazing. In regard to the second listed item, discussions at the LDEF Materials Workshop '91 indicated that some technologists feel that the current U. S. supply of pure potassium silicate paint binder for Z-93 might be questionable in the future, while others were not as concerned. The final item in the new materials category regards the need for a flexible white thermal control coating with demonstrated long-term LEO durability. The PCBT coating developed by the MAP Company in France has shown promise in a 9-month exposure (in a FRECOPA cannister) during the LDEF missions and in another short LEO flight (ref. 22). Ground simulation testing requirements in the coatings category are also listed in table 5.

Polymers and Films

Table 6A outlines the findings of the LDEF materials studies on polymeric materials and polymer films. The first two clear findings are illustrated in figs. 22 through 24. The Teflon surface of Ag/FEP blankets was eroded by atomic oxygen as shown in the scanning electron microscope photomicrograph at the right of fig. 22 for a specimen which saw a high AO fluence (refs. 23 and 24). The small salt crystal on the surface of the Teflon was possibly deposited on the launch pad prior to the LDEF insertion flight; the crystal is highly resistant to atomic oxygen and shielded the Teflon under it from erosion. The height of the "mesa" (and, thus, the depth of erosion) is approximately 0.0012-inch; based on short-term LEO exposure data in LEO (ref. 25), the predicted erosion depth was on the order of 0.00015-inch. This may be an example of AO/UV synergism wherein a threshold of UV exposure is reached after which the erosion is accelerated, as postulated in ref. 26. The morphology of the erosion around the "mesa" is consistent with that seen in many AO-eroded polymer specimens from space and from ground simulation AO beam facilities. The two microscopic profiles on the left of fig. 22 were made using a scanning tunneling microscope on an FEP surface that was shielded from AO and one which had a low AO fluence during the flight. The shielded surface is smooth, even at the hundred-nanometer level; the low AO fluence surface at the lower left (compared to the high fluence surface at the right) shows that the erosion mechanism is similar for both low and high fluence exposures. The post-flight visual appearance of the low-fluence surface was transparent and specular, similar to that of control specimens; the high-fluence surface was quite different, milky and diffuse, leading to supposition that the thermal control properties of this widely used second-surface mirror blanket material had been significantly degraded (fig. 23). Fortunately, that supposition was disproved, as shown in fig. 24, which is a plot of α_s/ϵ ratios for Ag/FEP samples from a number of LDEF locations. Samples from rows 6 through 11 received much higher AO fluences than those from rows 1 through 5 (fig. 7) but all samples retained the α_s/ϵ ratio of control specimens excepting one sample from row 8, which had a heavy contamination stain on it (ref. 27). The visual appearance change of the uncontaminated Ag/FEP was entirely due to a change in reflectance type from specular to diffuse, but not in magnitude of total reflectance.

Figs. 25 and 26 illustrate the effect of meteoroid and debris impacts on silvered Teflon thermal blankets: A delaminated area (vapor-deposited silver/Inconel coating delaminated from the FEP Teflon) from a fraction of a centimeter to several centimeters in diameter surrounded the sub-

millimeter-diameter craters made by the impacts (fig. 25). The ability of Ag/FEP to function as a second-surface mirror thermal control blanket is affected. Fig. 26 qualitatively indicates this finding. An Ag/FEP sample flown on LDEF with impact crater and delamination diameters of approximately 0.5mm and 10mm, respectively was photographed on its front face with an infrared camera while transient heating was applied to the rear face with an infrared lamp. The resultant "thermal lag" in the delaminated area is evident; the implication is that thermal energy absorbed by the silver surface from solar heating in LEO will not be readily conducted into the Teflon to be radiated to space from the blanket surface. The LDEF blankets most severely affected by this phenomenon had about 5 percent of the area delaminated; from an engineering point of view, this should not result in significant losses of thermal control capability for Ag/FEP blankets. For much longer LEO flights than LDEF's, however, this phenomenon must be considered.

The effects of the LDEF environment on mechanical properties of FEP film from the Ag/FEP thermal blankets are indicated in fig. 27 (ref. 27), which shows data from films exposed to the space environment and control specimens flown on LDEF which were protected from the environment. Although the Teflon surface was eroded by the atomic oxygen exposure on rows 7 to 11 (and, thus, load carrying capability of the film was reduced), the tensile strength was not affected. However, on LDEF rows 1 to 6, where AO fluence was low, tensile strength was reduced by approximately 30 percent from that of the control specimens. This finding was apparently due to the effects of long-term solar ultraviolet radiation exposure of the FEP film surface; erosion of the affected surface layer by AO resulted in no degradation of the film strength (based on the remaining cross-sectional area, after erosion). Ref. 28 also presents data on this phenomenon. Polyethylene films on LDEF exhibited similar effects.

Some film specimens received 10-month exposures in cannisters which were opened to the LEO environment after LDEF was inserted into its orbital trajectory and were closed 10 months later, protecting the surfaces from further exposure for the balance of the mission (ref. 29). Photographs of four such specimens from experiment A0134 are shown in fig. 28; the experimental siloxane-modified polyimide, PIPSX-6 resisted atomic oxygen erosion much better than other polymers flown on LDEF. Fig. 29 shows the results of the full 5.8-year LDEF exposure on polymer films on the same LDEF leading edge experiment tray which were up to ~0.25-mm thick, sized for the planned 1-year LDEF mission. They were completely eroded by atomic oxygen during the 5.8-year flight (ref. 29).

Other clear findings listed in table 6A include the recognition of LDEF contamination and the importance of considering contamination effects in the analysis of LDEF polymeric materials' surfaces. The finding that atomic oxygen erosion of Kapton is linearly predictable with AO fluence (ref. 4), based on comparison of LDEF data with data from previous space flights, has important implications for Kapton's use as "witness" specimens in AO ground laboratory exposures which attempt to simulate LEO effects, with LDEF data as the baseline for comparison before extrapolation to other flight conditions is attempted. Other polymeric materials, such as polystyrene and PMMA, exhibited greater erosion than predicted for the LDEF exposure (based on previous flight data), similar to that described above for FEP Teflon. LDEF specimen analyses indicate that the atomic oxygen erosion mechanism involves minimal chemical changes, if any, to the polymer films (ref. 30). Some film specimens appear to have been exposed to extensive heating; this may be another "microenvironment" effect. Carbon films were attacked by atomic oxygen, somewhat more slowly than most of the polymer films, but at a high enough rate to require surface protection for long LEO flights.

The unexplained findings for polymers and polymer films (table 6A) include the erosion findings discussed above, the sources of thermal effects, and the degree of confounding of polymer surface analyses due to the molecular contamination.

Table 6B lists new polymeric material development requirements for durability in long term LEO environments and ground simulation testing requirements, based on LDEF polymers and polymer film analyses thus far. No current polymeric material appears to be completely resistant to atomic oxygen and/or UV attack. If such polymers can be developed, they must have the additional attribute of non-contamination of other materials on a spacecraft due to outgassing, reaction products from AO or other LEO environmental parameter interactions, etc. Ground simulation testing requirements listed in table 6B are largely self-explanatory. The final item listed (definition of thermal "lag") will require tests of specimens of significant size in non-contaminating vacuum chambers.

Polymer-Matrix Composites

One of the important benefits of the attitude stability of LDEF during its entire flight is the capability to examine identical or similar materials from different locations on the LDEF exterior. Fig. 30 shows the location of four classes of graphite-fiber reinforced polymer-matrix composite materials, with examples of several materials for the epoxy- and polyimide-matrix composites. The LDEF location, AO fluence, and vacuum ultraviolet radiation fluence are tabulated for each exposure location and additional environmental parameters are listed. In general, as indicated during the discussions at the LDEF Materials Workshop '91, the data on space environmental effects on these composite materials from various principal investigators studies and the MSIG evaluations was remarkably consistent. Anomalies revealed in those investigations may well be due to "microenvironment" effects, discussed previously.

Table 7 outlines the findings of LDEF materials studies on polymer-matrix composites. The first clear finding, surface degradation of uncoated composites, is illustrated in fig. 31 in scanning electron microscope photomicrographs of a small wedge cut from a 4-ply, $[\pm 45]_s$ specimen of T300/ 5208 (Gr/Ep) composite exposed on LDEF Experiment A0134 (on tray 9B, thus on an LDEF experiment tray closest to the leading edge) (ref. 31). Virtually one ply of composite material (approximately 0.012cm) was eroded away during the 5.8-year exposure. The epoxy matrix eroded somewhat more rapidly than the graphite fibers. An ash-like residue remained on the eroded surface after the flight. Fig. 32 shows a compilation of chemical- and mechanical-property data from specimens on the same experiment tray (9B). The chemical properties (infrared spectra, T_g and molecular weight distribution) are for the polysulfone-matrix P1700 specimens. They show no bulk polymer property changes in the composite due to the exposure; similar findings were found for the other composites. The mechanical property chart of tensile modulus for all composites tested in LDEF Experiment A0134 (lower right), shows good correlations between the 3 types of control specimens and reasonable consistency with the erosion data illustrated in fig. 31.

Fig. 33 illustrates an important LDEF finding to spacecraft designers who require polymeric-matrix composites for critical low-Earth orbit applications, because of the combination of very low coefficient of thermal expansion that can be "tailored" into these composites and their low weight and high specific moduli compared to other candidate spacecraft materials: Very thin inorganic coatings on the surfaces of polymeric composites completely prevent AO erosion (ref. 32). A vapor deposited, 1200Å-thick aluminum coating protected the T300/934 (Gr/Ep) from AO, with negligible weight penalty. No coating delamination from the composite surface was noted after approximately 34000 thermal cycles in LEO. Similar results were found for a variety of inorganic coatings, including Ni and SiO₂.

The dimensional stability of composite materials after long term exposures in Earth orbit has been a concern of spacecraft designers. LDEF experiment AO180 on tray D12 (90° to the LDEF leading edge) was devoted to this concern and generated excellent data to define the problem, measuring thermal expansion in orbit on a tape recorder, as composite specimens were being thermally cycled during each orbit (ref. 33). Fig. 34 depicts a few of the results. The graph

on the right, of microstrain as a function of temperature for a stainless steel calibration tube, illustrates the high quality of the experimental data. The graph in the center of fig. 34 shows that some dimensional changes do occur in a unidirectional graphite/epoxy composite in the longitudinal direction. The graph on the left is for the same composite, in the transverse direction. During the first 40 days in orbit, this transverse specimen shrunk significantly, approximately 500 cm/cm of microstrain. When LDEF returned to Earth, this dimensional instability was found to be completely reversible and to be due almost entirely to moisture desorption in orbit and absorption of moisture from the Earth's atmosphere after return from orbit. Thus, it is possible that preconditioning of composites to remove moisture prior to flight could substantially reduce, if not eliminate, dimensional instability of polymer-matrix composites in orbit.

Other clear findings on LDEF polymer-matrix composite specimens are listed in Table 7, including items related to optical properties, meteoroid and debris impacts and thermal cycling. More information in these areas can be found in ref. 2. The unexplained findings in polymer-matrix composite materials on LDEF include (as for most other materials) the effects of contamination. The second unexplained finding, the differences in AO erosion morphologies of Gr/Ep reinforced with 5-mil tape are depicted in the left side photomicrograph of figure 33. The "ash" residue on AO-eroded composite surfaces appeared to vary with the composite material. The lack of degradation of uncoated composite material mechanical properties may simply be due to the degree of erosion on the fiber and its interface with the matrix.

New materials development requirements in polymer-matrix composites concentrate on scaleup and thermal cycling adherence verification for coatings, plus the development of flexible coatings. Ground simulation testing requirements (Table 7) are similar to those noted for other materials categories, including size of specimens, synergistic effects of simulated space environment parameters, and analytical modelling of such effects.

Metals, Ceramics, and Optical Materials

Table 8 outlines the findings of LDEF materials studies on metals, ceramics, and optical materials. Most of these findings are described in more detail in refs. 2 and 4. A key clear finding regarded structural metals, aluminum and titanium alloys. Their mechanical properties were unaffected by the LDEF 5.8-year LEO exposure (refs. 34, 35, and 36 and discussions at LDEF Materials Workshop '91), although certain minor surface effects were noted in the highest AO fluence regions (refs. 37 and 38). No coldwelding was found (refs. 39 and 40). Aluminum coated stainless steel was verified to be a very stable mirror/reflector for extended LEO exposures. The molecular contamination on many LDEF surfaces, discussed previously, appeared to be the most prevalent effect on most metallic and ceramic structural materials; it affected the properties of optical materials. The exceptions to this general finding are discussed in the following paragraphs.

As shown in fig. 15, discussed previously, thin anodized coatings on aluminum alloys showed small but measurable increases in the ratio of solar absorptance to thermal emittance as a result of the LDEF exposure. This effect was apparently due to a combination of light contamination and atomic oxygen effects on the surface (ref. 38).

All metallic film coatings excepting tin and platinum showed at least some slight evidence of surface oxidation of the LDEF Leading Edge (ref. 41); silver, osmium, and copper showed heavy oxidation (refs. 41, 42, and 43), as illustrated for a vapor-deposited silver coating on an optical glass substrate in fig. 35.

Both aluminum- and magnesium-matrix composites were exposed on LDEF in experiment AO134. The aluminum metal-matrix composite showed no evidence of degradation due to the 5.8-year exposure. The P100 graphite fiber reinforced magnesium alloy composite was not notably

degraded from a structural point of view, but some magnesium oxidation was evident at the specimen edges, where the graphite fibers intersected the surface (fig. 36).

Graphite reinforced borosilicate glass composites with no protective coatings were highly stable during the LDEF flight (ref. 44). The chart on the left of fig. 37 shows the coefficient of thermal expansion (CTE) of this material as a function of temperature for specimens exposed on LDEF leading edge (LE) and trailing edge (TE) trays, compared to that of a control specimen. At the time of the LDEF launch, in 1984, this material was experimental; the CTE values shown are within the material variability. No CTE changes due to the 5.8-year exposure should be inferred. The photograph at the right shows a Gr/GI exposed LE specimen cross section, with the specimen surface at the top. Only the graphite fibers which were on the specimen surface were eroded by atomic oxygen; even a few μm of glass surrounding the fiber completely prevented AO erosion for the entire flight.

Other clear findings on these classes of materials relate to the LEO stability of ceramics and glasses (unless damaged by meteoroid and debris impacts), effects on optical properties of glass in the ultraviolet regions of the spectrum (probably largely related to molecular contamination), and the increased absorptance of some black coatings, Table 8. Unexplained findings, new materials development requirements, and ground simulation testing requirements are similar to those discussed previously for other material classes.

Systems-Related Materials

This materials category covers lubricants, adhesives, seals, mechanical fasteners, solar cells, and batteries, with materials aspects studies conducted jointly by the LDEF Systems and LDEF Materials Special Investigation Groups; a detailed exposition of findings is presented in ref. 45. In general, LDEF systems functioned well; the system materials met their requirements. Table 9 outlines some specific findings. Clear findings included the need to protect lubricants from direct contact with the LEO environment and to carefully lubricate fasteners to prevent galling during installation, if post-flight disassembly is required. All seals on LDEF were protected from direct exposure to atomic oxygen and electromagnetic/particulate radiation; they functioned well. Some acrylic and RTV adhesives (ref. 35) degraded in one experiment, but silicone adhesives performed well in another (ref. 46).

FINDINGS IN OTHER LDEF DISCIPLINES

As shown in fig. 3, the four LDEF Special Investigation Groups include those involved in the disciplines of ionizing radiation, meteoroid and debris, systems, and materials. The interim findings of the latter have been detailed in the preceding sections of this report. The findings of the other SIGs are detailed in refs. 2, 45, 47, 48, and 49 and are outlined in figs. 38, 39, and 40, which are self-explanatory. Additional information on LDEF thermal and solar illumination environments is presented in refs. 50, 51, and 52.

LDEF MATERIALS CONTRIBUTIONS TO SPACE TECHNOLOGY

As noted in the introduction, the promise that LDEF offered (ref. 1) for providing unparalleled data on long-term space environmental effects on materials in low-Earth orbit is being fulfilled. Fig. 41 is a perspective of LDEF data in comparison to previous sources of ground-

simulation and flight-experiment data. Ground-simulation testing is generally limited to simulation of one or simultaneous simulation of two or three, or sequential simulation of the key space environmental parameters which cause material degradation in LEO. However, there are many environmental parameters, both natural and induced, which may become the key parameters for a particular mission or application. Those which have been considered for Space Station Freedom (SSF) Work Package 2 are listed in figs. 42 and 43. Real time flight test data is indispensable to determine whether the ground simulation exposure provides a reasonable simulation of the materials degradation mechanism(s) involved. Thus, ground simulation tests alone are often inadequate for LEO SEE simulation.

Previous flight data from Mir, Solar Max, and Space Shuttle Orbiter Payload Bay experiments (fig.41) have significant limitations in environment definition, specimen material definition and control specimens, and exposure duration. LDEF overcame all these limitations with a relatively long exposure in the proposed SSF orbit (albeit only one-fifth of the proposed life of the SSF structure), well-defined experiments, and the stable orbital attitude which is a key to direct and unambiguous analyses of materials degradation and degradation phenomena.

Fig. 44 lists the variety of NASA and U. S. Department of Defense space mission categories for which LDEF materials data can make important contributions during the planning and design phases. Focusing in on Space Station Freedom, fig. 45 paraphrases a letter from the prime SSF Phase 2 contractor concerning their recent utilization of LDEF materials data (ref. 53). Thermal control materials and coatings data were of particular interest for radiator applications. The verification of long-term stability of absorptance and emittance of anodized aluminum in LEO and the preliminary characterization of contamination were of importance to design considerations for the SSF aluminum alloy truss structure. The revised atomic oxygen fluence model has been utilized to design for materials erosion, particularly in "grazing AO flux" areas. The need for outer layer surface protection for multilayer blanket insulations on SSF for long mission lives was established with LDEF data.

CONTINUING LDEF MATERIALS STUDIES

The LDEF materials studies to date represent approximately 70 percent of the currently planned MSIG observation and data collection activities, ~25% of planned data comparisons with current environmental degradation models and damage theories, ~50% of generation of new environment and damage models, and ~10% of materials data bases and archives development. Given the quantity and quality of archived LDEF materials available, much more than the current plan could be done, but funding limitations have constrained all but the highest priority activities. Another limitation regarding specimen analysis for data collection, especially for polymeric materials, concerns post-exposure effects in Earth storage on surfaces which have been exposed to the LEO environment (refs. 29 and 30). MSIG support for materials analysis on polymeric and metallic materials and on composite materials will decline in 1992 and 1993, with the focus gradually changing to phenomenological understanding, documentation, archiving, and data basing. LDEF specimens and hardware will be archived and will be available to researchers worldwide in the foreseeable future, through the LDEF Science Office and NASA.

Projected MSIG ground-based simulation testing activities (which can now utilize LDEF data as a baseline or "sanity check" on the ability of the ground test to adequately simulate LEO effects and phenomena) are listed for contamination-related tests and LDEF-exposure/ground-exposure effects correlation in fig. 46. Projected MSIG environmental modeling activities are listed for contamination-related modeling, exposure effects modeling, and environmental parameter modeling in fig. 47. Some of these are currently in progress and others have been planned, but some will suffer from lack of funding support. A plan for a detailed study of LDEF contamination

mechanisms to provide a unified perspective of large spacecraft contamination for future space missions is outlined in fig. 48; however, implementation of this plan is beyond the scope of current MSIG resources.

CONCLUSIONS

This paper has presented a broad overview of interim findings of materials observations and analyses from ongoing studies of specimens from the National Aeronautics and Space Administration Long Duration Exposure Facility. These findings are summarized in Table 10. The column at the upper left lists materials which demonstrated high resistance to degradation for the entire 5.8-year flight. The column at the upper right lists materials which may be perfectly adequate for flights up to several years in LEO but which, if unprotected, exhibited various degrees of degradation during the LDEF flight. As a result of these findings, new materials development requirements and general ground simulation testing requirements have been identified, as listed in the lower parts of Table 10.

In general, LDEF met or surpassed all of its goals regarding the generation of long-term data on spacecraft materials. The ongoing studies outlined herein indicate LDEF to be the definitive source of long-term exposure verification of low-Earth orbit effects on materials. The quantitative data / micro-environment / mechanistic understanding being developed will strongly contribute to future spacecraft design and new materials development guidelines. LDEF furnishes an unprecedented opportunity to provide a unified perspective of unmanned low-Earth orbit spacecraft contamination mechanisms and interactions. The LDEF materials data bases under development should become the basis of a new family of design guidelines for space environmental effects on materials.

ACKNOWLEDGEMENTS

The author is pleased to express his appreciation for the efforts of the outstanding LDEF planners and scientific investigators, and particularly the members of the LDEF Materials Special Investigation Group, whose remarkably competent efforts made this review paper possible. Special thanks go to Phil Young, Lou Teichman, Wayne Slem, Joan Funk, Bill Kinard, Arlene Levine, and Maureen Sgambelluri of the NASA-Langley Research Center; Bruce Banks of the Lewis Research Center; Jim Mason and Joel Edelman of the Goddard Space Flight Center; Ann Whitaker, Roger Linton, Jim Zwiener, and Tom Parnell of the Marshall Space Flight Center, and the MSIG support laboratory staff at Boeing Defense and Space Co., led by Gary Pippin and Harry Dursch. As I approach retirement from a long NASA career in aerospace materials research, I know that my associations with the LDEF community will always be remembered as one of the unforgettable highlights of my life.

REFERENCES

1. Teichman, Louis A. and Stein, Bland A. (Compilers): NASA/SDIO Space Environmental Effects on Materials Workshop. NASA Conference Publication 3035, 1989.
2. Levine, Arlene S. (Editor): LDEF - 69 Months in Space: First Post-Retrieval Symposium. NASA Conference Publication 3134, 1992.

3. Clark, Lenwood G.; Kinard, William H.; Carter, David J. Jr.; and Jones, James L. Jr. (Editors): The Long Duration Exposure Facility (LDEF). NASA SP-473, 1984.
4. Stein, Bland A. and Young, Philip R. (Compilers): LDEF Materials Workshop '91. NASA Conference Publication 3162, 1992.
5. Kinard, William H.; Martin, Glenna D.; and O'Neal, Robert L.: Initial Results from the Long Duration Exposure Facility Postretrieval Observations. AAS Paper 91-15, 1991.
6. Stein, Bland A. and Young, Philip R. (Compilers): LDEF Materials Data Analysis Workshop. NASA Conference Publication 10046, 1990.
7. Visentine, J.T.; Leger, L.J.; Kuminecz, J.F.; and Spiker, I.K.: STS-8 Atomic Oxygen Effects Experiment. AIAA Paper 85-0415, 1985.
8. a. Anon.: Preliminary Report on LDEF Related Contaminants. Boeing Defense and Space Co. preliminary report to LDEF MSIG. Available from LDEF Science Office, NASA - LaRC, MS 404, Hampton, VA 23665-5225.
b. Anon.: Long Duration Exposure Facility (LDEF) Experimenter Users Handbook. LDEF No. 840-2, Change No. 3, October 1980. Available from LDEF Science Office, NASA - LaRC, MS 404, Hampton, VA 23665-5225.
9. Crutcher, E. R.; Nishimura, L. S.; Warner, K. J.; and Wascher, W. W.: Migration and Generation of Contaminants from Launch through Recovery: LDEF Case History. In LDEF-69 Months in Space, NASA Conference Publication 3134 (A. Levine, editor), Part 1, 1991, p. 121.
10. Crutcher, E. R.; Nishimura, L. S.; Warner, K. J.; and Wascher, W. W.: Quantification of Contaminants Associated with LDEF. In LDEF-69 Months in Space, NASA Conference Publication 3134 (A. Levine, editor), Part 1, 1991, p. 141.
11. Crutcher, E. R. and Warner, K. J.: Molecular Films Associated with LDEF. In LDEF-69 Months in Space, NASA Conference Publication 3134 (A. Levine, editor), Part 1, 1991, p. 155.
12. Harvey, G. A.: Organic Contamination of LDEF. In LDEF-69 Months in Space, NASA Conference Publication 3134 (A. Levine, editor), Part 1, 1991, p. 179.
13. Maag, C. R. and Linder, W. K.: Measured Space Environmental Effects to LDEF During Retrieval. In LDEF-69 Months in Space, NASA Conference Publication 3134 (A. Levine, editor), Part 1, 1991, p. 85.
14. Young, P.R. and Slep, W.S.: An Analysis of LDEF-Exposed Silvered FEP Teflon Thermal Blanket Material. NASA TM 104096, 1991.
15. Crutcher, E. R. and Wascher, W. W.: Particle Types and Sources Associated with LDEF. In LDEF-69 Months in Space, NASA Conference Publication 3134 (A. Levine, editor), Part 2, 1991, p. 101.
16. Plagemann, W. L.: Space Environmental Effects on the Integrity of Chromic Acid Anodized Coatings. In LDEF-69 Months in Space, NASA Conference Publication 3134 (A. Levine, editor), Part 2, 1991, p. 1023.
17. Wilkes, D. R.; Brown, M. J.; Hummer, L. L.; and Zwiener, J. M.: Initial Materials Evaluation of the Thermal Control Surfaces Experiment (S0069). In LDEF-69 Months in Space, NASA Conference Publication 3134 (A. Levine, editor), Part 2, 1991, p. 899.

18. Zwiener, J. M.; Herren, K. J.; Wilkes, D. R.; Hummer, L. L.; and Miller, E. R.: Unusual Materials Effects Observed on the Thermal Control Surfaces Experiment (S0069). In LDEF-69 Months in Space, NASA Conference Publication 3134 (A. Levine, editor), Part 2, 1991, p. 919.
19. deGroh, K. K. and Banks, B. A.: Atomic Oxygen Undercutting of LDEF Aluminized-Kapton Multilayer Insulations. In LDEF-69 Months in Space, NASA Conference Publication 3134 (A. Levine, editor), Part 2, 1991, p. 781.
20. Dyer, J. R.: Applications of Absorption Spectroscopy of Organic Compounds. Prentice-Hall, Englewood Cliffs, NJ, 1965.
21. Hurley, C. J.: Long Duration Exposure Facility Experiment M0003-5: Thermal Control Materials. In LDEF-69 Months in Space, NASA Conference Publication 3134 (A. Levine, editor), Part 2, 1991, p. 961.
22. Guillaumon, J-C.: Thermal Control Paints for Satellites. Presented at the Canadian Space Agency Space Station Program Forum: Protection of Materials and Surface Finishes from the Low Earth Orbit Space Environment, Toronto, Canada, Feb. 1992.
23. Banks, B. A.; Dever, J. A.; Gebauer, L.; and Hill, C. M.: Atomic Oxygen Interactions with FEP Teflon and Silicones on LDEF. In LDEF-69 Months in Space, NASA Conference Publication 3134 (A. Levine, editor), Part 2, 1991, p. 801.
24. Young, P.R. and Slempp, W.S.: An Analysis of LDEF-Exposed Silvered FEP Teflon Thermal Blanket Material. NASA TM 104096, 1991.
25. Visentine, J.T.; Leger, L.J.; Kuminecz, J.F.; and Spiker, I.K.: STS-8 Atomic Oxygen Effects Experiment. AIAA Paper 85-0415, 1985.
26. Koontz, S; Leger, L.; and Albyn, K.: Vacuum Ultraviolet Radiation/Atomic Oxygen Synergism in Materials Reactivity. Journal of Spacecraft and Rockets, May-June 1990.
27. Rousslang, K.; Crutcher, R.; and Pippin, G.: Results of Examination of Silvered Teflon from the Long Duration Exposure Facility. In LDEF-69 Months in Space, NASA Conference Publication 3134 (A. Levine, editor), Part 2, 1991, p. 847.
28. Brinza, D. E.; et al.: Vacuum Ultraviolet (VUV) Radiation-Induced Degradation of Fluorinated Ethylene Propylene (FEP) Teflon Aboard the Long Duration Exposure Facility (LDEF). In LDEF-69 Months in Space, NASA Conference Publication 3134 (A. Levine, editor), Part 2, 1991, p. 817.
29. Young, P.R. and Slempp, W.S.: Characterization of Selected LDEF-Exposed Polymer Films and Resins. In LDEF Materials Workshop '91.(Bland A. Stein and Philip R. Young, compilers). NASA Conference Publication 3162, 1992.
30. Young, P. R. and Slempp, W. S.: Chemical Characterization of Selected LDEF Polymeric Materials. In LDEF-69 Months in Space, NASA Conference Publication 3134 (A. Levine, editor), Part 2, 1991, p. 687.
31. Slempp, W.S.; Young, P.R.; Witte, W. G., Jr., and Shen, J. Y.: Effects of LDEF Flight Exposure on Selected LDEF Polymer Matrix Resin Composite Materials. In LDEF-69 Months in Space, NASA Conference Publication 3134 (A. Levine, editor), Part 2, 1991, p. 1149.

32. Young, P.R.; Slemp, W.S.; Witte, W. G., Jr., and Shen, J. Y.: Characterization of Selected LDEF Polymer Matrix Resin Composite Materials. Proceedings of the 36th International SAMPE Symposium and Exhibition, 1991.
33. Tennyson, R. C., Mabson, G. E., Morison, W. D., and Kleiman, J: Preliminary Results from The LDEF/UTIAS Composite Materials Experiment. In LDEF-69 Months in Space, NASA Conference Publication 3134 (A. Levine, editor), Part 2, 1991, p. 1057.
34. Stein, B. A. and Pippin, H. G.: Preliminary Findings of the LDEF Materials Special Investigation Group. In LDEF-69 Months in Space, NASA Conference Publication 3134 (A. Levine, editor), Part 2, 1991, p. 617.
35. Meshishnek, M. J.; Gyetvay, S. R.; and Jagers, C. H.: Long Duration Exposure Facility Experiment M0003 Deintegration/Findings and Impacts. In LDEF-69 Months in Space, NASA Conference Publication 3134 (A. Levine, editor), Part 2, 1991, p. 1073.
36. Spear, W. S. and Dursch, H. W.: LDEF Mechanical Systems. In LDEF-69 Months in Space, NASA Conference Publication 3134 (A. Levine, editor), Part 3, 1991, p. 1549.
37. Miglionico, C., et al.: Effects of Space Environment on Structural Materials. In LDEF-69 Months in Space, NASA Conference Publication 3134 (A. Levine, editor), Part 2, 1991, p. 663.
38. Plagemann, W. L.: Space Environmental Effects on the Integrity of Chromic Acid Anodized Coatings. In LDEF-69 Months in Space, NASA Conference Publication 3134 (A. Levine, editor), Part 2, 1991, p. 1023.
39. Mason, J. B.; Dursch, H.; and Edelman, J: Systems Special Investigation Group Overview. In LDEF-69 Months in Space, NASA Conference Publication 3134 (A. Levine, editor), Part 3, 1991, p. 1217.
40. Assié, J-P. and Condé, E.: Microwelding (or Cold-Welding) of Various Metallic Materials Under the Ultra-Vacuum LDEF Experiment AO138-10. In LDEF-69 Months in Space, NASA Conference Publication 3134 (A. Levine, editor), Part 3, 1991, p. 1613.
41. Gregory, J. C., et al.: Interactions of Atomic Oxygen With Material Surfaces in Low Earth Orbit: Preliminary Results from Experiment AO114. Presented at LDEF First Post-Retrieval Symposium, Kissimmee, FL, June, 1991.
42. Linton, R. C.; Kamenetzky, R. R.; Reynolds, J. M.; and Burriss, C. L.: LDEF Experiment A0034: Atomic Oxygen Stimulated Outgassing. In LDEF-69 Months in Space, NASA Conference Publication 3134 (A. Levine, editor), Part 2, 1991, p. 763.
43. Peters, Palmer N.; Gregory, J. C.; Christi, L. C.; and Raikar, G. N.: Effects on LDEF Exposed Copper Film and Bulk. In LDEF-69 Months in Space, NASA Conference Publication 3134 (A. Levine, editor), Part 2, 1991, p. 755.
44. Tredway, W. K. and Prewo, K. M.: Analysis of the Effect of Space Environmental Exposure on Carbon Fiber Reinforced Glass. United Technologies Research Center Report R91-112542-4, 1991.
45. Dursch, H. W., et al.: LDEF Systems Special Investigation Group Interim Report. Available from LDEF Science Office, NASA - LaRC, MS 404, Hampton, VA 23665-5225.

46. Whitaker, A. F. and Young, L. E.: An Overview of the First Results on the Solar Array Materials Passive LDEF Experiment (AO171). In LDEF-69 Months in Space, NASA Conference Publication 3134 (A. Levine, editor), Part 3, 1991, p. 1241.
47. Benton, E. V. and Parnell, T. A. (Editors): Ionizing Radiation Exposure of LDEF. Available from LDEF Science Office, NASA - LaRC, MS 404, Hampton, VA 23665-5225.
48. Armstrong, T. W. and Colborn, B. L.: Scoping Estimates of the LDEF Satellite Induced Radioactivity. Available from LDEF Science Office, NASA - LaRC, MS 404, Hampton, VA 23665-5225.
49. See, T. H., et al.: Meteoroid and Debris Impact Features Documented on the LDEF. Available from LDEF Science Office, NASA - LaRC, MS 404, Hampton, VA 23665-5225.
50. Berrios, W. M.: LDEF Post-flight Thermal Analysis: Orbital/Thermal Environment Data Package. Available from LDEF Science Office, NASA - LaRC, MS 404, Hampton, VA 23665-5225.
51. Berrios, W. M. and Sampair, T. R.: LDEF Calculated Flight Temperature Data Package. Available from LDEF Science Office, NASA - LaRC, MS 404, Hampton, VA 23665-5225.
52. Berrios, W. M. and Sampair, T. R.: LDEF Solar Illumination Data Package. Available from LDEF Science Office, NASA - LaRC, MS 404, Hampton, VA 23665-5225.
53. Babel, H. W., McDonnell Douglas Space Systems Corporation: Letter to D. R. Tenney, NASA - Langley Research Center, dated October 1, 1991.

TABLE 1

LAUNCH:

- April, 1984 (into 255-mile orbit)

RETRIEVAL:

- January, 1990 (from 178-mile orbit)

EXPERIMENTS:

- 57 Technology, Science, and Applications Experiments
- Potential for >25000 test specimens from experiment trays and structure

PARTICIPANTS:

- >200 Principal Investigators from 9 Countries
 - 33 Industry
 - 7 NASA Centers
 - 21 University
 - 4 DoD Laboratories
- 4 Special Investigation Groups, >75 Participants
 - Materials
 - Meteoroid and Debris
 - Systems
 - Ionizing Radiation

Long Duration Exposure Facility information.

TABLE 2

HIGH VACUUM:

- 10^{-6} to 10^{-7} torr

UV RADIATION:

- 100 - 400 nm; 4,500 to 14,500 equivalent sun hours

ELECTRON AND PROTON RADIATION:

- $\sim 2.5 \times 10^9$ Rads surface fluence

ATOMIC OXYGEN:

- $\sim 10^5$ to 8.8×10^{21} atoms/cm² (wake- to ram-facing)

METEOROID AND DEBRIS IMPACTS:

- >36000 particles from ~ 0.1 mm to ~ 2 mm
- High fluence on ram-facing surfaces

COSMIC RADIATION:

- ~ 6 Rads
- ~ 20 tracks Thorium and Uranium

THERMAL CYCLING:

- $\sim 34,000$ cycles
- [$\pm 20^\circ\text{F}$] to [$\sim -30^\circ\text{F}$ to $\sim +190^\circ\text{F}$]

LDEF exposure conditions.

TABLE 3

<u>Clear Findings</u>	<u>Confusing/Unexplained Findings</u>
<ul style="list-style-type: none"> • All polymers were attacked by AO • Metals and oxides protect against AO • LDEF mission environments defined: AO and total solar exposures, contamination history • "Microenvironment" analysis methodology in development for detailed understanding of SEE • AO fluence models must be revised to account for thermal velocity distribution • Impacts occur in temporal bursts • Widespread contamination occurred • Data bases required for both design and research communities 	<ul style="list-style-type: none"> • Sources of contamination • Contamination mechanisms • AO mechanisms • AO/UV synergism

Environmental parameters and data bases.

TABLE 4

<u>Clear Findings</u>	<u>Confusing/Unexplained Findings</u>
<ul style="list-style-type: none"> • Molecular contamination was extensive • Multiple sources, external and internal • Surface temperature dependent • Cross-contamination from Shuttle sources • Environmental interactions with AO & UV • Leading edge deposits more transparent • Particulate contamination was deposited pre-flight, in-flight, post-flight; can be differentiated • Opportunity to provide unified perspective of unmanned LEO spacecraft contamination mechanisms 	<ul style="list-style-type: none"> • Sources of silicones/silicates • Deposition mechanisms • Contribution of AO degradation products • Effects on analyses for other space environmental effects

New Materials Development Requirements:

- Alternate, non-silicone materials
- Non-contaminating lubricants, polymers

Ground Simulation Testing Requirements:

- Re-evaluation of current outgassing criteria/tests for long-term missions
- Combined exposure testing and analytical modeling
- System level testing and analytical modeling

LDEF Contamination.

TABLE 5

<u>Clear Findings</u>	<u>Confusing/Unexplained Findings</u>
<ul style="list-style-type: none"> • Chromic Acid Anodized Aluminum stable • Z-93, YB-71, PCB-Z white TC paints and D-111 black TC paint are stable • A276 affected by AO and UV • Potassium silicate binders are stable; organic binders are not stable • UV accelerates AO erosion of Teflon; FEP erodes more rapidly than predicted • Microcracking in Ag/FEP • Surface crazing of clear silicone coatings • Atomic-oxygen undercutting of polymer substrates under protective coatings 	<ul style="list-style-type: none"> • Fluorescence shift from UV to VIS (under UV rad.) • Black chromium gave variable results • S-13GLO gave variable results • Role of UV, e⁻, p⁺ in AO erosion of FEP

New Materials Development Requirements

- Thin silicate overcoats for AO protection
- New silicate source for Z-93
- Application process for Ag/FEP
- Durable flexible coating to replace S-13GLO

Ground Simulation Testing Requirements

- Temperature effects on AO, UV degradation
- Single/combined effects data for analytical modeling
- In situ measurement capabilities for AO and UV testing
- Addition of e⁻ and p⁺ to simulation facilities
- Verified accelerated testing and analytical modeling

Thermal Control Coatings and Protective Treatments.

TABLE 6A

<u>Clear Findings</u>	<u>Confusing/Unexplained Findings</u>
<ul style="list-style-type: none">• Ag/FEP blankets remained functional, but eroded by AO• No Ag/FEP changes in α/ϵ; diffuse reflectance increased• Sizeable delaminations of Ag from FEP at meteoroid/debris impacts; thermal "lag"• FEP, polyethylene mechanical properties affected by UV• Siloxane-modified materials resist AO• Non-silicone polymers attacked by AO• Contamination is important effect• AO erosion of Kapton linearly predictable• Greater erosion than predicted for FEP, polystyrene, PMMA• Minimal chemical change from AO exposures• Extensive heating of some films• AO attack on carbon films	<ul style="list-style-type: none">• More erosion on some materials than predicted -- UV/AO synergism effects?• Thermal effects• Effects of contamination

Polymers and Films.

TABLE 6B

New Materials Development Requirements:

- Non-contaminating materials resistant to AO attack
- Non-contaminating materials resistant to UV degradation

Ground Simulation Testing Requirements:

- High fluence AO testing (directed beam)
- High fluence UV/VUV testing
- Simultaneous AO/UV exposure testing and analytical modeling
- Verified accelerated testing and analytical modeling
- Large area exposures for mechanical testing
- Thermal cycling
- Temperature effects
- Quantitative definition of thermal "lag" at delaminations in silvered Teflon second-surface-mirror thermal blankets

Polymers and Films (concluded).

TABLE 7

<u>Clear Findings</u>	<u>Confusing/Unexplained Findings</u>
<ul style="list-style-type: none"> • AO causes surface degradation of uncoated composites; no bulk polymer property changes • Thin inorganic coatings prevent AO erosion • Outgassing dictates dimensional stability of Gr/Ep; other CTE changes minor • Optical properties: No change for Gr PMC except on LDEF LE; fiberglass darkened • Sequential effects of impact/AO erosion • Thermal cycling causes microcracking • No catastrophic failure from impacts 	<ul style="list-style-type: none"> • Effects of contamination on AO erosion rates • Differences in AO erosion morphologies; stripes on T300/934 and T300/5208 with 5-mil tape • Differences in appearance and quantity of "ash" on AO-eroded specimens • No AO degradation of mechanical properties except on LDEF leading edge

New Materials Development Requirements:

- Scale up of coating process to full size parts
- Flexible coatings (for composite springs, etc.)

Ground Simulation Testing Requirements:

- Current capabilities adequate for individual effects
- Capacity and size for AO inadequate
- Synergistic effects (AO, UV, thermal cycling, vacuum, contamination)
- AO simulation on UV degraded LDEF specimens
- Analytical modeling of individual parameter and synergistic effects

Polymer-Matrix Composites.

TABLE 8

<u>Clear Findings</u>	<u>Confusing/Unexplained Findings</u>
<ul style="list-style-type: none"> • Structural Al and Ti alloys are unaffected • Many surfaces are contaminated • 1000Å Al coating on stainless steel is a very stable mirror/reflector • Thin anodized coatings on Al show small but measurable α/ϵ increases • Heavy oxidation of Ag and Cu • All metallic films except Sn and Pt show some oxidation • Al-matrix composites are not degraded; Mg-matrix composites oxidize at edges • Gr/glass composites are stable • Ceramics and glasses are generally stable unless damaged by impacts • Optical properties of glasses are affected in UV spectral regions only • Black coatings become more absorbing 	<ul style="list-style-type: none"> • Sources of contamination

New Materials Development Requirements:

- Non-contaminating, craze-resistant clear coatings
- Non-contaminating flexible coatings

Ground Simulation Testing Requirements:

- Synergistic effects (AO, UV, thermal cycling, vacuum, contamination)
- Analytical modeling of synergistic effects

Metals, Ceramics, and Optical Materials.

TABLE 9

<u>Clear Findings</u>	<u>Confusing/Unexplained Findings</u>
<ul style="list-style-type: none"> • Lubricants--OK only when protected • Fasteners--no cold welding failures; galling evident • Seals--no failures (all protected) • Adhesives--a few indications of failure • Solar cells--degradation due to impacts • Batteries--no space-related failures 	<ul style="list-style-type: none"> • Dynamic effects • Solar cells--minor degradation in output, possibly due to contamination, UV, AO

New Materials Development Requirements:

- Non-contaminating dry film lubricants for exposed applications
- Non-contaminating seals for exposed applications

Ground Simulation Testing Requirements:

- Combined thermal vacuum / UV / AO / dynamic testing

Systems-Related Materials.

TABLE 10

<u>Resistant Materials</u>	<u>Degraded Materials</u>
<ul style="list-style-type: none"> • Chromic acid anodized aluminum alloys • Many metals and Al-matrix composites • Ceramics, glasses, and Gr/glass composites • YB-71, Z-93, PCB-Z, D-111 paints • Inorganic coatings • Some siloxane-based polymers • Al-coated stainless steel reflectors 	<ul style="list-style-type: none"> • Various thermal control coatings • Silicone conformal coatings • Polymers • Polymeric matrix composites • Silver & copper • Ag/FEP second surface mirrors • Exposed lubricants

New Materials Development Requirements:

- Non-contaminating, atomic-oxygen-resistant polymers and polymer-matrix composites
- AO-durable flexible polymer for electrical insulation
- Replacement for Ag/FEP with low α_s/ϵ
- Flexible white paint replacement for S-13GLO
- Non-contaminating lubricants and seals for exposed applications
- Durable transparent coatings
- Efficient concepts for hypervelocity impact resistance

Ground Simulation Testing Requirements:

- Synergistic effects testing and analytical modeling
- Validated accelerated tests for combined UV, AO, thermal cycling

Summary of interim findings on LDEF materials.

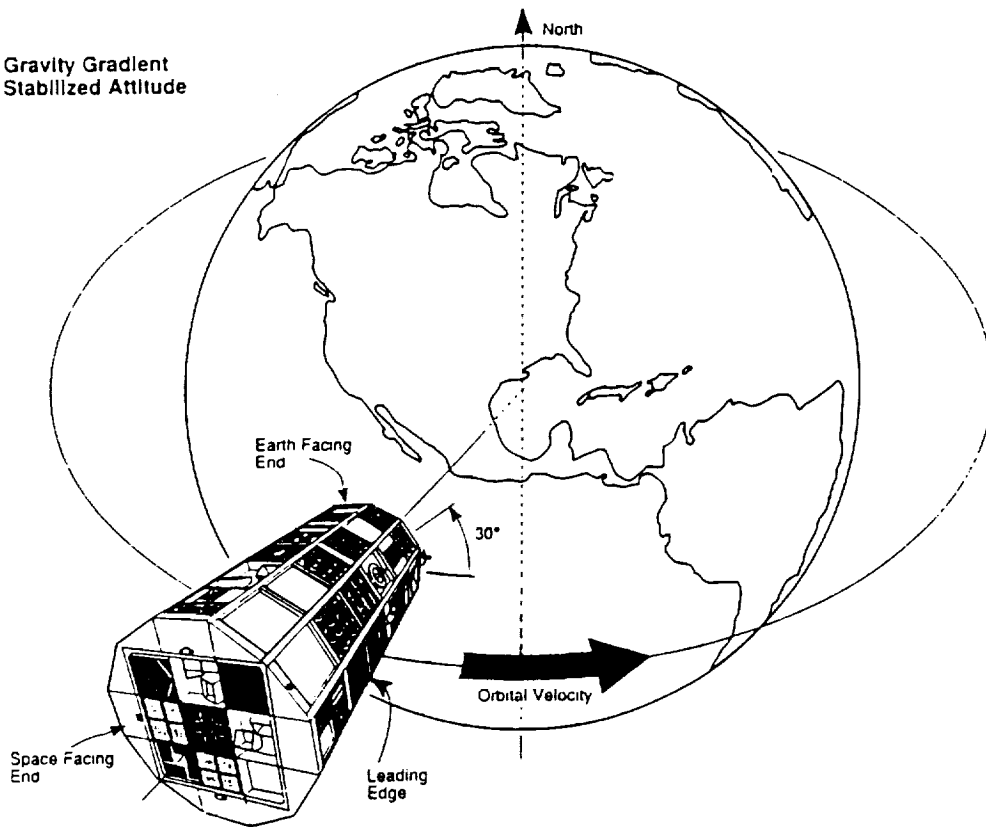


1. LDEF in orbit, April 1984.

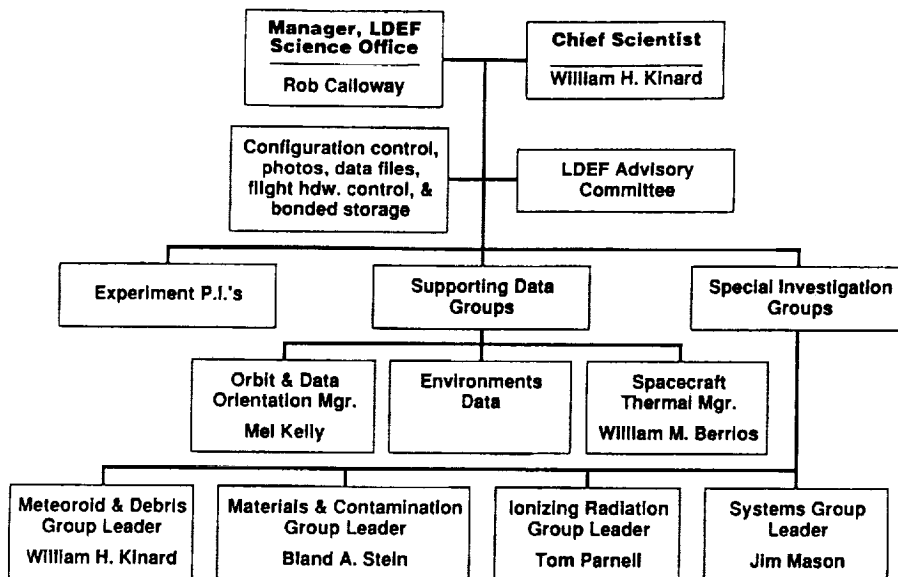


2. LDEF retrieval after 5.8 years in low-Earth orbit, January 1990.

- Gravity Gradient Stabilized Attitude



3. LDEF orientation.



4. LDEF Science Team.

Materials Issue	Data Available from LDEF
<ul style="list-style-type: none"> • Stability of Material Properties <ul style="list-style-type: none"> - Optical - Mechanical - Thermal - Physical - Chemical 	<ul style="list-style-type: none"> • Polymers, Metals, Composites, Ceramics, Glasses, Coatings, Films
<ul style="list-style-type: none"> • Combined Space Environment Effects Models 	<ul style="list-style-type: none"> • AO, Electrons, Protons, UV, ΔT, M & D, Vacuum • Control Specimens on LDEF and in Ground Storage
<ul style="list-style-type: none"> • Atomic Oxygen Effects 	<ul style="list-style-type: none"> • Erosion Rates and Mechanisms • Modifications to Fluence Models
<ul style="list-style-type: none"> • Meteoroid/Debris Impact Effects 	<ul style="list-style-type: none"> • Delamination of Blankets, Composites • Crater/Impact Particle Chemistry
<ul style="list-style-type: none"> • Contamination 	<ul style="list-style-type: none"> • Molecular & Particulate Levels/Chemistry

5. LDEF data available to address current issues in space environmental effects on materials.

SPONSOR: Long Duration Exposure Facility - Materials Special Investigation Group

OBJECTIVES:

- In-depth exposition of LDEF Materials Findings from Principal Investigators and MSIG
- Workshop discussions and theme reports on LDEF materials disciplines, data-basing requirements, ground simulation testing and analytical modeling needs, and future flight experiments

TUTORIAL AND WORKSHOP DISCUSSION DISCIPLINES:

- | | |
|--|--|
| <ul style="list-style-type: none"> • LDEF Materials, Environmental Parameters, and Data Bases • LDEF Contamination • Metals, Ceramics, and Optical Materials • Lubricants, Fasteners, Adhesives, Seals, Solar Cells, and Batteries | <ul style="list-style-type: none"> • Thermal Control Coatings, Protective Coatings, and Surface Treatments • Polymers and Films • Polymer-Matrix Composites |
|--|--|

ATTENDANCE:

- ~200 technologists from the International Space Materials Community

REPORT:

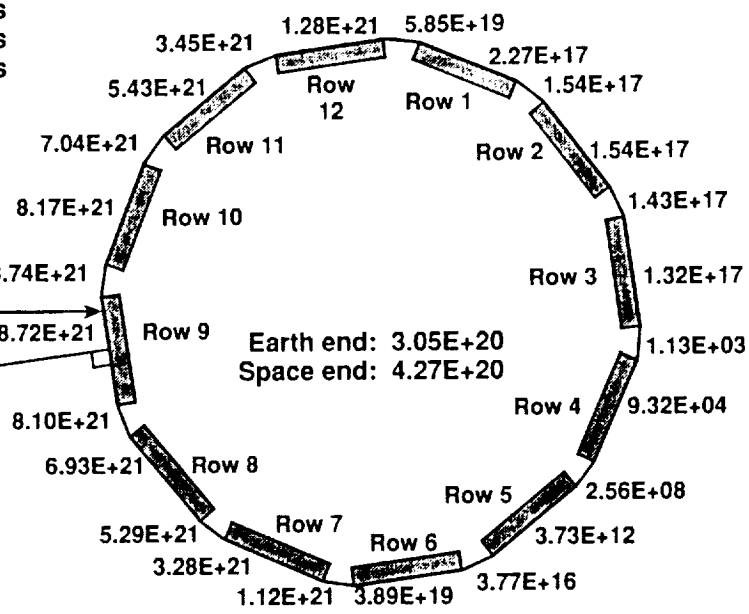
- NASA Conference Publication

6. LDEF Materials Workshop '91.

Yaw: 8.1 degrees
 Pitch: 0.8 degrees
 Roll: 0 degrees

Ram direction
 fluence:
 $8.81E+21$ Atoms
 Per Sq. Cm.

Z-Axis
 (Ram
 vector)
 8.1 degrees

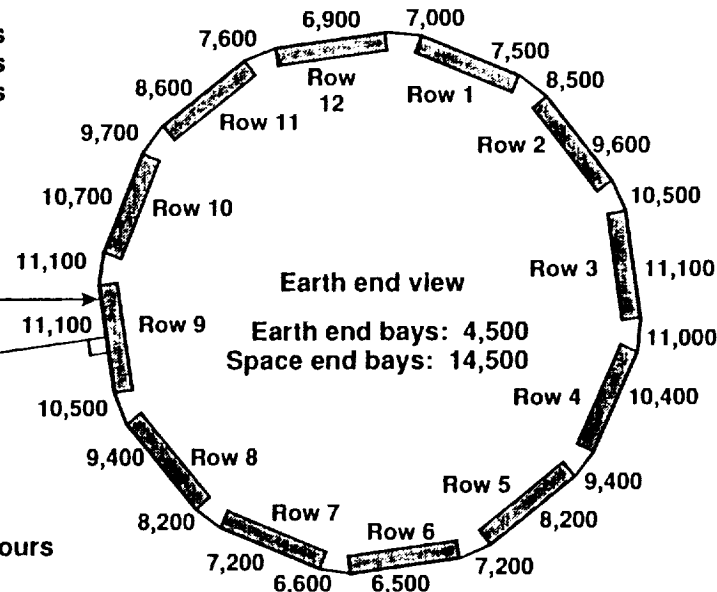


Atomic oxygen fluences at end of mission for all row, longeron, and end bay locations including the fluence received during the retrieval attitude excursion.

7. Atomic oxygen fluence for each LDEF tray location.

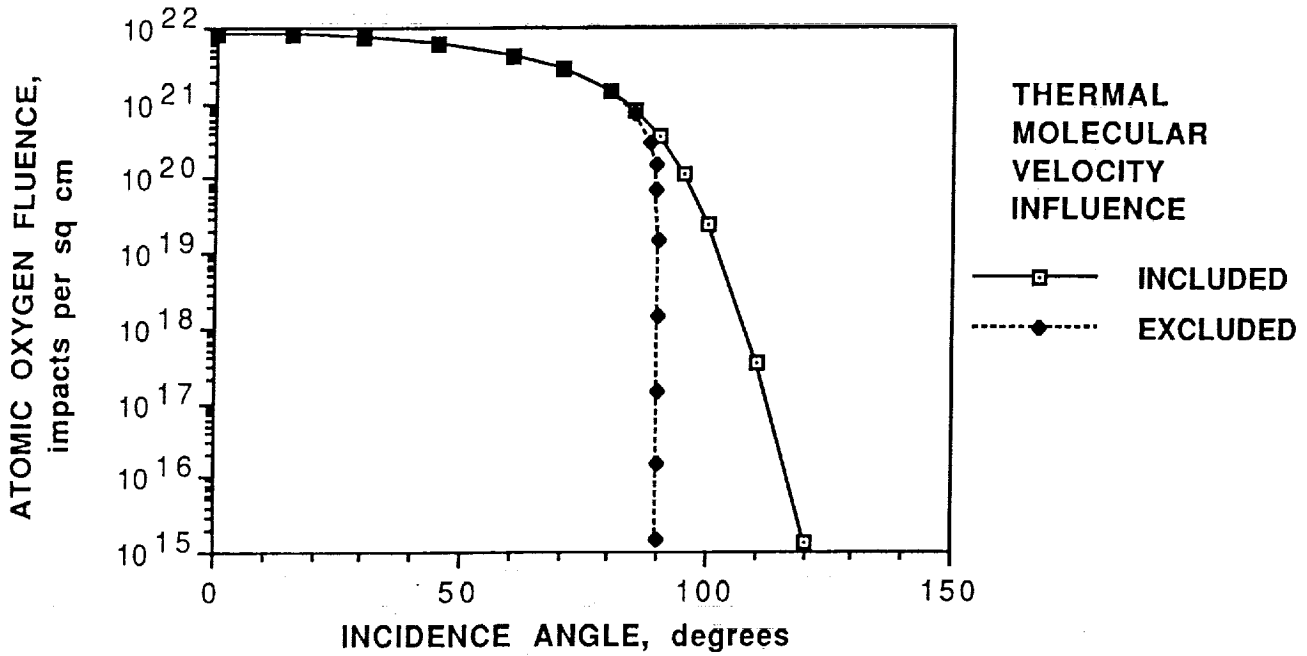
Yaw: 8.1 degrees
 Pitch: 0.8 degrees
 Roll: 0 degrees

Z-Axis
 (Ram
 vector)
 8.1 degrees



Equivalent sun hours
 Summation:
 Solar form factor x Hours +
 Earth form factor x Albedo x Hours

8. Equivalent sun hours at end of mission for each LDEF tray location.



9. Effect of thermal molecular velocity on atomic oxygen fluence.

- MATERIALS DATA BASE -

GOALS

- DEVELOP COMPREHENSIVE LDEF MATERIALS DATA BASE WITH INPUTS FROM PIs AND SIGs
 - USER FRIENDLY
 - ACCESSIBLE BY INTERNATIONAL COMMUNITY
 - MAINTAINED BY NASA

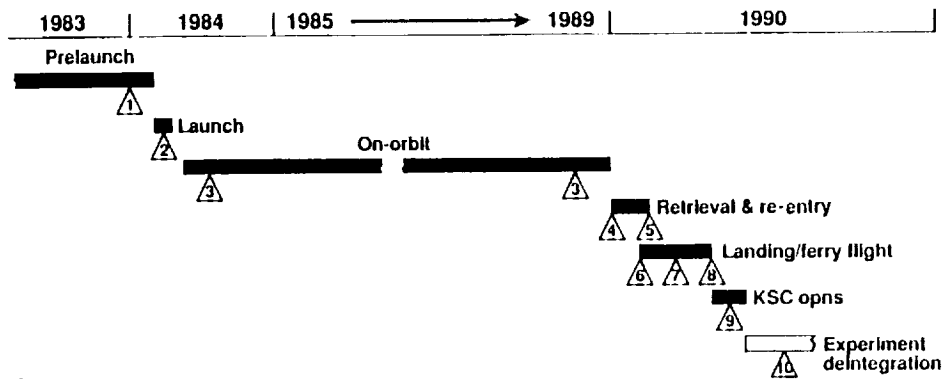
PROCEDURES

- UTILIZE NASA-MSFC MAPTIS DATA BASE METHODOLOGY
- DEFINE REQUIREMENTS
 - MULTI-USER ACCESS
 - MULTI-FILE ACCESS
 - SAMPLE IDENTITY AND LOCATION CODES
- DEFINE, EVALUATE AND STORE DATA
 - NARRATIVE FILES / PHOTOGRAPHIC (STILLS/VIDEOTAPE) FILES / OTHER GRAPHICS FILES
 - COMPARISONS WITH CONTROL SPECIMEN DATA AND DEGRADATION MODELS
 - LABORATORY-TO-LABORATORY DATA VARIABILITY

DELIVERABLES

- "MINI" DATA BASES: 1992 AND 1993
- COMPUTERIZED DATA BASES PLUS HANDBOOK(S) BY 1994

10. MSIG materials data base initial plan.

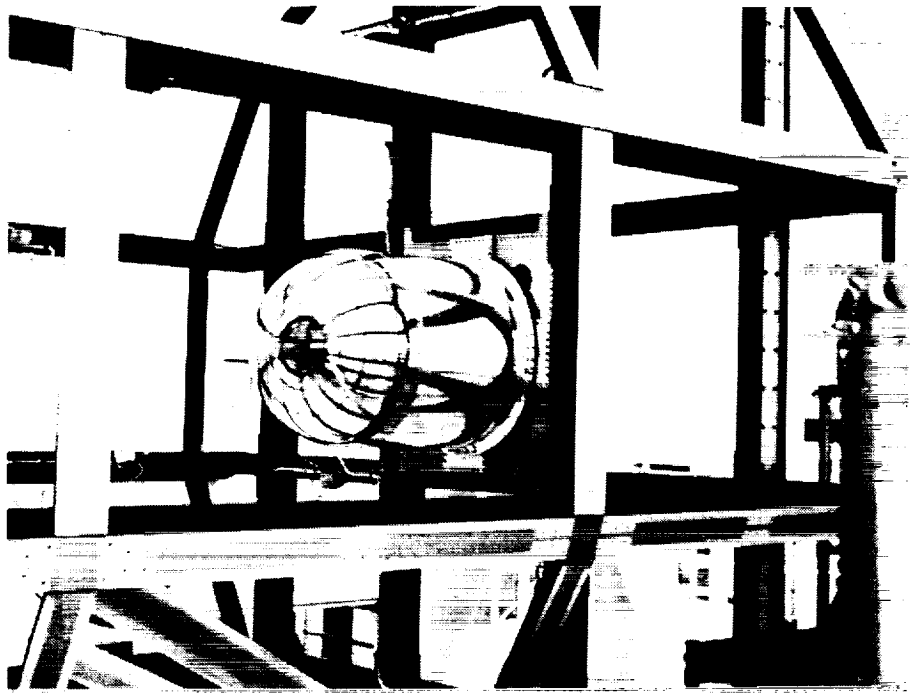


- 1 Pre-launch; Condition of LDEF prior to launch: > MIL STD 1246 level 1000 C for some trays.
- 2 Launch; During launch particulate contaminants are redistributed and Shuttle Bay Debris is added.
- 3 On-orbit; Contaminants are modified and new contaminants are generated in the orbital environment.
- 4 Retrieval; Grappling jars particles and films free, some may have relocated.
- 5 Re-entry; During re-entry particles and molecular contaminants relocate or are created.
- 6 Landing; The Shuttle is exposed to the Edwards Environment, accumulation of natural dusts.
- 7 Ferry flight; High humidity conditions, high velocity flow, thermal and pressure stresses occur.
- 8 Ferry flight; HEPA filter fibers appear on tape lifts after exposure to new filter.
- 9 KSC Ground operations; Ground operations prior to SAEF 2 include many manipulations of LDEF in complex environment.
- 10 De-integration; SAEF 2 exposure.

11. Contamination exposure history of LDEF.

- SAMPLING OF LDEF CONTAMINATION
 - Examined and photographically documented >2000 items of LDEF hardware
 - Collected >200 tapelifts from significant LDEF surfaces
 - Photographic examples shown in poster display
- SURFACE CHEMISTRY: OPTICAL MICROSCOPY, ELECTRON MICROSCOPY, ESCA, SIMS, MICRO FTIR, OPTICAL CRYSTALLOGRAPHY
 - 14 silvered Teflon thermal control blankets
 - Silicon-containing films conspicuously absent from AO-exposed Ag/FEP
 - Particle population on Ag/FEP increases with proximity to edges of trays
 - >90 anodized aluminum tray clamps
 - Impact-penetrated particulate contaminants well documented
- PARTICLE COUNT ANALYSIS
 - Selected areas of 22 trays
 - 24 tapelifts
 - 16 tray clamps
 - Particle counts for large (>100µm) particles higher than expected, based on current models

12. Scope of LDEF contamination analyses.



13. Molecular contamination on LDEF aluminum alloy structural elements.



14. Example of particulate contamination: Orbit-modified carbon fiber composite particle.
(Magnification 350X)

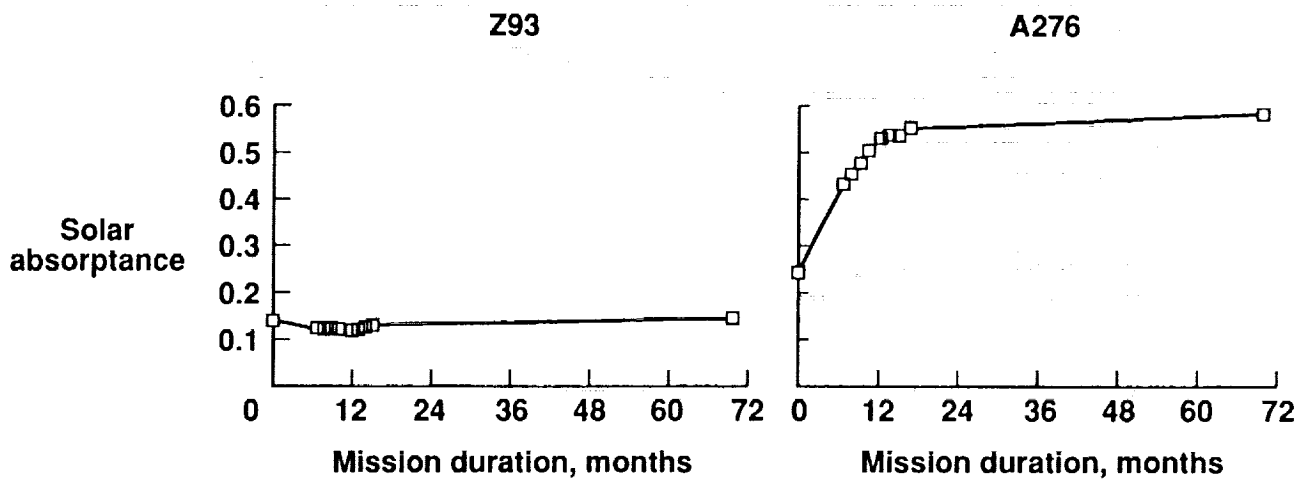
SPECIMENS AND LOCATIONS	α_s	ϵ	α_s/ϵ
Exposed Side of Clamps; All Areas of LDEF ¹	0.34	0.15	2.24
Unexposed Side of Clamps; All Areas of LDEF ¹	0.34	0.16	2.12
Control; In Storage on Earth ²	0.36	0.18	2.00

¹Average of measurements from 228 clamps, 3 data points per clamp

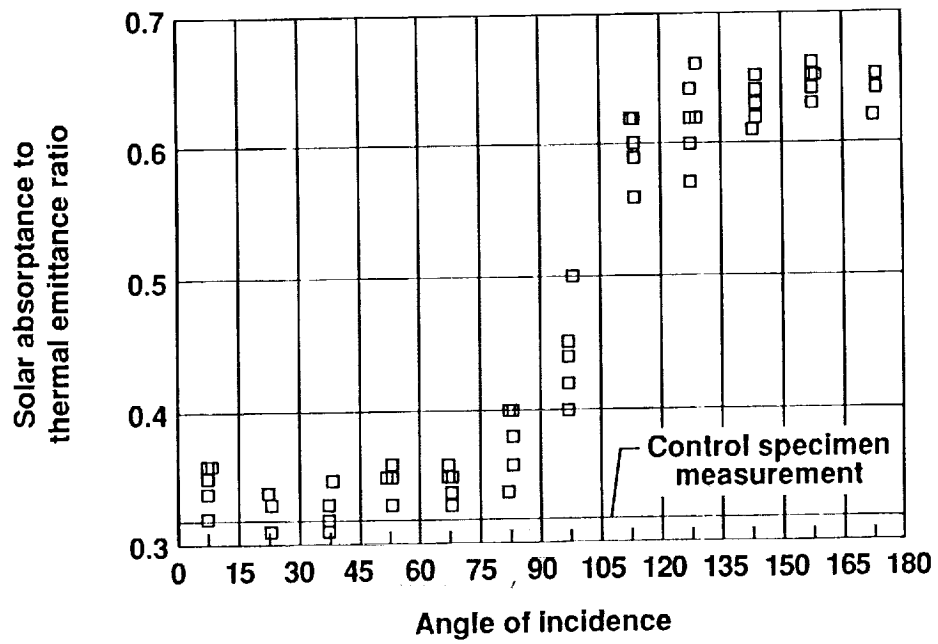
²Average of measurements from 4 control specimen clamps, 3 data points per clamp

15. Absorptance and emittance properties of anodized aluminum (6061-T6) clamps on LDEF.

**LDEF Experiment S0069
Tray A9**



16. Solar absorptance of white thermal control paints on LDEF.

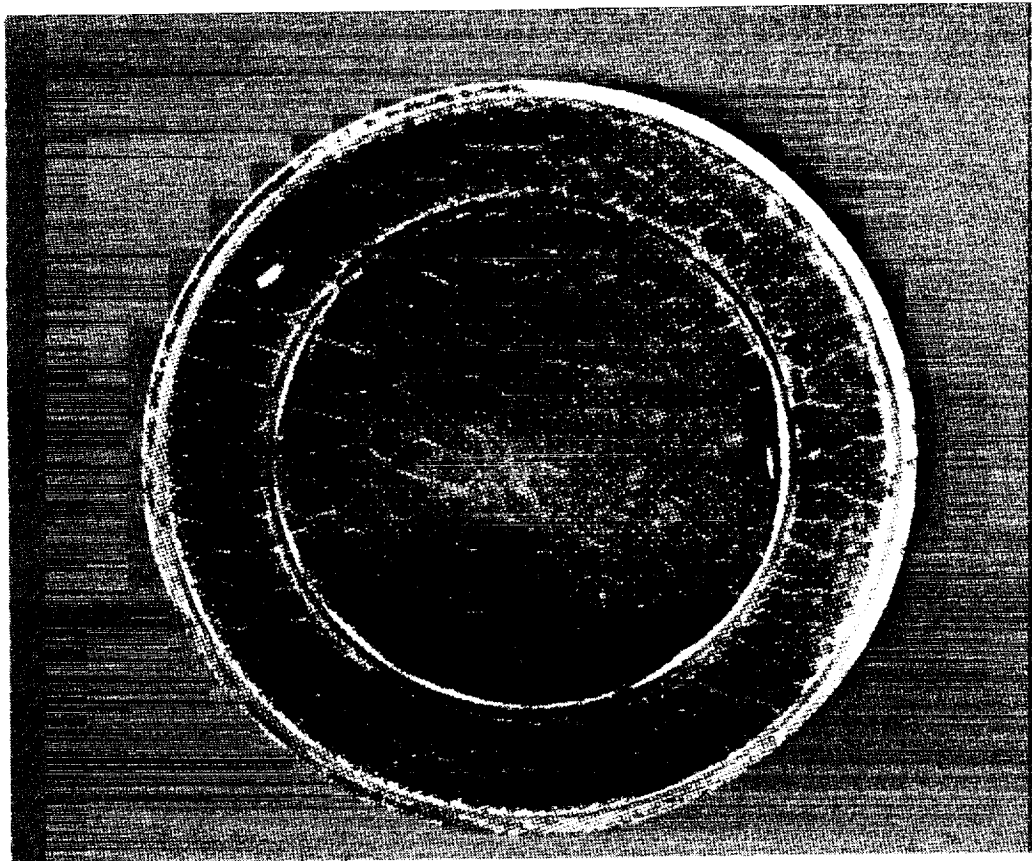


17. Absorptance to emittance ratio versus angle of incidence for A276 paint disks.

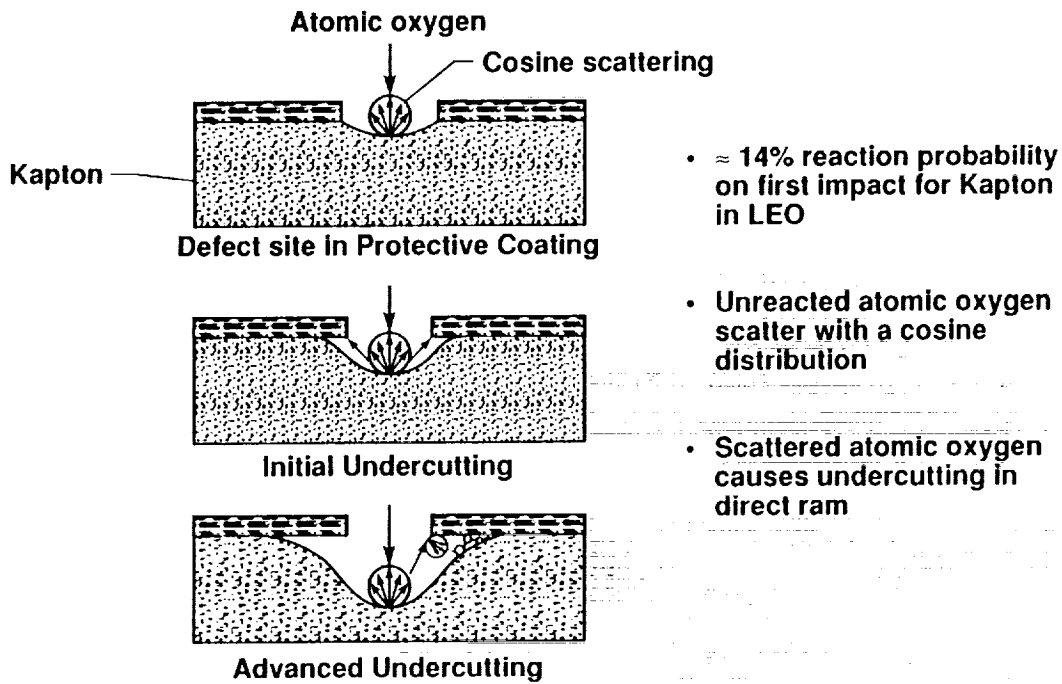


18. Microcracking in silver/Inconel layer and discoloration during of Ag/FEP second-surface mirror thermal blankets during LDEF flight. (Magnification approximately 100X)

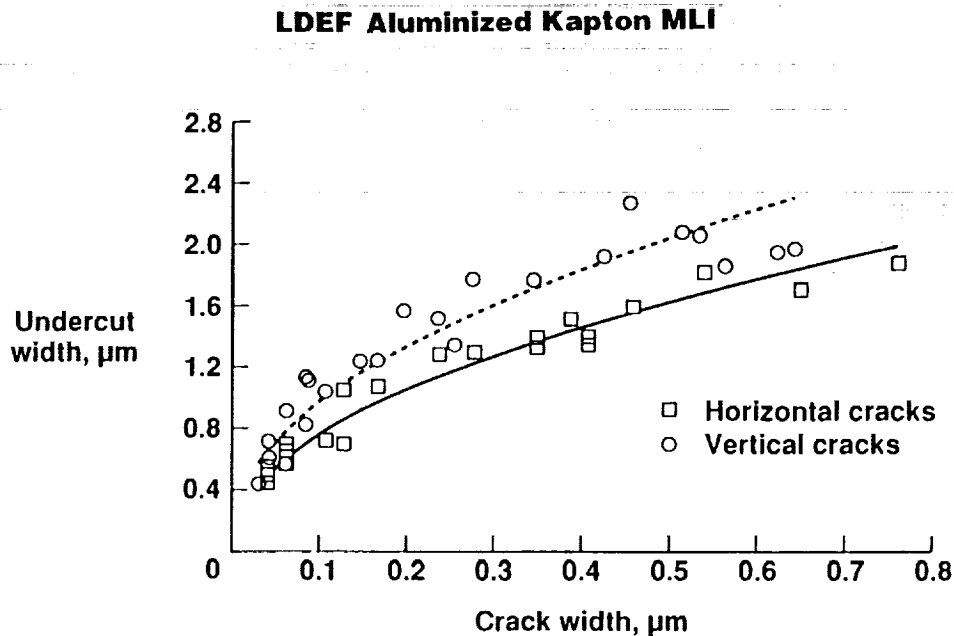
ORIGINAL PAGE
BLACK AND WHITE PHOTOGRAPH



19. Surface crazing of clear silicone coating during LDEF flight.

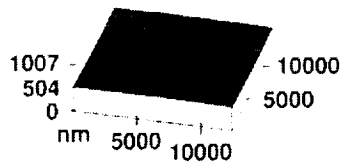


20. Atomic oxygen undercutting of coated polymeric materials on LDEF.

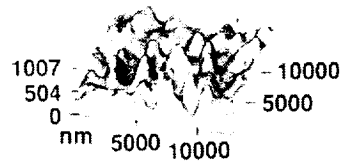


21. Atomic oxygen undercut widths in cracked multilayer insulations.

**Scanning tunneling
electron microscope profiles
of blanket surface**

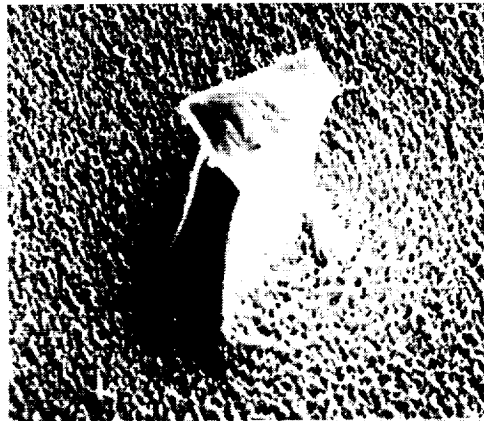


**Surface shielded
from atomic oxygen**



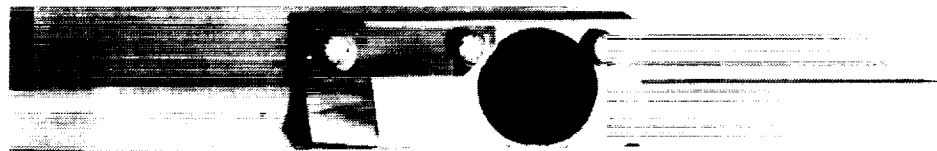
**Surface exposed
to atomic oxygen**

**Electron microscope picture
of blanket surface**

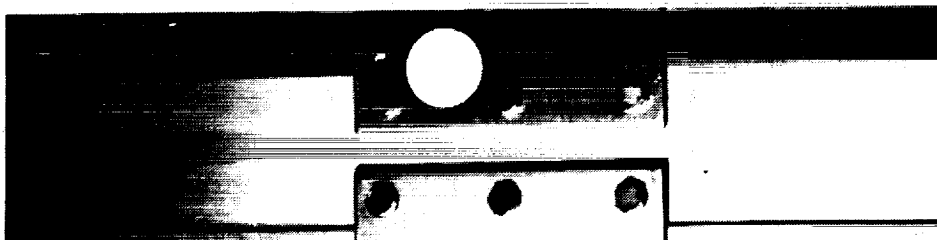


**Salt crystal on Teflon surface
shielded small region –
allowed exact measurement
of surface erosion depth.**

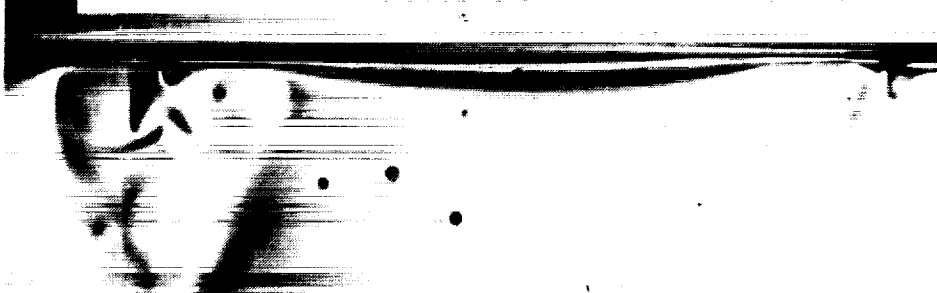
22. Atomic oxygen erosion of FEP Teflon on LDEF.



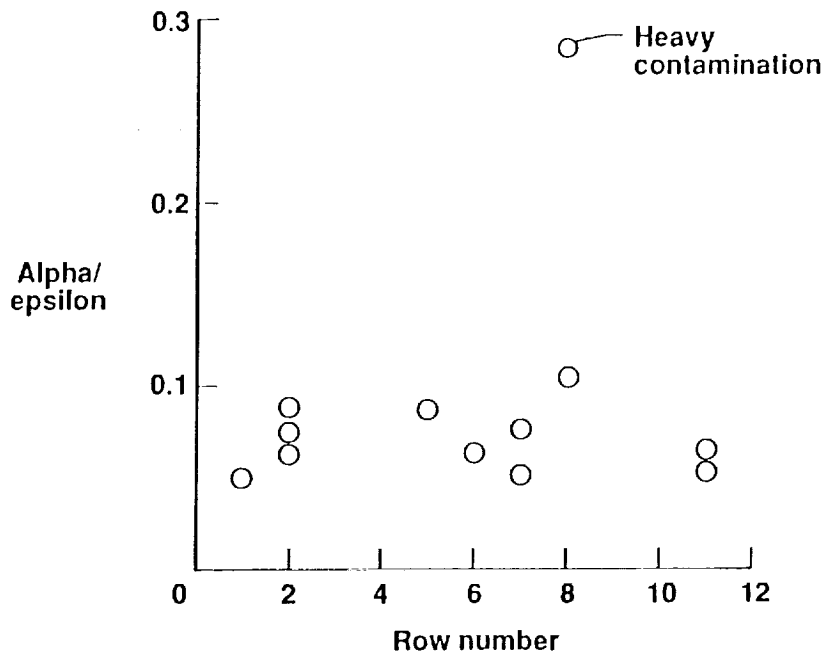
Tray F2 - Low fluence atomic oxygen exposure



Tray C8 - High fluence atomic oxygen exposure

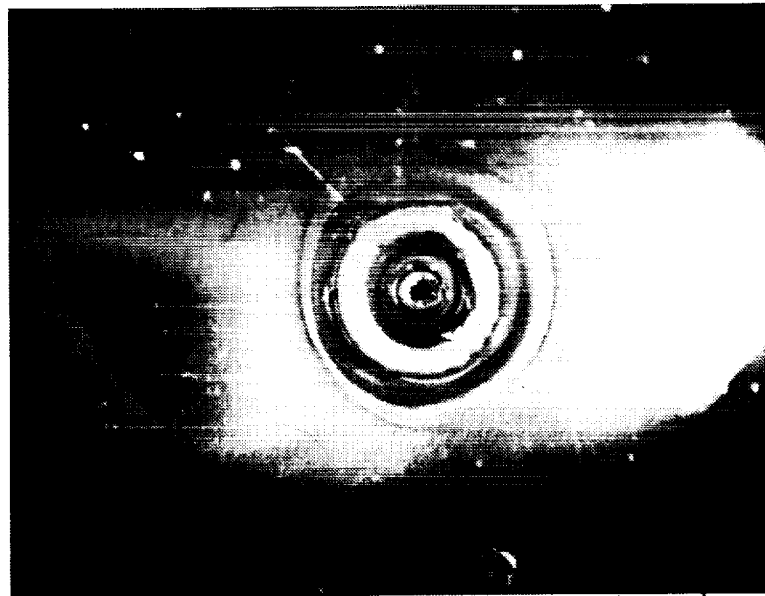


23. LDEF silver/Teflon second surface mirror thermal blankets.



24. Absorbance/emittance ratios for silvered Teflon (FEP) blankets on LDEF.

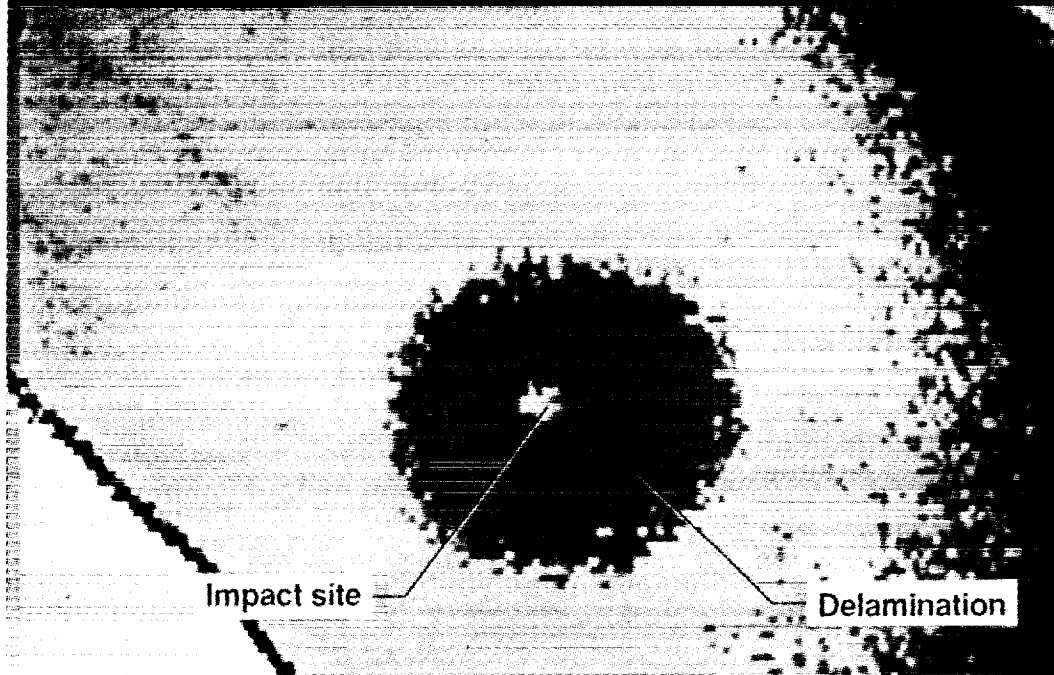
Low magnification (x16)



1 mm

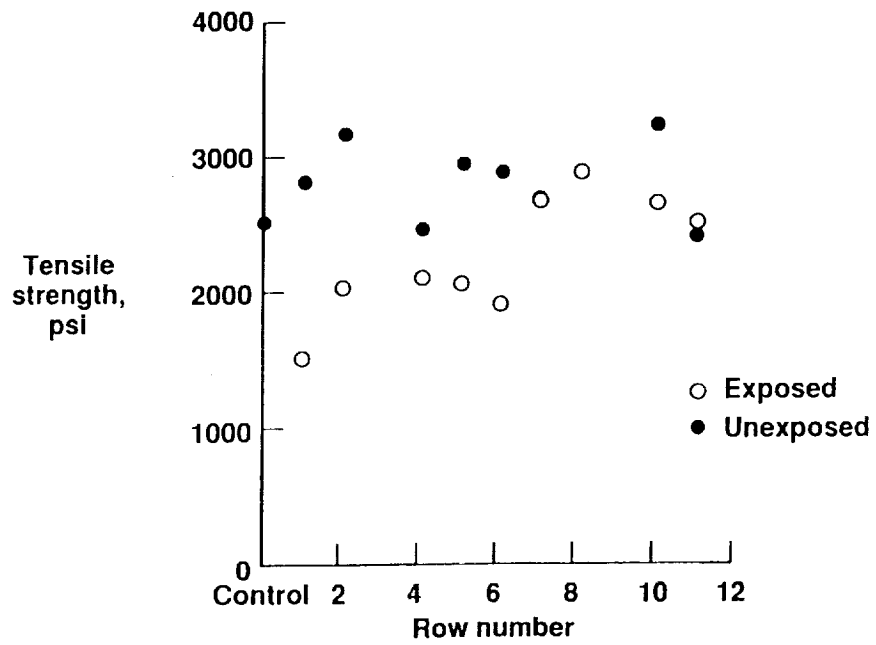
25. Photomicrograph of micrometeoroid impact on LDEF silvered Teflon thermal blanket.

LDEF A0178 Thermal Blanket

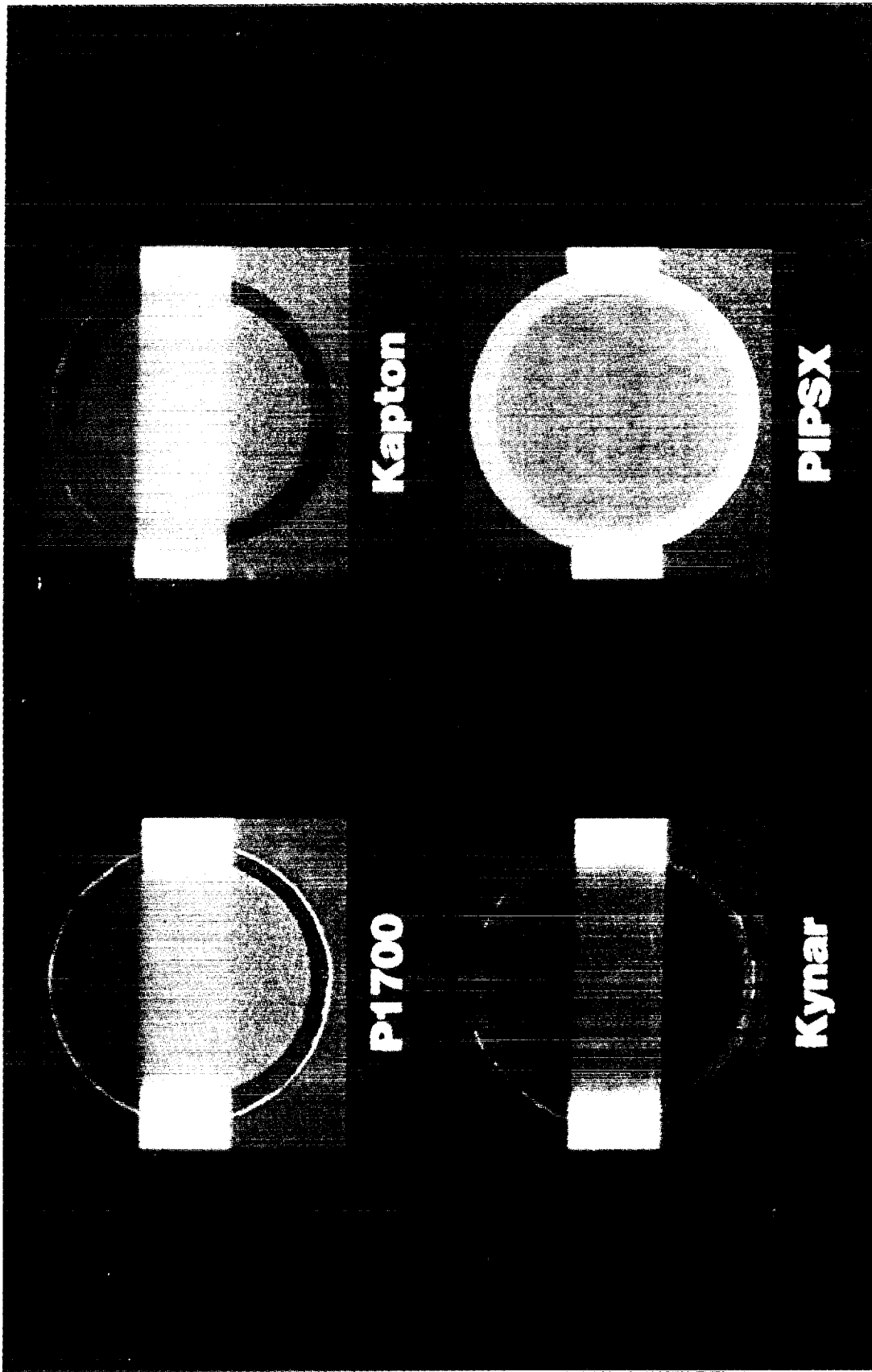


- Impact diameter ~0.5mm
- Delamination diameter ~10mm
- Infrared camera photograph
- Transient heating in air

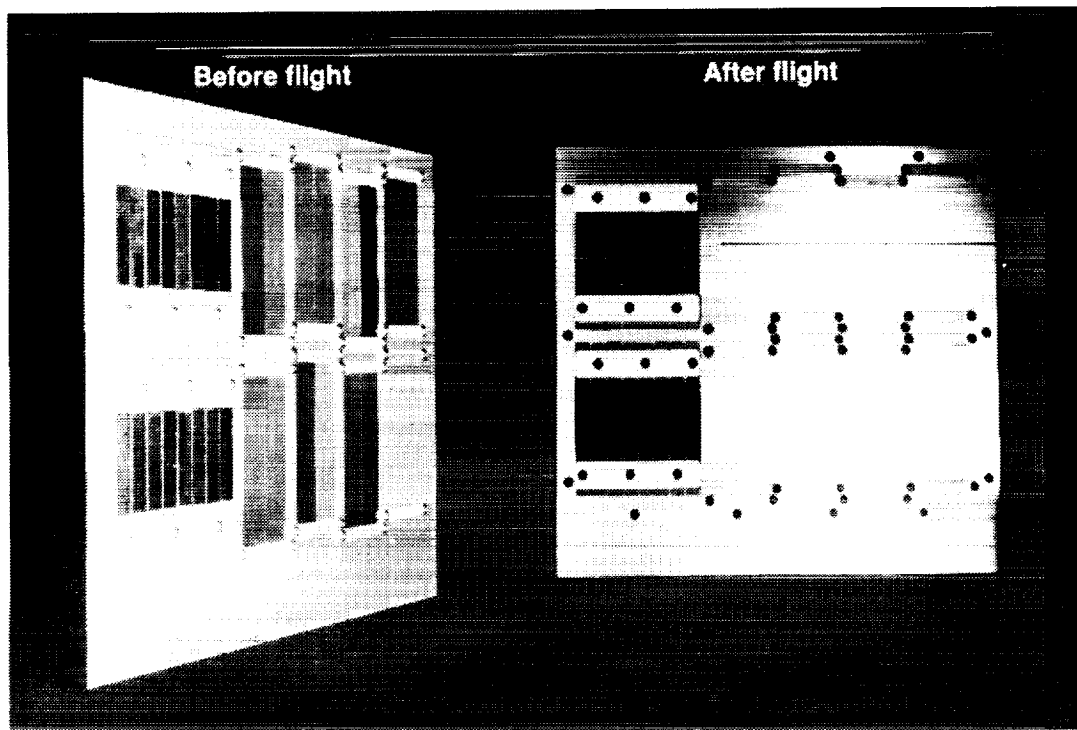
26. Thermal lag in delaminated silvered Teflon.



27. Tensile strength of FEP film from silverized Teflon blankets on LDEF as a function of row number.



28. Effect of 10-month LDEF exposure on four polymer films on LDEF experiment tray B9.



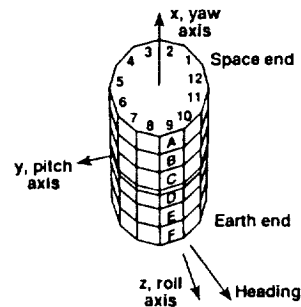
29. Langley polymer film experiment; 5.8-year exposure on LDEF tray B9.

Row no.	Angle off RAM (°)	AO fluence (10 ²¹ a/cm ²)	VUV (ESH x 10 ³)	Epoxy				Polyimide		Bismaleimide F178A/T300	Polysulfone P1700/T300
				934/T300	934/P75	CE339/GY70	5208/T300	PMR/C6000	LARC/C6000		
9	8	8.72	11.1	✓	✓	✓	✓	✓			✓
8	-38	6.93	9.4	✓	✓	✓	✓	✓			
7	-68	3.28	7.2					✓		✓	
12	82	1.28	6.9	✓			✓				
1	112	0.0002	7.5	✓					✓		✓
3	172	0.0001	11.1	✓	✓	✓	✓	✓			

Additional Environmental Parameters

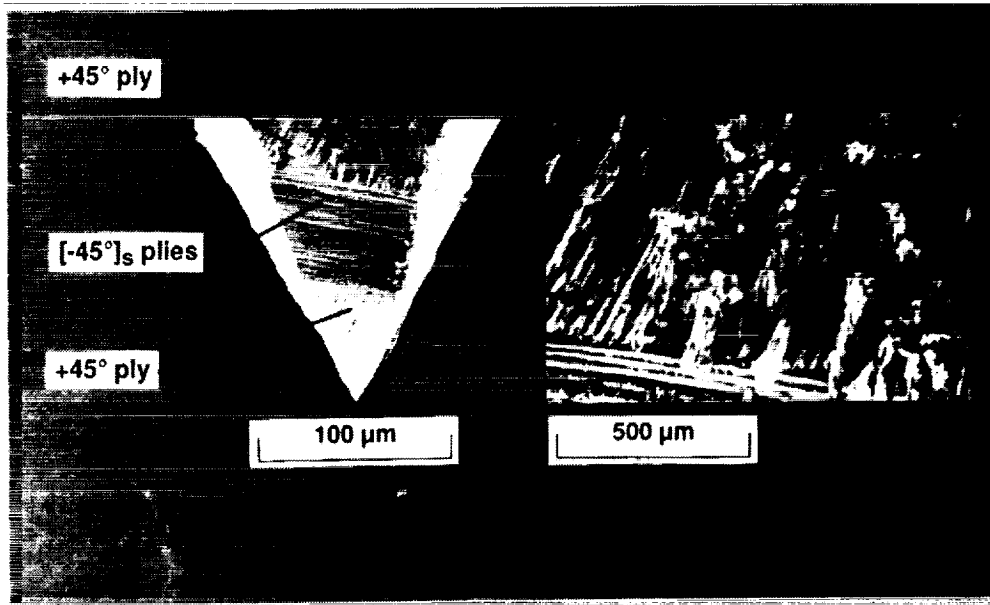
Thermal Cycles: ~34,000 (-20 to 160°F, ±20°)
 Particulate Radiation:
 e- and p+: 2.5 x 10⁵ rad
 Cosmic: <10 rad
 Vacuum: 10⁻⁶ - 10⁻⁷ torr
 Micrometeoroid and Debris: 34,336 impacts (0.5mm - 5.25mm)
 Altitude/Orbital Inclination: 255-180 nm/28.5°

LDEF Sketch and Orbital Orientation



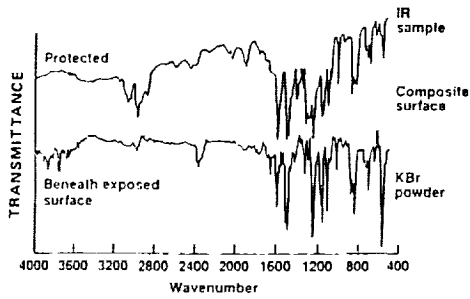
30. Selected LDEF-exposed composite materials.

SEM OF LDEF EXPOSED 5208/T300 COMPOSITE [±45]_s



31. Scanning electron microscope photomicrographs of LDEF-exposed T300/5208 (Gr/Ep) composite.

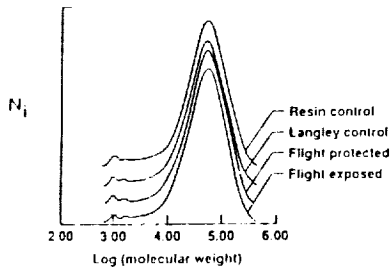
INFRARED SPECTRA



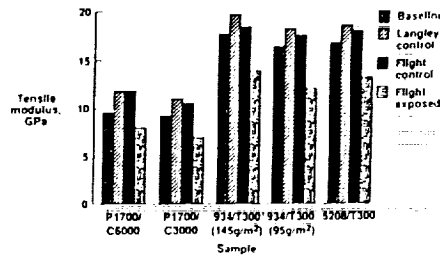
GLASS TRANSITION TEMPERATURE

Sample	T _g (°C)	Contacted side
Langley Control	167*	Random
	167*	
	170*	
	166*	
Flight Protected	164*	Side A
	166*	Side B
Flight Exposed	170*	Exposed side
	171*	
	169*	Nonexposed side
	171*	

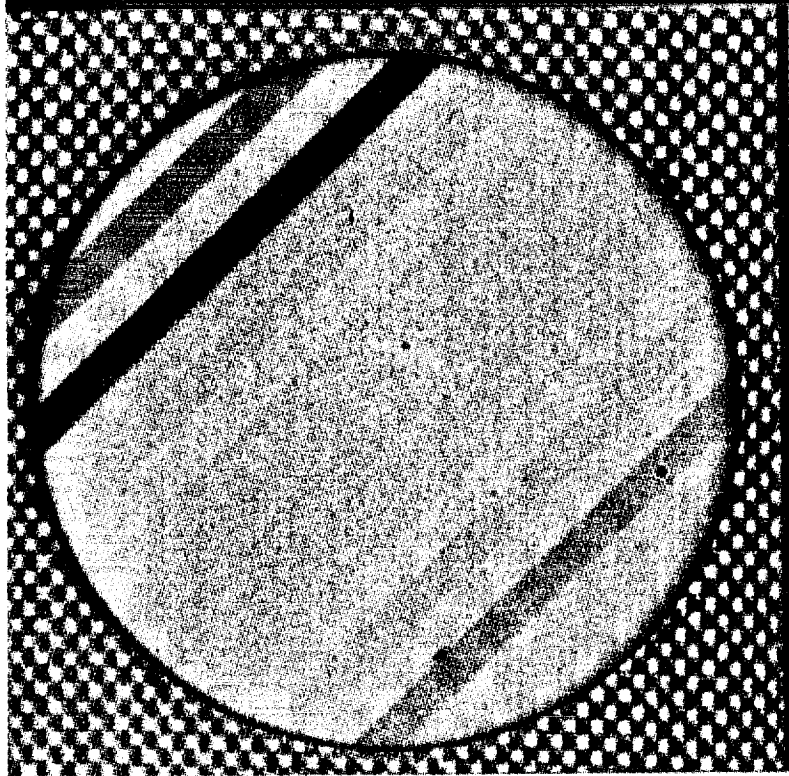
MOLECULAR WEIGHT DISTRIBUTION



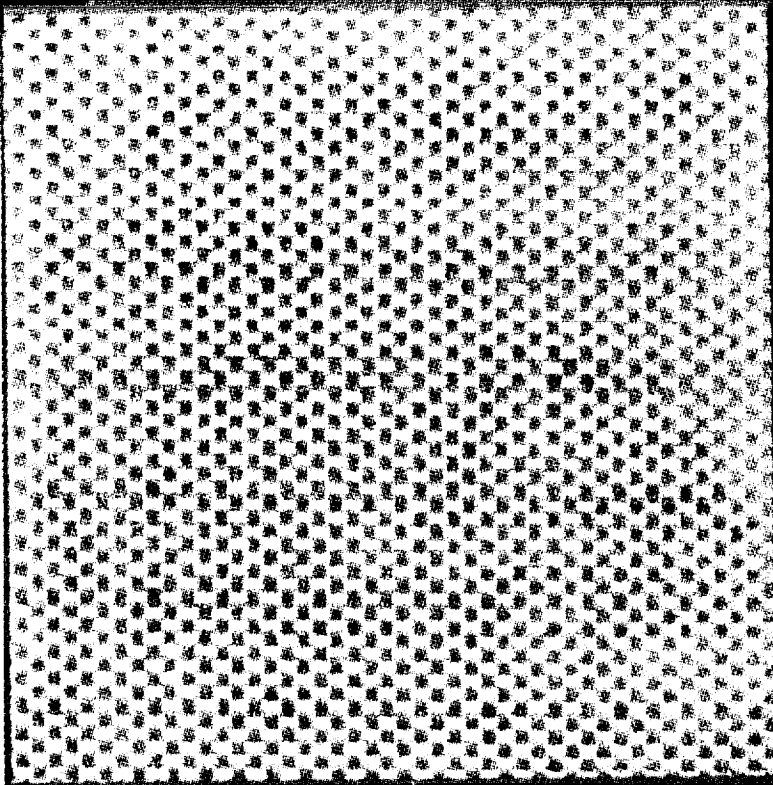
MECHANICAL PROPERTIES



32. Chemical and mechanical properties of LDEF-exposed composite materials.



Uncoated

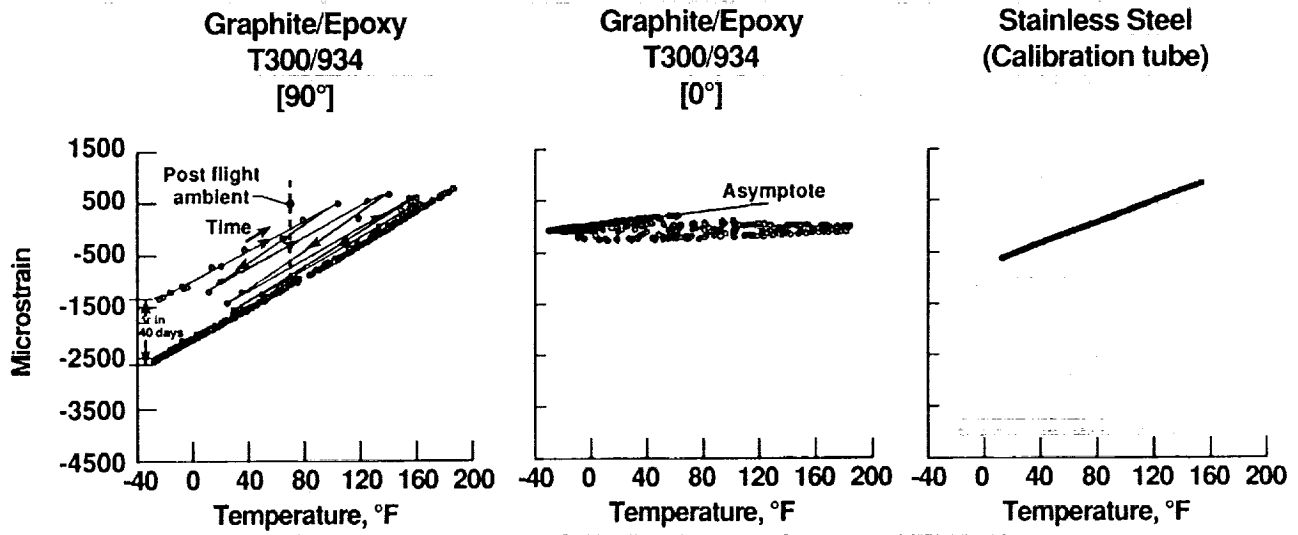


Coated: 1200A Aluminum

0.5 in.

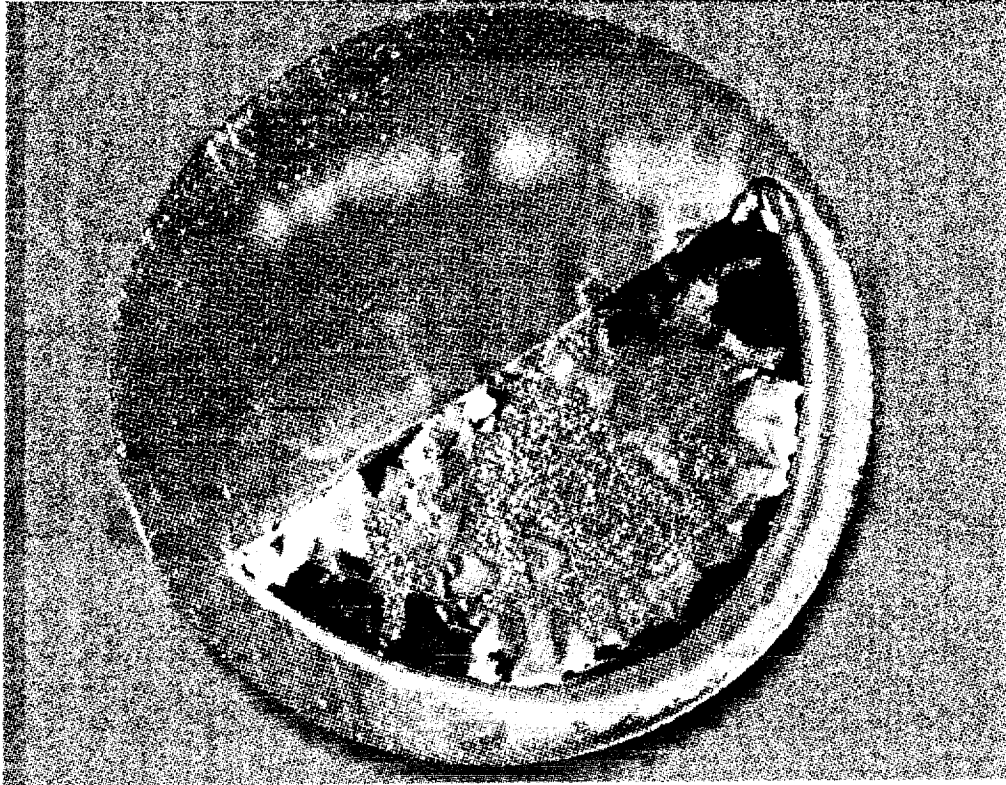
33. Comparison of coated and uncoated T300/934 (Gr/Ep) composite after 5.8-year LEO exposure on LDEF.

LDEF Experiment A0190 Tray D12



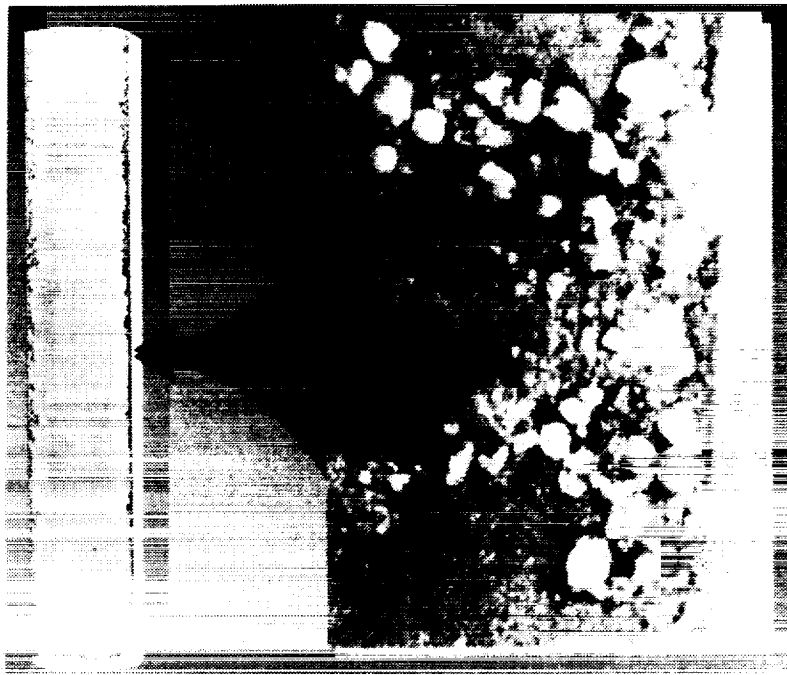
34. Dimensional stability of composites and metals on LDEF.

Optical Glass Substrate

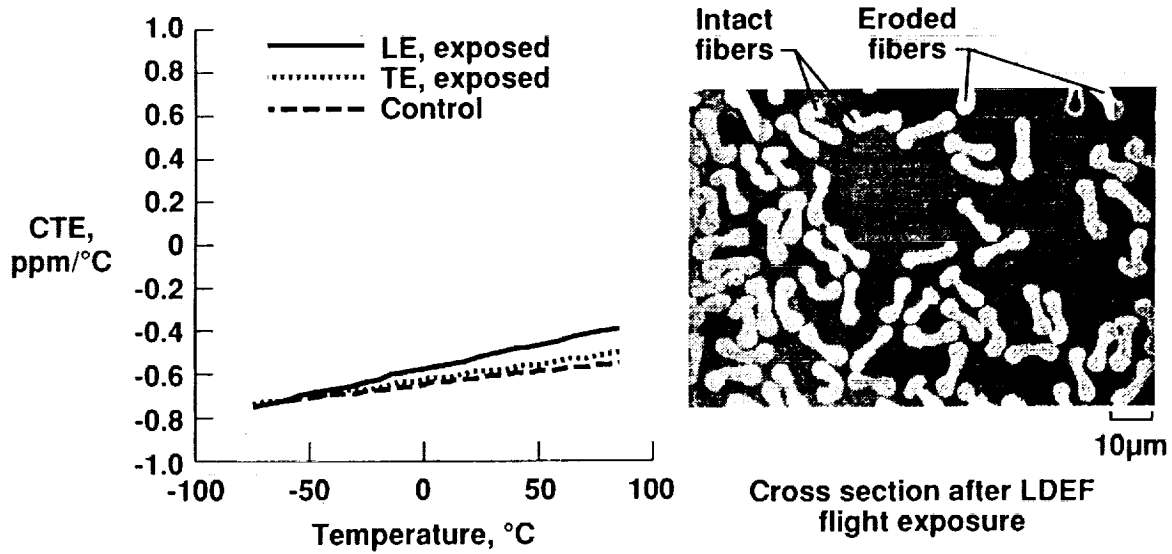


LDEF Experiment A0114
Tray C9

35. Oxidation of silver coating during LDEF flight.



36. Oxide growth on graphite fiber reinforced magnesium alloy metal-matrix composite specimen on LDEF.



37. Long-term durability of graphite/glass composites on LDEF.

- Directionality of trapped protons important to stabilized spacecraft
 - Current proton environment model gives factor of 3 errors
- Crew in Space Station Freedom flying above 400 Km will exceed 1-year dose limits in many locations
- Maximum radiation doses for SSF electronics specified from LDEF data
- Induced radioactivity not a significant radiation hazard for SSF
- Neutrons are significant secondary particles
 - Neutrons and cosmic rays produce measurable radioactivity
- ^7Be discovered on leading surfaces of LDEF
 - Inspired new atmospheric science investigations
- Fe nuclei observed with energies between galactic and anomalous cosmic rays (Partially ionized solar flare particles?)
- Activation measurements provide data base for environmental modeling
- Heavily ionizing recoil nuclei measured with good statistics
 - Short range, high-LET particles significant in electronic/biological damage

38. LDEF ionizing radiation findings.

- Unmelted meteoroids can be captured for origin/evolution studies
- Impact events are not random; affected by meteor showers, space operations
- Impacting particles have heterogeneous structure and composition
 - Chondritic compositions, silicates, sulfides identified
 - Beta micrometeoroids (blown away from the sun) identified
- Debris particles include metal and paint flakes
- Damage at impact sites affected by combined LEO environment parameters
- Thin plastic bumper sheets are effective in protecting against impacting particles
- SP-8013 Meteoroid Model requires modification
 - Premature meteoroid flux "roll-off" in model
 - Surface degradation greater than model predicts
 - Anisotropic meteoroid distribution, velocity, and directionality incorrect
- Current debris models require modification
 - underestimate debris in elliptical orbits
- SP-8042 cratering and penetration equations require modification

39. LDEF meteoroid and debris findings.

- No LDEF systems-level failures attributed to the natural LEO environment
- No bulk metallurgical changes in aluminum and titanium alloys
- Viscous damper passive stability concept worked well
 - Viable attitude control concept for SSF
- Uncoated hard optical materials, seals, batteries, heat pipes, wiring harnesses, radiometers, calorimeters, reflectometers, semiconductor diode lasers, LEDs, and adhesives generally performed well
 - A few acrylic adhesive joints failed
 - Some outgassing/contamination from connectors
- No evidence of cold welding; fastener galling observed
 - High quality fasteners / lubrication required for extended LEO missions
- Electromechanical relays continue to be a problem
- Contamination and drifting of conductive materials are hazards
- Solar cells were degraded by meteoroid/debris impact, UV / AO, contamination
- Lubricants showed some degradation where directly exposed to LEO environment
- Uncoated soft optical materials (e.g.- KRS-5 and KRS-6) were degraded
- Thermal cycling delaminated some dielectric and metallic coatings
- Preliminary optical materials data base generated

40. LDEF systems findings.

PRE-LDEF

- GROUND TESTS: Inadequate for LEO simulation
- SOVIET MIR DATA: Limited Value; environment poorly defined
- SOLAR MAX: 2-year mission; no designed materials experiments
- SHUTTLE PAYLOAD BAY DATA: Short, accelerated exposures

LDEF

- 5.8-year LEO exposure; mostly in Space Station Freedom orbit
- Well-defined materials, systems, and science experiments
 - State-of-the art materials
 - Ground and flight control specimens
- Stable orbital attitude
 - Broad range of exposure fluences for key environmental parameters (AO, UV, thermal cycles, etc.)
 - Real-time synergism of environmental effects

41. LDEF generated unique, high-quality, long-term data on space environmental effects on materials in low-Earth orbit.

NATURAL ENVIRONMENTS

ENVIRONMENT

- Orbital Atmosphere: Density and Composition
- Plasma
- Charged Particle and Electromagnetic Radiation
- Meteoroids and Space Debris
- Magnetic and Gravitational Fields
- Thermal
- Physical Constants
- Atomic Oxygen
- Ultraviolet Radiation
- Humidity

MISSION PHASES

- Ground Handling
- Launch
- Landing
- On-Orbit: External
- On-Orbit: Internal

* From McDonnell Douglas Space Systems Company Environmental Criteria Document 1F01920
for SSF Work Package 2

42. Space environmental effects considerations for Space Station Freedom: Natural environments.

INDUCED ENVIRONMENTS

ENVIRONMENT

- Electromagnetic
- Electrostatic
- Vibration
- Acoustics
- Shock
- Linear and Angular Acceleration
- Pressure
- Low Velocity Impact
- Thermal
- Internal Contamination
- External Contamination
- Plasma
- Radiation
- Plume Impingement
- Forces and Moments
- Spacecraft Glow
- Oxygen Concentration

MISSION PHASES

- Ground Handling
- Launch
- Landing
- On-Orbit: External
- On-Orbit: Internal

* From McDonnell Douglas Space Systems Company Environmental Criteria Document 1F01920
for SSF Work Package 2

43. Space environmental effects considerations for Space Station Freedom: Induced environments.

- Space Station Freedom
- Long-term Earth observation satellites
 - Platforms
 - Optical benches
 - System components
- Deep-space observatories in LEO
 - Precision reflectors
 - Electromagnetic sensors
- Space transportation systems
 - Earth-to-orbit
 - Orbital transfer
- Communications satellites
- Surveillance satellites
- Active defense systems
 - Long-term inactivity in LEO
 - Electronics protection

44. LDEF materials data applies to a variety of NASA and Department of Defense missions.

- Data on atomic oxygen erosion of Silvered Teflon
 - Used to define predictive erosion models for SSF radiator coating
- Long-term stability of Z-93 white thermal control coating was verified
 - Z-93 selected for large thermal radiators on SSF
- Anodized aluminum alloy long-term durability in LEO was verified
 - Anodized Al selected for SSF truss structure
- Most other thermal control coatings were degraded by LDEF exposure
 - Confirmed ground-based simulation test results
- Contamination distribution on LDEF was characterized
 - Used in thermal model development for SSF truss structure
- Revised atomic oxygen fluence model generated for orbiting spacecraft
 - Used to design for material erosion on SSF
- MLI blanket surfaces degraded during LDEF mission
 - MLI will require outer layer surface protection for SSF applications

45. Utilization of LDEF materials data in Space Station Freedom design.

CONTAMINATION-RELATED TESTS

- Evaluate potential molecular contamination precursors in UV exposures
- Investigate adequacy of current outgassing tests / criteria for spacecraft materials
- Determine the role of silicon-containing contamination on AO erosion rates
- Investigate the migration of silicone species on spacecraft surfaces

LDEF-EXPOSURE / GROUND-EXPOSURE EFFECTS CORRELATION

- Expose LDEF polymer films, composites, and coatings to AO / UV / tensile loads, individually and simultaneously, and evaluate effects
- Expose specimens of LDEF external surfaces and thermal control paints to elevated temperatures (which could be reached by contact with very high α/ϵ materials) and evaluate effects

46. Projected LDEF MSIG ground-based simulation testing activities.

CONTAMINATION-RELATED MODELING

- Develop an LDEF molecular contamination model
- Integrate models for contamination + UV + AO effects on surface chemistry

EXPOSURE EFFECTS MODELING

- Correlate observed equivalent dose effects of UV and/or AO in ground base facilities with LDEF data
- Assess potential post-retrieval effects on LDEF materials
 - Radical / reactive chemistry
 - Interaction between specimens and storage containers
 - Oxygen bleaching
 - Artificial light
 - Temperature and humidity

ENVIRONMENTAL PARAMETER MODELING

- Develop models for LDEF "micro-environments"
 - Shadowing due to scuff plates, trunnions, support beam
 - Indirect scattering from scuff plate on tray A4 thermal blanket
 - Gaps between trays

47. Projected LDEF MSIG environmental parameter modeling activities.

OBJECTIVE: Detailed study of LDEF contamination mechanisms to provide a unified perspective of spacecraft contamination

BACKGROUND: MSIG Preliminary study of LDEF contamination; supporting data for LDEF PIs

APPROACH:

- Detailed chemical/morphological characterization of contaminants on LDEF structure, experiment trays, and systems
 - Molecular contamination
 - Particulate contamination
- Identify source(s) of contaminants
- Document features indicative of orbital exposure and define contamination mechanisms consistent with LDEF flight parameters and the LEO environment
- Model the internal and external "LDEF atmosphere" from launch to retrieval
- Characterize the LDEF mission in terms of contamination
 - Sources, mechanisms, and resultant effects
 - Lessons learned

TESTS AND ANALYSES:

- Analytical light microscopy
- Automated image analysis
- Fourier Transform infrared spectroscopy
- Microchemical techniques
- Electron beam techniques

DELIVERABLES: Report and data base on LDEF contamination with implications for future space missions

48. Plan for detailed study of LDEF contamination.

LDEF Materials, Environmental Parameters, and Data Bases

Co-Chairmen: Bruce Banks and Mike Meshishnek
Recorder: Roger Bourassa

THE UNIVERSITY OF CHICAGO
DIVISION OF THE PHYSICAL SCIENCES
DEPARTMENT OF PHYSICS

PHYSICS 354: QUANTUM MECHANICS
LECTURE 10: THE HARMONIC OSCILLATOR

PROFESSOR J. JOYNT
LECTURER D. KANE

WINTER 2020

PHYSICS 354
LECTURE 10

10/10/2020

LDEF
ATOMIC OXYGEN FLUENCE
UPDATE*

Roger J. Bourassa and J. R. Gillis
Boeing Defense and Space Group
Seattle, WA

INTRODUCTION

The definition of LDEF atomic oxygen exposure involves theoretical prediction of fluxes, modeling of shielding and scattering effects, and comparison of predicted with observed atomic oxygen effects on LDEF experiments. Work is proceeding as follows: atomic oxygen fluxes and fluences have been recalculated using a more detailed orbit prediction program; a micro-environments program is being developed to account for the effects of experiment geometry on atomic oxygen flux; and, chemical and physical measurements are being made on copper grounding straps to verify correspondence between predicted exposures and observed surface property variations. These three areas of work are reported briefly herein.

PRECEDING PAGE BLANK NOT FILMED

* Work done under NAS 1-18224, Task 12

LDEF ATOMIC OXYGEN FLUENCE UPDATE, AO FLUENCE CALCULATION

Atomic oxygen fluxes and fluences for LDEF have been recalculated using a more accurate procedure for establishing orbit altitude. The calculation reported at the First LDEF Post-Retrieval Symposium, Reference (1) was based on altitudes determined by way of a point-mass, elliptical-orbit routine assuming a spherical earth. These simplifying assumptions could introduce error in the calculated atomic oxygen environment. Atomic oxygen flux calculations are very sensitive to altitude accuracy.

Both the original calculation and the refined calculation are based on state vectors prepared, courtesy of Cheryl Andrews of NASA Johnson Space Center, from NORAD elements which are in turn based on ground observations of LDEF recorded during the mission. The refined calculation was made using a Long Term Earth Satellite Orbit Prediction Program to determine orbit position and orbit average conditions between tabulated state vectors. The general course of calculation was to start at a state vector and then continue with simple adjustments to drag coefficient to minimize differences between calculated and observed positions of the spacecraft. Once significant error developed, the calculation was restarted using a later state vector as the starting position. Twenty-one such spans of calculation were needed to cover the LDEF mission. Calculated orbital data were tabulated for 5.75-minute intervals for the mission. In the original calculation, orbit average flux was determined from the first sixteen orbits following each state vector. The principal features of orbit calculation are summarized in Figure 1.

The method of determining atomic oxygen fluxes from the orbital data is unchanged from the method reported earlier, Reference (1).

ORBITAL MECHANICS

- Eighth order gravitational harmonics
- Perturbations of sun and moon
- Atmospheric drag
- Daily observed solar activities

MISSION TREATMENT

- Calculation spans: twenty-one ranging from 381 days to 11 days duration
- Position and velocity vectors: tabulated at 5.75-minute intervals for the mission
- Drag coefficient: adjusted to match calculated with reported state vectors
- Standard deviation of altitude (calculated with observed), 103 points: 0.61 km
- Mean altitude error, 103 points: -0.13 km

ATOMIC OXYGEN MODEL (Unchanged)

- Thermal molecular velocity: kinetic theory treatment
- Atmospheric Model: NASA MSIS-1986
- Atmospheric velocity: co-rotation of earth's atmosphere
- Outputs: flux and mission total fluence for each tray and longeron

Figure 1. Features of the LDEF atomic oxygen exposure calculation.

LDEF ATOMIC OXYGEN FLUENCE UPDATE, AO FLUENCE CALCULATION

The results of the revised calculation are summarized in Figure 2. The revised calculation found ram direction fluence to be 4.3% greater than that reported initially. However, this value is an average difference for the entire mission. Fluences for shorter periods of time differ by as much as 18% between the two calculations. The difference could be significant for experiments that were not open for the entire flight. The results of the revised calculation should be used for LDEF materials evaluations.

Fluences for trailing surfaces show a relatively greater difference between calculations. The revised calculation gives lower values than the original calculation, for example: the fluence for Row 3 was calculated originally as $3.71E03$ atom/sq cm compared with a revised value of $1.33E03$ atoms/sq cm. The difference is attributed to a small difference in average atmospheric temperature between the two determinations of orbit altitude. However, fluences on trailing surfaces are shown to be insignificant by either calculation at angles greater than about 105 degrees to ram. The data reported in Figure 2 are for the free, orbital flight of LDEF. They do not include exposure of the vehicle during or after retrieval.

The revised calculation incorporates the best information available on pitch and yaw angles as determined by Dr. Bruce Banks, NASA Lewis Research Center (Reference 2). The yaw angle is 8.1 degrees with the spacecraft turned so that the ram direction lies between Rows 9 and 10. Pitch angle is 0.8 degree with the space end of the vehicle pitched forward. The 0.8-degree forward pitch causes a significant difference between space-end and earth-end atomic oxygen exposures.

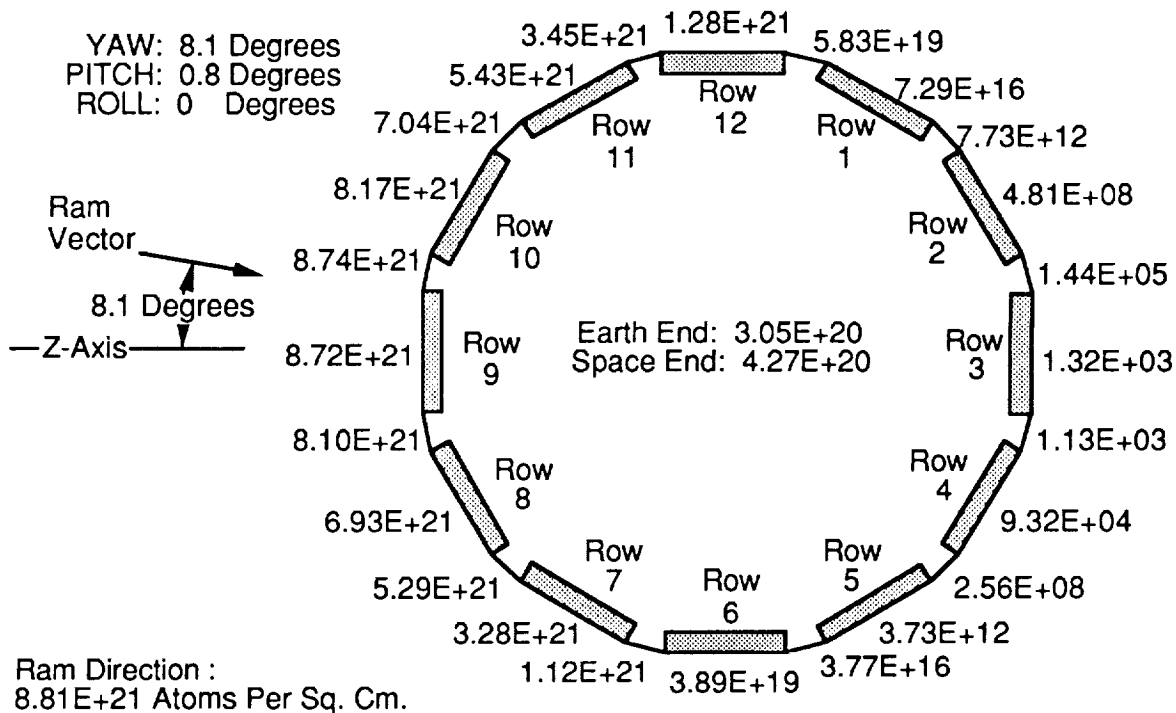


Figure 2. Revised atomic oxygen fluences for LDEF at the end of orbital flight. Fluences incurred during retrieval are not included in the totals shown.

LDEF ATOMIC OXYGEN FLUENCE UPDATE, AO MICROENVIRONMENTS PROGRAM

A microenvironments program is being developed to handle the effects of shadowing, scattering and reflection of atomic oxygen from objects near an exposed area of a spacecraft. Thus far, a program has been developed using available routines to account for shadowing. The general layout of the program is shown in Figure 3. A geometric routine is used to describe the shape and arrangement of hardware items in numerical terms. A ray tracing routine is used to determine the field of view for selected points on an experiment. Flux intensity as a function of direction is determined and intensity is summed over the field of view to yield total flux. The calculation is repeated for other points. Pictorial and graphical presentations of atomic oxygen exposure for the experiment are generated from the geometric inputs and calculated fluxes.

Scattering and reflection routines will be added to the program described. The program developed thus far is computationally efficient. About one minute of machine time is required per one hundred points of calculation.

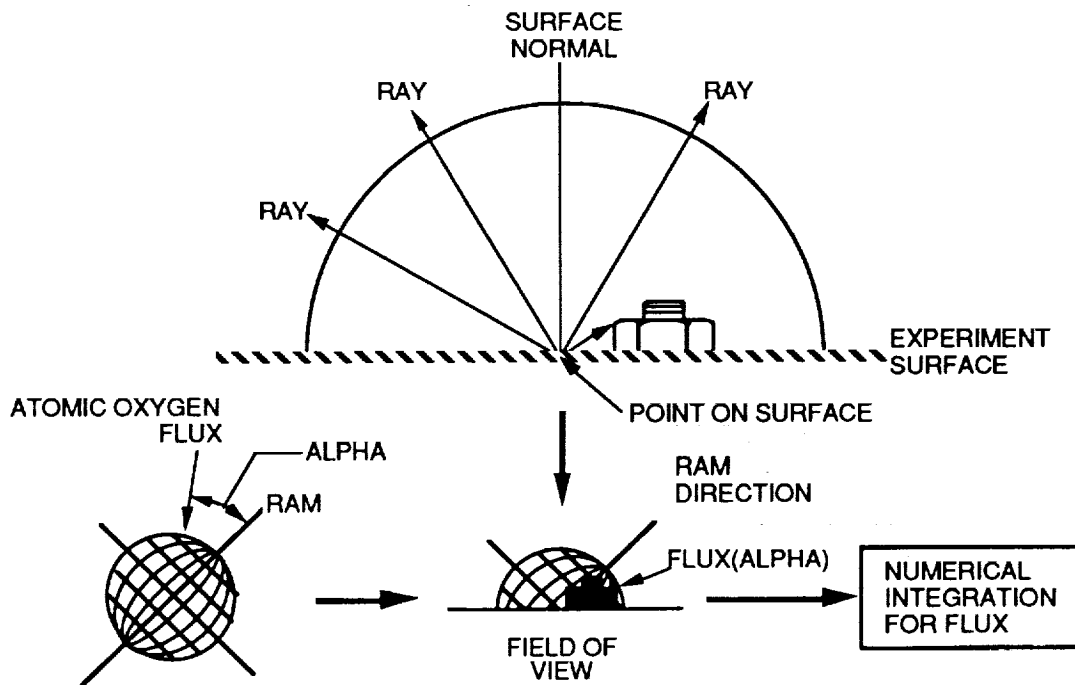


Figure 3. The field of view from a point on the spacecraft surface is obstructed by a fastener.

LDEF ATOMIC OXYGEN FLUENCE UPDATE, AO MICROENVIRONMENTS PROGRAM

Figure 4 shows the results of a preliminary calculation made with the microenvironments program. For trial calculation purposes, an experiment tray with simple geometry was assumed. The tray shown is three inches deep. Lateral tray dimensions are 46" x 34". A 12-inch diameter cylinder, 4.5 inches in height is attached to the bottom of the tray. The tray is positioned so that the viewer faces the 34-inch wide end of the tray. The angle between ram vector and the normal vector is 38 degrees. Atmospheric composition, temperature, and velocity were taken at average values for the LDEF flight.

The shadows on the bottom of the tray to the right of the cylinder show shielding caused by the cylinder. Lighter tones represent higher atomic oxygen fluxes. It will be noted that some shielding of the tray bottom is shown just upstream (left side) of the cylinder. This is because atomic oxygen arrives from all directions; thus the cylinder in fact causes some reduction in flux at the tray bottom even where the bottom surface is open to the ram direction. At the left edge of the tray, it can be seen that the vertical, 3-inch wall causes shielding of the bottom surface. The calculation is also valid for surfaces at any angle and for curved surfaces. Thus, the vertical surface at the right edge of the tray is shown to receive less flux than the vertical surface at the far end. The cylinder receives more flux on its left side (curved vertical surface) than on its right side. The flux on the cylinder cover is comparable to that at the tray bottom. The effects shown in Figure 4 are caused only by shadowing. The next step in the program development will be the addition of routines to handle scattering and reflection of incident atomic oxygen.

Figure 4 appears on the following page.

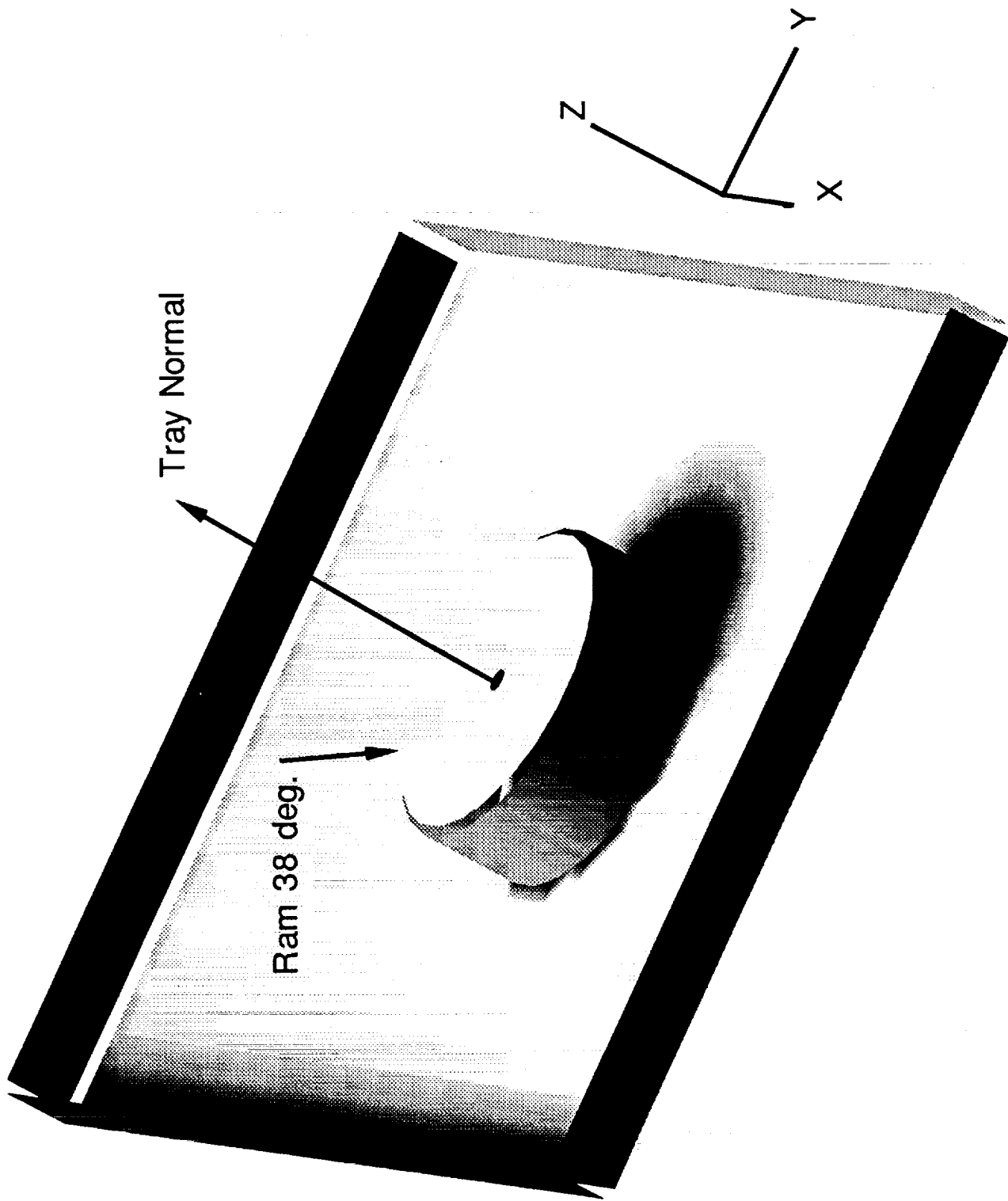


Figure 4. AO microenvironments checkout calculation using an assumed experiment configuration and average LDEF flight conditions.

LDEF ATOMIC OXYGEN FLUENCE UPDATE, AO MICROENVIRONMENTS PROGRAM

Figure 5 illustrates how data generated with the microenvironments program can be used to analyze atomic oxygen exposures of complex surfaces. The variation of atomic oxygen flux on the cylindrical surface of the geometric model shown in Figure 4 is shown plotted as a function of angle in Figure 5. The values of flux used for the plot were taken on a line around the cylinder 2.25 inches above the tray bottom. The plot shows that atomic oxygen flux does not go completely to zero on the trailing side of the cylinder, although it declines very rapidly as angle is increased beyond about 100 degrees. This result agrees with results obtained previously with the analytical model.

The value of flux calculated by the microenvironments program for points on the tray bottom a few inches from the cylinder ($3.64E13$ atoms/cm²-sec) is in agreement with the average mission flux value for experiments on Row 8 of LDEF calculated by analytical integration of the flux equation for a plane surface. This result helps to validate the numerical integration routine.

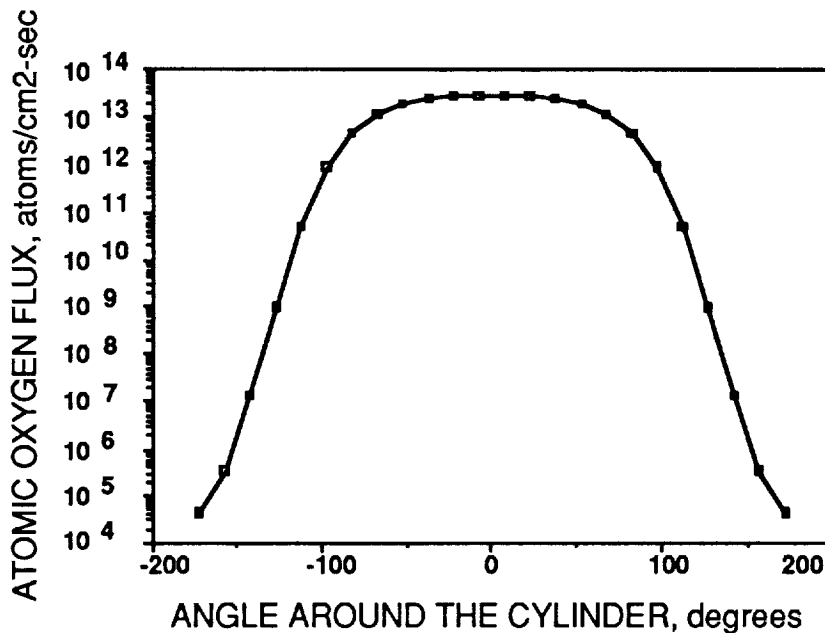


Figure 5. Variation of atomic oxygen flux around the cylindrical surface.

LDEF ATOMIC OXYGEN FLUENCE UPDATE, AO EFFECTS ON COPPER GROUNDING STRAPS

Figure 6 shows the grounding strap for experiment Tray C-05 (Reference 3). The strap connects the tray thermal control blanket to a clamp fastened to the longeron between experiment Rows 5 and 6. The surface of the clamp is 113.1 degrees from the incident ram vector. At the edge of the clamp, the strap is bent down against the tray frame. The surface of the tray frame is 128.1 degrees from the ram vector. The photo shows some imperfection in fit-up between the strap and the frame and between the strap and the clamp. The strap was not originally intended as a test material. However, the arrangement does provide two surfaces that were exposed to the space environment for 6 years at angle to the incident ram vector that are known approximately.

Twelve such grounding straps are available from LDEF covering a wide range of incident angles for both leading and trailing surfaces. The surface properties of these straps are of interest. They provide data on the response of copper exposed in low earth orbit to varying levels of atomic oxygen and ultraviolet radiation. Also, examination of the strap surfaces provides a check on calculated exposures supplementing similar verifications of exposure based on tests of other materials.

Several surface properties of the copper grounding straps can be readily determined; solar absorptance, thermal emittance, and ESCA measurements of chemical composition. Also, reflected light from first and second surfaces of thin oxide coatings causes variations in reflectance. Methods of determining film thickness by way of optical interference effects are being examined. Thus far, data are available from solar absorptance and thermal emittance measurements.

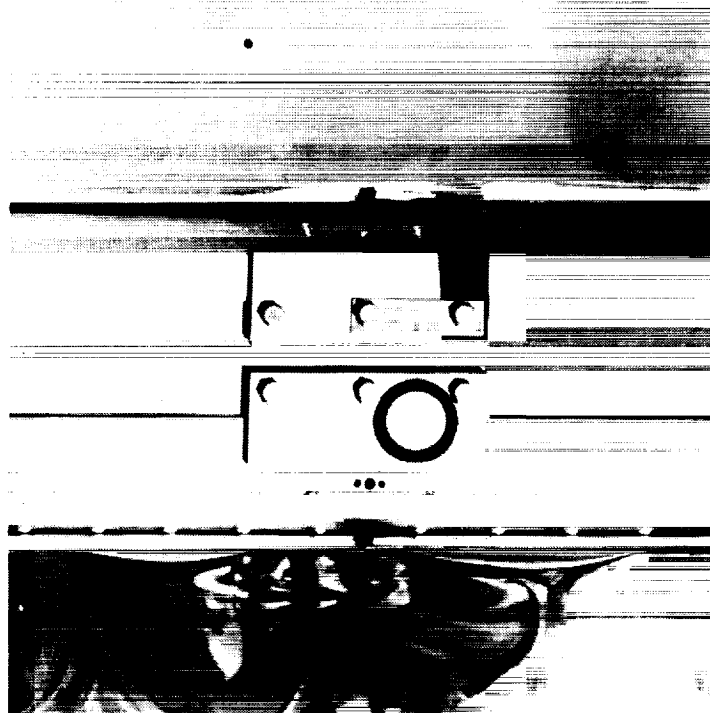


Figure 6. Grounding strap for the thermal control blanket of LDEF Tray C-05.

LDEF ATOMIC OXYGEN FLUENCE UPDATE, AO EFFECTS ON COPPER GROUNDING STRAPS

Possible factors causing absorptance and emittance to change are atomic oxygen exposure, solar exposure, and contamination. For copper grounding straps on leading surfaces of LDEF, contamination is not considered to be a factor. The surfaces were cleaned by atomic oxygen. On leading surfaces, the effects of the other two factors cannot be separated mathematically because they varied together. Both atomic oxygen exposure and solar exposure decreased with increasing incident angle. Atomic oxygen exposure decreased from $7.78E20$ atoms/cm² at Tray A-10 to $7.71E16$ atoms/cm² at Tray B-07. Solar exposure decreased from 10,700 to 7,100 equivalent sun hours for these experiments.

The variation in atomic oxygen exposure is greater than that for solar exposure and was chosen as the only independent variable for Figure 7. The data for absorptance and emittance at zero atomic oxygen fluence were taken on unexposed control material stored on earth during the LDEF flight. Figure 7 shows that solar absorptance is significantly increased by exposure in space. When solar absorptance is plotted against atomic oxygen fluence, the resulting function accounts for 88 percent of the deviation in sample values, although some of this effect may be caused by co-variation of solar exposure with atomic oxygen exposure.

No significant trend was found in the thermal emittance of copper grounding straps as a function of exposure on leading LDEF surfaces.

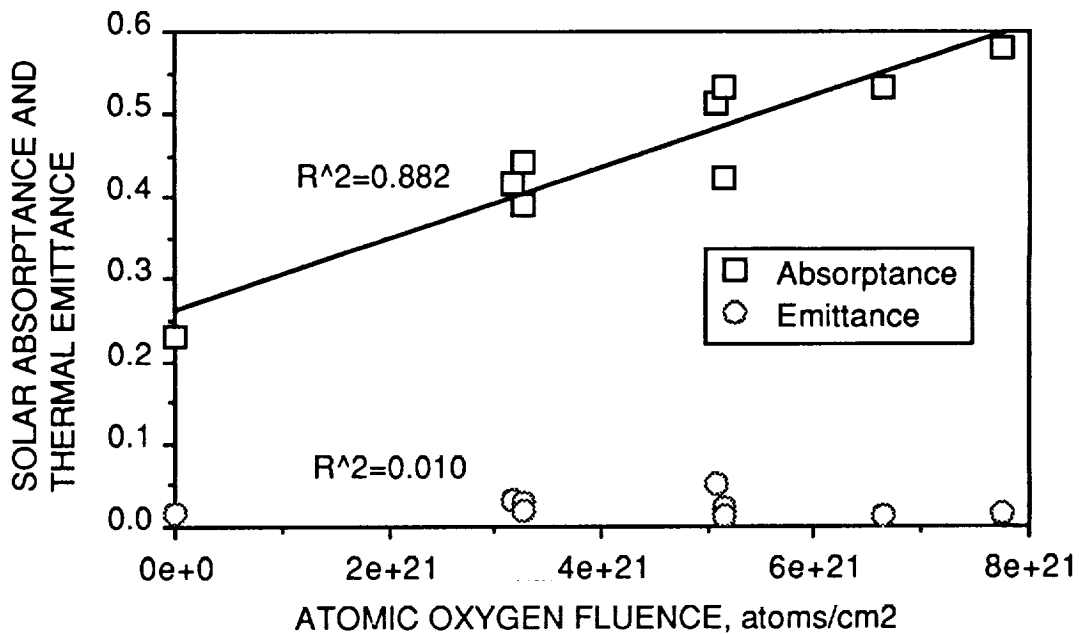


Figure 7. Absorptance and emittance of copper grounding straps on leading surfaces vs atomic oxygen exposure.

LDEF ATOMIC OXYGEN FLUENCE UPDATE, AO EFFECTS ON COPPER GROUNDING STRAPS

On trailing surfaces of LDEF the atomic oxygen exposure was near zero. The most likely variables affecting absorptance and emittance are contamination and solar exposure. Figure 8 shows solar absorptance and thermal emittance measurements on copper grounding straps from trailing experiments on LDEF plotted as functions of solar exposure in equivalent sun hours. The data given for zero hours exposure were taken from unexposed control material stored on earth during the LDEF flight.

Figure 8 shows a moderate dependence of solar absorptance on solar exposure. However, solar absorptance measurements for the exposed samples cluster about an average and do not show a consistent increase with increasing solar exposure. Most of the deviation in plotted values results from differences between the control sample and the exposed samples. The trend may be caused by contamination. If this is true then absorptance of the strap surfaces could be independent of solar exposure.

No significant difference in thermal emittance was noted between the control sample and samples exposed on LDEF's trailing experiments.

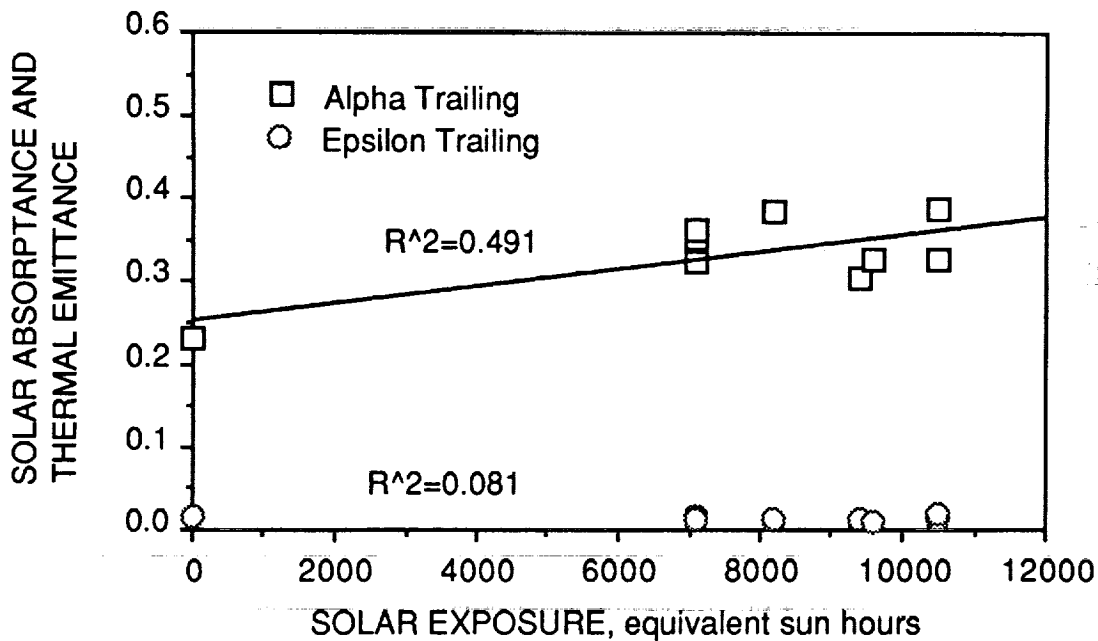
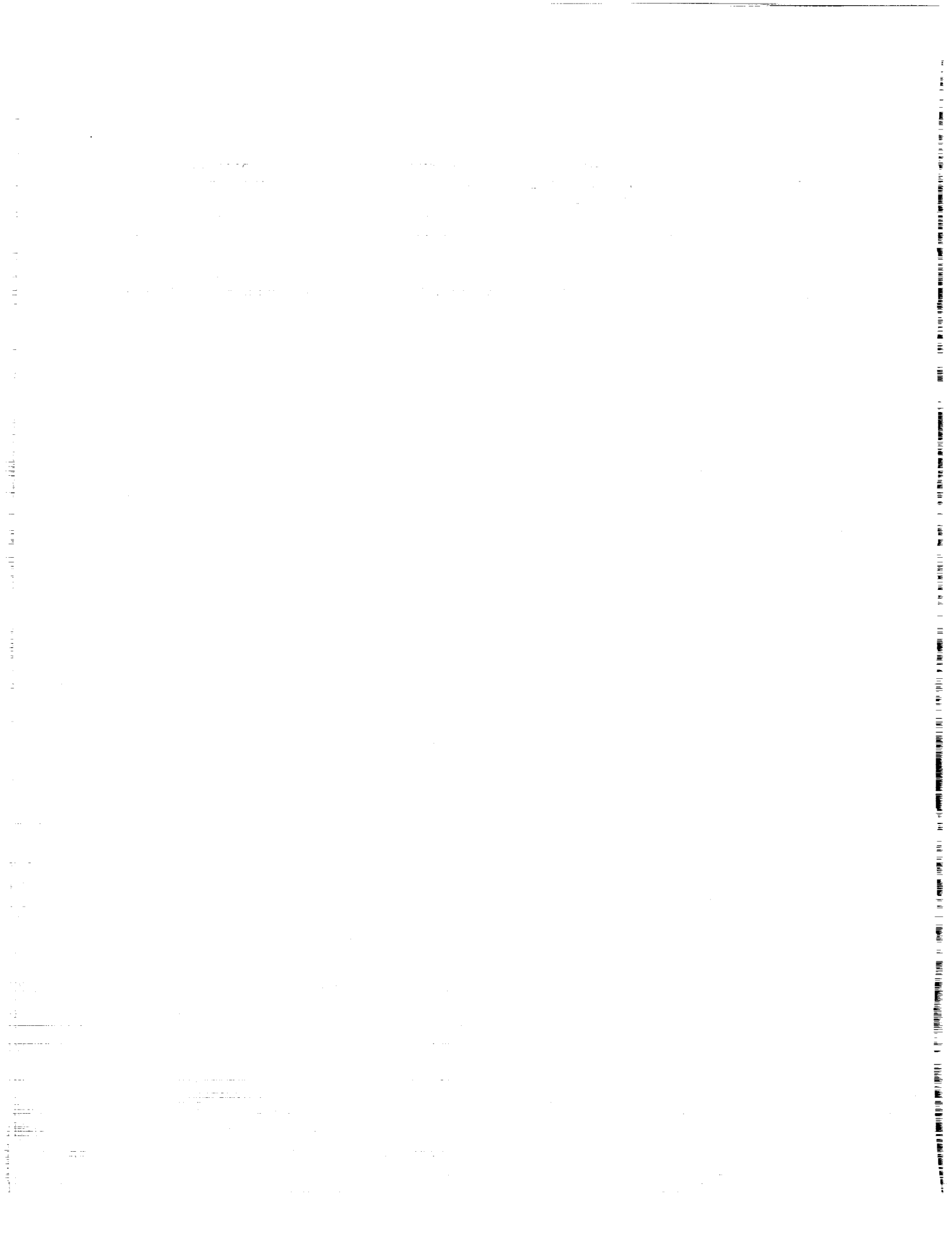


Figure 8. Absorptance and emittance of copper grounding straps on trailing experiments vs solar exposure.

REFERENCES

1. R. J. Bourassa, J. R. Gillis and K. W. Rousslang, Atomic Oxygen and Ultraviolet Radiation Mission Total Exposures for LDEF Experiments, First LDEF Post-Retrieval Symposium, Orlando, FL (June 2-8, 1991).
2. Dr. Bruce Banks, LDEF Yaw And Pitch Angle Estimates, LDEF Materials Workshop '91, November 1991.
3. Photo Number: KSC-390C-1110.06, LDEF Survey, SAEF II, Kennedy Space Center, Florida, February 1990.



LDEF YAW AND PITCH ANGLE ESTIMATES

Bruce A. Banks
NASA Lewis Research Center
Cleveland, Ohio

Linda Gebauer
Cleveland State University
Cleveland, Ohio

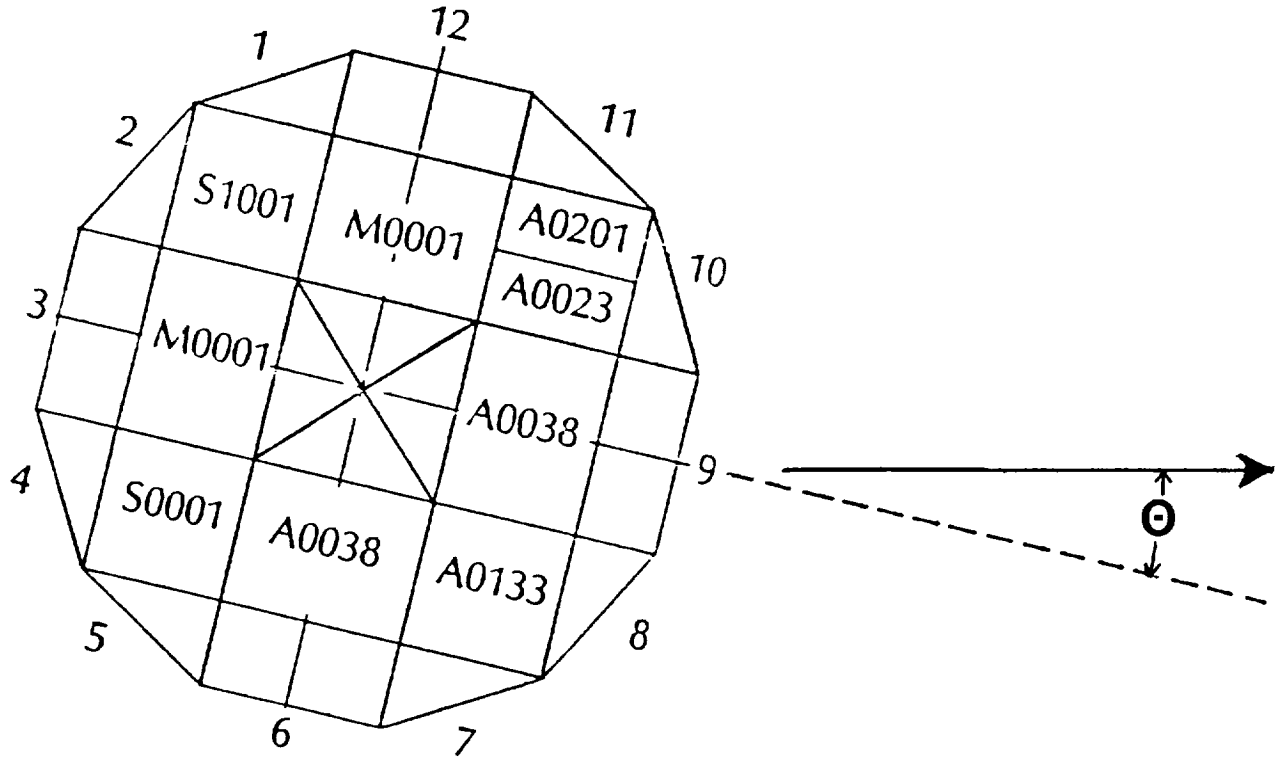
INTRODUCTION

Quantification of the LDEF yaw and pitch misorientations is crucial to the knowledge of atomic oxygen exposure of samples placed on LDEF. Video camera documentation of the LDEF spacecraft prior to grapple attachment, atomic oxygen shadows on experiment trays and longerons, and a pinhole atomic oxygen camera placed on LDEF provided sources of documentation of the yaw and pitch misorientation. Based on uncertainty-weighted averaging of data, the LDEF yaw offset was found to be $8.1 \pm 0.6^\circ$, allowing higher atomic oxygen exposure of row 12 than initially anticipated. The LDEF pitch angle offset was found to be $0.8 \pm 0.4^\circ$, such that the space end was tipped forward toward the direction of travel. The resulting consequences of the yaw and pitch misorientation of LDEF on the atomic oxygen fluence is a factor of 2.16 increase for samples located on row 12, and a factor of 1.18 increase for samples located on the space end compared to that which would be expected for perfect orientation.

ACKNOWLEDGMENT

The authors gratefully acknowledge the assistance of Robert O'Neal of the Langley LDEF Project Office who greatly contributed to the assessment of the LDEF yaw and pitch orientation.

YAW OFFSET



Viewgraph #2:

For the purposes of this investigation, a positive yaw offset is a rotation of the LDEF spacecraft about its long axis in a clockwise direction as viewed from above looking down at the space end.

LDEF YAW MISORIENTATION

<u>Source</u>	<u>LDEF Yaw Misorientation, degrees (Allowing Greater Atomic Oxygen Exposure of Row 12 Than Row 6)</u>	<u>Uncertainty, Degrees</u>
Video Camera Documentation of Cloud Movement relative to LDEF prior to grapple attachment	Banks, NASA LeRC 8.3	± 1.1
Shadows behind on Earth End	Banks, NASA LeRC 7.0	± 1.4
Pin Hole Camera	Gregory, University of Alabama in Huntsville 8.0	± 0.4
Nut Plate Shadows on Longerons	Banks, NASA LeRC 4.3	± 1.0
Nut Plate Shadows on Tray 9C	Banks, NASA LeRC 7.4	± 0.5
Nut Plate Shadows on Transverse Flat-Plate Heat Pipe Experiment S1005	Linton & Vaughn, NASA MSFC 11.0	± 1.0
Nut Plate Shadows on Solar Array Materials Passive LDEF Experiment A0171	Linton & Vaughn, NASA MSFC 12.0	± 1.0
Nut Plate Shadows on Thermal Control Surfaces Experiment S0069	Linton & Vaughn, NASA MSFC 11.5	± 1.0

Viewgraph #3:

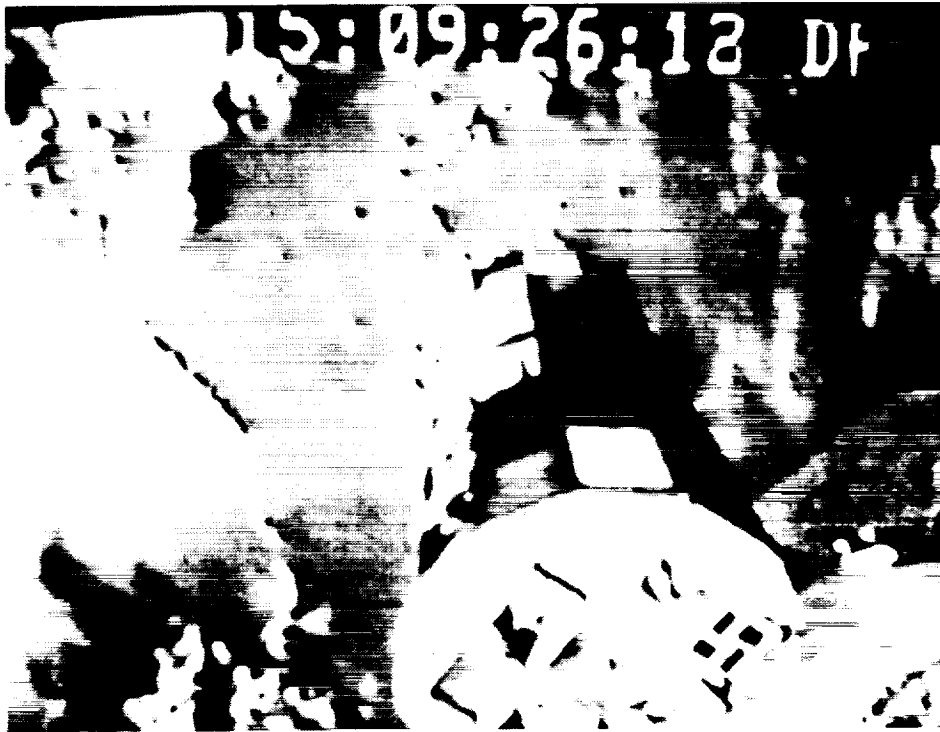
This table lists the various yaw offsets measured by LDEF investigators. The first measurement listed and the fourth through the eighth measurements will be discussed later. The second measurement listed is that of the atomic oxygen shadows of both heads on the LDEF's earth end. The third measurement listed is that of Dr. John Gregory's pinhole camera. This was the only device on the LDEF spacecraft which was specifically intended to measure the LDEF's orientation. The pinhole camera consisted of a 0.5 mm (0.020") diameter pinhole in a 3.25 cm (1.28") radius silver-coated stainless steel hemisphere. Although the silver was highly oxidized as a result of overexposure caused by scattered atomic oxygen, a clear visualization of the arrival direction of atomic oxygen was observed. The uncertainties listed are probable errors.

ORIGINAL PAGE
BLACK AND WHITE PHOTOGRAPH



Viewgraph #4:

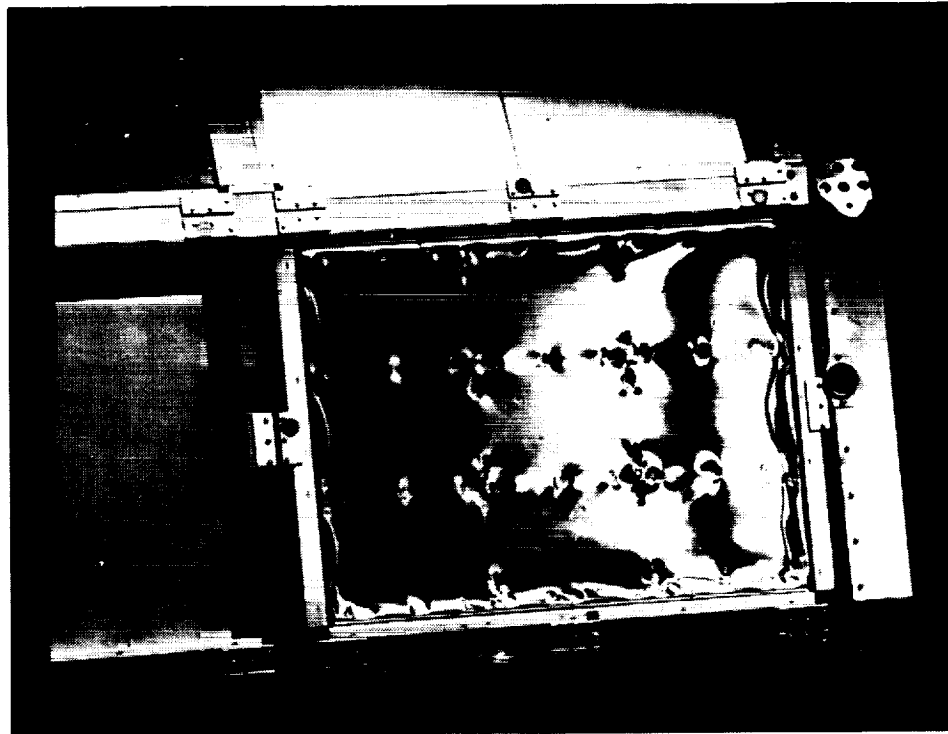
This picture is a copy of the video camera photos prior to retrieval. The orientation of the LDEF spacecraft was noted by observing the tray edges on the space end. The direction of travel of the LDEF spacecraft with respect to ground is noted by the specific cloud formations.



Viewgraph #5:

This photo shows the LDEF spacecraft 22 seconds after the prior photo. Note some of the same cloud formations can be seen displaced from their previous positions. Lines that were drawn connecting the cloud formation allowed the direction of travel to be measured with respect to the LDEF orientation. To properly perform this measurement, corrections were made to account for the angle under which the LDEF spacecraft was observed to predict what the actual yaw offset would be. As can be seen from the previous yaw offset summary table, the video camera yaw misorientation was in agreement with the pinhole camera and shadows behind both heads on the earth end if one considers the uncertainties.

ORIGINAL PAGE
BLACK AND WHITE PHOTOGRAPH



Viewgraph #6:

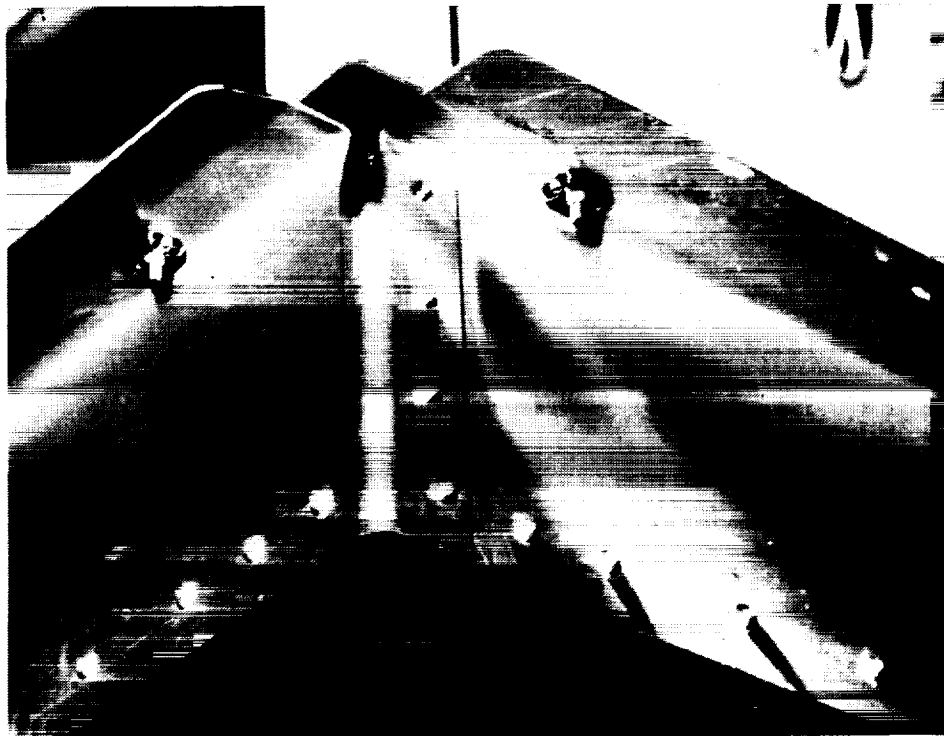
This photo shows the openings in the tray corners, as well as the nut plates on the tray flanges, which were used pre- and post-flight to attach protective covers over the experiments.



Viewgraph #7:

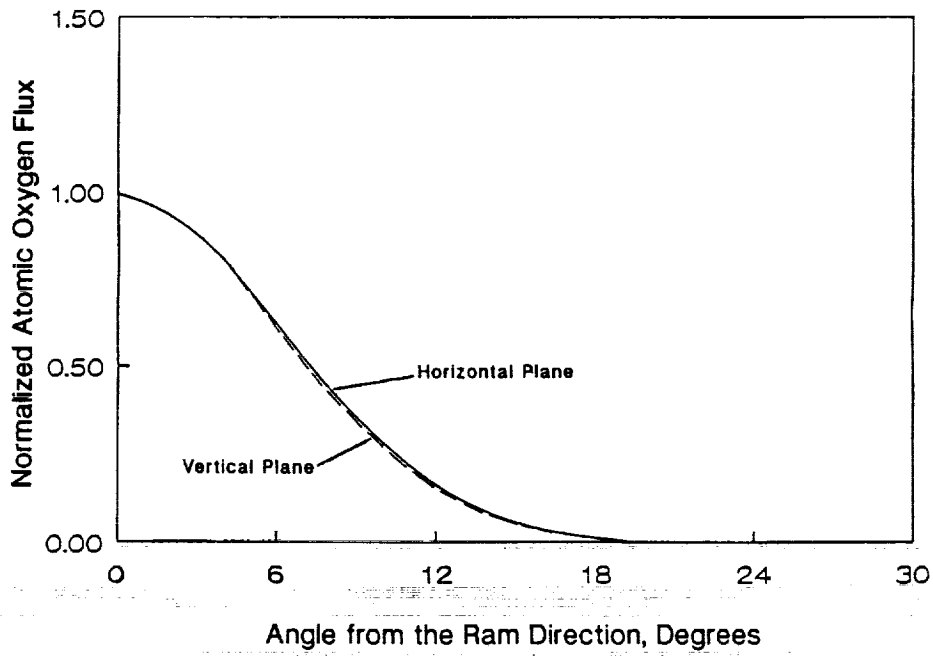
This photo shows the detailed configuration of typical tray corner openings, and nut plates which had 10-32 screw hole apertures, allowing atomic oxygen to enter into the LDEF interior.

ORIGINAL PAGE
BLACK AND WHITE PHOTOGRAPH



Viewgraph #8:

This photograph of an LDEF tray on row 11 bay A shows the typical atomic oxygen darkened contaminant streak on the LDEF tray sides as a result of atomic oxygen entrance into the LDEF interior through the openings in the corners of the trays. Note in this photo, the nut plates have the screws attached because the protective coverlet has been installed post-flight. The contaminant on this corner was analyzed and found to contain silicon, as well as carbon. Based on numerous other measurements, it is probable that silicone contaminants from within LDEF were oxidized to form silicates, which also contain other hydrocarbon contaminants. Note also that the rivet heads on the bottom of the tray make atomic oxygen shadows which point back to the direction of the opening of the tray.



Viewgraph #9:

This plot shows the atomic oxygen arrival angular distribution for LDEF assuming 1227 K atoms, 411 kilometers altitude, and 28.5° orbital inclination. Because the atomic oxygen atoms are hyperthermal, arriving atomic oxygen has a distribution of arrival directions, causing the atomic oxygen streaks within the trays to be broad, rather than thin lines.

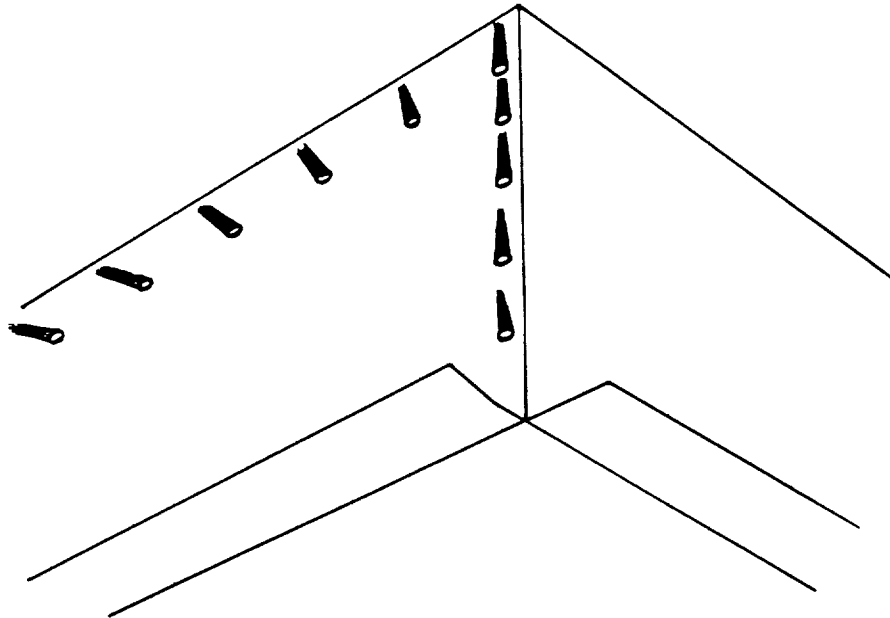
ATOMIC OXYGEN INCIDENT ANGULAR DISTRIBUTION



411 km altitude
1227 K atoms
28.5° inclination

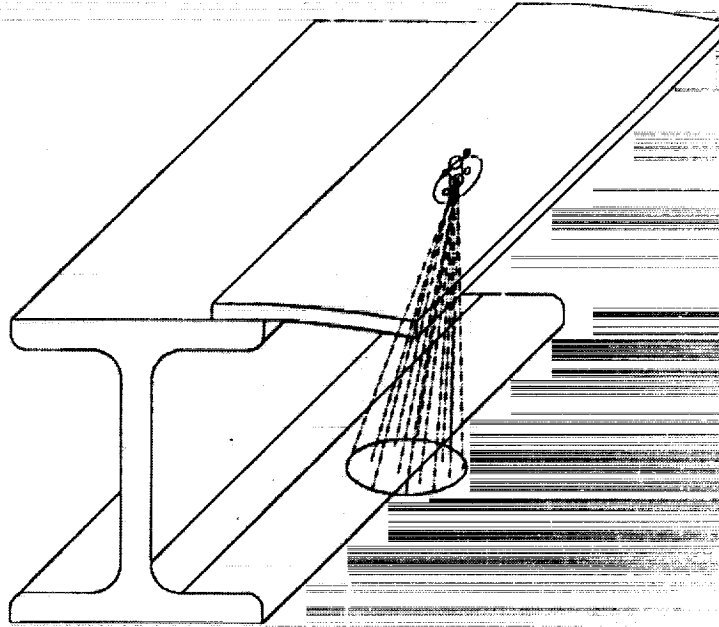
Viewgraph #10:

This plot shows the same angular distribution plotted in polar coordinates.



Viewgraph #11:

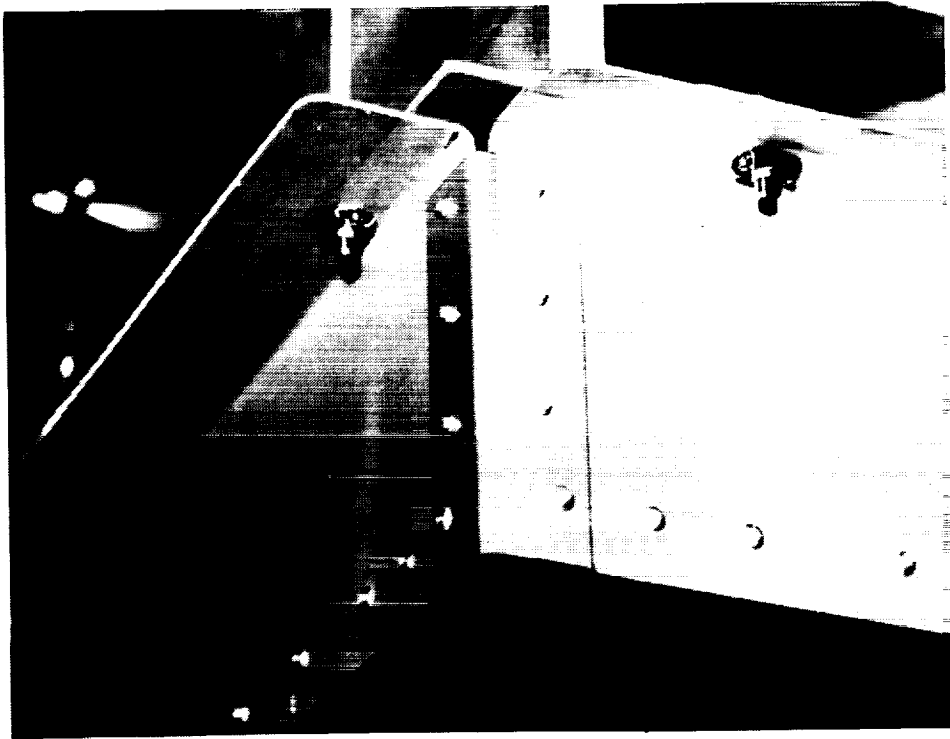
Because atomic oxygen arrives from a variety of incoming angles, all streaks behind the rivet heads on the tray point back to the opening, rather than specifically to the direction of the main arrival of atomic oxygen. The intensity of the streaks is perhaps a better measure of the direction arrival. That is to say, where the streaks are darkest are where the central arrival direction is most likely. Thus the broad distributed arrival of atomic oxygen through the tray corners does not allow accurate measure of the LDEF yaw orientation. The smaller openings of the 10-32 nut plates, on the other hand, did allow more accurate ground measurements.



Viewgraph #12:

Nut plate measurement shadows on the longerons indicated a 4.3° yaw misorientation with a probable error of $\pm 1^\circ$.

ORIGINAL PAGE
BLACK AND WHITE PHOTOGRAPH



Viewgraph #13:

This photo of the LDEF tray from row 9, Bay C shows faint nut plate streaks which were useful for both the yaw and pitch measurements. Similar measurements from other trays were made by Roger Linton and Jason Vaughn of NASA Marshall Space Flight Center as well as the authors. The quality of the measurements relies heavily upon uniformity of arrival of silicone-containing contaminants. Areas of high spacial gradients in contaminant flux may have misoriented atomic oxygen streaks. Efforts were made by the author to measure only streaks which had high degrees of symmetry.

**Generic
Measurement**

**Yaw Misorientation
(allowing greater atomic oxygen exposure of row 12)**

Video Camera Documentation
Prior to Grapple Attachment

8.3 ± 1.1

Shadows Behind Nuts on Earth End

7.0 ± 1.4

Pin Hole Camera

8.0 ± 0.4

Nut Plate Shadows

9.2 ± 1.0

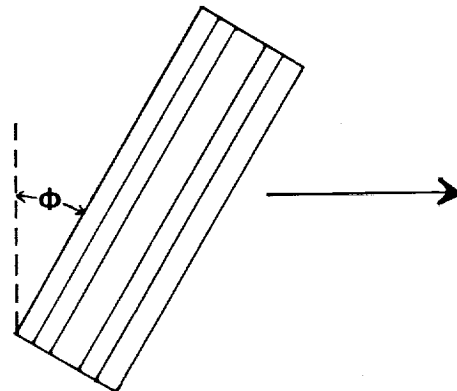
AVERAGE

8.1 ± 0.6

Viewgraph #14:

This summary chart lists the generic types of yaw misorientation measurements. For each generic yaw misorientation measurement, the angles specified are the averages of all investigators' information with their assigned probable error estimates. The overall average is an uncertainty weighted average of the various generic measurements, along with its probable error.

PITCH OFFSET



Viewgraph #15:

This drawing shows the LDEF as viewed from the side where the pitch angle is considered positive if the space end is leaning forward in the direction of travel.

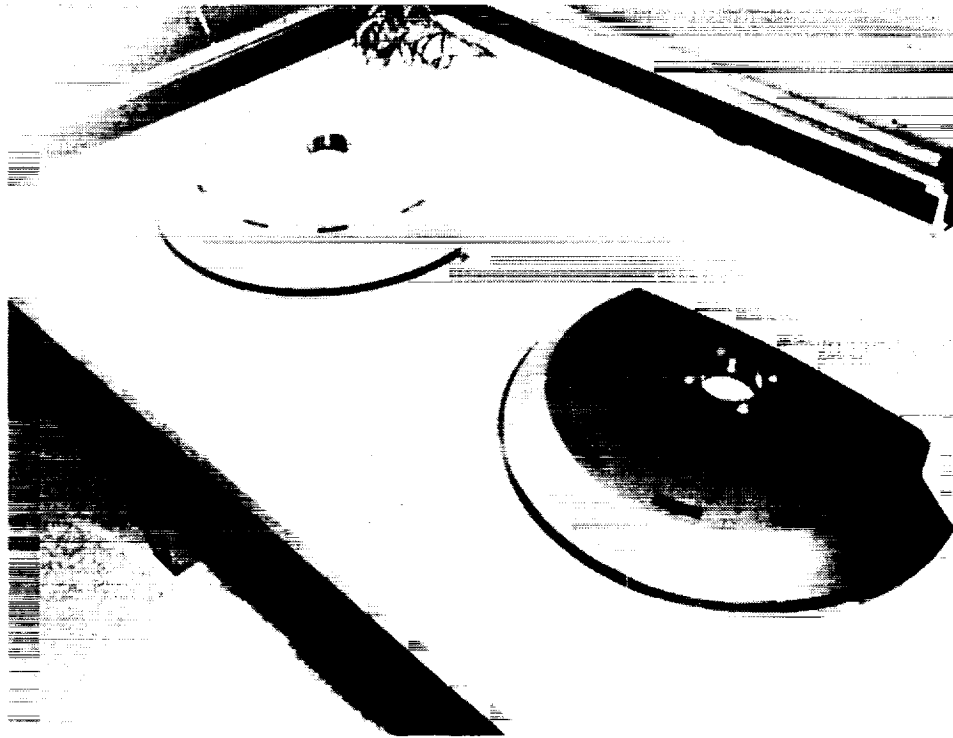
LDEF PITCH ANGLE MISALIGNMENT DATA SOURCES

<u>Source</u>	<u>Pitch Angle, degrees (Space End Forward is +)</u>
1. Pinhole Camera from AO114 on 9C	1 ± 0.4
2. Nut Plate Shadow on Longeron Flange under 9B	0 ± 1.0
3. Scuff Plate Shadows from Trunnions on Row 9	No Shadows Observed
4. Grapple Alignment Pin Shadow from 10C	No Shadows Observed
5. Be ⁷ Populations on Space and Earth End Tray Clamps compared to those around LDEF	Not Measured
6. Nut Plate Shadows on Tray Sides Parallel to Longerons on Tray 9C	$0.66 \pm .35$
7. Solar Absorptance of A-276 Paint Spots on Space and Earth Ends compared to around LDEF	$\left. \begin{array}{l} -1.72 + 8.5 \\ -7.2 \end{array} \right\} \text{Space End}$
	$\left. \begin{array}{l} -40.5 + 4.6 \\ -3.9 \end{array} \right\} \text{Earth End}$
8. Shadows of Tray Corner Openings on LDEF Internal Structures	Data Unavailable
9. Mass Model Gravity Gradient Stabilization Prediction of Pitch Angle	Data Unavailable
10. Experiment Exposure Control Canister Drive Screw Shadows on S0010 on 9B	No Shadows Observed

Viewgraph #16:

This table shows the various sources of information for determination of the LDEF pitch angle. As can be seen, many of the potential sources of data revealed no results or data which had high probable errors relative to the magnitude of the measurement. The first source of information, the pinhole camera from Dr. John Gregory's experiment on AO114 on Row 9C, is one of the more definitive measurements. The pinhole camera was specifically designed to measure the LDEF spacecraft orientation, and had a measurement in excess of its probable error. On the other hand, the nut plate shadow on longeron flange under 9B had a probable error in excess of the measurement, and it therefore is deemed non-usable as a source of data. Atomic oxygen shadows from the trunnions on Row 9, and the grapple alignment pins on tray 10C were not observable, and therefore no information was gained from items 3 and 4. Similarly, because the Be⁷ calculations were not measured on the space or earth end tray clamps, calculations of the pitch were not possible to be made to compare with the Be⁷ calculations around LDEF. The nut plate shadows on the tray sides parallel to longerons on tray 9C did provide meaningful data. The solar absorptance from paint spots on the space and earth end produced highly uncertain data with questionable reliability based on contamination issues. Items 8, 9, and 10 had potential to provide information, however, no observations or data was found available to produce meaningful numbers.

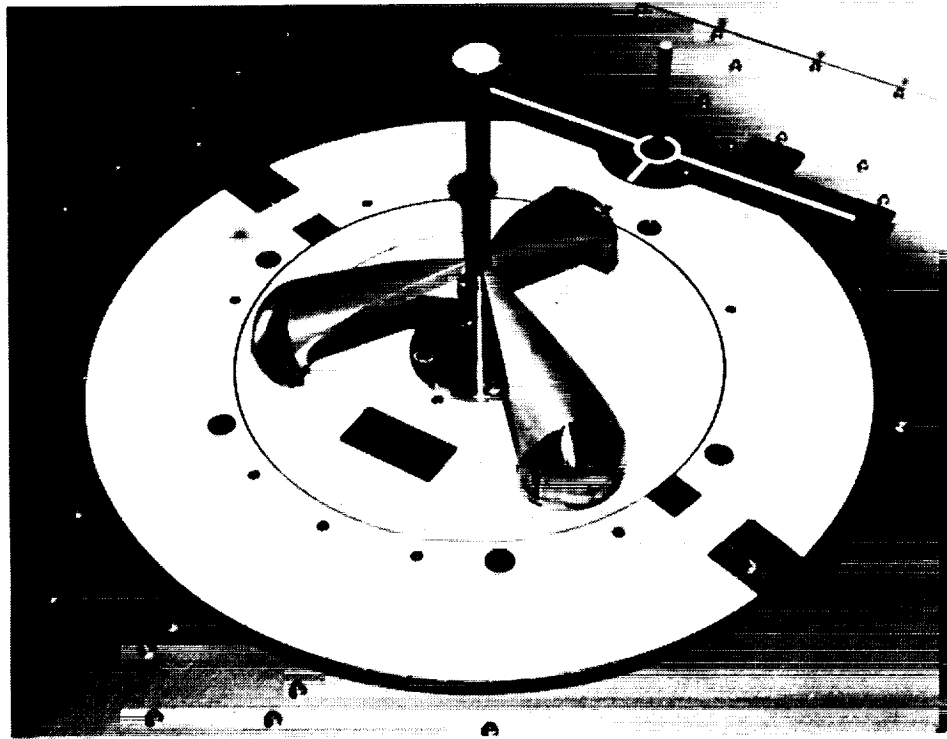
ORIGINAL PAGE
BLACK AND WHITE PHOTOGRAPH



Viewgraph #17:

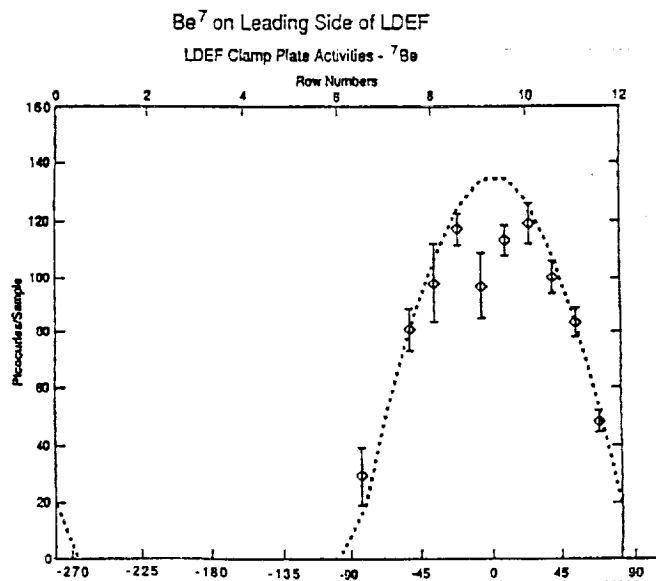
This is a photograph of the scuff plates showing the lack of atomic oxygen shadows from the trunnions.

ORIGINAL PAGE
BLACK AND WHITE PHOTOGRAPH



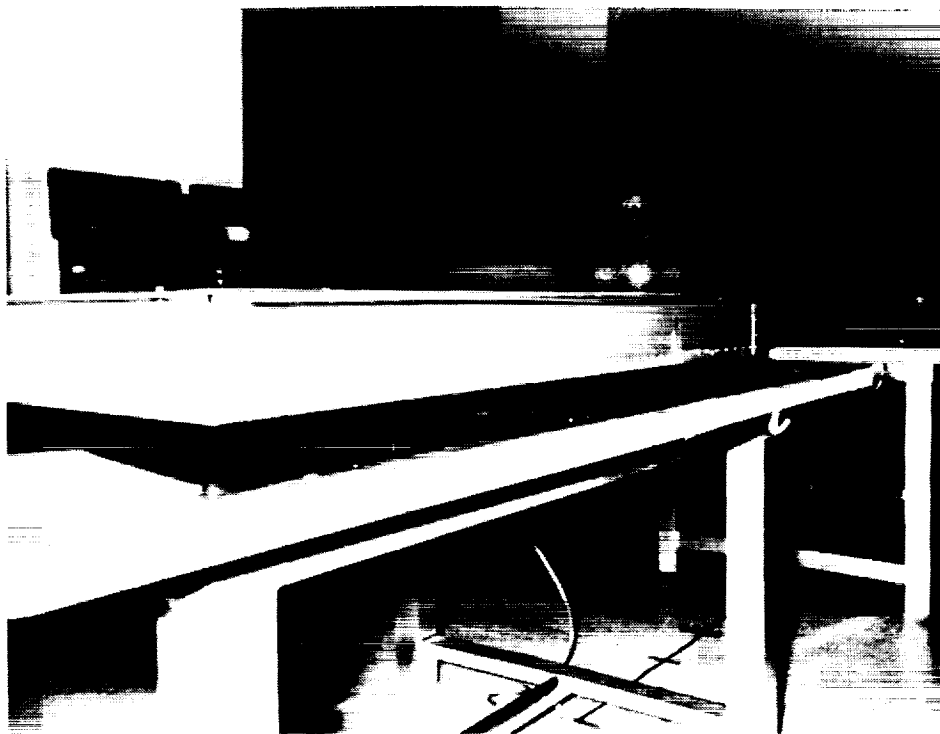
Viewgraph #18:

This is a photo of the grapple fixture which did not reveal atomic oxygen shadows from the grapple alignment pin.



Viewgraph #19:

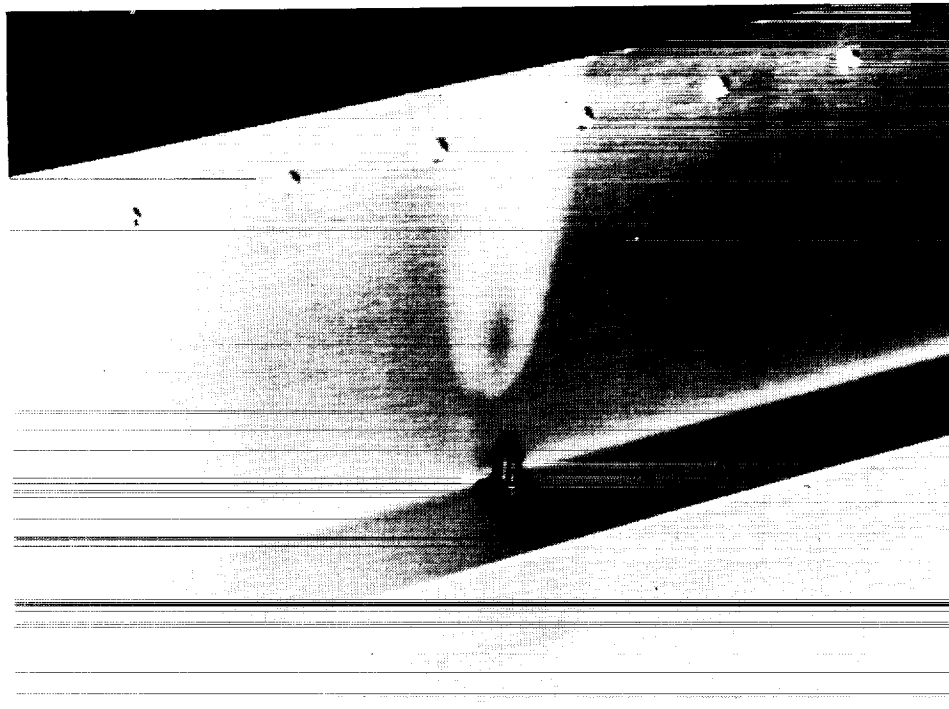
The Be⁷ calculation as a function of angle around LDEF held potential to determine pitch angle information if space or earth end data was taken. However, because no such data was taken, correlations with this plot were not possible.



Viewgraph #20:

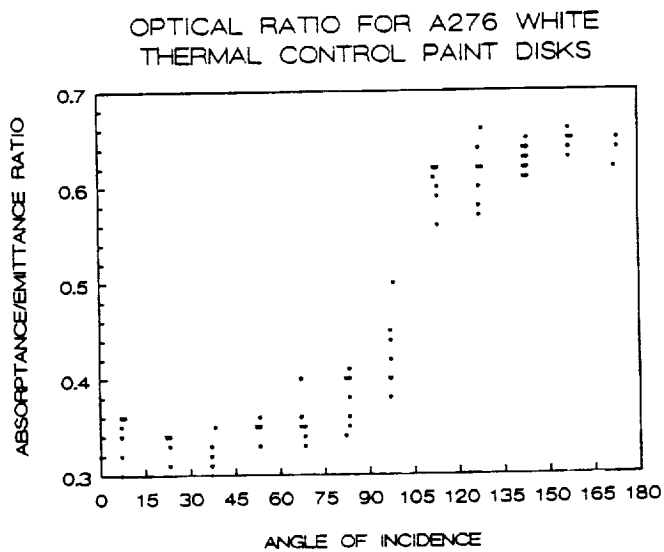
This is a photograph of the tray 9C showing atomic oxygen streaks on the sides of the tray as a result of its entrance through 10-32 screw holes from the nut plates on the tray flanges. The streaks were found to contain silicon, which is thought to be in the form of silicates as a result of atomic oxygen interaction with arriving silicone contaminants.

ORIGINAL PAGE
BLACK AND WHITE PHOTOGRAPH



Viewgraph 21:

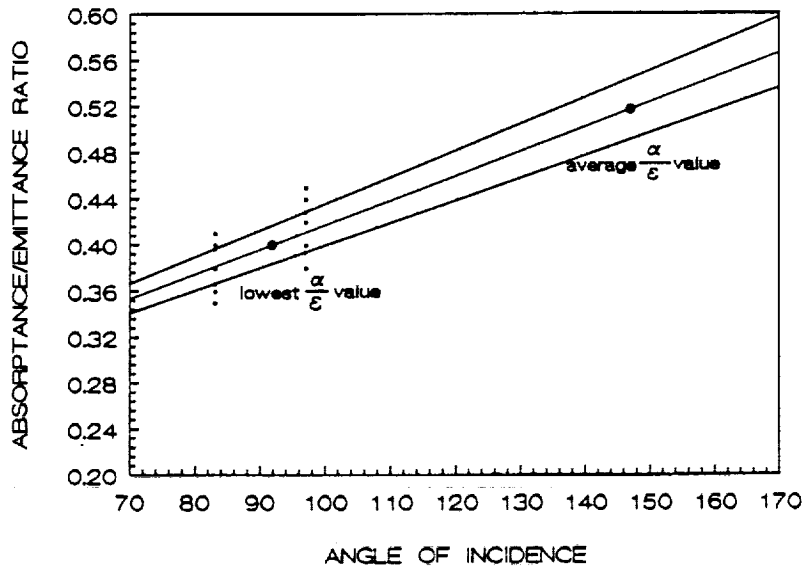
This is a photograph of the row 10 side of tray 9C showing the ground atomic oxygen streak associated with the nut plate aperture. Such streaks were used to calculate the pitch angle for LDEF.



Viewgraph #22:

This plot shows the solar absorptance-to-thermal emittance ratio as a function of position around LDEF for A276 white thermal control paint disks. Through knowledge of the earth and space end thermal control paint solar absorptance-to-thermal emittance ratio, one can estimate the angle of the surface with respect to the ram direction.

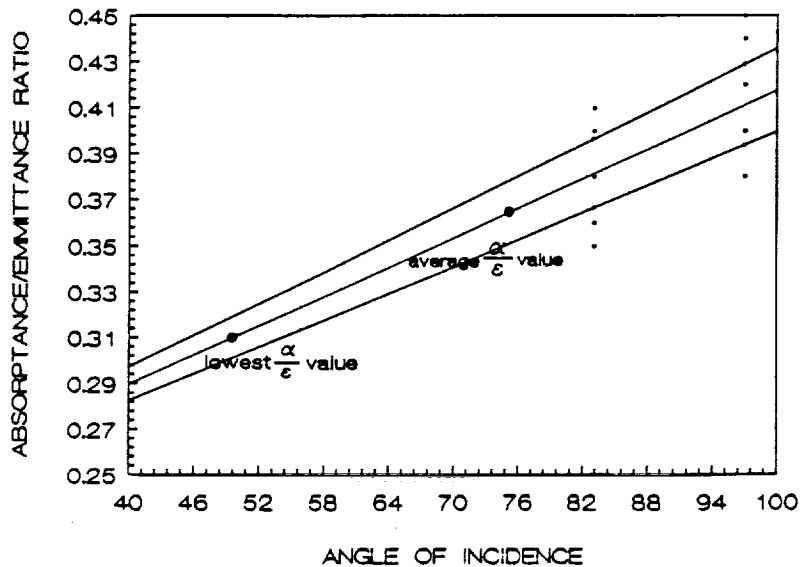
LDEF PITCH ANGLE FROM A276 DISKS
Space end data



Viewgraph #23:

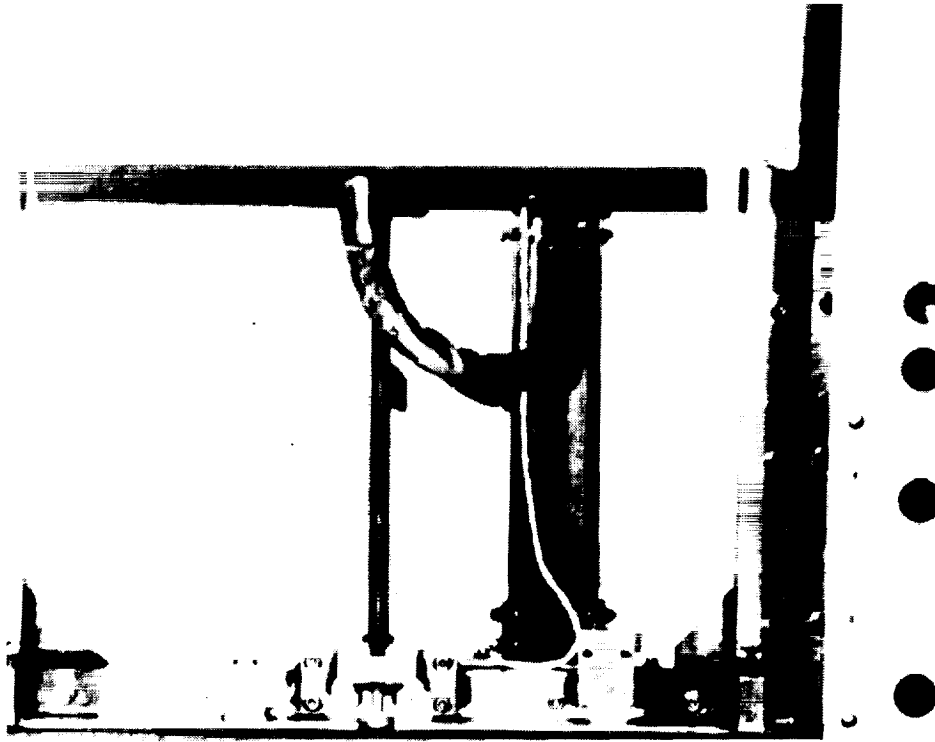
The small dots near 90° angle of incidence are the solar absorptance-to-thermal emittance ratio of the paint spots closest to 90° angle of incidence, or a zero pitch offset. As can be seen from the photo, paint spots from the space end with the lowest alpha over epsilon value or average alpha over epsilon value, produced a greater than 90° angle of incidence, which implies pitch angles of -1.72 or -56.9°. The wide variation between the lowest and the average alpha over epsilon value is probably a result of the widely varying level of contamination on the space end, which also currently contributes to the lack of reliability of this measurement.

LDEF PITCH ANGLE FROM A276 DISKS
Earth end data



Viewgraph #24:

The earth end data produced pitch angles which were also highly negative and with large uncertainties. The highly negative pitch angles are probably a result of the earth end surfaces being cleaner, possibly as a consequence of lower contamination, or being warmer. Thus the earth end paint spot data cannot be highly relied upon.



Viewgraph #25:

The experiment exposure control canister drive screw did not produce atomic oxygen shadows. Shadows shown in this figure are a result of room illumination, rather than atomic oxygen interactions.

LDEF PITCH ANGLE

Generic Measurement

Pinhole Camera from AO114 on 9C	1.0 ± 0.4
Nut Plate Shadows on Tray Sides Parallel to Longerons on Tray 9C	0.66 ± 0.35
<hr/>	
Average	0.8 ± 0.4

Viewgraph #26:

This table summarizes the LDEF pitch angle data which is considered meaningful for calculation of an overall average pitch angle of $0.8 \pm 0.4^\circ$, where the overall average pitch angle is a weighted average of the two generic types of measurements which provided meaningful data, and the uncertainty is the probable error.

SUMMARY

	<u>Degrees</u>	
LDEF YAW OFFSET	8.1 ± 0.6	(Allowing higher atomic oxygen exposure of Row 12 than planned)
LDEF PITCH OFFSET	0.8 ± 0.4	(space end tipped forward)

Viewgraph #27:

This table summarizes the final LDEF yaw and pitch offset angles and their associated probable errors.

Effect of Yaw and Pitch Offset on Atomic Oxygen Fluence

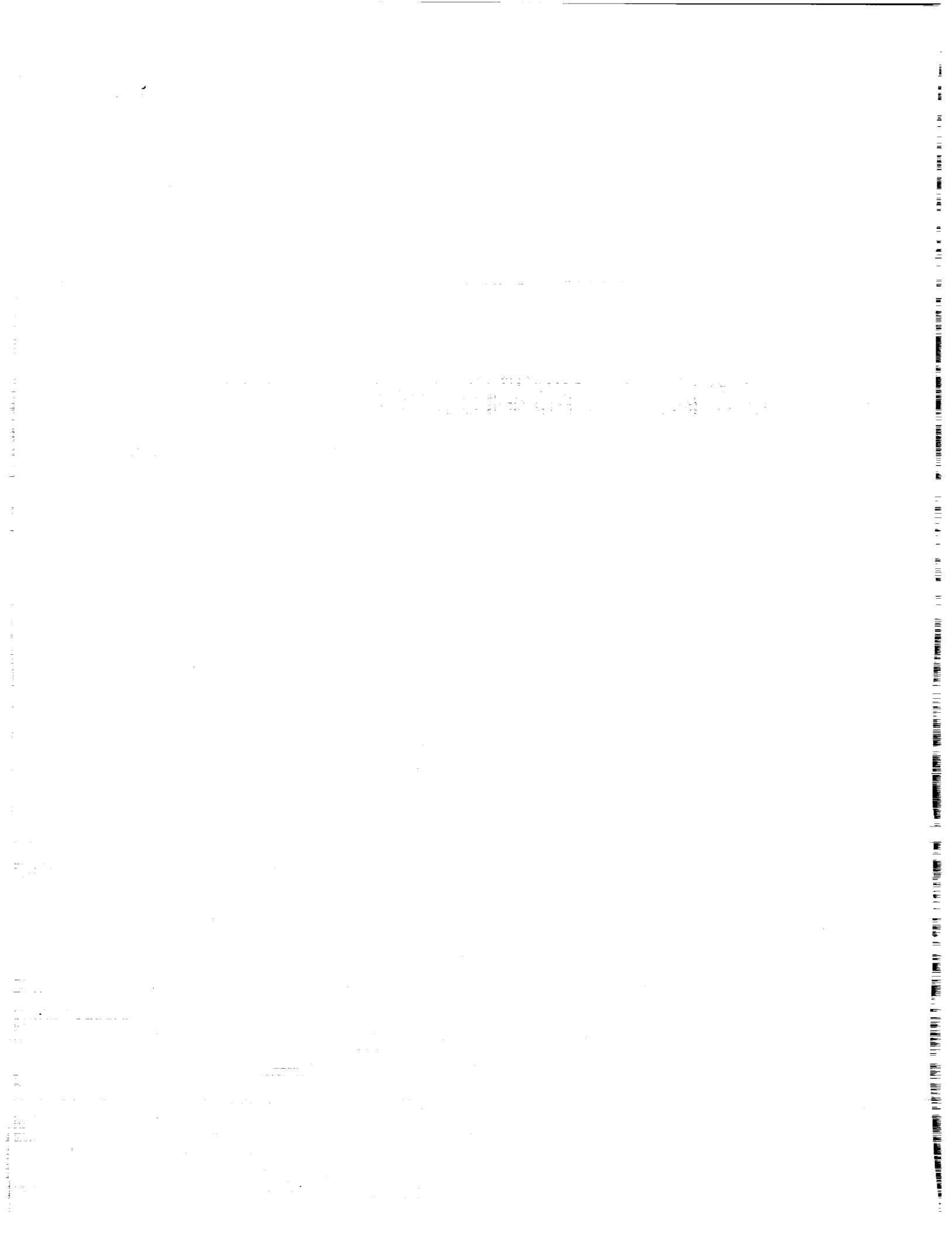
<u>Location</u>	<u>Fluence Relative to Zero Offset</u>
Row 12	2.16
Row 6	0.13
Space End	1.18
Earth End	0.87

Viewgraph #28:

This table illustrates the consequences of the yaw and pitch offset on surfaces which are most affected by the LDEF misorientation. As can be seen, the yaw offset effects have far greater relative changes on the atomic oxygen fluence than the smaller pitch offset does.

LDEF Contamination

Co-Chairmen: Wayne Stuckey and Steve Koontz
Recorder: Russell Crutcher



MATERIALS SIG QUANTIFICATION AND CHARACTERIZATION
OF SURFACE CONTAMINANTS

Russ Crutcher
Boeing Defense and Space Group
Kent, Washington

ABSTRACT

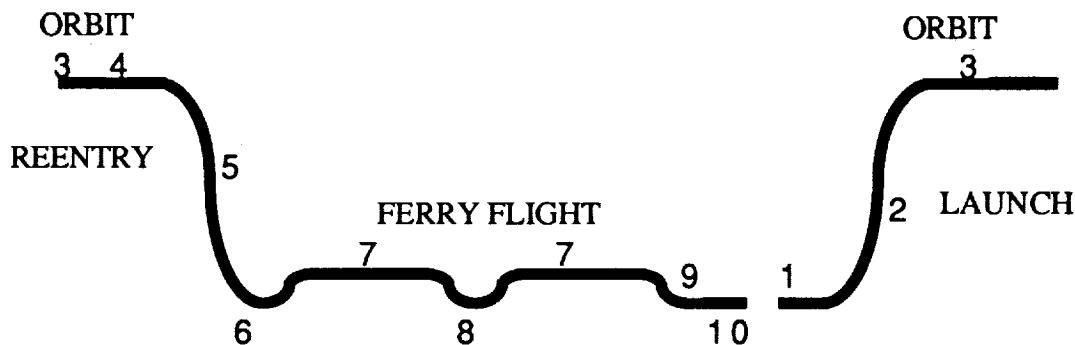
When LDEF entered orbit its cleanliness was approximately a MIL-STD-1246B Level 2000C. Its burden of contaminants included particles from every part of its history including a relatively small contribution from the shuttle bay itself. Although this satellite was far from what is normally considered clean in the aerospace industry, contaminating events in orbit and from processing after recovery were easily detected. The molecular contaminants carried into orbit were dwarfed by the heavy deposition of UV polymerized films from outgassing urethane paints and silicone based materials. Impacts by relatively small objects in orbit could create particulate contaminants that easily dominated the particle counts within a centimeter of the impact site.

During the recovery activities LDEF was 'sprayed' with a liquid high in organics and water soluble salts. With reentry turbulence, vibration, and gravitational loading particulate contaminants were redistributed about LDEF and the shuttle bay. Atomic oxygen weakened materials were particularly susceptible to these forces. The ferry flight exposed LDEF to the same forces and again redistributed contaminants throughout the bay.

Once in SAEF-2 there was a steady accumulation of particulate contaminants. These included skin flakes, paper fiber, wear metals, sawdust, and pollen to name a few. Some surfaces had a tenfold increase in their particle loading during their stay in SAEF-2. A few of the cleaner surfaces experienced a hundredfold increase.

INTERVALS IN THE HISTORY OF LDEF WITH DISTINCT CONTAMINATION ENVIRONMENTS

LDEF has been exposed to a variety of discrete environments over its lifetime. The prelaunch environment was a time when the new surface of trays, clamps, and the superstructure of LDEF were exposed to assembly debris, skin flakes, hair and fiber, insects, minerals, etc. The remnants or modified forms of these materials show the effects of exposure to all subsequent LDEF environments. The launch phase exposed LDEF to materials characteristic of the Shuttle Bay. These included bay liner materials, tile fiber and debris, and a variety of other contaminants common in the Shuttle bay but not unique to the bay. The launch environment is characterized by decompression, vibration, and a general acceleration force of about three times normal gravitation. These effects promote the migration of larger particles in the bay toward vents and toward surfaces that are normal to and face the acceleration vector. Once in orbit the environment is dominated by the orientation of the satellite with respect to the ram vector and atomic oxygen, to the thermal and ultraviolet light exposure, and to micrometeorite and debris impacts. Position four below marks the effects of grappling and docking operations. The first significant, although very low, acceleration loading after nearly six years in orbit occurred when the grapple arm attached to LDEF. Numerous objects, from as large as solar cell panel samples to small flakes of aluminum foil, began drifting from LDEF. Some relocation of materials from one LDEF surface to another probably occurred at this time. Reentry and landing exposed the orbitally degraded surfaces of LDEF to turbulent repressurization, acceleration and vibration loading, and to the reactive atmospheric gases, including water vapor. It also provided an environment in which cross contamination with the Shuttle Bay could occur. On the ground the Shuttle was exposed to natural minerals and other common airborne materials. The ferry flights exposed LDEF to decompression, repressurization, thermal cycling, and high humidity. Intervening stops during the ferry flight exposed LDEF to other contaminants. Once at Kennedy the ground operations prior to SAEF-2 exposed LDEF to a variety of particulate contaminants that were free of the effects of orbital exposure. Organic fibers, pollen grains, and insect debris were among the most obvious new contaminants. In SAEF-2 exposure to these types of materials continued with abraded floor materials, more pollens, skin flakes, and disassembly debris being added. The subject of this presentation is an overview of the changes in the contaminant distribution and character from grappling (4) to the final handling in SAEF-2 (10).



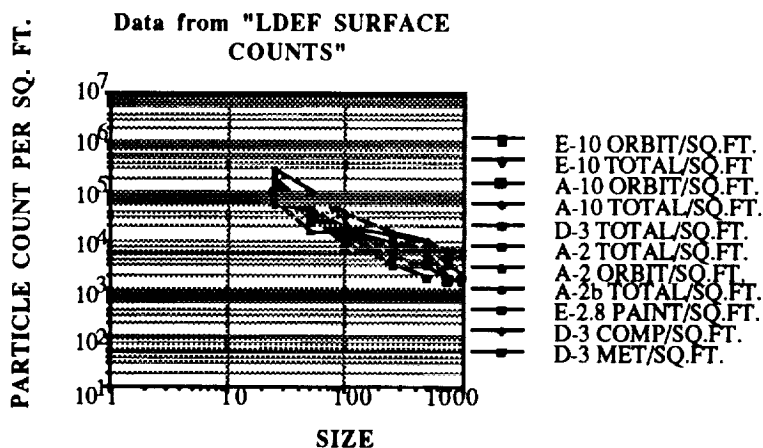
1. Condition of LDEF prior to launch: >MIL-STD-1246B, level 1000C for many trays.
2. During launch particulate contaminants are redistributed and Shuttle Bay debris is added.
3. Contaminants are modified and new contaminants are generated in the orbital environment.
4. Grappling jars particles and films free; some may have relocated on LDEF.
5. During reentry particles and brittle molecular contaminant films relocate.
6. The shuttle is exposed to the Edwards environment, accumulation of natural dusts.
7. High humidity, high gas flow velocities, thermal and pressure stresses occur.
8. HEPA filter fibers appear on tapelifts after exposure to new filters.
9. Ground operations prior to SAEF-2 include many manipulations to LDEF in complex environments.
10. SAEF-2 exposure.

Contamination Exposure History of LDEF

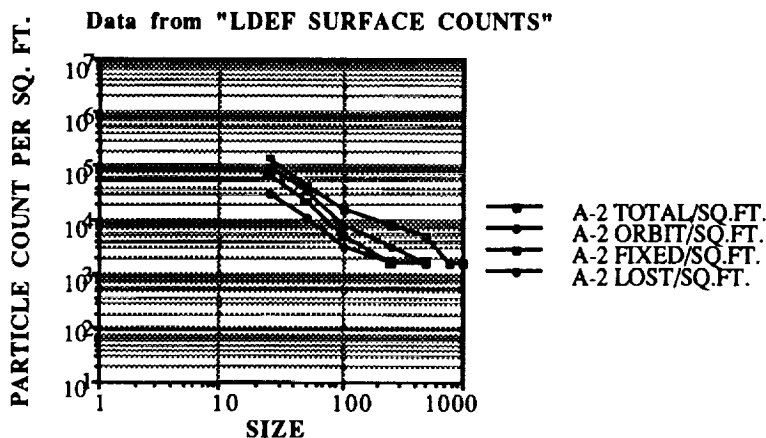
INCREASE IN SURFACE CONTAMINATION FROM ORBIT TO FINAL PACKAGING IN SAEF-2

On trays A-2, A-10, and E-10 particle counts were made on selected areas to determine the cleanliness of the surface in orbit, the migration of particles present in orbit during recovery operations, and the cleanliness as received from SAEF-2. The surfaces counted for each of these trays were silver backed Teflon. The particles present in orbit could be identified by the silhouette of the particle on the surface, indicating that the surface had been protected during its orbital exposure. For the leading edge trays exposed to a high fluence of atomic oxygen (A-10 and E-10) the silhouette was a small area of surface not eroded to the same extent as immediately adjoining areas. For tray A-2 the silhouette was the area protected from the brown returning molecular contaminants. All of the particles present during orbit were indicated by the term "Orbit". Some of the particles present in orbit were still present when the sample was analyzed. These were particles that had a silhouette of themselves on the surface beneath them. Such particles were indicated as "Fixed" particles. The count of particles actually present on the surface as received from SAEF-2 was indicated by the term "Total". The total count after SAEF-2 was from about two to four times the number of particles present on the surface during orbit.

The upper graph illustrates that the analyses of the particle population from Teflon surfaces, composite surfaces (D-3 COMP), metal surfaces (D-3 MET), and painted surfaces (E-2.8 PAINT) all seem to be within the same order of magnitude.



Particle Counts From LDEF Surfaces, Total Counts of all Particles and Counts Of Those Particles Present During Orbit.



Tray A-2 Detailed Particle Count of Total Particles, Those Present During Orbit, Those Fixed During Orbit and Still Present, and Those Present During Orbit Now Missing.

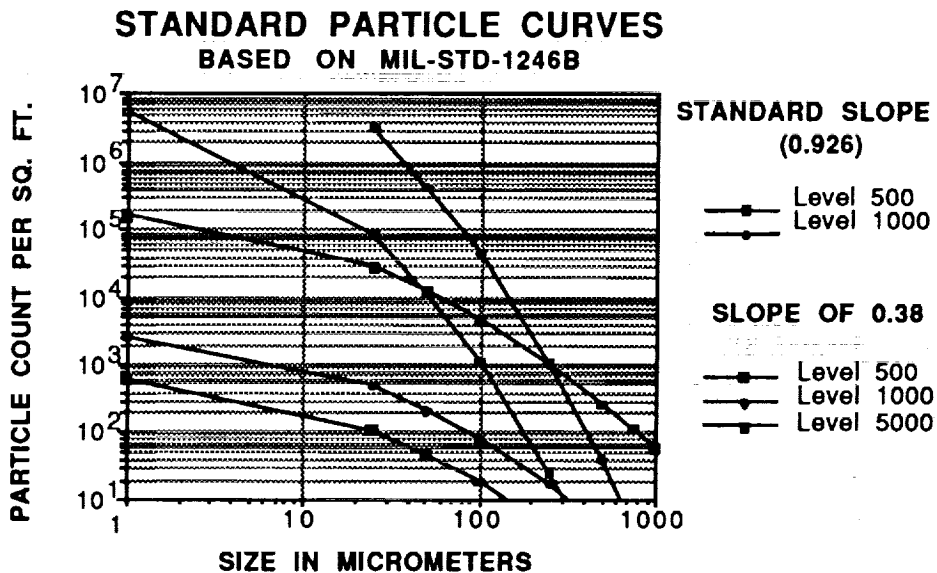
MIL-STD-1246B PARTICLE DISTRIBUTION CURVES AND LOG/LOG SQUARED CURVES WITH A DIFFERENT SLOPE

MIL-STD-1246B establishes cleanliness levels based on a particle size distribution assumed to be linear when the log of the cumulative number of particles greater than a specified diameter is plotted by the square of the log of the diameter. The standard further establishes the slope of the resultant line to be 0.926.

The log/log squared particle distribution with a slope of 0.926 was based on empirical data generated by measuring the removal efficiency by size for a standard material whose mass increased by the cube of the diameter. This is not the general case. The mass of a fiber varies linearly with its longest diameter. Pollens and spores decrease in density with increasing diameter. Skin cells have a mass that increases by the square of their diameter.

Pollens and fibers are not randomly sized but have specific dimensions characteristic of their origin. The 0.926 slope has a built in assumption that the particle population is the same for each size particle. The sedimentation rate for large particles is much greater than that for small particles; so even though there are more small particles, the large particle population becomes disproportionately represented on surfaces collecting particle fallout. As a result, though the log/log squared distribution still seems reasonable, the actual distribution seen on surfaces is often better characterized using an alternative slope. For many of the surfaces on LDEF slopes as low as 0.38 are indicated.

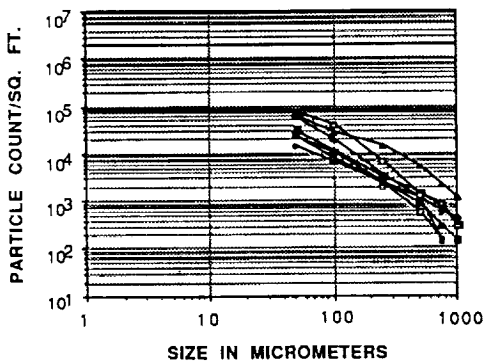
When identifying a cleanliness class using MIL-STD-1246B some arbitrary sized particle must be selected to establish the level if the particle distribution curve does not have a slope of 0.926. A particle distribution with a slope of 0.38 and one particle per square foot greater than 5000 micrometers could be assigned a cleanliness level of 1000 for particles less than 250 micrometers or a level 500 based on particles smaller than 50 micrometers.



PARTICLE DISTRIBUTION CURVES AND LDEF ASSOCIATED PARTICLE COUNTS

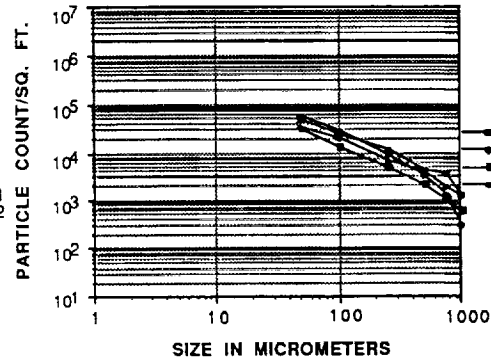
These charts are based on the results of tapelift samples from the Shuttle Bay and the Transportation Canister collected when LDEF was located within each respective container. The particle count distribution by size curves for the Shuttle Bay and for the Transportation Canister are much more shallow than the 0.926 slope used for the MIL-STD-1246 curves. The Shuttle Bay samples collected in the OPF are very close to a slope of 0.38. All of the particle count data for LDEF is shown in graphical form. The graphical format is used because the particle distribution is not conducive to the assigning of a MIL-STD-1246B cleanliness level. The significance of a list of numbers is also less informative than seeing the shape of the distribution. Unusual distributions such as that in the pre-transportation Transportation Canister sample are easily seen in a graphical format.

SHUTTLE BAY, EDWARDS



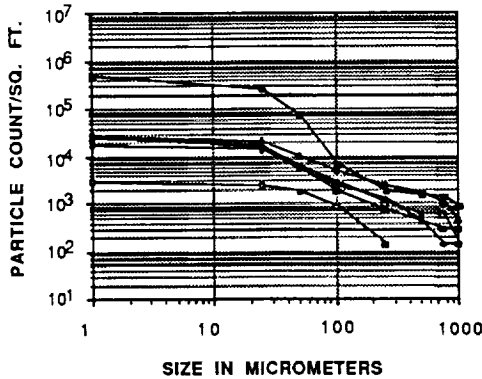
- Rt PreOp
- Lt PreOp
- Rt PostOp
- Lt PostOp
- Purge Duct
- Rt PreFerry1
- Rt PreFerry2

SHUTTLE BAY, OPF



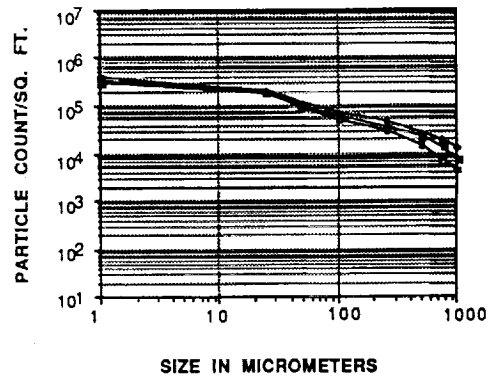
- Rt PostFerry2
- Aft
- Lt PostFerry
- Lt PreFerry

CANNISTER, OPF (Pre-Trans.)



- Slide 1
- Slide 2
- Slide 3
- Slide 4
- Slide 5
- Control

CANNISTER, O&C (Post-Trans)

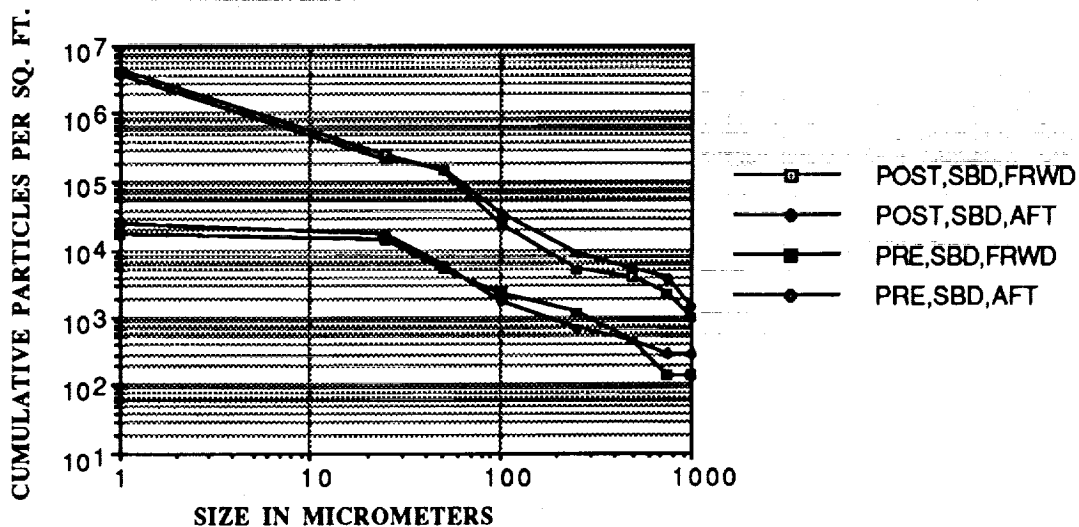


- Slide 6
- Slide 7
- Slide 8

DISTRIBUTION OF PARTICLES IN THE TRANSPORTATION CANISTER BEFORE AND AFTER TRANSPORTING LDEF

The Transportation Canister was relatively clean prior to transporting LDEF from the OPF to the O&C building based on tapelift samples collected from the floor of the Canister. Most of the particles were small metal fragments. Many of these were in a line as a result of scratches on the surface of the Canister floor. Some of these fragments were bound together with an organic binder. Skin particles, paper fiber, clean room wiper residue, starch grains, sand grains, and vinyl flooring residue were also present. After transporting LDEF the particle count increased by nearly an order of magnitude or more. The second set of lifts were collected from approximately the same location as the first set. LDEF debris was a major reason for the increase in the number of particles but other sources also made a significant contribution. The LDEF debris was identifiable as very thin metal foils, Kapton particles, and fine ash particles. These materials accounted for over half of the increase. The balance was spray paint residues, paper fibers, calcite, starch, soil particles, pine pollen, and rust. The size distribution of the LDEF debris ranged from submicrometer to millimeters in greatest dimension. The non-LDEF debris was predominantly between five and one hundred micrometers with some of the fibers exceeding the millimeter range in length. The proportion of LDEF debris to other contaminants was smaller than had been expected. This may have been due to much of the more easily removed LDEF debris having been already removed by the earlier activities or having been moved to locations on LDEF where they were stable with LDEF in the fixed, row 12 top, configuration. The accumulation of more contaminants on the Canister floor not directly attributable to LDEF suggests that the upward facing surfaces of LDEF would receive contaminants from the Canister cover. These contaminants would include paper fibers, pollens, etc. The two plots of the particle size distribution before transporting LDEF are very close to one another, as are the two plots for the samples collected after transportation. This would seem to indicate that this was not a localized effect but was representative of what occurred during transport.

**TAPELIFT COUNTS FROM THE TRANSPORTATION
CANISTER BEFORE AND AFTER TRANSPORT OF LDEF**

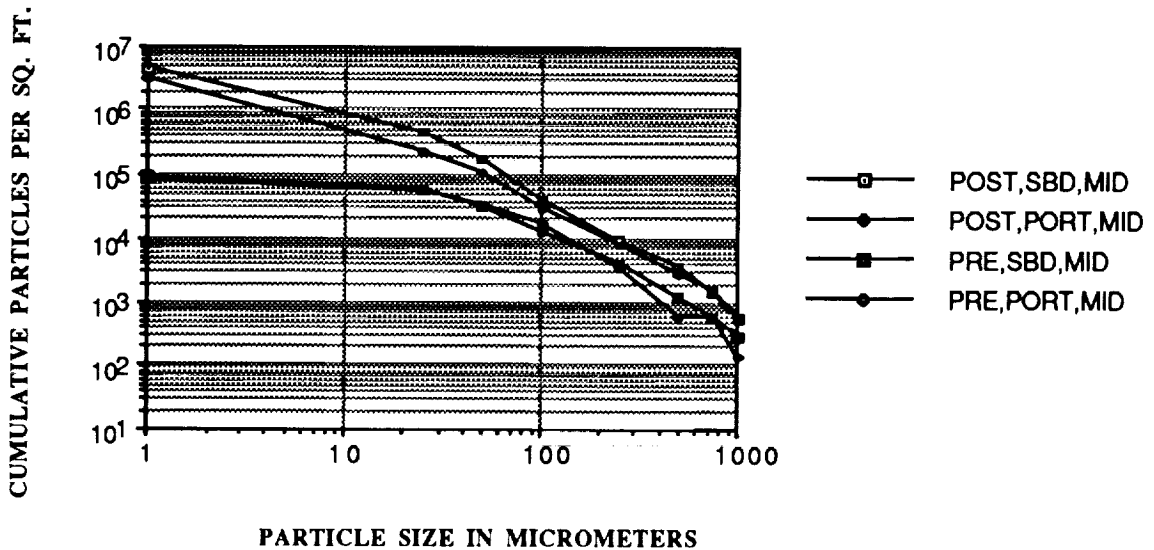


DISTRIBUTION OF PARTICLES IN THE LATS BEFORE AND AFTER TRANSPORTING LDEF

The LATS was not nearly as clean as the Transportation Canister before the transport of LDEF. Tapelift samples collected from the port and starboard sides of the LATS floor near the middle of LATS had particle counts that were a factor of ten greater than was found on the pre-transport Transportation Canister for particles smaller than one hundred micrometers.

After transport of LDEF the particle size distribution curves for the LATS samples were nearly the same as the post-transport samples from the floor of the Transportation Canister. The contribution from LDEF however was much less. Less than a third of the increase was due to LDEF particles. Cleaning residues, spray paint residues, pollens, insect parts, paper and clothing fiber, and black foam particles were more common. The LATS activities probably contributed more new contaminants to LDEF than did the Transportation Canister.

TAPELIFT COUNTS FROM THE LATS BEFORE AND AFTER TRANSPORTATION OF LDEF TO SAEF-2

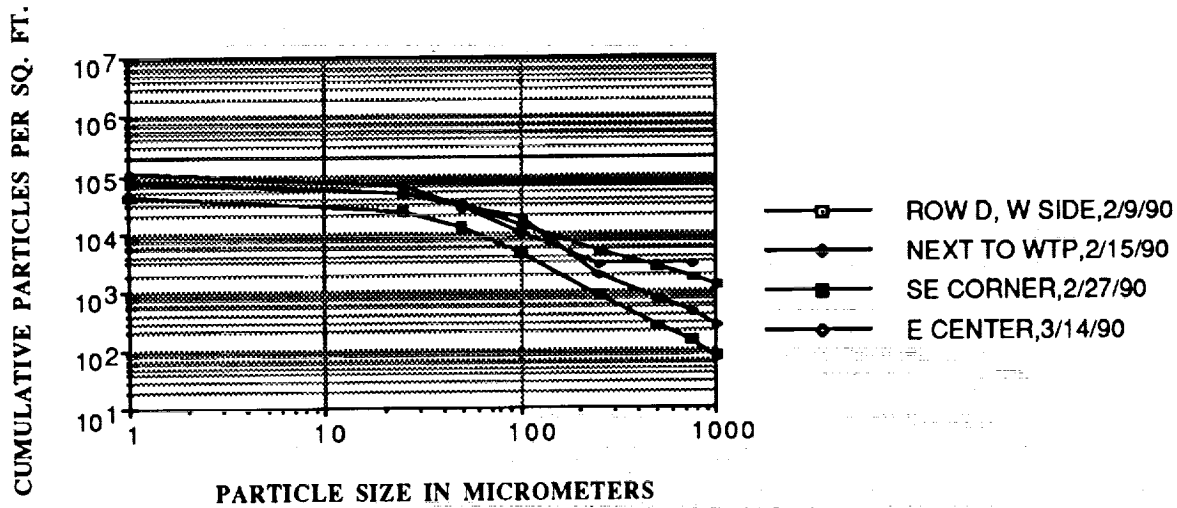


SURFACE CLEANLINESS OF LATS BASED ON PARTICLE FALLOUT PAD AND TAPELIFT ANALYSIS IN SAEF-2

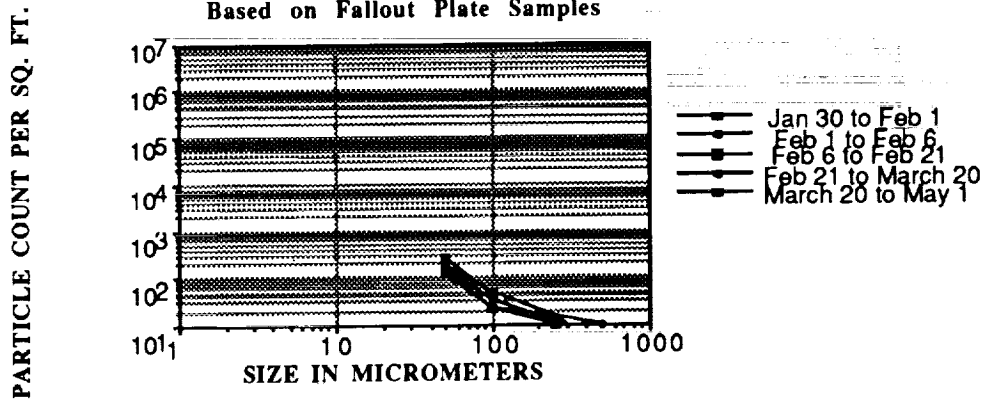
The floor of the LATS was cleaned regularly (daily) to reduce the opportunity for the mechanical transport or lofting of debris to LDEF. The tapelift samples were collected at midday on the days noted. The surfaces sampled were areas of low traffic. The sample collected on the fifteenth of February was taken adjacent to one of the fallout pads. These samples indicate a relatively low cleaning efficiency and a rapid sedimentation rate.

The fallout pad data should be lower than the tapelift results in that the fallout pad collects only fallout and not mechanically transferred debris, but the difference in these two plots indicates that the fallout pad data grossly underestimates LDEF's exposure. Considering only the one hundred micrometer particles the fallout pad results summed for the entire exposure interval of the open trays, Jan. 30 to Feb. 21, would amount to less than a thousand (MIL-STD-1246B, Level 500).

SUMMARY OF LATS PARTICULATE CLEANLINESS BASED ON TAPELIFT SAMPLES



LATS AVERAGE PARTICLE FALLOUT PER 24 HR. Based on Fallout Plate Samples

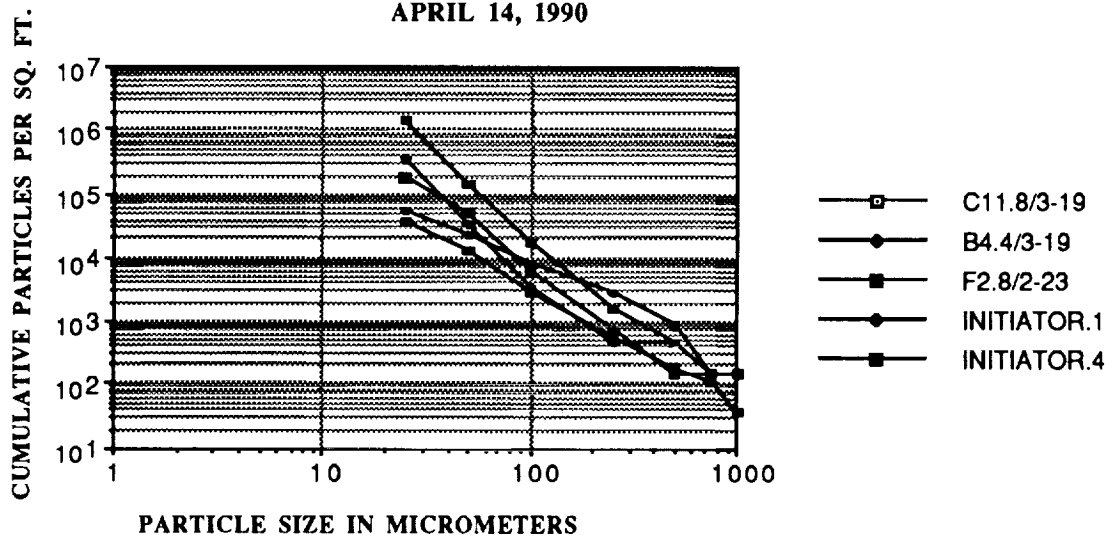


TAPELIFT RESULTS FOR LDEF SURFACES UNDER TRAY CLAMPS AND FROM THE INTERIOR OF LDEF

Tapelifts were collected from the surface of LDEF that had been covered with tray clamps prior to the removal of the trays. The legend indicates the tray clamp under which the sample was collected and the date on which that clamp had been removed (for example, the first entry below indicates the sample was collected from under the eighth tray clamp of tray C-11. This clamp had been removed with the tray on the 19th of March and the surface had been exposed to the SAEF-2 environment until the sample was collected on the 14th of April). It had been anticipated that the particle distribution would reflect the duration of SAEF-2 exposure. This was not the case. Although high particle counts were seen the type of particle was biased toward manufacturing and assembly residues and not so much toward the typical SAEF-2 debris. The particle population under clamp 8 of tray F-02 was about the same as that under clamp 4 of tray B-04 even though the F-02 area had been exposed in SAEF-2 for nearly three weeks longer. All of the samples from under the tray clamps were more contaminated than the tray surfaces or the other exposed surfaces of LDEF. This suggests that the tray clamps retained contaminants that were removed from other surfaces following integration. Surfaces not protected by tray clamps (INITIATOR samples and those shown in the lower chart) are nearly an order of magnitude cleaner. The contaminants on these other surfaces are also different indicating populations of the type seen on the tray surfaces.

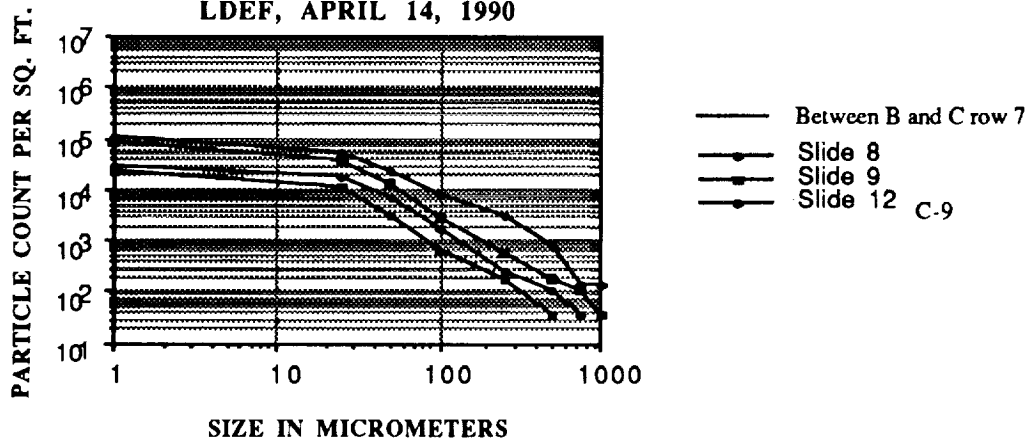
TAPELIFT DATA FROM LDEF SURFACE COLLECTED

APRIL 14, 1990



PARTICLE SIZE IN MICROMETERS

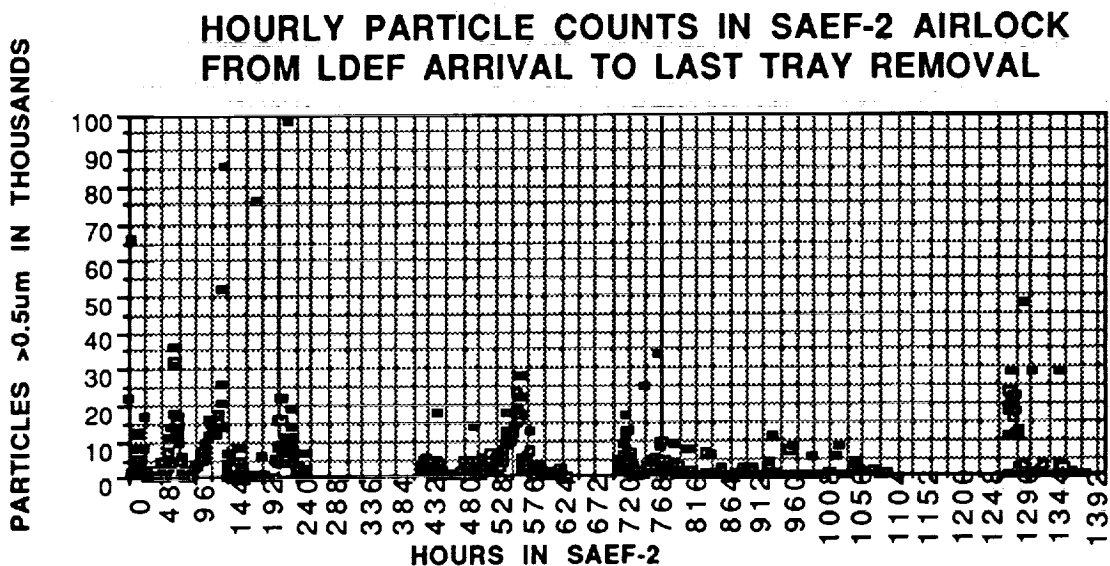
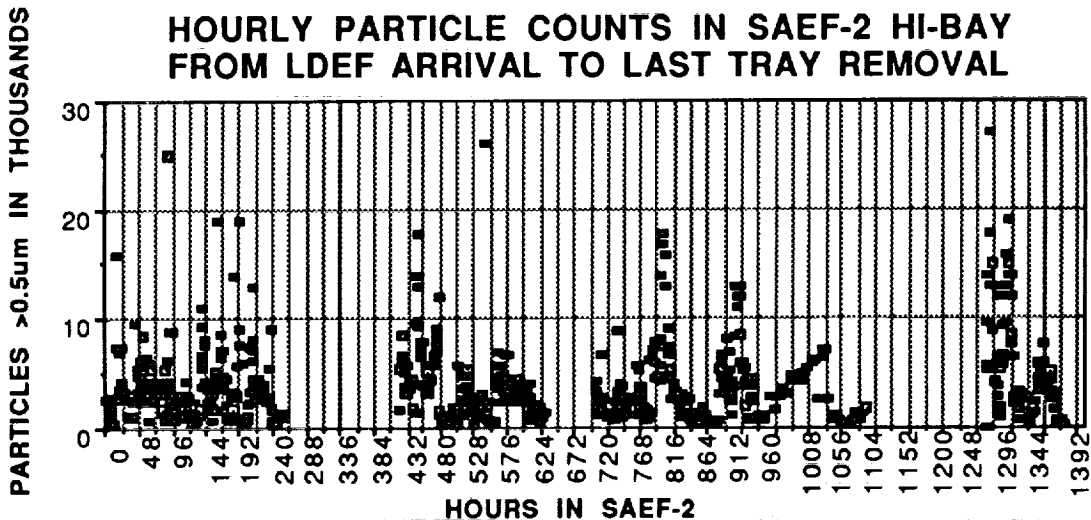
LDEF, APRIL 14, 1990



SIZE IN MICROMETERS

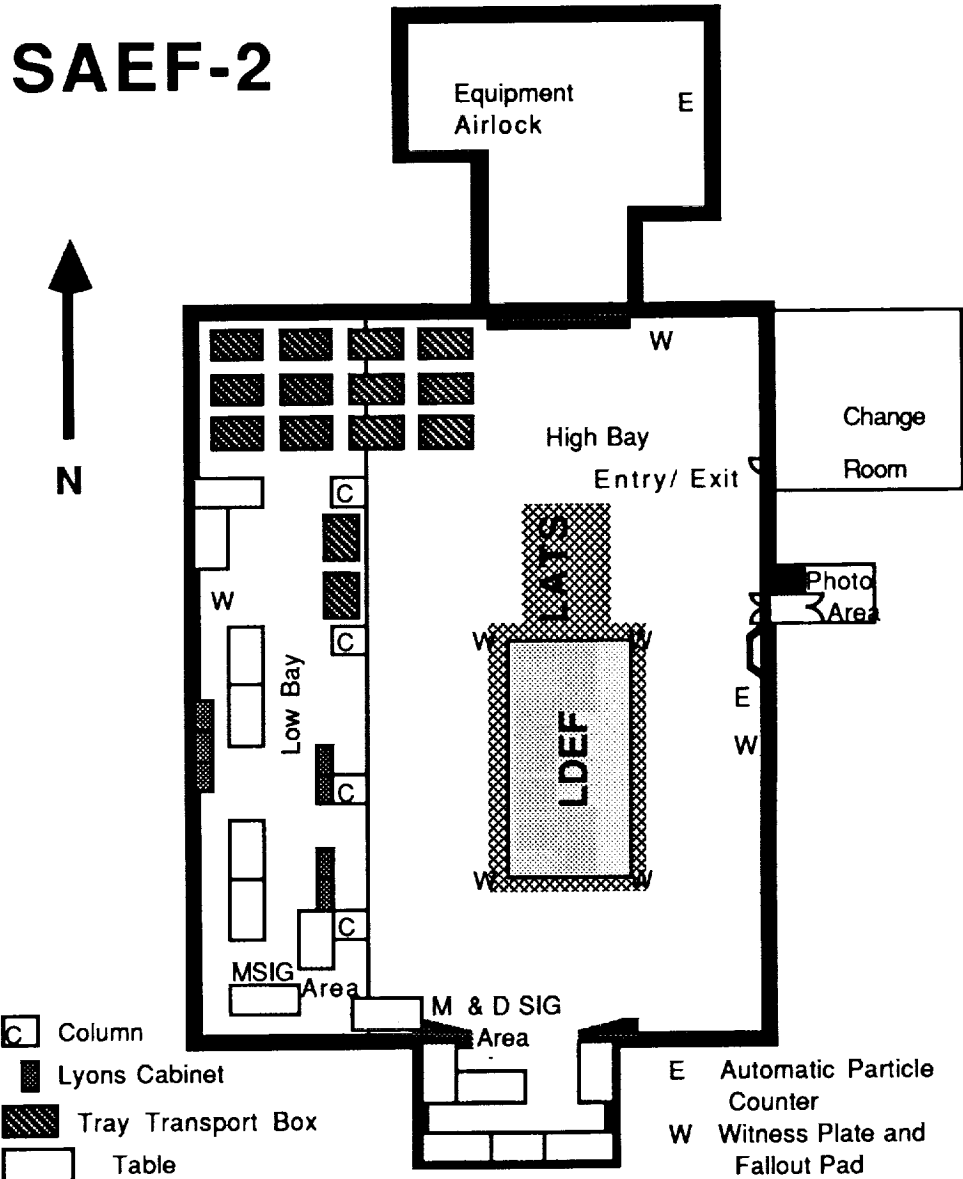
AIRBORNE PARTICLE COUNTS $>0.5 \mu\text{m}$ FOR THE SAEF-2 CLEANROOM HIGH BAY AND THE EQUIPMENT AIRLOCK

The graphs below show the particle count at each hour mark recorded during LDEF's exposure to the SAEF-2 environment. The hourly counts in the High Bay cleanroom never exceeded thirty thousand. Individual counts on one occasion exceeded one hundred thousand but that was a transient condition associated with the moving of a scaffold that was above and adjacent to the particle counter. This event lasted only a few minutes and the airborne particle count dropped back well below one hundred thousand before the next hour mark. The scaffolding was moved periodically but it was normally closer to LDEF and didn't significantly disturb the particle counter. In the Airlock the particle counts were typically higher. When materials were entering the Airlock from outside the count would exceed one hundred thousand. The particle count would recover generally within an hour. The airborne particle counts indicated that the air being supplied to SAEF-2 was being effectively scrubbed by the HEPA's. In a conventional non-laminar flow cleanroom with a single sensor mounted ten feet high on the wall relatively little information is gathered with regard to the larger particle population (five micrometers and greater).



SAEF-2 FLOOR PLAN WITH LDEF ON LATS

The locations of the wall mounted airborne particle monitors and the floor or LATS bed fallout pads are shown in this illustration.

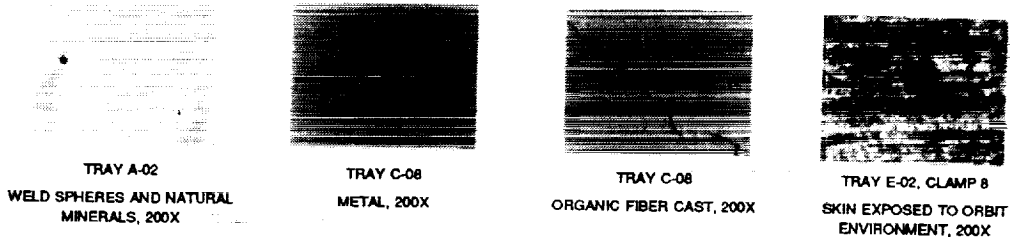


PARTICLES THAT INDICATE DEBRIS FROM TRAY ASSEMBLY AND PARTICLES THAT ARE TRACEABLE TO SPECIFIC SOURCES

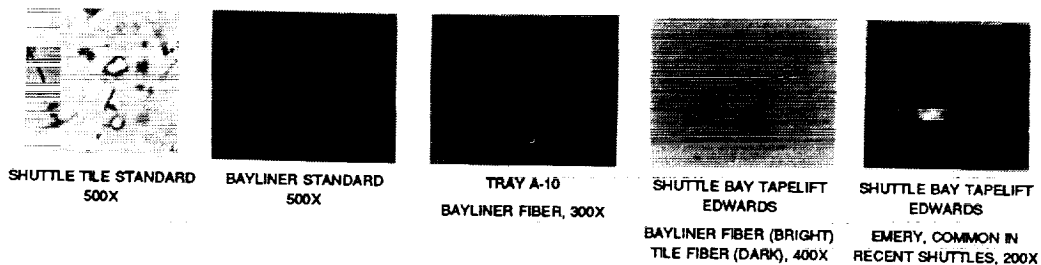
Particles that accumulated during assembly up through launch and that were present in orbit can be distinguished from more recent particles by shadow effects on the underlying surface associated with the particles. On the trailing side tray A-02 the weld sphere and the mineral particle are associated with a shadow in the deposited molecular film indicating their presence early in the mission. The wear metal particle seen on tray C-08 protected part of the surface it covered from atomic oxygen exposure during the mission. Organic particles present early in the mission also provided protection for the underlying surface but only so long as they survived the attack of atomic oxygen. When they were finally consumed the underlying surface was protected only by what ash remained. The temporary protection provided by these particles resulted in a silhouette of the particle on the surface detected as a less eroded area. Where shadow effects were not easily seen the particle itself could indicate its long term orbital exposure, such as the example of the skin cell on clamp 8 of tray E-02. These particles are all typical of residues from tray assembly operations.

The Shuttle Bay was also a source of particles. Two materials characteristic of the Shuttle are the glass fibers from the Shuttle thermal protection tiles and the Teflon coated glass particles from the liner of the Shuttle Bay. When some of the glass fibers collected in the Shuttle and on LDEF were compared to standard samples from these sources they were found to be the same.

ASSEMBLY DEBRIS TRACER PARTICLES

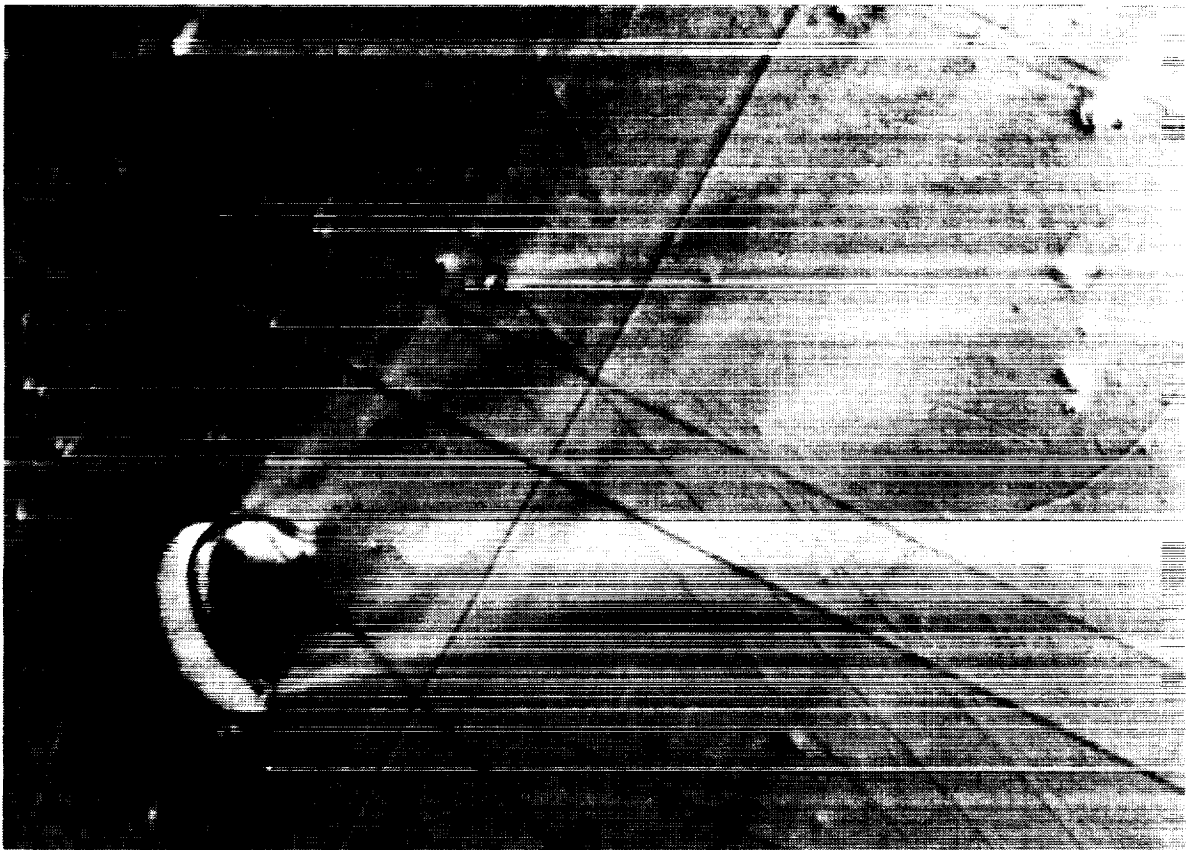


SHUTTLE BAY TRACER PARTICLES



FEATURES INDICATING A PARTICLES PRESENCE DURING ORBIT

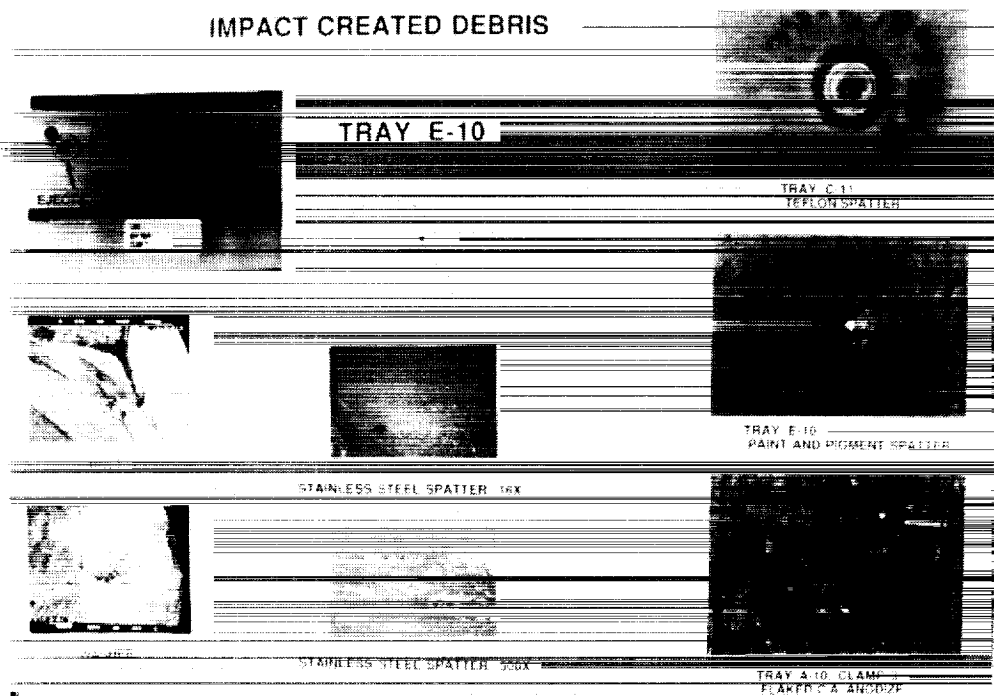
This photograph shows an area of the surface on tray A-04. Particles present during orbit have a shadow (bright area) associated with them. Particles removed after the formation of the shadow leave only the shadow to indicate their past presence (small bright spot near center of photo). The halo around each particle is believed to be the result of outgassing materials held by capillary attraction at the interface between the particle and the tray surface. The "plume" pattern is believed to be the effect of the molecular flow over the surface.



ORIGINAL PAGE
BLACK AND WHITE PHOTOGRAPH

PARTICLES GENERATED IN ORBIT

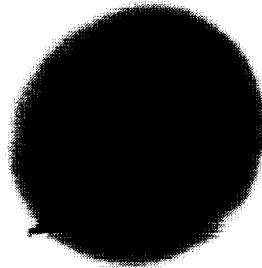
Micrometeorites or space debris impacts on the surface of LDEF created particles that could deposit on LDEF. The photographs on the left of this foil characterize one such event when a micrometeorite impacted with the side of a stainless steel bolt on tray E-10. Examples of other materials releasing particles as a result of impacts are given for Teflon on tray C-11, paint on tray E-10, and chromic acid anodize on tray A-10.



PARTICLES DEPOSITED AS LIQUID DROPLETS

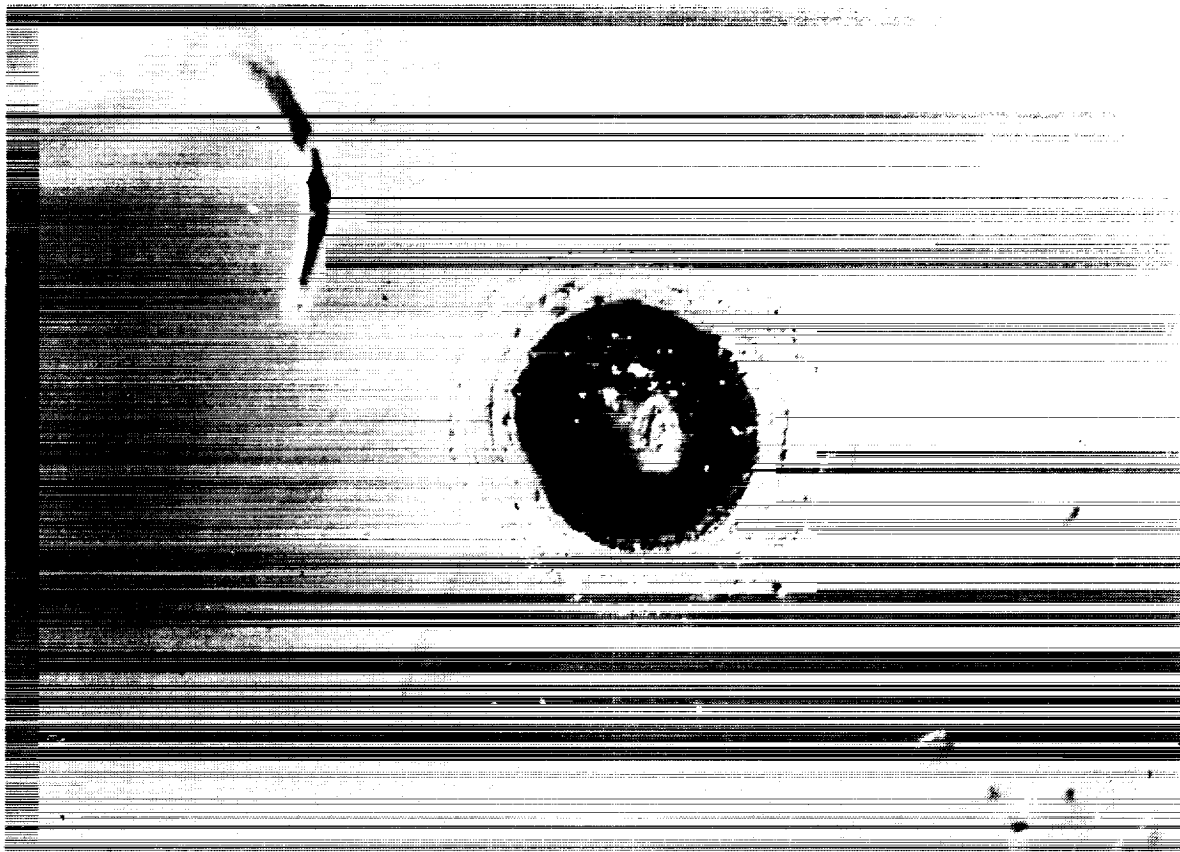
A number of brown spots were found distributed widely over the surface of LDEF. These spots were circular or globular in shape indicating the effects of surface tension on their formation. Within these deposits particles were generally distributed concentrically about the center of the droplet. This is all consistent with the deposition of liquid aerosols on the surface. There are many sources for liquid aerosols during assembly, during orbit, and following recovery.

This photograph illustrates one of at least four types of brown spots seen on LDEF. This type is characterized by a high residual material content and significant organic content. It was collected from under tray clamp number four of tray B-08 and had been deposited on the frame of LDEF prior to the integration of the experiment trays.



PARTICLES DEPOSITED AS LIQUID DROPLETS

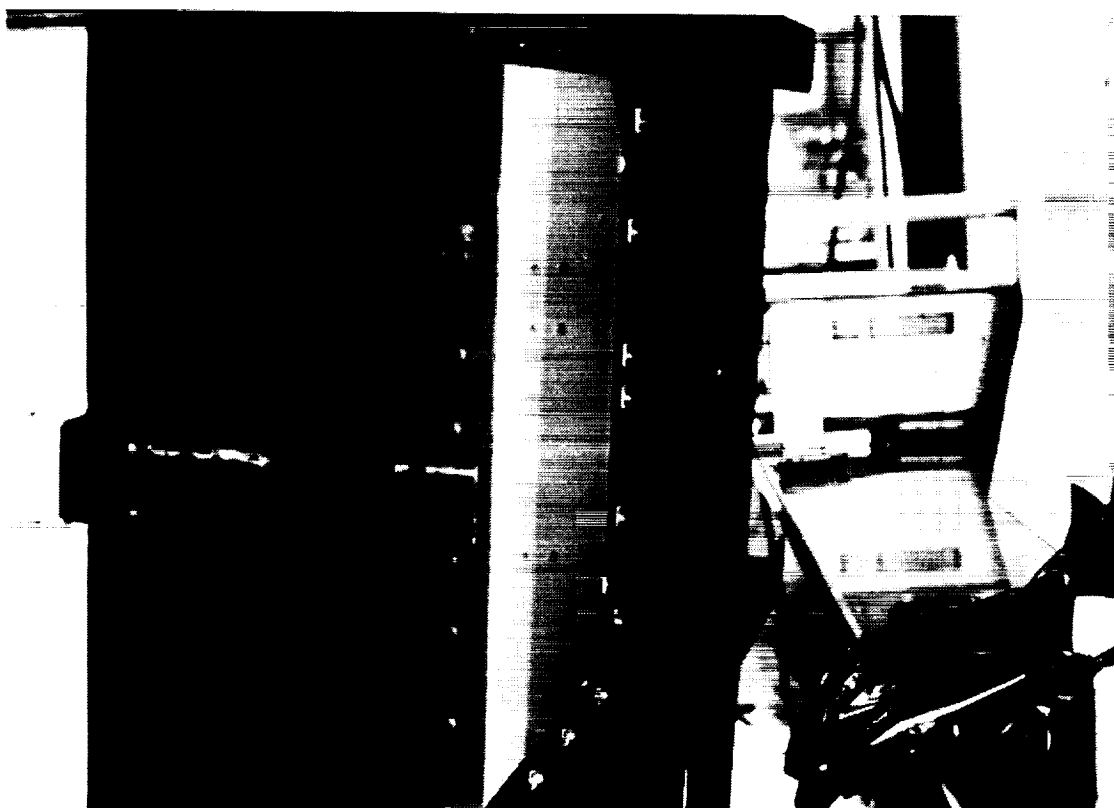
This type of brown spot is characterized by concentric rings of particles outside of the central deposit. Skin cells are common in this droplet. This is typical of "sneeze" type residues deposited before orbital exposure. This droplet was photographed in SAEF-2 and was found on the surface of experiment A0187-2, tray C-03.



ORIGINAL PAGE
BLACK AND WHITE PHOTOGRAPH

MOLECULAR FILM DEPOSITED ON INTERIOR SIDE OF TRAY F-06

Molecular films were visually detected either by the brown discoloration seen on light surfaces or the thin film interference colors caused by them on black surfaces. This photograph illustrates the interference color effect* seen on the ram facing side panel of tray F-06. Each red band beginning with the brown-red near the edge just before the first blue band corresponds to a thickness of approximately 100 nanometers (0.1 micrometers) added to the film's thickness. Notice the continuation of the pattern on the next brace.

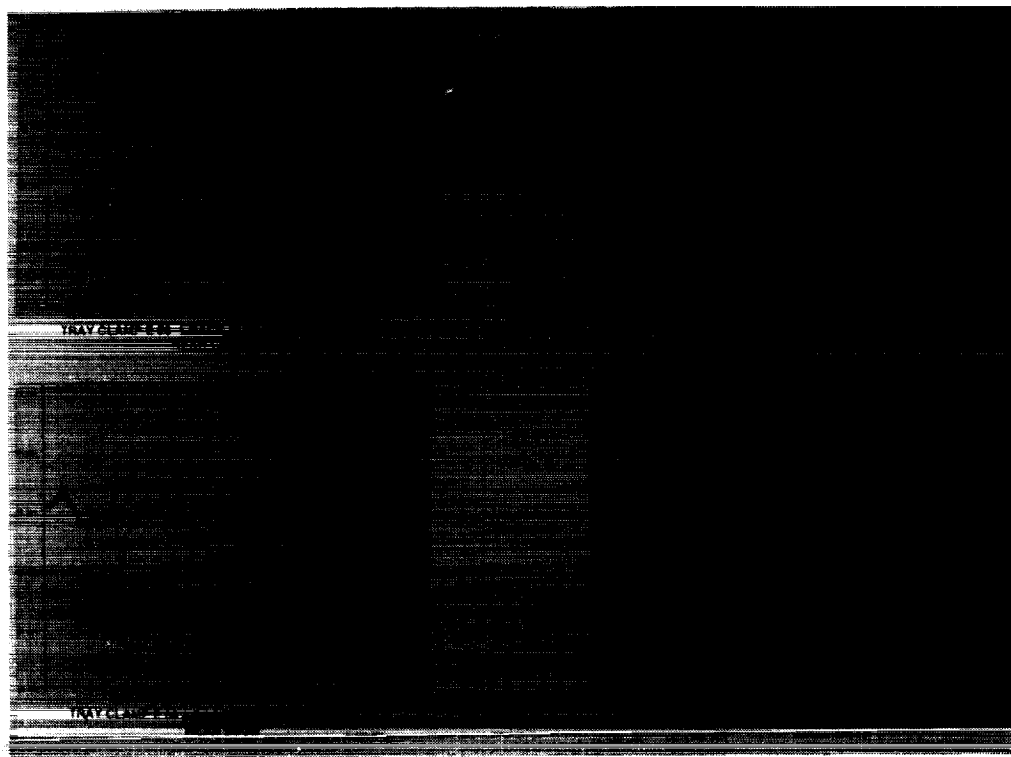


ORIGINAL PAGE
BLACK AND WHITE PHOTOGRAPH

*Shown in black and white only.

TYPICAL INFRARED SPECTRA OF MOLECULAR DEPOSIT

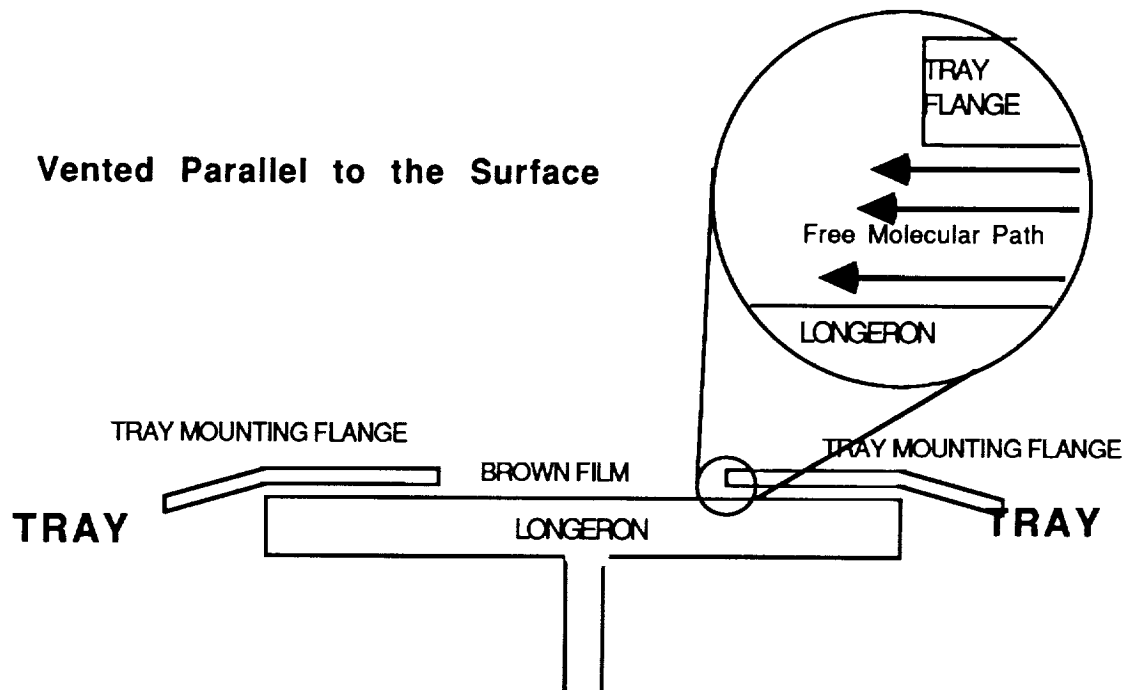
The infrared spectra of the brown film from most locations were remarkably similar. On the right of this foil are the spectra from the earth end frame of LDEF and from the space end frame. The same basic functional groups are indicated in similar proportions. The spectra on the left side are an example of the organic materials detected as residues between the tray clamps and shims on LDEF.



VENT PATH FROM INTERIOR OF LDEF ALONG THE EDGE OF TRAYS

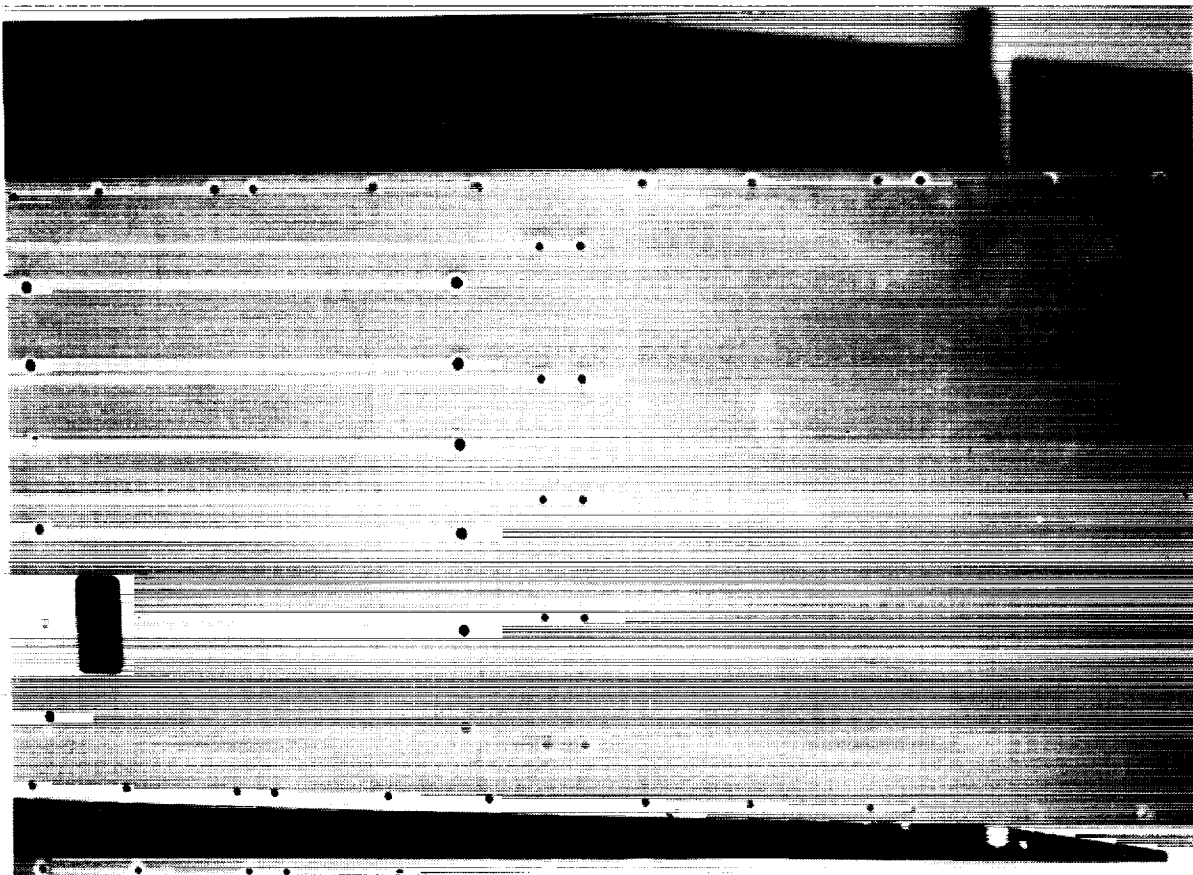
Many of the vent paths on LDEF consisted of narrow openings between parallel plates of metal. The edge of the trays are an example of such a path. Molecules escaping from the interior along such a path would tend to parallel the surface of LDEF. Any encounter with another molecule would have a fifty percent probability of directing the molecule toward the surface of LDEF. This may help explain the relatively high deposition efficiency exhibited by the exterior surface of LDEF.

VCM Vented Parallel to the Surface



HANDPRINT ON TRAY F-06

On the tan stained surface of the floor of tray F-06 a lighter colored pattern could be seen. This pattern is a palm print. The trays were handled without gloves and while working with this tray it began to tip. One of the individuals handling the tray put up his hand to stop the tray. The cleanliness requirements for LDEF didn't require a control of surface organics or particles that were not obvious to the unaided eye so no attempt at wiping the tray clean was made. This pattern is of interest for two reasons. First, it illustrates the conditions under which LDEF was assembled. Second, it creates questions regarding the mechanism that turned the tray floor tan where it was "cleaner" but not where it had been contacted by a bare hand. In some other areas fingerprints were seen that had turned black from exposure to ultraviolet light.



ORIGINAL PAGE
BLACK AND WHITE PHOTOGRAPH

**Z306 MOLECULAR CONTAMINATION
AD HOC COMMITTEE RESULTS**

Johnny L. Golden

**Boeing Defense & Space Group
Seattle, WA 98124-2499**

Phone: 206/773-2055, FAX: 206/773-4946

LDEF external surfaces which did not receive significant amounts of atomic oxygen were observed to be coated with a brown contamination, apparently the result of a condensed organic residue darkened due to UV radiation exposure. During the initial Materials Special Investigation Group (MSIG) Meeting after LDEF deintegration, held in Seattle - July 1990, this organic contamination was the subject of much discussion. The amount of contamination was thought to be significant and its source was immediately believed to be the Z306 black thermal control coating used to coat the entire inner surface of LDEF. Due to the size of the structure, it was not feasible to bake-out the coating. However, initial data on the contamination film was confusing in that significant amounts of silicon was observed by several different researchers. Silicon (from silicone) was not expected to be a potential outgassing product of the Z306 polyurethane coating. To investigate the connection between external contamination and the interior paint, a MSIG ad hoc committee was formed.

Committee Members

**PHILIP R. YOUNG, NASA Langley Research Center
WAYNE K. STUCKEY, The Aerospace Corporation
DAVID E. BRINZA, Jet Propulsion Laboratory
KENNETH W. ROUSSLANG, University of Puget Sound
JOHNNY L. GOLDEN, Boeing Defense & Space Group**

The ad hoc committee's objective was to develop a plan of attack for analysis of the interior paint, which would in turn determine the extent of external contamination induced by its presence. The approach developed to meet the committee objective was defined as the following four tasks. First, we needed as much historical background as possible into the coating used on LDEF and how it was applied. Any test specimens of LDEF-era paint were also of interest. Second, we needed a thorough examination of the contaminant film. Third, we would characterize the specimens of Z306 paint that we could obtain, particularly concentrating on the outgassed condensables. And fourth, we would attempt to duplicate the characteristics of the LDEF contamination by conducting simulated UV exposure of outgassed condensables from Z306 paint.

OBJECTIVE

To Develop And Implement A Test Plan For The Analysis Of LDEF Interior Thermal Control Paint, Determining Possible Connection With The Brown Deposits Found On External Structures

APPROACH

- TASK 1. OBTAIN HISTORICAL INFORMATION AND TEST SPECIMENS**
- TASK 2. CONTAMINANT CHARACTERIZATION**
- TASK 3. CHARACTERIZATION OF COATINGS AND OUTGASSED CONDENSABLES**
- TASK 4. SIMULATED UV EXPOSURE OF OUTGASSED CONDENSABLES**

Under Task 1, the following information was obtained.

LDEF interior surfaces were painted by a number of different people at different sites. This compounds the difficulty with treating all aspects of the Z306 application issue with certainty.

The standard finish used was a single coat of 9924 wash primer followed by one to four coats of Z306. As an illustration of the different groups involved with painting, MIL-P-23377 epoxy primer has been observed as having been used on some of the experiment trays.

In all cases, those involved with the painting of LDEF structures have indicated that the application of Z306 was conducted strictly in accordance with the vendor specification. This is pertinent information, since there had been some unsubstantiated reports of silicone oil being added to the Z306 to aid in its application. Polyurethanes are extremely sensitive to silicones and their presence will result in coating flaws such as "fisheyes". No documentation concerning the use silicones in Z306 has been obtained.

**TASK 1. OBTAIN HISTORICAL INFORMATION
AND TEST SPECIMENS**

- Structures Painted By LaRC, By Subcontractors, And By Experimenters (Trays)
- Chemglaze 9924 Primer (0.0005 inch), Followed By Z306 Topcoat (0.0015 to 0.0050 inch)
Note: MIL-P-23377 Epoxy Primer Used On Some Trays
- Coatings Applied Per Vendor Specification

Several test specimens were obtained by the ad hoc committee. Flight specimens were obtained from the backs of experiment trays. The difficult specimens to obtain were the specimens which could be used as controls, since the present investigation was not a planned experiment (generally the case with all MSIG investigations). Remarkably, a 6" x 6" witness coupon of Z306 was obtained from the structure painting process. In addition, 1" disks of Z306 that were sprayed at about the same time as LDEF were obtained from NASA LaRC. A section of A0178 thermal control blanket was obtained (these blankets were coated with Z306 on the back). The final control specimens were unsprayed samples of currently available Z306 and 9924 coatings.

**TASK 1. OBTAIN HISTORICAL INFORMATION
AND TEST SPECIMENS (Continued)**

- **Flight Specimens**
 - **Samples From Back Of Trays**
- **Controls**
 - **1 - 6"x6" Panel Of LDEF Coating (Carol Kiser)**
 - **1" Disks With LDEF Era Coating (Wayne Slomp)**
 - **8"x12" Section Of A0178 Thermal Blanket, Flight Control (Dublin Inst., ESA-ESTEC)**
 - **Current Vintage Z306 & 9924 Coatings**

Chemical characterization of the contamination deposit was initially made using IR spectroscopy. The spectra are shown in figures 1-6, and were taken from opposing surfaces on LDEF. With the exception of the spectra taken for the deposit on tray C12, all the IR spectra are remarkably consistent. The spectra indicate O-H, N-H, and C-H stretching absorption bands, as well as carbonyl and silicate type bonds. All of the spectra exhibit 'broadening', indicating that the chemical bonds or groups identified are in varied chemical environments.

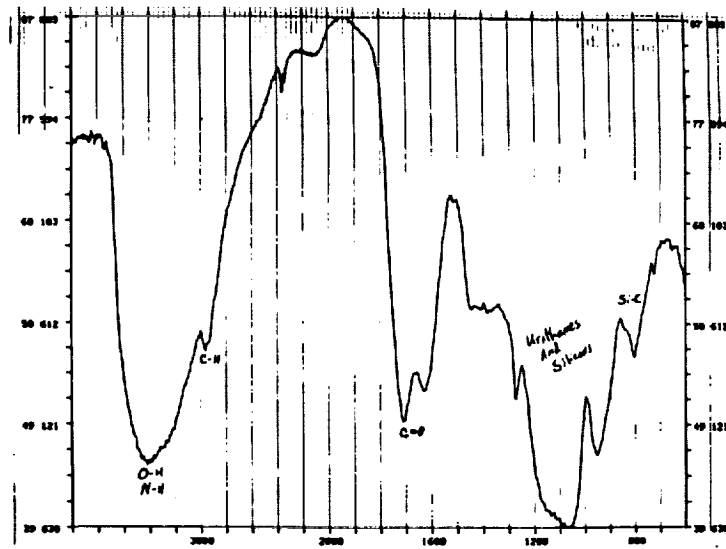
Elemental analysis of the contaminant was made with the use of EDX, shown in figures 7 & 8. Previously reported results of the contaminant at tray C12 have shown that particular deposit to contain phosphorus, a consequence of the outgassing of phosphate esters from the C12 experiment. The EDX for space and earth end deposits do not indicate phosphorus, but do indicate silicon. Trace amounts of chloride and sulfur were also observed.

ESCA was also used by NASA LaRC to characterize the contaminant film. Observations indicate that the silicon portion of the contaminant is generally in silicate form (specimens were from the LDEF leading edge) but some measurements did detect silicone.

At the time of the Materials Workshop, it was agreed that more elemental analysis was needed. Since the Workshop, data obtained by Aerospace Corp on tray D8 indicates the contaminant to contain 28.4% C, 4.1% H, 25.8% O, 18.9% Si, 0.7% N, and trace levels of Cl, F, and P.

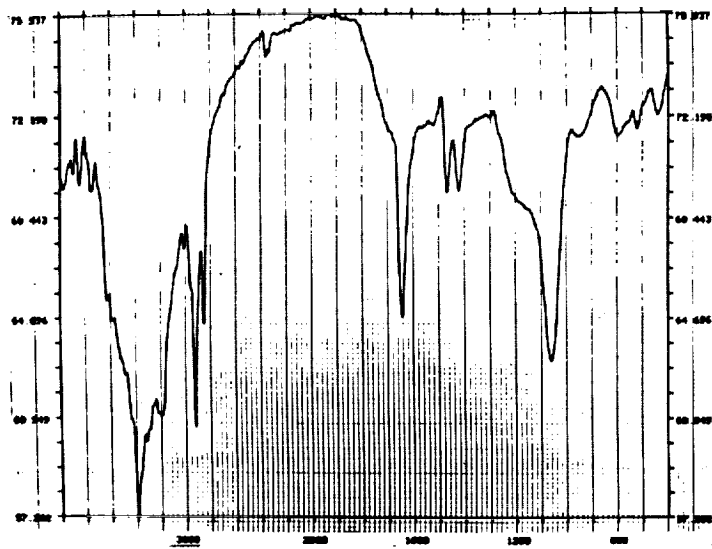
TASK 2. CONTAMINANT CHARACTERIZATION

- **IR Spectroscopy Indicates O-H, N-H, C-H, C=O, And Silicate Bonds In "Broadening" Chemical Environments**
- **Elemental Analysis Indicates Presence of Silicon In General; Phosphorus In Particular Around Tray C12**
- **Silicon Is Generally In Silicate Form, Some Measurements Detect Silicone**
- **Need Better Elemental Analysis**



Space End Brown Film, Longeron 13

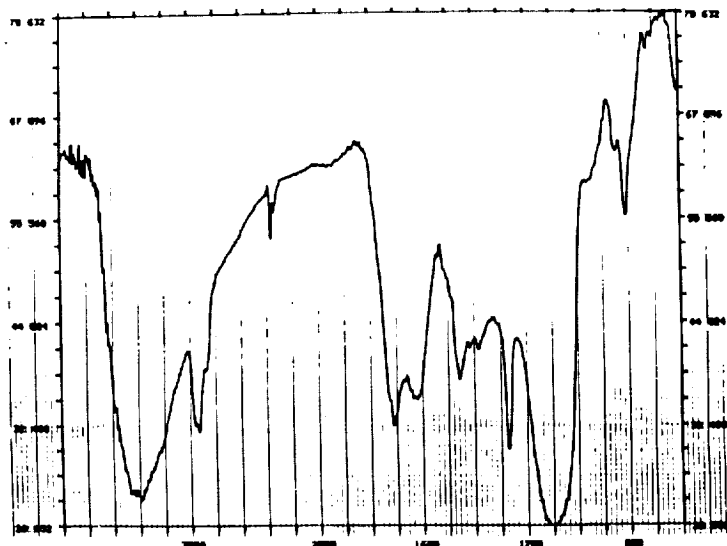
FIGURE 1.



Tray Clamp F12-7: Shim Deposit On Back Surface

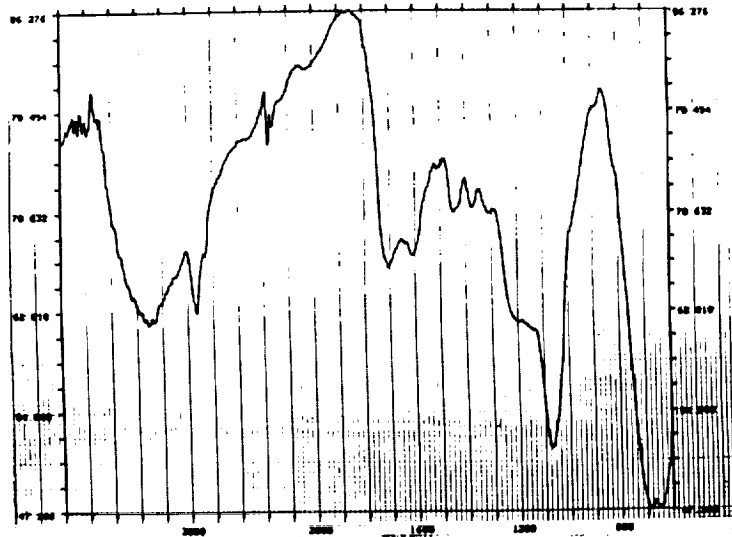
FIGURE 2.

Original figures unavailable at time of publication.



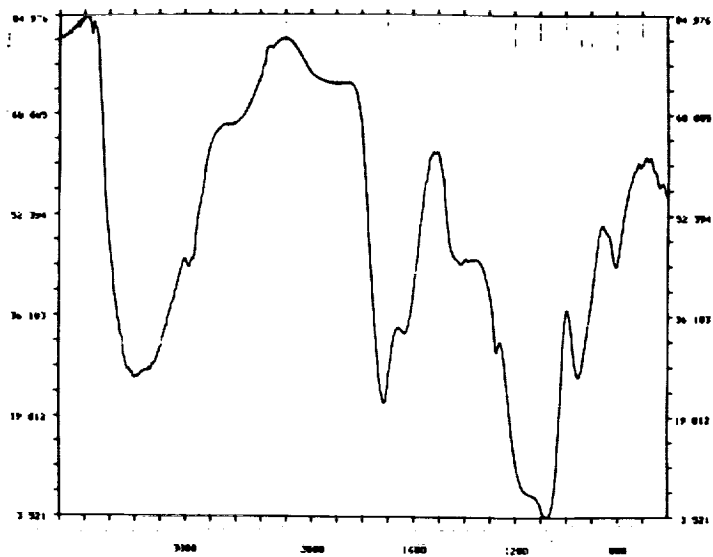
Tray Clamp E06-1: Back Surface Beside Shim, Beveled Edge

FIGURE 3.



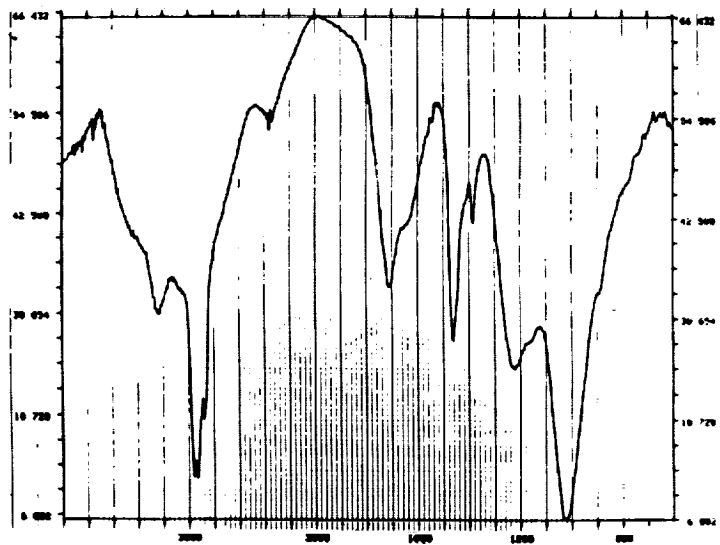
Tray H06: Brown Film On Protected Surface

FIGURE 4.



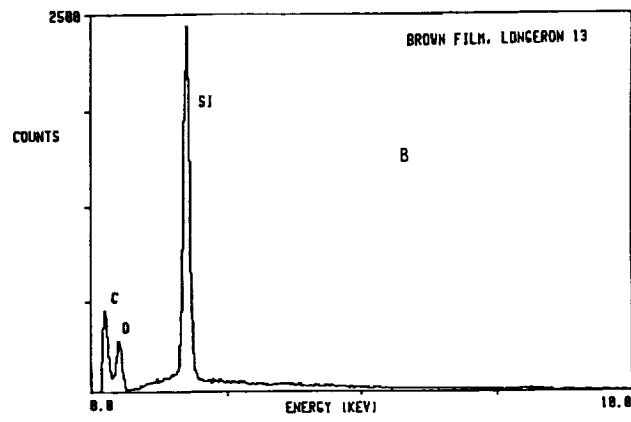
Earth End Frame Brown Film, Beside Tray G12

FIGURE 5.



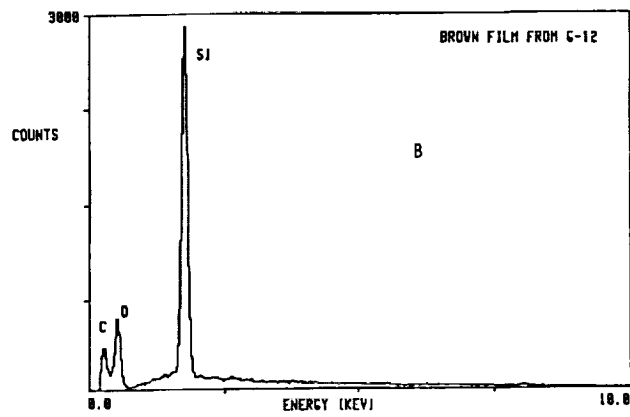
Tray C12: Brown Film

FIGURE 6.



EDX Elemental Survey Of Brown Film, Space End Longeron 13

FIGURE 7.



EDX Elemental Survey Of Brown Film, Earth End Longeron 12

FIGURE 8.

Characterization of the control specimen coatings and outgassed condensables was conducted. IR spectra were obtained for the paint films and are shown in figure 9 (for Z306) and figure 10 (for 9924).

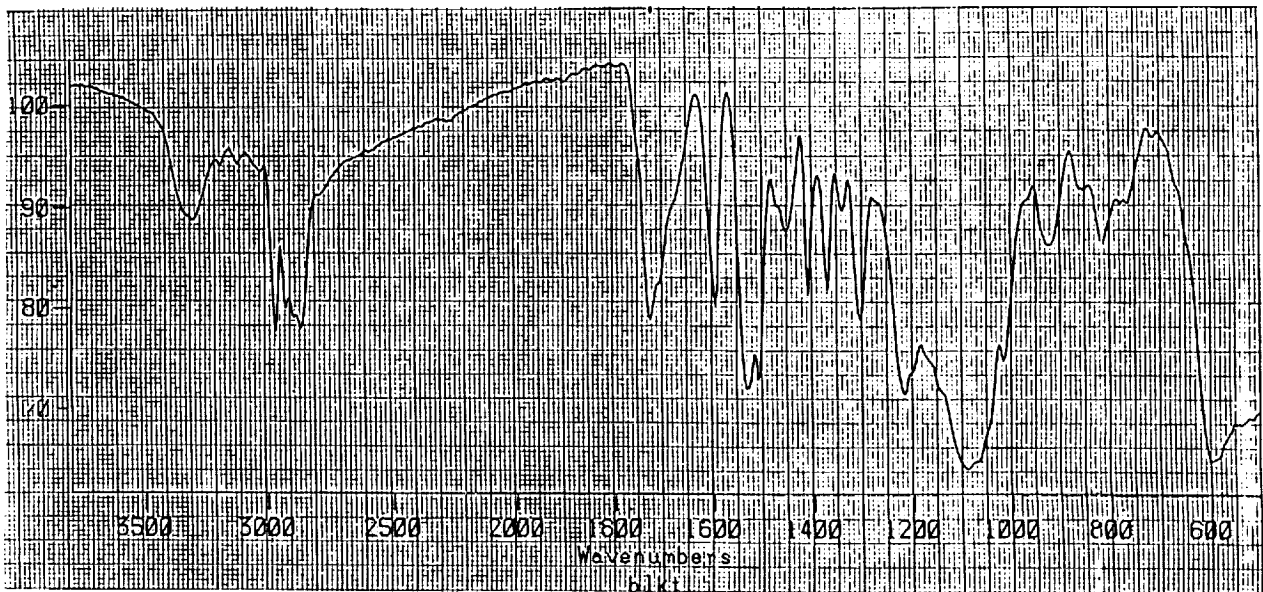
Solvent extractions were also made of the control paint specimens in an attempt to characterize the extractable fractions. Several different solvents were used in the extraction analyses, and the IR spectra resulting from these extractions are shown in figures 11-13. Quantitative measurements of the amounts of extractables in test specimens were measured at JPL. Disk control specimens of LDEF-era Z306 were observed to contain 1-2% extractable aliphatic hydrocarbon, whereas newly painted control specimens contained only 0.1%. Neither of these specimens contained extractable silicone.

Outgassing data of interest to the present analysis is shown in Table 1. Characterization of the collected condensables is shown in figures 14-16. A difference spectra, subtracting the condensables spectra from the paint spectra, is shown in figure 17. The difference spectra is comparable to the spectra for amorphous silica, shown in figure 18. Finally, an IR spectra of the condensables from the thermal blanket velcro adhesive is shown in figure 19.

Cross-sectioning and subsequent chemical analysis of test specimens was conducted. On an LDEF flight specimen thermal blanket, silicone was detected on the surface. Cross-sections of paint specimens showed silicon throughout the paint film, but this is in the form of silicate used as part of the paint pigment package.

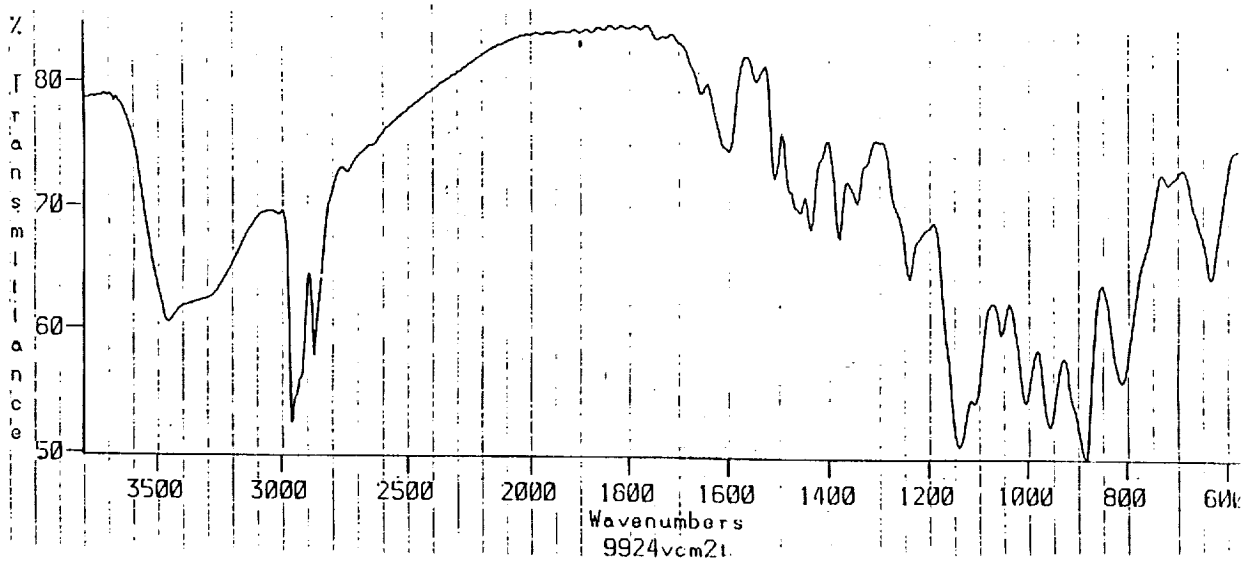
TASK 3. CHARACTERIZATION OF COATINGS AND OUTGASSED CONDENSABLES

- **IR Spectroscopy Of:**
 - **Paints Themselves**
 - **Solvent Extractions**
 - **Methylene Chloride, MEK, Petroleum Ether, Hexane, THF Used**
 - **1 - 2% Extractable Aliphatic HC In Disk Control Specimens**
 - **0.1% In Newly Painted Controls**
 - **Collected Condensables**
- **Cross-Section And Elemental Analysis**
 - **Silicone At Surface Of Thermal Blanket Coatings (LDEF Flight Specimen)**
 - **Silicon Observed Throughout Paint Films**



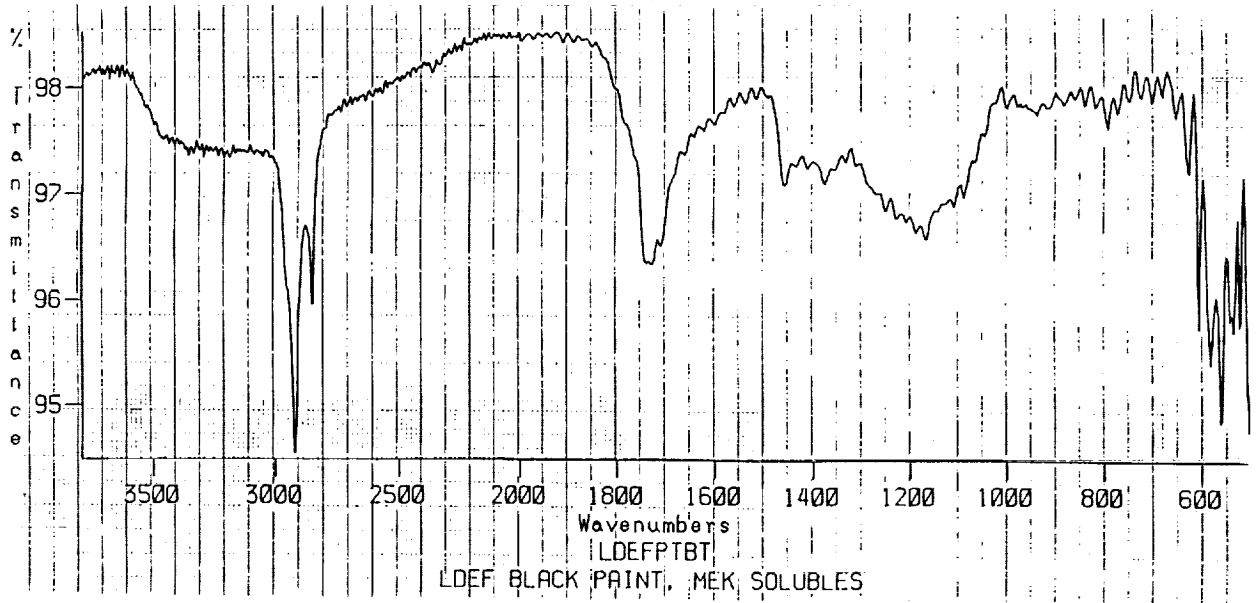
Chemglaze Z306 Thermal Control Paint

FIGURE 9.



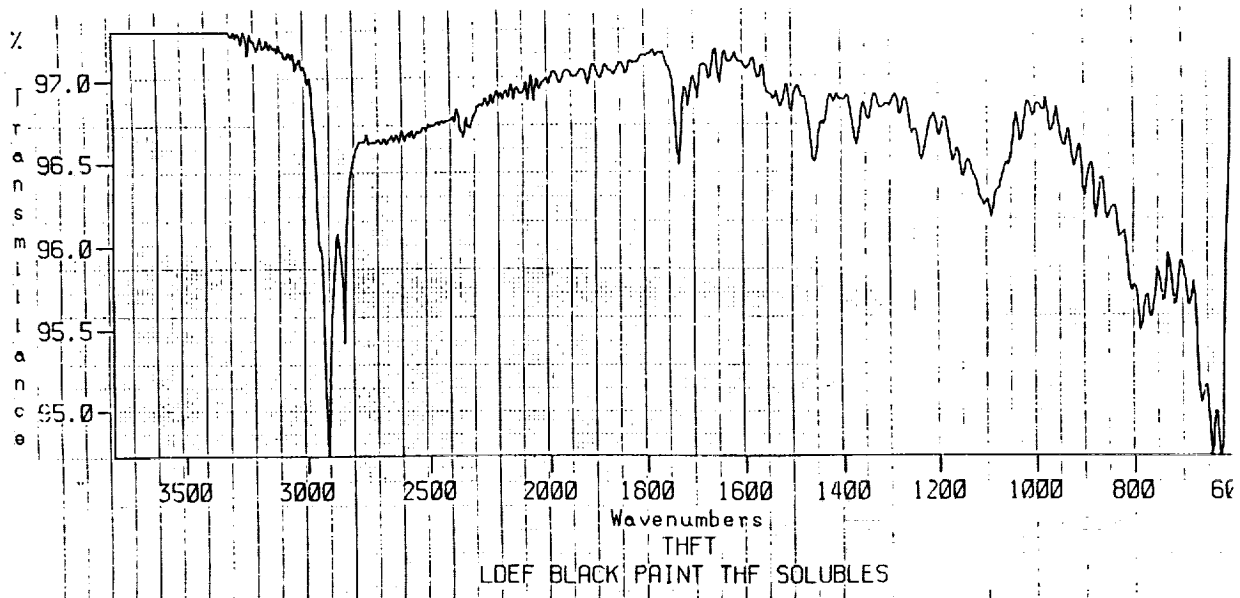
Chemglaze 9924 Primer

FIGURE 10.



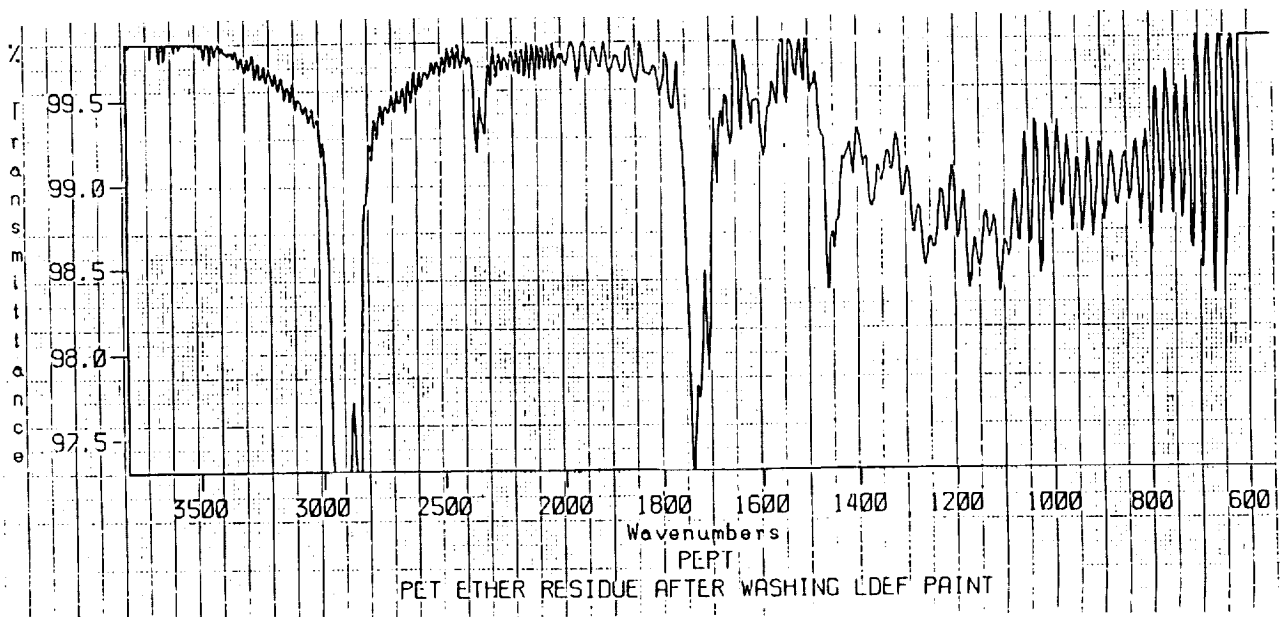
Chemglaze Z306 Paint, MEK Solubles

FIGURE 11.



Chemglaze Z306 Paint, THF Solubles

FIGURE 12.



Chemglaze Z306 Paint, Petroleum Ether Solubles

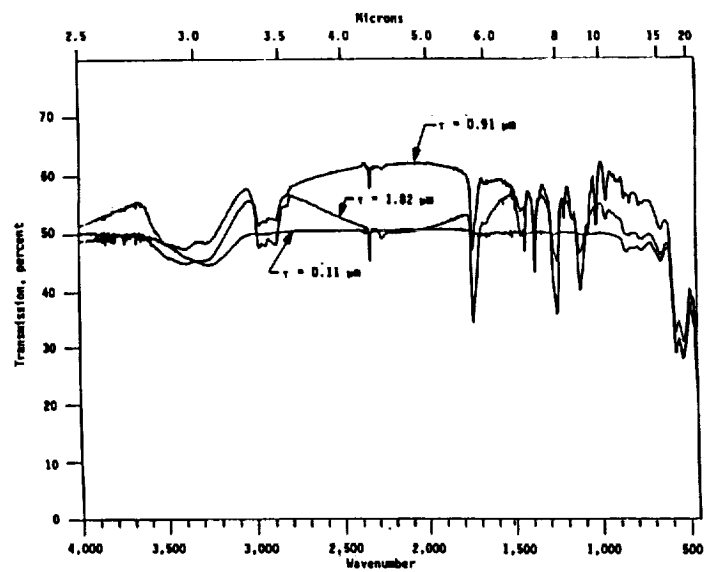
FIGURE 13.

Outgassing data indicates that the primers are significant sources of condensable materials. All data measured by the committee is for a seven day outgassing period, rather than the 24 hours used in the standard outgassing test (NASA SP-R-0022A). Comparison is also made to available literature data, which used the standard outgassing period.

TABLE 1.

RESEARCH & ENGINEERING	Z306 MOLECULAR CONTAMINATION AD HOC COMMITTEE RESULTS	
	<small>Boeing Defense & Space Group</small>	
OUTGASSING DATA		
MATERIAL	TML	VCM
Z306	1.08%	0.04% (0.03%) ¹
9924	10.2%	0.14%
Z306-9924	4.13%	0.06% (0.07%) ¹
MIL-P-23377	2.36%	0.11%
A0178 RTV ADHESIVE (7 DAY OUTGASSING)	(0.22%) ² 0.53%	(0.02%) ² 0.06%
<p>1 A.P.M. Glassford, Lockheed M&S (1978) 2 MSFC-HDBK-527F, 24 Hour Outgassing (1988)</p>		

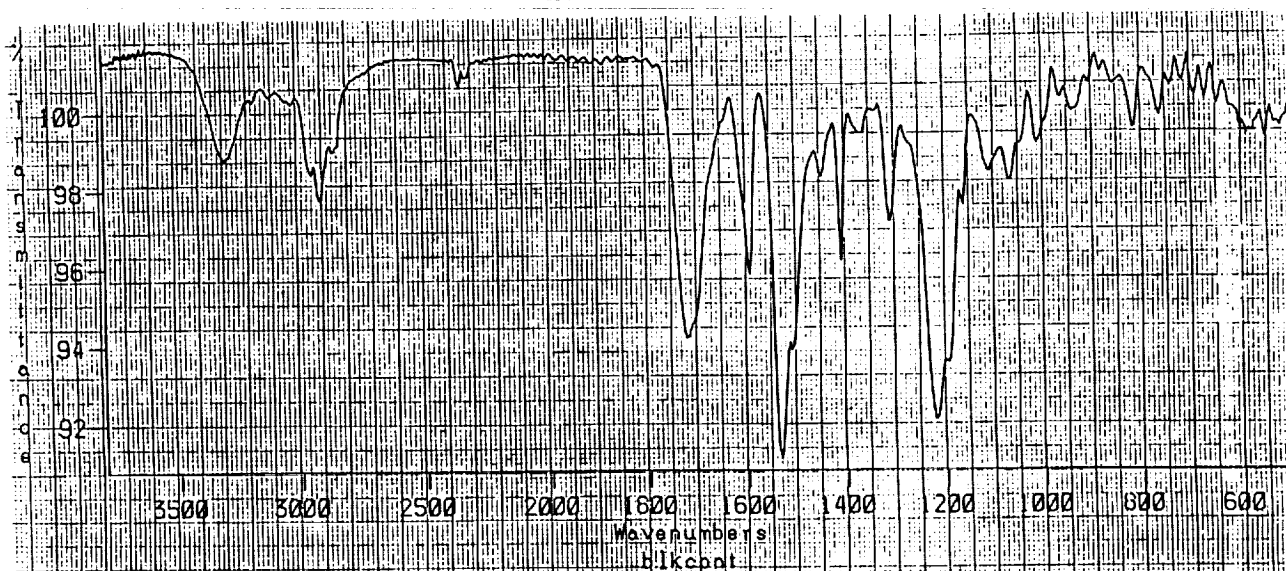
IR spectra of condensed outgassing contaminants from Z306 was obtained by Wood, et al., for three film thicknesses.



B.E. Wood, et al., Surface Effects of Satellite Material Outgassing Products, AEDC-TR-89-2, p.33, June 1989

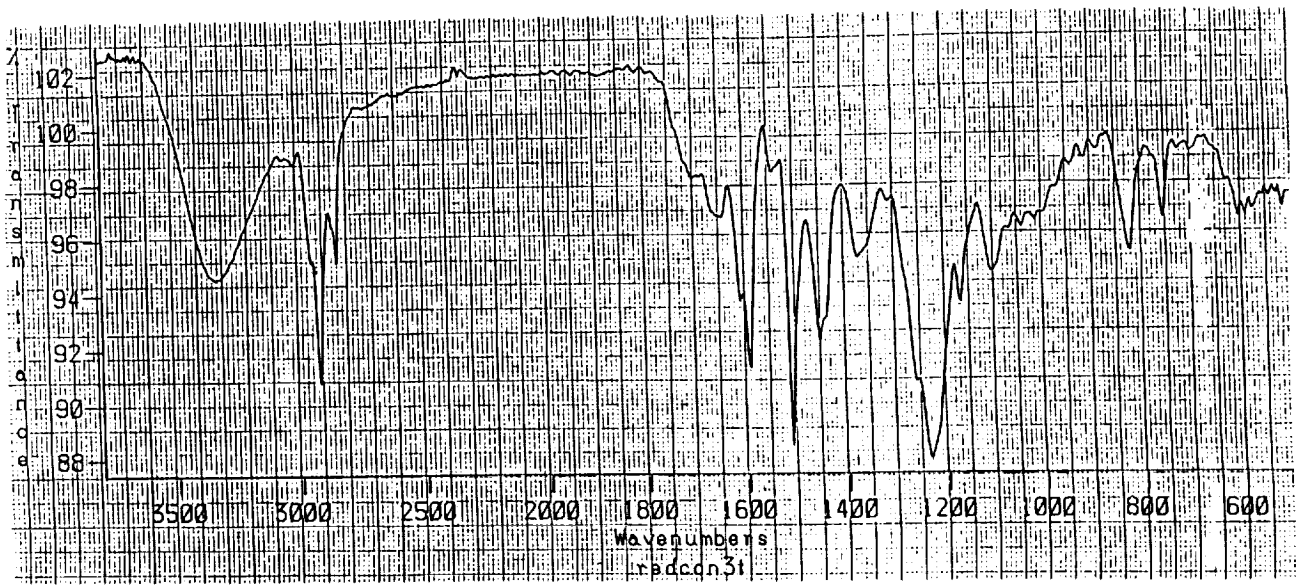
FIGURE 14.

Condensables from Z306 were all apparently removed with MEK. The solvent was used to transfer the condensate to a salt window, and was then allowed to evaporate prior to measuring the IR spectrum for the condensate. A following rinse of the condensate collector plate with petroleum ether, a good solvent for silicones, did not yield a spectrum.



MEK Wash Of Z306 Condensables

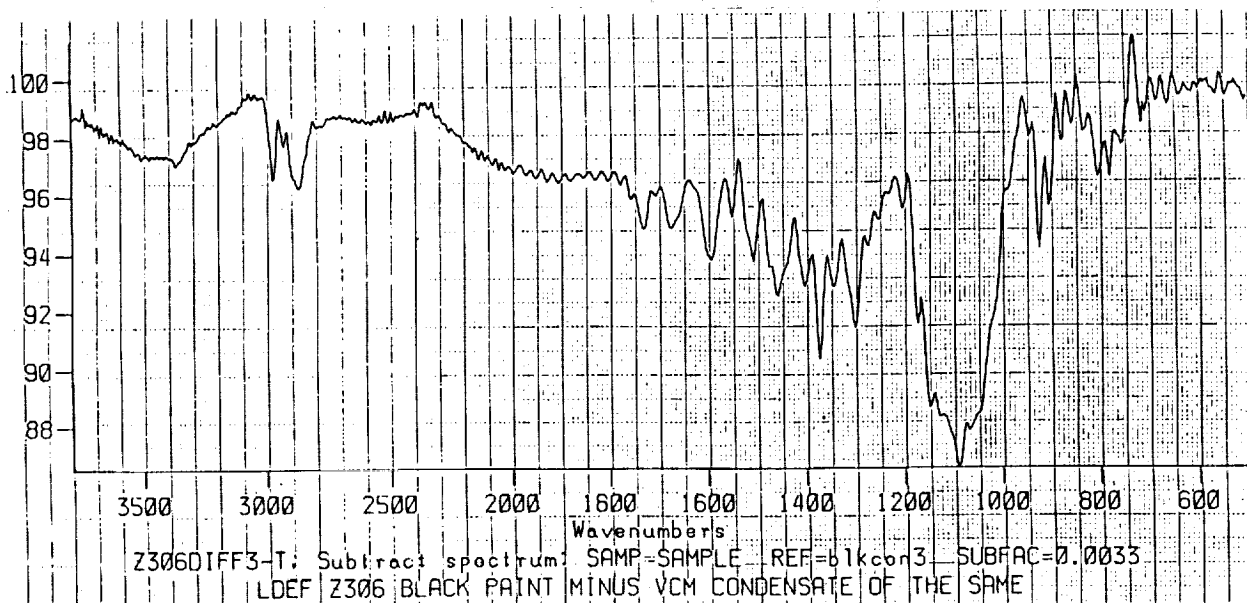
FIGURE 15.



MEK Wash Of 9924 Condensables

FIGURE 16.

The principal difference between the Z306 paint and its condensables is the silicate absorption band at 1100 wavenumbers. Silicate materials are common fillers or extenders used in paint pigments.

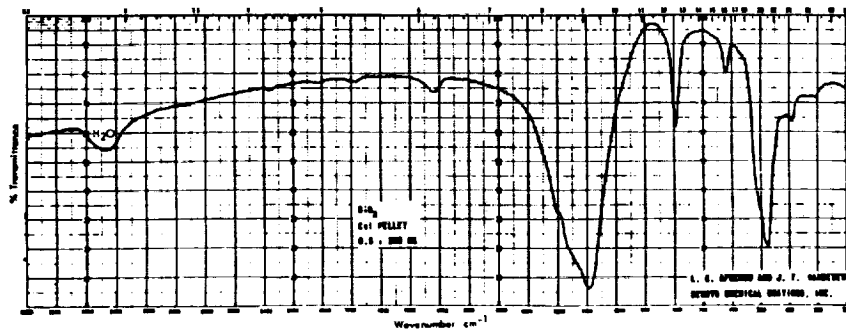


Difference Spectrum, Z306 Paint - Z306 Condensables

FIGURE 17.

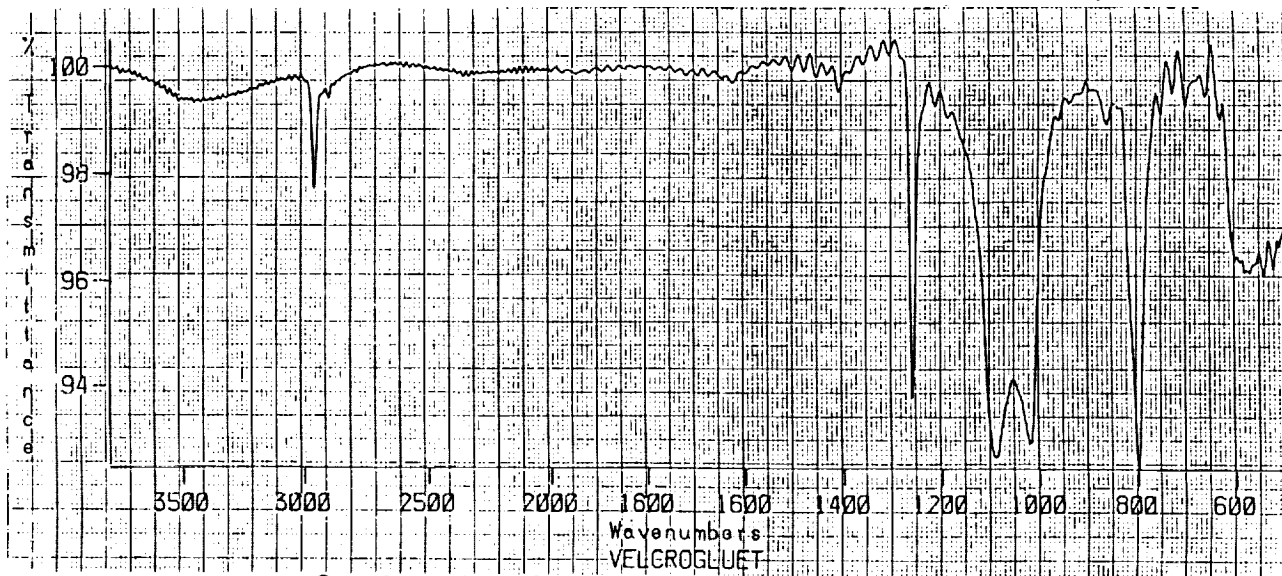
Example IR spectra of amorphous silica, obtained from a paint coatings supplier.

Amorphous silica Diatomaceous earth		4661
O ₂ Si	PREP Cell disc .5/300 mg PATH REGION SOLVENT	NSRDS-COLENTZ CLASS III structure verified
SiO ₂	SPECTROMETER Beckman IR-12 Gratings biased at 3330, 1330, 445, 220 cm ⁻¹	STATE solid M.P. B.P. CONTRIBUTOR DeSoto, Inc. DATE RECORDED



Amorphous Silica Spectrum

FIGURE 18.



**Condensables From Adhesive Attaching Velcro
To A0178 Thermal Blanket, Flight Control Specimen**

FIGURE 19.

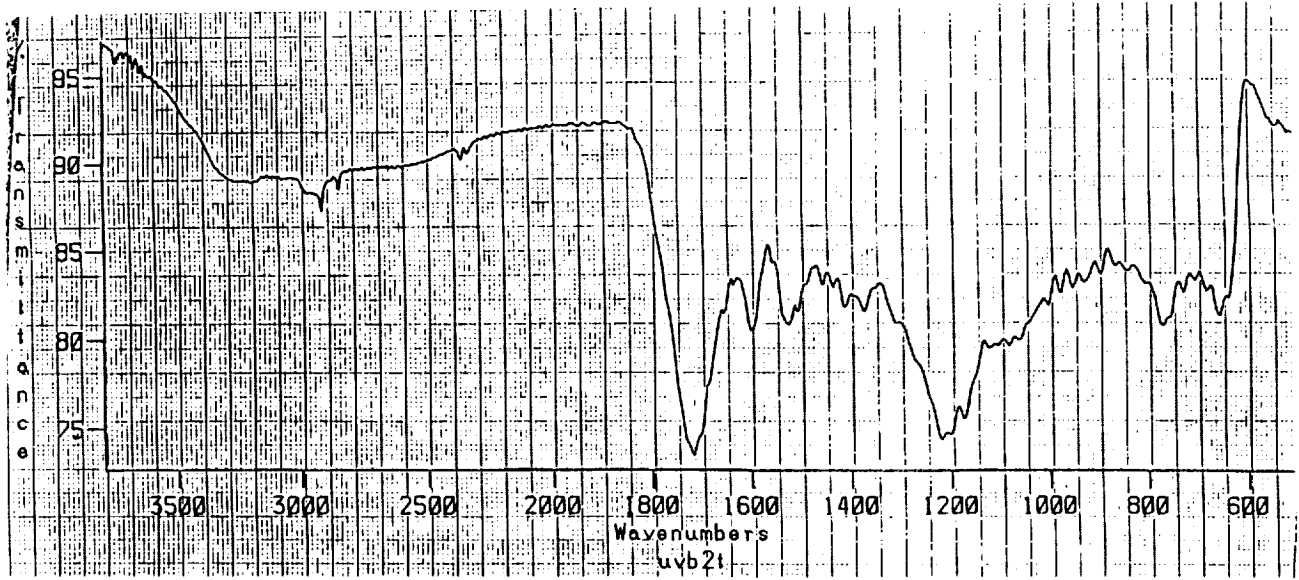
The final ad hoc committee task was an attempt to form the contaminant film observed on LDEF surfaces through the simulated UV environment exposure of Z306 condensables. This task was conducted in two parts. First, condensables were irradiated with a low power UV source in air. The results are shown in figure 20. Broadening of the IR absorption peaks was accomplished (compare to figure 14), indicating that the condensable material is being modified and the primary functional groups are being influenced in several ways due to a varied chemical environment. A similar effect is noted for the 9924 primer in figure 21.

The second part of task 4 was to use the optics degradation simulation chamber at Arnold Engineering Development Center. Z306 paint was outgassed onto a germanium collector plate, where the condensables could be irradiated with simulated UV radiation at one-sun intensity for 200 hours. The germanium plate was subsequently removed and the spectra of figure 22 obtained. A spectra of the space end brown film contaminant is shown in figure 23 for comparison.

An interesting comparison of the the LDEF contaminant can be made with the UV photodeposited silicone oil shown in figure 24.

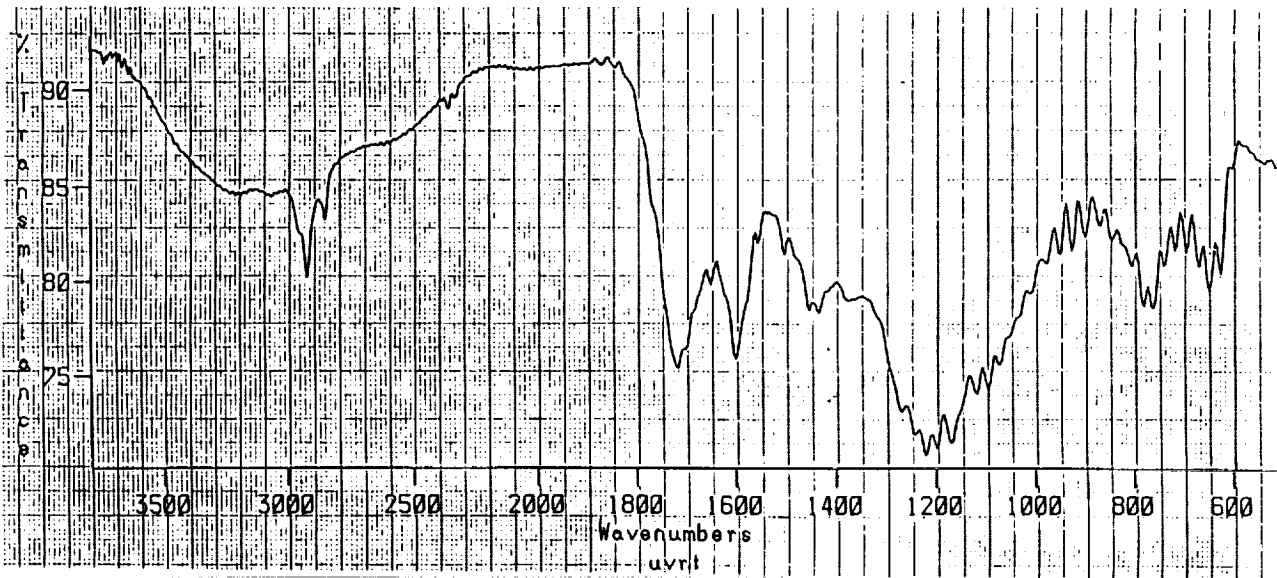
TASK 4. SIMULATED UV EXPOSURE OF OUTGASSED CONDENSABLES

- **IR Spectroscopy Of Condensables Irradiated In Air With
254nm UV Source (3.3 W/sq. m)**
- **IR Spectroscopy Of Condensables At AEDC**



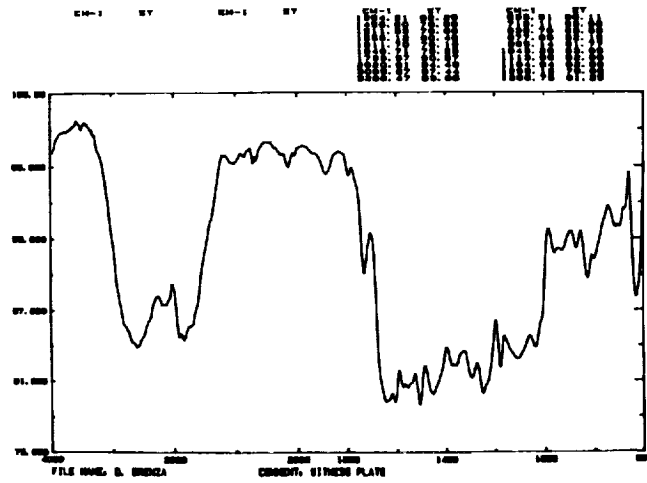
Chemglaze Z306 Condensables After UV Exposure In Air

FIGURE 20.



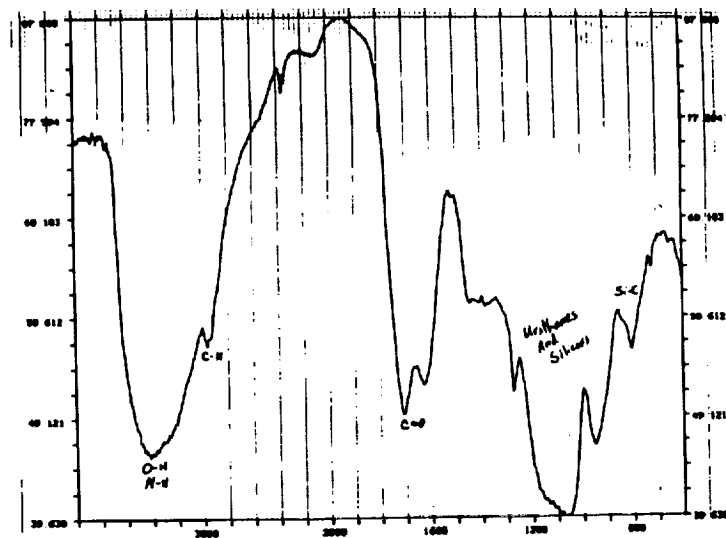
Chemglaze 9924 Condensables After UV Exposure In Air

FIGURE 21.



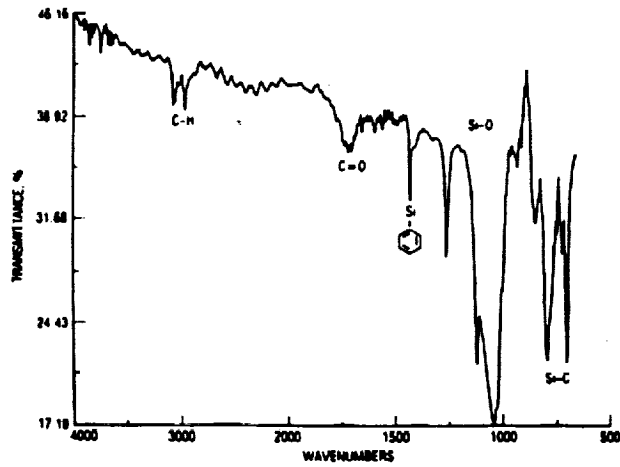
UV-Irradiated Z306+9924 Outgassing Film (AEDC)

FIGURE 22.



Space End Brown Film, Longeron 13

FIGURE 23.



UV Photodeposit of DC-704 Silicone Oil, T. B. Stewart, et al.,
Photolysis Of Spacecraft Contaminants, The Aerospace Corp.,
SD-TR-89-45, July 1989

FIGURE 24.

CONCLUSIONS

Several conclusions were drawn by the Z306 molecular contamination ad hoc committee. Conclusions can be made about the contaminant film. The contaminant, with the most notable exception of the area around tray C12, is consistent in IR spectra from opposite sides and ends of LDEF. This contaminant contains several organic functional groups in varied chemical environments, and also contains silicon, principally in silicate form when it can react with atomic oxygen.

Outgassing and extraction measurements indicate that the Z306, and especially its primer, are significant sources of molecular contamination. Many characteristics of the contaminant film can be attributed to paint condensables by comparing IR spectra. However, no evidence could be found that the paint coatings are a source of silicone contamination.

UV irradiation of outgassed condensables from Z306 produced some characteristics of the IR spectra obtained with LDEF contamination. What is lacking, however, is a source of the significant levels of silicon detected in the contaminant film.

Therefore, silicones from other sources, in addition to the outgassing from the Z306 and the primers used, were the primary contributors to the molecular contamination observed on LDEF.

CONCLUSIONS

- **Spectroscopic Evidence Indicates LDEF Contamination Films Contain Silicon, Principally In Silicate Form, And Several Organic Functional Groups In Varied Chemical Environments**
- **Z306 And Its Primer (9924 Or MIL-P-23377) Are Significant Sources Of Molecular Contamination, But Not Of Silicone Contamination**
- **UV-Irradiation Of Outgassed Condensables From Z306 Produces Some But Not All Of The Characteristics Exhibited By LDEF Molecular Contamination**
- **Silicones, Z306, And Primer Were The Primary Contributors To The Observed Molecular Contamination On LDEF**

POINTS OF INTEREST

To stimulate further thought on the subject of the LDEF molecular contamination, several points of interest can be raised which were discussed by the committee during its investigations.

The first point concerns the source of silicon which has been observed in the LDEF molecular contamination film. Since the committee was not able to determine that Z306 was the source of the silicon, what other sources might there be? One source would be the silicone adhesive that was used for bonding velcro tape to thermal control blankets. The amount of adhesive used for this purpose has been estimated at more than 3 kilograms. This is not intended as a criticism of the particular experiments or experimenters which used this bonding system. Many other potential sources of silicone have been identified on LDEF. The point is that the silicone had to come from somewhere, and the cumulative silicone adhesive and potting compounds used on LDEF must be the source.

Finally, the relative uniformity in the IR spectra obtained for contaminant films from various LDEF surfaces leads to either, and perhaps both, of the following two points. One possibility is that the contaminant film has reached a chemical equilibrium with the LEO environment, essentially achieving environmental stability. The other possibility is that the contamination mechanism that produced these films was not line-of-sight, suggesting a significant departure from the classical contamination control design approach.

POINTS OF INTEREST

- **Silicone Adhesive Used For Bonding Velcro Tape To Thermal Blankets**
Estimate 2 g Adhesive/Tape, 2 Tapes/Attachment, 48 Attachments/Tray, 17 Trays
Yields >3 kg Silicone Adhesive
- **Numerous Potential Sources Of Silicone Contamination Have Been Identified**
- **Relatively Uniform Spectra For Contaminant Films From Various Location Indicates:**
 - **Equilibrium Chemistry In Contamination Products (Environmental Stability)**
 - **Non Line-Of-Sight Contamination Mechanisms**

**LONG DURATION EXPOSURE FACILITY (LDEF)
CONTAMINATION MODELING**

Tim Gordon
Applied Science Technologies
P.O. Box 621134
Littleton, CO 80162
Phone: (303) 973-7708

Ray Rantanen
ROR Enterprises
4043 South I-25
Castle Rock, CO 80104
Phone: (303) 688-9428

SUMMARY

The Integrated Spacecraft Environments Model (ISEM) was used to model the LDEF induced neutral molecular environment at several different times and altitudes during the mission. The purpose of this effort was to provide the community with an estimate of the neutral molecular environment to assist in phenomenology studies.

INTRODUCTION

The objectives of this modeling effort were twofold. First, to model the overall vehicle induced neutral environment and to determine the flux of various molecular species on different surface locations. Secondly, to use the overall modeling results as input for the modeling of the molecular flux through a small aperture (vacant screw hole) into the vehicle interior. This second modeling effort was of interest because of very noticeable brown deposition patterns on interior surfaces in close proximity to the aperture. It was believed that understanding the molecular

environment in the vicinity of the aperture would help in determining the mechanism which produced the deposition pattern.

INTEGRATED SPACECRAFT ENVIRONMENTS MODEL (ISEM)

ISEM is a collisional molecular transport code which computes the molecular density and flux in a three dimensional modeling volume for any number of user defined molecular species.

MODELING PARAMETERS

Three different periods in the LDEF mission were modeled to obtain representative results over the mission lifetime. These periods were representative of the beginning, middle and end of the mission timeline and corresponded to orbital altitudes of 463 km, 417 km, and 333 km respectively. Table 1 shows the ambient values for the six different ambient molecular species modeled at the three periods. The values were obtained using the atmosphere-predicting model MSIS86 and represent annual and orbital position averaged values for the periods modeled.

Table 2 shows the outgassing and erosion rates used for the modeling. External surfaces were modeled as having an average uniform outgassing rate which decreased with time. The initial outgassing rates were based on test data and the percentages of various materials present. Outgassing from internal surfaces was allowed to escape to the external environment via the numerous holes around the experiment trays. The external outgassing rate was assumed to decrease with an e folding time of 6000 hours. The internal outgassing rate was assumed to decrease with an e folding time of 7000 hours. The e folding times were based on Skylab measurements, taking into account differences in materials and materials control between the two programs. The average erosion rate was assumed to be 15% of Kapton for all the surfaces. The erosion rate given in Table 2 is for a surface normal to ram; a cosine dependence (relative to the velocity vector) was assumed for non-normal surfaces.

GEOMETRY MODEL

LDEF was modeled as the geometric structure shown in Figure 1. Based on data at the time of the modeling, the geometric structure was rotated 10 degrees relative to ram as shown in Figure 2.

GENERAL MODELING RESULTS

Density

ISEM was used to compute the density of every tracked species throughout the three dimensional modeling volume for the mission beginning, middle, and end cases described previously. Figures 3, 4 and 5 show the total iso-density contours for a plane of values from the three dimensional modeling volume. The total density value is the sum of ambient species, surface reemitted ambient species, internal and external outgassed species, and the scatter portions of all species. The contour values have been normalized to the total undisturbed ambient density at the respective altitude. Figure 3 shows the total iso-density contours for the early mission case at an altitude of 463 km. A slight ram buildup can be seen in front of the vehicle (velocity vector from left to right), but the density around the vehicle is dominated by the outgassing. Figure 4 shows the total iso-density contours for the middle mission case at an altitude of 417 km. In this figure one can see a significant ram buildup and a distinct wake region. The density in the wake region is dominated by the outgassing. Figure 5 shows the total iso-density contours for the late mission case at an altitude of 333 km. There is a strong density buildup in front of the vehicle due to ambient and erosion products. The wake is very well defined and although the densities are much less than on the ram side the density in the wake region is still dominated by the outgassed species. Figure 6 is an iso-density contour plot of only the erosion products. The plot shows a strong ram angle dependence.

Flux

From the standpoint of surface materials interaction with the molecular environment, molecular flux of the different species is much more important than density. Flux of each tracked species was computed to each of the LDEF facets. Figures 7 through 10 show the surface incident flux at the three modeled altitudes for O, O₂, N, and N₂ respectively. In the figures the surface incident flux is plotted as a function of incidence angle as measured from the ram direction. The term "direct" on the plots refers to flux of molecules which have not had a collision; they still retain the kinetic energy of the orbital velocity (in the spacecraft reference frame). Figure 11 shows the flux of outgassed and erosion products at the three modeled altitudes. Note that there is no direct flux in these plots because only transport via scattering can produce the return flux of these species to the external surfaces (this is not necessarily true on the scale of individual trays).

SMALL SCALE MODELING RESULTS

The second portion of the modeling effort was to model the molecular flux through a small aperture and the resulting incident flux on an internal surface (the side of an experiment tray). Figure 12 shows the geometrical relationship of the aperture and the internal surface. Figure 13 shows the energy distribution in the spacecraft reference frame of atomic oxygen and nitrogen in terms of electron volts. Figure 14 shows the angular distribution in the spacecraft reference frame of atomic oxygen due to the ambient thermal velocity distribution. Figure 15 shows the incident flux distribution of atomic oxygen on the internal surface due to flow through the small aperture. The flux distribution on the surface is due primarily to the thermal distribution of atomic oxygen. The dotted lines indicate the approximate cone angle of the observed deposition pattern.

CONCLUSIONS

We believe that the internal deposition modeled was due to atomic oxygen fixing of internally outgassed contaminants present on internal surfaces. The pattern observed is consistent with the thermally distributed flux of ambient atomic oxygen in the spacecraft reference frame.

The atomic oxygen erosion rates at the end of the mission were comparable to initial outgassing rates of LDEF surfaces. Return flux of erosion species near the end of the mission were an order of magnitude greater than the return flux of outgassed products early in the mission.

ACKNOWLEDGMENTS

We would like to acknowledge the financial support of Dr. Ann Whitaker at NASA Marshall Space Flight Center. We would also like to thank Ralph Carruth at MSFC for his technical and logistical assistance.

Table 1. Average Ambient Atmosphere Density Values
(MSIS 86)

Species #/cm ³	Date		
	4/84	4/87	1/90
O	2.59x10 ⁷	3.48x10 ⁷	9.03x10 ⁸
O ₂	7.52x10 ³	1.43x10 ⁴	6.06x10 ⁶
N	6.65x10 ⁵	7.44x10 ⁵	3.28x10 ⁷
N ₂	4.23x10 ⁵	7.26x10 ⁵	2.03x10 ⁸
He	3.47x10 ⁶	3.85x10 ⁶	5.07x10 ⁶
H	1.63x10 ⁵	2.30x10 ⁵	2.66x10 ⁴
Total Density	3.06x10 ⁷	4.04x10 ⁷	1.15x10 ⁹
Temperature (K)	920	829	1303
O Flux/cm ²	2.0x10 ¹³	2.x10 ¹³	7.0x10 ¹⁴

Table 2. Outgassing and Erosion Rates

Rate g/cm ² /sec	463 km	417 km	333 km
	4/84	4/87	1/90
External	2.0 x 10 ⁻⁹	2.6 x 10 ⁻¹¹	1.4 x 10 ⁻¹²
Internal	2.0 x 10 ⁻¹⁰	5.6 x 10 ⁻¹²	4.8 x 10 ⁻¹³
Erosion	6.3 x 10 ⁻¹¹	8.5 x 10 ⁻¹¹	2.2 x10 ⁻⁹

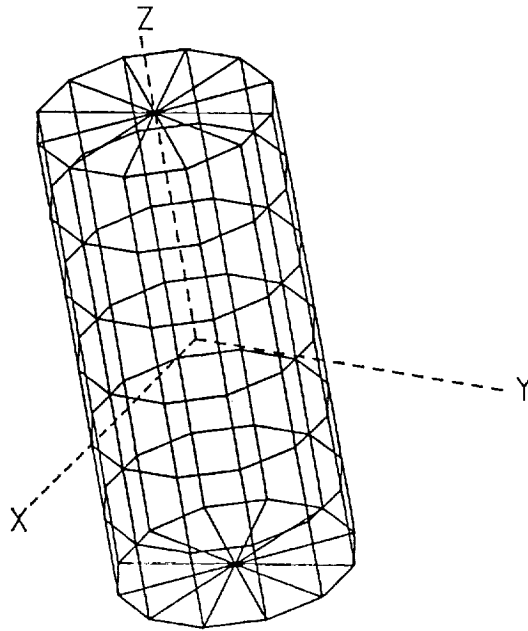


Figure 1. LDEF geometry model.

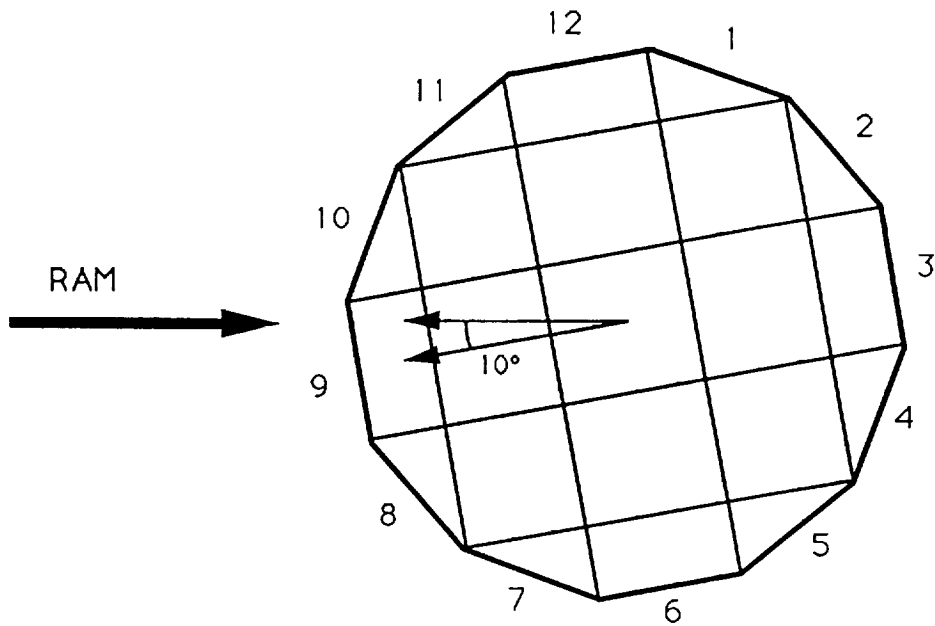


Figure 2. LDEF facet identification (from Earth end).

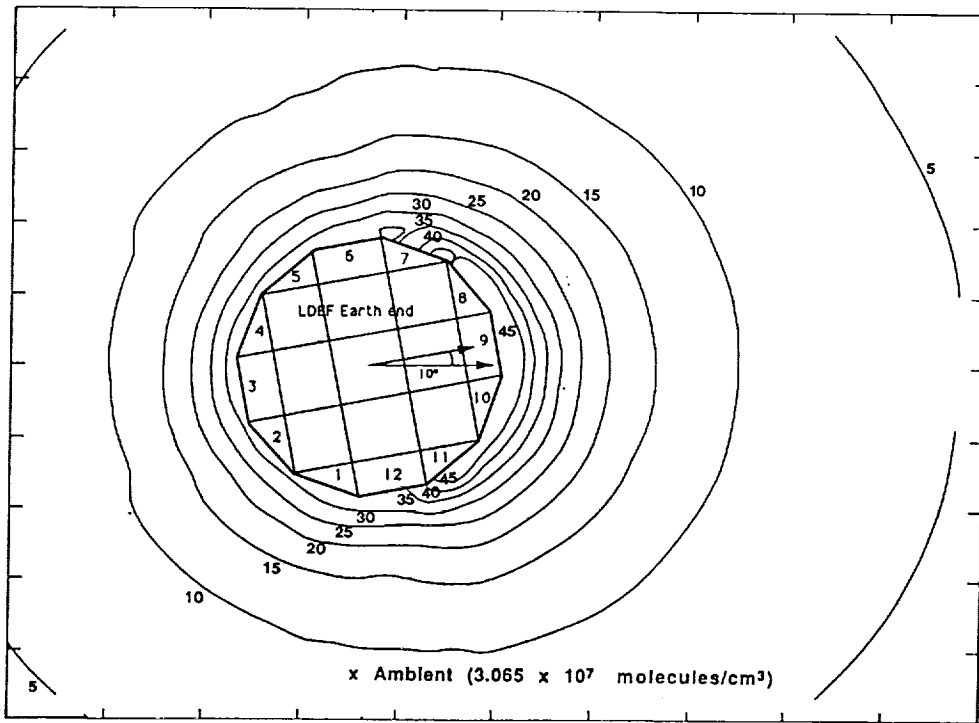


Figure 3. Total density at 463 km.

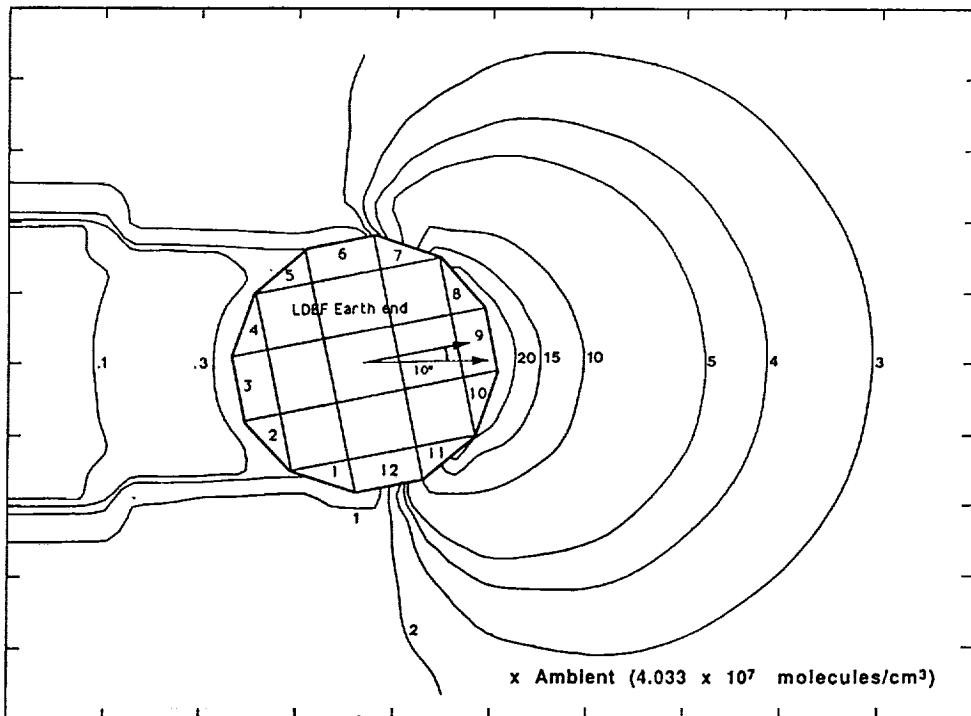


Figure 4. Total density at 417 km.

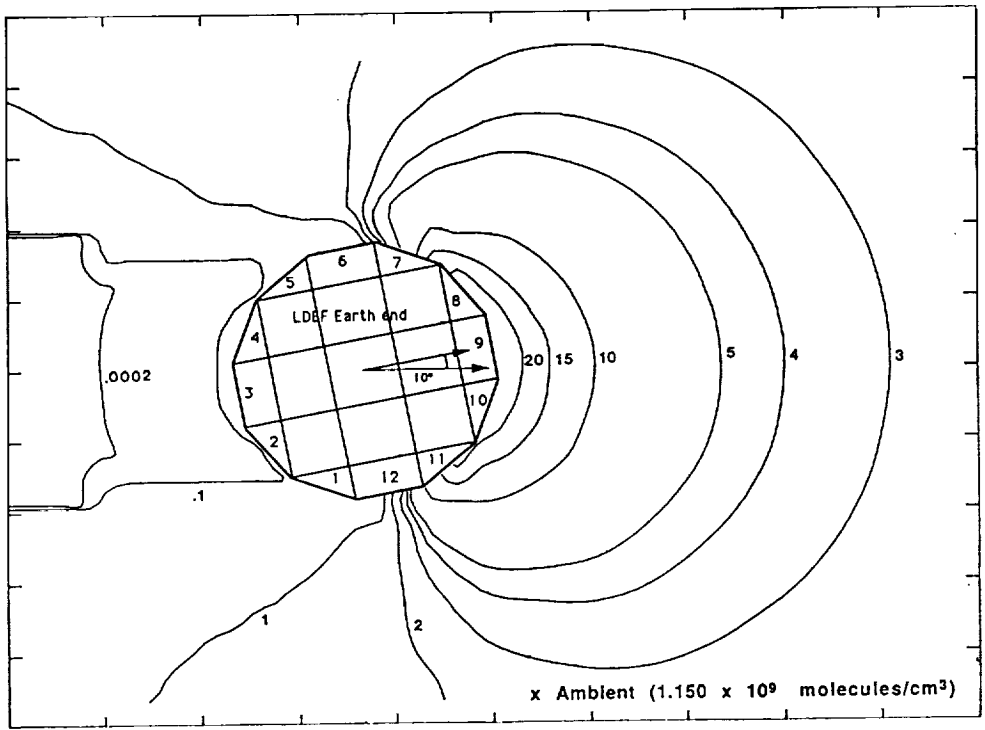


Figure 5. Total density at 333 km.

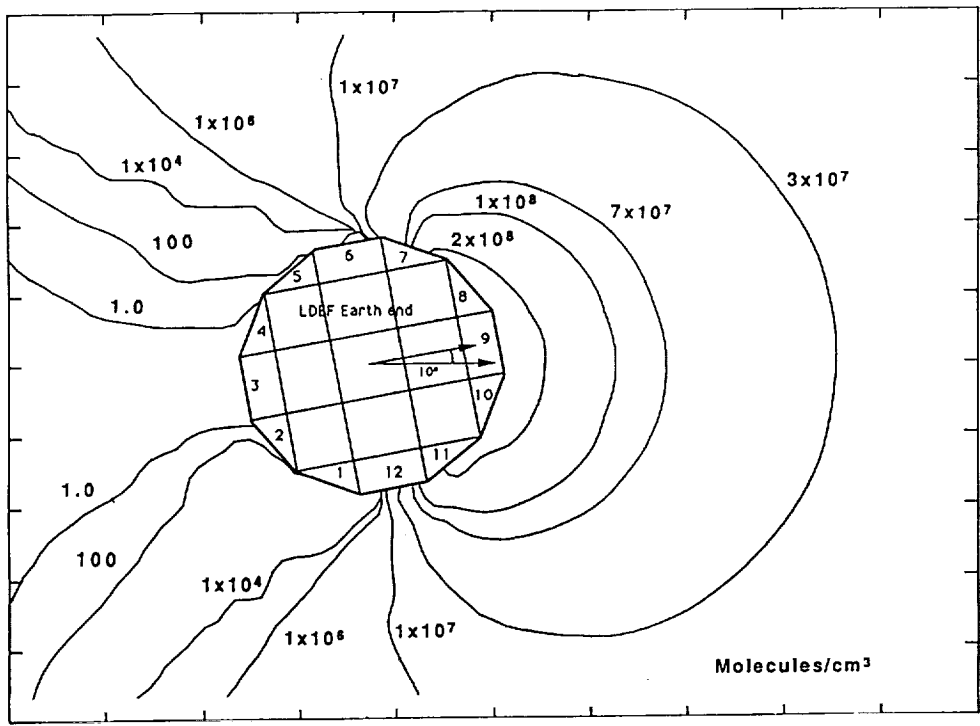


Figure 6. Density of erosion products at 333 km.

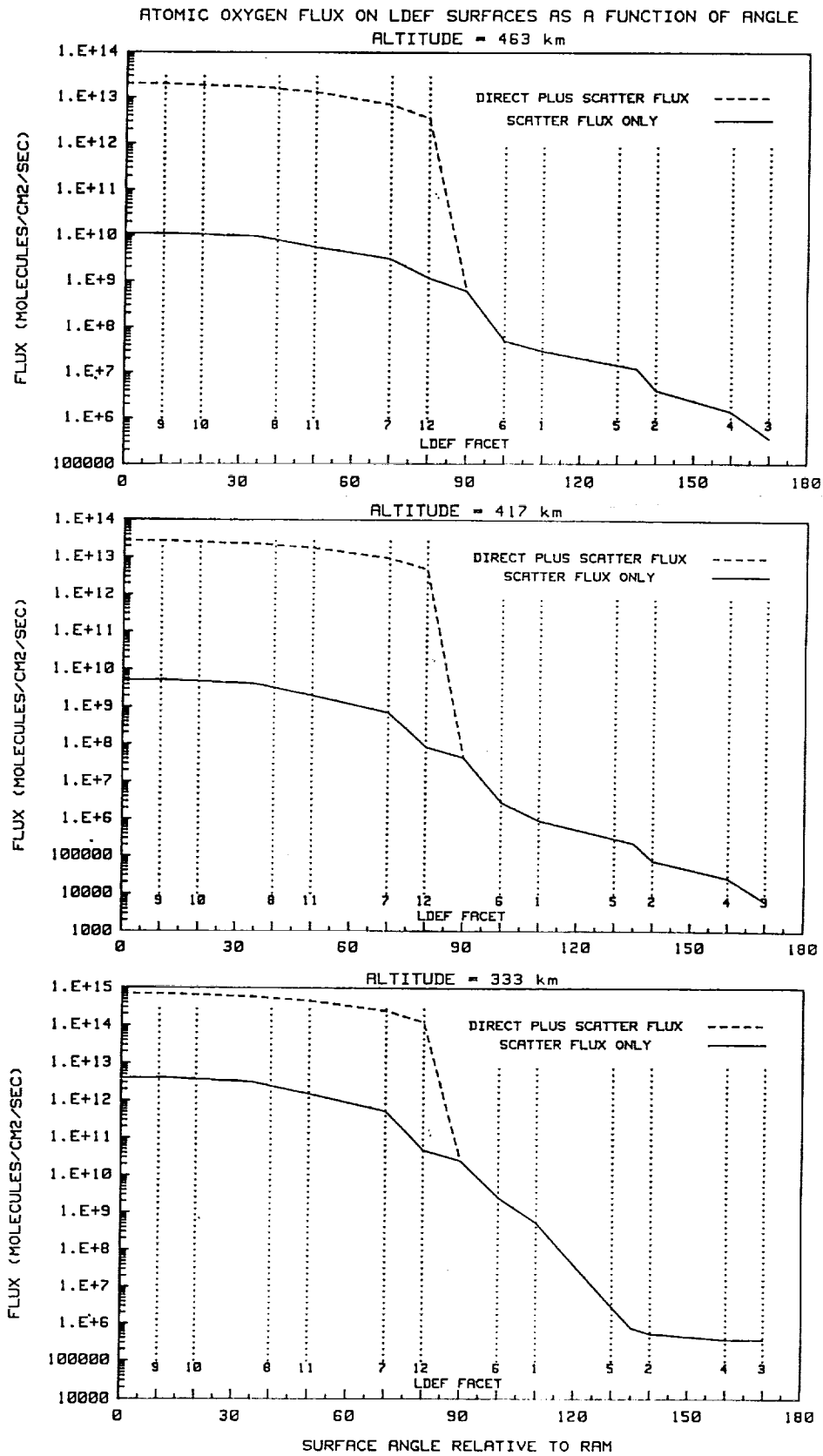


Figure 7. Atomic oxygen flux on LDEF surfaces.

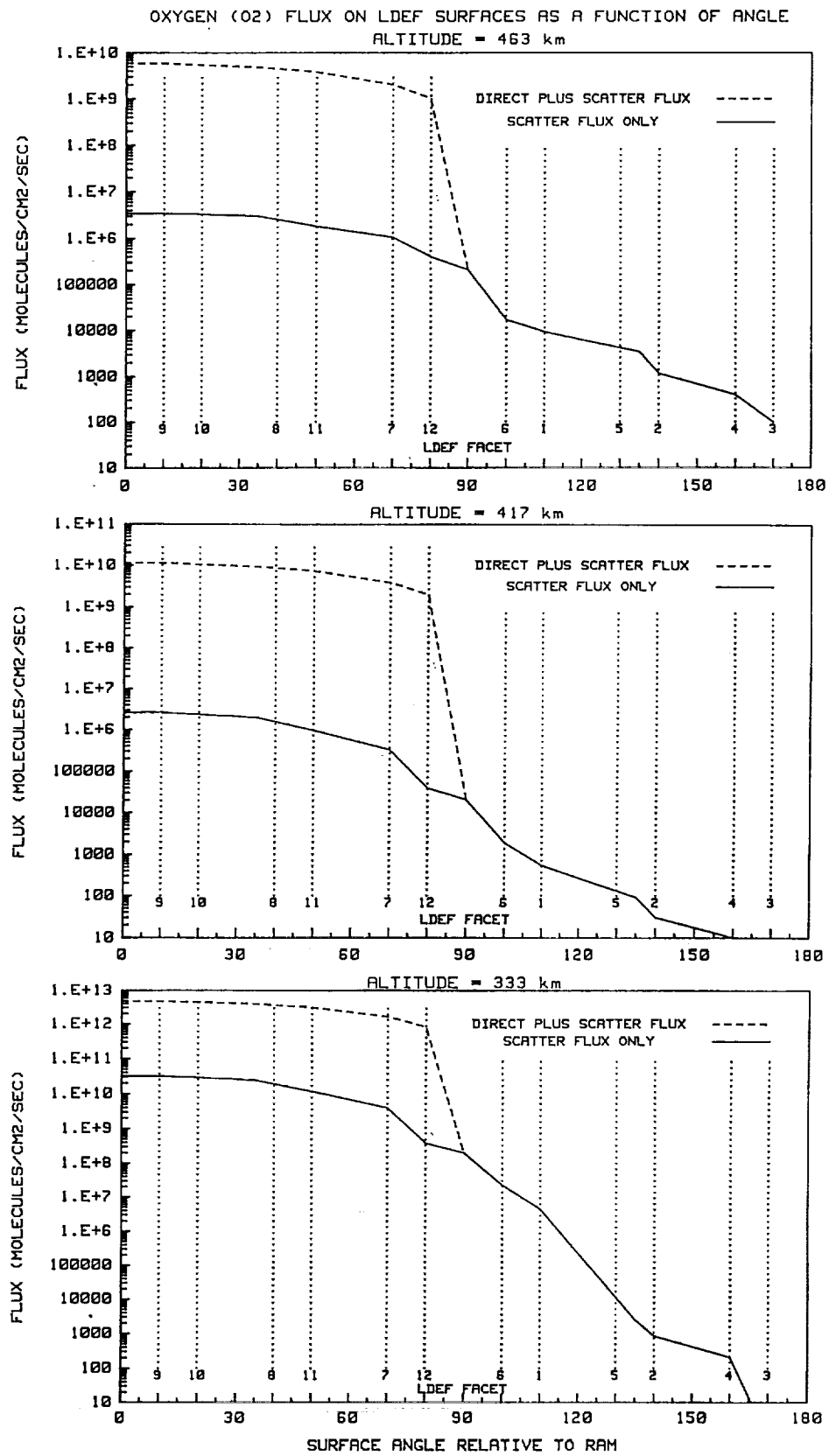


Figure 8. Oxygen flux on LDEF surfaces.

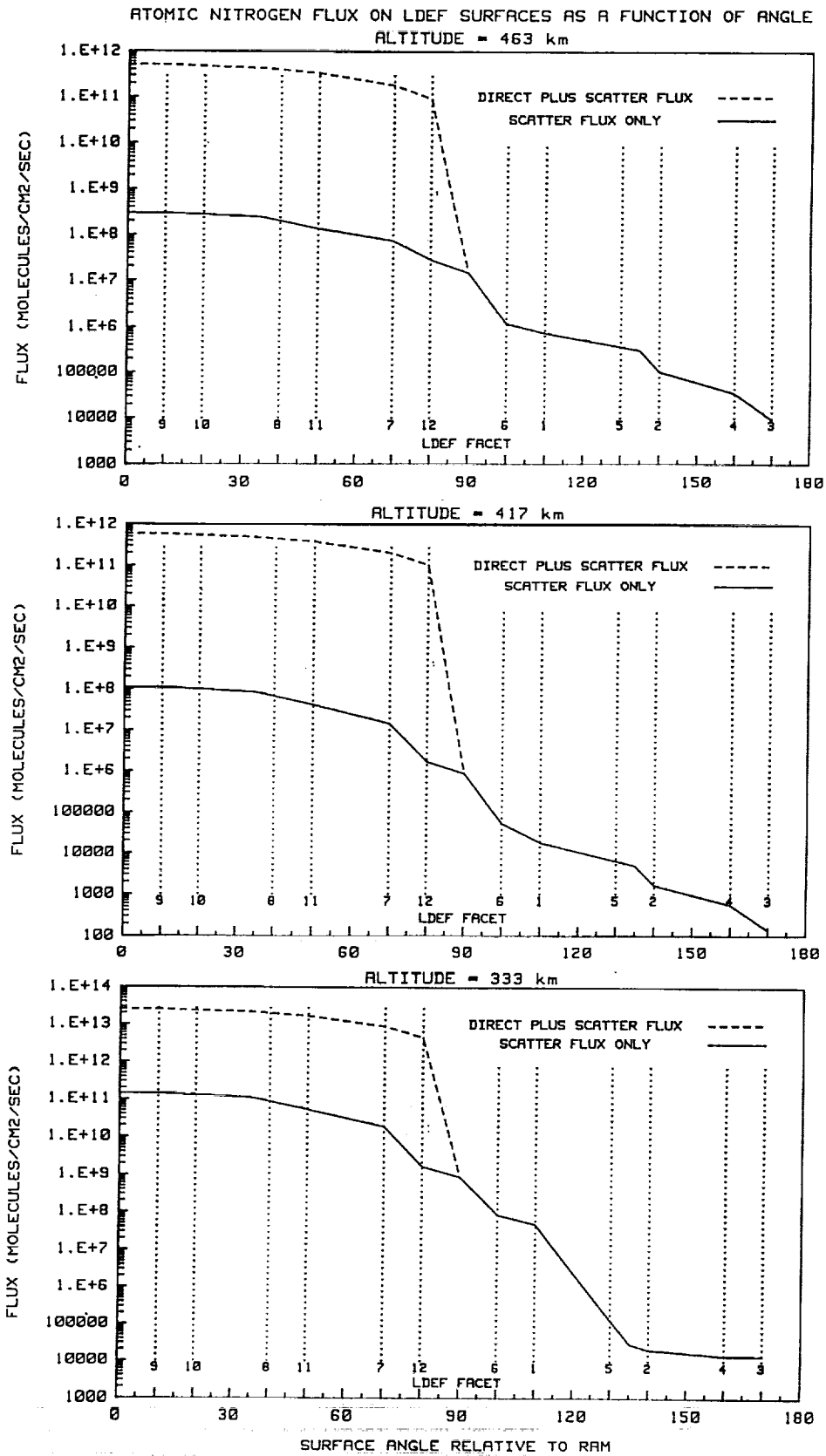


Figure 9. Atomic nitrogen flux on LDEF surfaces.

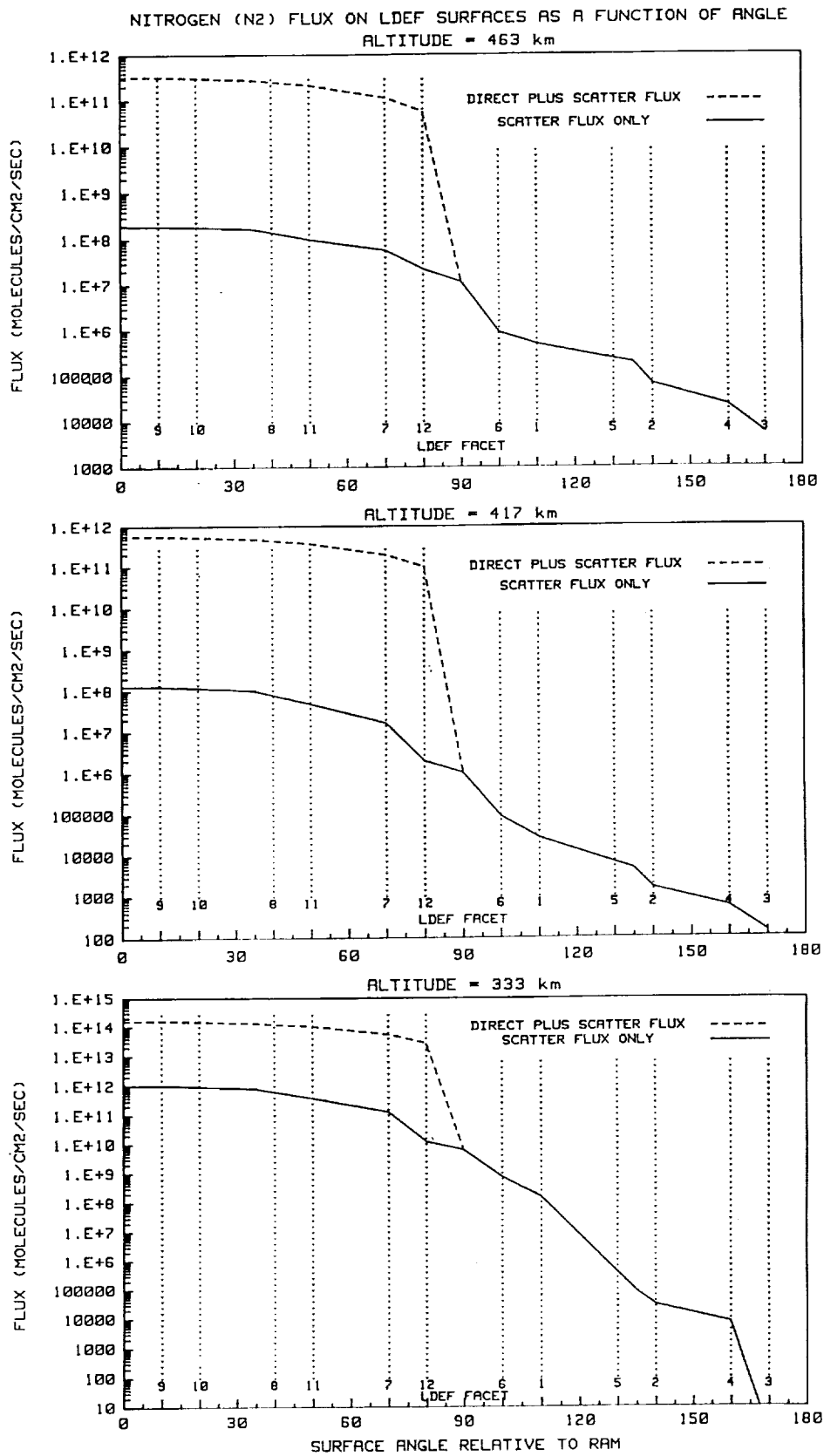


Figure 10. Nitrogen flux on LDEF surfaces.

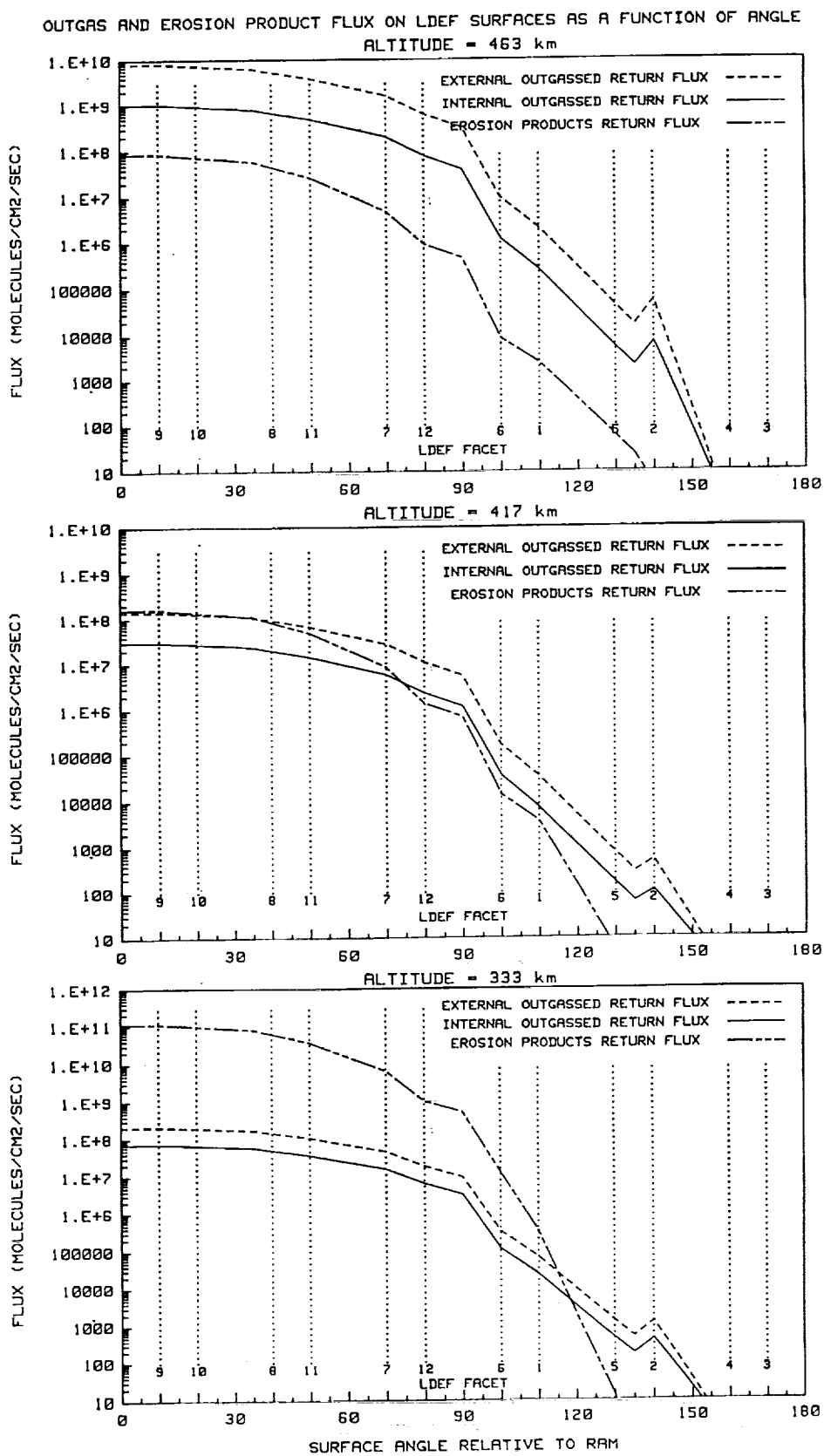


Figure 11. Outgassed and erosion products flux on LDEF surfaces.

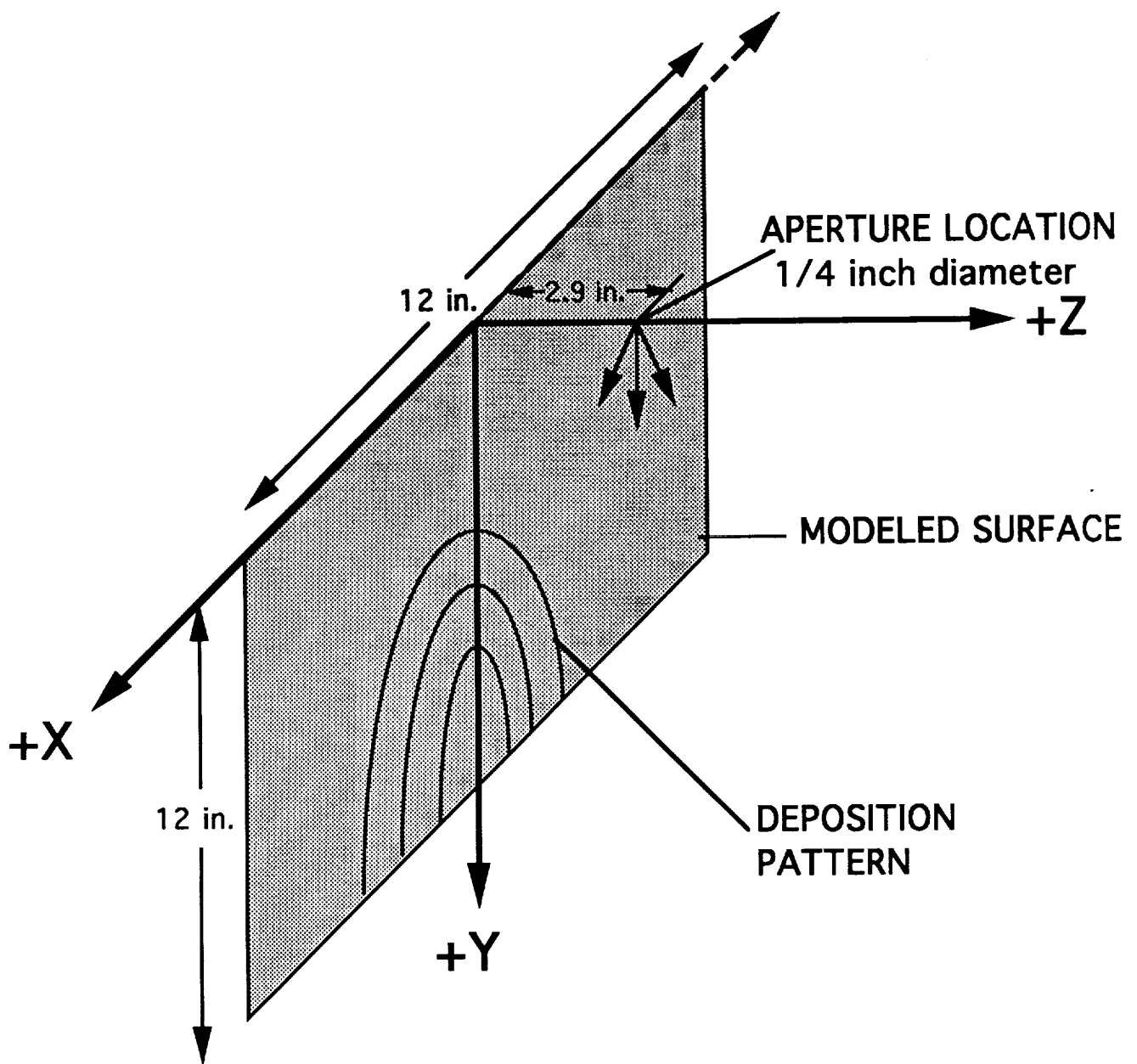
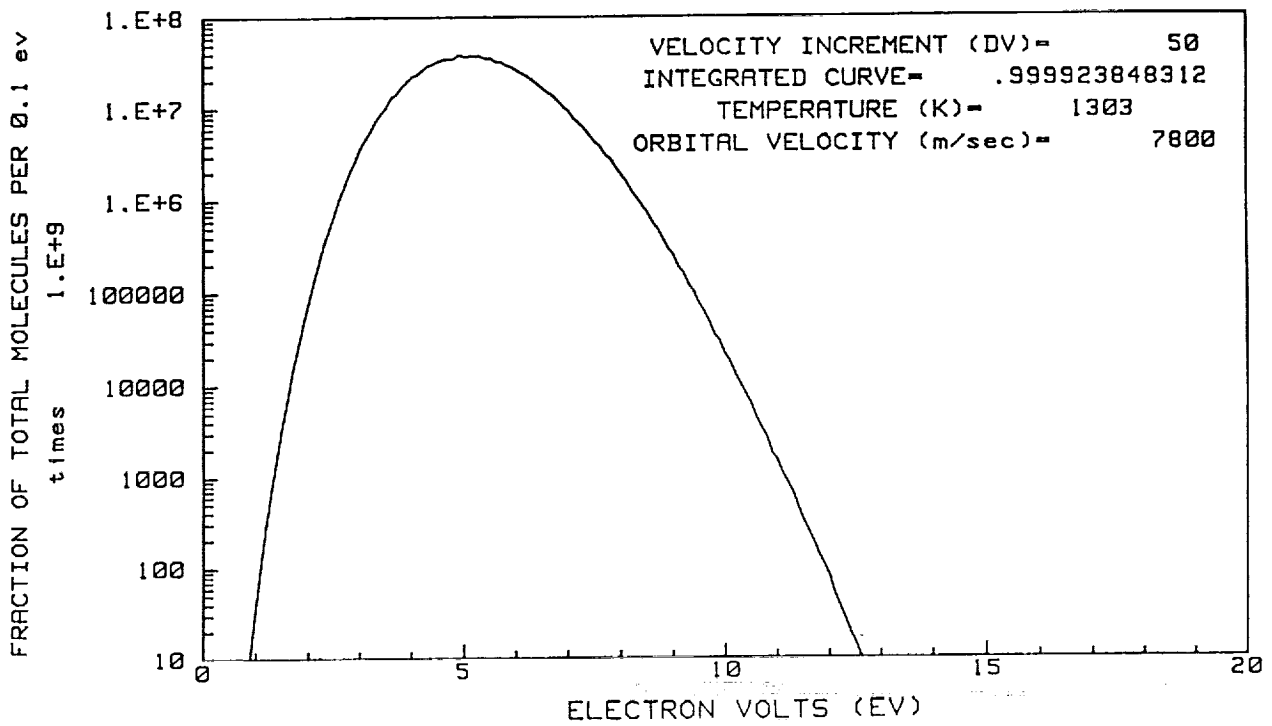


Figure 12. Internal surface deposition model geometry.

EV DISTRIBUTION OF INCIDENT AMBIENT ATOMIC OXYGEN



EV DISTRIBUTION OF INCIDENT AMBIENT NITROGEN

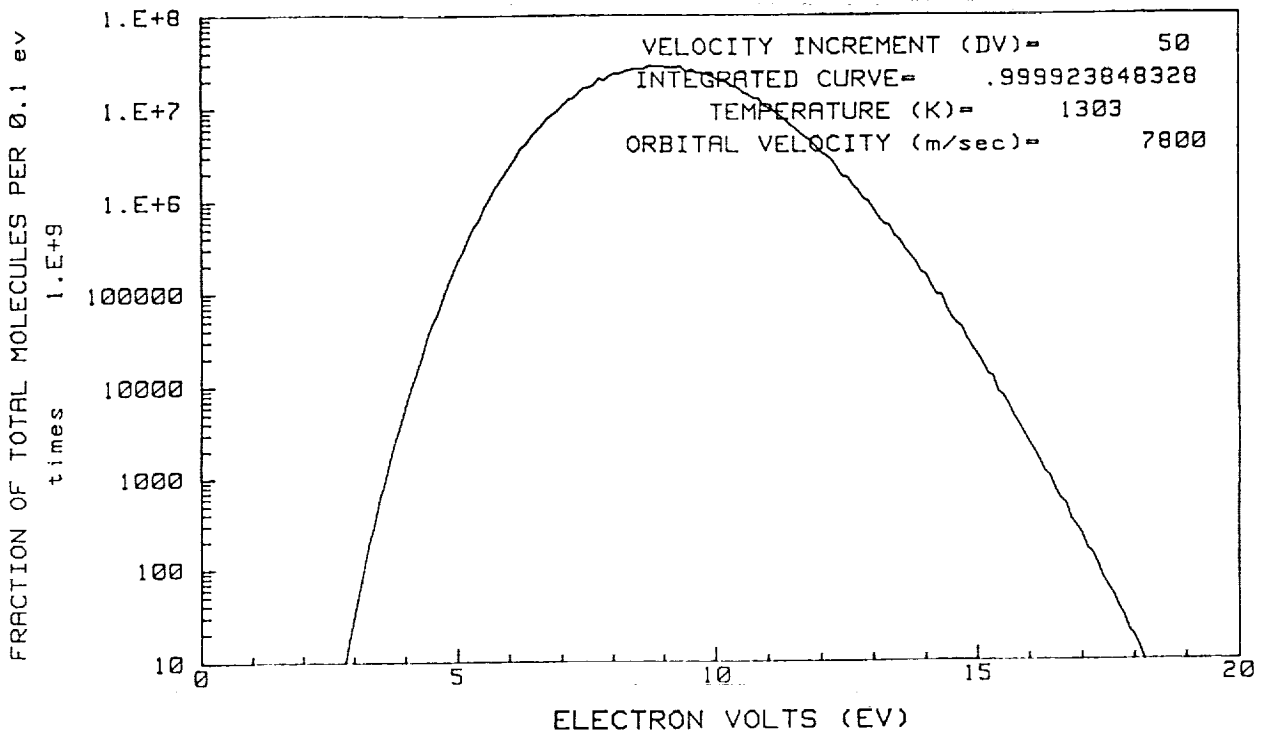


Figure 13. Energy distribution of atomic oxygen and nitrogen.

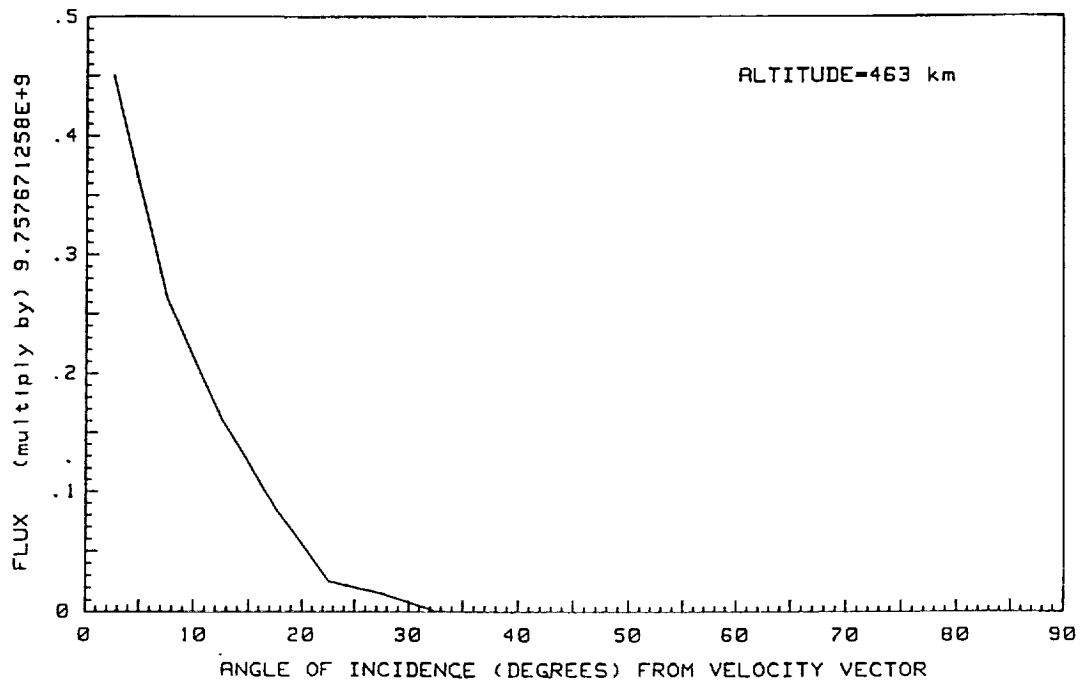


Figure 14. Atomic oxygen angular distribution from ram direction.

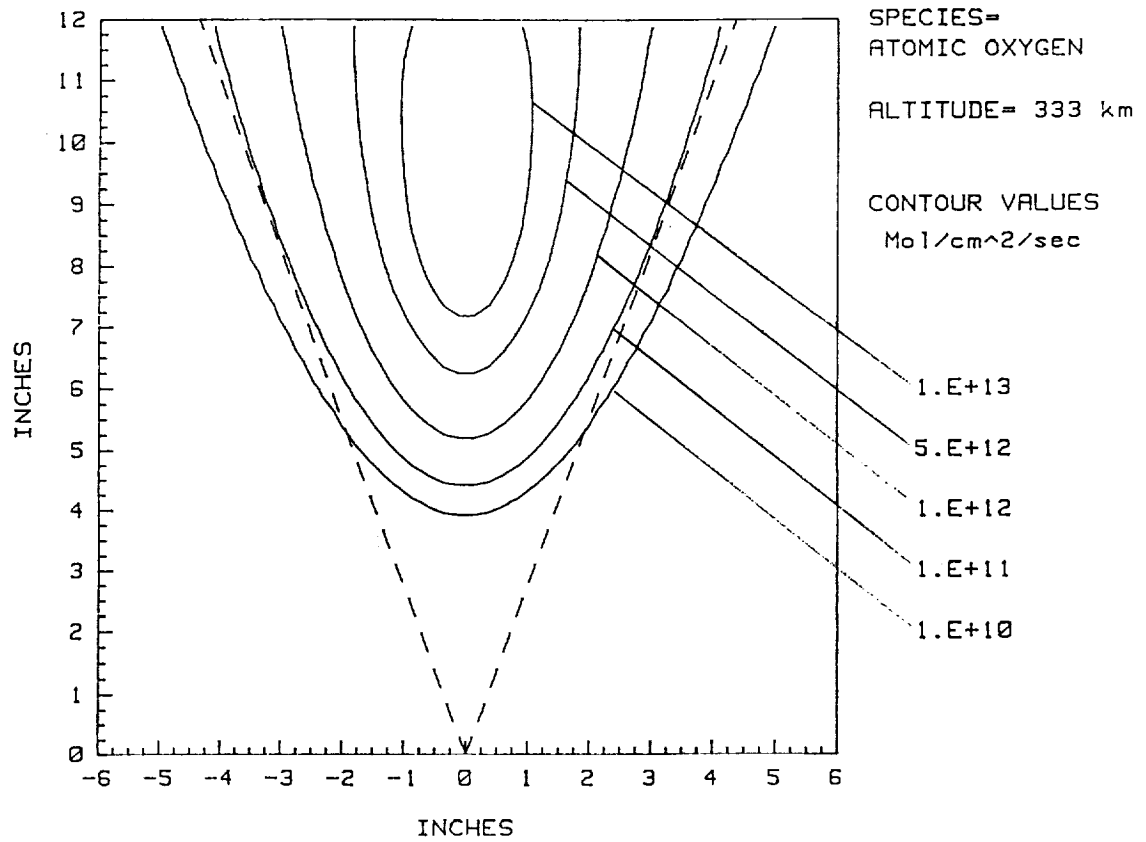
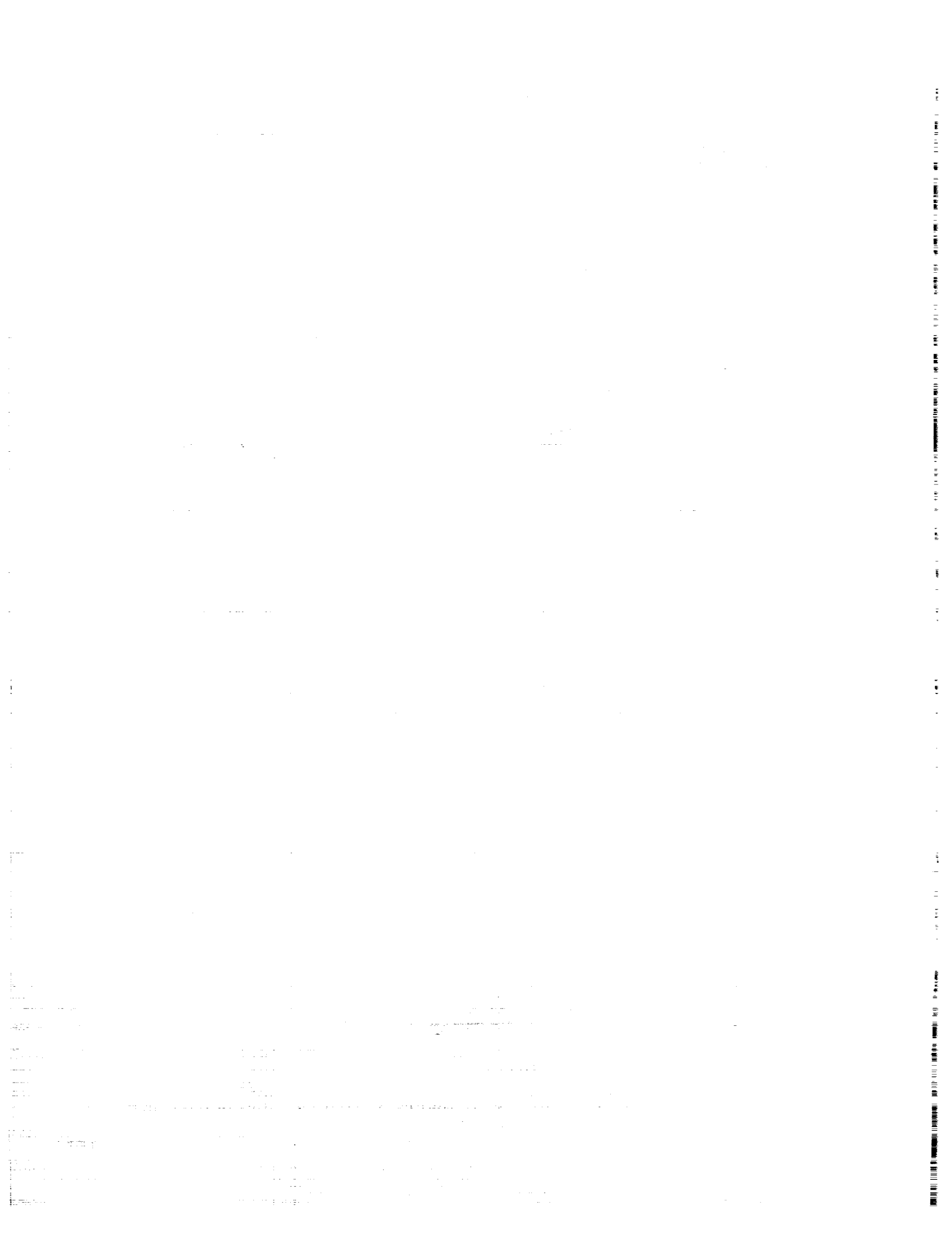


Figure 15. Iso-flux contours of atomic oxygen on internal surface.



SURFACE CONTAMINATION ON LDEF EXPOSED MATERIALS *

C. S. Hemminger
The Aerospace Corporation
El Segundo, CA 90245
Phone: 310/336-1619; Fax: 310/336-5846

ABSTRACT

X-ray photoelectron spectroscopy (XPS) has been used to study the surface composition and chemistry of Long Duration Exposure Facility (LDEF) exposed materials including silvered Teflon (Ag/FEP), Kapton, S13GLO paint, quartz crystal monitors (QCMs), carbon fiber/organic matrix composites, and carbon fiber/Al alloy composites. In each set of samples, silicones were the major contributors to the molecular film accumulated on the LDEF exposed surfaces. All surfaces analyzed have been contaminated with Si, O, and C; most have low levels (<1 atom %) of N, S, and F. Occasionally observed contaminants included Cl, Na, K, P, and various metals. Orange/brown discoloration observed near vent slots in some Ag/FEP blankets were higher in carbon, sulfur, and nitrogen relative to other contamination types. The source of contamination has not been identified, but amine/amide functionalities were detected. It is probable that this same source of contamination accounts for the low levels of sulfur and nitrogen observed on most LDEF exposed surfaces.

XPS, which probes 50 to 100 Å in depth, detected the major sample components underneath the contaminant film in every analysis. This probably indicates that the contaminant overlayer is patchy, with significant areas covered by less than 100 Å of molecular film. Energy dispersive x-ray spectroscopy (EDS) of LDEF exposed surfaces during secondary electron microscopy (SEM) of the samples confirmed contamination of the surfaces with Si and O. In general, particulates were not observed to develop from the contaminant overlayer on the exposed LDEF material surfaces. However, many SiO₂ submicron particles were seen on a masked edge of an Ag/FEP blanket.

In some cases such as the carbon fiber/organic matrix composites, interpretation of the contamination data was hindered by the lack of good laboratory controls. Examination of laboratory controls for the carbon fiber/Al alloy composites showed that preflight contamination was the most significant factor for all the contaminants generally detected at < 1 atom % , or detected only occasionally (i.e., all but Si, O, and C). Flight control surfaces, including sample backsides not exposed to space radiation or atomic oxygen flux, have accumulated some contamination on flight (compared to laboratory controls), but experimentally, the LDEF exposed surface contamination levels are generally higher for the contaminants Si and O.

For most materials analyzed, Si contamination levels were higher on the leading edge surfaces than on the trailing edge surfaces. This was true even for the composite samples where considerable atomic oxygen erosion of the leading edge surfaces was observed by SEM. It is probable that the return flux associated with atmospheric backscatter resulted in enhanced deposition of silicones and other contaminants on the leading edge flight surfaces relative to the trailing edge. Although the Si concentration data suggested greater on-flight deposition of contaminants on the leading edge surfaces, the XPS analyses did not conclusively show different relative total thicknesses of flight-

* This work was supported by Air Force Space Systems Division contract F04701-88-C-0089.

deposited contamination for leading and trailing edge surfaces. It is possible that atomic oxygen reactions on the leading edge resulted in greater volatilization of the carbon component of the deposited silicones, effectively "thinning" the leading edge deposited overlayer. Unlike other materials, exposed polymers such as Kapton and FEP-type Teflon had very low contamination on the leading edge surfaces. SEM evidence showed that undercutting of the contaminant overlayer and damaged polymer layers occurred during atomic oxygen erosion, which would enhance loss of material from the exposed surface.

INTRODUCTION

In the course of LDEF post-retrieval investigations, XPS has been used to study the surface composition and chemistry of exposed materials including Ag/FEP, Kapton, S13GLO paint, QCMs, carbon fiber/organic matrix composites, and carbon fiber/Al alloy composites. One objective of this study was to compare typical surface contamination types and coverages on leading and trailing edge LDEF exposed surfaces for a variety of materials. Analysis of anomalies and other "nonrepresentative" areas was generally avoided in an attempt to maximize data acquisition for areas with average exposure to the space environment. XPS is an excellent surface analysis technique for the study of contaminant overlayers. Each XPS analysis provides an average semi-quantitative surface composition over an area approximately 4 x 5 mm, with an analysis depth of 50 to 100 Å. All elements can be detected except hydrogen and helium. The details of electron energies and peak shapes give information about the chemical state of many elements in the sample surface. Minimal sample preparation of LDEF exposed materials was required for XPS analysis, and the analysis was nondestructive unless the surface components were radiation sensitive. Surface charging of insulators and semiconductors does not pose a major problem for the XPS technique, allowing straightforward analysis of surface oxides and contamination layers. Complementary SEM/EDS analysis was used to look at many of the same samples. EDS analysis provides an average semi-quantitative surface composition over the area rastered by the electron beam, with an analysis depth of $\leq 1 \mu\text{m}$.

EXPERIMENTAL

The LDEF exposed materials and their reference samples investigated in this study are listed in Table I. The LDEF experiment and exposure position of the samples is included in the Table, where the notation "D9" indicates bay D/row 9 of LDEF. Some materials were analyzed with no sample preparation other than mounting on an appropriate sample stub. Most, as indicated in Table I, were cut to provide samples that could be introduced into the analysis system. Additional information about the materials is given in Table II.

The LDEF exposed and reference samples were analyzed by XPS using a VG Scientific LTD ESCALAB MK II instrument. The samples were mounted on sample stubs with strips of tantalum foil or with double-sided tape. Survey scans from 0 to 1100 eV binding energy were acquired to qualitatively determine the sample surface composition. Analysis areas were about 4 x 5 mm in size and analysis depth was about 50 - 100 Å. Data acquisition with a Mg K α and an Al K α source was used to check for all the elements of interest. High resolution elemental scans were subsequently run to obtain semi-quantitative elemental analyses from peak area measurements and chemical state information from the details of binding energy and shape. Measured peak areas for all detected

elements were corrected by elemental sensitivity factors before normalization to give surface mole %. The quantitation error on a relative basis is $\leq 10\%$ of the measurement for components with a surface concentration >1 mole %. Large uncertainties in the relative elemental sensitivity factors can introduce absolute errors of a factor of 2 or even greater. The detection limit is about 0.1 surface mole %, but spectral overlaps between large peaks and small peaks can make it impossible to detect minor components, particularly when more than one chemical state is present for a given element.

A JEOL 840 SEM with an EDAX 9900 EDS system was used for the SEM/EDS analyses. Nonconductive surfaces were coated by carbon evaporation to minimize surface charging effects.

RESULTS AND DISCUSSION

Contamination on Composite, Paint, and QCM Surfaces

The XPS data for the carbon fiber/Al alloy composite samples are shown in Table III. The entire XPS signal should come from the 2024 Al alloy surface foil, which was shown to be intact by SEM, and its contamination overlayer. The flight surfaces had visible discoloration. The exposed side of the trailing edge sample had a pale brown stain. The exposed side of the leading edge sample had a rainbow-like light dispersion in some areas, and its backside had a very pale brown stain. The laboratory and flight control surfaces did not have visible discoloration. The flight control sample had been mounted on the backside of the D4 cassette.

The laboratory control surfaces were contaminated with C, Si, N, Na, K, Ca, F, Cl, P, and S. Pre-launch contamination was clearly significant. This points out how laboratory control samples can be critical to the assessment of on-flight contamination and material modification. The flight control surfaces and sample backsides (another commonly used "flight control") had higher concentrations of Si contamination than the lab control surfaces by more than a factor of 2. The observed variability for Si (7 to 28%) on these four surfaces was a factor of 4, showing the inherent inaccuracy of using only flight controls for comparison to the exposed surfaces. The contamination on the leading edge sample backside surface was particularly high, possibly due to preflight or postflight contamination. The Si concentration on the exposed surfaces was a factor of 2 higher than on the flight controls. Si contamination was about 25% higher on the leading edge exposed surface than on the trailing edge exposed surface. Si was detected predominantly as SiO_2 on both exposed flight surfaces and on the leading edge sample backside; this assignment was based on a $\text{Si}2p$ binding energy of 103.5 ± 0.2 eV after charge correction. On the other surfaces, the $\text{Si}2p$ peak was detected at lower binding energy, 102.9 ± 0.3 eV, which indicated surface silicone or possibly mixed silicone/silicate/silica. It was not possible to determine the source of carbon on the flight surfaces: it could come from silicone and/or hydrocarbon deposition and/or from the preflight contaminant overlayer.

Aluminum was detected as the oxide, Al_2O_3 , on all sample surfaces, as would be expected for air-exposed alloy. It is possible that postflight air oxidation could mask on-flight changes. Only the predominant chemical state of the alloy surface could be detected in the presence of the contaminant overlayer. The weak Al signal ($<1\%$) on the exposed flight surfaces implies a contaminant coverage at least comparable to the depth probed by XPS, 50 to 100 Å. In the case of noncontinuous or nonuniform coverage, the average thickness of the contaminant overlayer could be substantially

greater. Stronger Al signals (3 to 11%) on the control and trailing edge backside surfaces indicate relatively lower contaminant thickness/coverage.

The XPS data for the carbon fiber/organic matrix composites are shown in Table IV. The composites were designated as A, B, and C, and had been fabricated with differences in the matrix. The "L" and "T" prefixes in Table IV indicate leading and trailing edge, respectively. No laboratory control samples were available for these samples, and the sample backsides were used as the flight controls. These carbon/poly(arylacetylene) (PAA) materials were under development at The Aerospace Corporation in 1984 as replacements for more traditional composites such as carbon/epoxy. The exposed leading edge surfaces were visibly eroded. SEM and optical microscopy showed the erosion to be irregular to a depth of about 5 mils.* The erosion morphology was dominated by crevasses parallel to the fibers, with triangular cross sections. The edges of the crevasses were well-defined and penetrated through both matrix and fibers. The exposed trailing edge samples and sample backsides exhibited no physical appearance changes due to exposure.

Comparison of Si concentration on leading and trailing edge surfaces showed a much broader range of values on the leading edge: 3 to 19% Si on the leading vs. 4 to 7% on the trailing edge. A comparison of the Si concentration on pairs of leading and trailing edge composites gave the widely varied ratios of 1.7, 4.8, and 0.4. Si contamination was highest on sample L-B, which had lower erosion than L-A and L-C. Composite B had the lowest resin content of the three: 22% by weight compared to 37% and 33% for composites A and C, respectively. It is unknown if the surface contamination plays a role in erosion crevasse initiation and enlargement. Si concentration on the sample backsides ranged from 2 to 4%. Si ratios for exposed leading edge surfaces to their backsides were 5.0, 6.3, and 0.8. Si ratios for exposed trailing edge surfaces to their backsides were 3.0, 2.0, and 1.8. The predominant chemical state of Si detected was SiO₂ on all of the exposed surfaces, both leading and trailing edges. The Si detected on the samples backsides was predominantly from silicone or mixed silicone/silicate/ silica. The lack of laboratory controls prevents conclusions about changes in the composite surface chemistry and about the wide range of minor contaminants, including N, F, S, Cl, Cu, Zn, Ni, Sn, Na, and P. One surface had 25% F; release cloth used in fabrication is the most likely source of fluorocarbon contamination. It is likely that preflight contamination is significant as a source of minor contaminants.

The XPS data for S13GLO paint are shown in Table V. There were no flight control or backside surfaces, nor were laboratory controls maintained. A laboratory reference was prepared for comparison from a current batch of S13GLO. Visible changes were seen in the flight surfaces. The trailing edge surfaces had brown discoloration, with some lighter lines and spots. Little discoloration was observed on the leading edge surfaces. Interpretation of surface contamination was complicated because the binder is methyl silicone, and by the lack of a same-batch laboratory control. On all flight exposed surfaces, the C signal decreased and the O signal increased, relative to Si. The Si2p binding energy and O to Si concentration ratio changed from silicone to SiO₂ on leading and trailing edge surfaces. Exposure to UV radiation and atomic oxygen in the space environment caused silicone degradation, with resulting formation of SiO₂ and loss of carbon through volatiles. This investigation was inconclusive on the question of silicone binder decomposition vs. silicone contaminants deposition/decomposition as the source of measured surface Si. It was observed that the leading edge surfaces had greater loss of carbon than trailing edge surfaces. The SEM analysis was inconclusive on whether a significant amount of binder was lost from leading edge surfaces due to atomic oxygen erosion. K and Zn from the pigment were detected on all flight samples, but not on

* J. J. Mallon, J. C. Uht, and C. S. Hemminger: Surface Analyses of Composites Exposed to the Space Environment on LDEF. Submitted for publication, 1991.

the reference. This may indicate some binder loss, but it may also be due to a difference between batches of S13GLO.

The XPS data for the QCM crystals are shown in Table VI. The reference crystals served as flight control samples for the sense crystals. Laboratory control samples have not been made available. The flight surfaces were not visibly altered by space environment exposure. The QCMs were disassembled at QCM research and all the crystals were cleaned in acetone at that time, before delivery to The Aerospace Corporation for analysis. Solvent washing can remove some surface contaminants and leave new residues. It is possible that these residues explain the observation that most of the crystal surfaces were contaminated with $\geq 50\%$ carbon. SEM/EDS analysis showed the thin 150Å top layers to still be present on all the crystals. Thus, the low signals for In, Zn, and Al, $< 1.5\%$ for all crystal surfaces, indicate average contamination coverage comparable to the depth of analysis. Si contamination was detected on all but one surface, a reference crystal. The Si surface contamination was higher on the leading edge surfaces relative to the trailing edge surfaces for both sense and reference crystals, but was highest for the leading edge sense crystals at 10 and 23%. The Si concentration leading edge/trailing edge ratio for the flight exposed sense crystals was 4 for the passive QCMs and 15 for the active QCMs. The predominant Si species on both leading edge exposed surfaces was SiO₂. On all other crystal surfaces, Si was detected as silicone or a mix of silicone/silicate/silica. Some of the surface contamination observed on the crystal surfaces may be due to other components of the QCMs, such as Sn and Pb from solder, or N and Ag from conductive epoxy.

Conclusions

An overview of the XPS analyses of LDEF exposed composite, paint, and QCM crystal surfaces shows their surface contamination to be nonuniform and complex. Interpretation of the data is hindered by the uncertainty of preflight and postflight contaminants, and by the lack of comparable laboratory and flight controls for each type of material. However, the following observations are consistent for all of these samples. Silicones were a major contributor to the accumulated molecular film. The predominant surface species of Si was identified as SiO₂ on almost all of the exposed flight surfaces, and as silicone or a mix of silicone/silicate/silica on flight controls including backside surfaces. It is thought that UV and atomic oxygen exposure causes decomposition of surface-deposited silicones, with SiO₂ as one of the products. For most pairs of samples, the Si contamination level was higher on the leading edge surface than on the trailing edge surface. Measured Si concentration leading edge/trailing edge ratios varied from 0.4 to 15, with a median of about 1.5 and an average of about 4. Atmospheric backscatter could play a major role in enhancing non-line-of-sight deposition of outgassed species onto the leading edge exposed surfaces.

It was not possible to use the XPS data to distinguish hydrocarbons or other organic species deposited during flight from the preflight, postflight, and substrate sources of surface carbon. The relative surface carbon concentration is generally higher on the trailing edge exposed surfaces than on the leading edge surfaces. There could be significant contributions to this carbon coverage from preflight and/or postflight contamination (available controls indicate that most samples have only minor Si preflight contamination). It is also possible that atomic oxygen reactions on the leading edge result in greater volatilization of the carbon component of the deposited silicones, effectively "thinning" the leading edge deposited overlayer.

It was difficult to assess changes in the surface chemical states of these samples because of their tendency to oxidize and hydrate in earth environment. Preflight and postflight surface chemical state could differ from on-flight condition. The flight control samples, including backsides, have accumulated some contamination. This contamination varied significantly in concentration from one control surface to the next, but on average was significantly thinner than on space environment exposed surfaces. Lower contaminant concentrations and higher substrate signals from the flight control surfaces are both consistent with this conclusion. Element signals from the substrate were weak, but were detected on every flight exposed surface where it was possible to differentiate between contaminant film and substrate components. This would be consistent with a contaminant film that has an average thickness of 50 to 100 Å. The contaminant overlayer is probably patchy, with significant areas covered by less than 100 Å, and other areas by greater than 100 Å of molecular film. No pattern of significant difference was noted between substrate signals for leading edge and trailing edge exposed surfaces. Thus, although the Si concentration data suggests greater on-flight deposition of contaminants on the leading edge surfaces, the substrate signal data shows that the XPS data is not conclusive on the relative thicknesses of flight-deposited contamination for leading and trailing edge surfaces.

Contamination on Polymer Surfaces

Polymeric materials on LDEF were represented in this study by exposed surfaces of Kapton and fluorinated ethylene (FEP) Teflon from Ag/FEP thermal control blankets. In general, polymer surfaces are clean and reproducible and stable in the earth environment. This simplified postflight analysis of LDEF exposed polymers and provided a good opportunity to observe carbon contamination and minor contaminants deposited on-flight. Good controls were available for the polymers, and preflight complications were found to be minimal for FEP and Kapton. Changes in the surface chemical state of the polymer surfaces were readily observed. These have been attributed to space environment exposure, though postflight exposures to air may have as-yet undetermined effects on damaged polymer surfaces.

A variety of visible changes were observed in the Ag/FEP surfaces on both leading and trailing edge samples. The exposed leading edge blanket surfaces appeared uniformly foggy or clouded. The exposed trailing edge blanket FEP surfaces were "patterned" in some areas with alternating transparent and clouded bands. Clouded areas were observed on many blanket edges, particularly near the bends between exposed and masked material ("transition zone"). Areas of orange/brown discoloration were notable near some of the keyhole-shaped vent slots along the edges of the Ag/FEP blankets.

The SEM and XPS results (Ref. 1) for the exposed Ag/FEP surfaces are summarized in Table VII. The leading edge samples, from row 7 to 11, all had roughened surfaces typical of high velocity atomic oxygen erosion of FEP, as seen in Figure 1 for FEP exposed on C11 compared to a featureless control surface. The highly textured surfaces gave rise to diffuse light scattering and the consequent cloudy appearance. The XPS data for the control surface showed carbon and fluorine only. The XPS analysis of the exposed surfaces showed that the surface composition of the FEP remaining after the erosion was indistinguishable in carbon and fluorine composition from the control, with trace amounts of some contaminants (Si, N, S, and Cl) and measurable oxygen present. This oxygen could be from the atomic oxygen interaction or from water adsorption from the atmosphere after retrieval. Water adsorption could be enhanced on the erosion-roughened surfaces

which have much higher surface area than the control. The surface chemistry of these leading edge samples was identical to clean FEP Teflon, judged by a comparison of the F:C mole ratio and the C1s peak shape. The C1s spectrum from the D7 blanket surface is shown in Figure 2a; curve-fitting revealed the major CF₂ peak at 292 eV and moderate CF and CF₃ peaks (approximately 10% each) at 289.5 eV and 294 eV, respectively. This matched the spectrum predicted for FEP with an approximate ethylene/propylene comonomer blend of 90%/10%. It appeared that deposited contaminants and damaged polymer were both removed during atomic oxygen erosion.

The FEP surfaces exposed on the trailing edge of LDEF underwent changes which were observed both by SEM and XPS. The surfaces lost the smooth, featureless texture of the unexposed FEP, even when the amount of contamination remained low, as indicated by low silicon concentration. SEM showed an intriguing variety of new surface textures. Within short distances on some trailing edge samples, both the surface morphology and surface contamination levels were observed to change dramatically, as seen in Figure 3. The FEP surfaces nearest to the trailing edge row 3 were moderately to heavily contaminated and the blanket surface areas which appear fogged or cloudy on the trailing edge had become sufficiently diffuse to change visibly. The contamination was very nonuniform. It is currently not clear if any causal relationship exists between observed morphology type and surface contamination build-up. It is possible that some morphologies will have a higher probability of trapping or adsorbing outgassed or backscattered species, thereby leading to greater surface contamination buildup. Further from row 3, FEP surfaces showed little texture development and no significant contamination except oxygen, possibly from postflight exposure. It is possible that low atomic oxygen exposure on rows 1, 5, and 6 was sufficient to remove the contaminant overlayer.

XPS data divided the trailing edge surfaces into two categories. The first was characterized by low contamination levels (Si < 1%) and a C1s spectrum, as in Figure 2b, that differs significantly from that of clean FEP, but does not have a major peak at 285 eV. The second category was characterized by moderate to high levels of surface contamination (Si, O, C, N, and S, and sometimes Cl) and a C1s spectrum dominated by a peak at 285 eV, as seen in Figure 2c and d. Contaminant carbon was distinguishable from FEP and degraded FEP carbon by binding energy, and was measured at $\leq 20\%$ of the total surface composition. The C1s peak at 285 eV is predominantly due to C-C bonds, and is thought to build up on the trailing edge surfaces from decomposition products of outgassed silicones and hydrocarbons. The C1s spectrum in Figure 2b arises from degradation of the FEP surface, for which the C1s spectrum is shown in Figure 2a. Curve-fitting shows that the decrease in intensity of the CF₂ peak at 292 eV is accompanied by major increases in intensity at 294 eV, 289.5 eV, and 287 eV, assigned to CF₃, CF, and C-(CF_n)₄, respectively. These changes are consistent with damage to the carbon backbone of the Teflon polymer resulting in molecular weight degradation, new chain terminations, branching, and crosslinking through free radical reactions. The solar ultraviolet (UV) radiation exposure of the LDEF surfaces is thought to have caused this FEP surface degradation. The FEP surfaces were also exposed to the stress of about 34,000 thermal cycles, but the maximum temperatures calculated for Ag/FEP blankets on LDEF are less than 0°C (Ref. 2) and not sufficient to break chemical bonds. Exposure of FEP to the XPS x-ray source for several hours induced similar shifts in the C1s spectrum; almost all of the FEP C1s spectra used for curve-fitting in this study were acquired during the first minute of sample exposure to the x-ray source to minimize surface degradation from the analysis itself. A recent study of the degradation of polytetra-fluoroethylene (PTFE) Teflon by 3 keV electrons showed very similar XPS C1s spectra changes to those seen in Figure 2b as a function of electron irradiation and subsequent heating to drive off volatiles (Ref. 3). Degradation of the PTFE was attributed to the type of damage described above.

The predominant chemical state of Si identified on the trailing edge FEP surfaces was SiO₂. Si concentrations were measured to be ≤ 20 mole %, indicating up to about 60% as the oxide. The contaminant film was definitely nonuniform over large areas, and was probably patchy on a submicron scale. Significant areas must be covered by $< 100 \text{ \AA}$ of deposited contamination, because fluorocarbon was detected on each FEP surface analyzed. The damaged FEP layer is probably thicker than the depth of analysis.

The Ag/FEP thermal control blanket edges were contaminated, in many cases more than the exposed surfaces. Therefore, the masked edges did not provide good flight "control" samples. The transition zone from the exposed surface to the masked edge was particularly prone to contamination build-up. This was probably the result of the combination of high out-gas flux and radiation. The blankets were bent down around the edges of the tray so that the blanket edges were not rigorously shielded from radiation. SEM images from one transition zone, seen in Figure 4, showed that during atomic oxygen erosion of the FEP surface, undercutting of the contamination and damaged polymer layer played a role in the development of a clean, highly textured surface. Area A, at the periphery of the exposed surface, had a characteristic atomic oxygen erosion pattern. Area D, closer to the blanket edge, was a surface with contamination coverage and UV degraded FEP. Area C, in the center of the transition zone, showed undercutting of the contamination and damaged polymer layer by atomic oxygen erosion. The development of submicron particles of SiO₂ was observed on some edge surfaces by SEM/EDS, as seen in Figure 5. Such particle development was not detected on any of the other samples included in this study. Areas of orange/brown contamination were observed on some Ag/FEP surfaces near keyhole-shaped vent slots in the blanket edges. XPS analysis showed these stains to be high in carbon, sulfur, and nitrogen relative to other contaminated areas. The source of contamination was not identified, but it appears to have contained an amine/amide functionality.

Only two samples of Kapton, from leading edge F9, have been analyzed to date, but the results complemented those for leading edge FEP Teflon. SEM analysis showed the leading edge Kapton had heavy atomic oxygen erosion. Contaminant build-up, as seen in Table VIII, was low due to that erosion, totalling < 4 surface mole % excluding oxygen. The observed surface oxygen concentration increases were associated with these contaminants as well as with polymer oxidation. A 5% increase in oxygen-containing surface functionalities was measured by C1s spectrum curve-fitting.

SUMMARY

XPS was used to study the average surface composition and chemistry of a variety of LDEF exposed materials. XPS gives excellent surface sensitivity and element detection for contaminant analysis, with minimal sample alteration. SiO₂ and other decomposition products of silicones exposed to the space environment were identified as the predominant surface contaminant for every type and location of material. Deposited carbon residues were distinguishable from preflight contamination on Ag/FEP surfaces. This carbon is thought to come from silicones decomposition and organic contaminants, including the source of the orange/brown stains which had increased carbon, sulfur, and nitrogen concentrations relative to other deposits. Most of the minor (< 1 atom %) and occasionally-observed contaminants on the LDEF exposed surfaces were attributed primarily to preflight contamination. This clearly demonstrated the need to maintain good laboratory controls during the study of space environmental effects on materials.

The flight controls (no direct line of sight to the space environment) were found to have accumulated some contamination, but generally less than exposed surfaces. The polymeric materials studied had low contamination on the leading edge surfaces due to atomic oxygen erosion. All other materials had higher average Si contamination on leading edge than on trailing edge surfaces, probably due to the return flux associated with atmospheric backscatter. For individual pairs of samples, measured Si concentration leading edge/trailing edge ratios varied from 0.4 to 15, with a median of about 1.5 and an average of about 4. Element signals from some substrates were weak, but were detected on every flight exposed surface where it was possible to differentiate between contaminant film and substrate components. This would be consistent with a contaminant film that has an average thickness of 50 to 100 Å. The contaminant overlayer is probably patchy, with significant areas covered by less than 100 Å, and other areas by greater than 100 Å of molecular film. No pattern of significant difference was noted between the intensity of substrate signals for leading edge and trailing edge exposed surfaces. Thus, although the Si concentration data suggested greater on-flight deposition of contaminants on the leading edge surfaces, the XPS analysis was not conclusive on the relative total thicknesses of flight-deposited contamination for leading and trailing edge surfaces.

ACKNOWLEDGMENTS

The author would like to acknowledge the many contributors to this work within The Aerospace Corporation, including T. Giants, S. Gyetvay, C. Jagers, T. Le, J. Mallon, N. Marquez, M. Meshishnek, G. Radhakrishnan, G. Steckel, W. Stuckey, C. Su, and J. Uht. In addition, I would like to thank H. G. Pippin of Boeing Aerospace & Electronics, W. Slemp of NASA Langley Research Center, E. Lan of McDonnell Douglas Astronautics Company, and D. Wallace of QCM Research for making samples available to us. I also thank D. Wheeler of NASA Lewis Research Center for his helpful discussions on Teflon radiation damage.

REFERENCES

1. C. S. Hemminger, W. K. Stuckey, and J. C. Uht: Space Environmental Effects on Silvered Teflon Thermal Control Surfaces. First LDEF Post-Retrieval Symposium, June 1991. NASA CP 3134, 1992.
2. W. M. Berrios and T. R. Sampair: LDEF Post Flight Thermal Analysis. LDEF Science Office, NASA Langley Research Center.
3. D. R. Wheeler and S. V. Pepper: X-ray Photoelectron and Mass Spectroscopic Study of Electron Irradiation and Thermal Stability of Polytetrafluoroethylene. *J. Vac. Sci. Technol.* vol A8, no. 6, Nov/Dec 1990, pp. 4046-4056.

TABLE I. I.D.E.F. EXPOSED MATERIAL AND REFERENCE SAMPLES INVESTIGATED

I.D.E.F. exposed material	Experiment and location	Sample preparation	Reference samples
Carbon fiber/Al alloy composite	M0003; D8 and D4	1/2 inch squares cut	Flight controls Laboratory controls
Carbon fiber/organic matrix composites	M0003; D9 and D3	1/2 inch squares cut	Backside flight controls
SI3GLO paint	M0003; D9 and D3	As-received	Laboratory reference
Quartz crystals from QCMs	M0003; D9 and D3	Crystals dismounted from QCMs and acetone-washed at QCM Research	Reference QCM crystals
Kapton	A0076; F9	1/2 inch square cut	Laboratory reference
Ag/FEP, thermal control blankets	A0004-1; F2 A0178; D1, A2, A4, F4, B5, C5, D5, C6, B7, D7, C8, A10, C11, D11	1/2 inch squares cut	Laboratory controls Masked edge flight controls
Ag/FEP, adhesively mounted thermal control sheets	M0003; D9 A0076; F9	1/2 inch squares cut	Laboratory references Masked edge flight controls

TABLE II. I.D.E.F. EXPOSED MATERIAL INFORMATION

I.D.E.F. exposed material	Supplier	Additional information
Carbon fiber/Al alloy composite	Fiber Materials, Inc.	GY70 graphite fibers, manufactured by BASF Structural Materials Inc., reinforcing Al alloy 201 matrix with 2024 Al alloy surface foils. Major components of 2024 alloy are 93% Al, 4.4% Cu, 1.5% Mg and 0.6% Mn.
Carbon fiber/organic matrix composites	The Aerospace Corporation	T300 woven fabric, manufactured by Amoco Performance Products, Inc., reinforcing poly(arylacetylene) materials that were under development at The Aerospace Corporation in 1984.
SI3GLO paint	I. I. T. Research Institute; coupons made by TRW	White thermal control paint. Zinc oxide pigment encapsulated in potassium silicate with a methyl silicone binder.
Quartz crystals from QCMs	QCM Research	Active QCMs used crystals with 9000 Å Al + Al ₂ O ₃ plus 150 Å In ₂ O ₃ top layer. The top layer on passive QCMs was 150 Å ZnS.
Kapton	E. I du Pont de Nemours & Co., Inc.	A polyimide.
Ag/FEP, thermal control blankets	Sheldahl	5 mil FEP Teflon, manufactured by E. I du Pont de Nemours & Co., Inc.
Ag/FEP, adhesively mounted thermal control sheets	Sheldahl	2 mil FEP Teflon, manufactured by E. I du Pont de Nemours & Co., Inc.

TABLE III. XPS DATA FOR CARBON FIBER/ALUMINUM ALLOY COMPOSITES

Sample		Surface Mole %, Normalized														
		Al	Mg	O	Si	C	Na	K	Ca	F	Cl	P	S	N	Sn	Cu
AL3-3, Leading Edge	Exposed	0.4	nds	65	29	6	tr	tr	nds	nds	tr	nds	nd	nd	nds	tr
	Backside	0.2	nd	65	28	4	2	nd	tr	tr	tr	nd	0.2	0.1	tr	tr
AL5-11, Trailing Edge	Exposed	0.7	nds	59	23	13	3	0.1	nds	0.3	0.2	nds	0.2	0.4	0.1	nds
	Backside	11	2	51	7	20	3	0.7	0.3	0.8	0.3	0.5	2	1	0.2	0.1
AL5-13, Flight Control	Side 1	5	0.8	43	11	37	0.7	0.2	0.3	0.6	0.4	0.2	0.3	1	0.2	tr
	Side 2	3	0.5	41	11	40	1	0.3	0.2	0.3	0.4	0.1	0.3	2	0.2	tr
AL3-14, Lab Control	Side 1	9	0.8	35	2	49	1	0.2	0.3	0.1	0.3	tr	0.4	2 ^v	nd	nds
	Side 2	8	1	35	3	49	1	0.2	0.3	0.1	0.2	0.3	0.3	2	nd	nds

tr = trace (<0.1)
 nd = not detected
 nds = not detected survey scan; no high resolution scan run

TABLE IV. XPS DATA FOR LDEF FIBER/ORGANIC MATRIX COMPOSITES

		Imaged?	Surface Mole %, Normalized										Ni	Sn	Na	P	
			C	O	Si	N	E	S	Cl	Cu	Zn						
L-A	Exposed	Yes	45	42	10	2		0.6		0.3							
	Exposed	No	44	44	8	1	0.4	0.5	tr	2	0.3						
	Backside	No	71	20	2	2	3	0.1	0.1	1	tr						
T-A	Exposed	No	51	36	6	2	3	tr	0.1	3	0.2		0.1				
	Backside	No	66	26	2	1	3	0.2	0.1	1							
L-B	Exposed	Yes	17	59	19	0.6	nd	0.3	0.1	2	tr	1		nd	0.3		
	Backside	Yes	59	31	3	2	2	0.2	0.2	2	nd			1	nd		
T-B	Exposed	Yes	45	23	4	0.9	25	0.1	0.1	1	0.1				0.1		
	Exposed	No	46	27	3	1	19	0.1	0.2	2	0.2				1		
	Backside	Yes	70	22	2	1	3	0.1	0.2	0.7	nd				0.2	nd	
L-C	Exposed	Yes	61	31	3	3	0.1	0.5	nd	0.3	nd		0.4	0.3	0.6		
	Backside	Yes	67	23	4	2	3	0.1	0.2	2	nd		nd	0.1	nd		
T-C	Exposed	Yes	47	39	7	2	0.4	0.2	0.4	5	0.4		tr	0.1	nd		
	Backside	Yes	65	24	4	1	0.3	nd	0.3	1	0.2		tr	nd	nd		
Release Cloth		No	39	4	0.7		56										

tr = trace
 nd = not detected in elemental scan
 blank = not detected in survey scan and no elemental scan acquired

TABLE V. XPS DATA FOR S13GLO PAINT

S13GLO Paint Sample		Surface Mole % (Normalized)									
		C	O	Si	K	Zn	N	S	Cl	Na	E
	Reference	44	30	26	0.2	nd	nd	nd	nd	nd	nd
L31V-18-17-1	Leading	12	56	27	1	0.5	2	0.3	0.5	0.3	0.1
L31V-18-18-2	Leading	13	56	27	1	0.5	2	0.2	0.5	0.3	0.1
T31V-18-17	Trailing	28	46	21	0.8	0.3	2	0.4	0.4	0.7	0.5
T31V-18-18	Trailing	27	47	21	1	0.2	2	0.4	0.4	0.8	0.4

TABLE VI. XPS DATA FOR QCM CONTAMINATION MONITORS

QCM		Surface Mole %, Normalized															
	Crystal	Top Layer	C	O	Si	In	Sn	Zn	S	Pb	K	Na	N	Cl	Al	Ag	
TP 329, Active	1	Sense	In ₂ O ₃	17	58	23	0.7	0.2	nd	0.1	nd	tr	0.3	0.8	tr	nd	nd
	2	Reference	In ₂ O ₃	53	31	1.9	6.4	1.0	0.1	0.1	0.5	0.1	1.0	4.5	0.2	nd	nd
TP 330, Passive	3	Sense	ZnS	48	35	10	nd	0.2	0.9	0.5	0.1	tr	0.4	3.5	0.1	1.4	nd
	4	Reference	ZnS	61	23	1.0	nd	0.2	2.0	5.5	0.3	tr	0.7	4.7	0.4	nd	1.2
TP 318, Active	5	Sense	In ₂ O ₃	68	25	1.5	nd	0.3	nd	0.1	0.3	nd	0.1	4.7	0.2	0.4	nd
	6	Reference	In ₂ O ₃	65	24	0.2	2.3	0.7	0.1	0.2	0.4	nd	0.1	6.3	0.1	nd	nd
TP 353, Passive	7	Sense	ZnS	67	25	2.3	nd	0.4	0.1	0.1	0.4	nd	0.1	4.5	0.3	nd	nd
	8	Reference	ZnS	68	20	nd	nd	0.3	1.4	3.9	0.3	tr	0.3	4.1	0.3	nd	0.6

tr = trace (<0.1)
 nd = not detected

TABLE VII. SUMMARY OF SEM AND XPS RESULTS

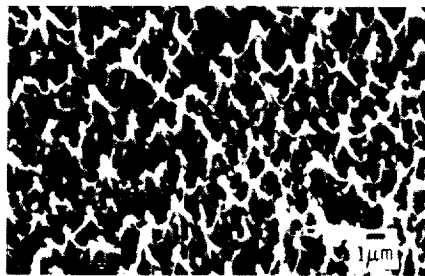
LDEF Row	SEM Morphology of Exposed FEP Surface	Bay	Surface Si%	Surface O%	CIs Envelope
1	Smooth; particulate contamination	D	0.2	2	Degraded FEP
2		A	0.7	6	Degraded FEP
2		F(Boeing)	2 - 8	11 - 32	Contamination
2	Puckered texture; more distinct in cloudy bands	F(NASA)	8 - 19	30 - 51	Contamination
3 (TE)					
4	Puckered and wrinkled textures in bands	F	0.2 - 7	4 - 31	Contamination
4		A	0.1	3	Degraded FEP
5	Slightly lumpy (B)	B, C, D	0.1	3 - 5	Degraded FEP
6	Some areas of puckered texture	C	<0.1	1 - 2	Degraded FEP
7	Eroded, sharp pinnacles (B)	B, D	<0.1	0.6	Clean FEP
8	Eroded, sharp pinnacles	C	<0.1	0.6	Clean FEP
9 (LE)		D, F	0.1 - 0.8	0.8	Clean FEP
10	Eroded, rounded peaks	A	0.1	0.6	Clean FEP
11	Eroded, sharp pinnacles (C)	C, D	<0.1	0.4	Clean FEP
12					
Control FEP	Smooth, featureless		<0.1	<0.1	Clean FEP

TABLE VIII. XPS DATA FOR KAPTON

Kapton Sample	Surface Mole %, Normalized								
	C	O	N	Si	Na	S	K	E	P
Reference	71	21	7.4	0.2	nd	0.1	nd	nd	nd
Exposed #1	62	28	6.8	2	1	0.4	0.3	0.1	tr
Exposed #2	64	27	6.8	1	1	0.3	0.2	0.1	tr

Scanning Electron Microscope Image

LDEF TRAY C11 EXPOSED TEFLON



CONTROL TEFLON SURFACE



Surface Composition Determined by X-Ray Photoelectron Spectroscopy

MOLE %

C	F	O	OTHER
27	72	0.4	TRACE SI, N, S, Cl
27	73	TRACE	NONE DETECTED

Figure 1. SEM images and surface composition of FEP. A leading edge surface with atomic oxygen erosion is compared to a featureless control surface.

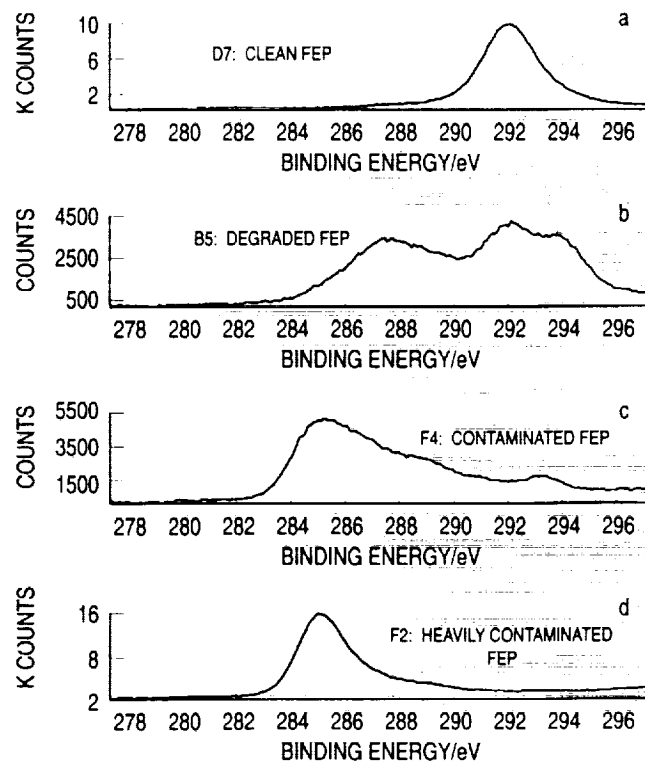


Figure 2a. XPS spectrum of the C1s peak of the D7 blanket surface. Representative of clean FEP.

2b. XPS spectrum of the C1s peak of the B5 blanket surface. Representative of degraded FEP.

2c. XPS spectrum of the C1s peak of the F4 blanket surface. Representative of contaminated FEP.

2d. XPS spectrum of the C1s peak of the F2 blanket surface. Representative of heavily contaminated FEP.

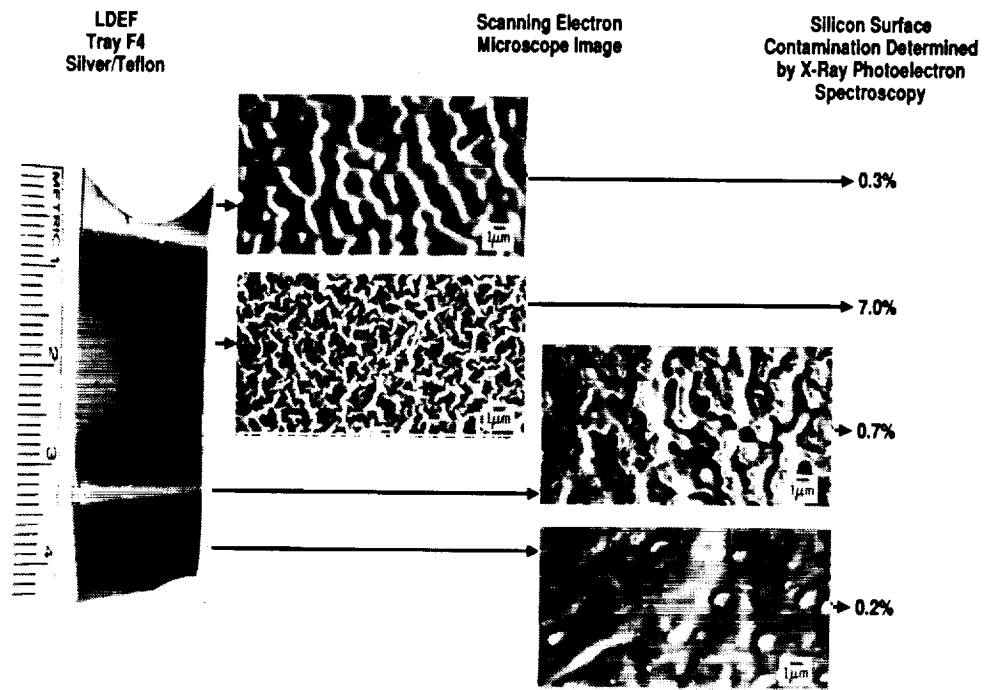


Figure 3. SEM images of surface morphology changes observed on a section of the trailing edge F4 blanket surface. The FEP surface appeared visibly patterned, as seen in the photograph on the left. The surface contamination, represented by Si concentration, was very nonuniform.

AO Erosion of A10 Thermal Blanket Edge Surface

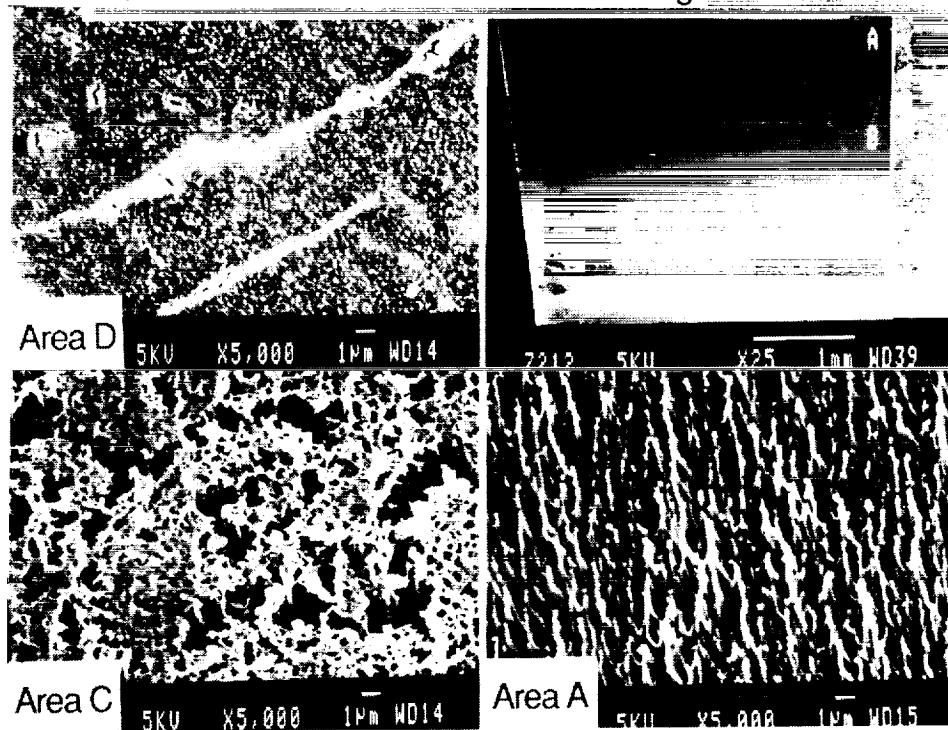


Figure 4. SEM images of a transition zone on the A10 blanket edge. Area A has the characteristic atomic oxygen erosion pattern. Area D is a surface with contamination coverage and UV degraded FEP. Area C shows undercutting of the contamination and damaged polymer layer.

C8: UNEXPOSED EDGE

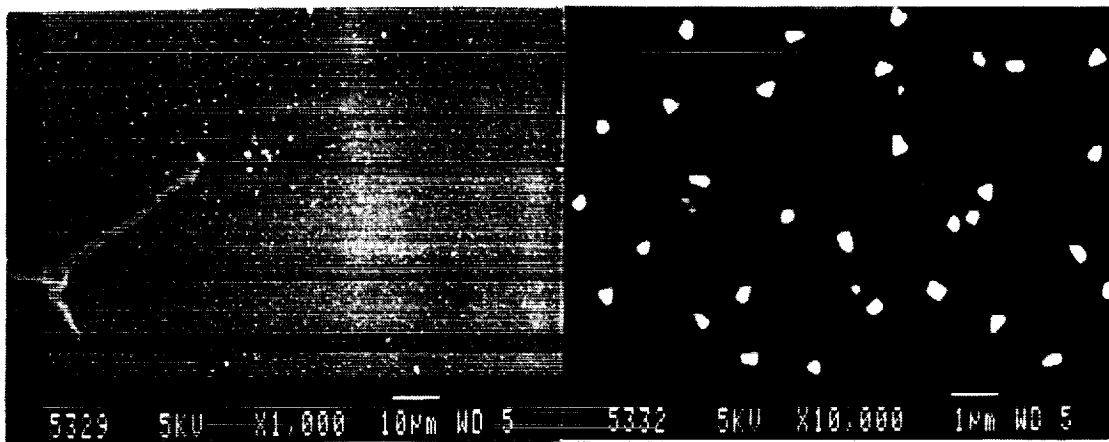


Figure 5. SEM images of submicron particles of SiO₂ on a masked edge surface of the C8 blanket.

SOURCES AND TRANSPORT OF SILICONE NVR

Gale A. Harvey

NASA Langley Research Center

Hampton, VA 23665-5225

Phone: 804-864-6742, FAX: 804-864-7790

SUMMARY

The retrieved LDEF had varying amounts of visible contamination films (brown stains) at many locations. FTIR spectra of heavy film deposits at vents and of optical windows from tray E5 indicated methyl silicone and silica in the contaminant films. Two possible sources of the methyl silicone are DC-710 phenyl methyl silicone in the shuttle-bay-liner beta cloth, and the shuttle tile waterproofing silane. It is concluded that much of the silicone and silica contamination came from ground operations and the orbiter.

INTRODUCTION

A brown stain of varying thickness was present on most of the retrieved LDEF (ref. 1). Several analyses have indicated significant silicone and silica in these stains (ref. 2). The source of the silicon, silica, or precursor silicones is not understood since most of the exposed surfaces of LDEF were anodized aluminum or urethane based paints. Organic silicones have strong absorptions in the 10 micrometer region of the spectrum. FTIR spectroscopy has been applied to LDEF samples, suspected silicones, and spacecraft facility witness plates at KSC in order to better understand the silicone contamination of LDEF.

MEASUREMENT TECHNIQUE

Fourier transform infrared spectroscopy (FTIR) was used for the identification of silicones and silica. The spectra are 4 cm^{-1} resolution and the spectrometer was optimized for the 5 to 10 micrometer region. The sample spectra are ratioed to a background spectrum to give transmission spectra. Sample residues are placed on IR transmitting windows (i. e., CaF_2 , MgF_2 , NaCl) and centered in the IR beam at the beam focus in the sample compartment. Additional information regarding FTIR spectroscopy for contamination analysis is in reference 3.

Solvent-wash plates are used in aerospace cleanrooms to measure accumulation of organic films. These witness plates are typically syringed with an aggressive solvent such as freon, chloroform, or methylene chloride. This solvent is allowed to evaporate in a fume hood and the residue is transferred to a weighing pan for mass measurement.

Organic films can also be removed from hardware or facility surfaces by wetting the surfaces with a solvent and then wiping the surface with an extracted cleanroom wipe (refs. 4, 5). The wipes are then extracted again by soaking for 30 minutes in spectroscopic grade isopropyl alcohol (IPA), the alcohol is evaporated, and the organic residue transferred to an IR window for measurement and analysis.

LDEF DATA

Some of the heaviest organic film deposits were on the ram direction edge of the 1/4 inch thick aluminum end plates (Figure 1). These end plates were at vent openings to the interior of LDEF and hence the organic films result primarily from outgassing from the interior. FTIR spectra of a scraping of film from an end plate is presented in figure 2. The absorption at 1260 cm^{-1} is identified as resulting from methyl silicone (SiCH_3). This absorption is normally spectral sharp and stable in frequency, and hence is a convenient and reliable indicator of a methyl silicone group in a molecule.

Calcium fluoride and magnesium fluoride windows were flown in tray E5 of LDEF. An IR spectrum of the calcium fluoride window is presented as figure 3. The 1260 cm^{-1} methyl silicone absorption is more pronounced here than in the vent scraping. The optical windows in tray E5 were mounted with Chorlastic R500 silicon rubber gaskets on the back side. Microscope examination revealed the windows had thin, brittle contamination films on both sides. However, the film on the center of the back surface of the magnesium fluoride window (figure 4) adhered to the gasket. The IR spectrum of only the front surface film is presented in figure 5. Again the 1260 cm^{-1} methyl silicone absorption is present. The broad absorption at 1050 cm^{-1} suggests silica. The 1260 cm^{-1} absorption in the front surface film suggests an external source rather than an interior source for much of the silicone.

The IR spectra of contamination on LDEF can be compared to spectra of typical spacecraft and cleanroom organic films. Figure 6 is the IR spectra of residue from Kapton multi-layer insulation which was used as a witness plate. Figure 7 is the IR spectra of residue from the cleanroom wipes used during integration and processing of the Upper Atmosphere Research Satellite (UARS). These spectra are dominated by strong carbonyl absorption at 1750 cm^{-1} and are not similar to spectra of contamination on LDEF.

Brown stains, similar to those on LDEF, have been reported in orbiter bays and on flight hardware. Such a stain in the Columbia bay after the LDEF retrieval is reported in reference 6. Photographs of faint brown stains in the Discovery bay after STS-48 were taken October 9, 1991, and are presented as figures 8 and 9. These stains suggest a possible nonpayload source of contamination.

BETA CLOTH OIL

Beta cloth is a woven fabric used for thermal control of spacecraft and is used to line much of the orbiters' bays. The fibers are about 10 micron diameter glass fibers coated with about a 10 micron layer of Teflon. Silicone oil is usually added to the fabric during manufacturing to enhance the mechanical properties (increase flexibility and reduce particle shedding) of the fabric. The DC-704 and DC-710 have vapor pressures of about 10^{-7} Torr at room temperature (ref. 7 and 8). Although the vapor pressure is low, all of this material is expected to outgas during long-term vacuum exposure. The expected mode of contamination at standard temperature and pressure is by contact transfer. The molecular structure for DC-704 (ref. 9) is presented as figure 10. Some beta cloths have as much as 100 mg/ft^2 of DC-710 extractable by soaking the cloth for 30 minutes in IPA. The beta cloth used in the Discovery bay for STS-48 had 10 mg/ft^2 of extractable silicone residue. The IR spectra of the residue from the Discovery bay liner beta cloth is presented in figure 11. The SiCH_3 absorption as well as the SiO absorptions are characteristically sharp and well defined in figure 11.

RTV-142 RESIDUE

RTV-142 is a silicone potting compound that was used on the UARS spacecraft and is believed to be representative of silicone potting compounds used sparingly on LDEF. Four measurements of NVR from RTV-142 were made. The four independent measurements are mass loss during vacuum bake, residue from 30 minute soak in IPA, mass spectroscopy via residual gas analyser, and baking in a vacuum gas cell.

The mass loss during a 24 hour bake at 70°C was ≈0.08 percent. The mass loss during a 24 hour bake at 160°C was ≈0.23 percent. The recovered NVR from a 30 minute soak in IPA was ≈0.5 percent. The IR spectra from the IPA soak is presented as figure 12. These spectra and 3.4 micrometer spectra indicate the residue is a phenyl methyl silicone. The RGA gives principal mass fragments of 15 (CH₃), 29 (CHO & C₂H₅), 31, and 43. Spectra of residue in the heated gas cell were similar to those from the IPA soak.

All of these tests indicated small mass loss of RTV-142 under vacuum. The higher mass recovered from IPA soaking compared to a 24 hour bake indicates slow outgassing.

PAYLOAD CHANGEOUT ROOM WASH PLATES

One foot square aluminum wash plates were exposed in the Payload Changeout Room (launch complex 39 PCR) during processing of the UARS spacecraft. Two wash plates were exposed during the period July 23 to August 13, 1991, near station 900 of the orbiter in the PCR. The plates were syringed with CH₂Cl₂ and the residues weighed. The residues were analyzed by the KSC Microchemical Analysis Branch (ref. 10). IR spectra of a transfer of residue with hexane is presented as figures 13 and 14. The spectra clearly show silicones, primarily dimethyl silicones. IR spectra of transfers of residue with CH₂Cl₂, a more aggressive solvent, show primarily carbonyl and C-O absorption. The hexane transferred residues indicate a light or volatile silicone.

STS-48 RESIDUES

A 14-inch by 14-inch square of 5 mil Kapton multi-layer insulation was attached to the UARS airborne support equipment (UASE) module during the STS-48 mission. The IR spectra of residue from an IPA syringe of this witness plate is presented as figure 15. Although only 0.01 mg of residue was recovered from this witness plate, SiCH₃ and SiO absorptions are strongly indicated. This witness plate was covered until August 13, 1991, and was retrieved from the shuttle bay October 9, 1991. The delay in retrieving this witness plate was due to the orbiter landing at Dryden rather than at KSC as planned, and conflicts in orbiter operations in the orbiter processing facilities.

Four dry wipes of the UARS Airborne Support Equipment (UASE) tool box, using extracted polyester wipes (ref. 4), were taken. IR spectra of a UASE dry wipe is presented as figure 16. Silicone absorption is indicated in the residue. However, some silicone is also indicated in residual residue of the control wipe (fig. 17) so caution should be exercised in interpretation of the UASE wipe data.

ORBITER TILE WATERPROOFING

The heat protective tile and upper surface external blankets of the orbiter are waterproofed to avoid unnecessary water absorption prior to launch. The waterproofing compound used for the STS-48 mission was dimethylethoxy silane (DMES). A diagram of the molecular structure of this material is presented as figure 18, and an IR spectrum is presented as figure 19. A strong SiH absorption is present at 2200 cm⁻¹ and methyl and methylene absorptions are also present at 2900 cm⁻¹.

This silane compound is used because it chemically reacts with the silica in the tiles to bond methyl silicones to the silica (ref. 11). About 200 pounds of DMES were used to waterproof the orbiter for STS-48*. DMES is extremely volatile; i. e., its vapor pressure is about 230 mm Hg at 20°C (ref. 12). The PCR wash plates suggest transfer of waterproofing compound in orbiter processing facilities.

A few drops of DMES were transferred to CaF₂ and NaCl windows placed on a deuterium lamp. A thin SiO₂ film (figure 20) was left on both of these windows. Therefore, DMES is a precursor to both methyl silicones (ref. 11) and silica.

DMES is not the silane used to rewaterproof the Challenger for the LDEF deployment. Hexamethyldisilazane (HMDS) was used to rewaterproof the Challenger for mission 41C.

* Palou, J., private comm., December 1991.

CONCLUSIONS

Several potential sources of silicone contamination from orbiter and spacecraft processing at KSC have been identified. The most suspect source is the orbiter tile waterproofing compound, a volatile silane. Further work is needed in order to better understand the role of the waterproofing compound in the production of the silicones and silica detected on LDEF.

REFERENCES

1. Harvey, G. A., "Organic Contamination of LDEF," Proc of First LDEF Post-Retrieval Data Conference, June 1991, NASA CP 3134, pp. 179-197, January 1992.
2. Crutcher, E. R., and K. T. Warner, "Molecular Films Associated with LDEF," Proc. of First LDEF Post-Retrieval Symposium, June 1991, NASA CP 3134, January 1992.
3. Harvey, G. A., and J. L. Raper, "Halogen Occultation Experiment (HALOE) Optical Witness-Plate Program," NASA TM 4081, February 1989.
4. Harvey, G. A., J. L. Raper, and D. C. Zellers, "Measuring Low-Level Nonvolatile Residue Contamination on Wipes, Swabs, and Gloves," *Microcontamination*, 8 (11): pp. 43-46, 69, 1990.
5. Raper, J. L., and G. A. Harvey, "Halogen Occultation Experiment (HALOE) Contamination Control Program," *Cleanroom Technology Forum Proceeding*, pp. 38-51 San Jose, CA, October 1991.
6. Maag, C. R., J. Houseman, and W. K. Linder, "Results of the Interim Operational Contamination Monitor (IOCM) as Flown on the STS-32 Mission," JPL Report D-8170, p. 150, March 1991.
7. Hall, D. F., T. B. Stewart, and R. R. Hayes, "Photo-Enhanced Spacecraft Contamination Deposition," AIAA 20th Thermophysics Conference, June 1985, Williamsburg, VA, p. 1-9, AIAA-85-0953.
8. Barrington, A. E., High Vacuum Engineering, Prentice-Hall, Inc., 1963.

9. Anon., Information about Silicone Fluids, Dow Corning, 1976.
10. Carman, W. R., "Analysis of NVR Samples STS-48 PCR Exposure," Laboratory Request MCB-0721-91, KSC Microchemical Analysis, September 1991.
11. Johnson, R. E., and D. Ford, "Studies of Silane Stability to Humidity and Temperature," LeTourneau University Research and Advanced Development Institute, April, 1990.
12. Anon., "Material Safety Data Sheet for Dimethylethoxysilane," HULS America Inc., 1992.

ACKNOWLEDGMENTS

Phil Klich (LaRC) and Sharon Straka (GSFC) assisted in obtaining HALOE and UARS witness plates at KSC. Barbara Lambert (GSFC) provided photographs of the Discovery bay. Jaime Palou (KSC) implemented the IR analysis of witness from the PCR. Bill Carman (KSC) performed the IR analysis of the PCR residues and reviewed the analysis in detail with the author. Tommy Leiffel (LaRC) provided samples of tile waterproofing compound (DMES).

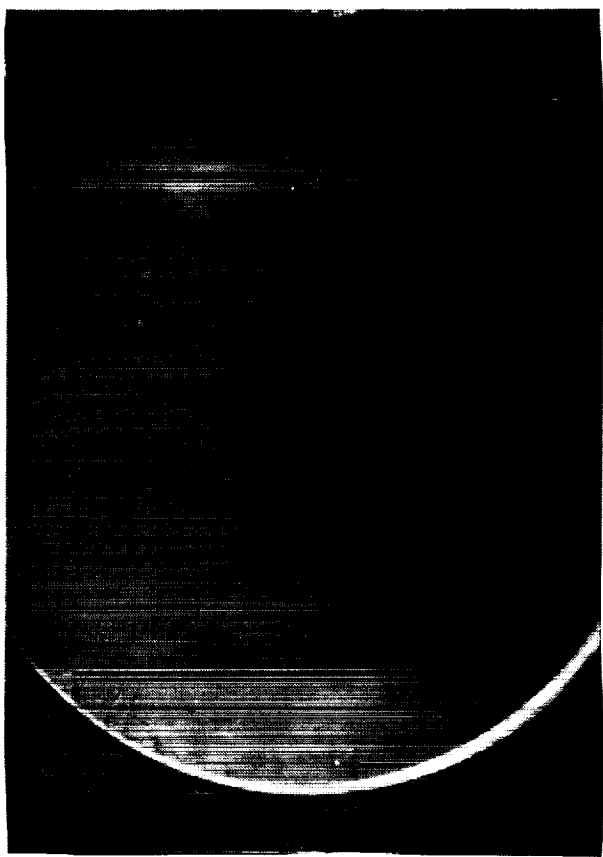


Figure 1. - Photograph of peeling contamination film near vent.

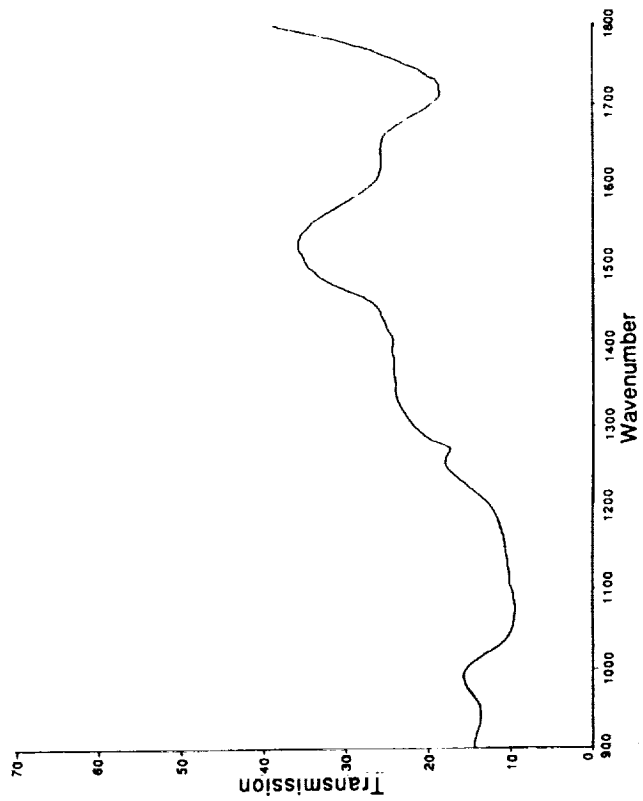


Figure 2. - IR spectrum of contamination film.

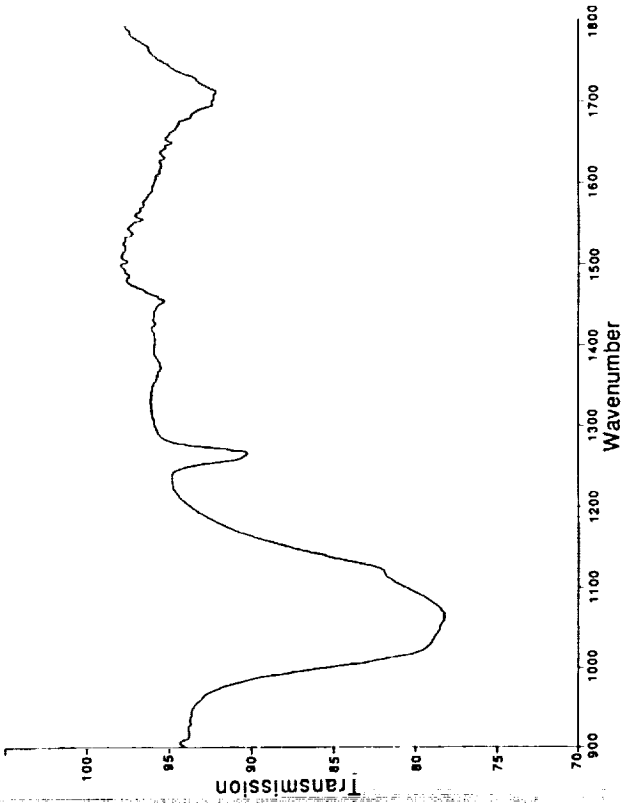


Figure 3. - IR spectrum of films on Caf2 optical window.



Figure 4. - Photograph of MgF2 optical window from tray E5.

0-3

ORIGINAL PAGE
BLACK AND WHITE PHOTOGRAPH

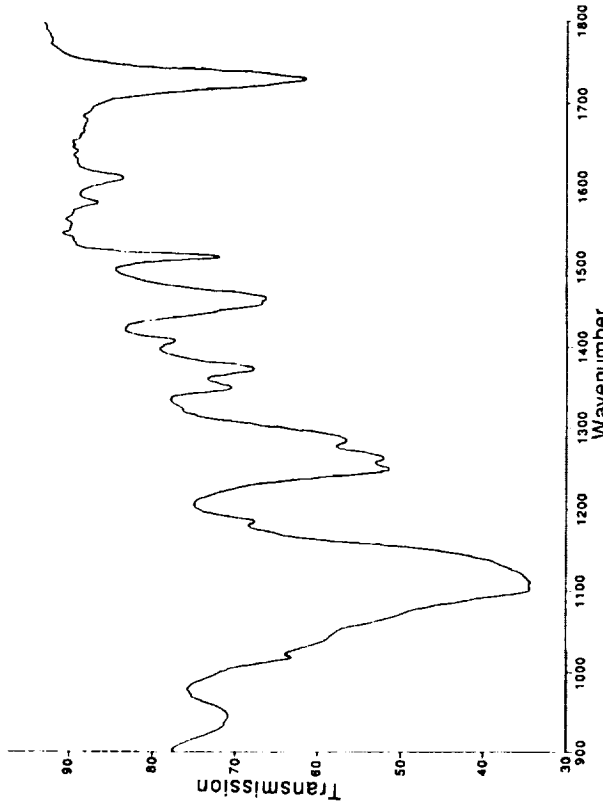


Figure 7. - IR spectrum of wipe residue.

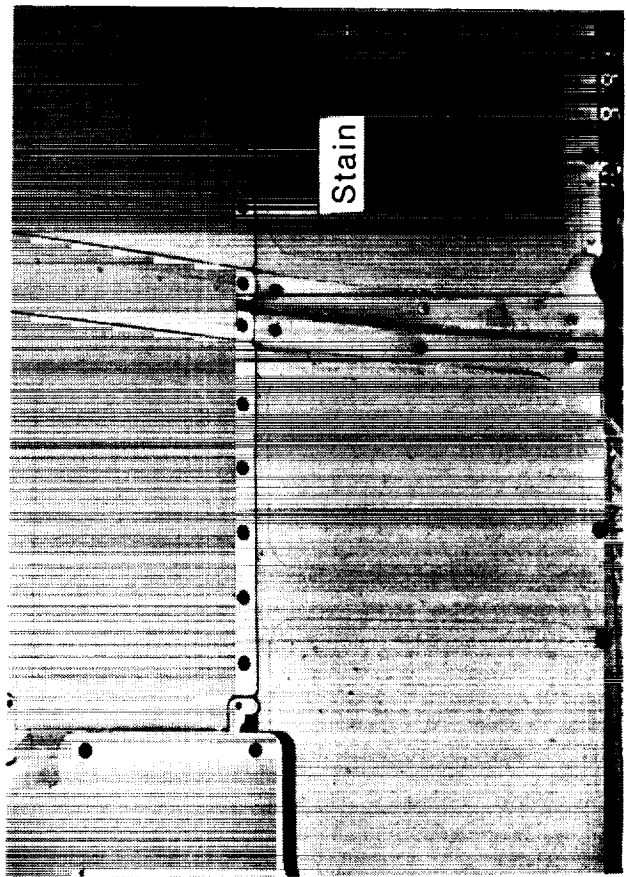


Figure 8. - Photograph of faint brown stain in postflight STS-48 bay.

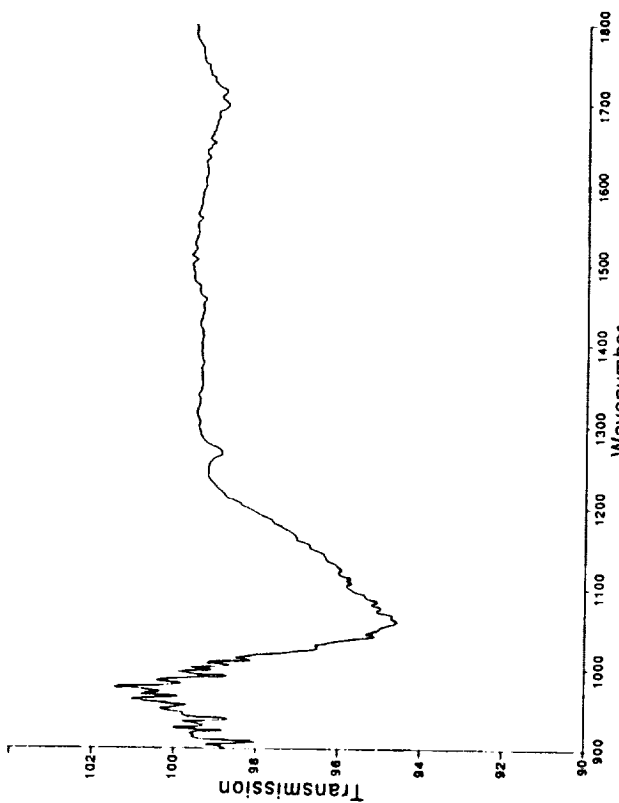


Figure 5. - IR spectrum of front surface on MgF2 optical window.

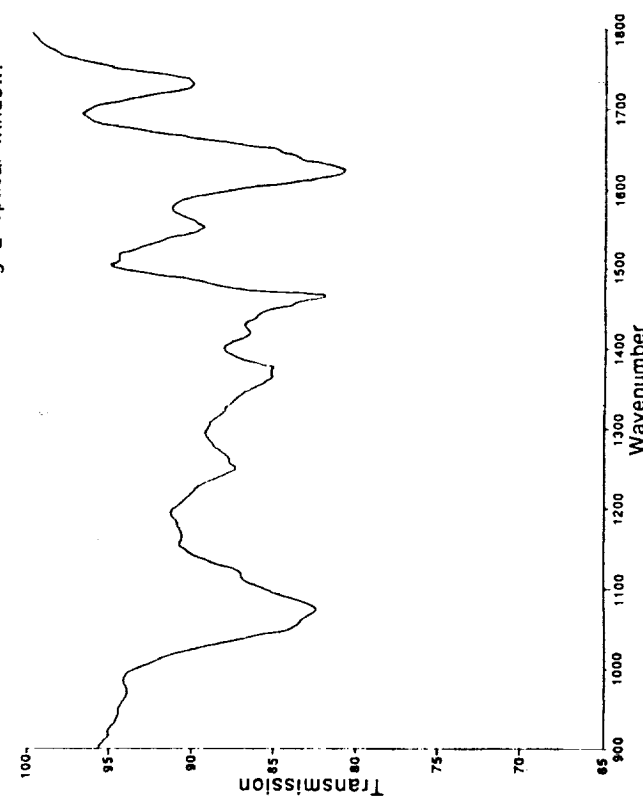


Figure 6. - IR spectrum of residue on ground control MLI witness.

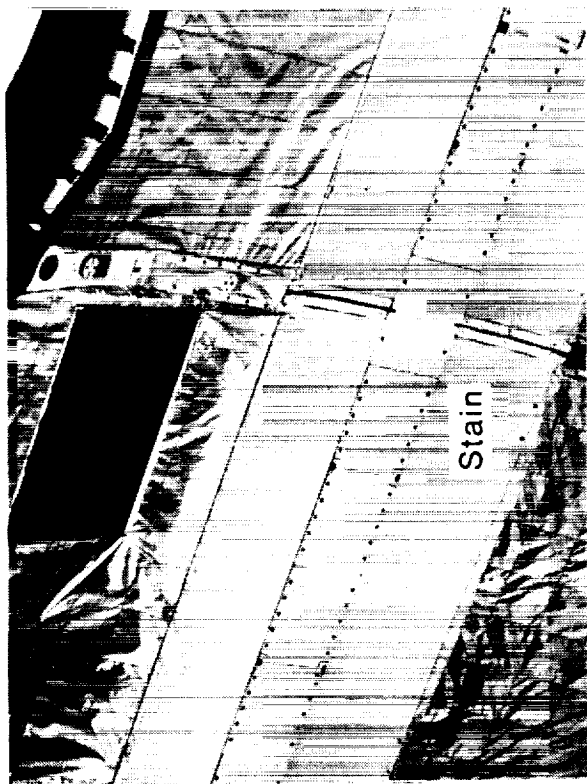
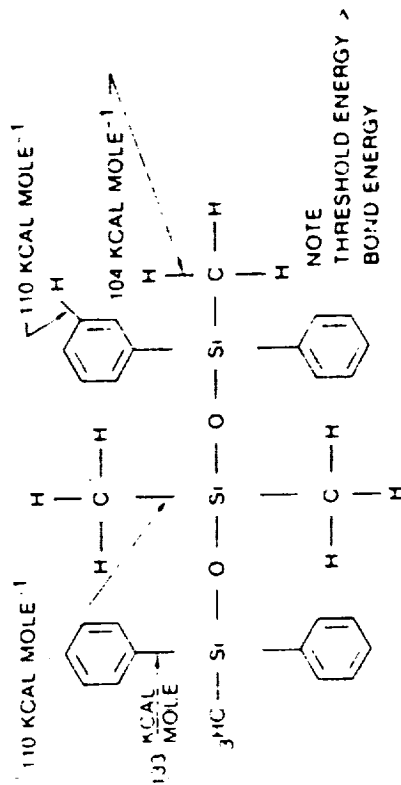


Figure 9. - Photograph of faint brown stain in postflight STS-48 bay.



Molecular structure and bond energies of likely scission points of methyl phenyl siloxane, a species commonly outgassed by silicone rubbers.

Figure 10. - Molecular structure of DC-704 oil.

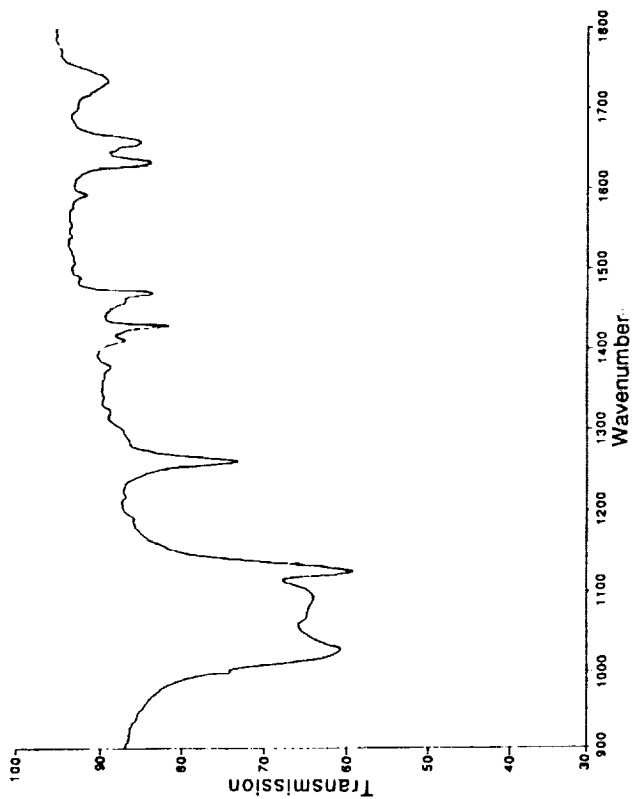


Figure 11. - IR spectrum of residue from STS-48 (Discovery) beta cloth.

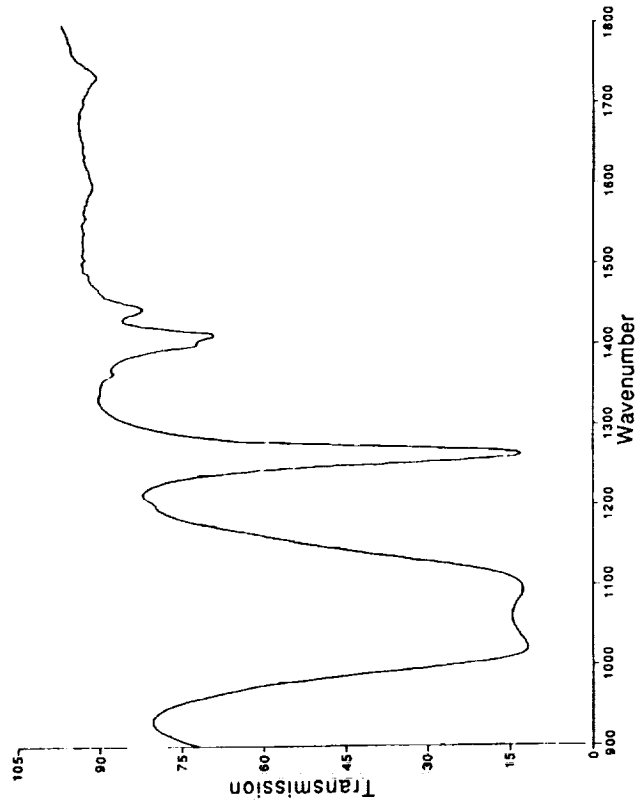


Figure 12. - IR spectrum of residue from RTV-142.

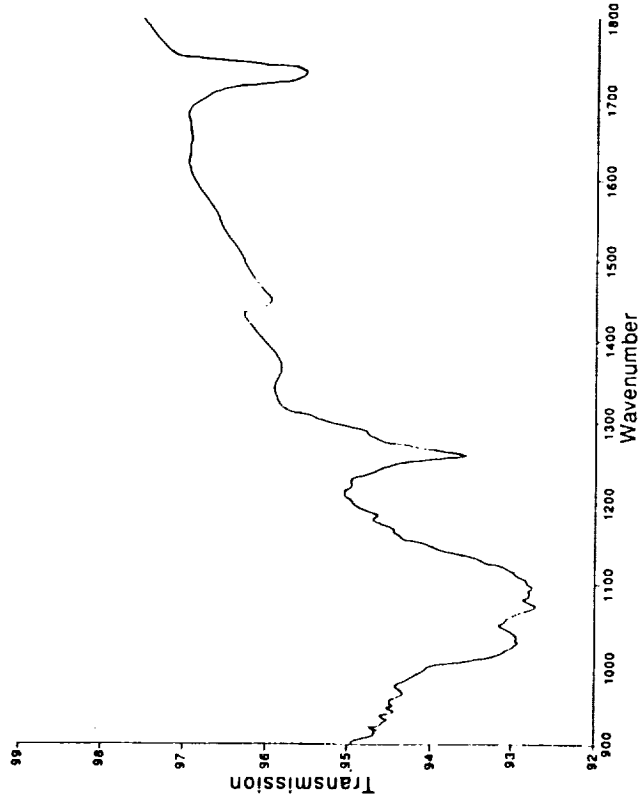


Figure 15. - IR spectrum of UARS/UASE flight MLI witness.

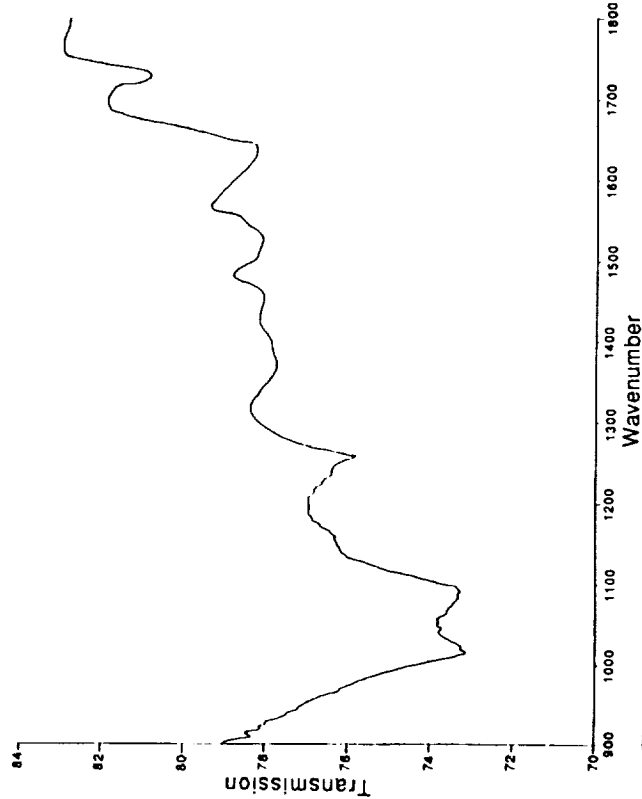


Figure 16. - IR spectrum of dry wipe UARS/UASE toolbox.

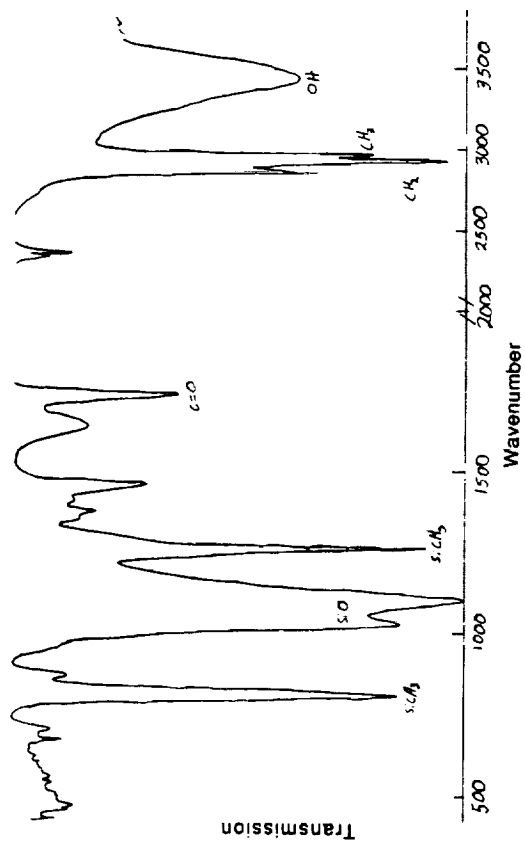


Figure 13. - IR spectrum of wash plate #056 residue from the PCR.

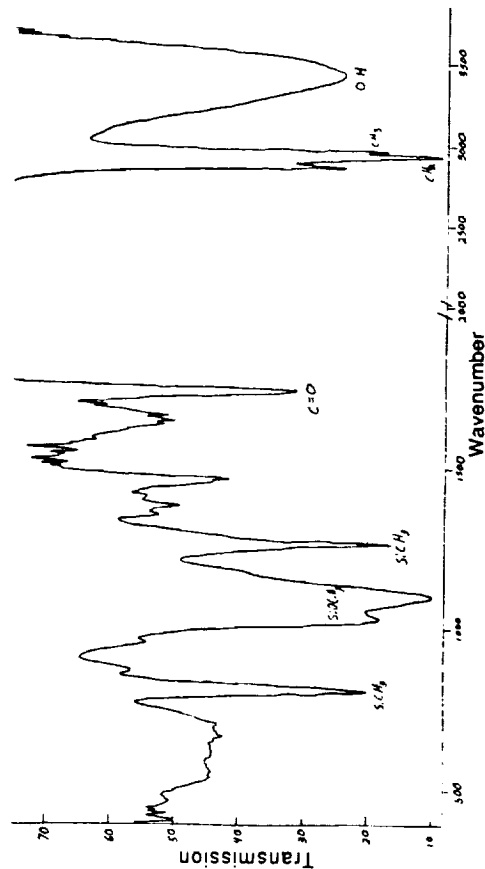


Figure 14. - IR spectrum of wash plate #047 residue from the PCR.

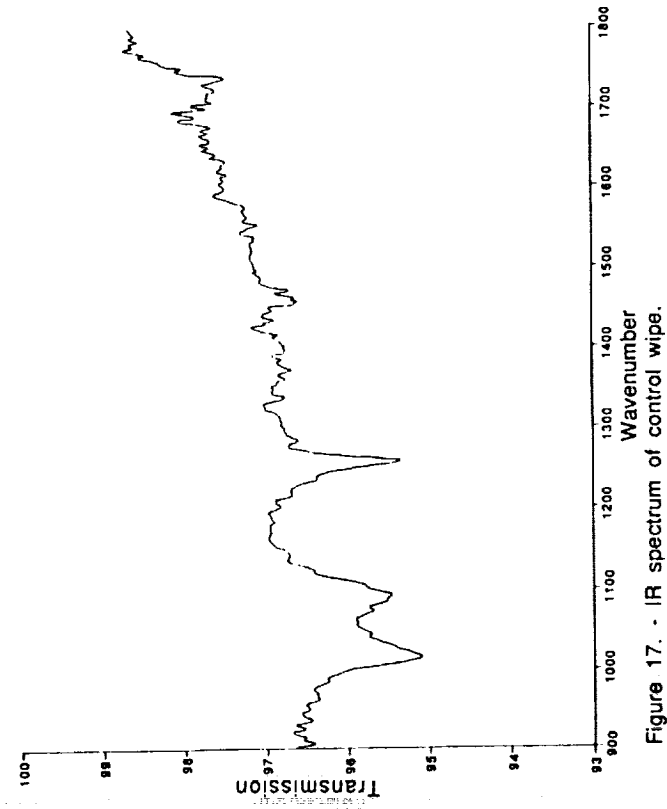


Figure 17. - IR spectrum of control wipe.

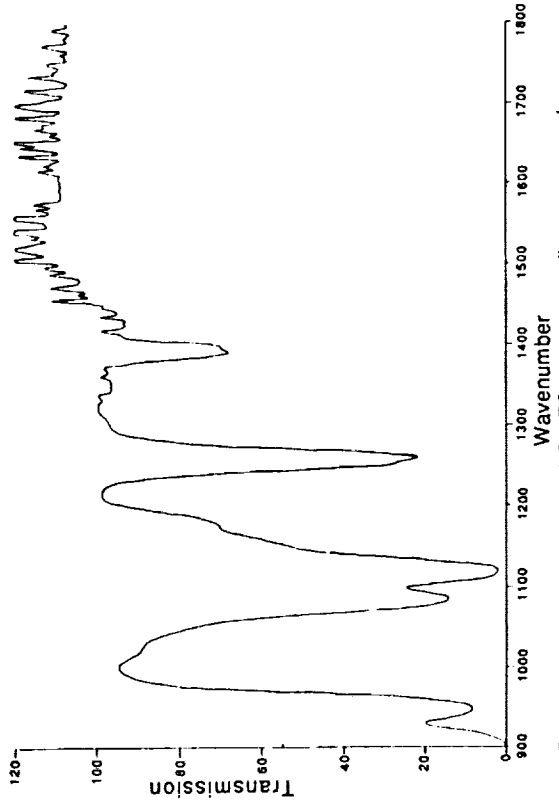


Figure 19. - IR spectrum of DMES rewaterproofing compound.

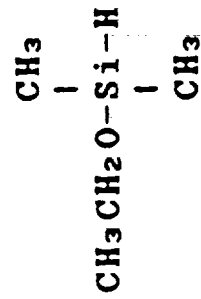


Figure 18. - Molecular structure of STS-48 rewaterproofing compound (DMES).

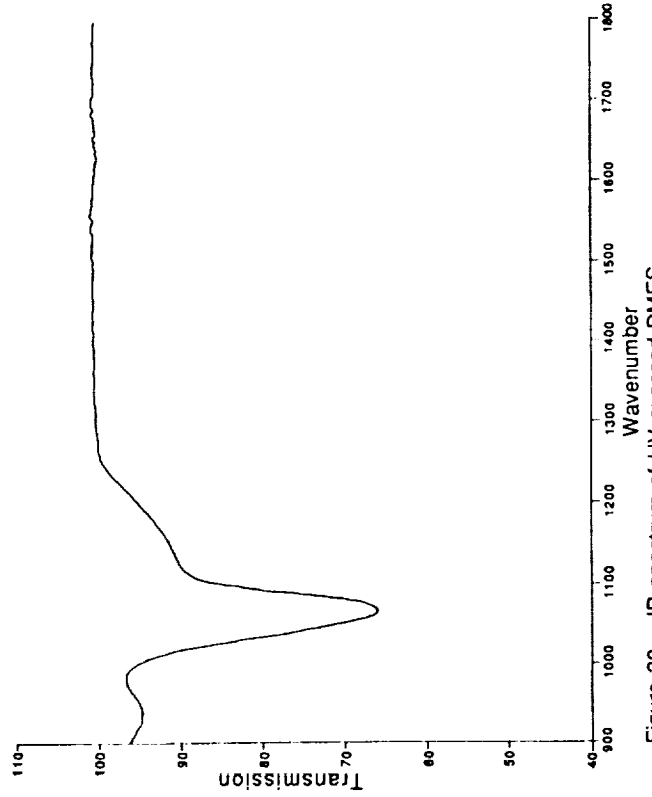
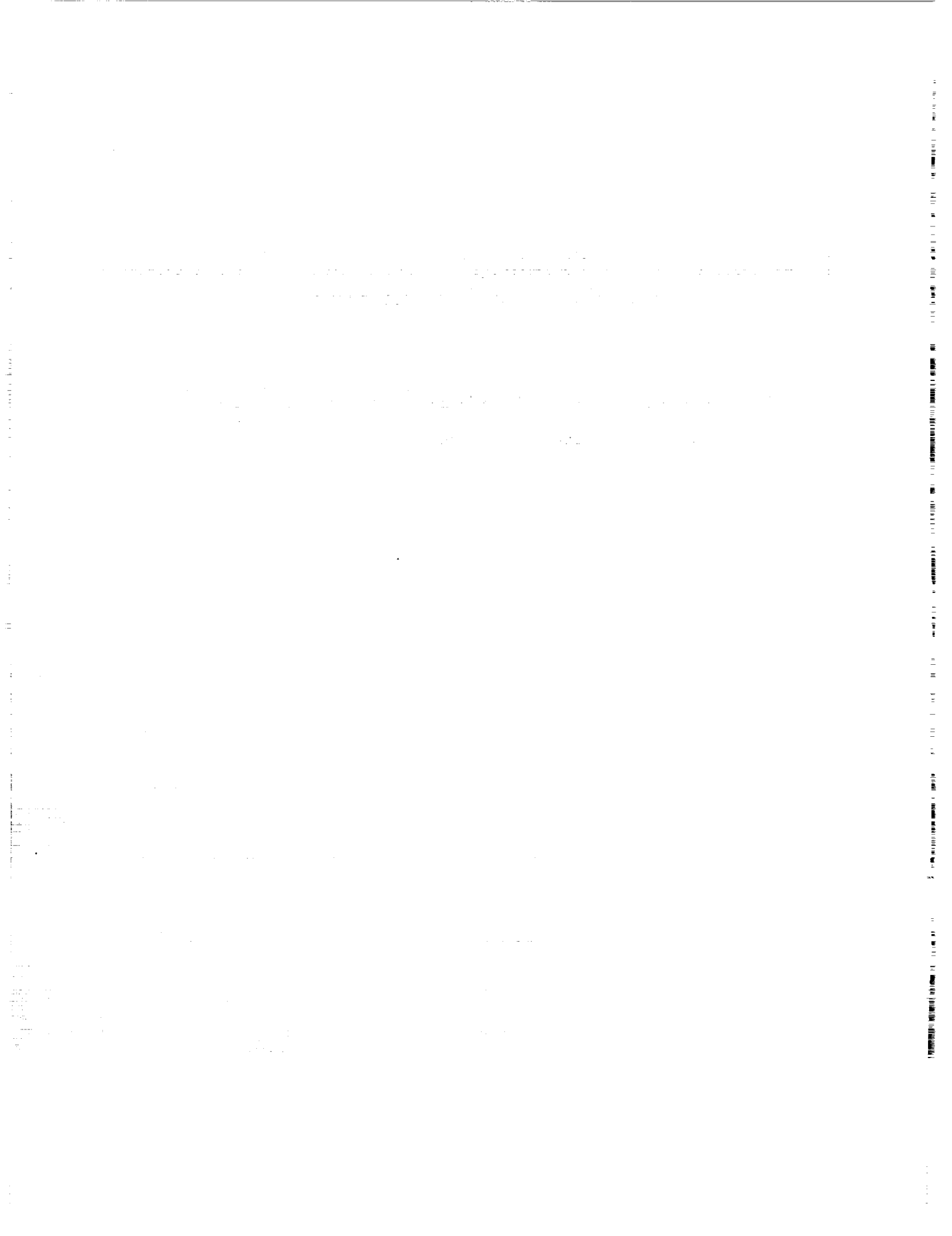


Figure 20. - IR spectrum of UV exposed DMES.

Thermal Control Coatings, Protective Coatings, and Surface Treatments

Co-Chairmen: Ann Whitaker and Wayne Slemp
Recorder: Johnny Golden



THERMAL CONTROL SURFACES ON THE MSFC LDEF EXPERIMENTS

Donald R. Wilkes
AZ Technology, Inc.
Huntsville, AL 35801

Ann Whitaker - A0171
James M. Zwiener - S0069
Roger C. Linton - A0034
David Shular - S1005
Palmer Peters - A0114
NASA Marshall Space Flight Center
Huntsville, AL 35812

John Gregory - A0114
University of Alabama/Huntsville
Huntsville, Alabama 35899

INTRODUCTION

There were five Marshall Space Flight Center (MSFC) experiments on the LDEF. Each of those experiments carried thermal control surfaces either as test samples or as operational surfaces. These materials experienced varying degrees of mechanical and optical damage.

Some materials were virtually unchanged by the extended exposure while others suffered extensive degradation. The synergistic effects due to the constituents of the space environment are evident in the diversity of these material changes. The sample complement for the MSFC experiments is described along with results of the continuing analyses efforts.

PRECEDING PAGE BLANK NOT FILMED

EXPERIMENT SURFACES EXHIBIT DIVERSE EFFECTS

The thermal control surfaces on the extended LDEF mission were exposed to a complex environment and experienced a wide range of effects due to this exposure.

Optical/Thermal

- Spectral Reflectance/Solar Absorptance
- Thermal Emittance
- Fluorescence

Physical

- Surface Roughening/Erosion
- Cracking/Peeling
- Weight Loss

Chemical

- Surface Effects
- Bulk Effects

mslg003

Figure 1. Effects of Space Environmental Exposure.

MSFC LDEF EXPERIMENTS

Marshall Space Flight Center (MSFC) had five experiments on the LDEF that exposed thermal control surfaces to the space environment. All five experiments had materials that were exposed to the RAM orbital direction and the atomic oxygen environment. Two of the experiments also had samples on the LDEF trailing edge and saw very little atomic oxygen. The Thermal Control Surfaces Experiment (TCSE - S0069) performed optical measurements on orbit. AO114 and AO171 samples were half covered (protected) and half exposed to the environment.

	S0069	AO114	AO171	AO34	S1005
Exposure-Leading Edge	X	X	X	X	X
-Trailing Edge		X		X	
-LDEF Row #	9	3, 9	8	3, 9	10
In-space Optical Measurements	X				
Samples Half Exposed/ Half Protected		X	X		

Figure 2. Summary of MSFC Experiments.

**THERMAL CONTROL SURFACES ON
THE MSFC EXPERIMENTS**

The five MSFC experiments had a wide range of thermal control surfaces in their sample complement. Most samples were either low α_S/ϵ_T coatings or black paints. Protective coatings of RTV670 and OI650 were applied over Chemglaze A276 white paint and Z302 black paint to prevent erosion by atomic oxygen.

	S0069 TCSE	AO114	AO171 SAMPLE	A0034	S1005
A276 White	X	X	X	X	
A276/OI650	X				
A276/RTV670	X				
S13G/LO White	X	X	X	X	
Z93 White	X	X		X	
YB71 White	X			X	
White TEDLAR	X		X		
Silver TEFLON	X				X
Chromic Acid Anodize	X				
Z302 Black	X	X	X		
Z302/OI650	X				
Z302/RTV670	X				
Z306 Black		X	X	X	
D111 Black	X				
401-C10 Black			X		
Z853 Yellow			X		
Tiodize K17 Black			X		
Tiodize K17 White			X		

Note: Teflon and Tedlar are trademarks of Dupont.

Figure 3. Materials Complement on MSFC LDEF Experiments.

THERMAL CONTROL SURFACES EMITTANCE CHANGES

The thermal emittance of most of the samples on the TCSE was essentially unchanged due to the extended LDEF exposure. The only exception was the 2 mil silver Teflon. Approximately 1 mil of this 2 mil Teflon material was eroded away by the incident atomic oxygen. The post-flight emittance of this material agrees well with laboratory measurements of 1 mil silver Teflon material.

Material	Emittance (ϵ_T)		$\Delta\epsilon_T$
	Pre-flt	Post-flt	
A276	.90	.93	.03
A276 w/RTV670	.91	.88	-.03
A276 w/OI650	.90	.89	-.01
Z93	.91	.92	.01
S13G-LO	.90	.89	-.01
YB71	.90	.89	-.01
YB71 over Z93	.85	.87	.02
Silver Teflon (2 mil)	.66	.46	.20
Silver Teflon (5 mil)	.81	.78	-.03
Silver Teflon (5 mil textured)	.82	.79	-.03
Chromic Acid Anodize	.84	.84	0

10e1200

Figure 4. Emittance Summary of TCSE Materials.

A276 WHITE PAINT

Chemglaze A276 is a polyurethane white paint manufactured by the Lord Chemical Company. It was anticipated that this material would be eroded by the atomic oxygen environment so clear protective overcoatings of RTV670 and OI650 were applied to some of the TCSE samples. Figure 5 shows the change in solar absorptance of the A276 samples on the TCSE, A0114 and A0171. Note that the unprotected A276 on the LDEF leading edge experienced very little change in properties over the LDEF mission and in fact was somewhat whiter after the mission. A276 has been shown to degrade readily under solar UV exposure, much like the A0114 trailing edge sample and the clear overcoated TCSE samples. The AO erosion of the unprotected A276 on the LDEF leading edge removed the UV damaged material leaving an undamaged surface. Also notice that even though the major portion of the AO fluence occurred late in the LDEF mission, there was sufficient AO present in the early stages to prevent most of the UV damage.

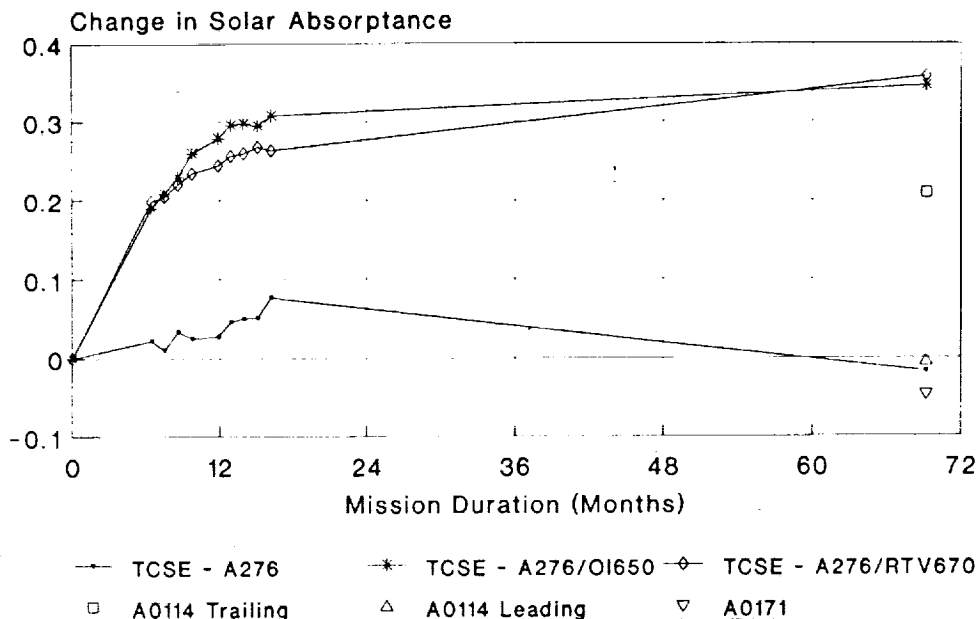


Figure 5. Performance of A276 White Paint.

A276 REFLECTANCE DATA

The detailed reflectance data for the TCSE A276 samples shows the spectral changes in this material after 15 months and post-flight. The spectra shows that the samples continued to degrade after 15 months at some wavelengths while improving at others.

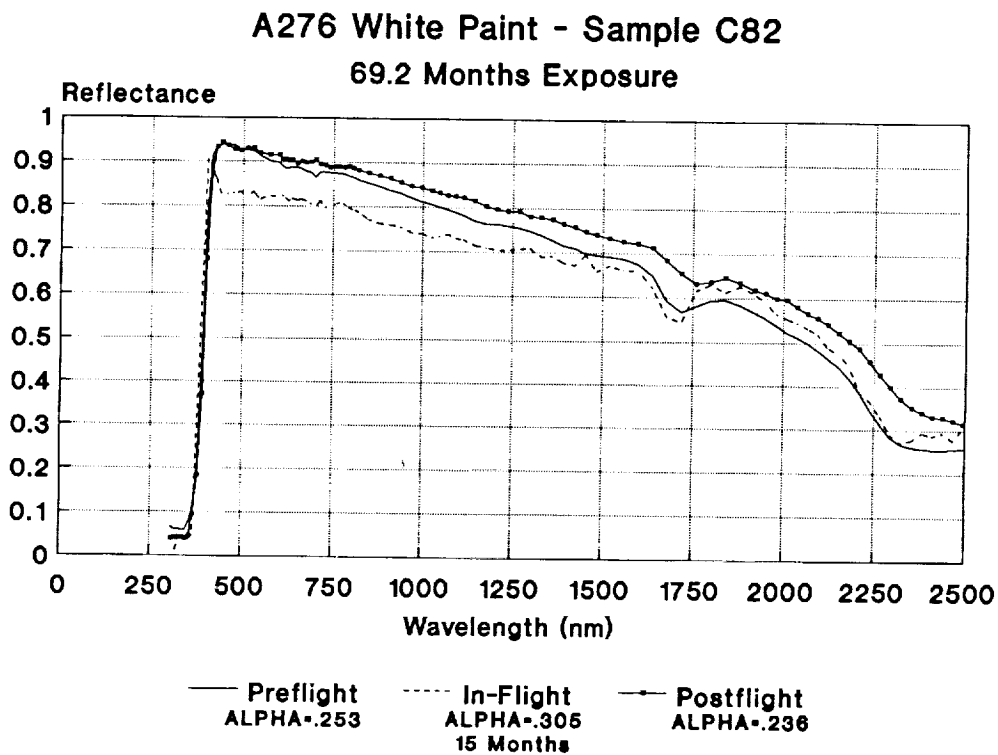


Figure 6. Reflectance Data for the TCSE A276.

A276/RTV670 White Paint - Sample C88
69.2 Months Exposure

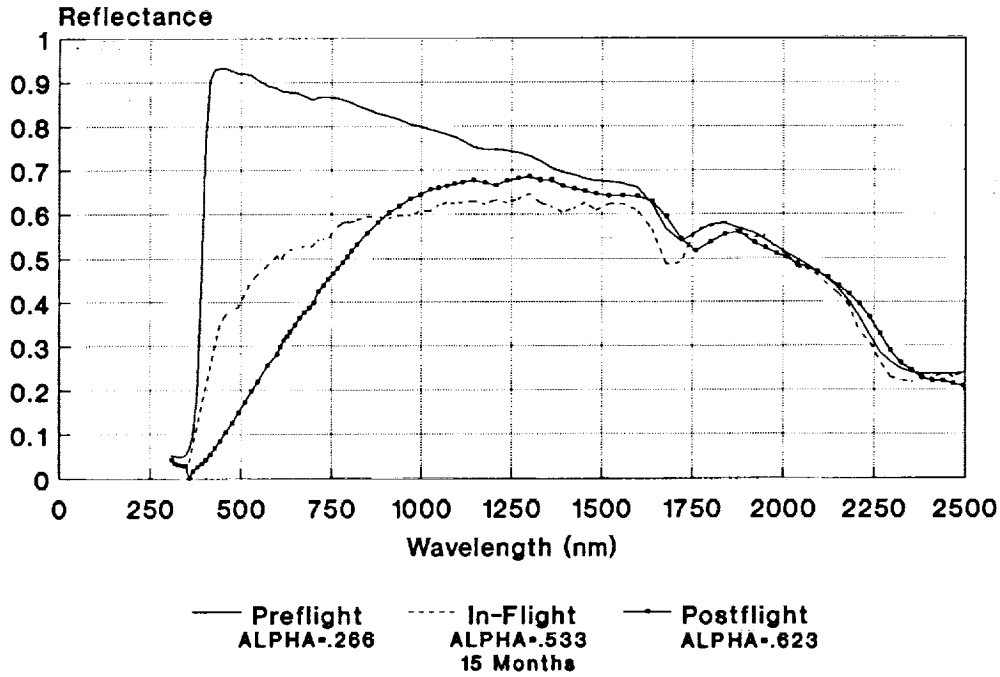


Figure 7. Reflectance Data for the TCSE A276/RTV670 Sample.

A276/OI650 White Paint - Sample C87
69.2 Months Exposure

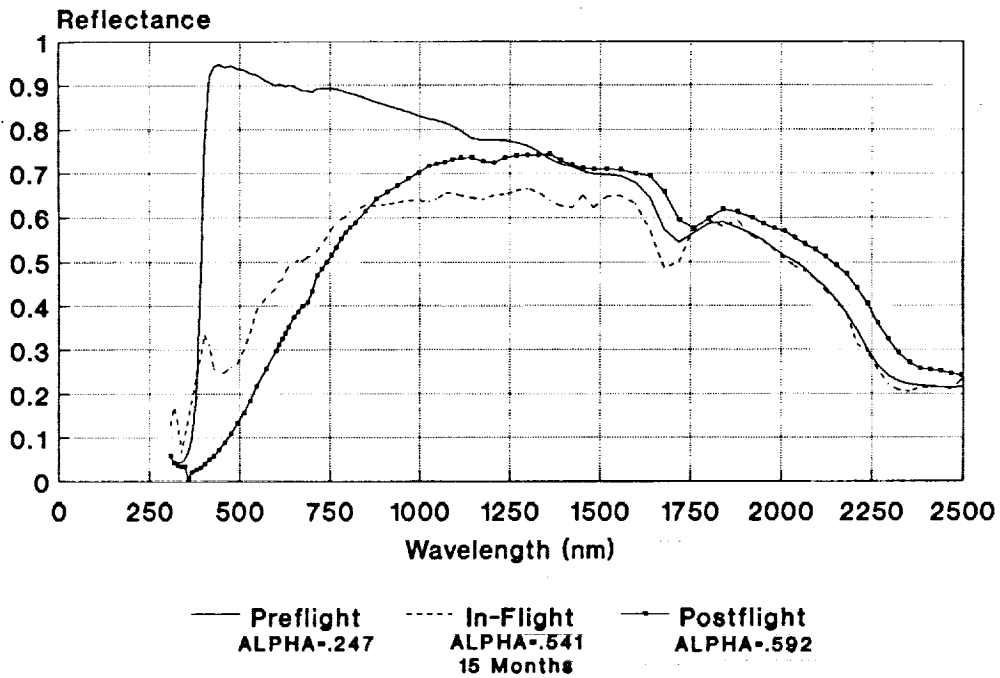
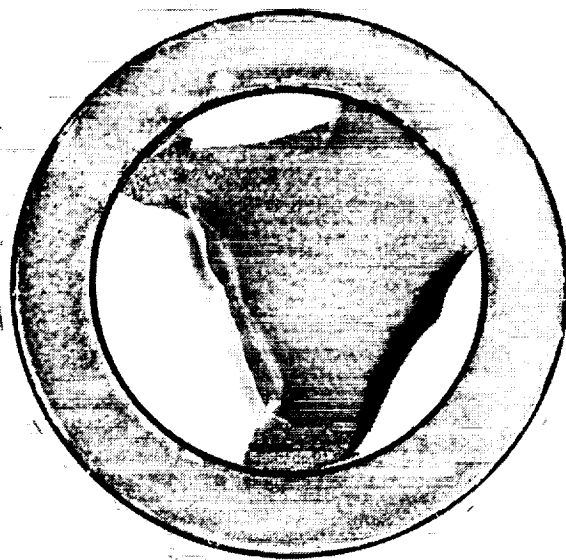


Figure 8. Reflectance Data for the TCSE A276/OI650 Sample.

OVERCOATED A276 WHITE PAINT

While the clear protective coatings protected the A276 from AO erosion, they also caused cracking and peeling of the combined coating. These two photographs show the effects on the TCSE calorimeter samples. These samples were thermally isolated and saw wide temperature excursions. Other samples of these coatings were not thermally isolated and, while they did crack, they did not peel away from the substrate.



A276/RTV670



A276/OI650

Figure 9. Photographs of Overcoated A276 Samples.

Z93 WHITE PAINT

Z93 is a white paint from the IIT Research Institute and was very stable for the extended LDEF mission. A small improvement in solar absorptance occurred early in the mission which is typical of potassium silicate coatings like Z93. Only a small degradation was seen for the remainder of the mission. The solar absorptance of Z93 was also not effected by the AO environment as shown by the A0114 trailing edge sample.

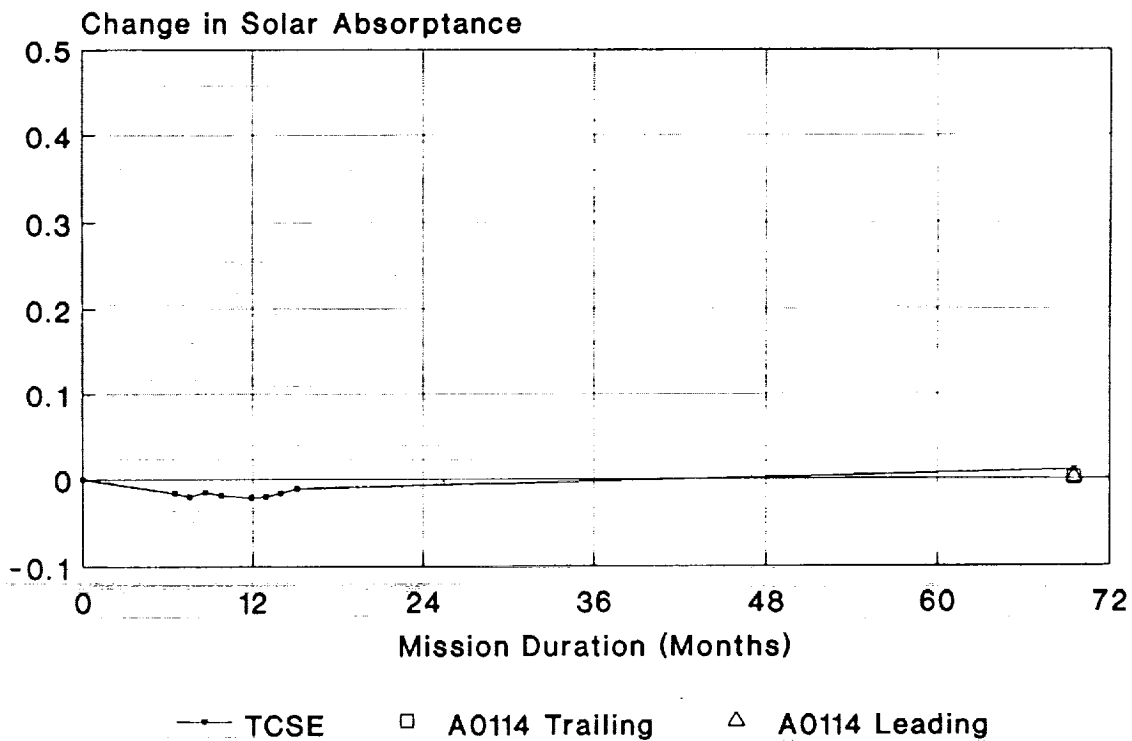


Figure 10. Performance of Z93 White Paint.

Z93 REFLECTANCE DATA

The post-flight detailed reflectance data for the A0114 leading edge and trailing edge samples also show that Z93 was very stable for the extended LDEF exposure.

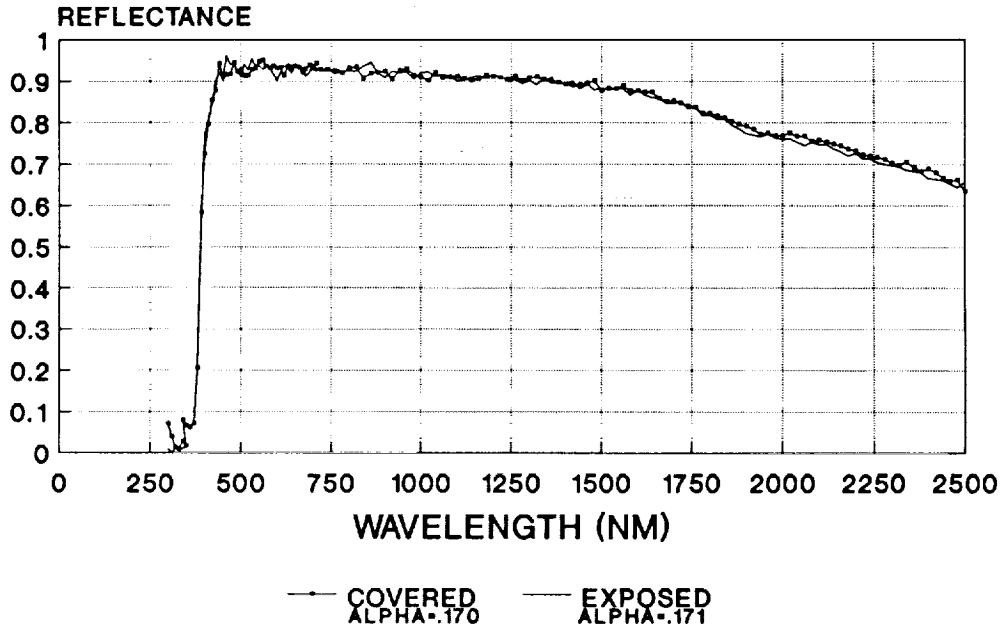


Figure 11. LDEF A0114 Z93 Trailing Edge Sample.

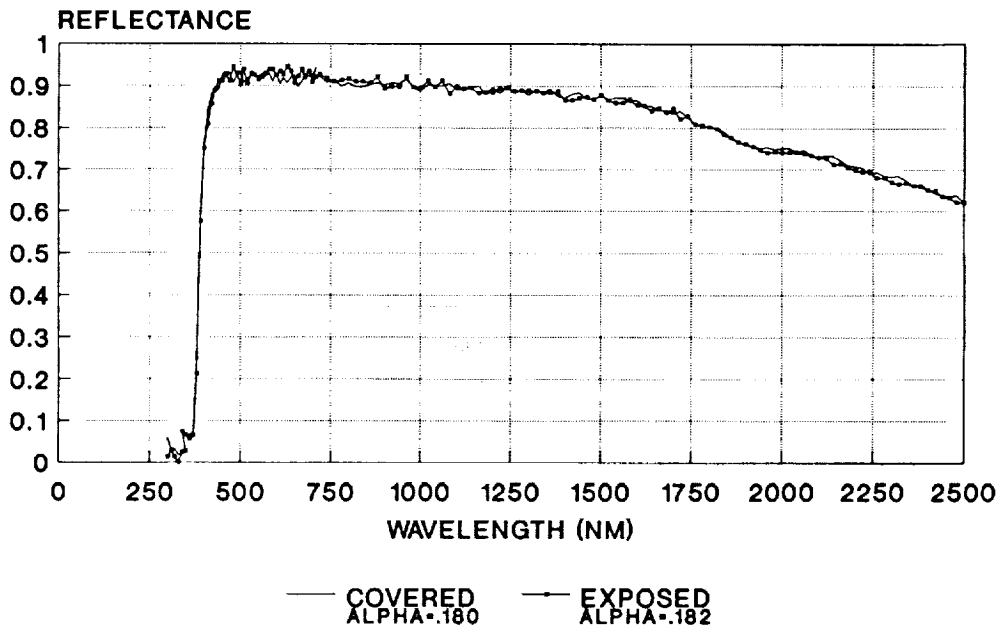


Figure 12. LDEF A0114 Samples Z93 Leading Edge Sample.

S13G/LO WHITE PAINT

S13G/LO is also a white paint from the IIT Research Institute and has been widely used on space hardware. Ground testing predicted that S13G/LO would degrade moderately in the solar UV environment. This material did degrade on the LDEF mission but degraded somewhat more than expected on the TCSE. The variation in overall degradation of S13G/LO between the three experiments was unexpected and unexplained at this time.

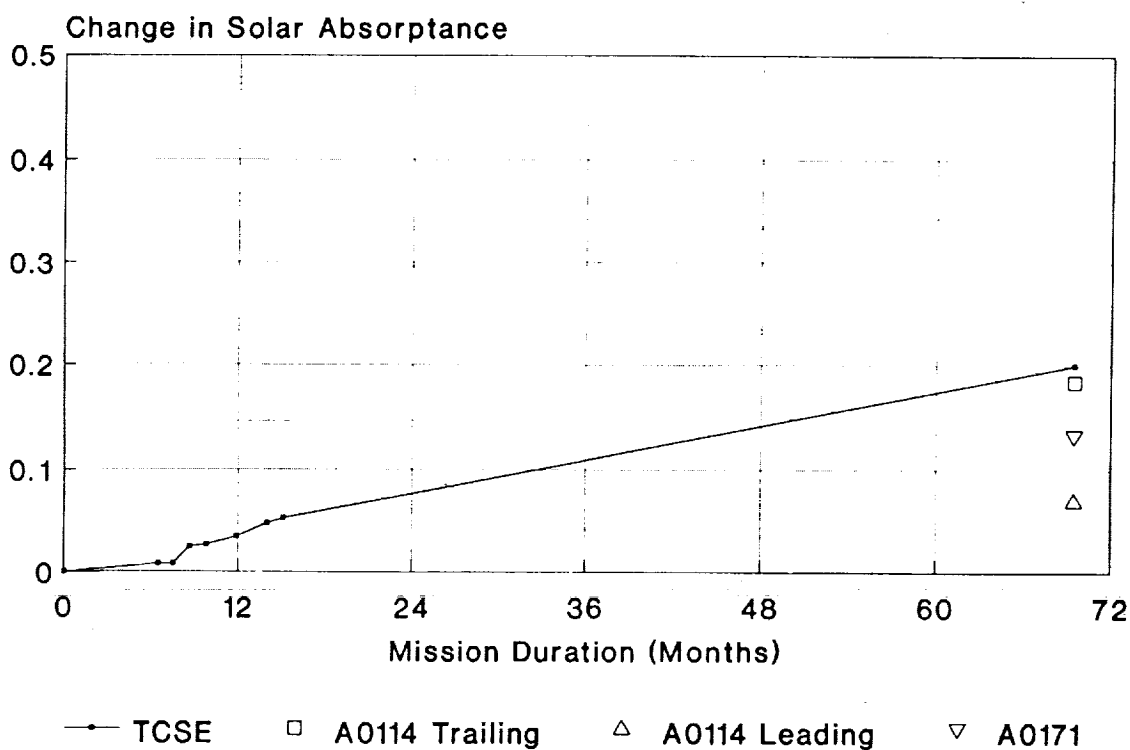


Figure 13. Performance of S13G/LO White Paint.

S13G/LO REFLECTANCE DATA

The reflectance measurements of the TCSE and A0114 samples show how the material degraded spectrally. The spectral data of the samples from the two experiments do not explain the differences in degradation rates, however.

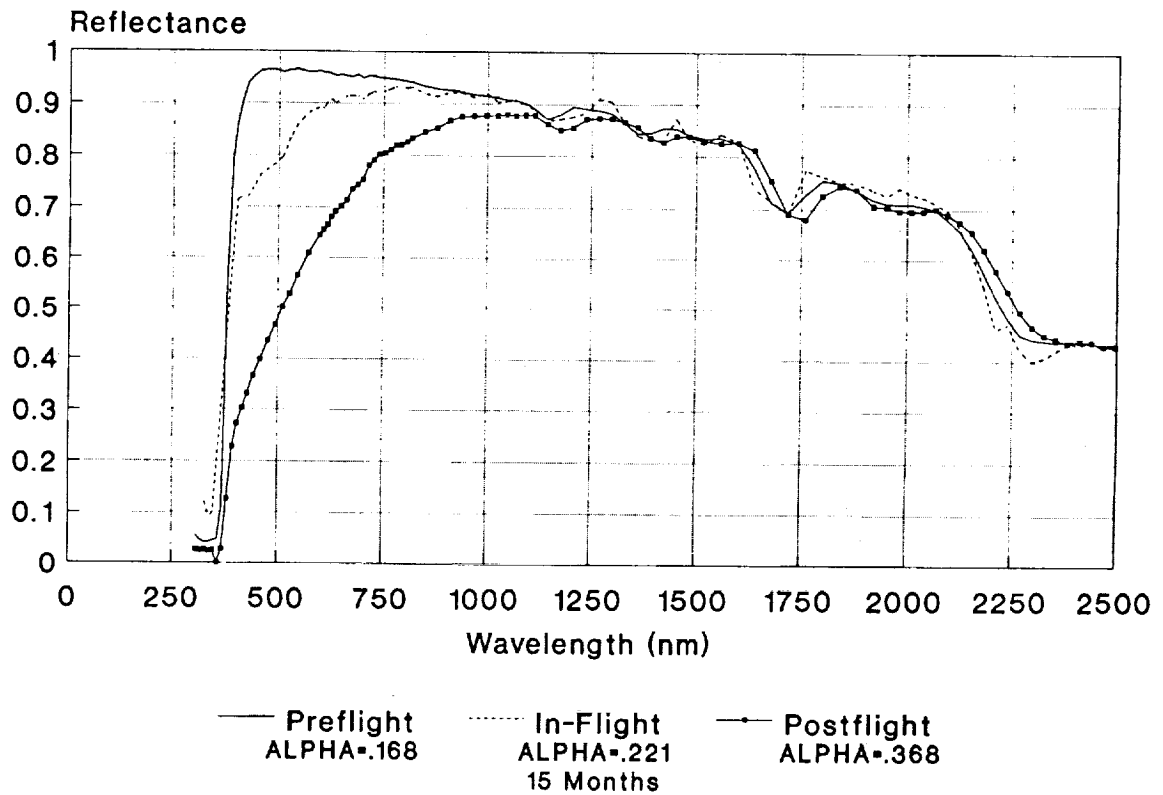


Figure 14. TCSE S13G/LO White Paint-Sample C92.

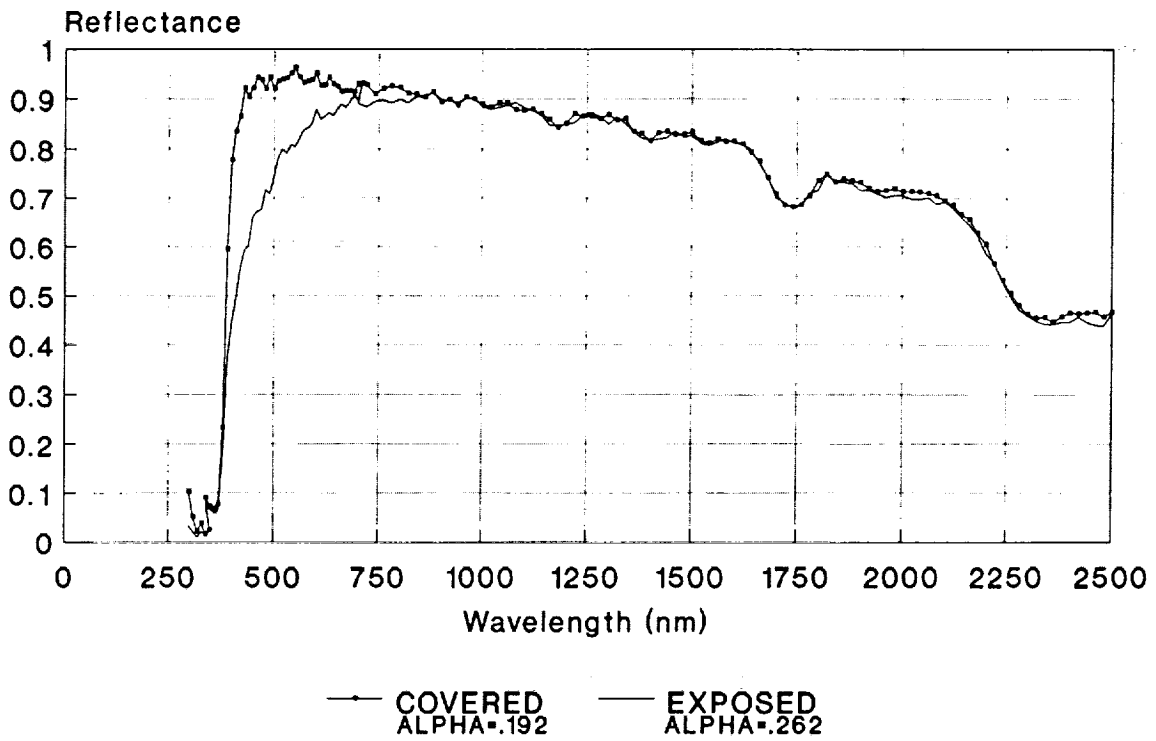


Figure 15. AO114 S13G/LO Leading Edge Sample.

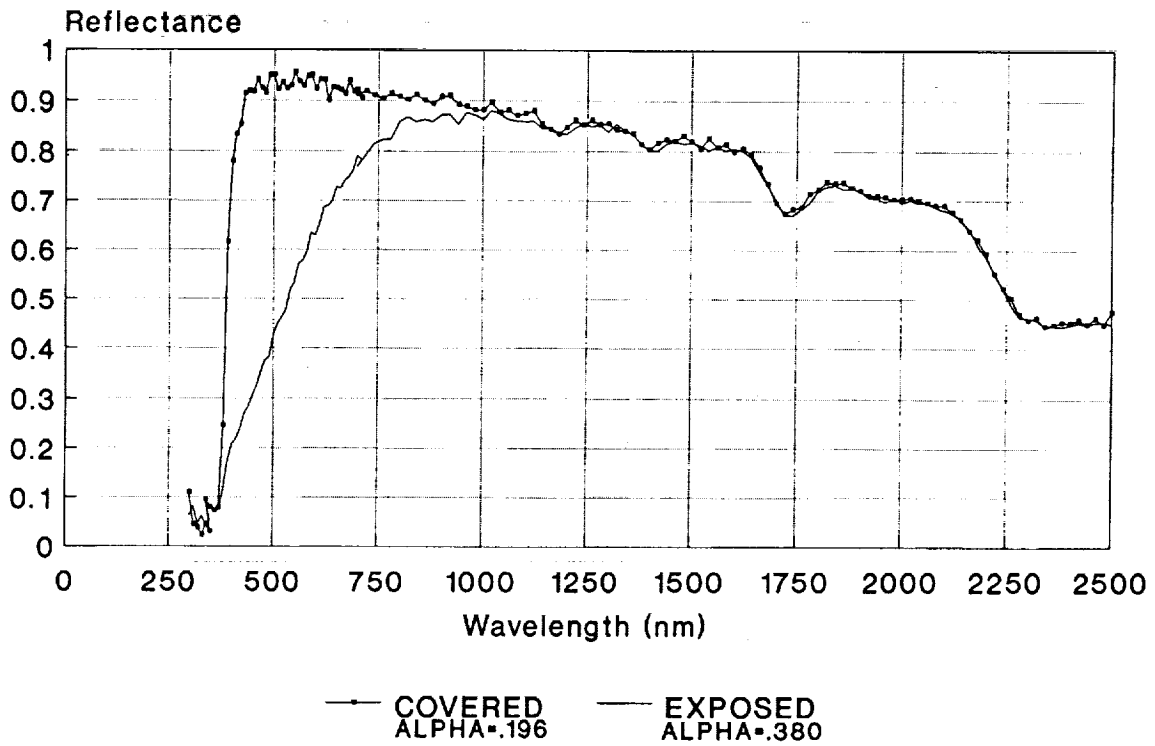


Figure 16. AO114 S13G/LO Trailing Edge Sample.

SILVER TEFLON

Both 2 mil and 5 mil silver Teflon samples were flown on the TCSE. The 2 mil material was also used on the TCSE front cover for thermal control. Experiment S1005 used 5 mil silver Teflon for thermal control of the transverse heat pipes. All the Teflon surfaces were eroded by the AO environment and had the typical whitish appearance observed on other silver Teflon surfaces exposed to the RAM AO environment. The 5 mil material applied with a P223 adhesive was optically very stable for the LSEF mission. The silver Teflon applied with the Y966 adhesive showed a wide variation in post-flight measurements between test samples and measurement positions on the TCSE cover.

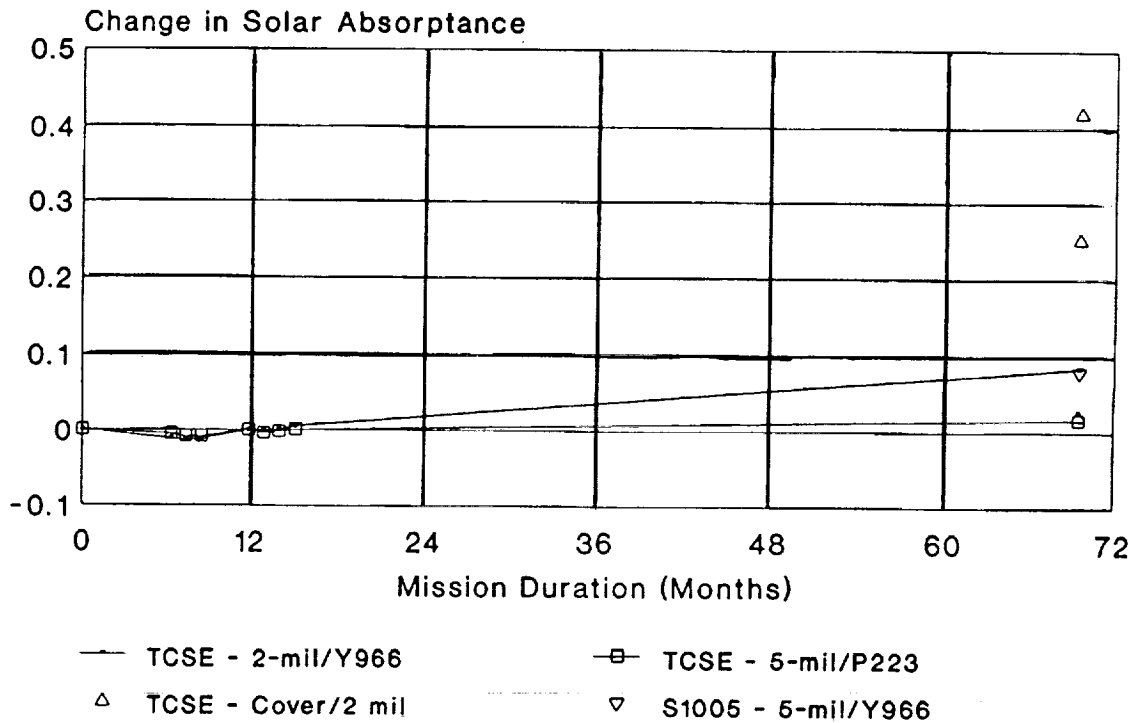


Figure 17. Performance of Silver Teflon.

TCSE FRONT COVER DEGRADATION

The front cover of the TCSE was covered with 2 mil silver Teflon and suffered significant degradation. This photograph shows the front cover. This cover is aluminum with the pre-adhesive silver Teflon film applied to it. The specular undamaged areas on the left and right sides and in the middle were protected by secondary covers. The streaky discoloration was caused by a cracking of the silver/inconel backing on the Teflon and the subsequent migration of components of the Y966 adhesive through the cracks into the silver and Teflon interface. This contaminant was then degraded to a dark brown by solar UV exposure. This cracking was caused by the application of the pre-adhesived silver Teflon including the removal of the paper backing and the working of the surface to remove air bubbles.



Figure 18. TCSE Front Cover.

SILVER TEFLON REFLECTANCE DATA

Samples were cut from several locations on the TCSE front cover and measured in the laboratory. These locations were selected to demonstrate the wide variation in surface degradation.

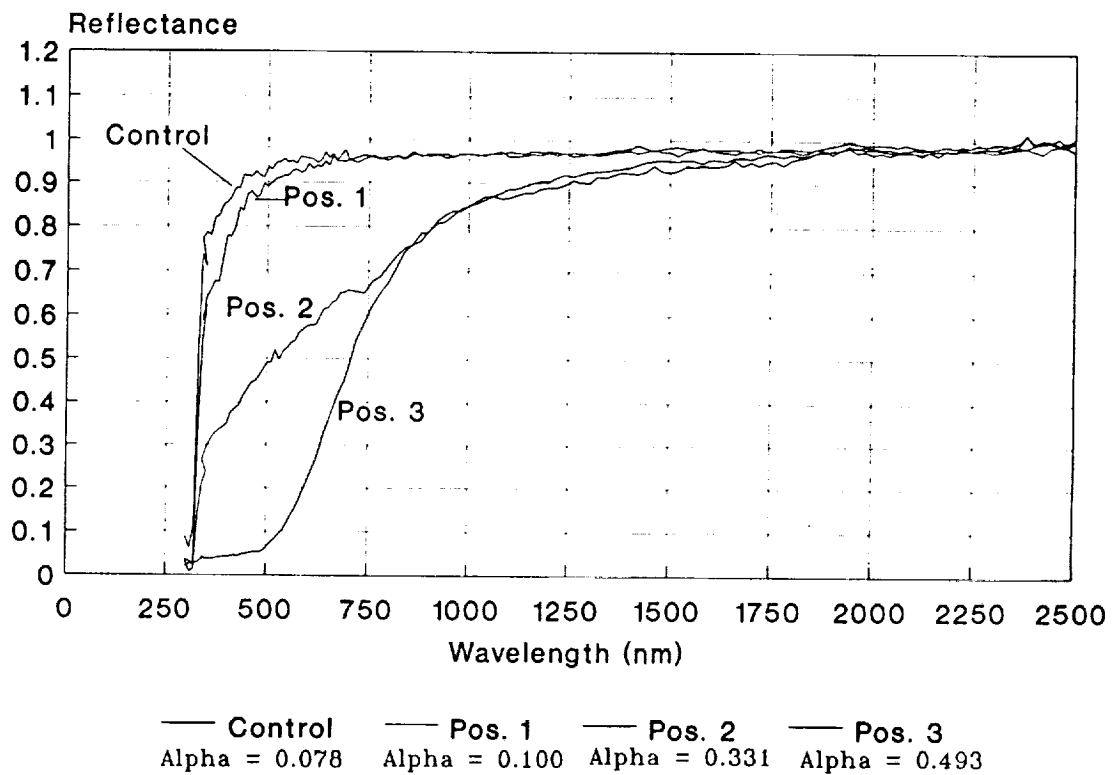


Figure 19. Measurements at Selected Locations on the Front Cover.

CHROMIC ACID ANODIZE

Two chromic acid anodize samples were provided by Wayne Slemp (LaRC) and were flown on the TCSE. One of the samples was exposed for the complete LDEF mission while the other was directly exposed for only the first 19.5 months of the LDEF mission. As can be seen from the data in Figures 20, 21, and 22 the two samples tracked well during the early stages of the mission as is shown by the TCSE in-flight measurements. The exposed sample, however, improved optically during the subsequent four years of exposure. This sample (69.2 month exposure) appears washed out and mottled while the other sample (19.5 month exposure) has an even coloring.

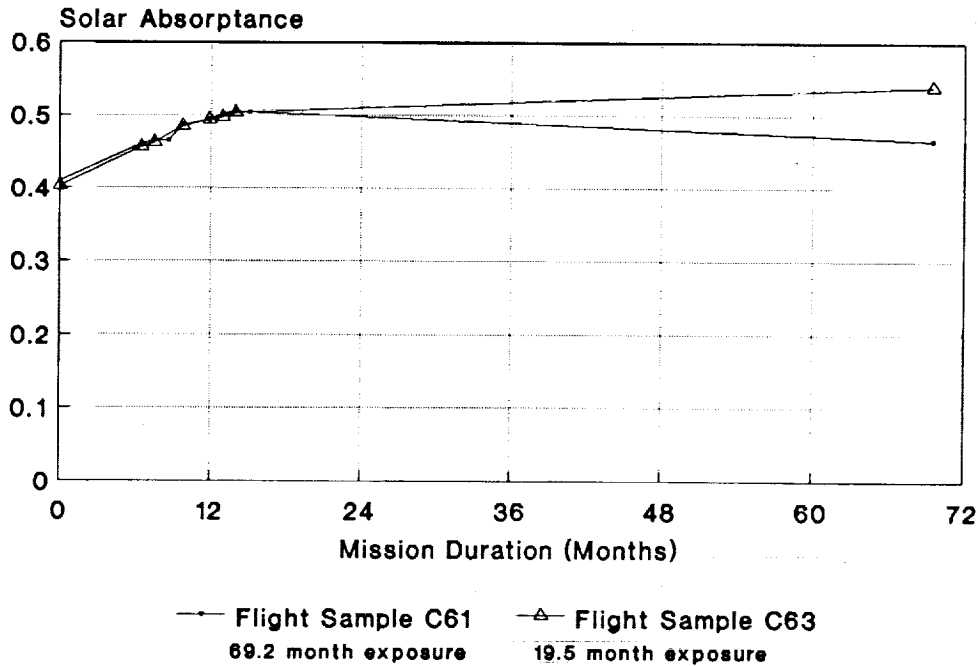


Figure 20. Performance of Chromic Acid Anodize.

Chromic Acid Anodize - Sample C63
19.5 Months Exposure

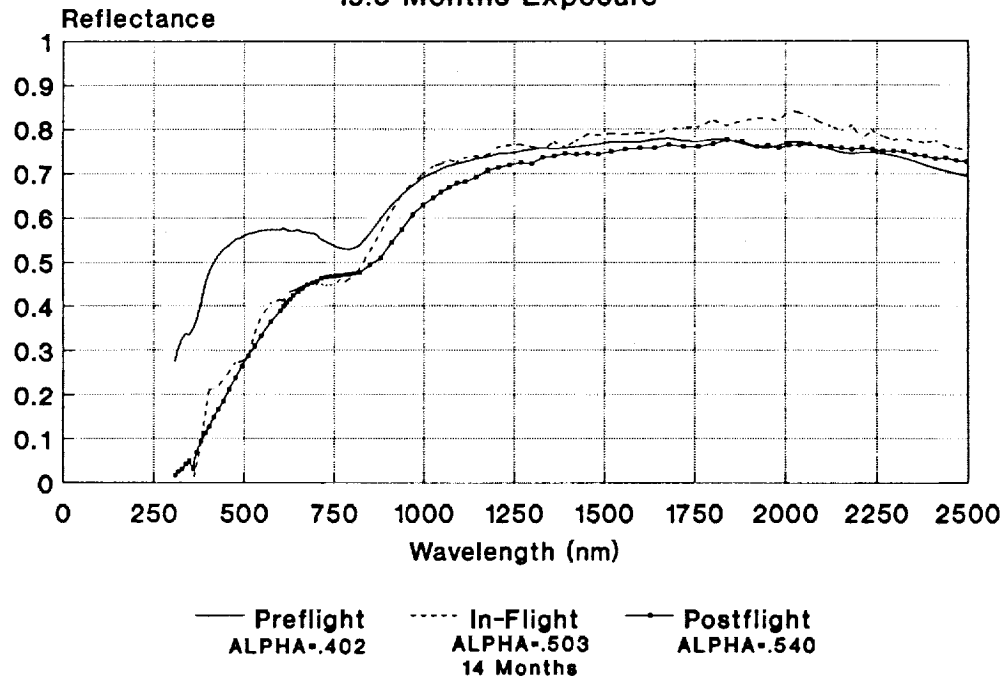


Figure 21. Reflectance Data for Chromic Acid Anodize.

Chromic Acid Anodize - Sample C61
69.2 Months Exposure

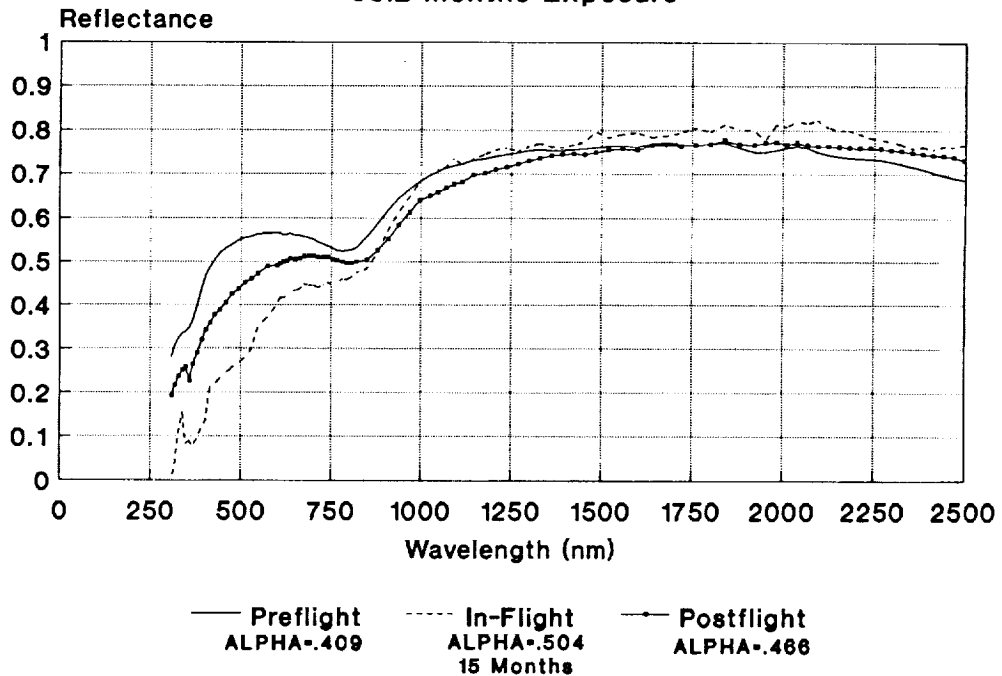


Figure 22. Reflectance Data for Chromic Acid Anodize.

YB71 WHITE PAINT

YB71 is another inorganic white paint from the IIT Research Institute. This YB71 sample was applied over a primer coat of Z93. As with Z93, YB71 was very stable for the extended LDEF exposure. This material exhibited a small initial improvement in reflectance (and solar absorptance) followed by a very low degradation rate.

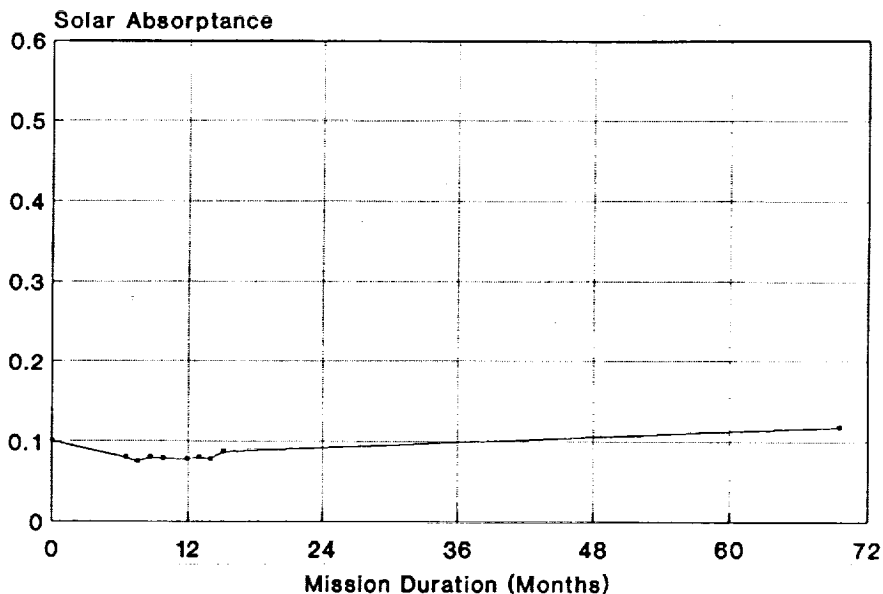


Figure 23. Reflectance Data for YB71 White Paint.

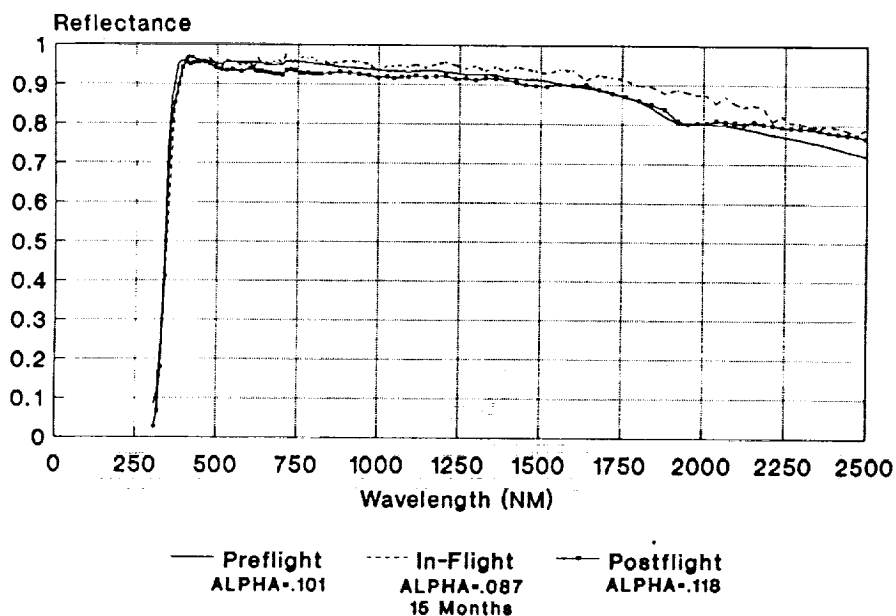


Figure 24. Performance of YB71 White Paint.

WHITE TEDLAR FILM

White Tedlar is another material that was expected to degrade over the 5.8 year LDEF mission due to solar UV exposure. Instead, the reflectance properties of this material improved slightly, as shown in Figures 25 and 26. The surface remained diffuse and white, similar to pre-flight observations. As with A276, Tedlar has been shown to be susceptible to AO erosion. The erosion effect of AO is the apparent reason for the lack of optical degradation of these flight samples.

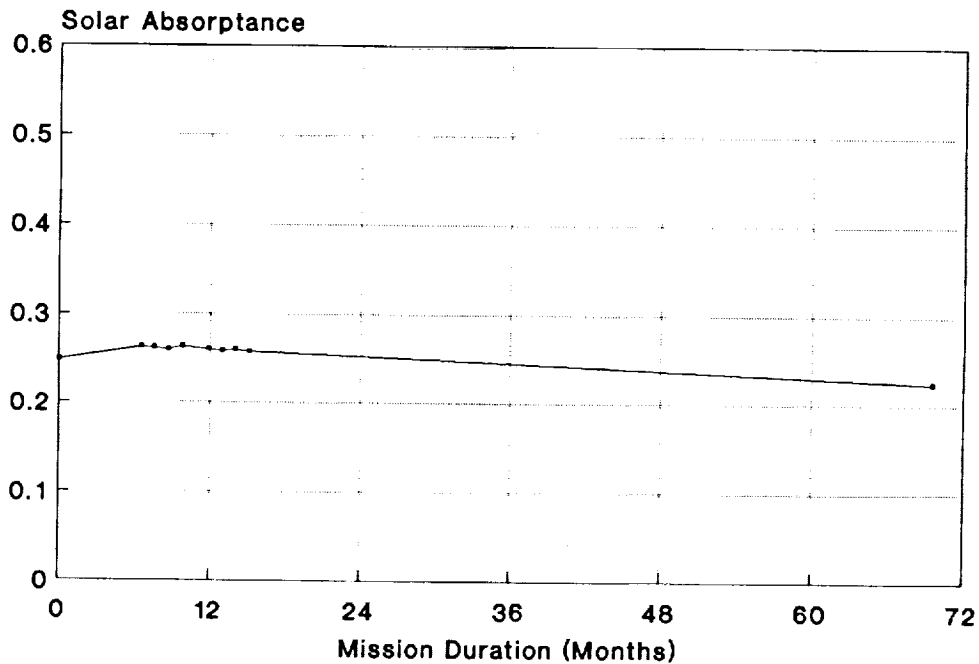


Figure 25. Reflectance Data for White Tedlar.

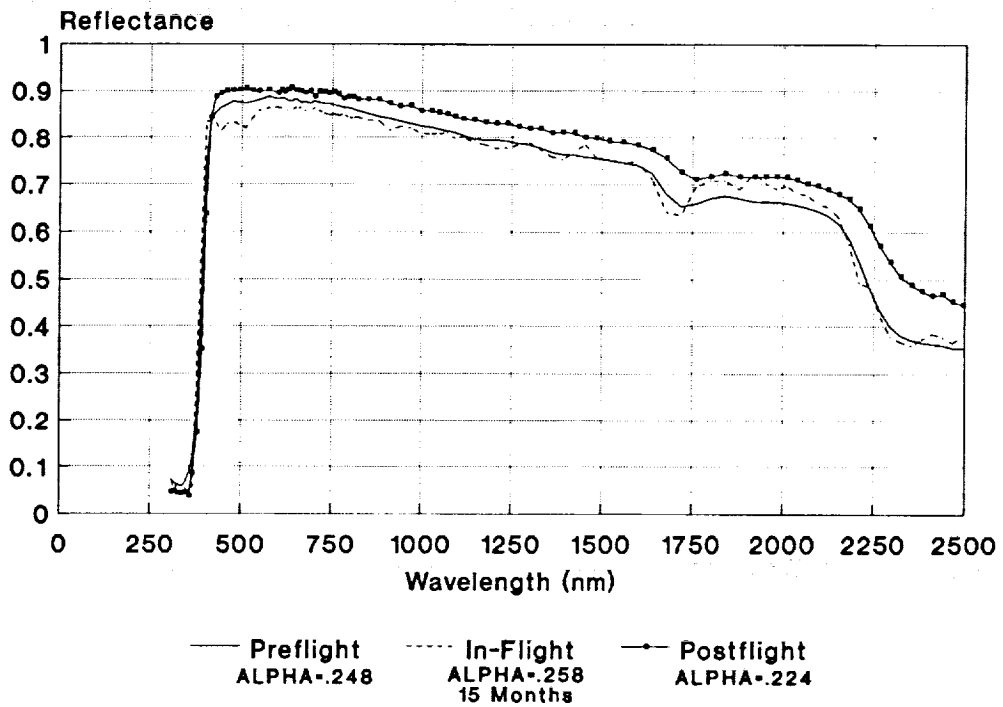
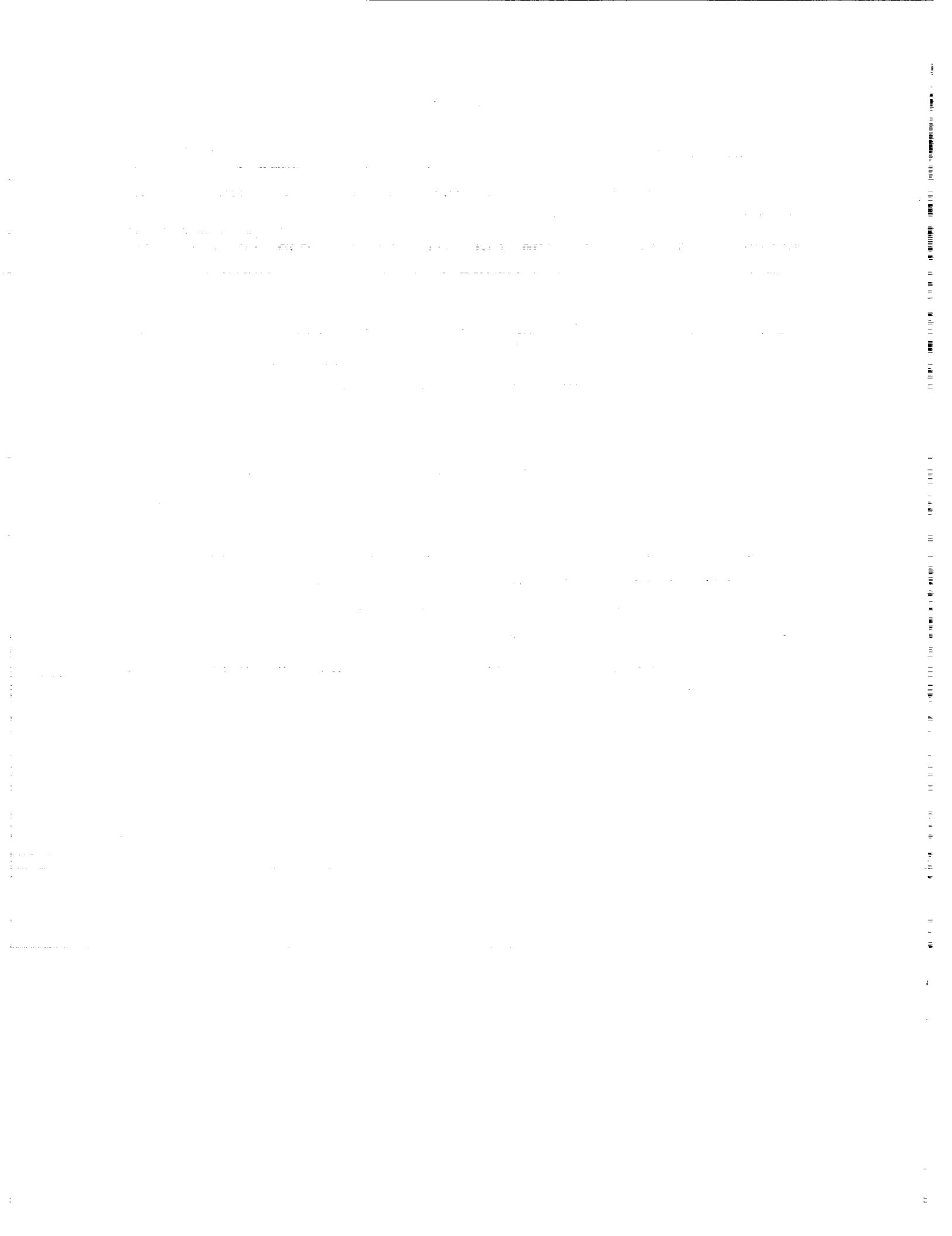


Figure 26. Performance of White Tedlar Film.

SUMMARY

The LDEF mission provided an excellent test bed for the behavior of materials in the space environment. The thermal control surfaces on the MSFC experiments experienced many types of mechanical and optical changes due to the LDEF space exposure. Some materials such as Z93 and YB71 were very stable for the extended exposure. Many other materials were significantly degraded both mechanically and optically. Some materials such as A276 and Tedlar were relatively stable optically but were significantly eroded by the AO environment. Silver Teflon was also eroded by AO but was optically stable where properly applied. The most significant problem with the silver Teflon was where the silver/inconel layers were cracked during the application of the pre-adhesived material. This problem points out the significance of the preparation and application process for long term stability of materials in the space environment.

With the diversity and complexity of the materials effects due to the extended LDEF mission, there remains many analyses to be performed to fully realize the benefits of the LDEF.



**ANODIZED ALUMINUM ON LDEF
A Current Status Of Measurements On
Chromic Acid Anodized Aluminum**

Johnny L. Golden
Boeing Defense & Space Group
Seattle, WA 98124-2499
Phone: 206/773-2055, FAX: 206/773-4946

Chromic acid anodize was used as the exterior coating for aluminum surfaces on LDEF to provide passive thermal control. Chromic acid anodized aluminum was also used as test specimens in thermal control coatings experiments. The following is a compilation and analysis of the data obtained thus far.

Solar absorptance and thermal emittance data for this summary was graciously provided by the following people.

SOURCES OF INFORMATION

- **Measurements Of α And ϵ From**
 - **T. R. Sampair, NASA LaRC / Lockheed**
LDEF Structure, Longerons, And Intercostals
 - **W. L. Plagemann, Boeing Defense & Space Group**
LDEF Tray Clamps
 - **W. S. Slemp, NASA LaRC**
Test Specimens
 - **D. R. Wilkes, AZ Technology, Inc.**
J. M. Zwiener, NASA MSFC
Test Specimens

Measurements reported by Tom Sampair for the solar absorptance and thermal emittance of chromic acid anodize on LDEF intercostals and longerons are shown in figures 1-4. During deintegration, readings were made on both exposed and unexposed areas of these structures (where covered by tray lips). Comparison is made in these figures to the Quality Assurance logs of 1978, made during LDEF part fabrication. Absorptance readings show significant variability from row to row. Absorptance measurements taken for leading edge surfaces are relatively unchanged, within the exhibited data scatter. However, trailing edge surfaces show significant increases in absorptance. Emittance readings for all exposed surfaces are not changed when compared to the QA logs. Unexposed surfaces, however, have a consistent increase in emittance compared to exposed surfaces.

LDEF INTERCOSTALS: AVERAGE ABSORPTIVITY Vs ROW LOCATION

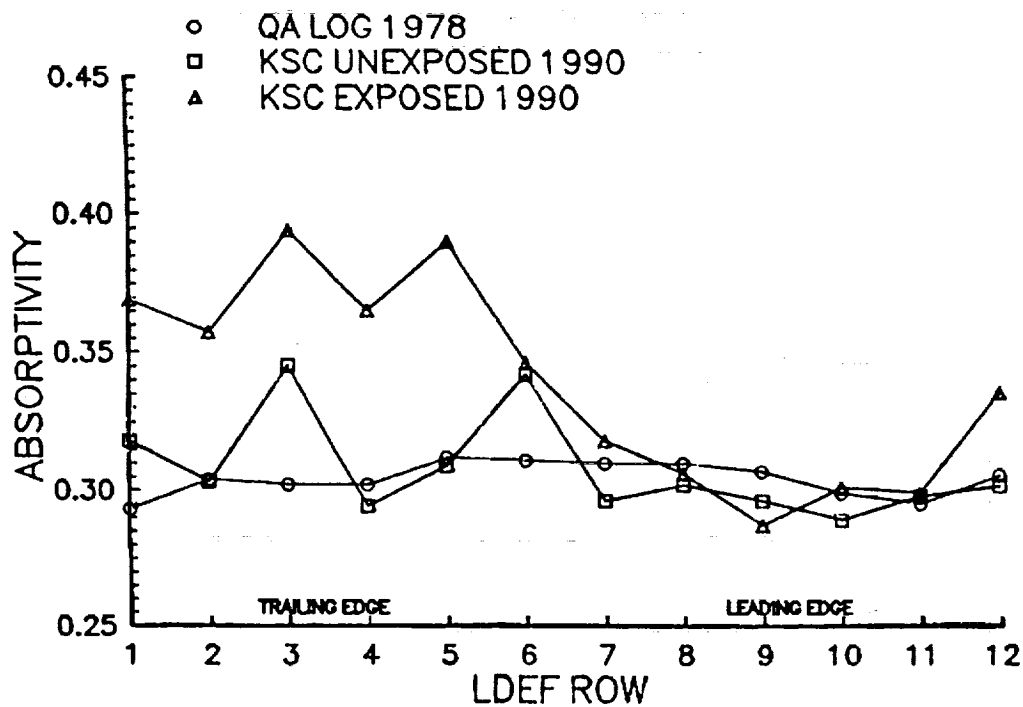


Figure 1.

LDEF LONGERONS: AVERAGE ABSORPTIVITY Vs ROW LOCATION

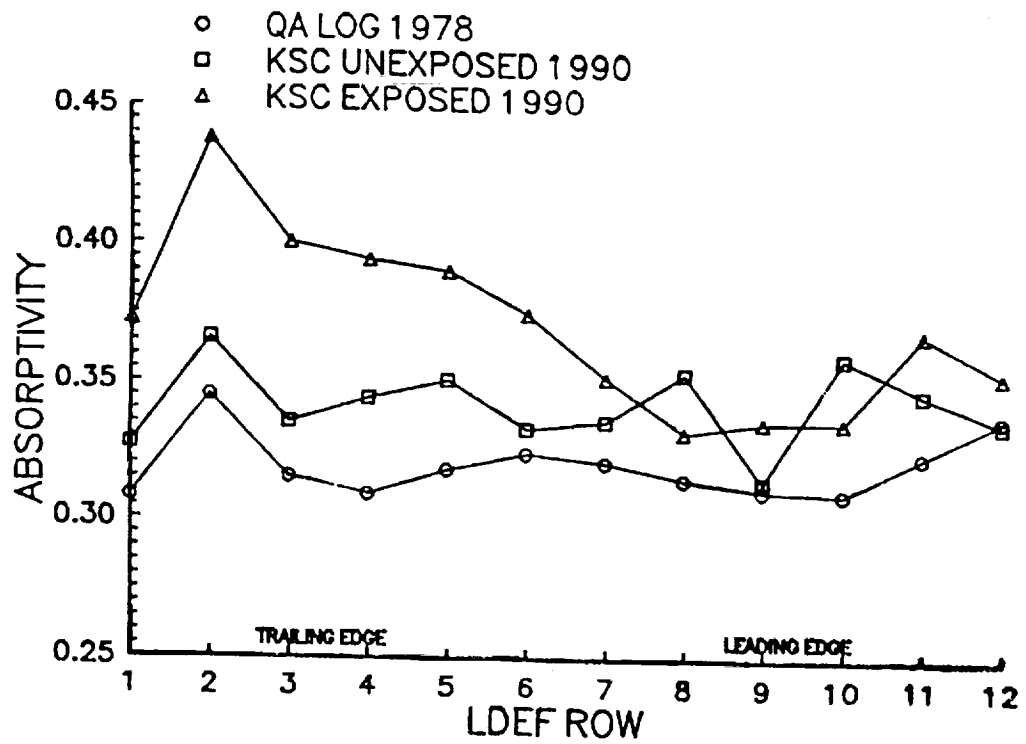


Figure 2.

LDEF INTERCOSTALS: AVERAGE EMISSIVITY VS ROW LOCATON

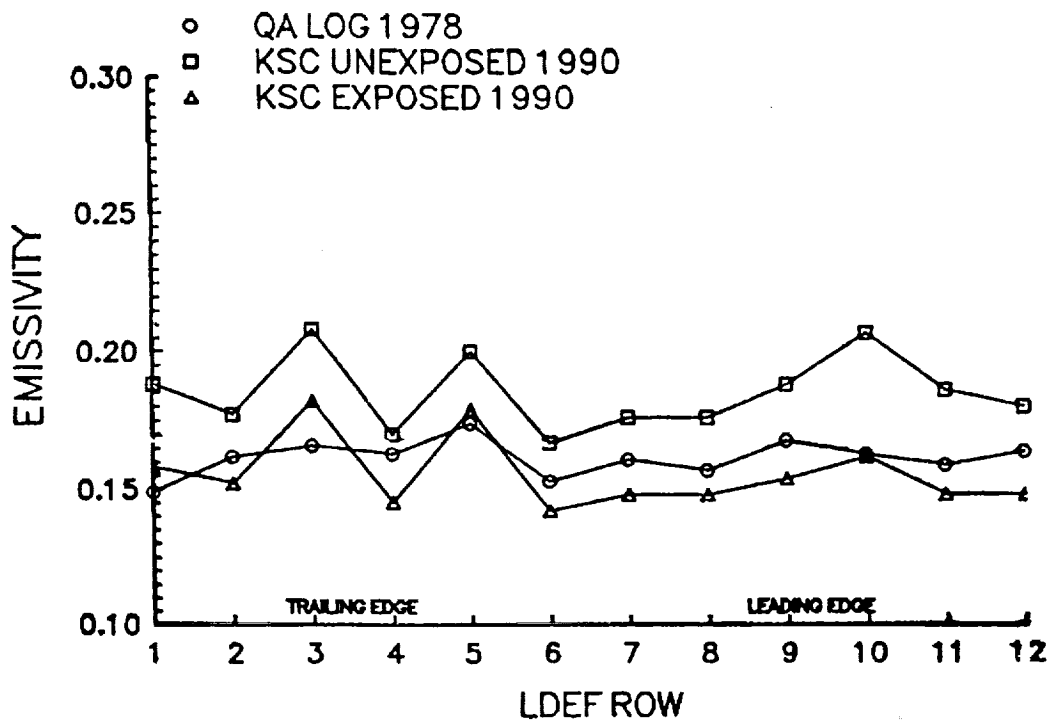


Figure 3.

LDEF LONGERONS: AVERAGE EMISSIVITY VS ROW LOCATON

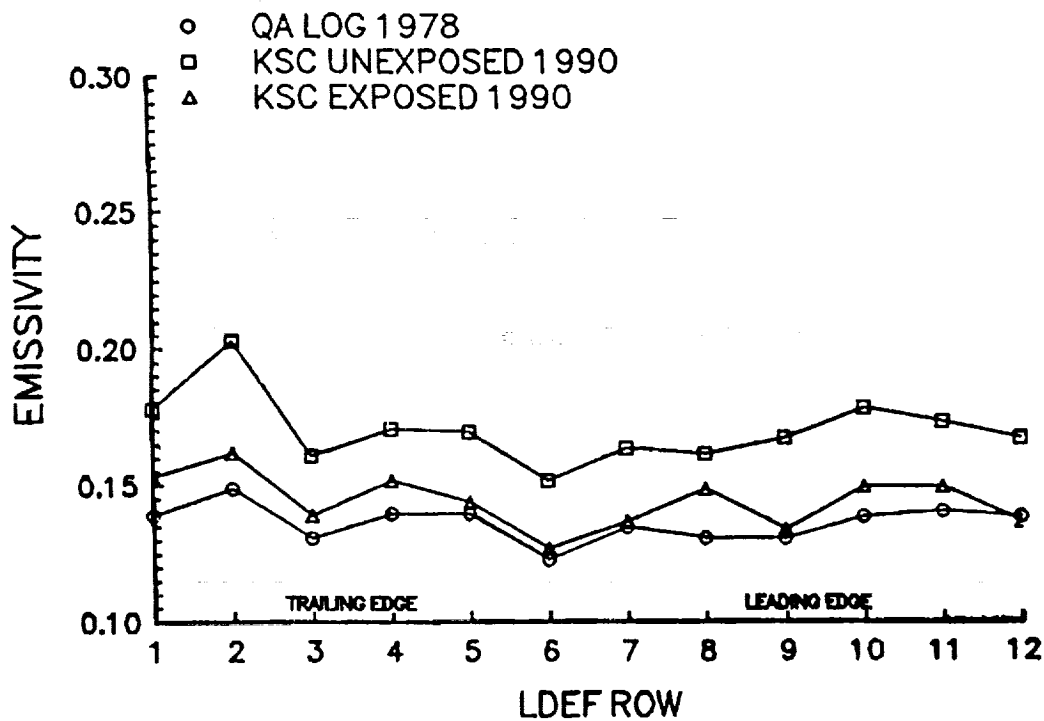


Figure 4.

Measurements reported by Wally Plagemann for optical properties of LDEF tray clamps are summarized in Table 1. When treated as averages, the anodize has suffered very little degradation as a result of space environmental effects.

Details of the tray clamp measurements are presented in various forms as figures 5 - 9. Figure 5 compares the absorptance readings for the exposed (front) and unexposed (back) surfaces of clamps as a function of LDEF location. A slight increase in absorptance for trailing edge surfaces is apparent. A similar plot of emittance is shown in figure 6. Although there is a 0.04 emittance unit spread to the readings, there is no difference apparent between leading and trailing edge clamps. There is, however, a slightly lower emittance for exposed surfaces than for unexposed surfaces, consistent with the readings reported for LDEF structure.

Solar absorptance versus UV exposure for LDEF side tray clamps is shown in figure 7. It appears that trailing edge specimens, as described previously, have higher absorptances than their counterparts on the leading edge. But there is no trend in absorptance change with UV exposure. A similar plot, figure 8, includes the readings for the earth and space end tray clamps. Finally, a plot of absorptance versus atomic oxygen fluence is shown in figure 9. Again the only change is a slight absorptance increase moving from high AO fluence (leading edge) to low AO fluence (trailing edge).

TABLE 1.

**Averages Of Measurements From Groups Of Tray Clamps
As Compared To Control Data**

Measurements On Flight Tray Clamps					Data From	Measurements
Unexposed	Exposed - Leading	Exposed - Trailing	Exposed - Space	Exposed - Earth	AIAA- 83-1492	On Unused Clamps
$\alpha - 0.34$ 0.01	$\alpha - 0.33$ 0.01	$\alpha - 0.35$ 0.02	$\alpha - 0.35$ 0.02	$\alpha - 0.35$ 0.01	$\alpha - 0.32$	$\alpha - 0.36$
$\epsilon - 0.16$ 0.01	$\epsilon - 0.15$ 0.01	$\epsilon - 0.15$ 0.01	$\epsilon - 0.16$ 0.02	$\epsilon - 0.17$ 0.01	$\epsilon - 0.16$	$\epsilon - 0.18$
$\alpha/\epsilon - 2.1$	$\alpha/\epsilon - 2.2$	$\alpha/\epsilon - 2.3$	$\alpha/\epsilon - 2.2$	$\alpha/\epsilon - 2.1$	$\alpha/\epsilon - 2.0$	$\alpha/\epsilon - 2.0$

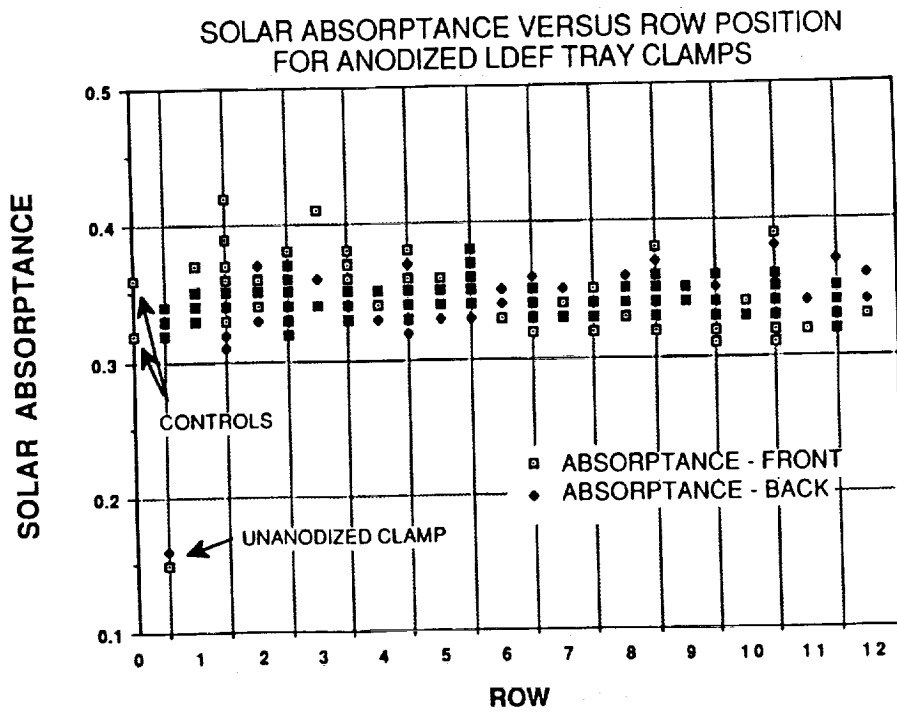


Figure 5.

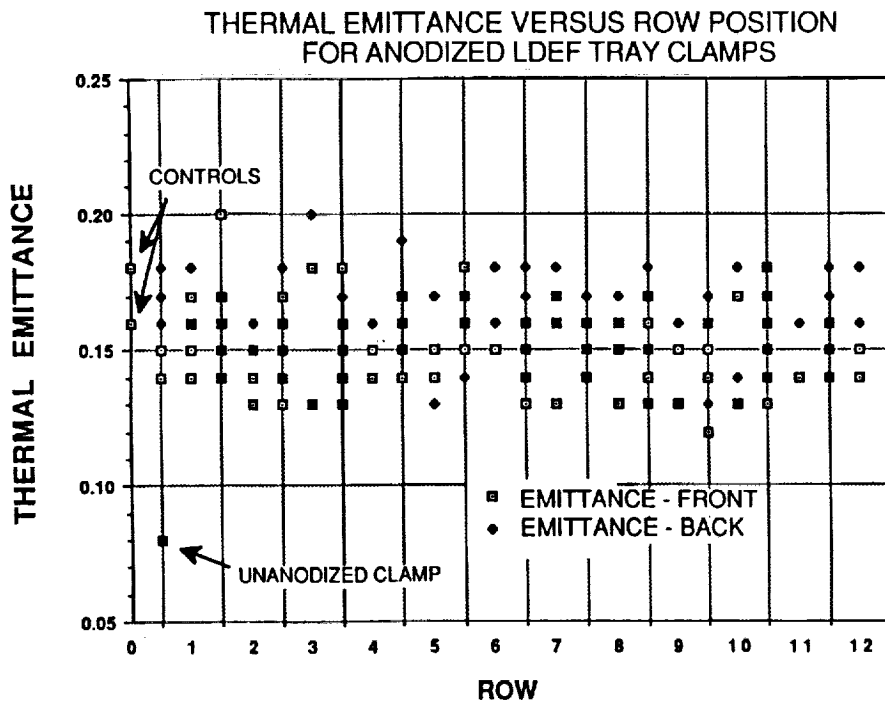


Figure 6.

SOLAR ABSORPTANCE VERSUS UV EXPOSURE
FOR RAM (LEADING EDGE) AND WAKE (TRAILING EDGE)
ANODIZED LDEF TRAY CLAMPS

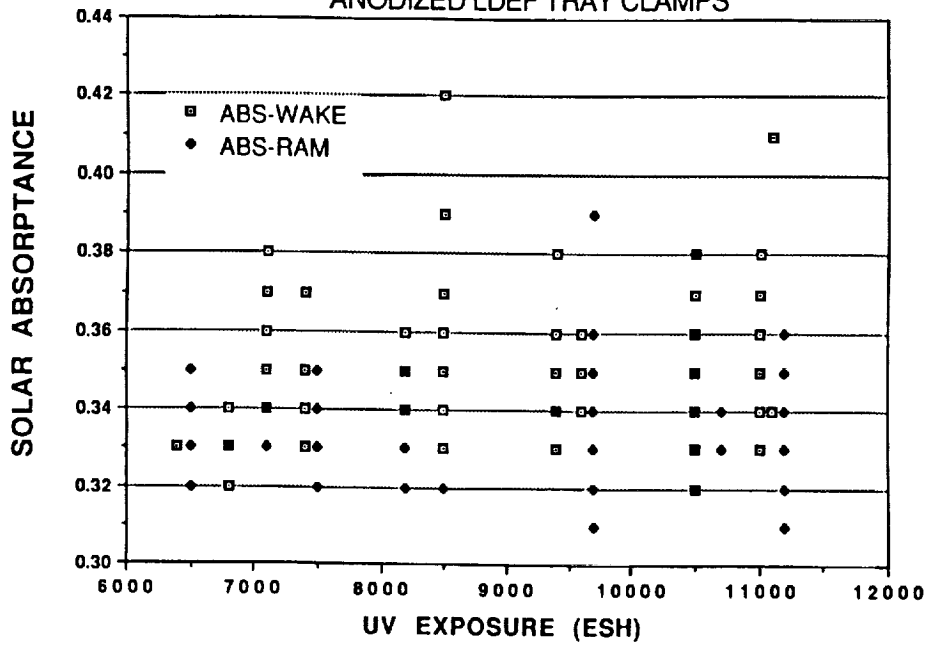


Figure 7.

SOLAR ABSORPTANCE VERSUS UV EXPOSURE
FOR ANODIZED LDEF TRAY CLAMPS

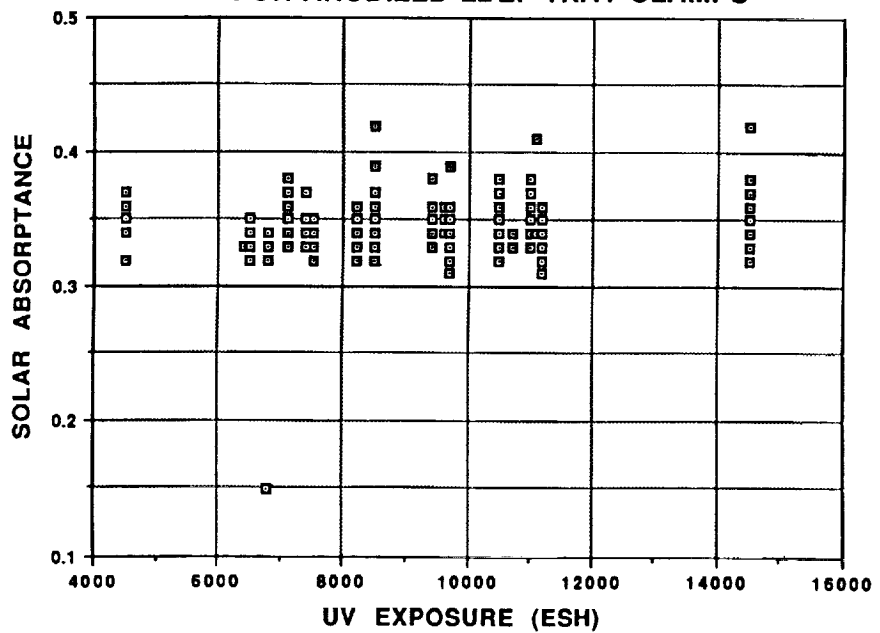


Figure 8.

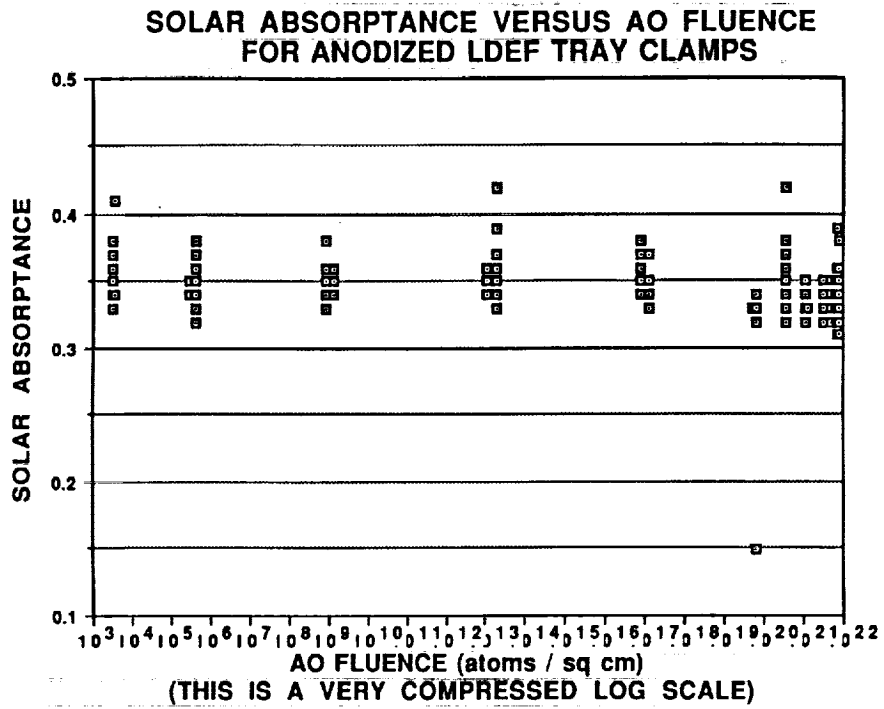


Figure 9.

Measurements reported by Wayne Slemp for chromic acid anodize on experiment S0010 are summarized in Table 2. Coatings of relatively constant absorptance (~10%) and varying emittance received two exposure levels at tray position B9 (8.7×10^{21} oxygen atoms/sq. cm and 11,200 ESH). Both absorptance and emittance readings at either exposure level are consistent with preflight measurements.

TABLE 2.

**NASA LaRC Experiment S0010 On
Chromic Acid Anodize (CAA)**

Coating	Preflight		10 Month Exposure		5.8 Year Exposure	
	α	ϵ	α	ϵ	α	ϵ
Thin CAA	0.295	0.16	0.299	0.17	--	--
	0.288	0.18	--	--	0.296	0.19
Medium CAA	0.292	0.43	0.287	0.43	--	--
	0.306	0.45	--	--	0.311	0.46
Thick CAA	0.33	0.71	0.337	0.71	--	--
	0.341	0.75	--	--	0.354	0.75

Measurements reported by Don Wilkes and Jim Zwiener for chromic acid anodize on experiment S0069 are summarized in Table 3. This experiment was located at tray position A9 (8.7×10^{21} oxygen atoms/sq. cm and 11,200 ESH). Two specimens of comparable absorptance and emittance were periodically measured for absorptance on this active experiment during the first 19.5 months of the LDEF flight. During that time, the absorptance of the anodize specimens increased significantly and consistently. One of the specimens was left exposed for the entire mission and recovered slightly (decreased) in absorptance. Emittance of the two specimens was not affected.

TABLE 3.

NASA MSFC And AZTEK Experiment S0069 Chromic Acid Anodize Specimens				
Specimen	Preflight	12 Months	19.5 Months	Postflight (69.2 Months)
C61	$\alpha - 0.41$ $\epsilon - 0.84$	$\alpha - 0.50$	--	$\alpha - 0.47$ $\epsilon - 0.83$
C63	$\alpha - 0.40$ $\epsilon - 0.84$	$\alpha - 0.49$	$\alpha - 0.54$ $\epsilon - 0.84$	--

There are several points that can be made in summary. First, there was some variability inherent in the absorptance and emittance measurements for LDEF chromic acid anodize coatings, due to both the anodizing process, and due to the differences in equipment and analysts used to make the measurements over the years. Data from tray clamps (and from LDEF structures) indicates this variability within one standard deviation is 0.02 for absorptance and 0.01 for emittance.

Next, absorptance changes for leading edge surfaces was minimal, with the exception being the results from Experiment S0069. The absorptance on trailing edge surfaces increased in general when compared to available control measurements.

Emittance changes were complex in that emittance appears to have slightly increased for unexposed surfaces, when compared to exposed surface or QA logs. However, these changes are of minimal significance when compared to inherent emittance variability or when treated relatively.

Based on the analyses thus far, indications are that chromic acid anodize is quite stable in the LEO environment, but that contamination did effect absorptance increases. Most leading edge surfaces were cleaned of this contamination by atomic oxygen.

• SUMMARY

- Variability Inherent In CAA Process From Tray Clamp Measurements Is $\pm 0.02 - 0.03$ In Both Absorptance And Emittance**
- Emittance Of Shielded Anodize Is Greater Than That Measured For Exposed Anodize**
- Absorptance Change On Leading Edge Surfaces Is Minimal, With Exception**
- Absorptance Increased on Trailing Edge Surfaces Compared to Unexposed Surfaces or to 1978 QA data**
- Results Indicate Absorptance Increases Are Due To Contamination Early In The LDEF Mission, Subsequently Removed From Leading Edge Surfaces By Atomic Oxygen**



PERFORMANCE OF THERMAL CONTROL TAPE
IN THE PROTECTION OF COMPOSITE MATERIALS

Rachel R. Kamenetzky
Ann F. Whitaker
NASA Marshall Space Flight Center
MSFC, AL

INTRODUCTION

The selection of materials for construction of long duration mission spacecraft has presented many challenges to the aerospace design community. After nearly six years in low earth orbit, NASA's Long Duration Exposure Facility (LDEF), retrieved in January of 1990, has provided valuable information on both the nature of the space environment as well as the effects of the space environment on potential spacecraft materials. Composites, long a favorite of the design community because of a high strength-to-weight ratio, were flown in various configurations on LDEF in order to evaluate the effects of radiation, atomic oxygen, vacuum, micrometeoroid debris and thermal variations on their performance. Fiberglass composite samples covered with an aluminum thermal control tape were flown as part of the flight experiment A0171, the Solar Array Materials Passive LDEF Experiment (SAMPLE). Visual observations and test results indicate that the thermal control tape suffered little degradation from the space exposure and proved to be a reliable source of protection from atomic oxygen erosion and UV radiation for the underlying composite material.

PRECEDING PAGE BLANK NOT FILMED

LDEF A0171 EXPOSURE CONDITIONS

The LDEF A0171 tray was located on the leading edge row 8A of the satellite, and was in orbit at an angle of ~38° from the ram vector. Table I shown below summarizes the environmental exposure conditions for the composite samples. Of particular significance in the evaluation of the thermal control tape performance is the high atomic oxygen fluence level and the large number of thermal cycles.

Table I LDEF A0171 Exposure Conditions

High Vacuum	10^{-6} to 10^{-7} Torr (estimated)
UV Radiation	10,471 ESH
Proton Fluence	10^9 p+/cm ² (0.5 to 200 Mev)
Electron Fluence	10^{12} to 10^8 e ⁻ /cm ² (0.5 to 3.0 Mev)
Atomic Oxygen	6.93×10^{21} atoms/cm ²
Micrometeoroid/ Space Debris	2 to 7 impacts per composite, <1mm
Thermal Cycles	~32,000 cycles (Temperature TBD)

COMPOSITE TEST SPECIMENS

Six "S" glass epoxy composite samples, 0.5" x 6" in size, were flown as part of flight experiment A0171, three of which were covered with an aluminum thermal control tape. Additionally, six composite control samples, three with the thermal control tape, remained in the lab for post flight comparison. The composite resin was supplied by Air Logistics and the "S" glass was from Owens Corning S-901 glass. The thermal control tape was a 2 mil aluminum with 2 mil pressure sensitive silicone adhesive SR574. Figure 1 below shows the basic flight configuration for the six plates which made up the A0171 tray experiment. The fiberglass epoxy composites, along with the aluminum covered fiberglass composites, are shown in the post flight condition in the upper right corner of plate III.

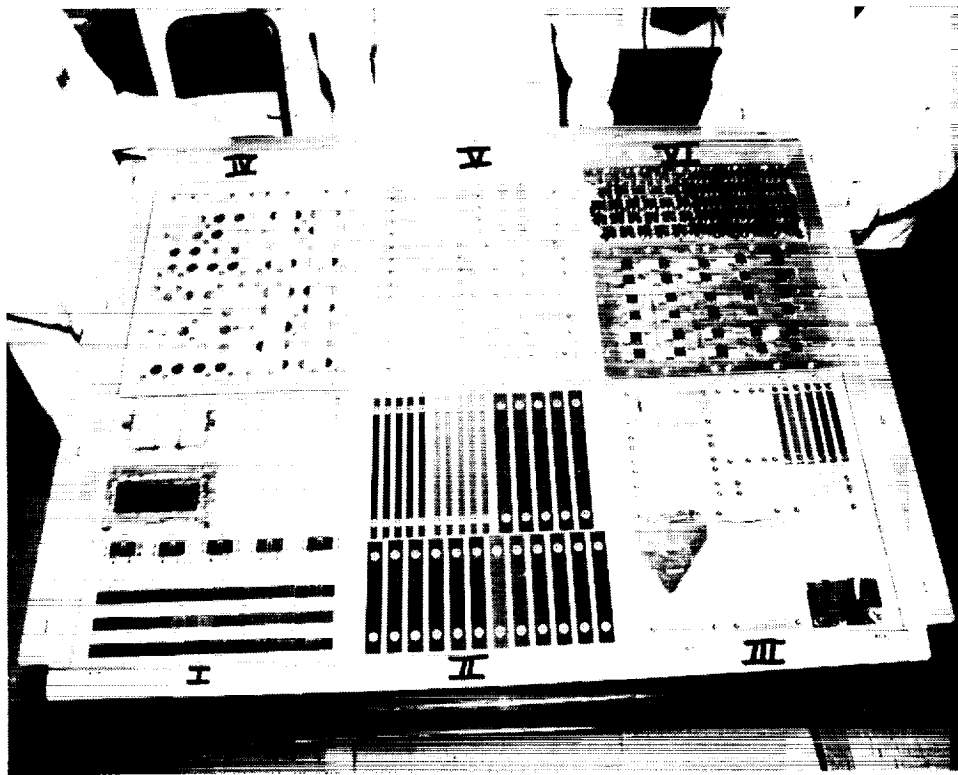


Figure 1. Flight experiment A0171, Solar Array Materials Passive LDEF Experiment (SAMPLE).

VISUAL OBSERVATIONS

In order to evaluate the effects of the space environment on the aluminum thermal control tape, comparative series of visual and mechanical tests were performed on the tape covered flight composite samples and the laboratory tape covered control composite samples. As seen in figure 2 below, no clear visual distinction can be made between the flight exposed samples and the control samples. However, because the tape was applied only to the surface of the composites, the edges of the flight samples were exposed to atomic oxygen and UV radiation. The flight sample edges showed clear signs of resin erosion in the composite matrix. A thin oxide layer was also evident on both the exposed and control tape surface. Further work is needed to better quantify the thickness of this oxide layer.

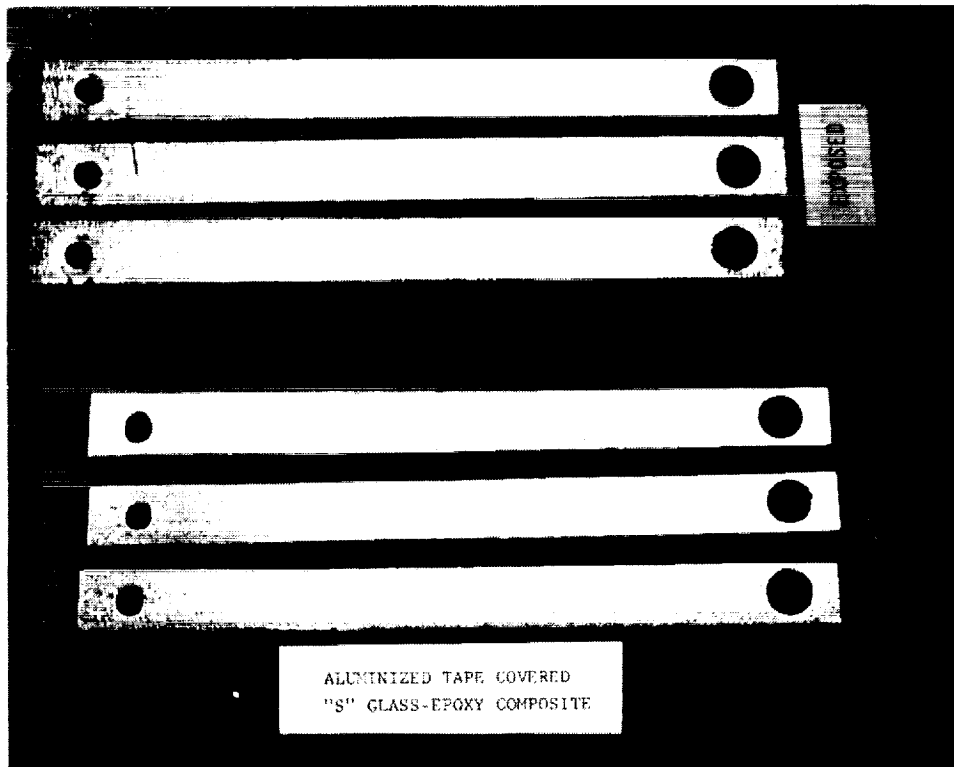


Figure 2. Tape covered fiberglass epoxy composite flight and control specimens.

ALUMINUM THERMAL CONTROL TAPE SEM PHOTOGRAPHS

The thermal control tape surface on the flight and control composite samples was examined using a scanning electric microscope (SEM). Figure 3 shown below compares the SEM photograph taken at 200x magnification for a control sample (left) and for a flight sample (right). Both the control and flight sample photographs show what appears to be fabrication "roll marks". The flight sample SEM photo, however, also shows evidence of a wave-like crest structure projecting from the surface of the tape.

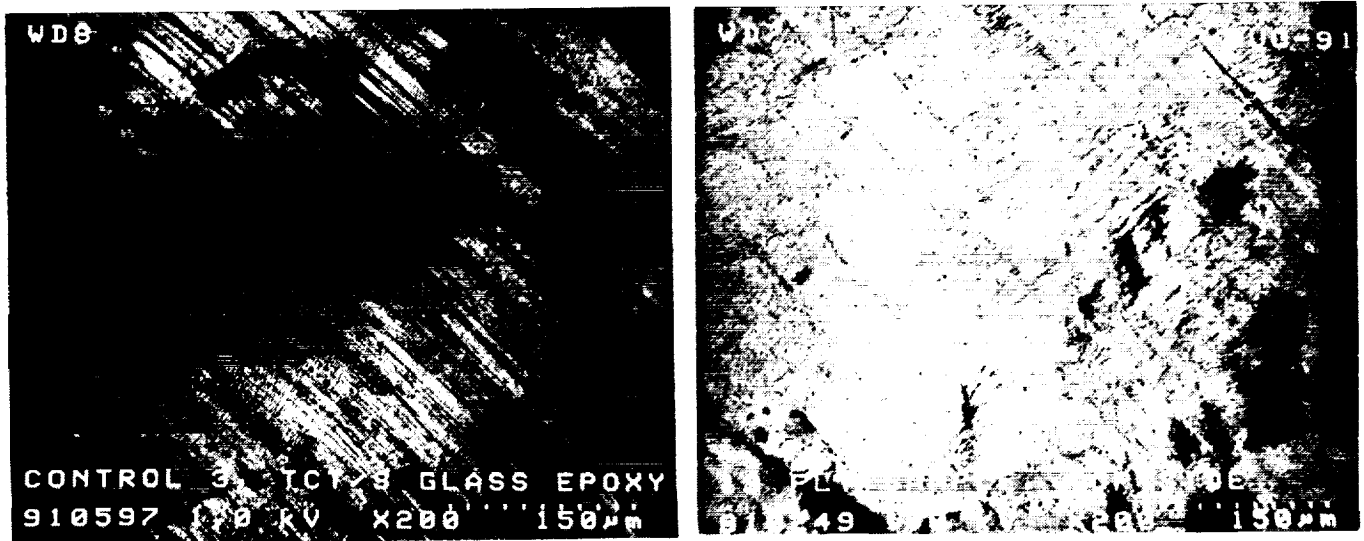


Figure 3. SEM photograph at 200x magnification of control tape surface (left) and flight tape surface (right).

ALUMINUM THERMAL CONTROL TAPE SEM PHOTOGRAPHS
(Continued)

Figure 4 shown below compares the SEM photograph taken at 1000x magnification for the same control sample (left) and flight sample (right) as contained in the earlier SEM photos. In this series of photos, a clear difference in the surface structure of the two tape specimens is easily seen. The wave-like structure of the flight tape is reminiscent of Luder's bands, a fatigue phenomena, and may be linked to the high number of thermal cycles that the flight samples underwent. Further analyses are required to confirm this phenomena.

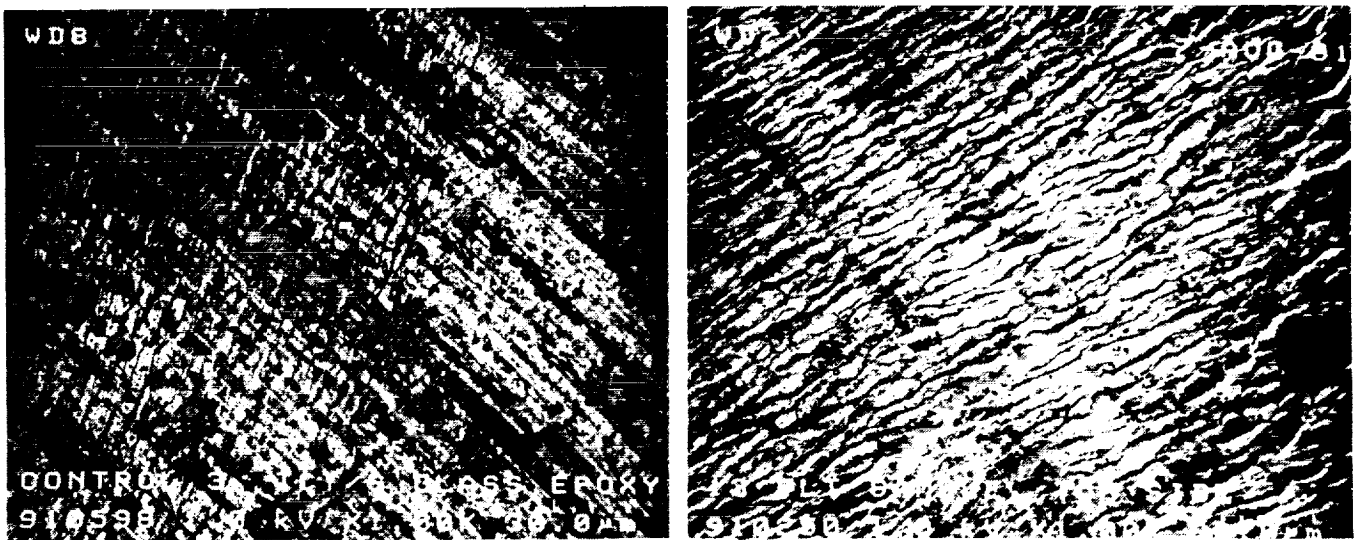
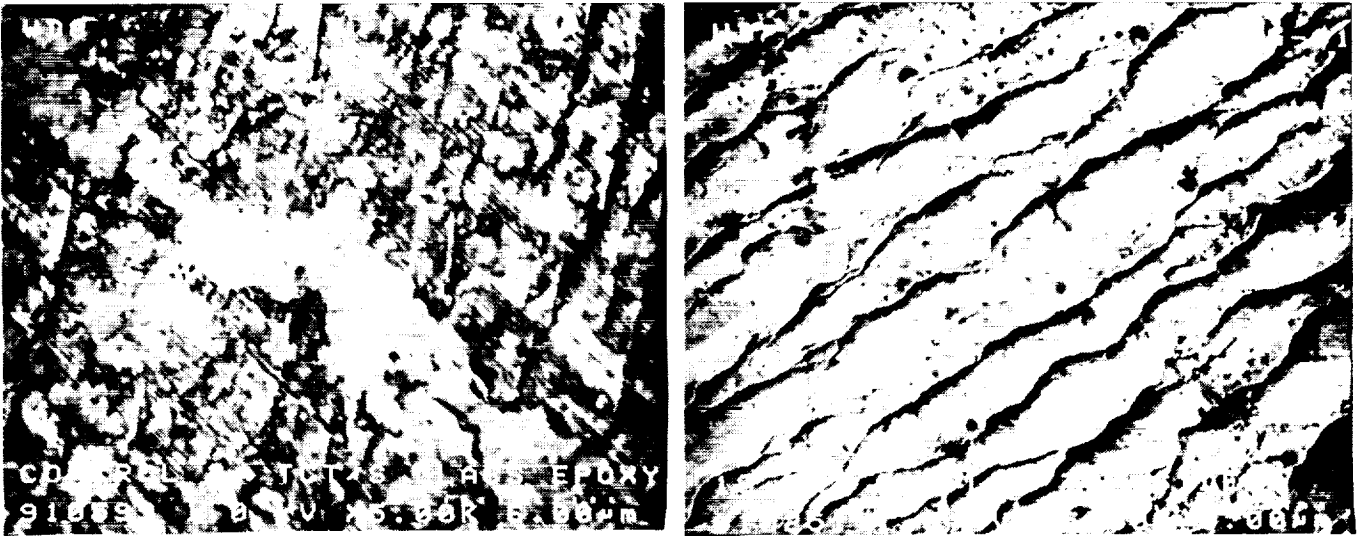


Figure 4. SEM photograph at 1000x magnification of control tape surface (left) and flight tape surface (right).

ALUMINUM THERMAL CONTROL TAPE SEM PHOTOGRAPHS
(Continued)

Finally, figure 5 below compares the SEM photograph taken at 5000x magnification for the control tape sample (left) and for the exposed tape sample (right). The contrast in surface texture between the flight tape and control tape is clearly evident.



Caption: Figure 5. SEM photograph at 5000x magnification of control tape surface (left) and flight tape surface (right).

MICROMETEOROID DEBRIS

Two of the flight taped covered glass epoxy specimens showed evidence of a single impact with micrometeoroid/space debris, with each impact measuring less than 1mm in diameter. While the thermal control tape was able to prevent damage to the composite substrate on one flight sample, the impact on the second sample did penetrate through to the composite substrate causing damage to the underlying fibers. Figure 6 shown below is the SEM photographs of the impact area for the non-penetrating impact (left) and for the penetrating impact (right).

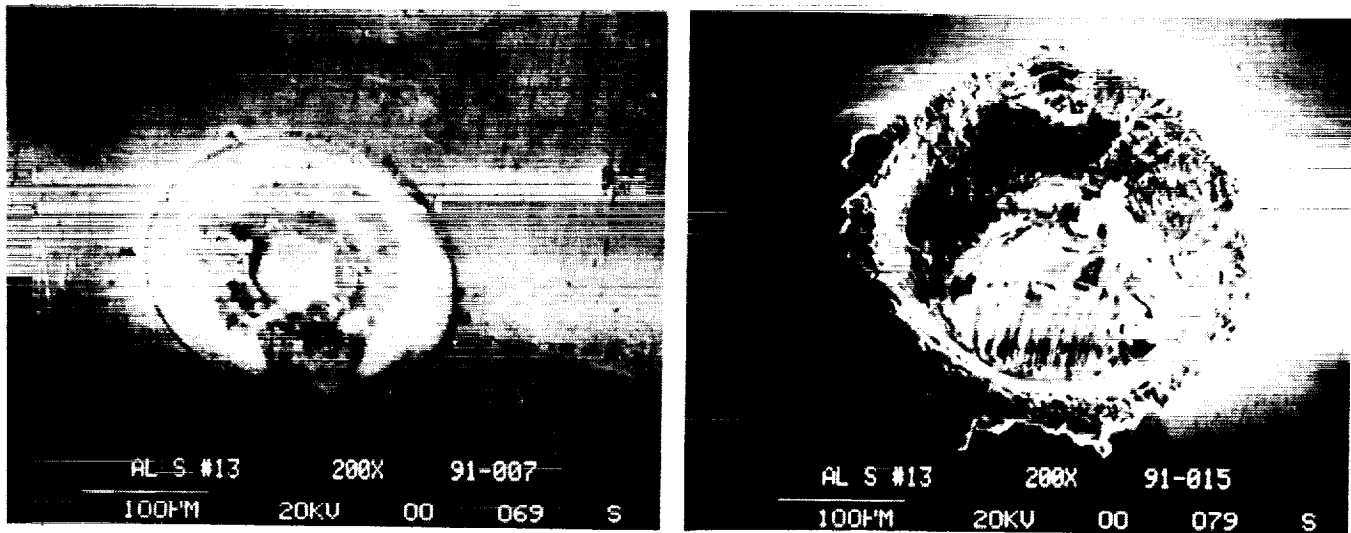


Figure 6. SEM photograph at 200x magnification of debris impacts on flight exposed tape covered fiberglass composites.

MECHANICAL AND OPTICAL PROPERTIES

Deterioration of composite materials by atomic oxygen/UV radiation is of considerable concern to the aerospace designer. Erosion of the composite matrix resin can lead to degradation in material mechanical strength. The thermal control tape proved successful in protecting the underlying composite from the atomic oxygen/UV radiation resin erosion as evident in the mass loss data. The mass loss for the "bare" composite was four times greater than for the tape covered composite. The small degree of mass loss on the tape covered specimens was due to erosion along the specimen edges where the composite was exposed. The tape silicone adhesive also proved to withstand the rigors of the environment, with the flight specimens showing an increase in peel strength over the control by a factor greater than 2 to 1. This increase in peel strength is again probably due to thermal cycling effects. Difficulties in conducting the peel tests on the flight tape specimens also suggested that the flight tape had become embrittled by the space exposure. This tape embrittlement theory is currently under investigation. The solar absorptance and IR emittance on the tape covered specimens showed little change between the flight and control specimens, with the differences in recorded values considered to be in the noise range of the portable instruments used to measure the properties. Table II below summarizes the mechanical and optical properties for the "bare" composite, control and flight, and for the aluminum tape covered composites, control and flight.

Table II Mechanical and Optical Properties

	Peel Strength (lb./in)	Mass Loss (mg/cm ²)	Solar α (avg.)	IR ϵ (avg.)
<u>Bare Composite</u>				
✓ Control	*****	*****	0.723	0.894
✓ Flight	*****	2.40	0.787	0.895
<u>Tape Covered Composite</u>				
✓ Control	1.9	*****	0.140	0.025
✓ Flight	4.6	0.59	0.103	0.020

CONCLUSION

The aluminum thermal control tape proved effective in protecting the underlying fiberglass epoxy composite from the rigors of the low earth orbit space exposure. Although SEM photos revealed morphology changes in the flight exposed tape surface, due at least in part to thermal cycling effects, the overall tape performance was not compromised. Mass loss data from the flight tape covered composite samples and "bare" composite samples clearly indicate that the aluminum tape prevented atomic oxygen/UV erosion of the composite matrix resin. The average peel strength for the flight exposed tapes increased by a factor of nearly 2.5 over the average ground based control tapes. Solar absorptance and IR emittance data on the aluminum tape varied little between flight exposed samples and control samples. The tape did not however provide complete protection from micrometeoroid/debris. One debris hit did penetrate the protective tape, causing damage to the composite substrate, while a second impact, originating most probably from a shuttle fluid dump, was unable to penetrate the tape.

FLUORESCENCE OF THERMAL CONTROL COATINGS ON S0069 AND A0114

James M. Zwiener, Richard J. Mell, Palmer N. Peters
NASA Marshall Space Flight Center
Huntsville, AL 35812

Donald R. Wilkes, Edgar R. Miller
AZ Technology
Huntsville, AL 35801

John C. Gregory
University of Alabama/Huntsville
Huntsville, AL 35899

INTRODUCTION

Many of the thermal control surfaces exposed to the space environment during the 5.8 year LDEF mission experienced changes in fluorescence. All of the thermal control coatings flown on LDEF experiments S0069 and A0114 were characterized for fluorescence under ambient conditions. Some of the black coatings, having protective overcoats, appear bright yellow under ultraviolet exposure. Urethane based coatings exhibited emission spectra shifts toward longer wavelengths in the visible range. Zinc oxide pigment based coatings experienced a quenching of fluorescence, while zinc orthotitanate pigment based and other ceramic type coatings had no measurable fluorescence.

CATEGORIES OR TYPES OF FLUORESCENCE EFFECTS OBSERVED

The specific fluorescence effects observed on the experiments can be divided into three categories as outlined in figure 1. Urethane binder type coatings including the black Z302 and the white A276 experienced similar shifts of fluorescence from the near ultraviolet toward the visible range. Zinc oxide pigmented coatings, using either the silicone or silicate binders, demonstrated the same quenching of original (pre-flight) fluorescence. Silver Teflon did not originally fluoresce, but now shows a weak, but measurable, fluorescence in the visible.

- URETHANE BINDER TYPE COATINGS
 - ▶ BLACK COATINGS
 - ▶ WHITE COATINGS
- ZINC OXIDE PIGMENTED COATINGS
 - ▶ SILICONE & SILICATE TYPE BINDERS
 - ▶ WHITE COATINGS
- SILVER TEFLON COATINGS
 - ▶ ACRYLIC ADHESIVE EFFECT

Figure 1. Three Categories of Fluorescence Effects Observed.

Note: Teflon is a trademark of Dupont.

PHOTOGRAPH OF THE VISUAL FLUORESCENCE OF S0069 SAMPLES

A pronounced visual demonstration of the post-flight fluorescence glow of the urethane type paints with protective atomic oxygen overcoats is provided in figure 2. Photographs were made using either white or ultraviolet lighting. Black Z302/OI650, under ultraviolet lighting, shows a bright visible yellow fluorescence. Even the white A276/OI650 shows a bright yellow fluorescence under ultraviolet lighting. The other samples lack sufficiently pronounced visible fluorescence for normal photographic observation.

ORIGINAL PAGE
BLACK AND WHITE PHOTOGRAPH

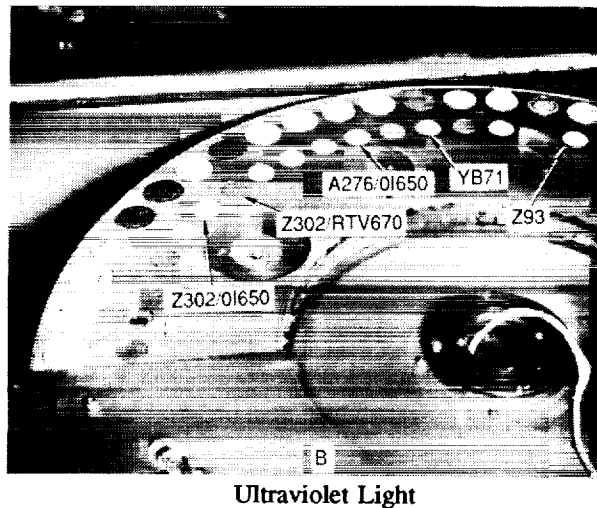
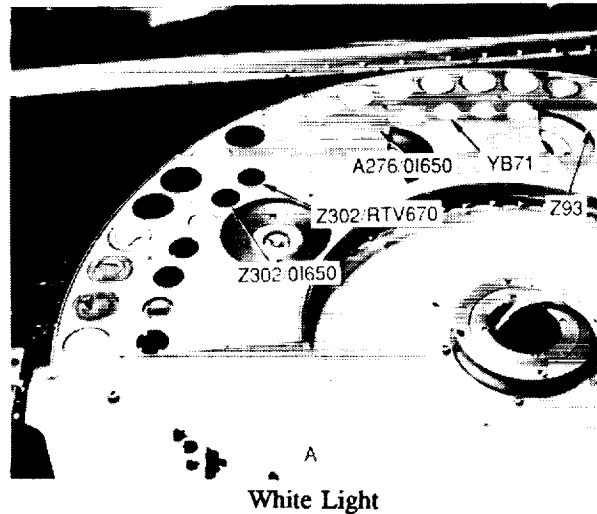


Figure 2. Fluorescence of Thermal Control Coatings Comparison of Samples Under White and Ultraviolet Light.

MEASUREMENT SETUP

Spectral measurements of the fluorescence of the samples from both the S0069 and A0114 were made using the instrumentation setup shown in figure 3. Monochromatic irradiation of the samples was provided using a mercury/xenon high pressure discharge source and attached prism monochromator. An excitation wavelength centered at 280 nm was used for all measurements described in this paper. All measurements utilized a test control sample of MgO to setup and verify consistent system response. In addition, sample controls were run for comparison.

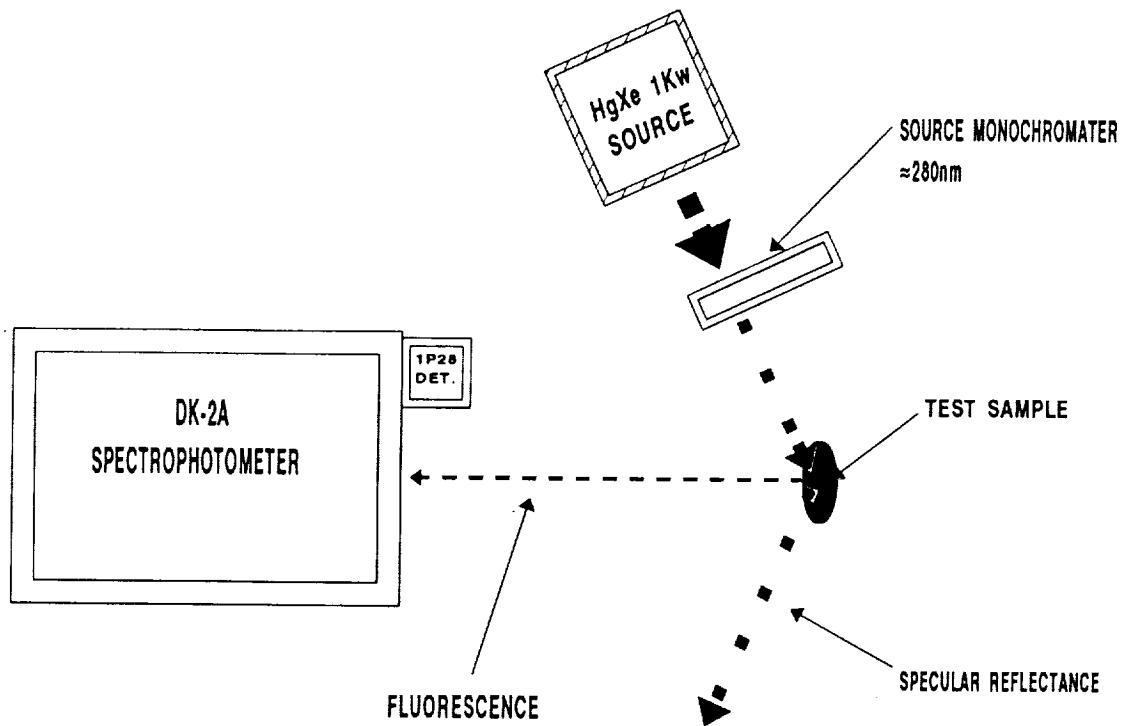


Figure 3. Schematic of Fluorescence Measurement.

FLUORESCENCE SPECTRA OF Z302

A typical example of the measured spectral fluorescence of the black Z302 samples is provided in figure 4. At about 280nm the scattered signal of the incident excitation light is recorded. An increase in the 280nm data indicates an increase in scatter or a decrease in absorptance, whereas a decrease could be attributed to an increase in the absorptance of the coating in the wavelength region. Since the unprotected Z302 is eroded by atomic oxygen, this increase over the ground control is most likely caused by a surface roughening. Note, this sample was exposed for only the 1.6 years and was still black. The Z302 sample exposed for the full 5.8 years was eroded down to the base primer, as can be seen in figure 2 (fourth sample from left, on outer row). The ground control sample shows a weak but measurable signal in the 400 to 500 nm wavelength range. In comparison the flight sample shows a shift of fluorescence into the visible region.

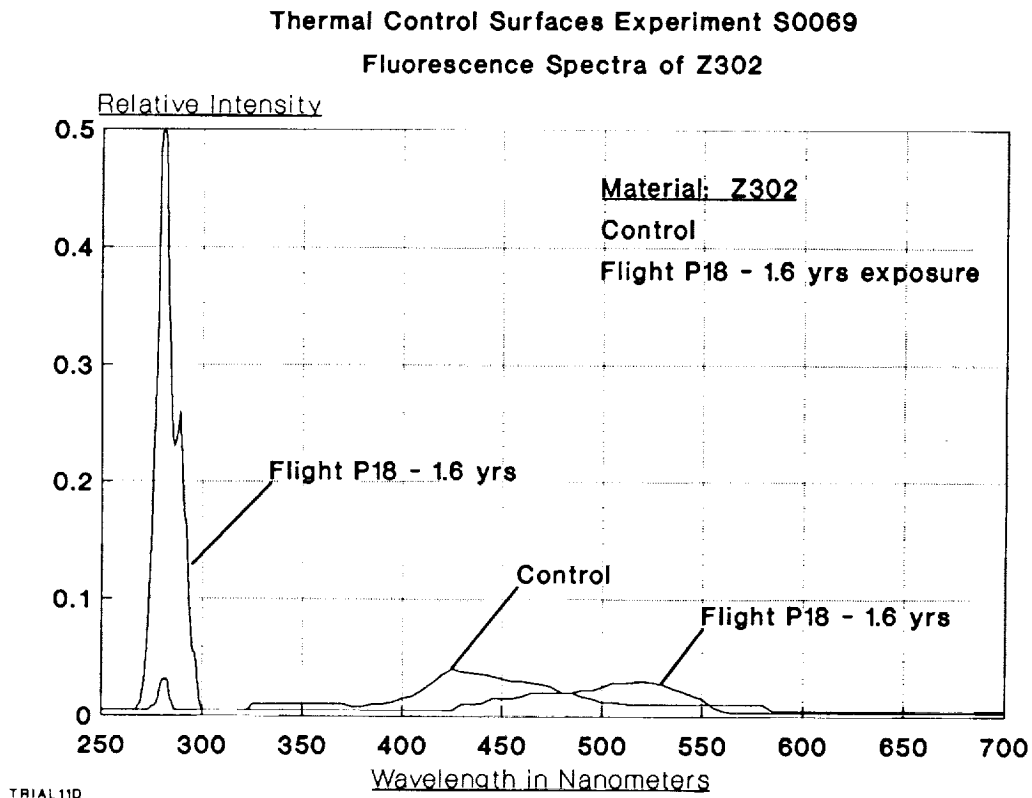


Figure 4. Fluorescence Spectra of Z302.

FLUORESCENCE SPECTRA OF Z302 WITH OI650 OVERCOAT

The brightest visual fluorescence was observed for the OI650 overcoated urethane based paint samples, as was shown in Figure 2. An example of the measured emission spectra is provided by the scan in Figure 5. It is interesting to note that the fluorescence of the Z302 and the OI650 are relatively distinct for the stored control sample; whereas, after flight exposure this distinction is not obvious. As compared to the Z302 sample, the Z302/OI650 emission shifts toward the visible region, but is considerably stronger. Although the data is not corrected for variations in instrumentation spectral response, the relative response between different scans at the same wavelength are comparable. A reference control was utilized to calibrate and maintain consistent total system response.

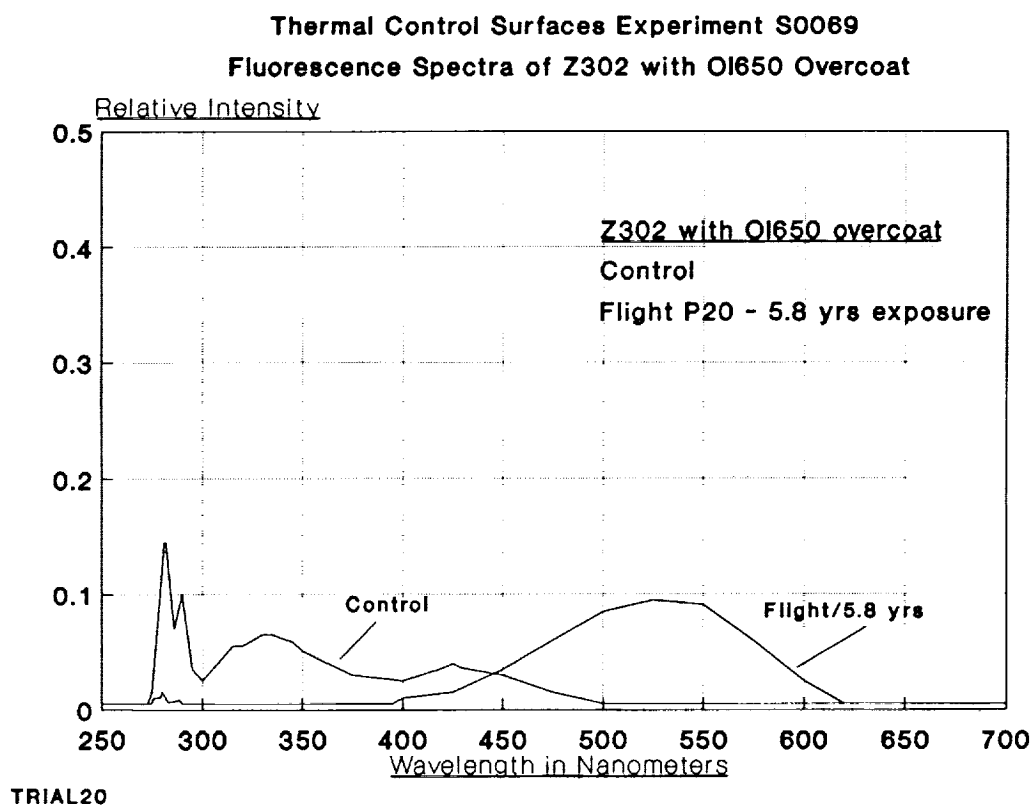
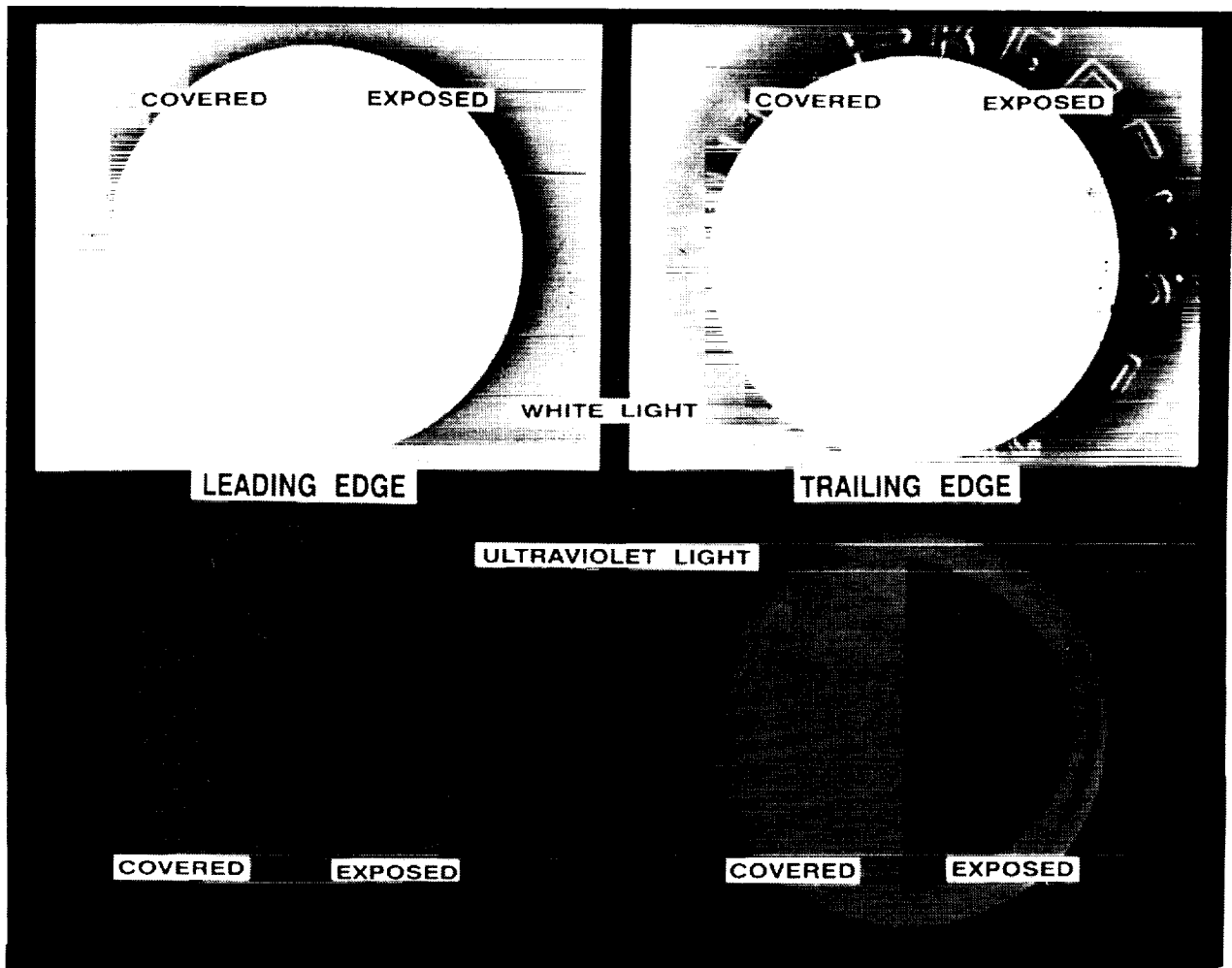


Figure 5. Fluorescence Spectra of Z302 with OI650 Overcoat.

Z93 WHITE PAINT VISIBLE FLUORESCENCE EFFECT

Photographs of Z93 samples from experiment A0114, under both visible and ultraviolet light (Figure 6), clearly show the quenching or reduction of the observed fluorescence emissions. These samples had covers that exposed only half of the surface. In white light, the exposed area is difficult to discern, whereas under the ultraviolet light it becomes very clear which area was exposed. Also note that the ram or leading edge sample and trailing edge sample experienced the same quenching of fluorescence. Comparison of the exposed to covered sample areas provides a good visible demonstration of the reflectance stability of this material to the low earth orbit space environment for extended periods.



White Light and Fluorescence of Z93
Samples from Experiment A0114

Figure 6. White Light and Ultraviolet Light Photographs of Z93.

FLUORESCENCE SPECTRA OF Z93 WHITE PAINT

Significant quenching of the fluorescence of the Z93 white paint occurred within the first 1.6 years of on-orbit exposure. Additional quenching occurred with continued exposure as shown in the fluorescence spectra in Figure 7. S13G/LO also showed a similar quenching of fluorescence. Both of these coatings are based on a ZnO pigment, but have different binders. Z93 has a silicate binder, whereas S13G/LO utilizes a silicone binder. Previous work reported by Zerlaut and Harada at IITRI (ref. 1) observed a decrease of fluorescence in the zinc oxide material after ultraviolet irradiation in vacuum. The original fluorescence was attributed to "interstitial zinc atoms or other crystal imperfections," with the decrease attributed to a "stabilization or approach of stoichiometry" after ultraviolet irradiation exposure.

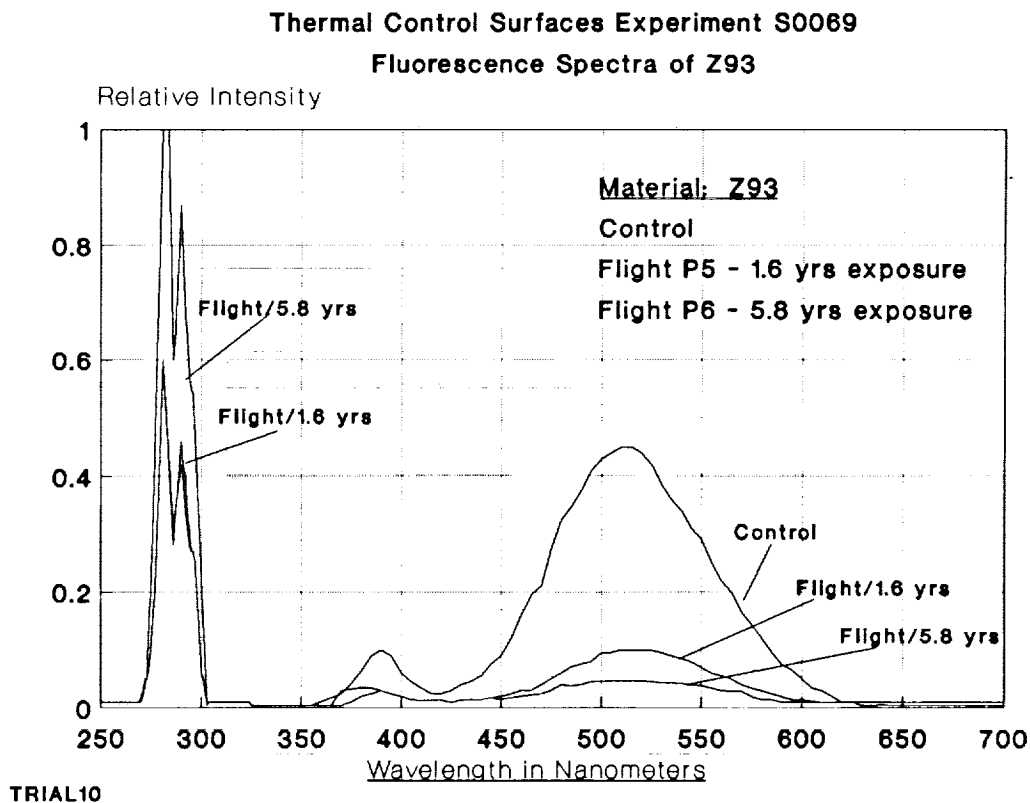


Figure 7. Fluorescence Spectra of Z93.

SILVER TEFLON SURFACE ON S0069 DURING ON-ORBIT RECOVERY

The first images returned of the front surface of experiment S0069 were similar to the on-orbit photograph shown in Figure 8. Originally the silver Teflon had the normal, specular mirror-like surface, but, as seen in the photograph, it has turned a diffuse whitish color with brown streaks. As reported previously, these brown streaks are caused by cracks in the silver/inconel layer which permits the adhesive (or components) to migrate between the Teflon/silver interface. After exposure to the space environment, mainly solar ultraviolet irradiation, the adhesive degrades to the observed brownish color. Note that the silver Teflon covered by the side panels still has the original mirror-like specular appearance.

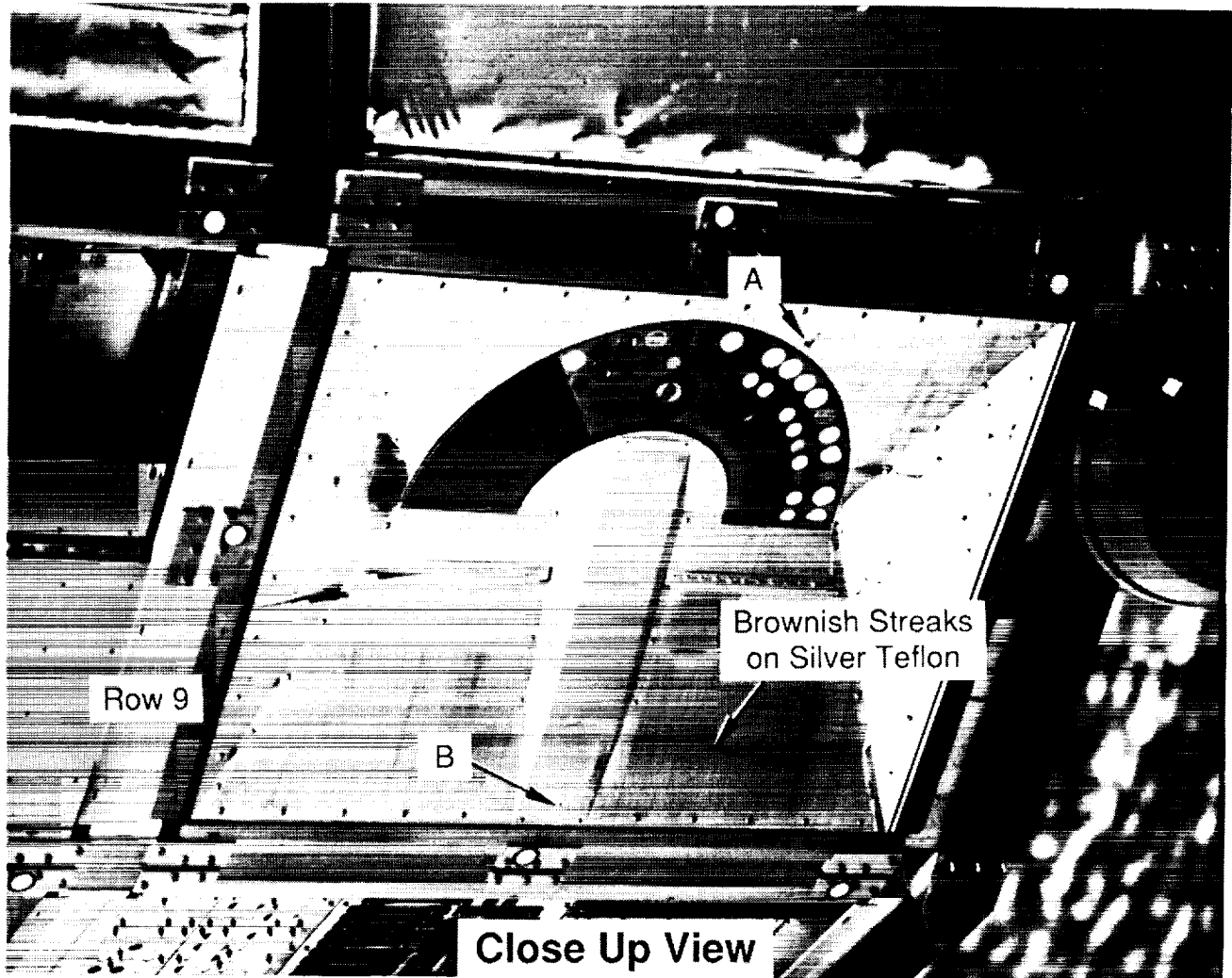


Figure 8. Close Up View of S0069 During Recovery.

FLUORESCENCE OF SILVER TEFLON SURFACE ON S0069

Several samples were cut from the front cover of S0069 in Figure 8 to determine if fluorescence could be detected. As can be seen in Figure 9, a weak but measurable fluorescence was obtained. This fluorescence is considerably less than the scattered light level, so that it cannot be detected during normal visual inspection with an ultraviolet light.

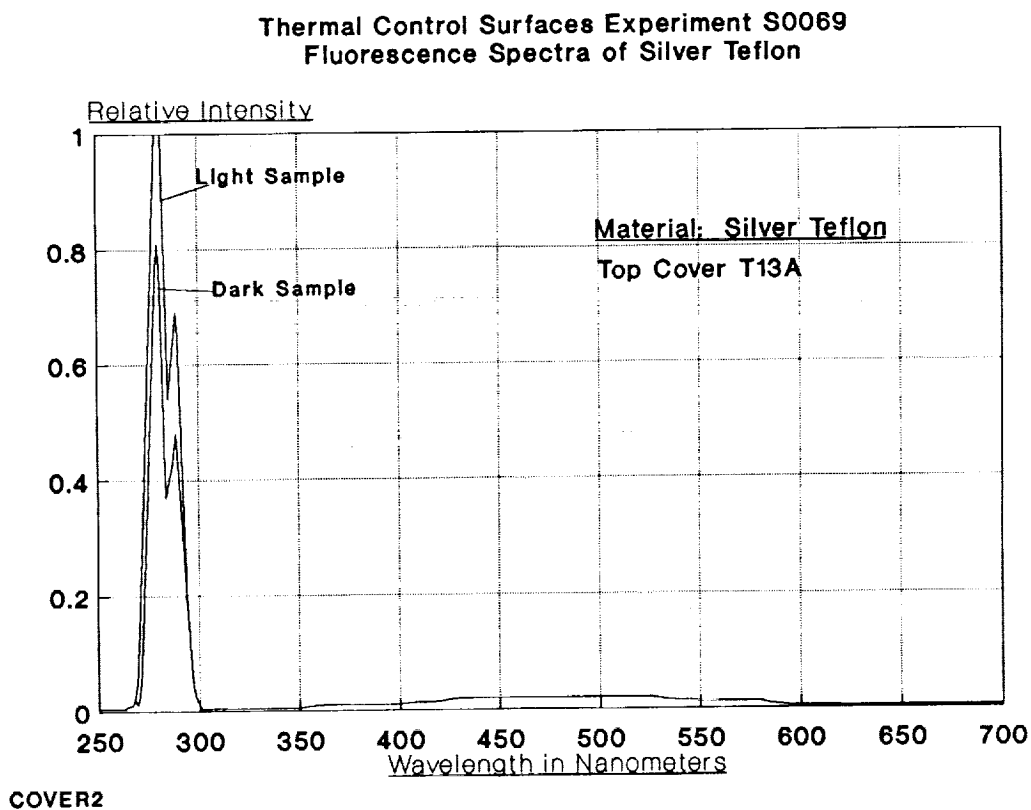


Figure 9. Fluorescence Spectra of Silver Teflon on S0069 After Recovery.

FLUORESCENCE OF SILVER TEFLON ADHESIVE 3M(966)

Samples of the acrylic adhesive used to bond silver Teflon to the S0069 front cover were exposed to simulated solar ultraviolet radiation for various times. These samples, including a control, were measured to see if they fluoresced and to determine the change, if any, from irradiation exposure. As can be seen from the data in Figure 10, not only did the original adhesive fluoresce, but after irradiation the emission shifts to the visual region, similar to what was observed on the flight material. As can be seen by comparing the emission spectra of Figures 9 and 10, the fluorescence of the ground sample is considerably stronger than the flight silver Teflon material. This can be attributed to several factors: the adhesive on the ground samples is totally exposed, while the flight samples have only very little surface area of the adhesive exposed along the silver/inconel cracks. In addition, the ground samples have only been exposed in air (no long term vacuum exposure) and were not covered with Teflon which could attenuate the signal. Further testing is under way to more accurately simulate the flight conditions.

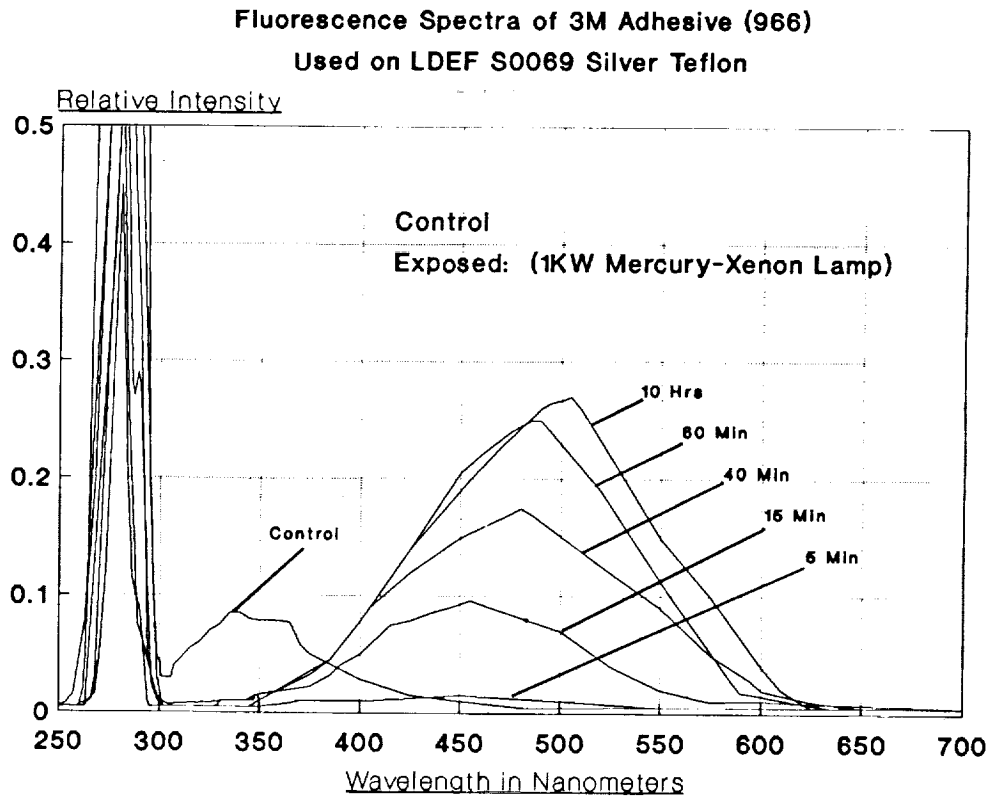


Figure 10. Fluorescence Spectra of 3M Adhesive (966) Used to Attach Silver Teflon to S0069 Front Cover.

SUMMARY OF FINDINGS

Fluorescence was detected on all thermal control surfaces flown and exposed to the space environment on S0069 and A0114 except the white Tedlar* and black ceramic paint D111 samples. In some cases the fluorescence was extremely weak as for the YB71 ceramic white paint using a zinc orthotitanate pigment. In other cases, the fluorescence was very striking, changing to the bright yellow emission under ultraviolet lighting. This change is similar to that shown by the black urethane, silicone overcoated Z302 samples.

The overall change in fluorescence emission characteristics can be classified into three types. Urethane based paints showed a shift in fluorescence from the near ultraviolet region toward the visible, while the zinc oxide pigment based paints exhibit a quenching of their fluorescence emission. In contrast, the silver Teflon material which does not itself show any measurable fluorescence, does exhibit a measurable fluorescence after recovery from the LDEF mission. This appears to be caused by the acrylic adhesive in the silver/inconel cracks.

Studies to fully document the fluorescence observed on experiments S0069 and A0114 are continuing, and will be reported in future papers.

* Tedlar is a trademark of Dupont.

REFERENCE

1. Zerlaut, Gene A. and Harada, Y: *Stable White Coatings*, Subcontract under NAS7-100, contract 950111, Interim Report No. IITRI-C207-27, January 9, 1964.

LONG DURATION EXPOSURE FACILITY
M0003-5
Thermal Control Coatings
on
DoD Flight Experiment

Charles J. Hurley
University of Dayton Research Institute
Dayton, OH

William Lehn
Nichols Research Corporation
Dayton, OH

INTRODUCTION

The M0003-5 thermal control coatings and materials orbited on the LDEF M0003 Space Environment Effects on Spacecraft Materials were a part of a Wright Laboratories Materials Directorate larger experiment. They were selected from new materials which emerged from development programs during the 1978-1982 time frame. Included were materials described in the technical literature which were being considered or had been applied to satellites. Materials that had been exposed on previous satellite materials experiments were also included to provide data correlation with earlier space flight experiments. The objective was to determine the effects of the LDEF environment on the physical and optical properties of thermal control coatings and materials. One hundred and two specimens of various pigmented organic and inorganic coatings, metallized polymer thin films, optical solar reflectors and mirrors were orbited on LDEF. The materials were exposed in four separate locations on the vehicle. The first set was exposed on the direct leading edge of the satellite. The second set was exposed on the direct trailing edge of the vehicle. The third and fourth sets were exposed in environmental exposure control canisters (EECC) located 30 degrees off normal to the leading and trailing edges.

The purpose of the experiment was to understand the changes in the properties of materials before and after exposure to the space environment and to compare the changes with predictions based on laboratory experiments. The basic approach was to measure the optical and physical properties of materials before and after long-term exposure to a low earth orbital environment comprised of UV, VUV, electrons, protons, atomic oxygen, thermal cycling, vacuum, debris and micrometeoroids. Due to the unanticipated extended orbital flight of LDEF, the thermal control coatings and materials in the direct leading and trailing edge were exposed for a full five years and ten months to the space environment and the canister materials were exposed for approximately one year to the full environment.

LDEF M0003 SUB-EXPERIMENTS

The individual experiments listed below were supplied by the organization named and integrated into the flight hardware trays by Aerospace Corporation. Deintegration was accomplished by the same organization.

#	NAME	ORGANIZATION
1	RADAR CAMOUFLAGE MATERIALS & EO SIGNATURE COATINGS	AVIONICS LAB
2	LASER OPTICS	WEAPONS LAB
3	STRUCTURAL MATERIALS	WEAPONS LAB
4	SOLAR POWER COMPONENTS	PROPULSION LAB
5	THERMAL CONTROL MATERIALS	MATERIALS LAB
6	LASER COMMUNICATION COMPONENTS	SPACE DIVISION/ McD-D ASTRONAUTICS
7	LASER MIRROR COATING	NAVAL WEAPONS CTR
8	COMPOSITE MATERIALS, ELECTRONIC PIECE PARTS, FIBER OPTICS	BOEING AEROSPACE
9	THERMAL CONTROL, ANTENNA, COMPOSITE MATERIALS, COLD WELDING	LOCKHEED MISSILE & SPACE CORP.
10	ADVANCED COMPOSITE MATERIALS	FLIGHT DYNAMICS LAB AEROSPACE CORP.
11	CONTAMINATION MONITORING	AEROSPACE CORP.
12	RADIATION DOSIMETRY	AEROSPACE CORP.
13	LASER HARDENED MATERIALS	McD-D ASTRONAUTICS
14	QUARTZ CRYSTAL MICROBALANCE	BERKLEY INDUSTRY
15	THERMAL CONTROL MATERIALS	AEROSPACE CORP.
16	ADVANCED COMPOSITE MATERIALS	AEROSPACE CORP.
17	RADIATION DOSIMETRY	AEROSPACE CORP.
18	THERMAL CONTROL COATINGS	AEROSPACE CORP.
19	ELECTRONIC DEVICES	AEROSPACE CORP.

LDEF IN THE ORBITER PROCESSING FACILITY

Fifty seven experiments were placed in a low earth orbit aboard LDEF on April 7, 1984 for a planned one year mission. The LDEF vehicle was recovered on January 12, 1990 from a degrading orbit by the Space Shuttle Columbia. After a landing at Edwards Air Force Base, California, the Space Shuttle, with LDEF still contained inside, was transported to Kennedy Space Center, Florida. LDEF was removed from the shuttle bay in the Orbiter Processing Facility (OPF) in late January 1990.

The photograph in figure 1 shows the extensive damage done to some of the experiments on the leading edge side and the space end of the vehicle. The M0003 experiment is located near the center of the vehicle at the scuff plate.

ORIGINAL PAGE
BLACK AND WHITE PHOTOGRAPH



Figure 1. LDEF in Orbital Processing Facility

LDEF in SAEF II

After completion of activities in the Orbiter Processing Facility, LDEF was transported to the Spacecraft Assembly and Experiment Facility II (SAEFII). This facility provided a controlled, clean working environment for the principal investigators and other observers to examine the various experiments. The photograph in figure 2 shows only a portion of the leading edge side of LDEF. The M0003 experiment is located to the far left of the photograph near the scuff plate.

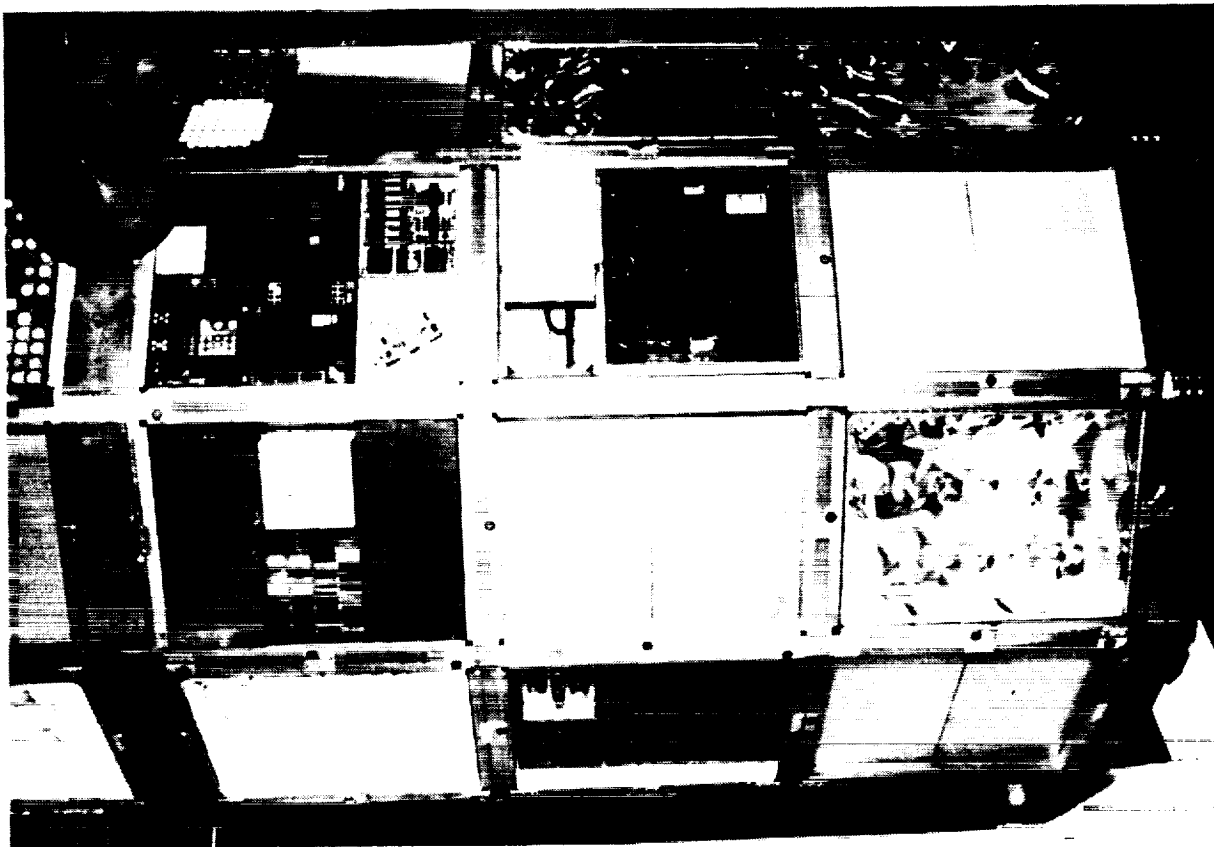


Figure 2. LDEF in SAEF II

**LDEF/WL/MD EXPERIMENT
THERMAL CONTROL MATERIALS
M0003-5**

THERMAL CONTROL MATERIALS

A SERIES

Pigmented Coatings	44
Metallized Polymer Films	28
Quartz Fabrics	8

B Series

Optical Solar Reflectors (second surface)	8
Gold Mirrors (first surface)	4
Silver Mirrors (first surface)	6
Aluminum Mirrors (first surface)	4

C Series

Metallized Polymeric Films	8
Metallized Bonded Films	14
Clear Films	10

Total	134
--------------	------------

M0003-5 LEADING EDGE EXPERIMENT

The M0003-5 experiment was located in a 3 inch deep leading edge tray designated as D9. It contained a variety of thermal control pigmented coatings, metallized polymer films, clear films and mirrors. The photograph in figure 3 shows the preflight layout of the materials. The thermal control coatings discs and mirrors are located on the right hand side of the tray.

ORIGINAL PAGE
BLACK AND WHITE PHOTOGRAPH

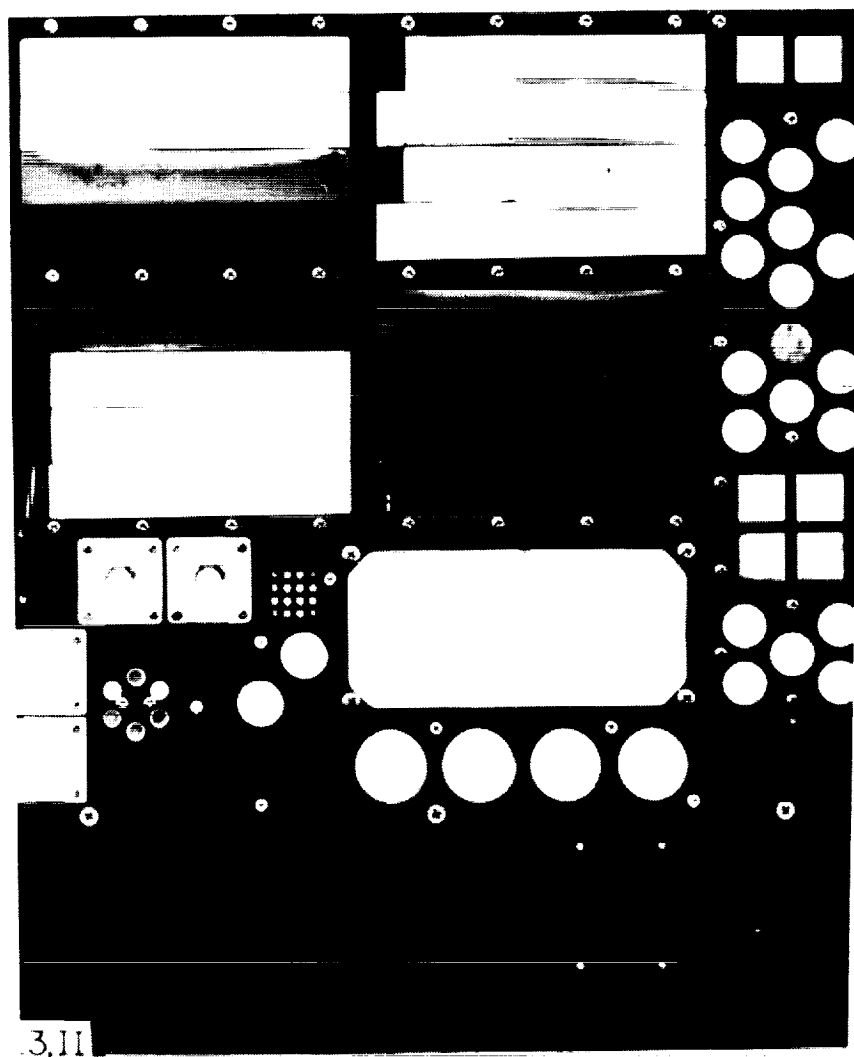


Figure 3. M0003-5 Pre flight Leading Edge Tray Experiment

RECOVERED LEADING EDGE M0003 TRAY

A photograph of the recovered M0003 leading edge tray originally located in the D9 position is shown in figure 4. Among the various areas of visible damage, note the condition of the polymeric films portion of the M0003-5 experiment located in the lower left quadrant of the tray. The thermal control material discs and squares are located in the far lower left quadrant. Atomic oxygen contributed some physical damage to the materials, especially the front surface. Silver mirrors and radiation contributed some color changes .

ORIGINAL PAGE
BLACK AND WHITE PHOTOGRAPH



Figure 4. M0003 Post Flight Leading Edge Tray

LDEF/M0003 IN SAEF II

The photograph in figure 5 shows the M0003 experiment and the surrounding trays. Note the extensive damage to the experiment located in tray D10 immediately above tray D9 M0003 experiment tray. Also observe the serious damage that occurred to the M0003-1 experiment located in the lower right quadrant of the tray. Damage is also evident to the M0003-5 polymer film materials. The thermal control discs are partially obscured by the scuff plate.

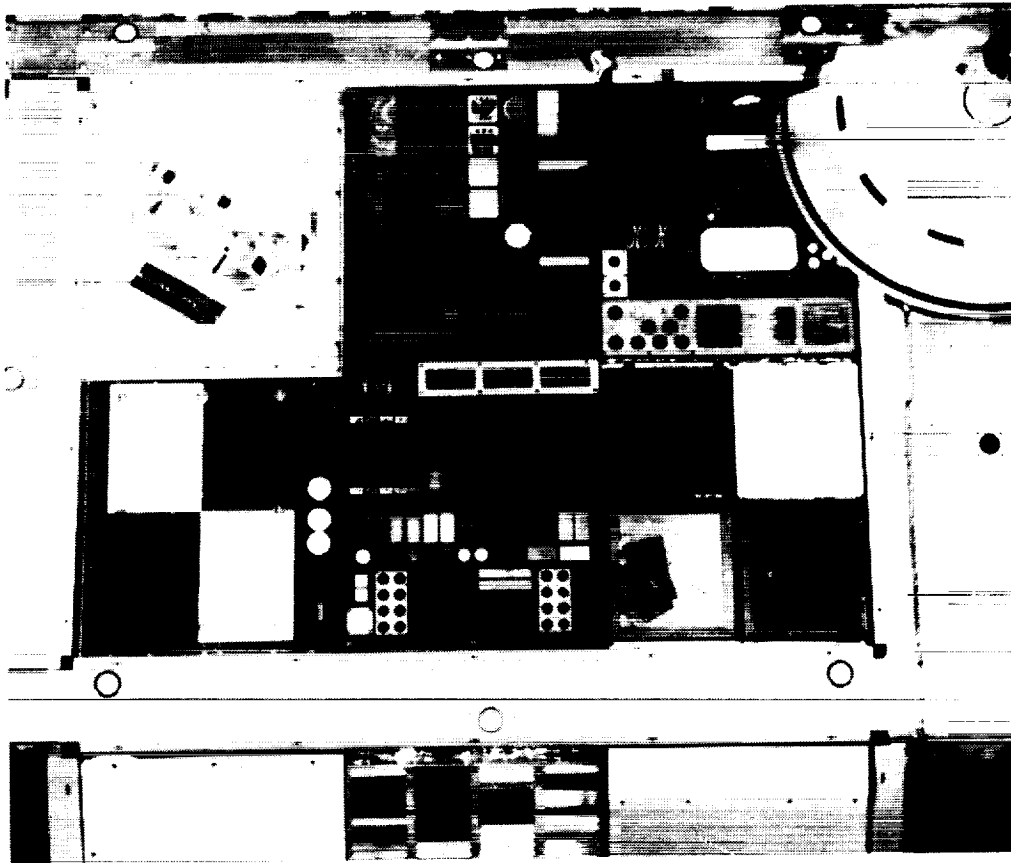


Figure 5. LDEF/M0003 IN SAEF II

M0003-5 POST FLIGHT LEADING EDGE TRAY CLOSEUP

The photograph in figure 6 below shows a closeup of the M0003-5 experiment materials. Note the extensive damage to the polymeric film strips. There is obvious physical damage, discoloration and debonding of the materials. The thermal control materials discs are located on the right hand side of the photograph. The most evident damage are the two front surface silver mirrors which were destroyed by atomic oxygen.

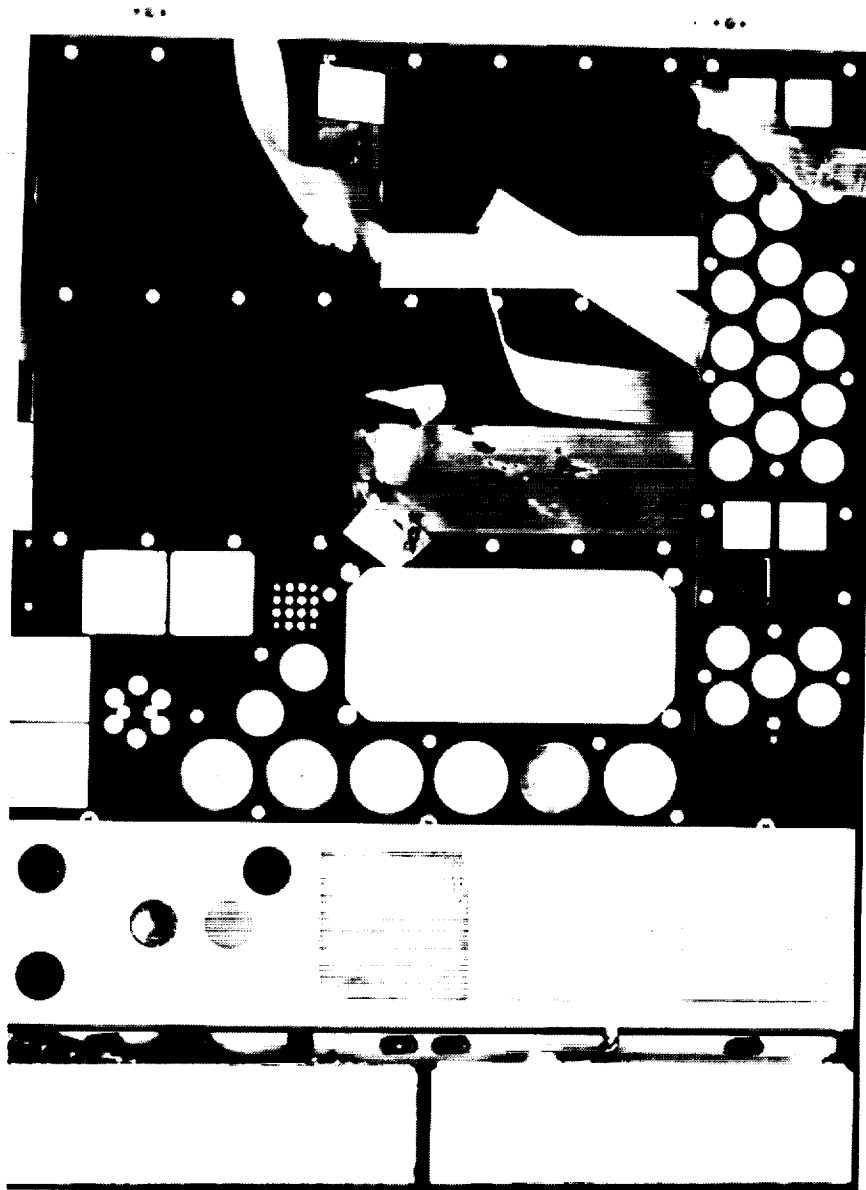


Figure 6. M0003-5 Post Flight Leading Edge Tray Closeup

M0003-5 PREFLIGHT TRAILING EDGE EXPERIMENT

The photograph in figure 7 shows the preflight thermal control coating discs and mirrors on the right side of the tray.

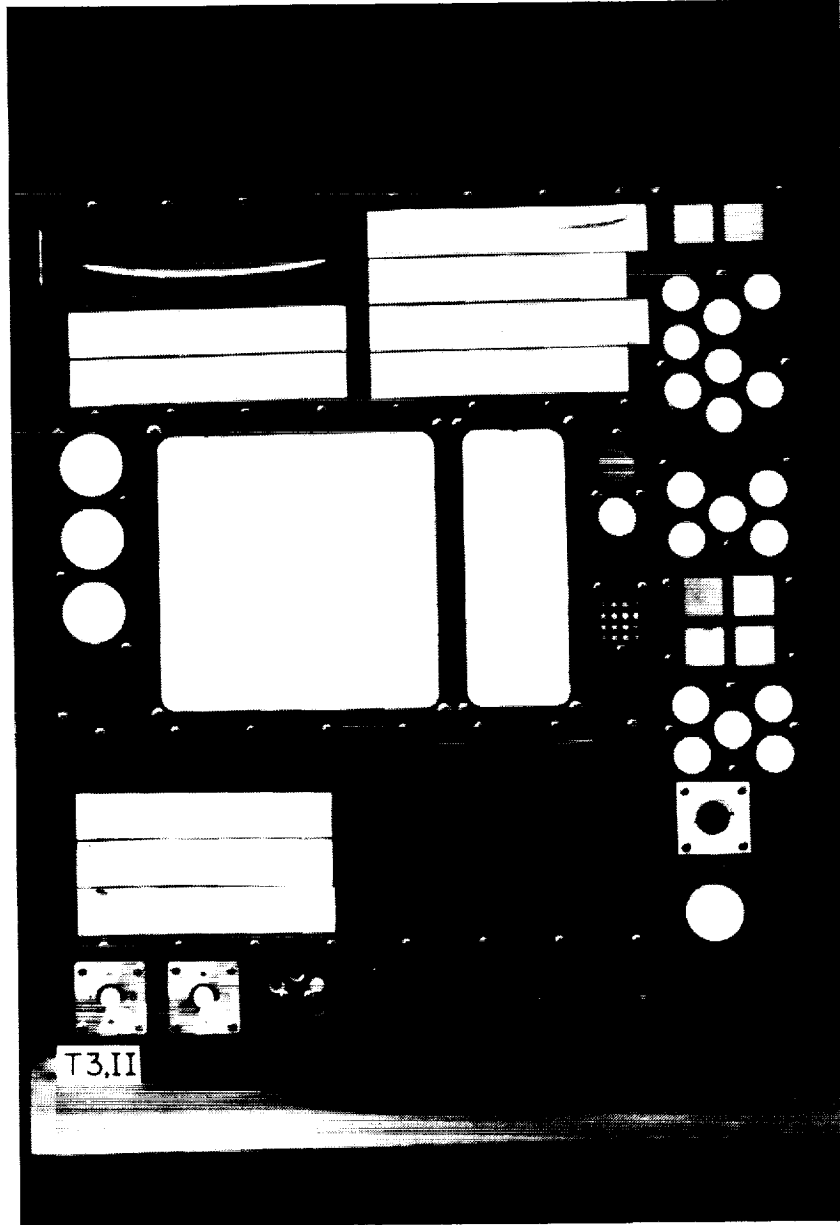


Figure 7. M0003-5 Preflight Trailing Edge Experiment

RECOVERED POST FLIGHT TRAILING EDGE M0003 TRAY

The photograph in figure 8 shows the post flight materials in the recovered trailing edge tray. Among the various areas of visible damage, note the condition of the M0003-5 polymeric film strips located in the upper right quadrant of the tray. The thermal control materials discs are located on the right side of the photograph. Contamination has discolored many of the specimens.

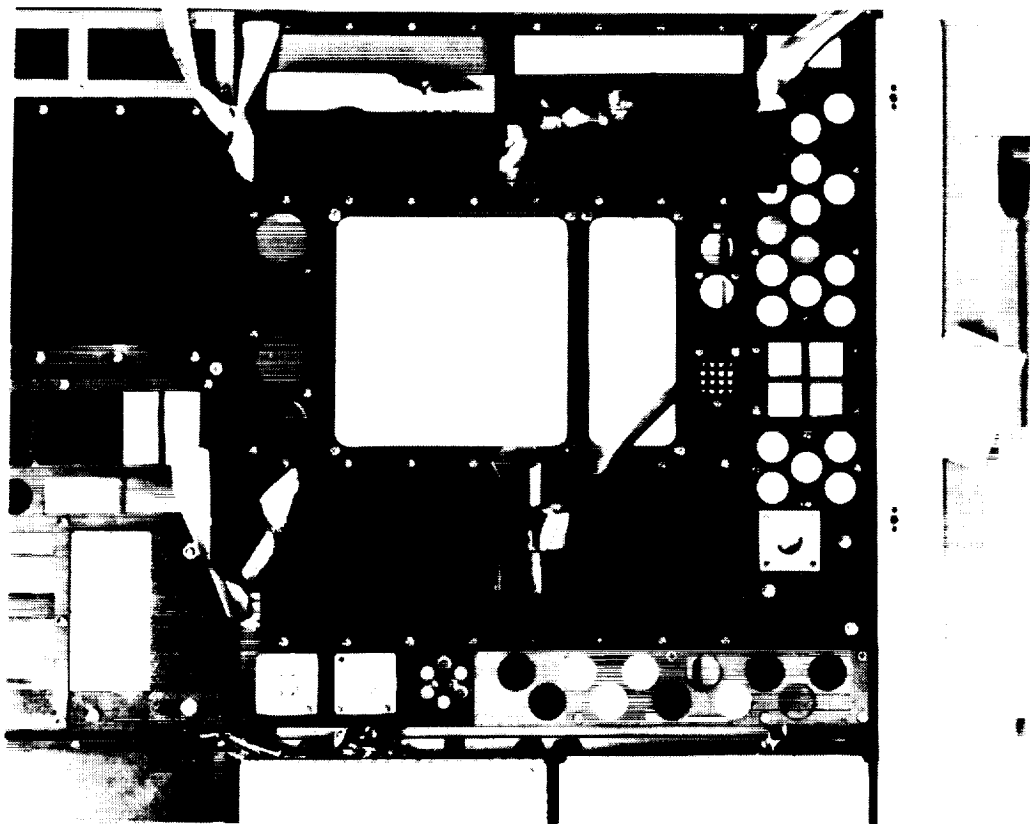


Figure 8. M0003 Post Flight Trailing Edge tray

M0003-5 POST FLIGHT TRAILING EDGE TRAY CLOSEUP

The photograph in figure 9 below shows a closeup of the M0003-5 experiment materials. Note the extensive damage to the polymeric film strips. The thermal control materials discs are located on the right side of the photograph. Contamination and radiation are responsible for the color changes in the materials.

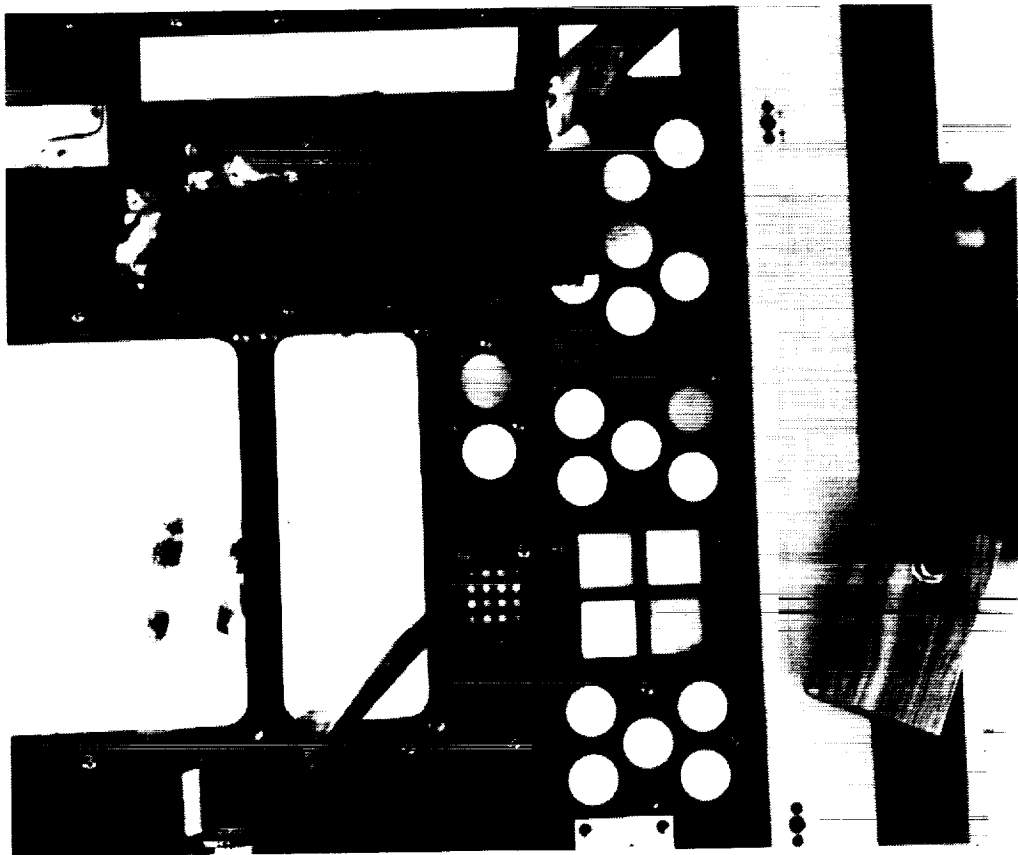


Figure 9. M0003-5 Post Flight Trailing Edge Tray Closeup

M0003-5 THERMO-OPTICAL DATA

Tables 1 through 5 provide a brief description of the materials in the M0003-5 experiment. The pre test and post test integrated IR emittance values from 2-20 microns are shown. UV-Vis-NIR reflectance values from 0.25 to 2.5 microns are also provided the for pretest and post test measurements.

Table 1. Thermo-Optical Data of M0003-5 Specimens A1 Through A6

SAMPLE ID	Material Description	Gier-Dunkle DB-100 2-20 μ pretest ϵ	Gier-Dunkle DB-100 2-20 μ post test ϵ	Bomem DA3 FTIR 2-12.5 μ post test ϵ	Beckman DK-2A 0.25-2.50 μ pretest α	Perkin-Elmer Lambda 9 0.25-2.50 μ post test α
C1-A*	Quartz fabric 581/FEP/Al		0.854	0.862	0.143	0.211
L3II-5-19-A1	Quartz fabric 581/FEP/Al	0.852	0.856	0.870	0.154	0.251
L6VI-5-7-A1	Quartz fabric 581/FEP/Al		0.855	0.867	0.149	0.215
T3II-5-19-A1	Quartz fabric 581/FEP/Al	0.850	0.854	0.863	0.142	0.289
T6VI-5-8-A1	Quartz fabric 581/FEP/Al		0.853	0.862	0.145	0.279
C1-A2	ITO/FEP/Ag/Inconel 5 mil		0.808	0.840	0.108	0.109
L3II-5-20-A2	ITO/FEP/Ag/Inconel 5 mil	0.812	0.811	0.848	0.104	0.109
L6VI-5-8-A2	ITO/FEP/Ag/Inconel 5 mil		0.810	0.842	0.114	0.096
T3II-5-20-A2	ITO/FEP/Ag/Inconel 5 mil	0.812	0.811	0.839	0.106	0.212
C1-A3	Porcelain Enamel	0.872	0.832	0.917	0.237	0.273
L3II-5-21-A3	Porcelain Enamel	0.869	0.832	0.920	0.249	0.327
L6VI-5-11-A3	Porcelain Enamel	0.871	0.830	0.916	0.248	0.285
T3II-5-21-A3	Porcelain Enamel	0.871	0.834	0.920	0.245	0.363
C1-A4	ITO/FEP/Ag/Inconel 2 mil		0.692	0.68*	0.111	0.099
L3II-5-22-A4	ITO/FEP/Ag/Inconel 2 mil	0.696	0.698	0.684	0.119	0.113
L6VI-5-12-A4	ITO/FEP/Ag/Inconel 2 mil		0.696	0.684	0.126	0.098
T3II-5-22-A4	ITO/FEP/Ag/Inconel 2 mil	0.691	0.697	0.684	0.122	0.142
C1-A5	Black Inorganic Coating D111		0.912	0.942	0.965	0.975
L3II-5-23-A5	Black Inorganic Coating D111	0.910	0.921	0.955	0.974	0.979
L6VI-5-13-A5	Black Inorganic Coating D111		0.922	0.958	0.972	0.981
T3II-5-23-A5	Black Inorganic Coating D111	0.909	0.918	0.952	0.971	0.982
C1-A6	Quartz Fabric 7 micron		0.855	0.856	0.239	0.307
L3II-5-24-A6	Quartz Fabric 7 micron	0.849	0.856	0.868	0.250	0.339
L6VI-5-16-A6	Quartz Fabric 7 micron		0.861	0.860	0.234	0.334
T3II-5-24-A6	Quartz Fabric 7 micron	0.851	0.863	0.868	0.239	0.426
T6VI-5-15-A6	Quartz Fabric 7 micron		0.860	0.859	0.224	0.354

M0003-5 THERMO-OPTICAL DATA

Table 2. Thermo-Optical Data of M0003-5 Specimens A7 Through A12

SAMPLE ID	Material Description	Gier-Dunkle DB-100 2-20 μ pretest ϵ	Gier-Dunkle DB-100 2-20 μ post test ϵ	Bomem DA3 FTIR 2-12.5 μ post test ϵ	Beckman DK-2A 0.25-2.50 μ pretest α	Perkin-Elmer Lambda 9 0.25-2.50 μ post test α
C1-A7	FEP/Ag/Inconel 2 mil		0.669	0.655	0.112	0.080
L3II-5-25-A7	FEP/Ag/Inconel 2 mil	0.667	0.640	0.616	0.104	0.092
L6VI-5-17-A7	FEP/Ag/Inconel 2 mil		0.658	0.637	0.108	0.085
T3II-5-25-A7	FEP/Ag/Inconel 2 mil	0.657	0.670	0.657	0.104	0.137
T6VI-5-7-A7	FEP/Ag/Inconel 2 mil		0.670	0.653	0.115	0.094
C1-A8	FEP/Ag/Inconel 5 mil		0.804	0.830	0.098	0.096
L3II-5-26-A8	FEP/Ag/Inconel 5 mil	0.798	0.801	0.829	0.104	0.117
L6VI-5-29-A8	FEP/Ag/Inconel 5 mil		0.802		0.104	0.084
T3II-5-26-A8	FEP/Ag/Inconel 5 mil	0.796	0.808		0.103	0.180
T6VI-5-14-A8	FEP/Ag/Inconel 5 mil		0.806		0.105	0.093
C1-A9	In2O3/FEP/Ag/Inconel 5 mil		0.811	0.843	0.149	0.129
L3II-5-27-A9	In2O3/FEP/Ag/Inconel 5 mil	0.808	0.814	0.844	0.139	0.126
L6VI-5-30-A9	In2O3/FEP/Ag/Inconel 5 mil		0.812	0.840	0.158	0.135
T3II-5-27-A9	In2O3/FEP/Ag/Inconel 5 mil	0.808	0.814	0.844	0.160	0.177
C1-A10	Kapton/Al 1 mil		0.672		0.319	0.356
L3II-5-28-A10	Kapton/Al 1 mil	0.649	0.677		0.299	0.390
L6VI-5-31-A10	Kapton/Al 1 mil		0.631		0.333	0.485
T3II-5-28-A10	Kapton/Al 1 mil	0.643	0.671		0.313	0.399
C1-A11	Kapton/Al 5 mil		0.864	0.902	0.456	0.486
L3II-5-29-A11	Kapton/Al 5 mil	0.850	0.863	0.901	0.453	0.499
L6VI-5-32-A11	Kapton/Al 5 mil		0.894	0.946	0.467	0.620
T3II-5-29-A11	Kapton/Al 5 mil	0.850	0.864	0.900	0.456	0.477
T6VI-5-6-A11	Kapton/Al 5 mil		0.865	0.901	0.458	0.480
C1-A12	In2O3/Kapton/Al 5 mil		0.780		0.370	0.407
L3II-5-30-A12	In2O3/Kapton/Al 5 mil	0.749	0.776		0.361	0.410
L6VI-5-33-A12	In2O3/Kapton/Al 5 mil		0.784		0.366	0.402
T3II-5-30-A12	In2O3/Kapton/Al 5 mil	0.750	0.776	0.835	0.357	0.417

Table 3. Thermo-Optical Data of M0003-5 Specimens A13 Through A17

SAMPLE ID	Material Description	Gier-Dunkle DB-100 2-20 μ pretest ϵ	Gier-Dunkle DB-100 2-20 μ post test ϵ	Bomem DA3 FTIR 2-12.5 μ post test ϵ	Beckman DK-2A 0.25-2.50 μ pretest α	Perkin-Elmer Lambda 9 0.25-2.50 μ post test α
C1-A13	White Inorganic Coating Z93		0.904	0.966	0.143	0.226
L3II-5-31-A13	White Inorganic Coating Z93	0.914	0.921	0.965	0.145	0.177
L6VI-5-34-A13	White Inorganic Coating Z93		0.920	0.966	0.151	0.161
T3II-5-31-A13	White Inorganic Coating Z93	0.903	0.921	0.966	0.149	0.166
T6VI-5-13-A13	White Inorganic Coating Z93		0.921	0.967	0.155	0.170
C1-A14	White Silicone Coating S13 GLO		0.897	0.953	0.161	0.213
L3II-5-32-A14	White Silicone Coating S13 GLO	0.894	0.893	0.945	0.148	0.266
L6VI-5-35-A14	White Silicone Coating S13 GLO		0.893	0.945	0.158	0.233
T3II-5-32-A14	White Silicone Coating S13 GLO	0.892	0.905	0.938	0.150	0.475
T6VI-5-5-A14	White Silicone Coating S13 GLO		0.910	0.950	0.154	0.238
C1-A15	White Inorganic Coating Zn2T1O4		0.909	0.962	0.094	0.152
L3II-5-33-A15	White Inorganic Coating Zn2T1O4	0.909	0.904	0.969	0.093	0.145
L6VI-5-36-A15	White Inorganic Coating Zn2T1O4		0.911	0.967	0.090	0.153
T3II-5-33-A15	White Inorganic Coating Zn2T1O4	0.910	0.904	0.966	0.087	0.162
T6VI-5-12-A15	White Inorganic Coating Zn2T1O4		0.911	0.968	0.089	0.150
C1-A16	White Inorganic Coating NS43G		0.910		0.259	0.301
L3II-5-34-A16	White Inorganic Coating NS43G	0.908	0.910		0.266	0.326
L6VI-5-37-A16	White Inorganic Coating NS43G		0.906		0.260	0.316
T3II-5-34-A16	White Inorganic Coating NS43G	0.908	0.909		0.257	0.301
T6VI-5-3-A16	White Inorganic Coating NS43G		0.908		0.262	0.303
C1-A17	White Silicone Coating Eu2O3 MeSi		0.928		0.131	0.170
L3II-5-35-A17	White Silicone Coating Eu2O3 MeSi	0.924	0.929		0.127	0.198
L6VI-5-38-A17	White Silicone Coating Eu2O3 MeSi		0.930		0.139	0.201
T3II-5-35-A17	White Silicone Coating Eu2O3 MeSi	0.924	0.930		0.133	0.328
T6VI-5-11-A17	White Silicone Coating Eu2O3 MeSi		0.929		0.140	0.228

M0003-5 THERMO-OPTICAL DATA

Table 4. Thermo-Optical Data of M0003-5 Specimens A18 Through A22

SAMPLE ID	Material Description	Gier-Dunkle DB-100 2-20 μ pretest ϵ	Gier-Dunkle DB-100 2-20 μ post test ϵ	Bomem DA3 FTIR 2-12.5 μ post test ϵ	Beckman DK-2A 0.25-2.50 μ pretest α	Perkin-Elmer Lambda 9 0.25-2.50 μ post test α
C1-A18	White Silicone Coating α Al ₂ O ₃ MeSi		0.880		0.093	0.134
L311-5-40-A18	White Silicone Coating α Al ₂ O ₃ MeSi	0.869	0.870		0.090	0.296
L6VI-5-39-A18	White Silicone Coating α Al ₂ O ₃ MeSi		0.882		0.097	0.227
T311-5-40-A18	White Silicone Coating α Al ₂ O ₃ MeSi	0.868	0.867		0.091	0.341
T6VI-5-2-A18	White Silicone Coating α Al ₂ O ₃ MeSi		0.901		0.089	0.224
C1-A19	White Silicone Coating PV100		0.862		0.196	0.236
L311-5-41-A19	White Silicone Coating PV100	0.858	0.870		0.198	0.270
L6VI-5-40-A19	White Silicone Coating PV100		0.865		0.198	0.249
T311-5-41-A19	White Silicone Coating PV100	0.859	0.858		0.196	0.395
T6VI-5-10-A19	White Silicone Coating PV100		0.859		0.193	0.270
C1-A20	WhiteSilicone Coating TiO ₂ MeSi		0.863		0.158	0.196
L311-5-42-A20	WhiteSilicone Coating TiO ₂ MeSi	0.862	0.862		0.157	0.205
L6VI-5-41-A20	WhiteSilicone Coating TiO ₂ MeSi		0.866		0.154	0.238
T311-5-42-A20	WhiteSilicone Coating TiO ₂ MeSi	0.862	0.862		0.156	0.372
T6VI-5-1-A20	WhiteSilicone Coating TiO ₂ MeSi		0.860		0.155	0.224
C1-A21	White Silicone Coating DC92-007		0.888		0.225	0.260
L311-5-43-A21	White Silicone Coating DC92-007	0.878	0.869		0.218	0.405
L6VI-5-42-A21	White Silicone Coating DC92-007		0.878		0.235	0.341
T311-5-43-A21	White Silicone Coating DC92-007	0.885	0.876		0.209	0.383
T6VI-5-9-A21	White Silicone Coating DC92-007		0.881		0.214	0.305
C1-A22	White Silicone Coating DC92-007		0.887		0.222	0.267
L311-5-44-A22	White Silicone Coating DC92-007	0.887	0.880		0.202	0.377
L6VI-5-43-A22	White Silicone Coating DC92-007		0.878		0.226	0.335
T311-5-44-A22	White Silicone Coating DC92-007	0.887	0.872		0.229	0.412

Table 5. Thermo-Optical Data of M0003-5 Specimens B1 Through B6

SAMPLE ID	Material Description	Gier-Dunkle DB-100 2-20 μ pretest ϵ	Gier-Dunkle DB-100 2-20 μ post test ϵ	Bomem DA3 FTIR 2-12.5 μ post test ϵ	Beckman DK-2A 0.25-2.50 μ pretest α	Perkin-Elmer Lambda 9 0.25-2.50 μ post test α
C1-B1	OSR OCLI S1-100					
L311-5-17-B1	OSR OCLI S1-100	0.801	0.804		0.078	0.060
L6VI-5-23-B1	OSR OCLI S1-100		0.804		0.078	0.053
T311-5-17-B1	OSR OCLI S1-100	0.801	0.807		0.074	0.113
T6VI-5-18-B1	OSR OCLI S1-100		0.805		0.081	0.056
C1-B2	OSR OCLI S1-100 w/conductive coating		0.783		0.090	0.133
L311-5-18-B2	OSR OCLI S1-100 w/conductive coating	0.778	0.787		0.089	0.076
L6VI-5-28-B2	OSR OCLI S1-100 w/conductive coating		0.787		0.089	0.078
T311-5-18-B2	OSR OCLI S1-100 w/conductive coating	0.778	0.782		0.089	0.120
T6VI-5-17-B2	OSR OCLI S1-100 w/conductive coating		0.783		0.090	0.066
C1-B3	OSR Au Mirror		0.022		0.276	0.292
L311-5-36-B3	OSR Au Mirror	0.015	0.024		0.237	0.258
L6VI-5-26-B3	OSR Au Mirror		0.026		0.245	0.258
T311-5-36-B3	OSR Au Mirror	0.018	0.027		0.247	0.279
T6VI-5-19-B3	OSR Au Mirror		0.030		0.247	0.248
C1-B4	OSR Al Mirror		0.040		0.143	0.132
L311-5-37-B4	OSR Al Mirror	0.027	0.061		0.158	0.134
L6VI-5-24-B4	OSR Al Mirror		0.044		0.151	0.111
T311-5-37-B4	OSR Al Mirror	0.027	0.044		0.159	0.171
T6VI-5-16-B4	OSR Al Mirror		0.044		0.153	0.139
C1-B5	OSR Ag Mirror		0.030			0.253
L311-5-38-B5	OSR Ag Mirror	0.012	0.687		0.105	0.864
L6VI-5-25-B5	OSR Ag Mirror		0.037		0.120	0.861
T311-5-38-B5	OSR Ag Mirror	0.012	0.494		0.101	0.270
T6VI-5-4-B5	OSR Ag Mirror		0.031		0.094	0.246
C1-B6	OSR Ag Mirror		0.024			0.206
L311-5-39-B6	OSR Ag Mirror	0.011	0.703		0.095	0.903
T311-5-39-B6	OSR Ag Mirror	0.012	0.025		0.095	0.384

SELECTED THERMO-OPTICAL DATA

The selected data listed in table 6 below is from the preceding thermo-optical data tables and is displayed in chart form in figures 10 and 11.

Table 6. Selected Thermo-optical Data

MATERIAL	LEADING-EDGE			TRAILING-EDGE		
	PRE	POST	DELTA	PRE	POST	DELTA
AQ/581/FEP/Al	0.154	0.251	0.097	0.142	0.289	0.147
ITO/FEP/Ag 5mil	0.104	0.109	0.005	0.106	0.212	0.106
Porcelain Enamel	0.249	0.327	0.078	0.252	0.363	0.111
ITO/FEP/Ag 2mil	0.119	0.113	-.006	0.122	0.142	0.020
Quartz Fabric 7u	0.250	0.339	0.089	0.239	0.426	0.187
FEP/Ag 2mil	0.104	0.092	-.012	0.104	0.137	0.033
FEP/Ag 5mil	0.104	0.117	0.013	0.103	0.180	0.077
In ₂ O ₃ /FEP/Ag 5mil	0.139	0.126	-.013	0.160	0.177	0.017
Kapton 1mil	0.299	0.396	0.097	0.313	0.399	0.086
Kapton 5mil	0.453	0.499	0.046	0.456	0.477	0.021
ITO/Kapton/Al 5mil	0.361	0.410	0.049	0.357	0.417	0.060
Z-93	0.145	0.177	0.032	0.149	0.166	0.017
S13GLO	0.148	0.266	0.118	0.150	0.475	0.325
ZnTiO ₄ ZOT	0.093	0.145	0.092	0.087	0.162	0.075
GFSC NS43G Yellow	0.266	0.326	0.060	0.257	0.310	0.044
Eu ₂ O ₃ MeSi	0.127	0.198	0.071	0.133	0.328	0.195
PV 100	0.090	0.296	0.206	0.091	0.341	0.250
TiO ₂ MeSi	0.157	0.205	0.048	0.156	0.372	0.216
DC92-007	0.218	0.405	0.187	0.209	0.383	0.174
OSR S1-100	0.078	0.060	-.018	0.074	0.113	0.039
OSR S1-100 ITO	0.089	0.076	-.013	0.089	0.120	0.031
OSR Au Mirror	0.237	0.258	0.021	0.247	0.279	0.032
OSR Al Mirror	0.158	0.171	0.013	0.159	0.171	0.012
OSR Ag Mirror	0.105	0.864	0.759	0.101	0.270	0.169
OSR Ag Mirror	0.095	0.903	0.808	0.095	0.384	0.289

M0003-5 ABSORPTANCE

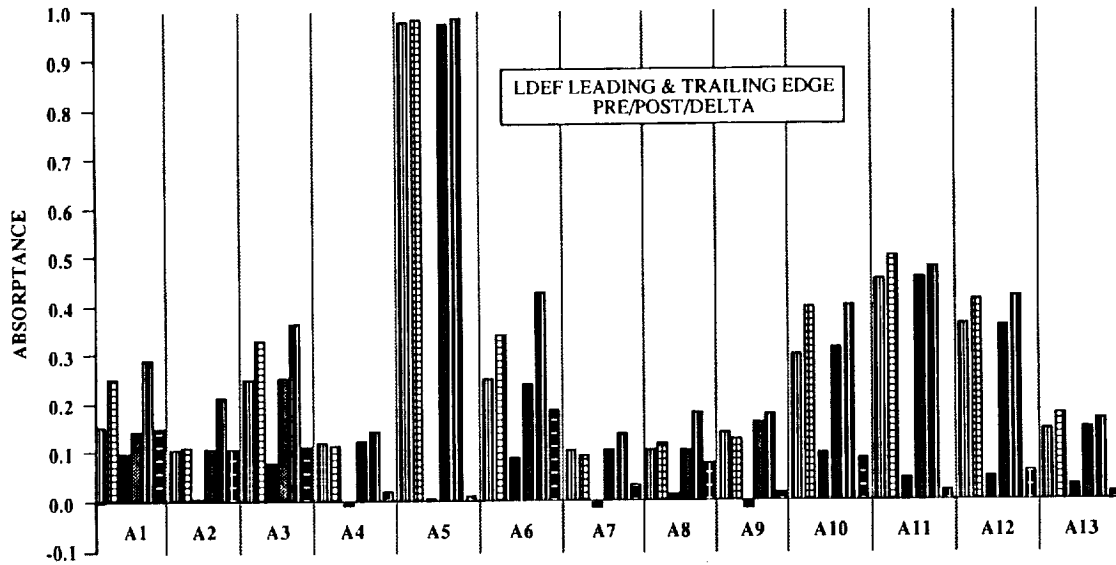


Figure 10. Absorbance Comparison Chart for Specimens A1 Through A13

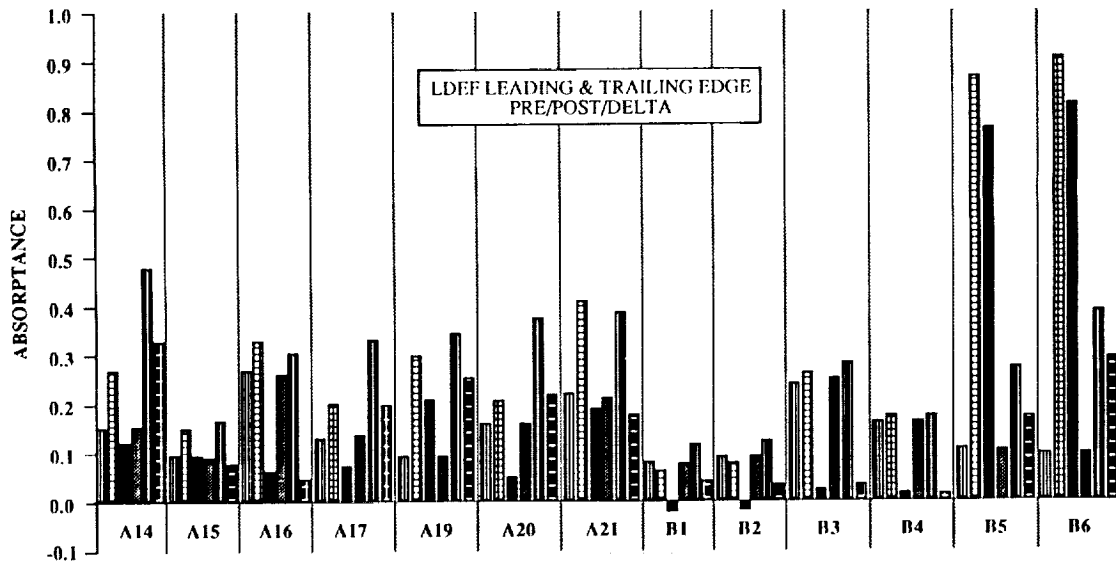


Figure 11. Absorbance Comparison Chart for Specimens A14 Through B6

QUARTZ FABRIC 7 micron

C1-A6 (Laboratory Specimen)

Some fabric fraying is present at the rim of the specimen. The adhesive bond between the Quartz fabric and the substrate appears to be intact.

A6-L3 (Leading Edge Specimen)

The exposed surface of the specimen exhibits a non-uniform distribution of a light-tan discoloration. The cloth weave shows no evidence of damage. The perimeter of the specimen is not discolored but the edges are frayed. The adhesive bond between the quartz fabric 7 micron and Al mounting disc appears intact.

A6-T3 (Trailing Edge Specimen)

The exposed surface of the specimen is discolored a yellowish tan. There is debris on the surface of the specimen. The weave pattern shows no evidence of damage. The perimeter of the specimen is not discolored, but the edges are frayed. The adhesive bond between the Quartz fabric 7 micron and the aluminum mounting disc appears intact.

A6-T6 (EECC Trailing Edge Specimen)

The exposed area of the specimen is nonuniformly discolored a light brown. The weave pattern is undisturbed except for one small localized area. The perimeter of the specimen is clean and white with frayed edges. The adhesive bond between the Quartz fabric 7 micron and the aluminum mounting disc appears intact.

A comparison photograph of the specimens is illustrated in figure 12; figure 13 compares the UV-Vis-NIR reflectance changes and figure 14 compares FTIR reflectance changes.

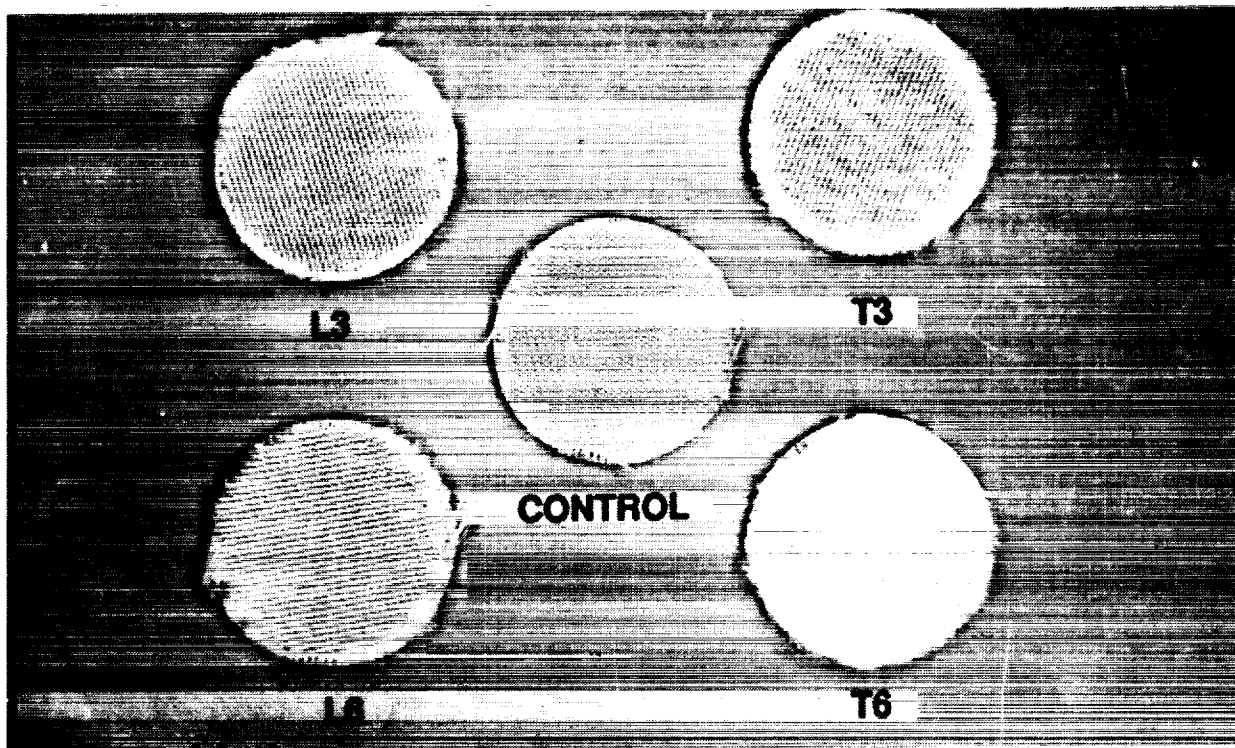


Figure 12. Comparison of Quartz Fabric 7 micron Specimens

QUARTZ FABRIC 7 micron

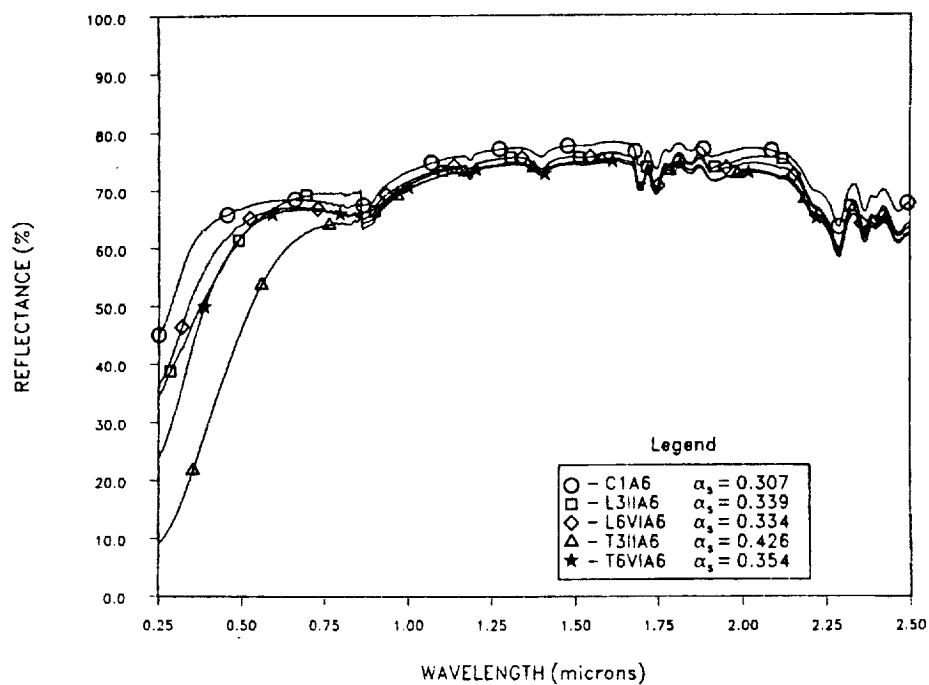


Figure 13. Comparison UV-Vis-NIR Reflectance Curves of Quartz Fabric 7 micron

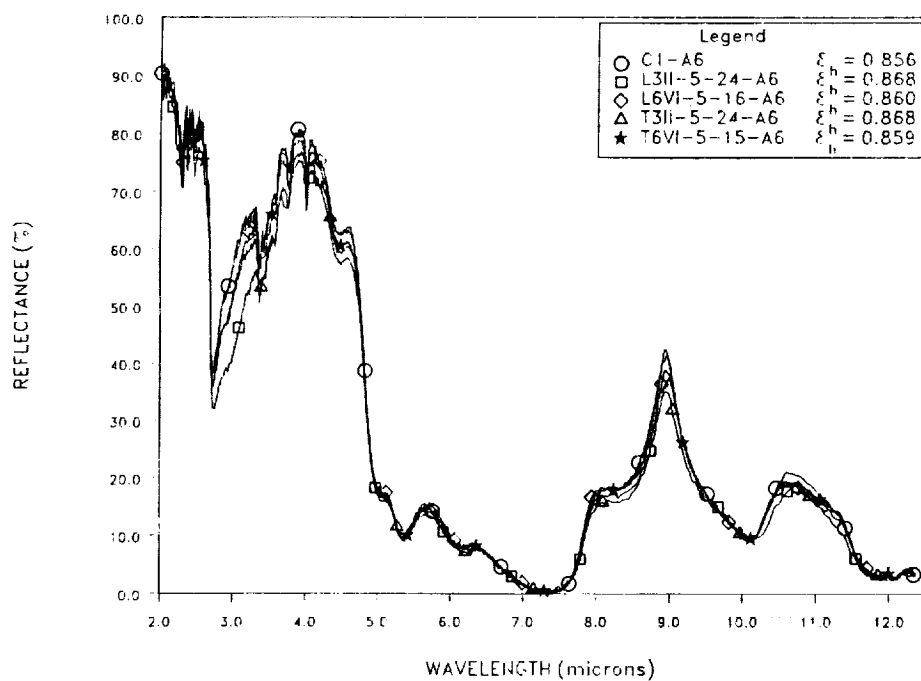


Figure 14. Comparison FTIR Reflectance Curves of Quartz Fabric 7 micron

In₂O₃/FEP/Ag/ INCONEL 5 mil

C1-A9 (Laboratory Specimen)

Specimen has surface scratches. There are small areas of yellow discoloration near the bond area. The metallized coating has pinholes. Some pinholes have tarnish rings surrounding the pinhole site. The adhesive bond between the In₂O₃ / F E P/Ag / Inconel / and Al mounting disc appears intact.

L3-A9 (Leading Edge Specimen)

The exposed surface area of the specimen is bright, shiny and reflective and has a slight haze. Fibers and particles are present on the exposed surface area. The exposed surface appears pitted or eroded. The weave pattern on the cloth used in preflight storage is embossed on the surface. There is a grayish black residue present in several areas near the perimeter covered by the mounting plate. The adhesive bond between the In₂O₃ / F E P/Ag / Inconel / and Al mounting disc appears intact.

T3-A9 (Trailing Edge Specimen)

The exposed surface area of the specimen is bright, shiny and reflective with a surface haze. Scuff marks are present on the surface as well as the imprint of the weave pattern from the cloth used in preflight storage. The adhesive bond between the In₂O₃ / FEP/ Ag/ Inconel and the aluminum mounting disc appears intact.

L6-A9 (EECC Leading Edge Specimen)

The exposed surface of the specimen is shiny and reflective with a slight haze. There is a weave pattern embossed on the surface from the protective cloth used during preflight storage. Surface scratches are present. The adhesive bond between the In₂O₃ / FEP / Ag / Inconel and the aluminum mounting disc appears intact.

A comparison photograph of the specimens is illustrated in figure 15; figure 16 compares the UV-Vis-NIR reflectance changes and figure 17 compares FTIR reflectance changes.

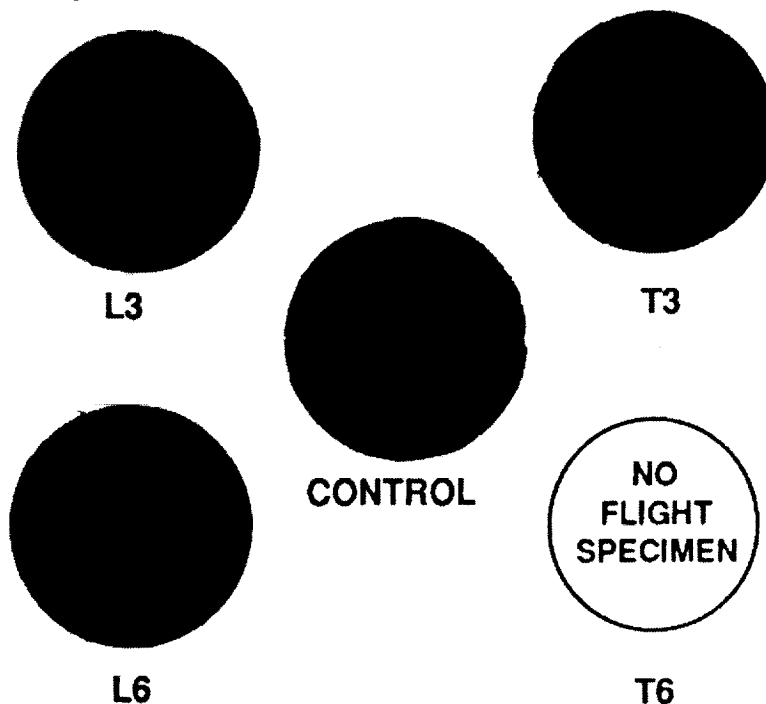


Figure 15. Comparison of In₂O₃/FEP/Ag/Inconel Specimens

In₂O₃/FEP/Ag/ INCONEL 5 mil

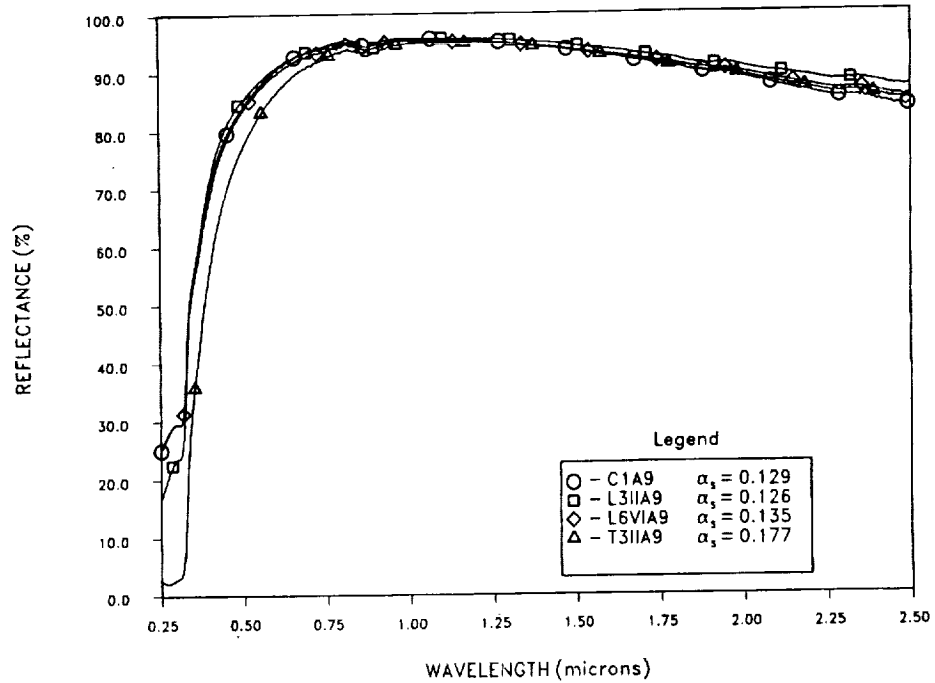


Figure 16. Comparison UV-Vis NIR Reflectance Curves of In₂O₃/FEP/Ag/ INCONEL 5 mil

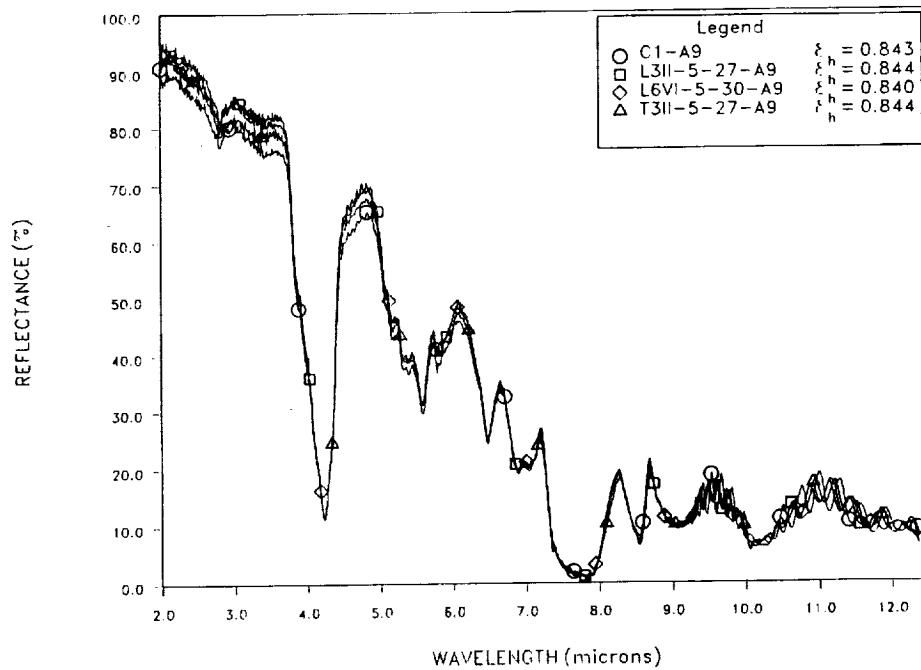


Figure 17. Comparison FTIR Reflectance Curves of In₂O₃/FEP/Ag/ INCONEL 5 mil

KAPTON/Al 5 mil

C-A11 (Laboratory Specimen)

Specimen appears to be in good condition. No apparent damage from long term storage.

L3-A11 (Leading Edge Specimen)

The exposed surface exhibits a hazy and discolored appearance. Surface scratches are present. A non uniform texture or weave pattern is present on the surface. Surface abrasion or pitting is indicated. Fibers and particles are present on the surface. The perimeter of the specimen covered by the mounting plate is undamaged and reflective, although some discoloration is present.

T3-A11 (Trailing Edge Specimen)

The exposed surface appears bright, shiny, reflective and is lighter in color than the perimeter area. There are thin lines or tracks abruptly beginning and ending on the surface. Fibers and particles are present on the surface. There is a yellowish discoloration in the form of a halo at the intersection of the exposed surface and the perimeter covering the specimen mounting plate. The perimeter is bright, shiny and reflective.

L6-A11 (EECC Leading Edge Specimen)

The exposed surface of the specimen is dull, nonspecular and orange red in color. Surface abrasion or erosion is apparent. There are bright colored particles present on the surface. The specimen appears to have shifted in the mounting plate at an early stage. The perimeter of the specimen appears undamaged, bright and reflective. There is debris around the perimeter.

T6-A11 (EECC Trailing Edge Specimen)

The exposed surface of the specimen is bright, shiny and reflective with a copper red color. A slight haze may be present. A smear is present near the edge of the specimen. Particles are present on the surface. The perimeter of the specimen is undamaged, shiny and reflective.

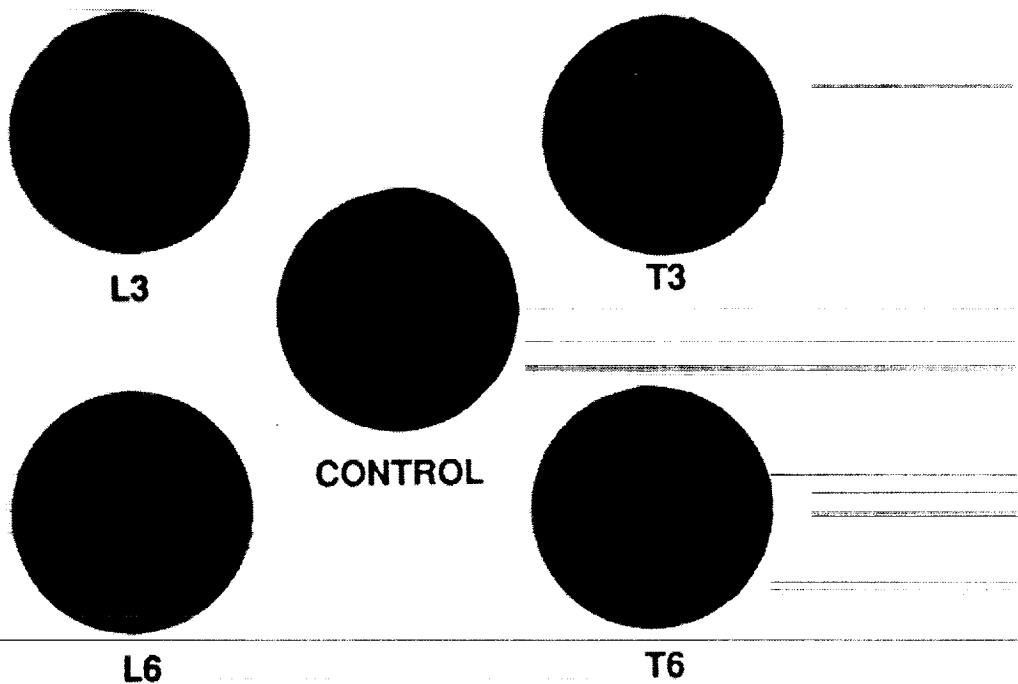


Figure 18. Comparison of Kapton/Al 5 mil Specimens

KAPTON/Al 5 mil

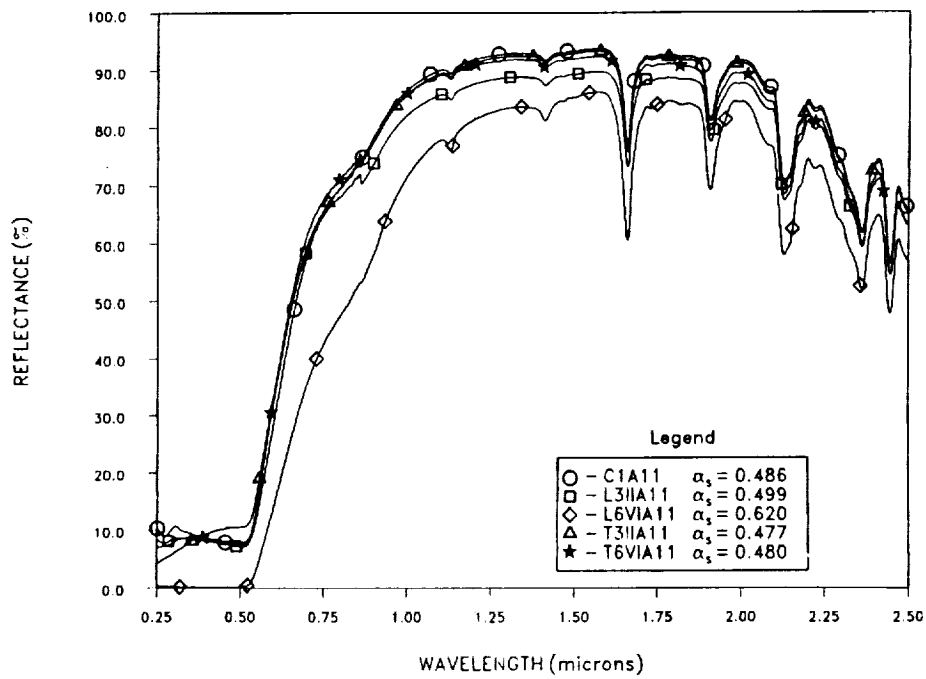


Figure 19. Comparison UV-Vis-NIR Curves of Kapton/Al 5 mil

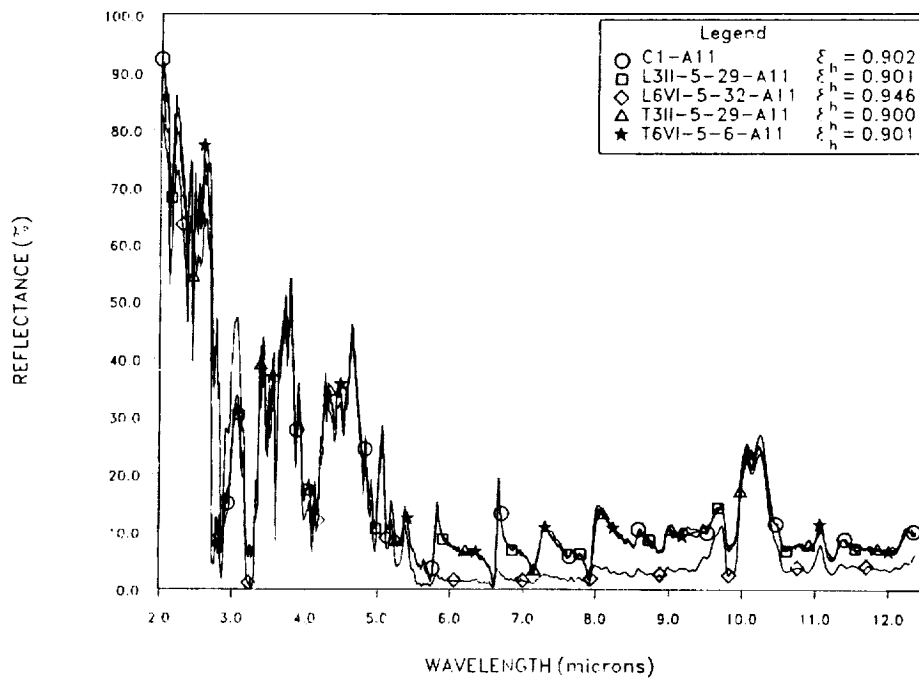


Figure 20. Comparison FTIR Curves of Kapton/Al 5 mil

In₂O₃/KAPTON/Al 5 mil

C1-A12 (Laboratory Specimen)

Specimen appears to be in good condition. No apparent damage from long term storage. The adhesive bond between the In₂O₃/Kapton/Al and the substrate appears to be intact.

L3-A12 (Leading Edge Specimen)

The entire specimen appears bright, shiny and reflective. Some surface scratches are present. Particles are present on the surface. The adhesive bond between the In₂O₃/Kapton/Al and the aluminum mounting disc appears intact.

T3-A12 (Trailing Edge Specimen)

The exposed surface appears darker than the perimeter area covered by the specimen mounting plate. There is a halo of dark yellow discoloration around the perimeter of the exposed surface. The specimen is bright, shiny and reflective. Surface scratches are present. Fibers and particles are present on the surface. The adhesive bond between the In₂O₃/Kapton/Al and the aluminum mounting disc appears intact.

L6-A12 (EECC Leading Edge Specimen)

Specimen is intact. The surface is bright yellow and reflective. There are some surface scratches present as well as a large amount of particles on the surface. There is a darker yellow halo near the perimeter of the specimen. The perimeter appears undamaged, bright and reflective. The adhesive bond between the In₂O₃/Kapton/Al and the aluminum mounting disc appears intact.

A comparison photograph of the specimens is illustrated in figure 21; figure 22 compares the UV-Vis-NIR reflectance changes.

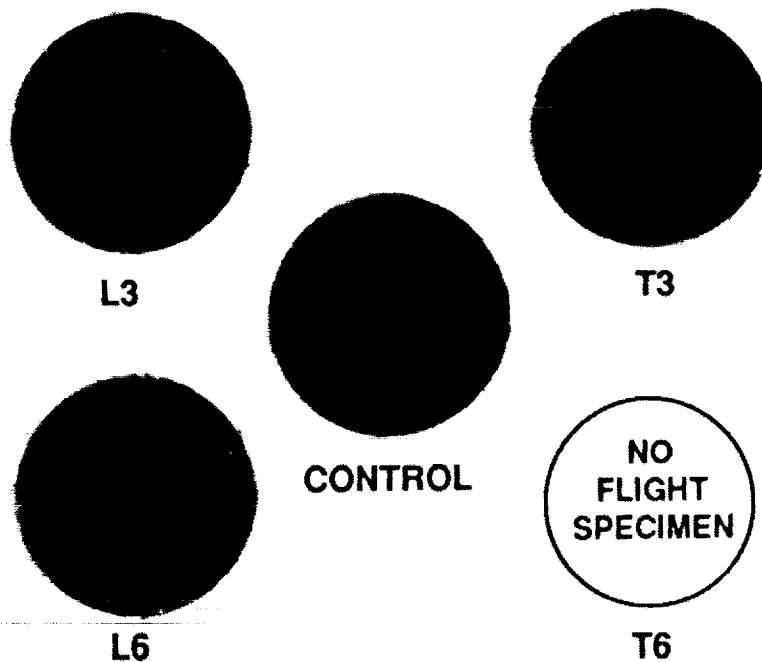


Figure 21. Comparison of In₂O₃/Kapton/Al Specimens

In₂O₃/KAPTON/Al 5 mil

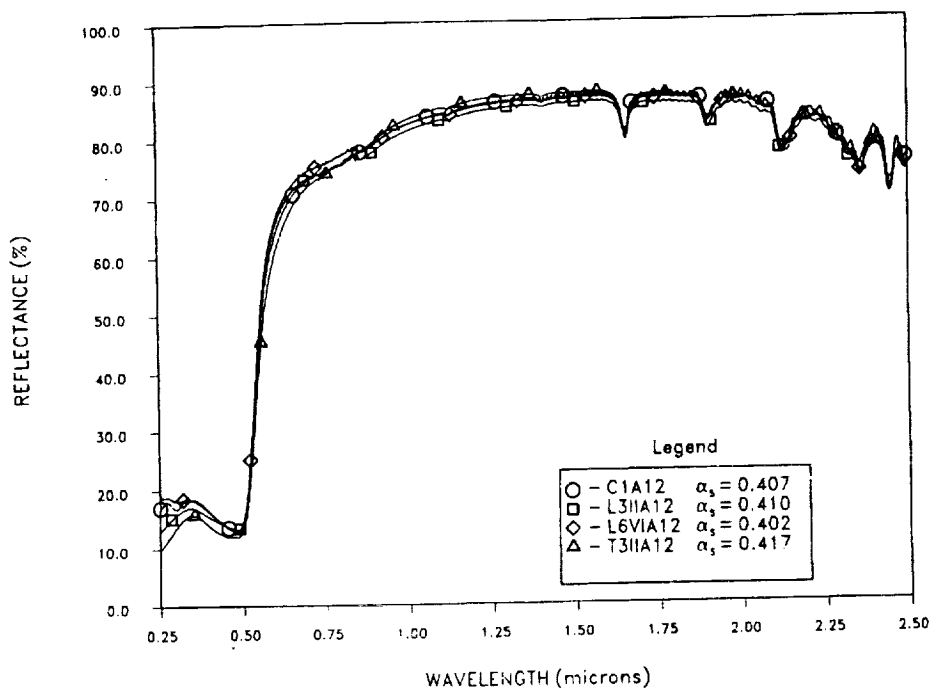


Figure 22. Comparison Curves of In₂O₃/Kapton/Al 5 mil

FTIR Unavailable

S-13 GLO WHITE SILICONE COATING

C1-A14 (Laboratory Specimen)

Specimen appears to be in good condition. No apparent damage from long term storage.

L3-A14 (Leading Edge Specimen)

The exposed surface of the specimen is bright yellow in color, nonspecular and has a slight sheen. The surface is rough and pebbled. A large piece of white debris (possibly Teflon) is present near the center of the specimen, as well as several metallic flakes. Other types of surface debris are also present. Several black marks are present at the periphery of the exposed area. Coating at the perimeter of the specimen is white, nonspecular and apparently undamaged.

T3-A14 (Trailing Edge Specimen)

The exposed surface of the specimen is discolored a dark tan-brown and is nonspecular. The surface is rough and pebbled with a localized area of a lighter tan color. Some debris is present on the exposed area. Coating at the perimeter of the specimen is white, nonspecular and apparently undamaged.

L6-A14 (EECC Leading Edge Specimen)

The exposed surface of the specimen is discolored a pale yellow and is rough in texture. Surface debris is present. The perimeter of the specimen is white with dark smears probably from the mounting plate.

T6-A14 (EECC Trailing Edge Specimen)

The exposed surface area of the specimen is discolored a light yellow. The surface has a slightly rough texture. Debris is present on the surface. The perimeter of the specimen is white and undamaged.

A comparison photograph of the specimens is illustrated in figure 23; figure 24 compares the UV-Vis-NIR reflectance changes.

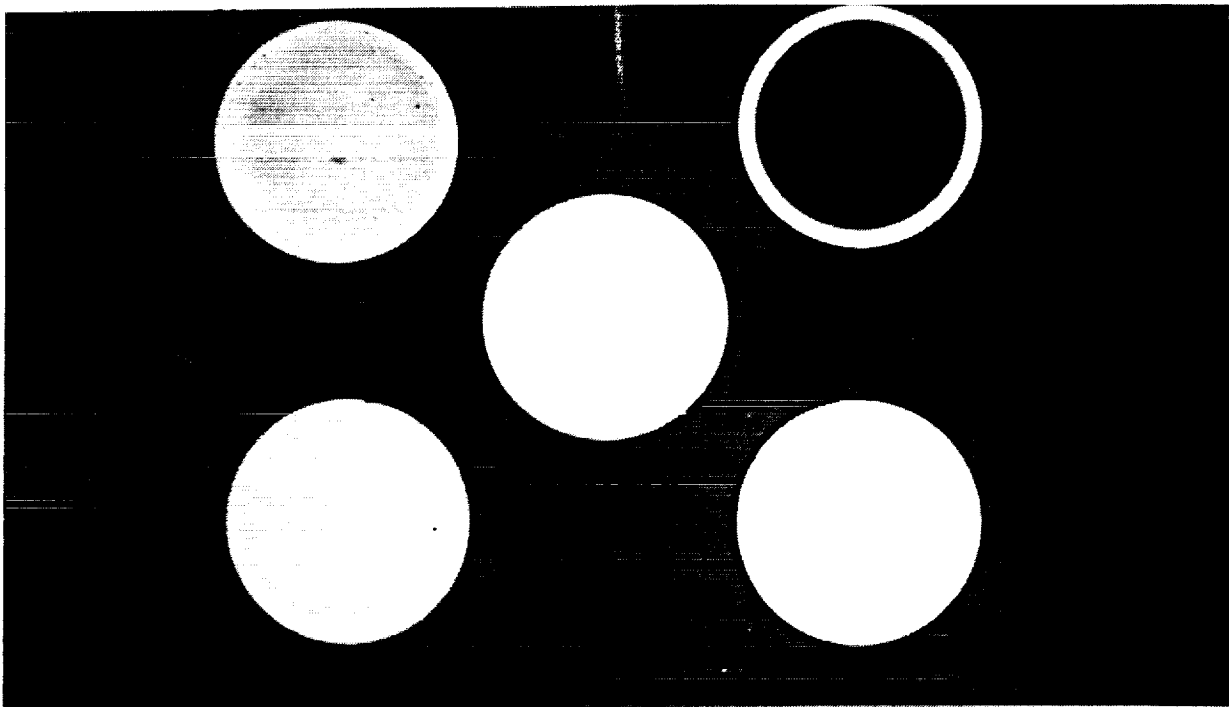


Figure 23. Comparison of S-13 GLO White Silicone Coating Specimens

S-13 GLO WHITE SILICONE COATING

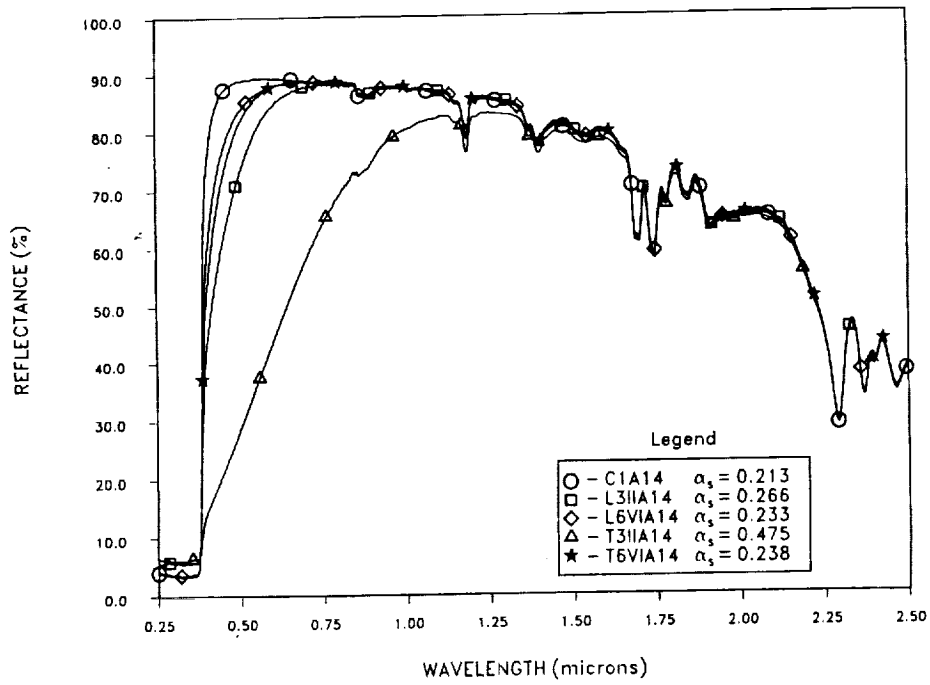


Figure 24. Comparison UV-Vis-NIR Reflectance Curves of S-13 GLO White Silicone Coatings

FTIR Unavailable

ZN₂TiO₄ WHITE INORGANIC COATING

C1-A15 (Laboratory Specimen)

Chipping is present in three areas of the specimen rim. One chipped area is large. One long scratch is also present on the rim.

L3-A15 (Leading Edge Specimen)

The exposed surface area of specimen is white and non-reflective. Several large cracks and a rough surface area are present on the exposed area. Black particles are present on the surface and there may be a slight discoloration. Approximately 30% of coating around perimeter is chipped and missing. Two cracks in coating are visible at the perimeter. A dark circular streak is present near the perimeter.

T3-A15 (Trailing Edge Specimen)

The exposed surface of the specimen is discolored a slight yellow. The surface is moderately rough and debris is present on the surface. The perimeter of the specimen is white with areas containing some dark particles or spots.

L6-A15 (EECC Leading Edge Specimen)

The exposed surface of the specimen is white and rough in texture. The surface appears crazed. The perimeter of the specimen has grayish smears, probably from the mounting plate. Chipping near the rim of the specimen is also evident.

T6-A15 (EECC Trailing Edge Specimen)

The exposed surface area of the specimen appears slightly discolored with a large area of rough texture. Debris is present on the surface. The perimeter of the specimen is chipped and remains white in color.

A comparison photograph of the specimens is illustrated in figure 25; figure 26 compares the UV-Vis-NIR reflectance changes and figure 27 compares FTIR reflectance changes.

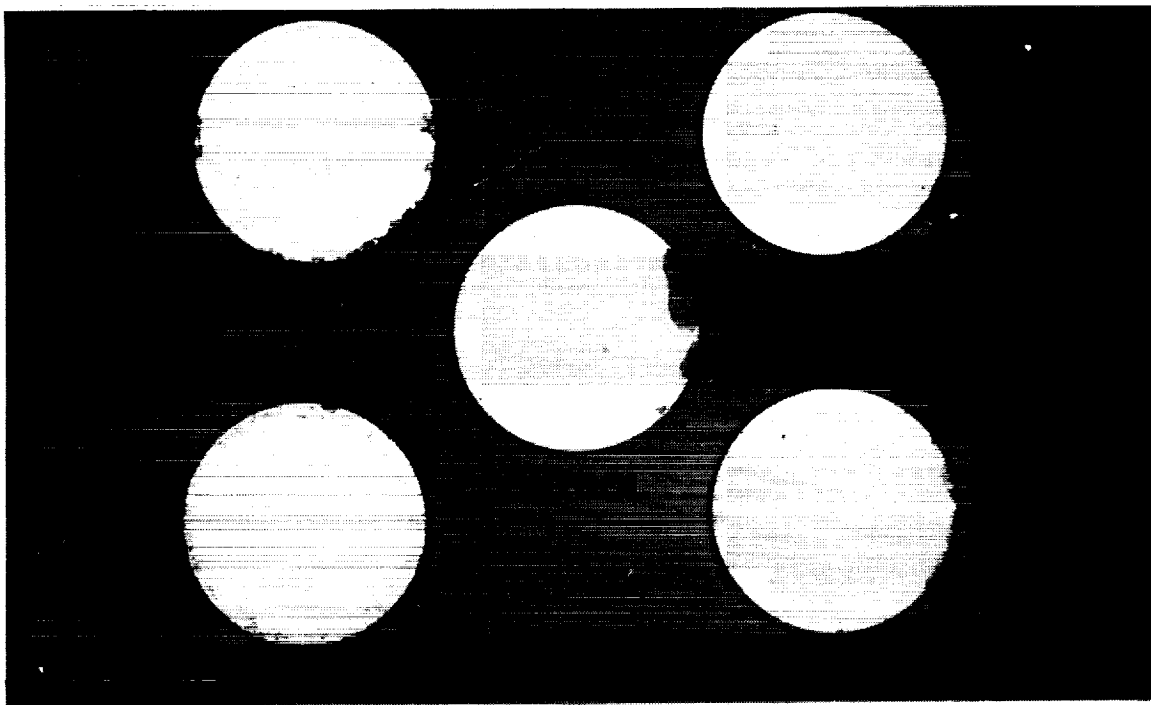


Figure 25. Comparison of Zn₂TiO₄ White Inorganic Coating Specimens

Zn₂TiO₄ WHITE INORGANIC COATING

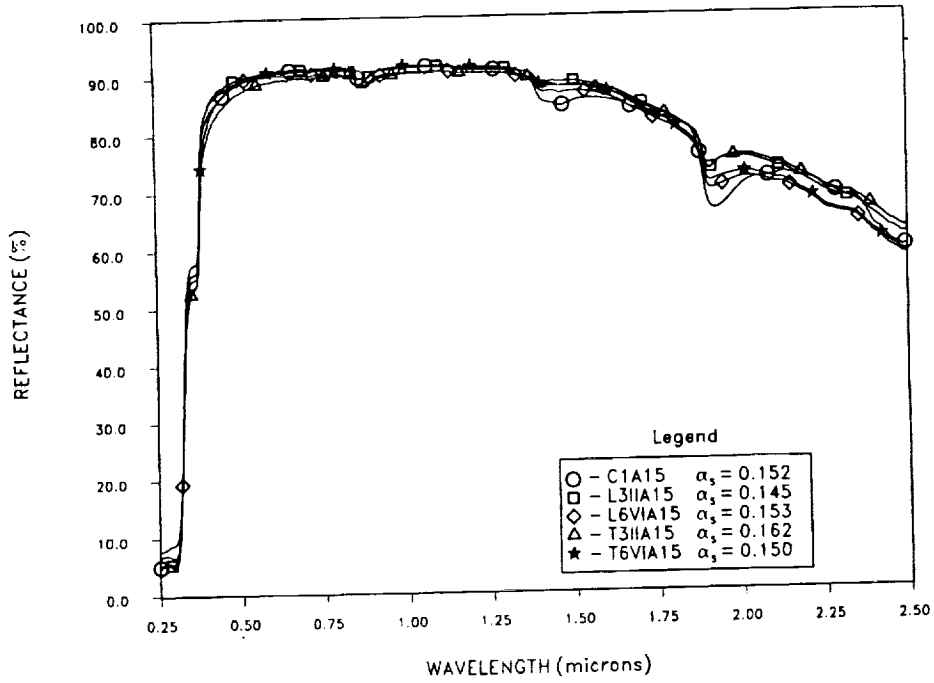


Figure 26. Comparison UV-Vis-NIR Reflectance Curves of Zn₂TiO₄ White Inorganic Coating

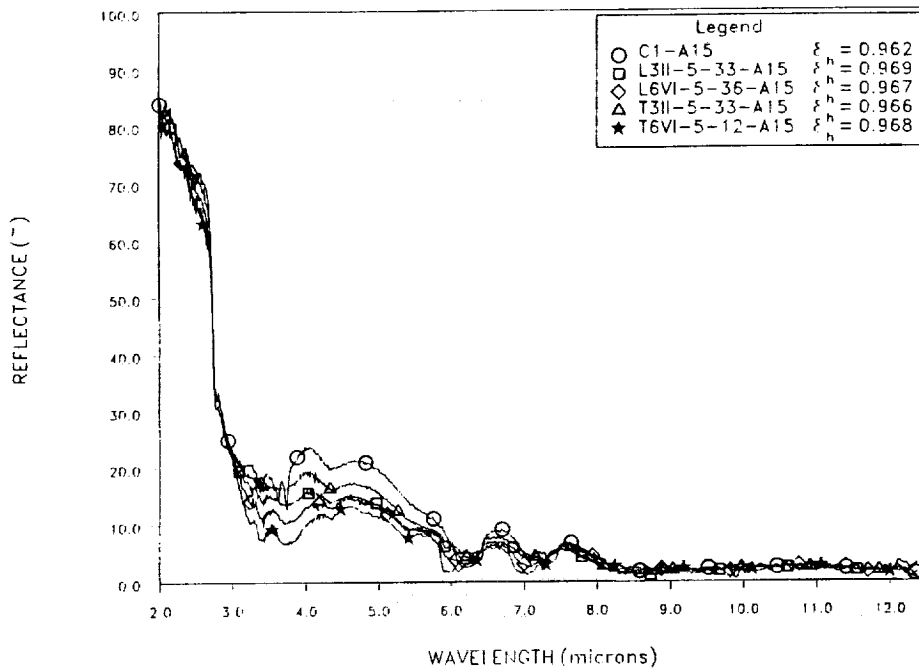


Figure 27. Comparison FTIR Reflectance Curves of Zn₂TiO₄ White Inorganic Coating

NS 43G WHITE INORGANIC COATING

C1-A16 (Laboratory Specimen)

Coating is yellow in color. Pinholes and bubbles are present in the coating. There is slight chipping on the rim of the specimen.

L3-A16 (Leading Edge Specimen)

The exposed surface of specimen is discolored to a light yellow, as well as the periphery of the specimen under the mounting plate. The surface of the entire specimen has a rough texture. Black particles are present in both exposed and unexposed surface area of specimen.

T3-A16 (Trailing Edge Specimen)

The entire surface area of the specimen is discolored a light yellow. The surface is moderately rough and contains considerable surface debris. There is a darker halo near the perimeter of the mounting plate.

L6-A16 (EECC Leading Edge Specimen)

The entire surface of the specimen is pale yellow in color and has a rough texture. Debris is present on the surface.

T6-A16 (EECC Trailing Edge Specimen)

The coating is discolored a light yellow over the entire specimen. A large amount of debris is present on the surface. Overall, the texture of the specimen is very rough.

A comparison photograph of the specimens is illustrated in figure 28; figure 29 compares the UV-Vis-NIR reflectance changes.

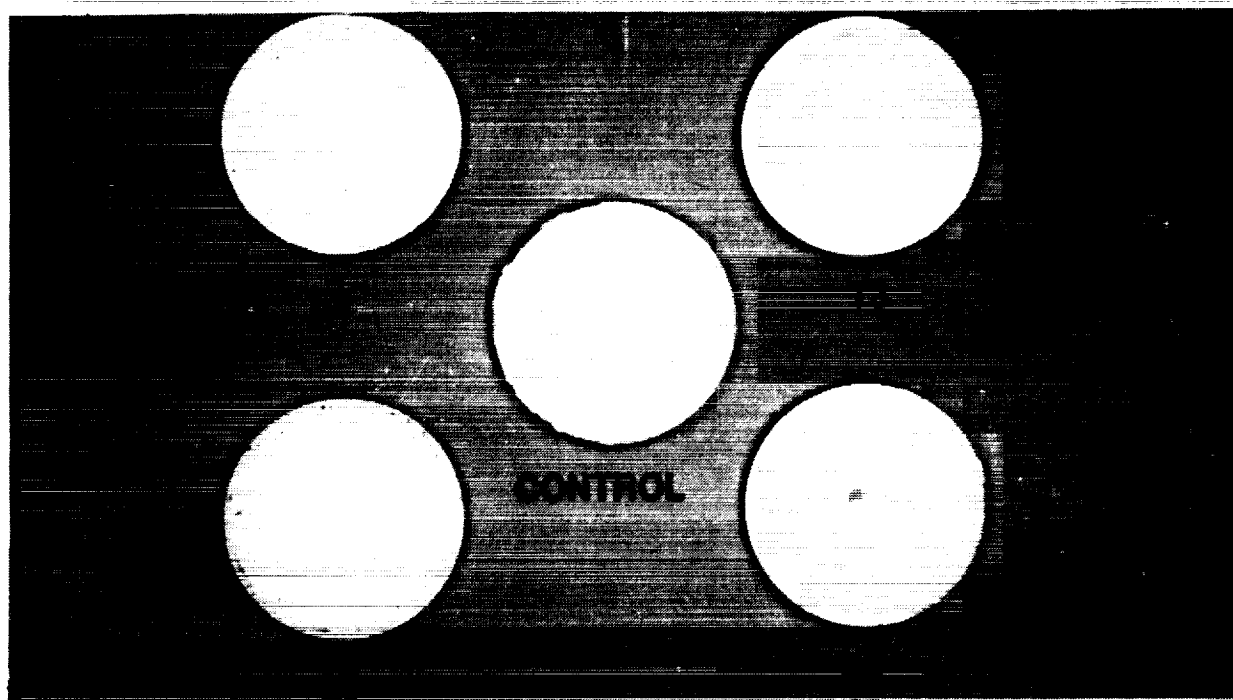


Figure 28. Comparison of NS 43G White Inorganic Coating

NS 43G WHITE INORGANIC COATING

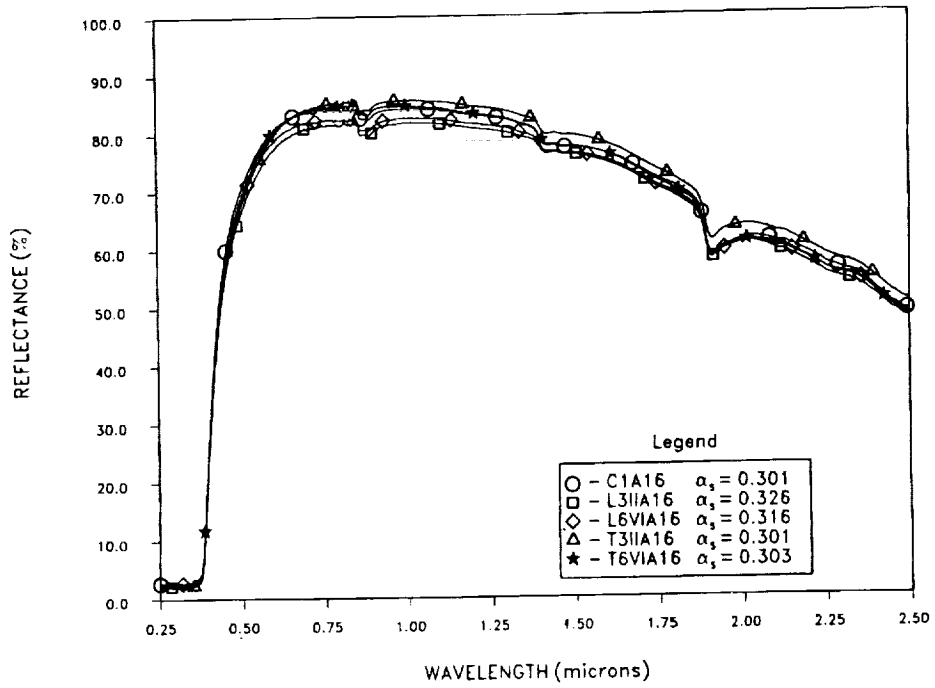


Figure 29. Comparison of UV-Vis-NIR Reflectance Curves of NS 43G White Inorganic Coating

FTIR Unavailable

a-4

DC92-007 WHITE SILICONE COATING

C1-A22 (Laboratory Specimen)

A fingerprint is present on the surface. The surface is glossy and has some surface dust.

L3-A22 (Leading Edge Specimen)

The exposed surface area of specimen is discolored a dark yellow, is moderately reflective and has extensive cracks in the coating. There are dark particles and fibers present on the exposed surface area. The coating perimeter of the specimen is white, reflective and slightly damaged.

T3-A22 (Trailing Edge Specimen)

The exposed surface area of the specimen is discolored a deep yellow-gold. There is an extensive network of cracks and fractures in the exposed area. There is a sheen or glazed appearance to the surface. Scuff marks and black particle debris are on the surface. The perimeter of the specimen is white, shiny, reflective and undamaged.

L6-A22 (EECC Leading Edge Specimen)

The exposed surface area of the specimen is yellow and slightly specular. The surface is rough in texture. A large amount of fibers and particles are present on the surface. The perimeter of the specimen is white and specular with debris.

A comparison photograph of the specimens is illustrated in figure 30; figure 31 compares the UV-Vis-NIR reflectance changes.

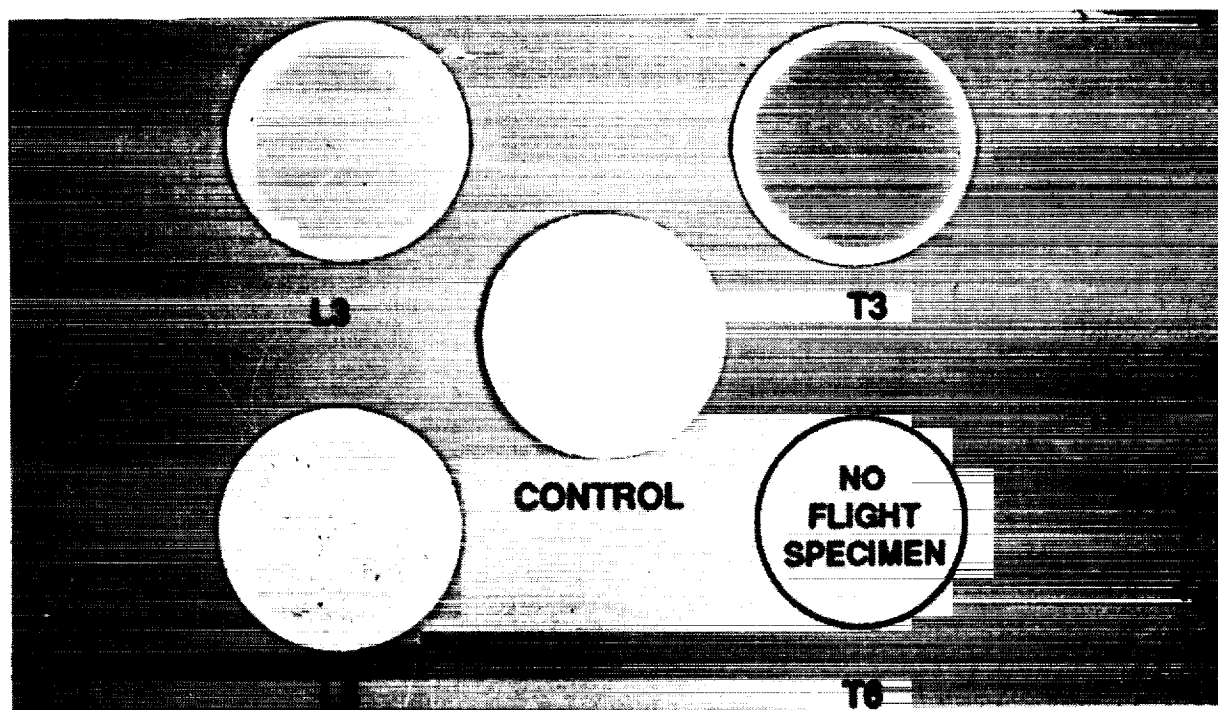


Figure 30. Comparison of DC92-007 White Silicone Coating Specimens

DC92-007 WHITE SILICONE COATING

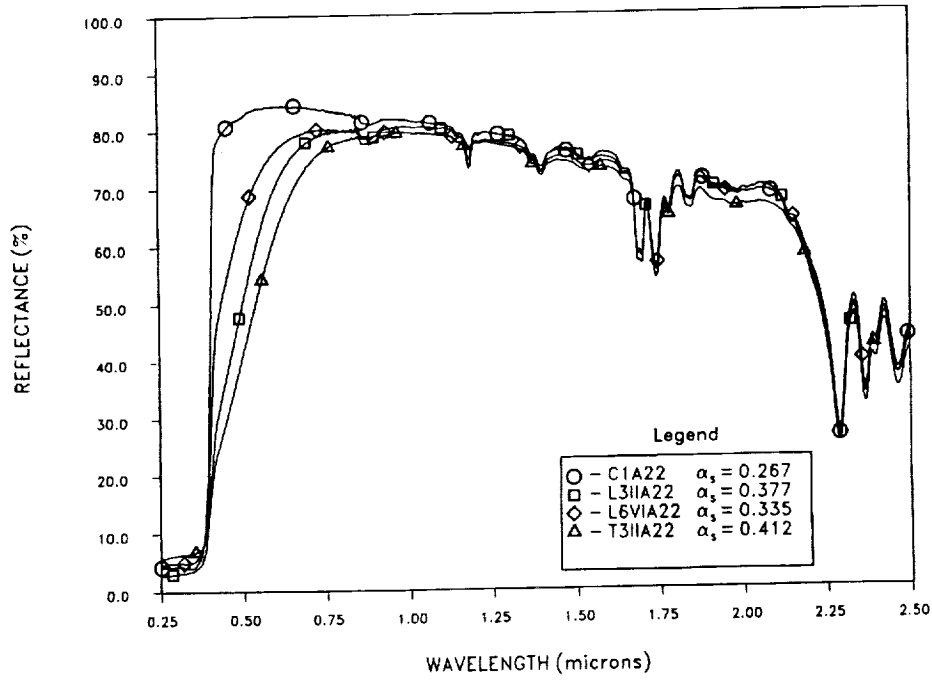


Figure 31 Comparison UV-Vis-NIR Reflectance Curves of DC92-007 White Silicone Coating

FTIR Unavailable

Ag MIRROR

C1-B6 (Laboratory Specimen)

Specimen is tarnished and has a fingerprint on the surface. Stains are also present.

L3-B6 (Leading Edge Specimen)

The exposed surface area of the specimen has been uniformly eroded, except at the perimeter of the specimen mounting plate. The edges of the specimen at the perimeter of the mounting plate are rough, distorted and eroded. The center of the surface has three circular indented areas, as well as several crater sites. The perimeter of the specimen is tarnished and shows evidence of fingerprints. The adhesive bond between the silver and aluminum mounting square appears intact.

T3-B6 (Trailing Edge Specimen)

The exposed surface area of the specimen is discolored a dark brown. The perimeter of the exposed area shows a darker brown discoloration. The perimeter of the specimen is discolored or tarnished. There is evidence of a fingerprint on one side of the specimen. A triangular shaped dark spot with a light center is present near the center of the specimen.

A comparison photograph of the specimens is illustrated in figure 32; figure 33 compares the UV-Vis-NIR reflectance changes.

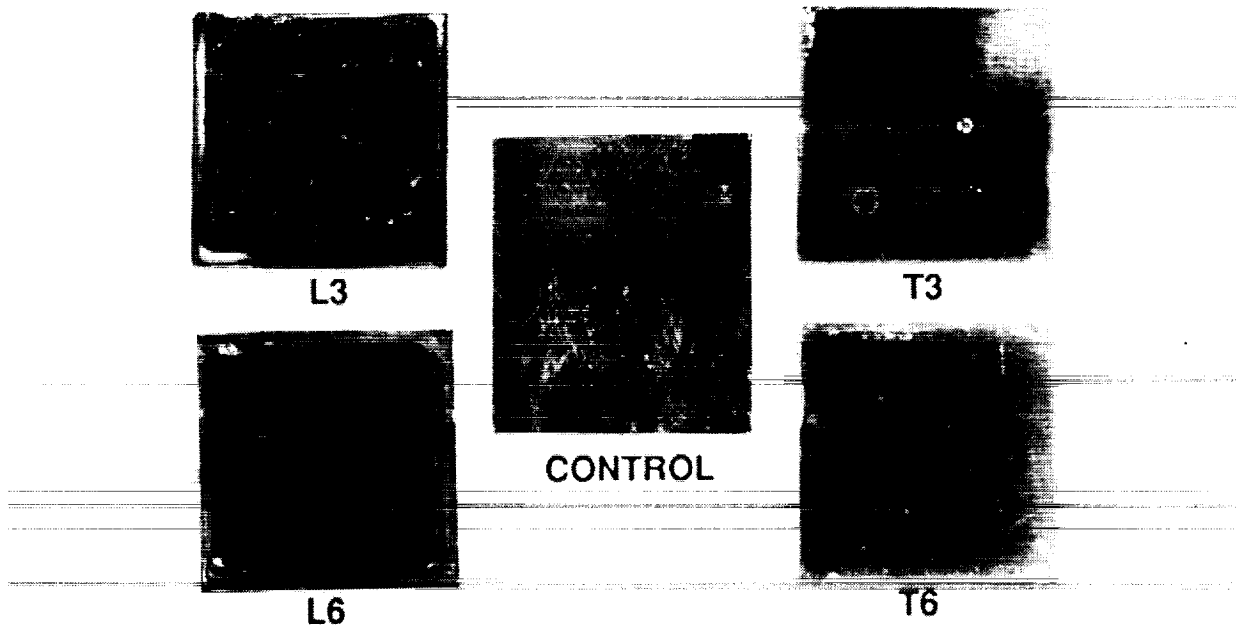


Figure 32. Comparison of Ag Mirror Specimens

Ag MIRROR

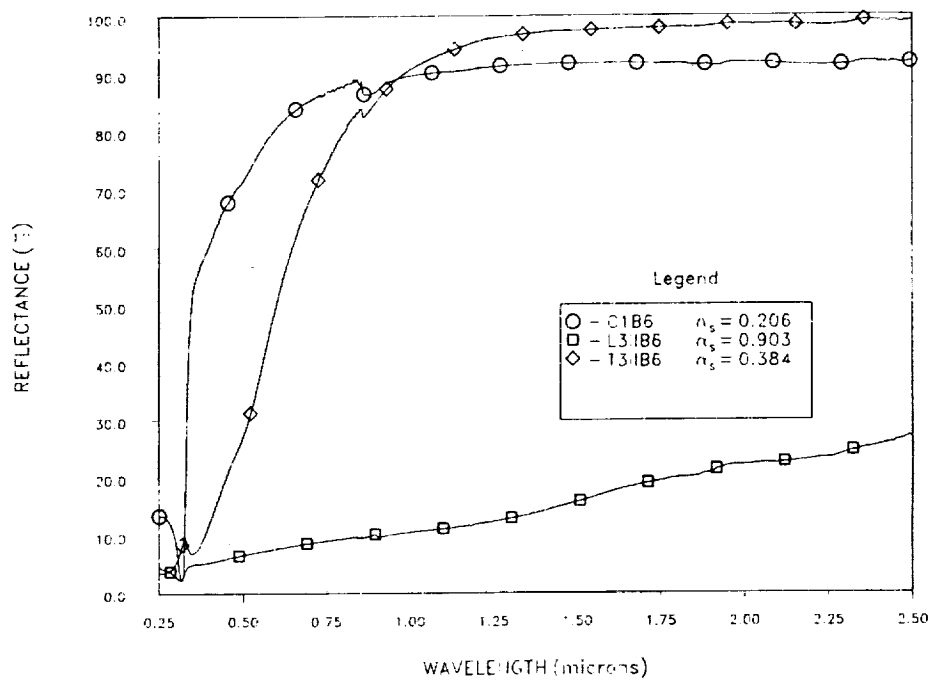


Figure 33. Comparison UV-Vis-NIR Reflectance Curves of Ag MIRROR

FTIR Unavailable

Ag MIRROR

C1-B5 (Laboratory Specimen)

Specimen is badly tarnished and has fingerprints as well as surface scratches.

L3-B5 (Leading Edge Specimen)

The exposed surface area of the specimen has been essentially eroded away leaving a black oxidized residue adhered to the adhesive. The remaining surface is rough and distorted. The perimeter of the specimen is intact, but tarnished. Localized areas of the aluminum mounting plate and adhesive bond are visible.

T3-B5 (Trailing Edge Specimen)

The exposed surface area of the specimen is nonuniformly discolored a light yellow. There is a significant micrometeoroid crater near the center. There are stains, smears and a possible fingerprint visible in the exposed area. There is a lighter band of discoloration around the perimeter of the exposed area. Surface debris is present. One edge of the specimen appears to be tarnished. The other three edges are shiny and reflective.

L6-B5 (EECC Leading Edge Specimen)

The exposed surface area of the specimen is heavily eroded and oxidized. Minute cracks are present on the surface. One spot is metallic in appearance and may be eroded through to the adhesive layer. The perimeter, at the mounting plate, is also severely eroded and oxidized. The perimeter is metallic in color and is heavily tarnished.

T6-B5 (EECC Trailing Edge Specimen)

The exposed surface area of the specimen is non-uniformly tarnished or contaminated a light tan color. Several spots or stains are present on the surface. Particles are present on the surface. The perimeter of the specimen appears tarnished a light grey color.

A comparison photograph of the specimens is illustrated in figure 34; figure 35 compares the UV-Vis-NIR reflectance changes.

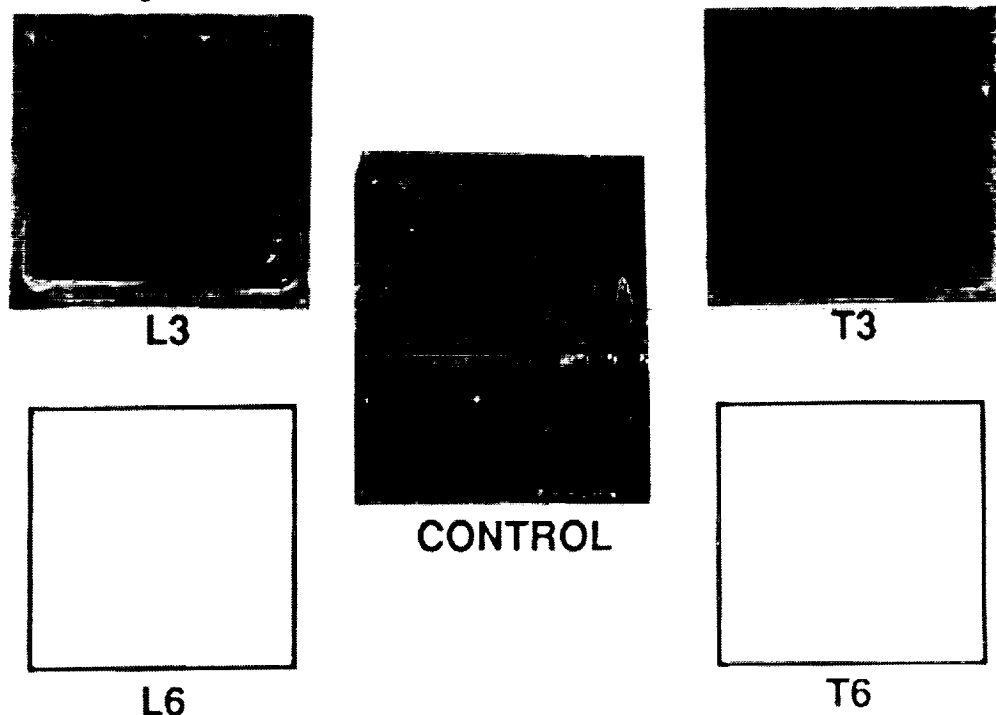


Figure 34. Comparison of Ag Mirror Specimens

Ag MIRROR

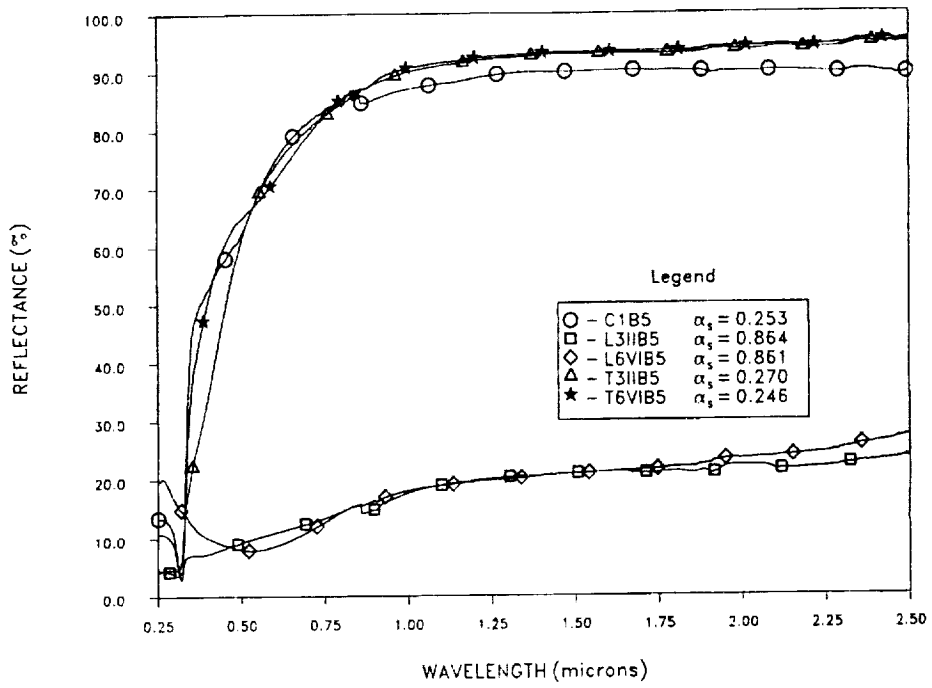


Figure 35. Comparison UV-Vis-NIR Reflectance Curves of Ag Mirror

FTIR Unavailable

LDEF M0003-5
WL/ML THERMAL CONTROL MATERIALS EXPERIMENT
PRELIMINARY OBSERVATIONS

- Solar absorptance changes were greater for trailing edge than leading edge materials.
- White coatings in organic binders exhibited more degradation than coatings in inorganic binders.
- Contamination effects were most pronounced on the trailing edge.
- Front surface silver mirrors were severely attacked by atomic oxygen.
- Polymeric leading edge materials displayed evidence of atomic oxygen attack.
- In₂O₃ coatings on Kapton and FEP reduced effects of atomic oxygen exposure.
- DC92-007 (TiO₂) and aAl₂O₃ coatings exhibited large changes in absorptance.
- Effects of scuff plate shadowing on leading edge samples have not been defined.

ELEMENT MATERIAL EXPOSURE EXPERIMENT BY EFFU

Yoshihiro Hashimoto, Masaaki Ito and Masahiro Ishii
Ishikawajima-Harima Heavy Industries Co., Ltd. (IHI)
Tokyo, 190-12, JAPAN

INTRODUCTION

The National Space Development Agency of Japan (NASDA) is planning to perform an "Element Material Exposure Experiment" using the Exposed Facility Flyer Unit (EFFU).

This paper presents an initial design of experiments proposed for this project by our company. The EFFU is installed on the Space Flyer Unit (SFU) as a partial model of the Space Station JEM exposed facility. The SFU is scheduled to be launched by H-II rocket in January or February of 1994, then various tests will be performed for three months, on orbit of 500 km altitude, and it will be retrieved by the U.S. Space Shuttle and returned to the ground. The mission sequence is shown in Figure 1.

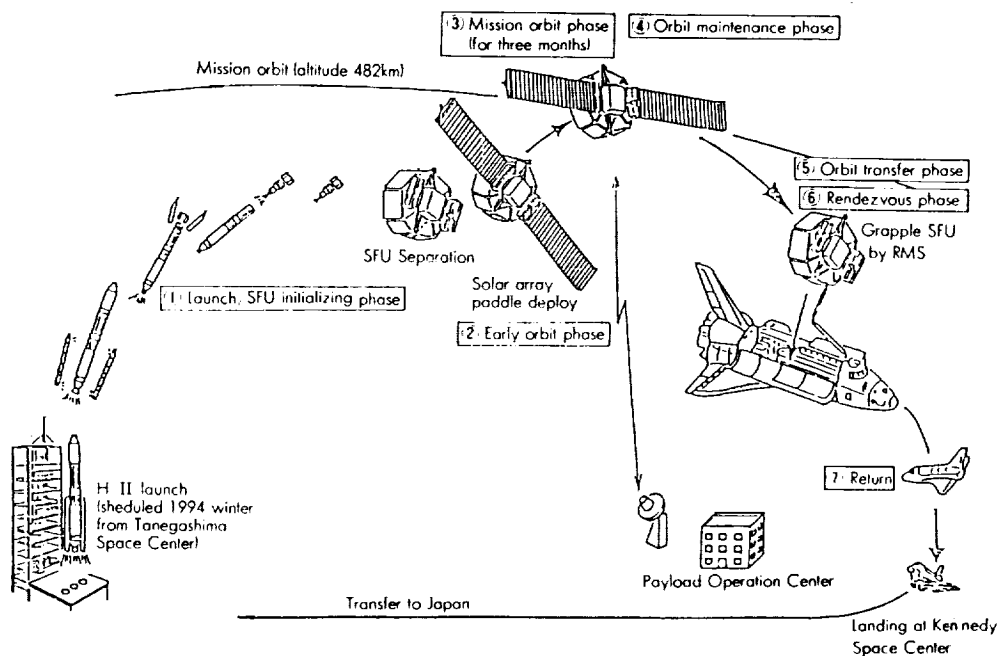


Figure 1. Flight operation profile of SFU.

PURPOSE AND MERIT OF THE EXPERIMENT

Two main purposes of the experiments are as follows:

- a. Confirmation of strength of element materials to be used in Japanese Experiment Module (JEM) of the Space Station Freedom against AO and/or UV in LEO.
- b. Research and Development for future projects.

In the LEO environment, the major factors contributing to the degradation of materials are AO and UV. In some cases, those synergistic effects must be more important.

SFU's basic attitude is "Solar pointing" (see Figure 2(a)). In this attitude, one surface faces the sun at all times and receives abundant irradiation of ultraviolet rays. To the others, no direct solar irradiation is given. As for AO irradiation, the plural panels receive atomic oxygen flux in the same manner (in sine curve). By using this advantage, three different irradiations are being applied; for example, AO, UV, and AO+UV.

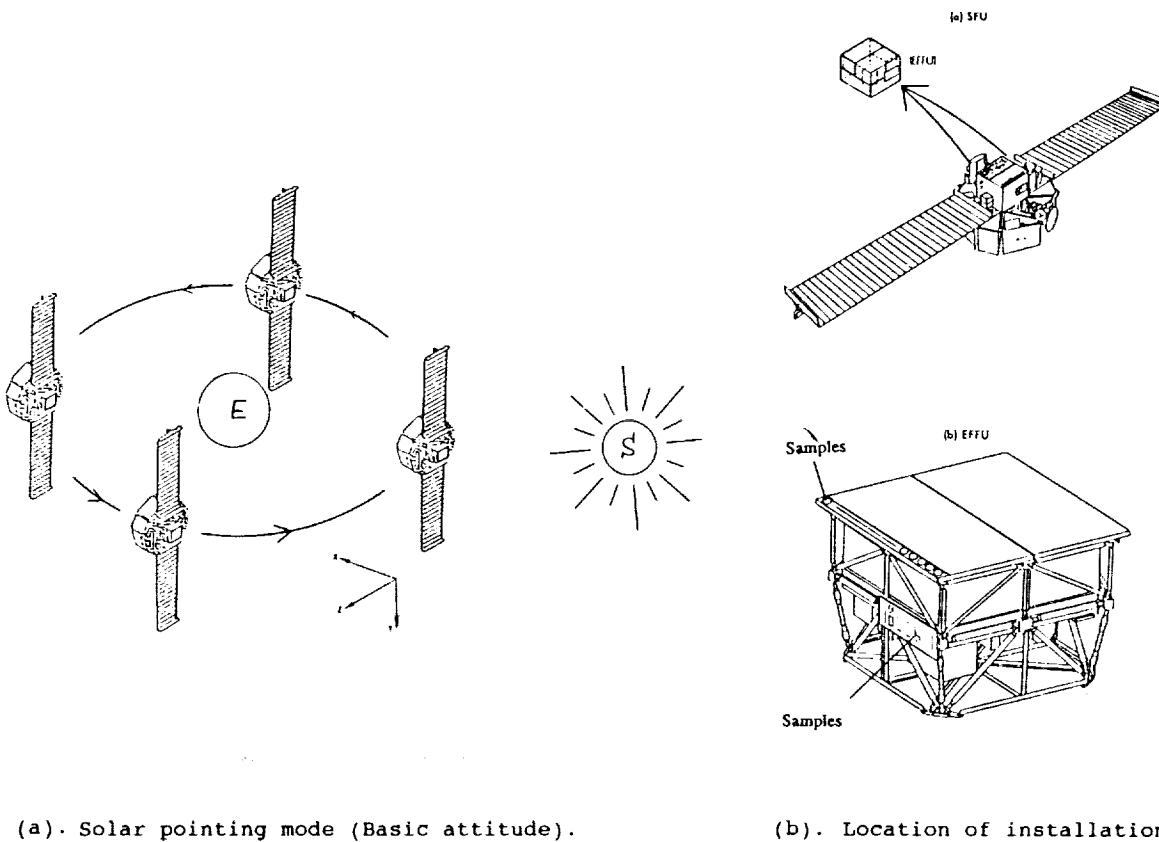


Figure 2. Installation and the flight.

FIVE MAIN EXPERIMENTS

Five main experiments proposed by IHI are shown in Table 1. Thermal control coatings and films are our concern because they are often used as the materials exposed to space and measurements of LEO component degradation urgently required. They include anodized, indium-tin-oxide and silicon-dioxide coatings and Teflons. Three themes are proposed for them (Themes 1, 2 and 4).

The only active monitoring performed by the exposure experiments at this time is temperature monitoring; this is done by one thermistor placed at the center of the sample panel prepared for this experiment. We have planned unique environment monitoring equipment to find out both the AO and UV flux (Theme 5).

As a research and development theme, "Comparison of damage among different direction arrangements of graphite crystals" is projected (Theme 3).

Purpose and background for each experiment theme are described in detail later.

Table I. Five Main Experiments

- | | |
|----|---|
| 1. | Comparison of durability characteristics among different anodizing processes. |
| 2. | Growth of erosion from coating defects. |
| 3. | Comparison of damage among different direction arrangements of graphite crystals. |
| 4. | Effects of UV, AO and their synergism on different types of fluorocarbon. |
| 5. | SFU orbit environment monitoring by Kapton. |

COMPARISON OF DURABILITY CHARACTERISTICS AMONG DIFFERENT ANODIZING PROCESSES

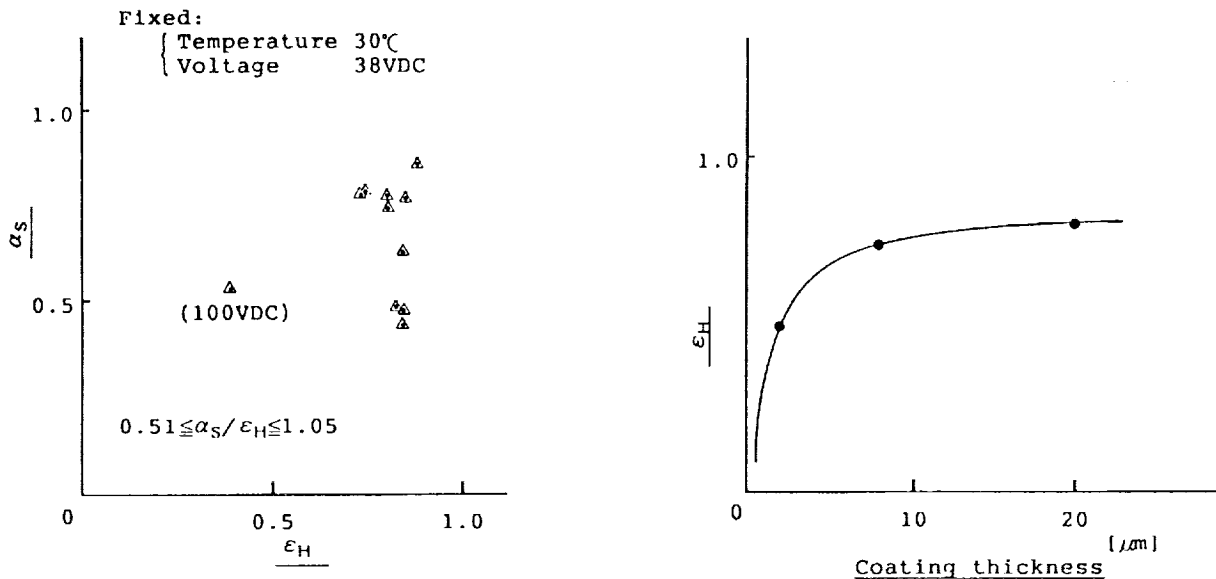
The Purpose of this experiment is to evaluate the strength of different anodized coatings under the LEO environment. The objects are coated with chromic, sulphuric and oxalic acid.

Aluminum anodizing is known to be stable against AO attack. Therefore, anodized aluminum foil used as the outer cover of multi-layered insulation can be very effective for long-life spacecrafts.

Different anodizing processes produce different surface optical properties. We expect that there also exists some differences of durability against AO/UV among those three types of coating.

Each type of coating has these characteristics as follows:

1. Chromic acid anodizing can give various α/ϵ by changing voltage and processing time (See Figure 3(a)).
2. Sulphuric acid anodizing provides low α adaptable as a radiator of spacecrafts.
3. Oxalic acid anodizing is said to be unaffected by UV and solar absorptance (α) is rather stable.



(a). Thermal optical properties obtained by various anodizing processes (Chromic acid). (b). Relation between ϵ_H and anodizing thickness (Sulphuric acid).

Figure 3. Thermal optical properties of anodized coating.

GROWTH OF EROSION FROM COATING DEFECTS

The purpose of this experiment is to evaluate the growth of erosion which will start from the coating defects under LEO.

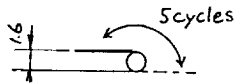
Indium-Tin-Oxide (ITO) or Silicon-dioxide (SiO₂) coated polymeric materials are known to be unaffected by atomic oxygen and can be applicable to JEM. Since ITO or SiO₂ is essentially brittle, however, some defects (like micro cracks) can be a starting point of erosion that cannot be avoided. Pin-holes by micro-meteoroids or debris, or perforations as air discharges, can also act in the same manner.

By knowing the quantity of the development of defects and why they are caused, these coatings can be applicable occasionally to JEM or Space Station Freedom— that is, for example, in limitation of duration of usage or in application suffering fewer AO/UV fluxes.

Three types of defects introduced in this experiment are shown in Figure 4, along with their sources.

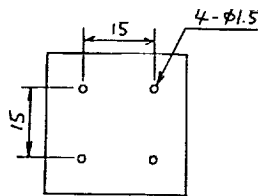
(1) Microcracks

5 cycles' bending of 180 against 1.6 mm diameter mandrel.

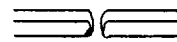


microcracks

(2) Air holes

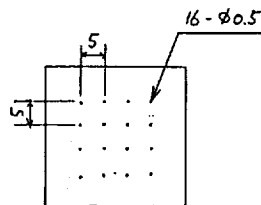


Perforation should precede coating



Air discharging hole

(3) Pin holes



Pinholing is preceded by coating



Pinhole

Figure 4. Making of "defects".

COMPARISON OF DAMAGE AMONG DIFFERENT DIRECTION ARRANGEMENTS OF GRAPHITE CRYSTALS

The purpose of this experiment is to compare damages among different direction arrangements of graphite crystals in carbon fibers.

In the process of calcining carbon fibers, temperature influences the direction arrangements of carbon graphite crystals. The highly developed and closed-packed structure of hexagon is very stable chemically. This means there can be some differences of durability in LEO among graphite crystals which have different direction arrangements. In this experiment, two different direction arrangements of graphite crystals, such as radial and quasi-onion, are to be exposed to space (see Figure 5).

In evaluation of damage of post-retrieval samples, these methods as written below, will be used.

- (1) Evaluate the reaction rate by means of measuring "mass loss".
- (2) Observe the differences in erosion by inspecting the surface and/or section by SEM or TEM.
- (3) Investigate the change of the crystal size and of the direction arrangements by means of x-ray diffraction.

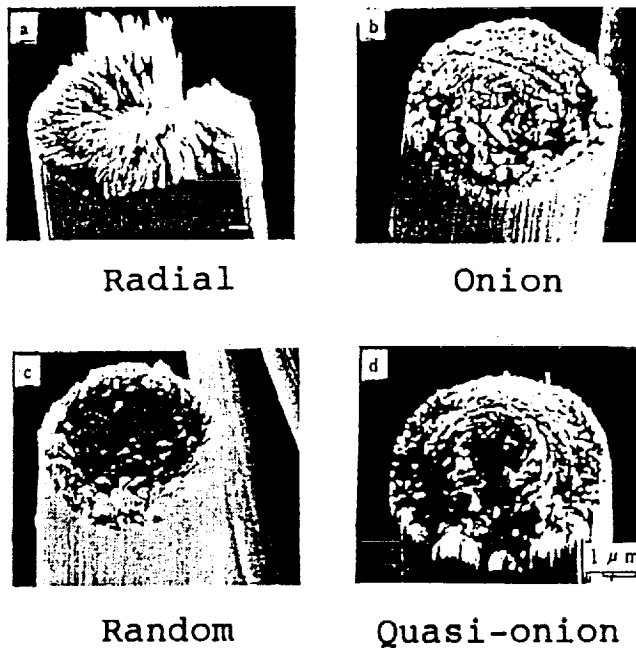


Figure 5. Coal-pitch carbon fibers (processed at 2500°C).

**EFFECTS OF UV, AO AND THEIR SYNERGISM
ON DIFFERENT TYPES OF FLUOROCARBON**

The purpose of this experiment is to evaluate the effects of UV, AO and their synergism on Teflon films (i.e. FEP, TFE and ETFE) that have different chemical compositions.

FEP, TFE and ETFE are fluorocarbons (Teflon) which have respective chemical compositions (See Table II).

Teflon is well known for its anti-UV characteristics and this can easily be confirmed in the ground simulation testing.

Regarding anti-AO characteristics, Teflon has been said to be strong because of space shuttle experiments and many ground testings, but the Teflon samples retrieved from SMRM are damaged, differing from the preceding results. In SMRM, synergism of AO and UV was investigated only qualitatively (ref. 1). Teflon used in this experiment was not pure fluorocarbon "TFE", but a copolymer of -CH₂- and -CF₂- (they are equivalent to ETFE). On the other hand TFEs are composed only of strong -CF₂- bondings and have no weak -CH₂- bonding. At this point TFEs can be expected to be stable satisfactorily in the LEO environment.

Table II. Chemical Composition of Teflons

Name	PTFE	PFA	FEP	ETFE
	<u>Polytetrafluoroethylene</u>	<u>Perfluoroalkoxy</u>	<u>Fluorinated Ethylene Propylene</u>	<u>Ethylene Tetrafluoroethylene</u>
Chemical Composition	$\left[\begin{array}{cc} \text{F} & \text{F} \\ & \\ -\text{C} & - & \text{C}- \\ & \\ \text{F} & \text{F} \end{array} \right]_n$	$\begin{array}{cccccc} \text{F} & \text{F} & \text{F} & \text{F} & \text{F} & \text{F} \\ & & & & & \\ -\text{C} & - & \text{C} & - & \text{C} & - & \text{C} & - & \text{C} & - & \text{C} & - & \text{C}- \\ & & & & & \\ \text{F} & \text{F} & \text{F} & \text{O} & \text{F} & \text{F} \\ & & & \text{Rf} & & \end{array}$	$\left[\left(\begin{array}{cc} \text{F} & \text{F} \\ & \\ -\text{C} & - & \text{C}- \\ & \\ \text{F} & \text{F} \end{array} \right)_x \left(\begin{array}{cc} \text{F} & \text{CF}_3 \\ & \\ -\text{C} & - & \text{C}- \\ & \\ \text{F} & \text{F} \end{array} \right)_n \right]$	$\left[\begin{array}{cccc} \text{H} & \text{H} & \text{F} & \text{F} \\ & & & \\ -\text{C} & - & \text{C} & - & \text{C} & - & \text{C}- \\ & & & \\ \text{H} & \text{H} & \text{F} & \text{F} \end{array} \right]_n$

Reference

1. R. H. Liang, K. L. Oda, S. Y. Chung and A. Gupta: *18th International SAMPE Technical Conference*, Oct. 7-9, 1986.

SFU ORBIT ENVIRONMENT MONITORING BY KAPTON

The purpose of this experiment is to acquire transient variation of irradiation fluence of AO in the flight orbit of SFU.

Parilene (Poliparaxylene) coated Kapton specimens are used. This coating is vapor deposited and processed to one side. Parilene can easily be controlled through its coating thickness—almost to the accuracy of $0.1 \mu\text{m}$. Being exposed to space, the Parilene layer of the sample is eroded at first by AO; the Kapton layer of the base appears in some months.

By preparing Parilene layer specimens of different thicknesses, we can precisely control the period of exposure time of Kapton (See Figure 6).

After the retrieval, examining the quantity of the surface erosion, (loss of thickness): Δt [cm], we can get such plotting as shown in Figure 7(a). Linearity of the erosion of Kapton with AO fluence is already confirmed in the LDEF experiment, so we first confirm this linearity again and then finally get the AO fluence characteristics shown in Figure 7(b).

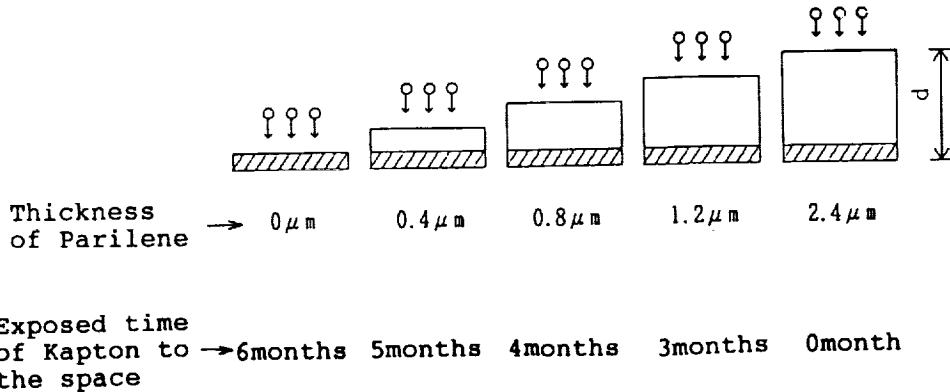
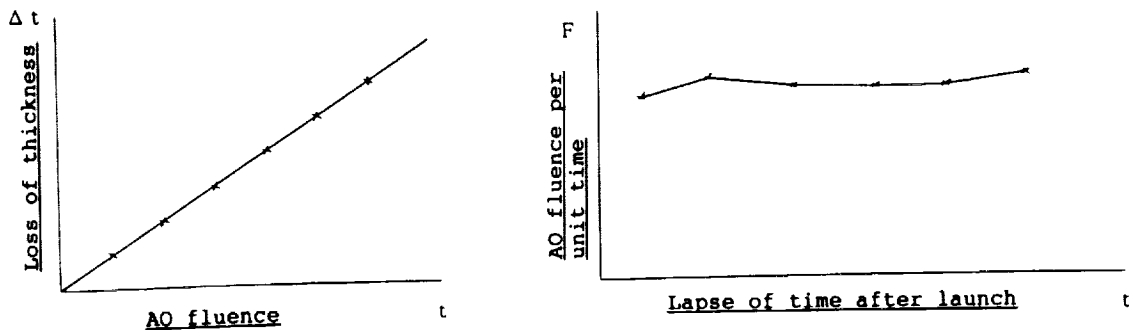


Figure 6. Mechanism of environment monitor.



(a) Erosion vs. period.

(b) AO fluence vs. elapsed time.

Figure 7. Expected plottings.

EXPECTED RESULTS AND SCHEDULE

Expected results brought from the *experiment* are summed up as follows:

1. After estimating declination quantity of each material during 10 years in LEO, we can confirm adaptability of those materials to JEM.
2. Confirmation and investigation can be achieved about the validity of ground simulation test equipment of AO irradiation.*
3. Base data for future development of space materials can be obtained (reaction data, etc.).

Schedule of this experiment is shown in Figure 8. Ground testing beforehand is very important because the number of the flight samples is limited. To reflect the results of this *experiment* in JEM's design, the schedule is very tight. JEM's system fabrication is to start in 1995.

The authors wish to express their sincerest appreciation to the session chairmen, workshop coordinators and the LDEF Chief Scientist for getting the chance to present this paper. To do this experiment successfully, advice, comments, and questions are very helpful and almost indispensable.

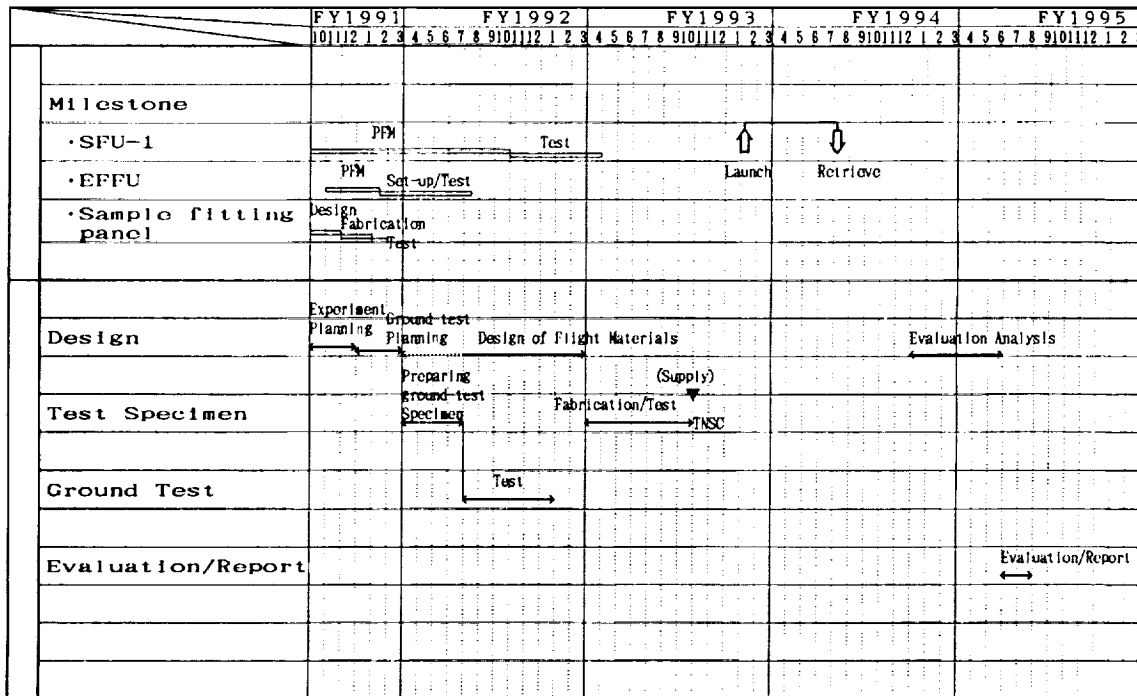


Figure 8. Schedule of the experiment

*IHI has developed its own equipment.

2

1
2
3
4
5
6
7
8
9
10
11
12
13
14
15
16
17
18
19
20
21
22
23
24
25
26
27
28
29
30
31
32
33
34
35
36
37
38
39
40
41
42
43
44
45
46
47
48
49
50
51
52
53
54
55
56
57
58
59
60
61
62
63
64
65
66
67
68
69
70
71
72
73
74
75
76
77
78
79
80
81
82
83
84
85
86
87
88
89
90
91
92
93
94
95
96
97
98
99
100

SKYLAB D024 THERMAL CONTROL COATINGS AND POLYMERIC FILMS EXPERIMENT

William L. Lehn
Nichols Research Corporation
4141 Col. Glenn Highway
Dayton, OH 45431

Charles J. Hurley
University of Dayton Research Institute
Dayton, OH 45469

INTRODUCTION

The Skylab D024 Thermal Control Coatings and Polymeric Films Experiment (ref. 1,2) was designed to determine the effects of the external Skylab space environment on the performance and properties of a wide variety of selected thermal control coatings and polymeric films. Three duplicate sets of thermal control coatings and polymeric films were exposed to the Skylab space environment for varying periods of time during the mission. The specimens were retrieved by the astronauts during extra vehicular activities (EVA) and placed in hermetically sealed return containers, recovered, and returned to the Wright Laboratory/Materials Laboratory WPAFB, Ohio for analysis and evaluation. Post flight analysis of the three sets of recovered thermal control coatings indicated that measured changes in specimen thermo-optical properties were due to a combination of excessive contamination and solar degradation of the contaminant layer. The degree of degradation experienced over-rode, obscured, and compromised the measurement of the degradation of the substrate coatings themselves. Results of the analysis of the effects of exposure on the polymeric films and the contamination observed are also presented. The D024 results were used in the design of the LDEF M0003-5 Thermal Control Materials Experiment. The results are presented here to call to the attention of the many other LDEF experimenters the wealth of directly related, low earth orbit, space environmental exposure data (ref. 3,4) that is available from the ten or more separate experiments that were conducted during the Skylab mission. Results of these experiments offer data on the results of low altitude space exposure on materials recovered from space with exposure longer than typical STS experiments for comparison with the LDEF results.

NASA SKYLAB SATELLITE

Skylab (SL 1) was launched 14 May 1973 on a Saturn V rocket and placed in a low earth, 415 km orbit with a period of 93 minutes. It was visited by three separate astronaut crews, SL 1/2, SL 1/3, and SL 4, who occupied the facility for a total of 171 days. During this time, it completed some 3900 orbits. The flight occurred during a period of waning, low solar activity. During launch the spacecraft lost its combined micrometeorite/thermal control (heat) shield, leaving the main body and the materials used to bond the external shields exposed. This resulted in a delay in the launch of the first astronaut crew, SL 1/2, while steps were taken to develop and package the "sun shade" as shown in figure 1. This shade was deployed by the first crew to bring the temperature of the Skylab living quarters down to a habitable level. A later crew delivered and installed the "solar sail" which was necessary to further lower the vehicle temperature. One solar array wing was also damaged and lost as a result of the launch problems.

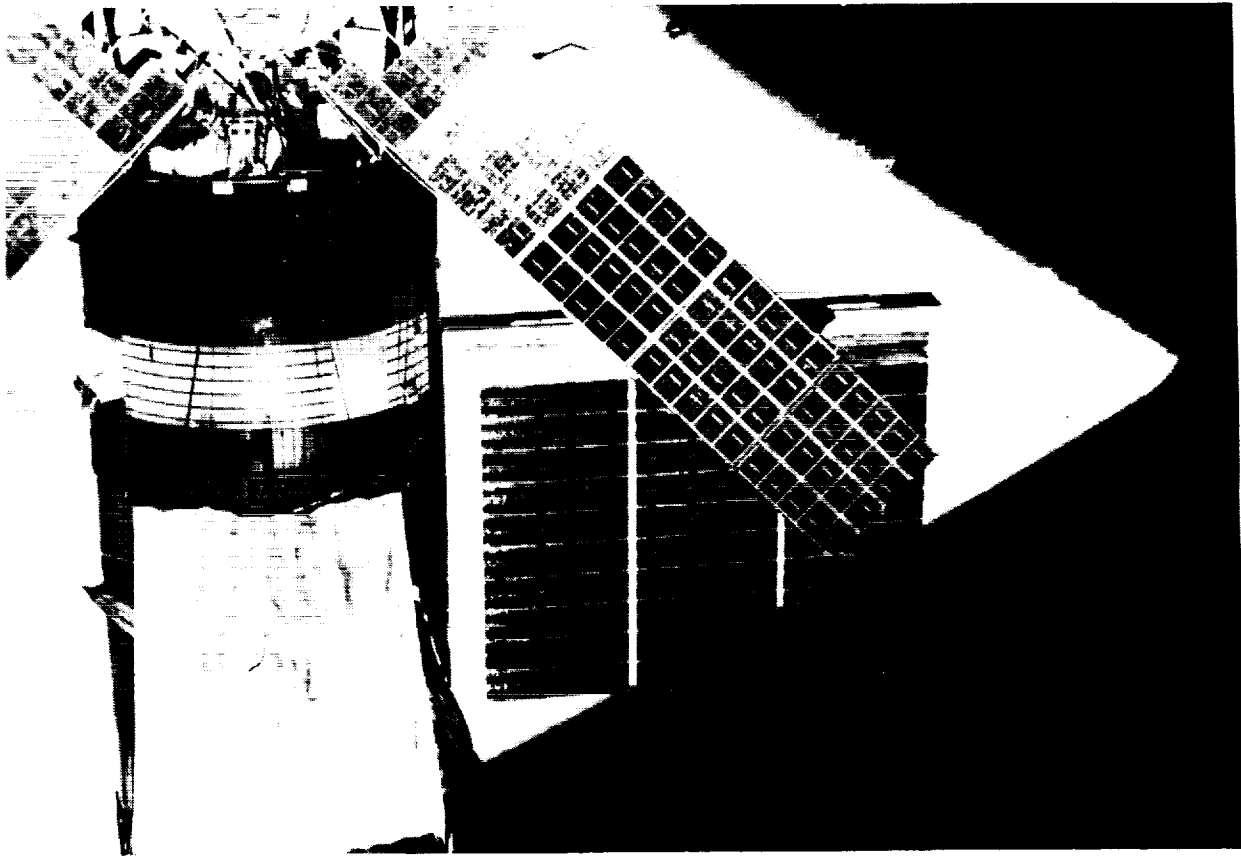


Figure 1. View of Skylab from the Command Module

DO24 EXPERIMENT LOCATION ON SKYLAB

The DO24 flight hardware consisted of four sample panels, two duplicate sample trays each containing 36 individual sample buttons coated with some 27 different selected thermal control coating materials and two duplicate sample trays each holding 8 different polymeric film specimens. The four trays along with two hermetically sealable return containers were mounted on the exterior of the Airlock Module (AM) near the Extra Vehicular Activity (EVA) hatch on the box structure at the right hand of the astronaut. The thermal control trays were mounted and oriented perpendicular to the sun vector of the solar inertially stabilized Skylab (except for selected EREP passes). In this configuration they were subjected to the maximum direct solar exposure. The polymeric films were located some 39° off axis from the solar vector. The first set of specimens, SL 1/2, were retrieved by the first crew after 35 days/550 hours of solar exposure and the second set, SL 1/3, after 131 days/2040 hours of solar exposure as shown in figure 2. The excessive contamination prompted the launch, deployment, exposure, and retrieval of a third set of samples by the SL 4 crew. These samples experienced 74 days/1150 hours of exposure. These samples were also badly contaminated.

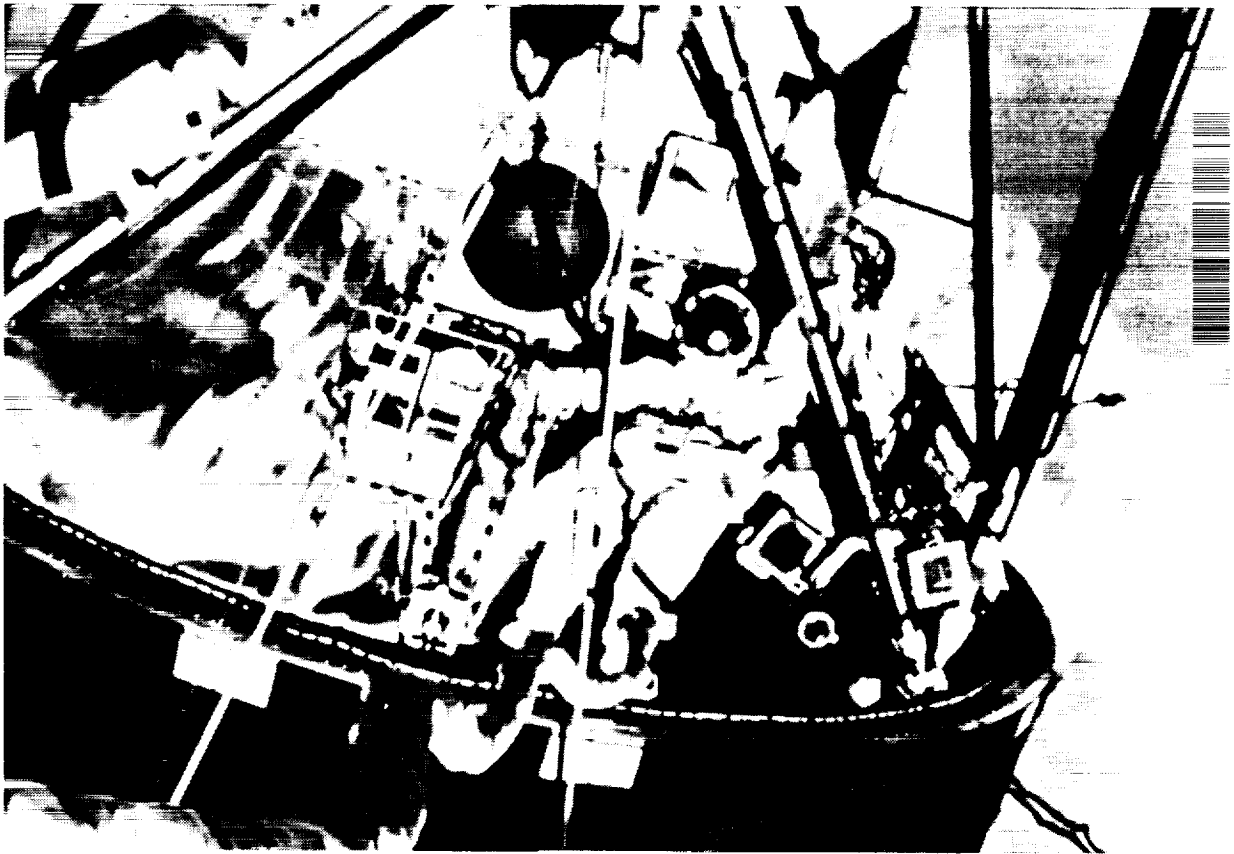


Figure 2. Astronaut Recovery of the DO24 Experiment

D024 THERMAL CONTROL COATINGS MATERIALS POST-FLIGHT SOLAR ABSORPTANCE CHANGES

The list of 36 selected thermal control coating materials flown on the D024 experiment along with the observed changes/delta in solar absorptance experienced are shown in Table 1. These changes all exceeded the expected changes based upon laboratory simulation data or values published in the literature.

MATERIAL	SL 1/2	SL4	SL 1/3
S13	0.091	0.117	0.284
S13G	0.092	0.091	0.237
Z93	0.095	0.006	0.179
SiO ₂ /MeSi	0.112	0.148	0.202
Eu ₂ O ₃ /MeSi	0.105	0.123	0.253
aAl ₂ O ₃ /MeSi	0.151	0.173	0.281
Anodized Al 0.5mil	0.310	0.204	0.273
FEP/Al	0.079	0.013	0.246
Fused Quartz/Al	0.057	0.006	0.208
AQ 5um	0.052	0.018	0.120
TiO ₂ /MeSi	0.147	0.089	0.302
3M Black Velvet	-.007	-.002	-.009
Microsheet/Ag	0.095	0.008	0.218
FEP/Ag	0.049	0.011	0.222
PV-100	0.142	0.125	0.258
aAl ₂ O ₃ /KSil	0.167	0.101	0.306
AQ 5um	0.081	0.039	0.105
AQ 5um Processed	0.052	-.018	0.120
AQ 10um	0.078	0.024	0.154
Zn ₂ TiO ₄ /MeSi	0.110	0.080	0.248
3D-QFY-Al 150 1/0	0.049	0.077	0.077
SiO ₂ /Al Interweave	0.064	0.034	0.080
ZrO ₂ /MeSi	0.211	0.247	0.314
CaTiSiO ₅ /MeSi	0.065	0.068	0.175
3D-QFY-150 1/0 VDA	0.117	0.019	0.096
FEP/Ag	0.049	0.002	0.152
Anodized Al 0.2mil	0.108	0.160	0.220
Anodized Al 0.5mil	0.131	0.204	0.273
LfgAL/SiAcrylic	0.099	0.019	0.145
S13G	0.105	0.122	0.251
Z-93	0.077	-.002	0.174
FEP/Al	0.064	0.071	0.157
3M Black Velvet	-.008	-.015	-.005
3M Black Velvet	-.011	-.006	-.006
Alzak Anodized Al	0.064	0.023	0.136
Zn ₂ TiO ₄ /MeSi	0.080	0.055	0.234

Table 1. DO24 Post Flight Absorptance Changes

D024 THERMAL CONTROL SPECIMENS AND TRAYS

The degradation/darkening of the thermal control coatings recovered by SL1/2 and SL 1/3 crews is apparent when compared with a set of preflight controls as shown in figure 3. The excessive discoloration is a result of excessive contamination followed by degradation/darkening of the contaminant layer by the solar exposure.

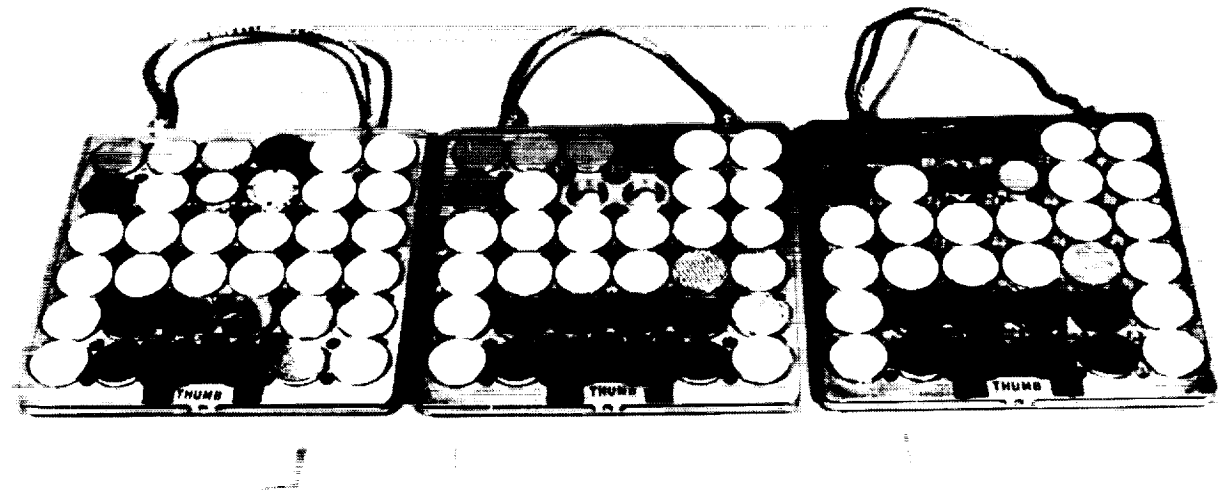


Figure 3. Comparison of DO24 Control and SL1/2 and SL1/3 Thermal Control Specimens

ORIGINAL PAGE
BLACK AND WHITE PHOTOGRAPH

D024 THERMAL CONTROL TRAYS LABORATORY CONTROL AND RECOVERED FLIGHT TRAYS

The degradation/darkening of the thermal control coatings due to contamination was also experienced on the SL 4 set of specimens and is apparent from the comparison of all three sets of specimens compared to a set of preflight controls as shown in figure 4. The SL 4 specimens were deployed after docking of the Command Module and recovered prior to undocking ruling out the Service Module Reaction Control System propellant by-products as a major source of contamination. Samples of the metallic silver coating on the surface of Sloan thickness monitor crystals exposed to the Skylab environment were badly degraded/oxidized. The reaction of the Ag with hydroxyl radicals formed due to the presence of large concentrations of water in the Skylab atmospheric "cloud" was proposed as a possible mechanism. The projected column densities of water vapor in the Skylab "cloud" also affected the sensitivity of measurements on other instruments. Atomic oxygen was mentioned but the role of "AO" in such phenomena was not really appreciated until the more recent Shuttle experiences.

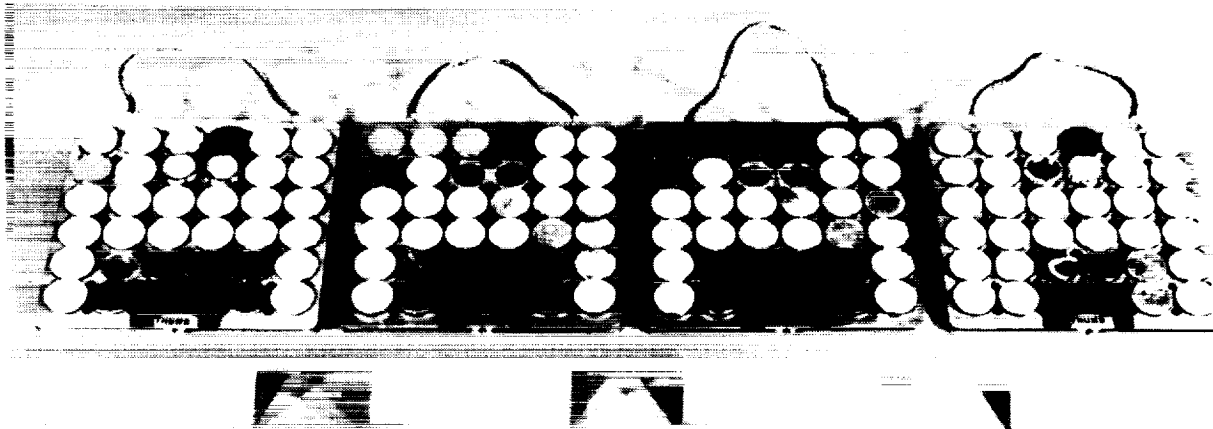


Figure 4. Comparison of Preflight and Post Flight Thermal Control Coatings Trays

SKYLAB CHANGES IN SOLAR ABSORPTANCE FOR SL1/2 - SL 4 - SL 1/3

The changes in solar absorptance for the thermal control coating materials flown on the three D024 Thermal Control Coating Trays have been plotted to show the changes which occurred and are shown in figure 5 and figure 6. The solar exposure times are: SL 1/2, 35 days/550 hours; SL 4, 74 days/1150 hours; and SL 1/3, 131 days/2040 hours. The primary increase in absorptance is due to the presence of contamination on the surfaces of the coatings. The degradation due to damage to the coating itself is largely obscured. There is some indication of the decrease in contamination level, lower values of absorptance for the SL 4 specimens. The values for the Ag and Au coated Sloan thickness monitor are not plotted. The Ag specimens were all severely oxidized all the way through the thickness to a blue/black amorphous mass. Areas of the Ag surface protected by the mechanical retaining ring were unchanged.

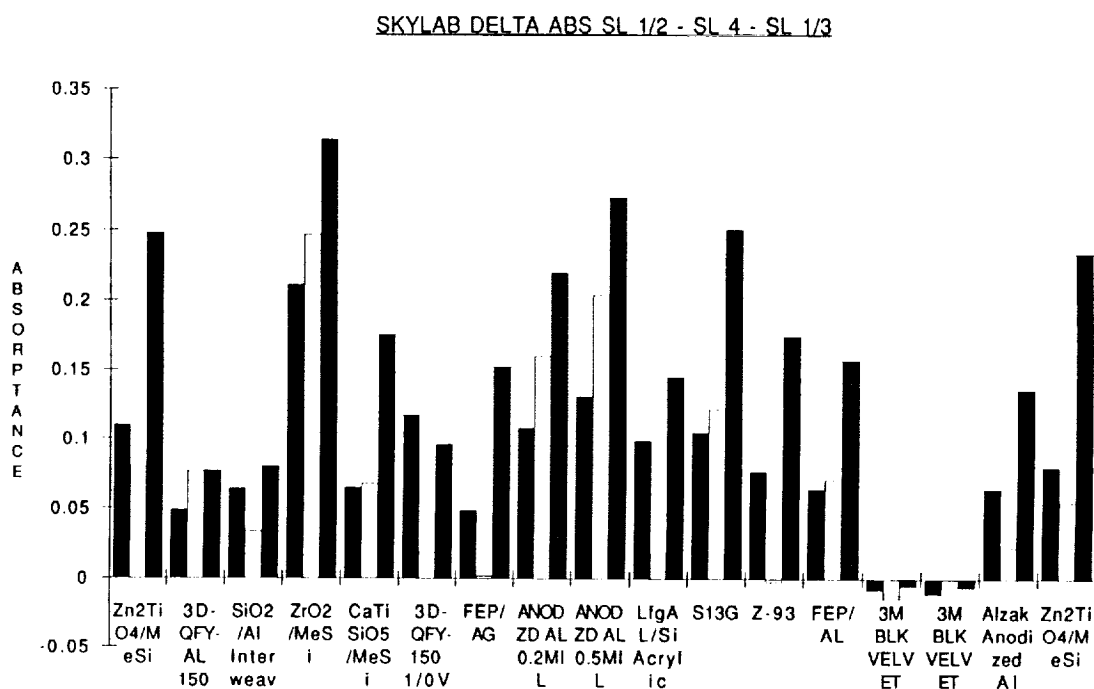


Figure 5. Solar Absorptance Changes for Thermal Control Coatings(Sl 1/2, SL 4, SL 1/3)

SKYLAB CHANGES IN SOLAR ABSORPTANCE FOR SL1/2 - SL 4 - SL 1/3

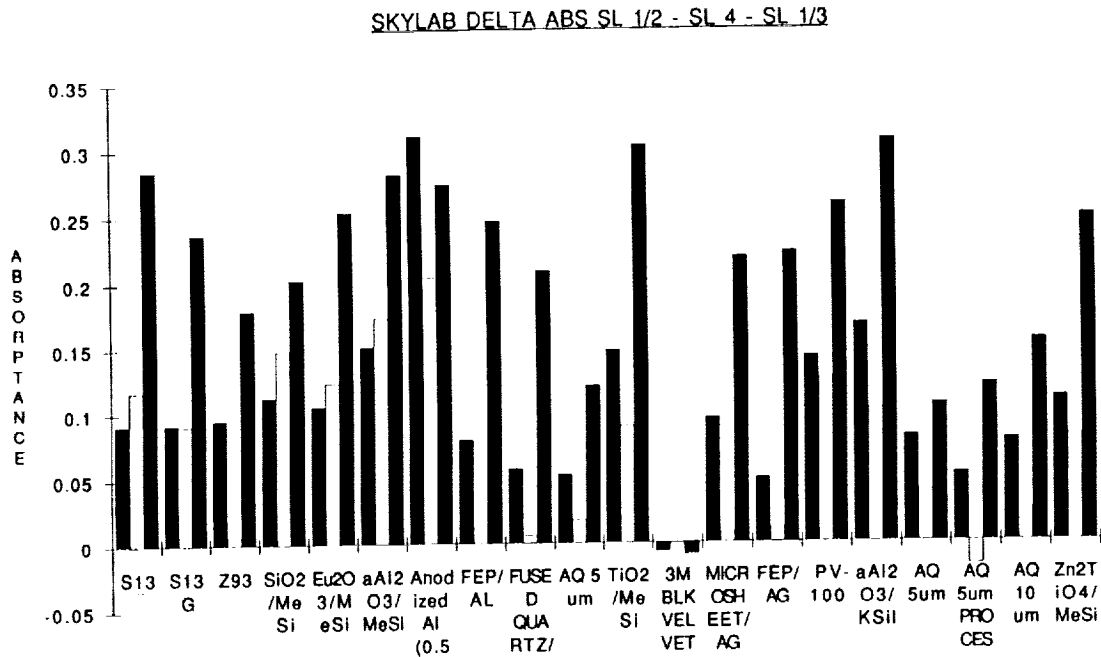


Figure 6. Solar Absorptance Changes for Thermal Control Coatings(Sl 1/2, SL 4, SL 1/3) Continued

EFFECTS OF SKYLAB EXPOSURE ON FUSED QUARTZ/AL

The effects of the Skylab exposure on a fused quartz/Al second surface mirror/OSR are shown in figure 7. The excessive degradation is attributed to the excessive contamination associated with the Skylab environment followed by further fixing and degradation of the contaminant layer by continued solar exposure.

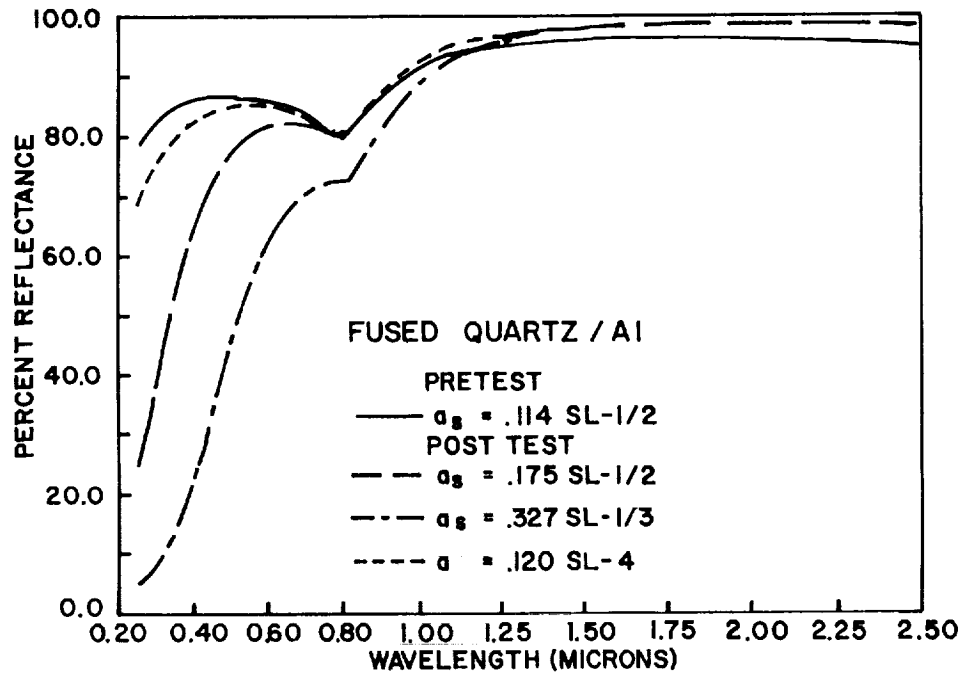


Figure 7. Effect of Skylab on Fused Quartz/Al

FEP SAMPLES RECOVERED FROM SKYLAB AND LDEF

The degradation in transmission of a sample of FEP Type A shows the effects of the contaminant layer. Comparison with the reflectance data of samples of FEP/Ag flown on LDEF are quite similar in appearance and indicate the presence of a degraded contamination layer as shown in figures 8 and 9.

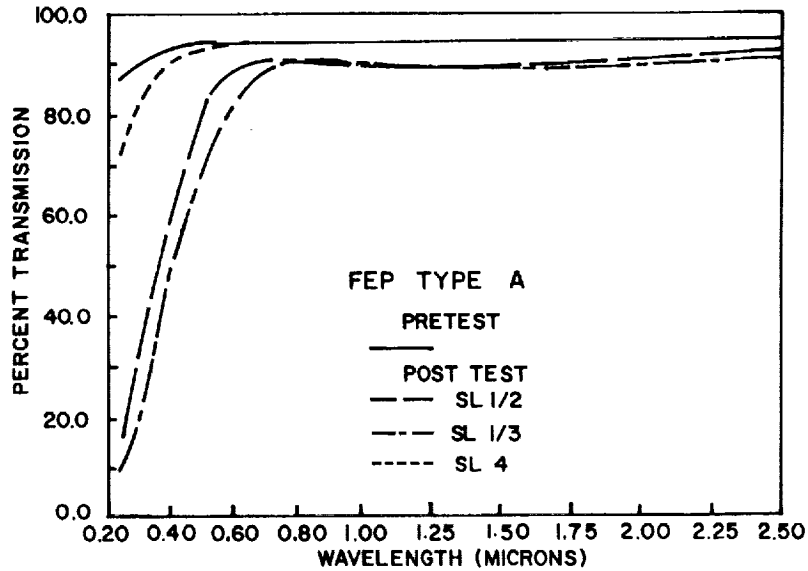


Figure 8. Effect of Skylab Exposure on FEP Type A

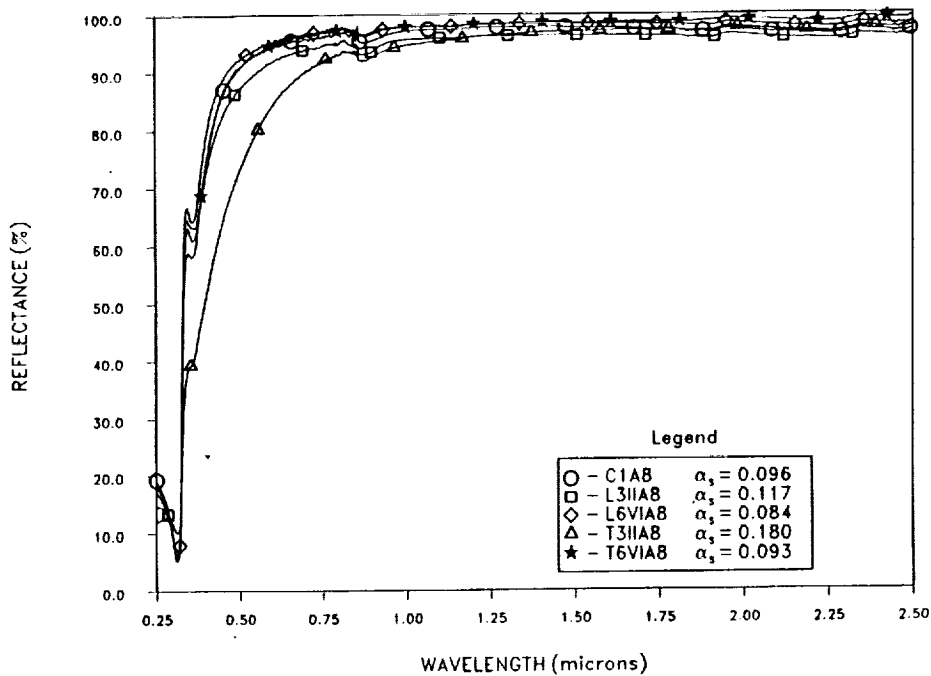


Figure 9. Effect of LDEF Exposure on FEP Type A

EFFECTS OF SKYLAB AND LDEF EXPOSURE ON S13 AND S13 GLO THERMAL CONTROL COATINGS

The pre- and post-flight reflectance spectra of samples of S13 and S13 GLO white thermal control coating paints flown on D024 and LDEF show similar changes. Contamination of these surfaces followed by degradation of the contaminant layer is proposed as the principal mechanism to account for these observed changes as shown in figures 10 and 11.

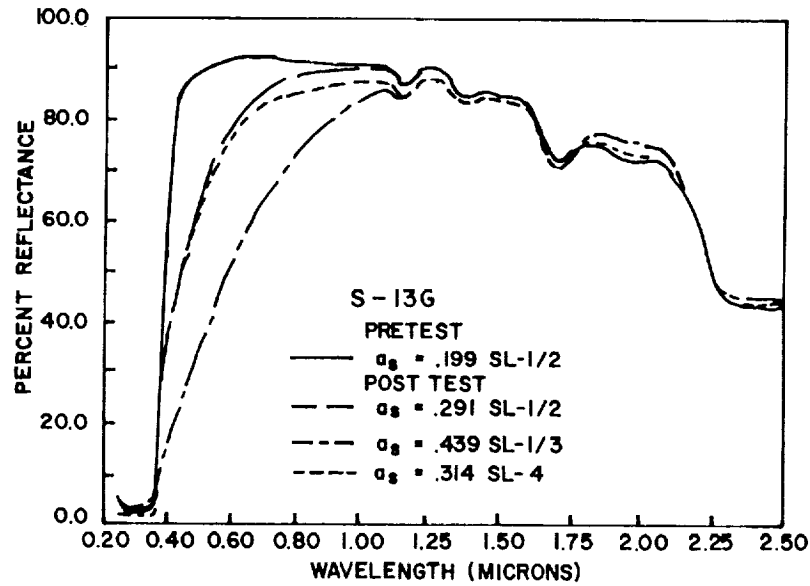


Figure 10. Effect of Skylab Exposure on S13 G

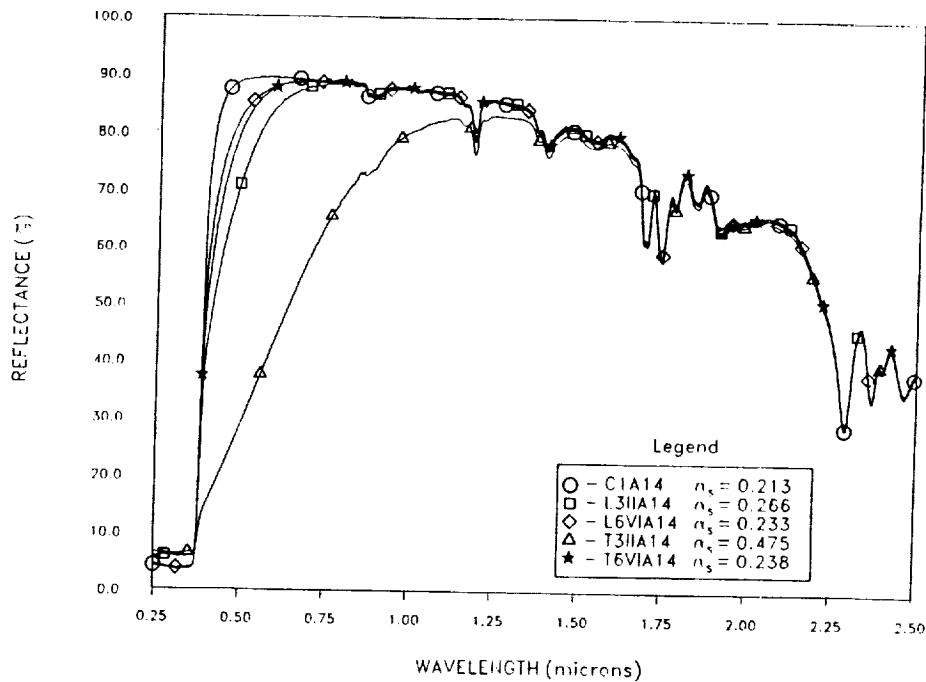


Figure 11. Effect of LDEF Exposure on S13 GLO

D024 POLYMERIC FILM STRIP TRAYS

Discrete shadow patterns of contamination were evident on all three sets of returned thermal control coating and polymeric film sample trays. They clearly demonstrated the excellent sun orientation maintained by the Skylab throughout the majority of the mission. Shadowed/clear areas exhibited only traces of contamination while the yellow/gold/brown areas showed the presence of SiO_x containing contaminants. Photos of the lower areas of the Apollo Telescope Mount displayed similar effects of degradation/shadowing in those areas exposed to the sun. Low molecular weight contaminants, which outgas, were free to deposit and re-evaporate and/or migrate along the spacecraft surfaces until they reached a solar exposed area, reacted with UV, and increased in molecular weight becoming fixed/immobile. There they continued to degrade and add further amounts of contaminants as the flight continued. A comparison of a preflight tray and a flight tray are shown in figure 12.

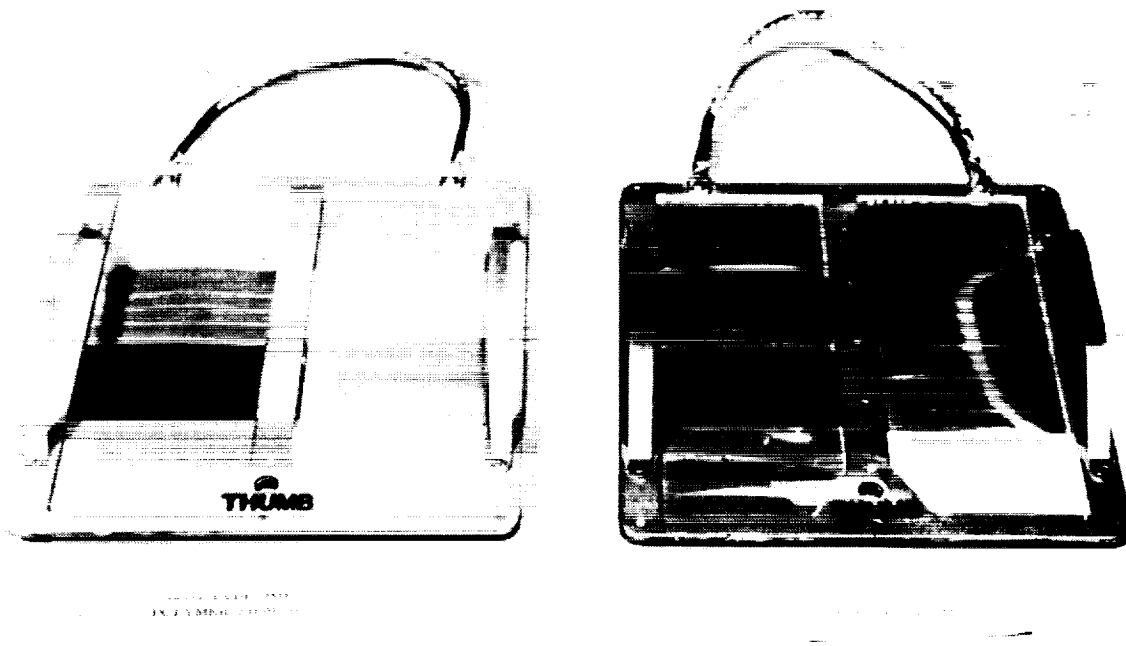


Figure 12. Comparison of DO24 Polymer Film Strip Trays

ORIGINAL PAGE
BLACK AND WHITE PHOTOGRAPH

D024 RETURN CONTAINERS

The presence of contamination is clearly evident by the shadow patterns displayed on the D024 Return Containers as shown in figure 13. The sharp line on the sides marks the shadowing which occurred while the containers were mounted extending down in the box structure. The excellent-solar inertial attitude orientation of Skylab is again readily apparent as is the angle of the containers relative to the sun vector.

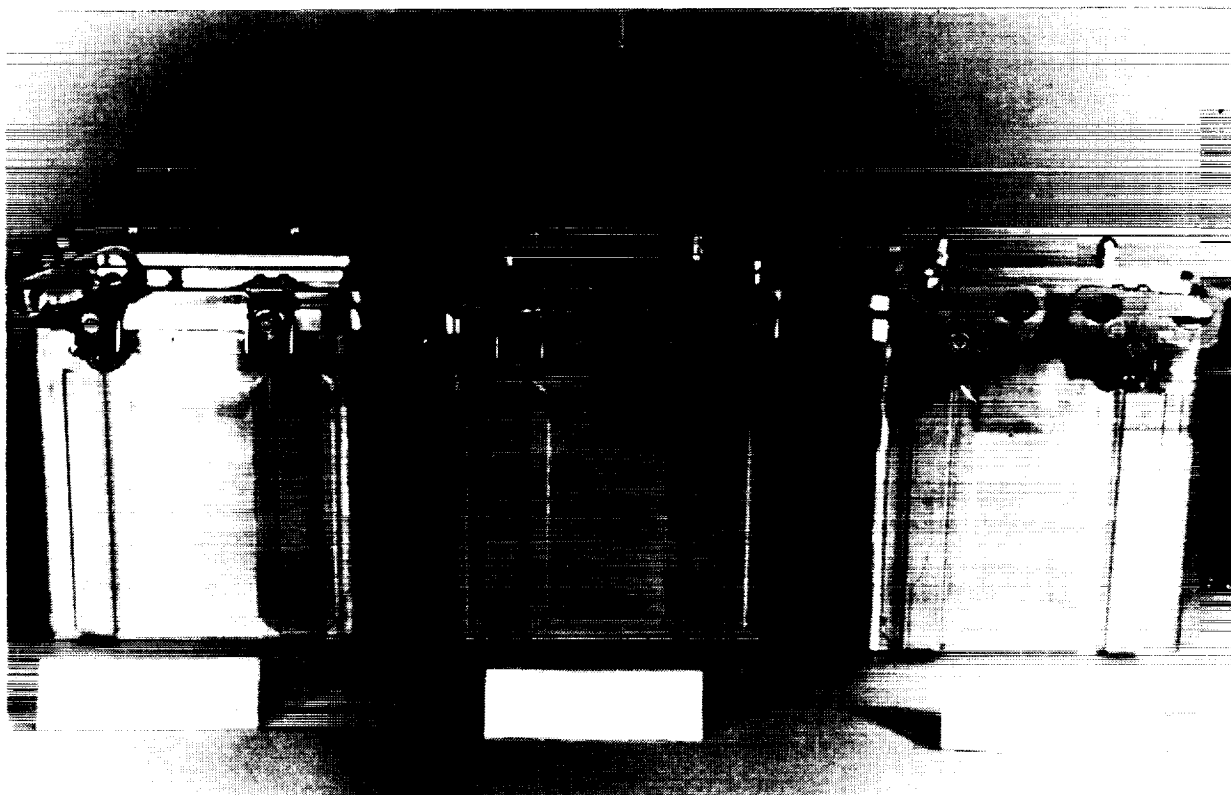


Figure 13. Comparison of D024 Flight Experiment Containers

ORIGINAL PAGE
BLACK AND WHITE PHOTOGRAPH

SKYLAB D024 POLYMERIC FILMS EXPERIMENT POST TEST SL 1/3

Results of the Skylab D024 Polymeric Films Experiment Post Test results from SL 1/3 are shown in table 2. Overall results from all three sets of returned specimens have been previously reported (ref. 2).

MATERIAL	%ELONGATION	TENSILE STRENGTH PSI X 10 ³	MODULUS PSI X 10 ⁶	YIELD PSI X 10 ⁶	REMARKS
Nylon 6/6	49.3	5.1	.23	4.0	Severe Crosslinking
Polyimide	37.2	11.3	.19	3.2	Slight Degradation
Polyphenyl Quinoxaline	4.4	6.5	.215	4.0	Moderate Degradation
FEP Type A	224.5	1.9	.037	0.7	Mild Crosslinking
Polycarbonate	53.9	4.5	1.6	3.2	Slight Degradation
Mylar	*12.9	8.1	.31	5.8	Degradation & Crosslinking
FEPXC20	248.0	1.6	.035	0.7	Increased Crosslinking
Teflon	105.8	1.2	.04	.07	Degradation & Slight Crosslinking

* Average of three tests.

Table 2. Tensile Properties of SL 1/3 Polymeric Films

CONTAMINATION HISTOGRAM FOR SKYLAB MDA

The contamination buildup as a function of time was measured by microbalances on the Skylab docking adapter. Crystals facing along the longitudinal axis registered the highest contamination rates. Crystals that faced away from the vehicle collected deposits presumably consisting of contaminants which originated from the space station and whose molecules were back-scattered by the atmosphere around the space station. Early in the mission, the crystal facing the command module was contaminated by the steering-rocket exhaust (ref. 3). A histogram is illustrated in figure 14.

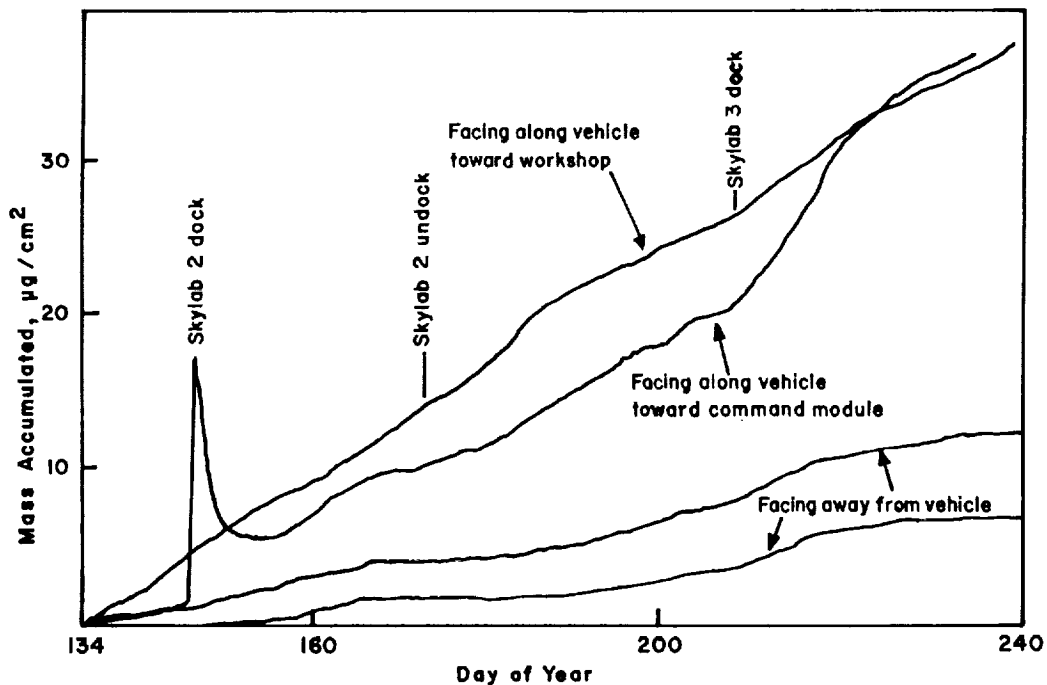


Figure 14. Histogram of Contamination for Skylab MDA

REFERENCES

1. Lehn, W. L.; and Hurley, C. J: AIAA/AGU Conference on Scientific Experiments of Skylab, Huntsville, AL, Oct. 30-Nov. 1974, AIAA Paper No. 74-1228.
2. Lehn, W. L.; and Hurley, C.J.: AIAA 10th Thermophysics Conference, Denver, CO, May 27-29, 1975, AIAA Paper NO. 75-689.
3. Lundquist, C.A.: Ed., "Skylab's Astronomy and Space Sciences," Scientific and Technical Information Branch, NASA, Wash. D.C., 1979, NASA SP-404.
4. Kendt, M.I.; and Wu, S.: editors, "Scientific Investigations On the Skylab Satellite," Progress in Astronautics and Aeronautics, Volume 48, American Institute of Aeronautics and Astronautics, New York, N. Y., 1976.

Polymers and Films (Including Ag/FEP)

Co-Chairmen: Phil Young and David Brinza
Recorder: Gary Pippin



Effects of the LDEF Environment on the Ag/FEP Thermal Blankets.

Francois Levadou
ESTEC, ESA
Noordwijk, The Netherlands

and

Gary Pippin
Boeing Defense and Space Group
Seattle, Washington

This presentation was made by Francois Levadou at the NASA Langley Research Center LDEF materials workshop, November 19-22, 1991. It represents the results to date on the examination of silvered teflon thermal blankets primarily from the Ultra-heavy Cosmic Ray Experiment and also from the blanket from the Park Seed Company experiment. ESA/ESTEC and Boeing conducted a number of independent measurements on the blankets and in particular on the exposed fluorinated ethylene-propylene (FEP) layer of the blankets. Mass loss, thickness and thickness profile measurements have been used by ESA, Boeing, and NASA LeRC to determine recession and average erosion yield under atomic oxygen exposure. Tensile strength and percent elongation to failure data, surface characterization by ESCA, and SEM images are presented. The Jet Propulsion Laboratory analysis of vacuum radiation effects is also presented. The results obtained by the laboratories mentioned and additional results from The Aerospace Corporation on samples provided by Boeing are quite similar and give confidence in the validity of the data.

Ag/FEP THERMAL BLANKET INVESTIGATION

BOEING and ESA/ESTEC

- **Mass loss, thickness and thickness profile**
- **Mechanical properties: elongation and tensile strength**
- **ESCA**
- **Contamination**

NASA LeRC and ESA/ESTEC

- **Erosion yield and recession**
- **SEM**

JPL

- **Vacuum UV radiation effects**
- **SEM**

The Ag/FEP blankets were the thermal protection for the Ultra-Heavy Cosmic Ray Nuclei Experiment(AO178). This experiment was in sixteen locations around the spacecraft.

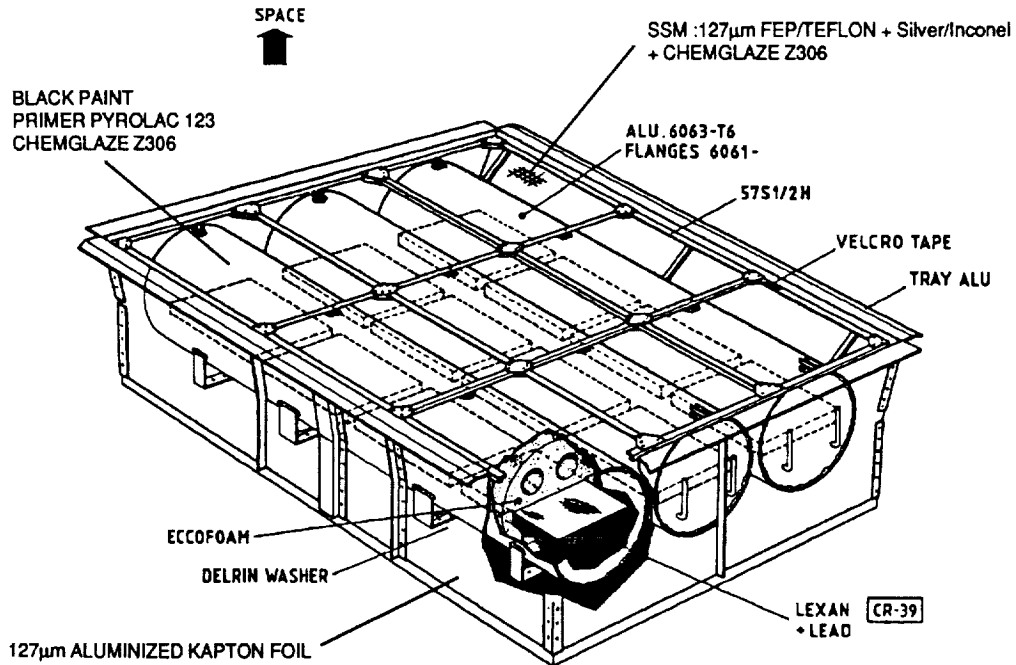
UHCRE [AO178]

ULTRA-HEAVY COSMIC RAY NUCLEI EXPERIMENT
A joint ESA/DIAS (Dublin Institute of Advanced Studies) experiment
which flew on NASA's LDEF

The main objective is a detailed study of the charge spectra of ultra-heavy cosmic-ray nuclei from zinc ($Z=30$) to uranium ($Z=92$) and beyond using solid-state track detectors.

Among 72 trays mounted around the periphery of LDEF, 16 were devoted to UHCRE.

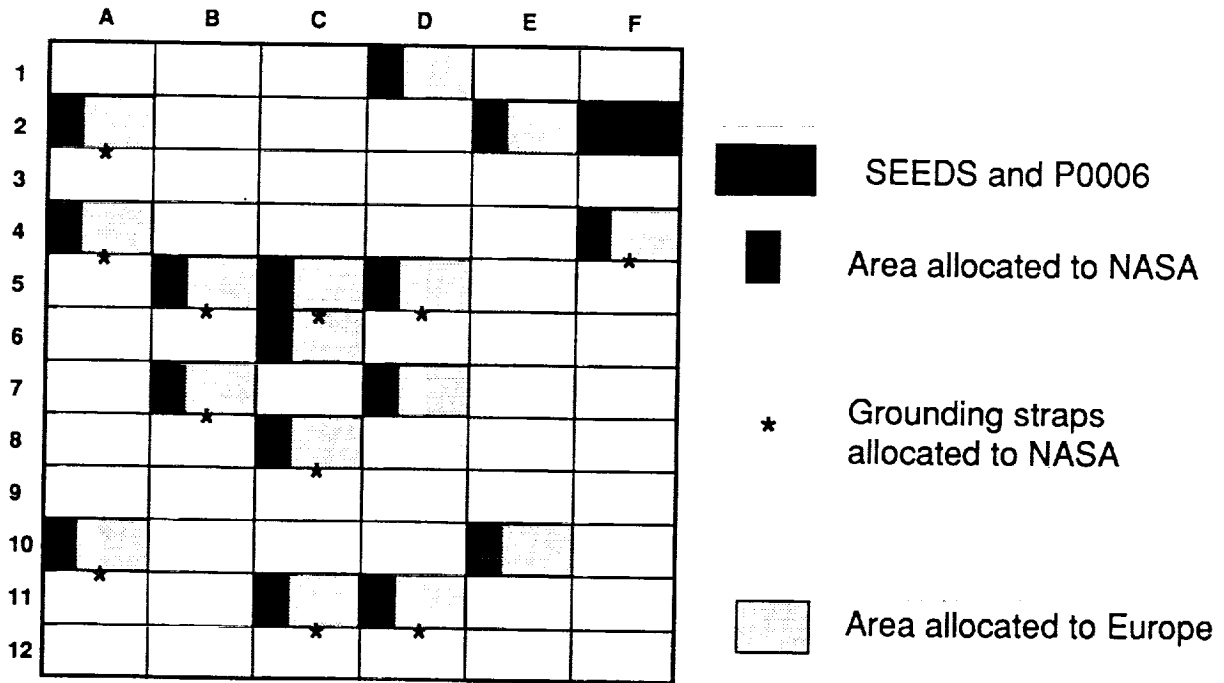
The thermal blankets were fastened to the frame of the tray using Astro-Velcro tape. Each of the blankets remained in place and each of the individual Velcro strips performed their function. The post-flight and pre-flight grip strengths of the Velcro were similar. The attachment location of each strip did provide a mechanical load on areas of each blanket because the fastened areas were not as free to expand and contract during thermal cycling as was the remainder of the blanket .



CONSTRUCTION OF UHCRE TRAY

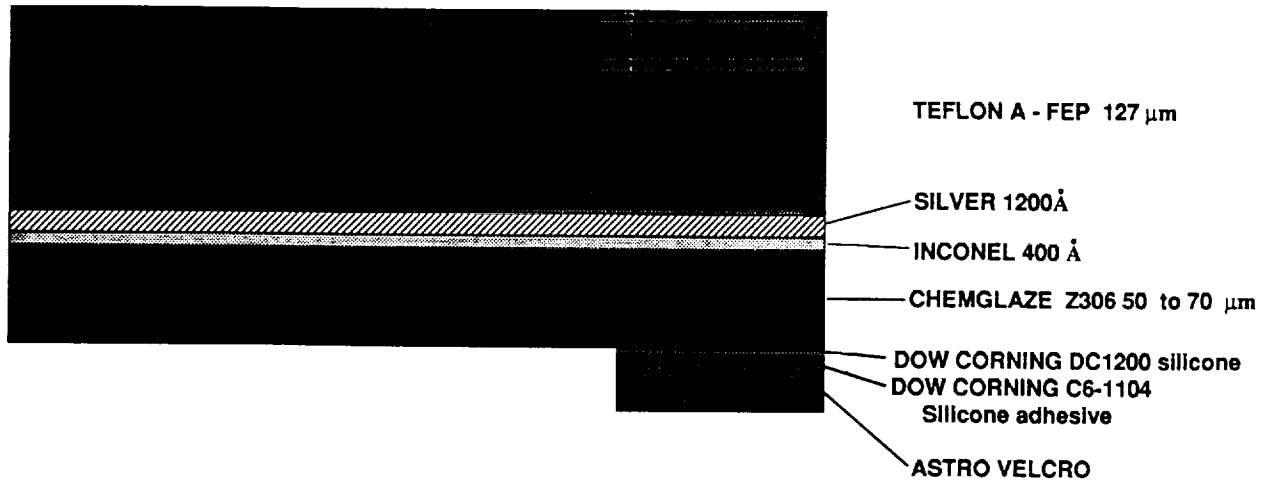
The light top frame supports the thermal tray FEP cover

The distribution of blanket locations on the spacecraft is shown in this figure. Two thirds of each blanket was retained by ESA and one third was provided to NASA. The blanket from location F2 was retained by NASA. Each blanket was electrically grounded to the main LDEF structure by copper straps attached to the Z-306 side of each blanket. Five copper straps were retained by ESA and twelve straps were sent to Boeing. Boeing received from NASA a strip approximately 4" wide by 16-18" long from the edge of the NASA portion of each blanket from AO178. Six strips about 2"x18" were provided from blanket F2.



LDEF UHCRE [A0178] Thermal blanket allocations

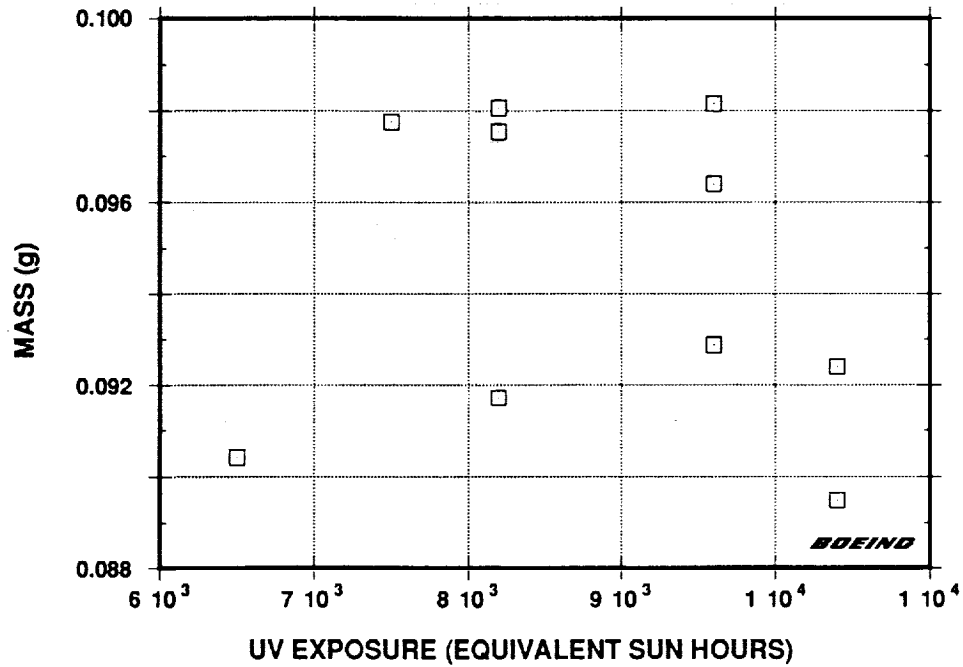
The FEP layer was exposed to the external space environment. The chemglaze Z-306 and the silicone adhesive holding the Velcro were facing the interior of the trays and exposed only to vacuum and mild thermal cycling.



UHCRE & SEEDS THERMAL BLANKETS
Scheldahl G401500 with Chemglaze Z306

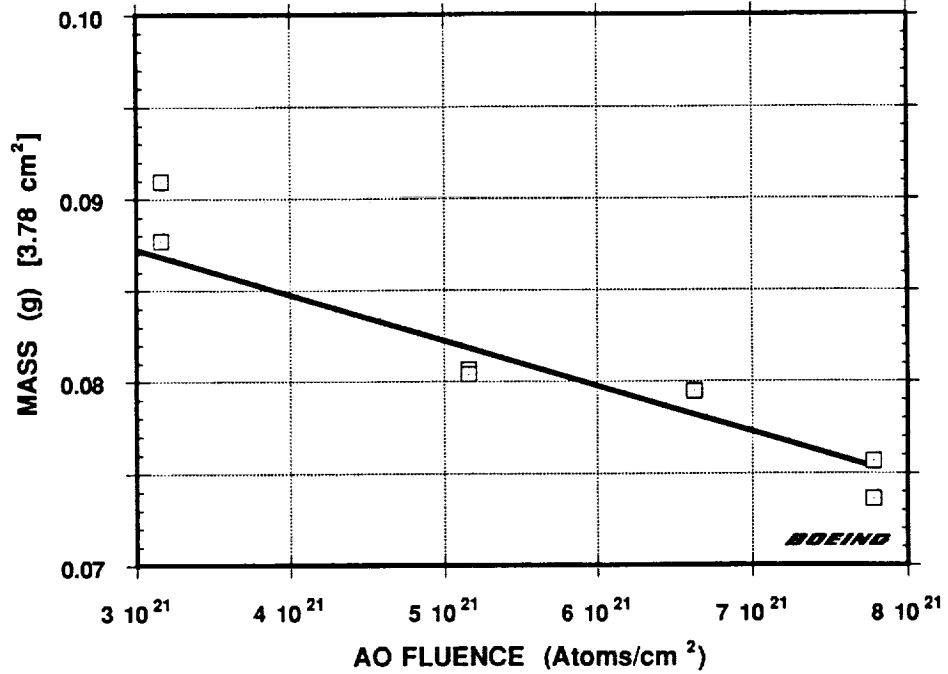
The wide variation in mass of specimens cut from the same die is partially due to natural thickness variation of the blankets as manufactured. The lack of any clear trend due to solar exposure indicates that the production of volatile UV degradation products, if this process occurs at all, is small.

Mass of FEP from Trailing Edge Exposed Specimens



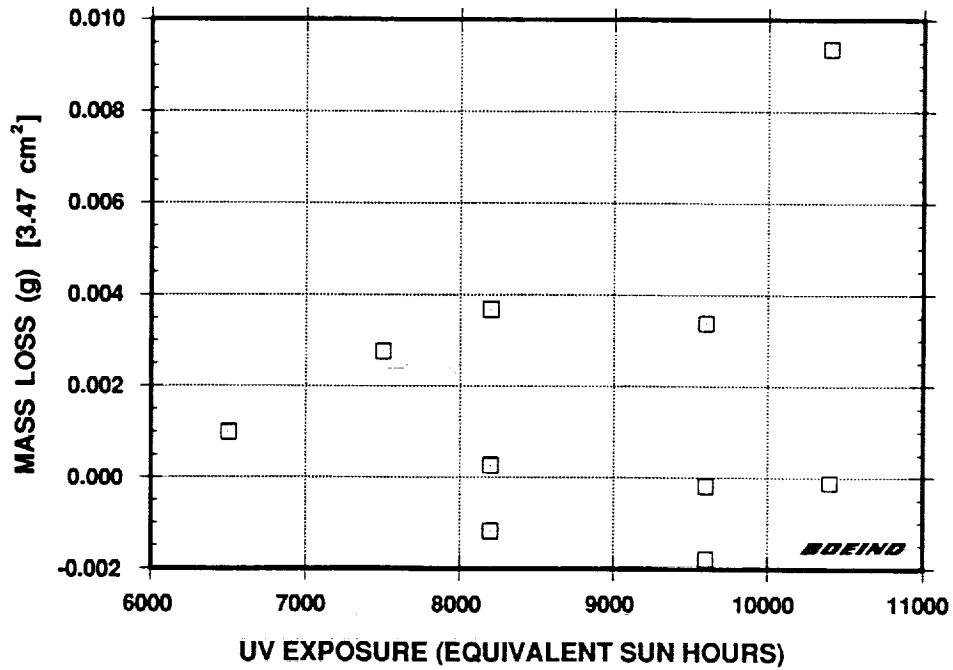
The masses of specimens taken from areas of blankets exposed to atomic oxygen, and cut with the same die, show a clear trend of increased recession with atomic oxygen exposure.

Mass of FEP from Leading Edge Exposed Specimens



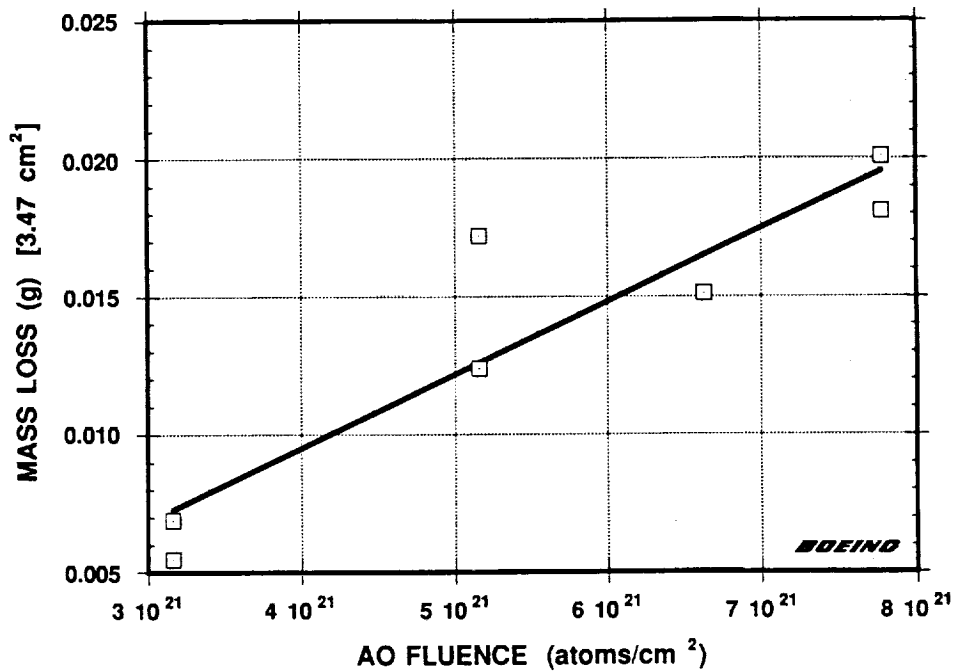
Mass differences between areas of each blanket exposed to only solar radiation and unexposed portions of the same blanket show essentially random distribution with respect to equivalent sun hours of solar exposure.

Mass Differences between Unexposed and Exposed FEP Specimens (Rows 1-6)



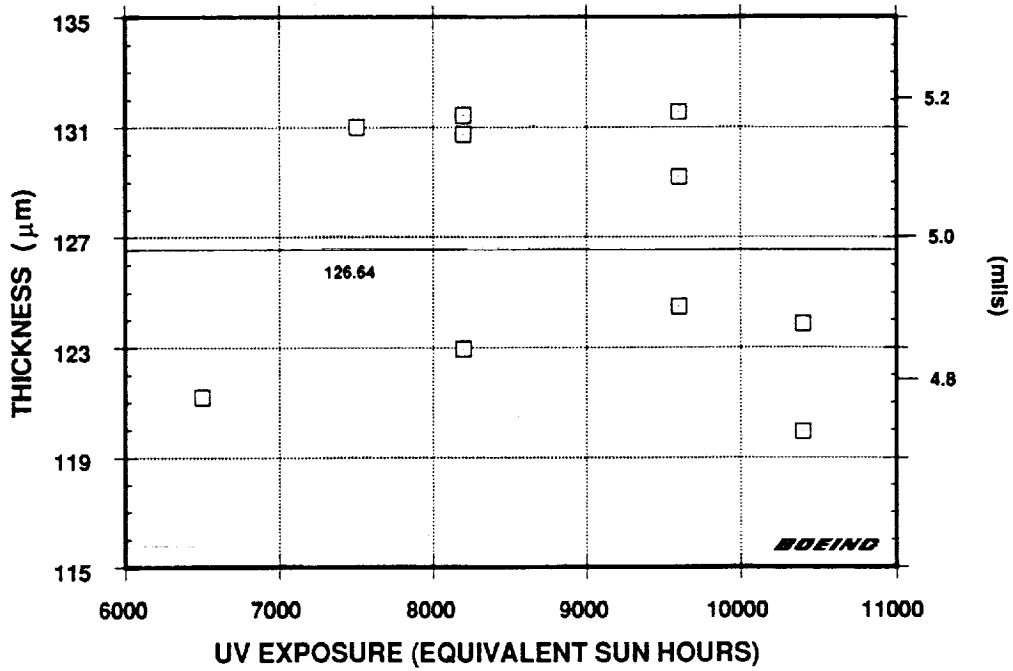
Mass differences between areas of each blanket exposed to atomic oxygen and solar ultraviolet radiation and unexposed portions of the same blanket show clearly increased mass loss with atomic oxygen fluence.

Mass Differences between Unexposed and Exposed Specimens (Rows 7-11)



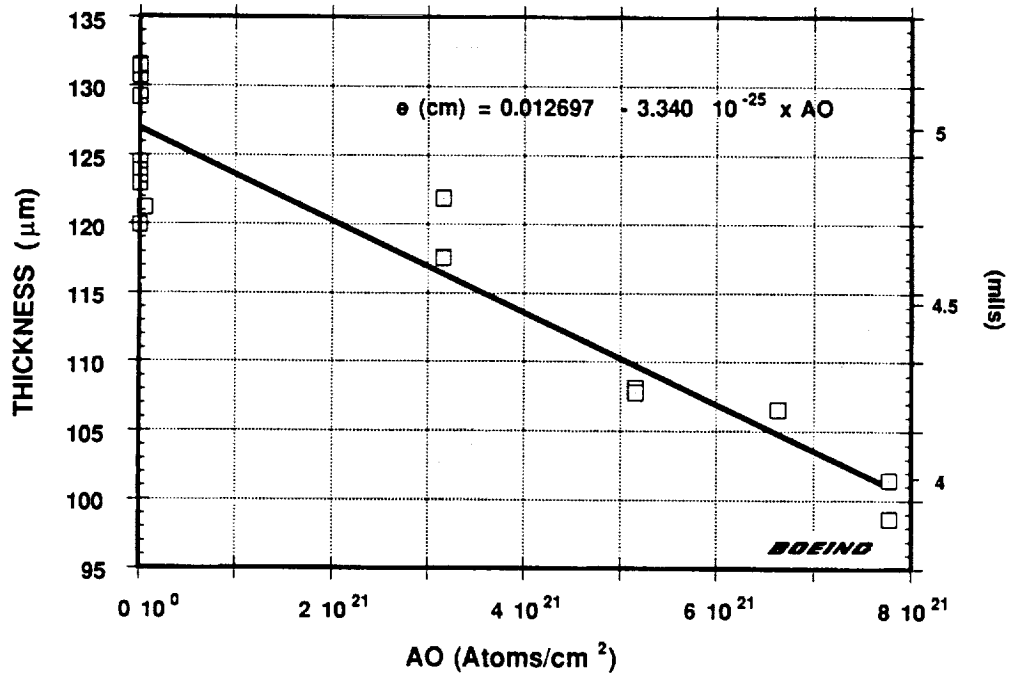
The thickness of the exposed specimens from the trailing edge was determined from the mass measurements and the assumption of 2.15 g/cm³ density for FEP.

Thickness of FEP from Trailing Edge Exposed Specimens



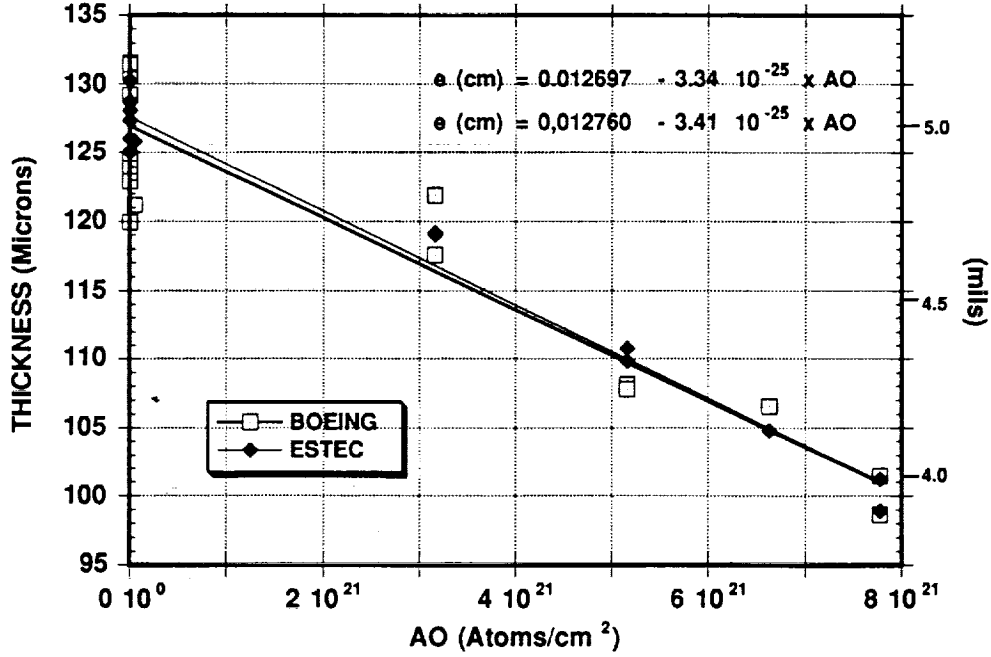
The thickness of leading edge exposed specimens measured at Boeing was determined from the mass measurements and the assumption of 2.15 g/cm³ FEP density. The data points at the left edge of the graph show the variation in the range of thicknesses for unexposed specimens from the trailing edge for comparison.

Thickness of FEP from Leading Edge Exposed Specimens



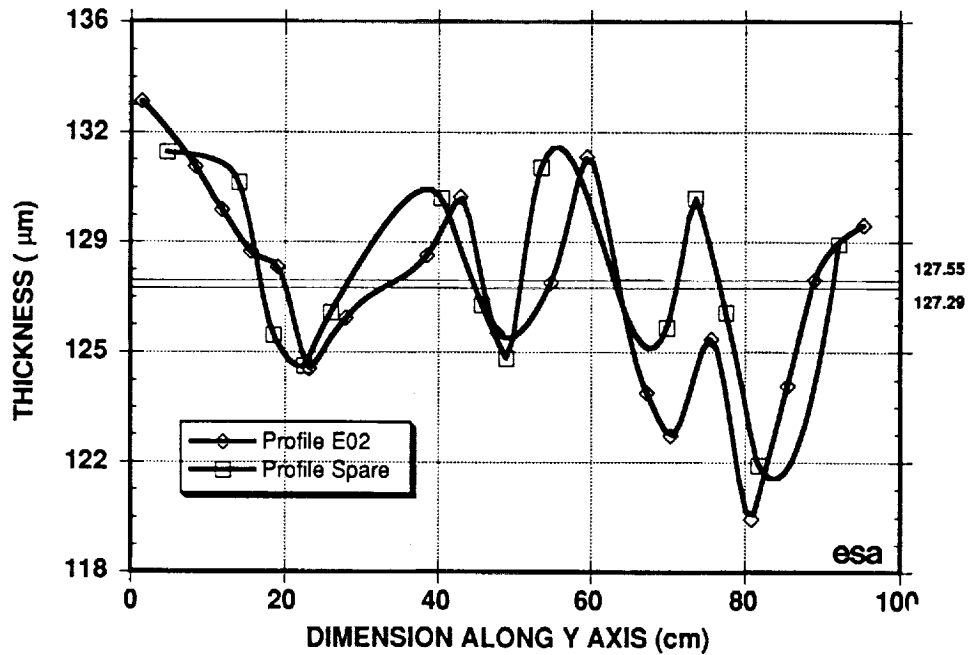
This chart shows the correlation between measurements at ESTEC and Boeing .
 The fits to the data give recession yields of 0.34×10^{-25} and 0.33×10^{-25} cm³ per atom, respectively.

Thickness of FEP from Leading Edge Exposed Specimens



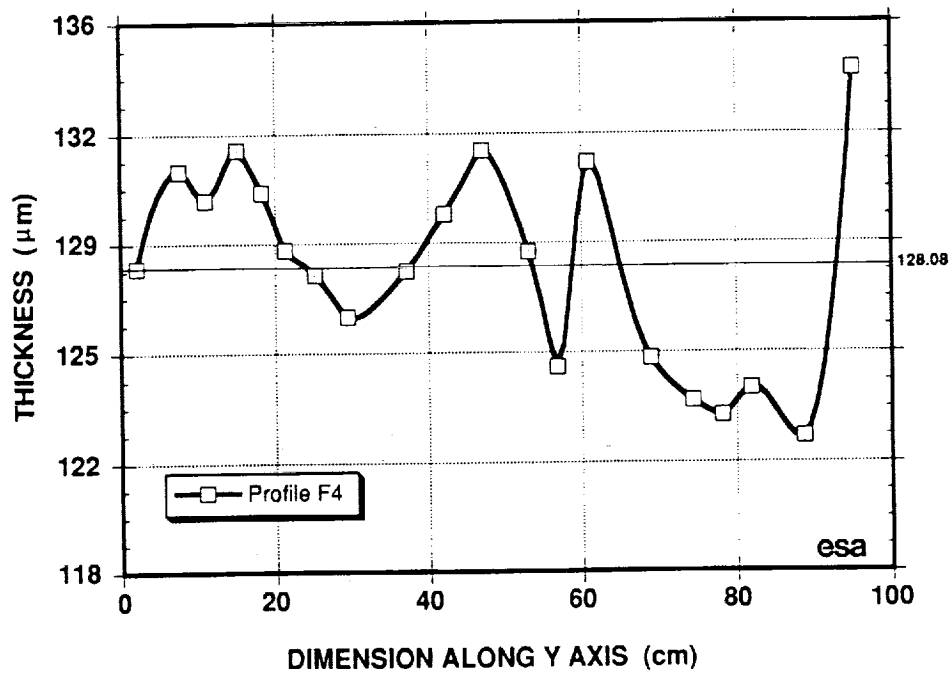
The variation in the blanket thickness along the length of a blanket is shown for blanket E02, which flew near the trailing edge, and a ground control blanket. The variation in manufactured thickness points out the need for care in obtaining recession data. Exposed and unexposed areas should be obtained from locations in as close proximity as possible to minimize the effects of the variation. A further point is that the thickness variation profiles for both the flown and ground stored blankets are quite similar.

Thickness Profile UHCRE Thermal Blanket



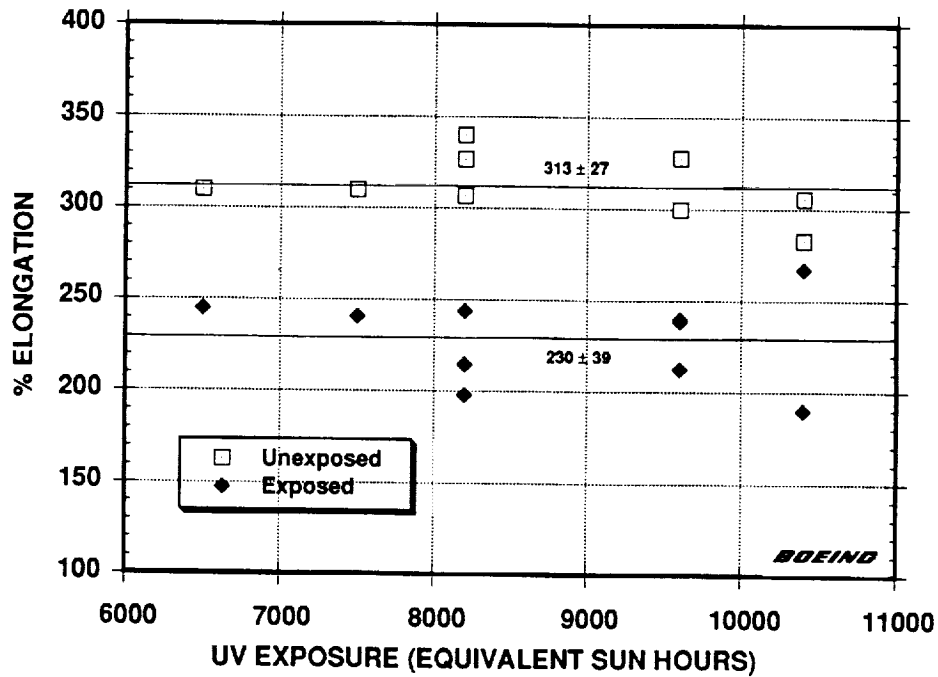
Additional data on thickness variation is shown for the blanket from tray F4. The trends are similar to the previous results.

Thickness Profile UHCRE Thermal blanket F4



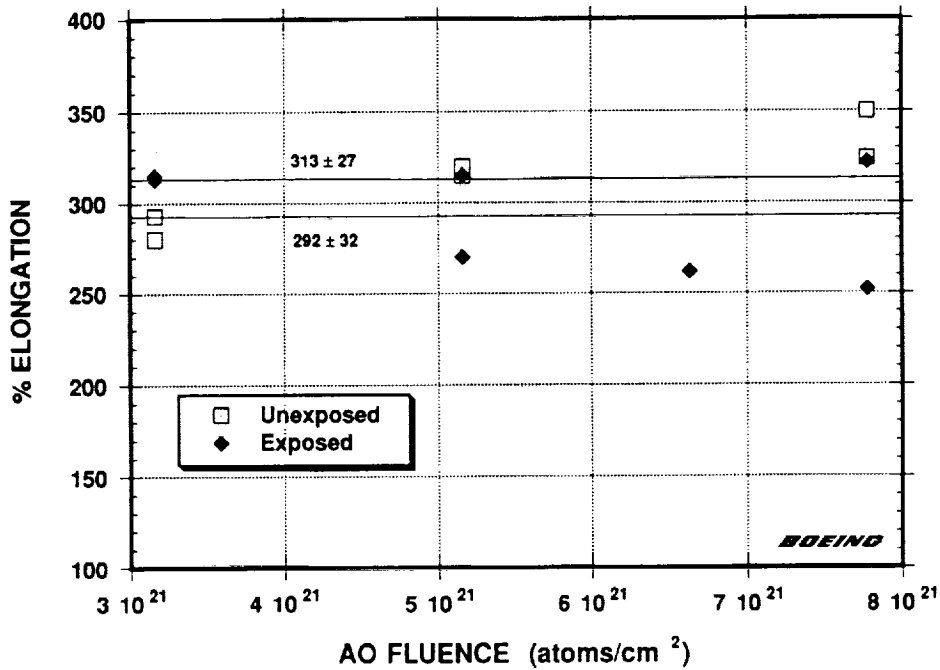
Tensile coupons were cut from both exposed and unexposed pieces of each blanket. Ultimate tensile strength and percent elongation at failure were measured. The results show that the exposed material has become imbrittled relative to the unexposed material. The unexposed material generally shows a percent elongation of about 300%; this is a typical value expected for FEP. It is also significant that the percent elongation of the exposed materials does not show a trend with hours of solar exposure. This implies the damage had essentially reached an equilibrium state prior to the 6400 equivalent sun hour exposure.

**% Elongation of FEP from Rows 1-6
Exposed and Unexposed Specimens**

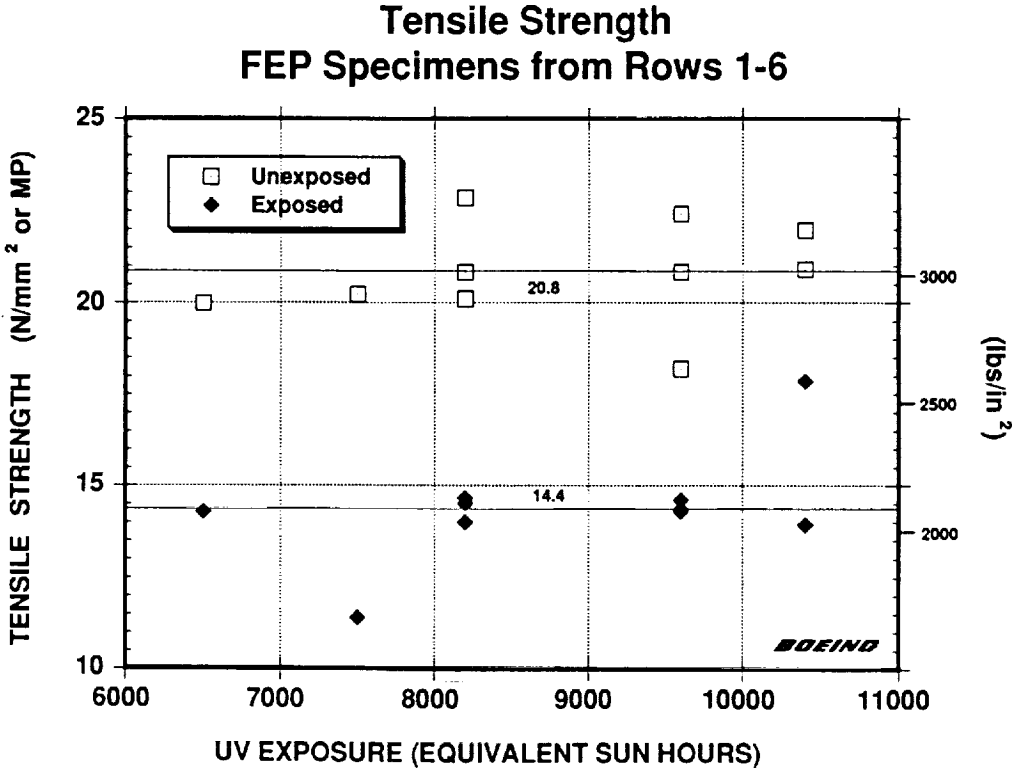


The percent elongation measurements for specimens from leading edge specimens show only slight differences between exposed and unexposed specimens. The averages between the two sets of measurements are not significantly different to a high degree of confidence. However, ESCA measurements do show differences between the surfaces of exposed and unexposed specimens. The imbrittled portion of the FEP material is being removed by surface oxidation, continually exposing fresh FEP. Thus, while the material is recessing, the oxygen is removing the observable effects of the ultraviolet-induced damage.

**% Elongation of FEP from Rows 7-11
Exposed and Unexposed Specimens**

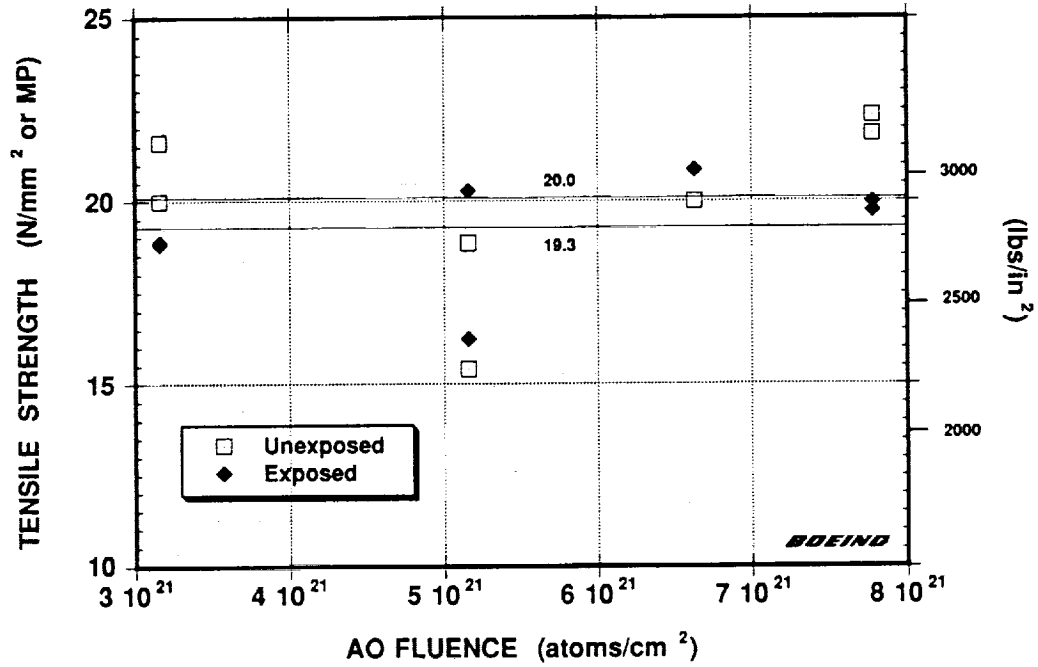


Ultimate tensile strengths for exposed and unexposed areas of blankets from the leading edge show essentially no difference within the uncertainty of the measurements.



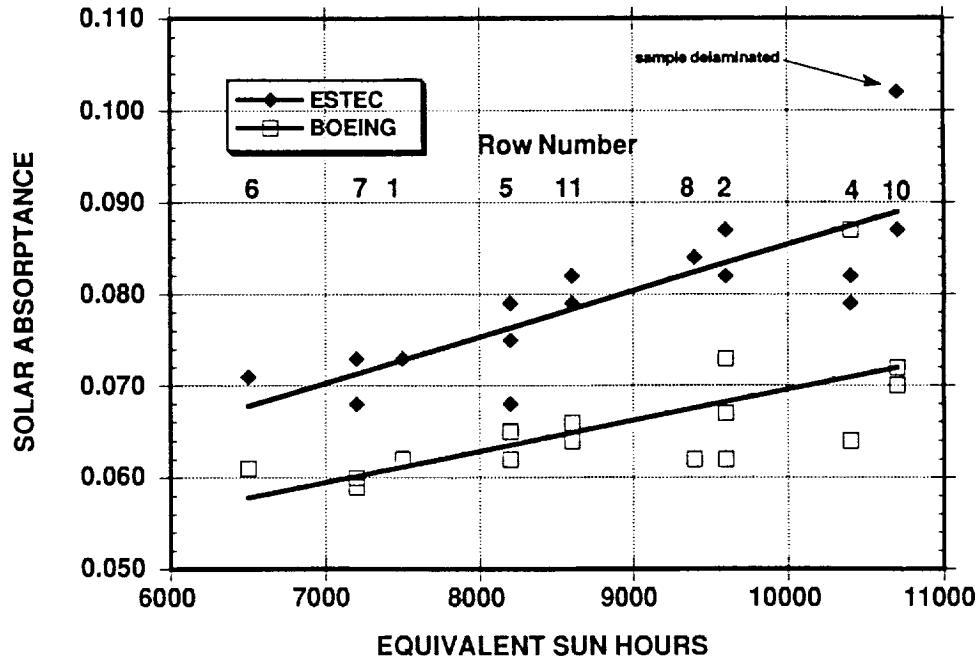
Ultimate tensile strength measurements on trailing edge specimens show the same pattern as the % elongation measurements. The exposed areas of the blankets have decreased mechanical strength relative to protected areas.

Tensile Strength FEP Specimens from Rows 7-11

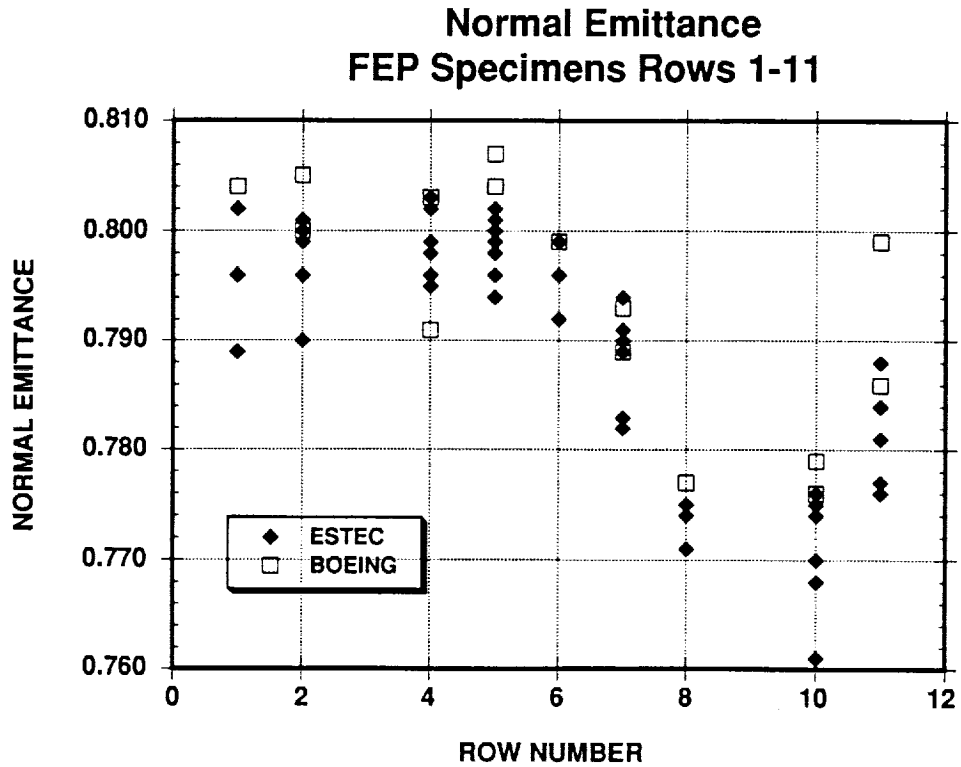


Measurements of solar absorptance vs equivalent sun hours of ultraviolet exposure made at both ESTEC and Boeing indicate a very slight increase in absorptance with increased solar exposure. It should be pointed out, however, that the absolute error associated with such measurements is at least ± 0.02 absorptance units. The differences between the absolute values obtained by the two laboratories are within this error and are most likely due to differences in calibration of the instruments used.

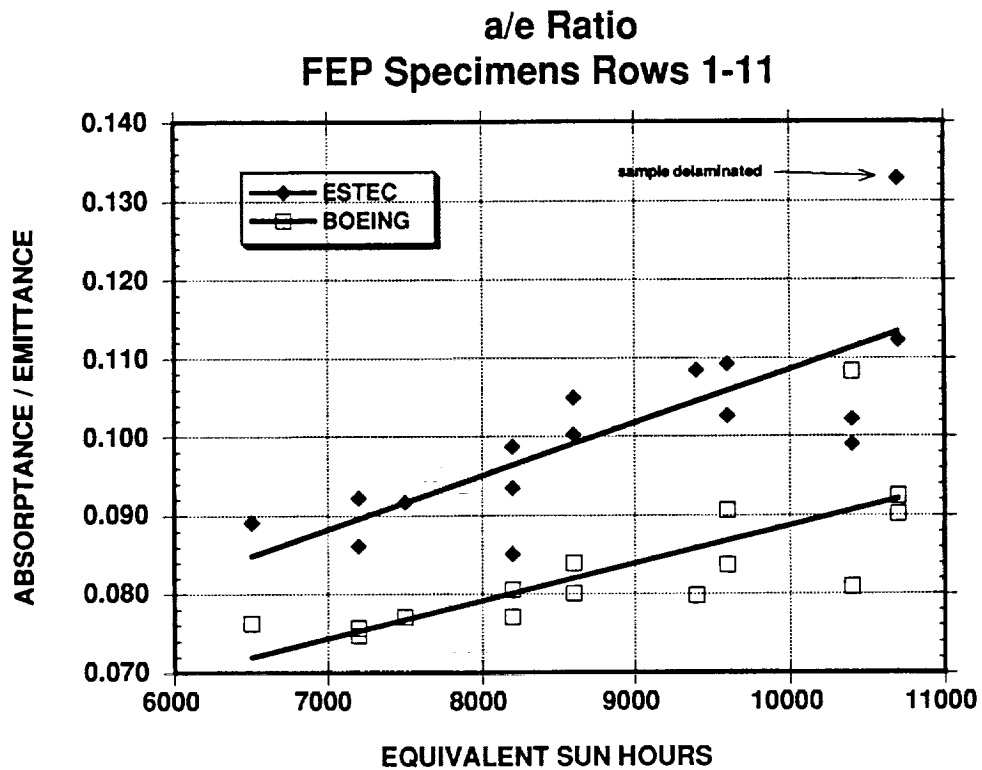
**Solar Absorptance vs UV Irradiation
FEP Specimens Rows 1-11**



The normal emittance measurements made at ESTEDC and Boeing show a small but reproducible decrease in the emittance of specimens exposed to atomic oxygen. This reflects the slightly decreased thickness of leading edge specimens. The spread in the data is due mainly to initial thickness differences rather than uncertainty in the measurements. The short term reproducibility of the equipment used (Geir-Dunkle DB100) is ± 0.003 .

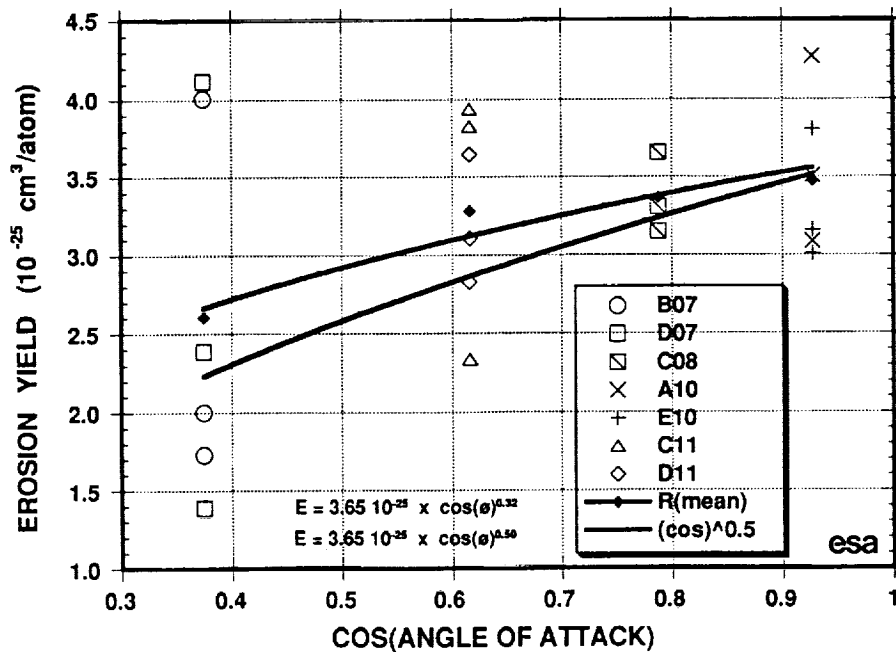


The absorptance to emittance ratio for the silver-backed FEP blankets increases with increased solar exposure. Measurements were made on areas of the blankets free from any noticeable impacts and represent the least damaged areas of the blanket. The fraction of areas punctured and delaminated by impact must be considered when determining the overall efficiency of this type of blanket as thermal protection.



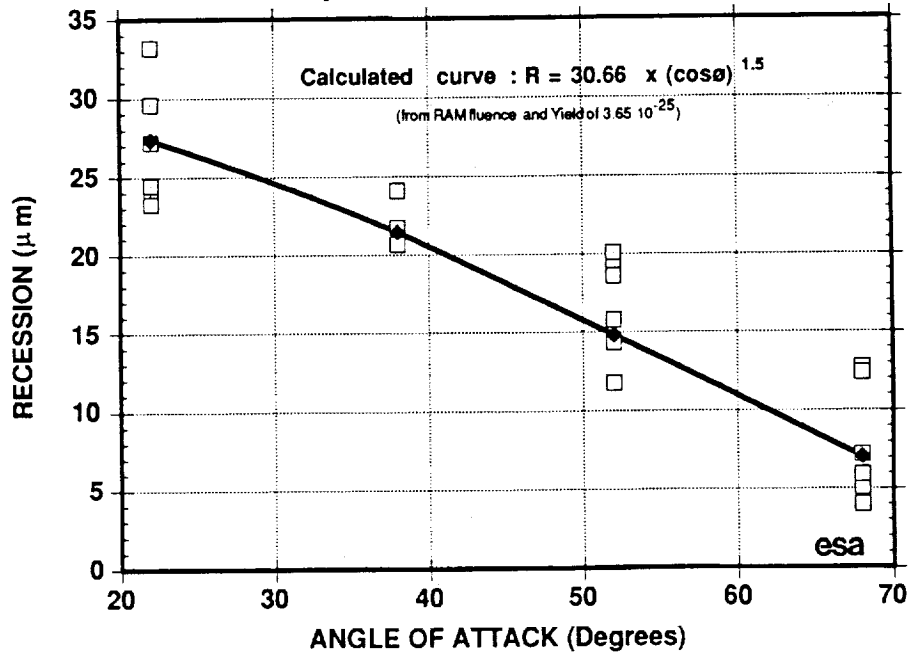
The erosion yield for individual measurements on specimens shows a wide range of values within each row. The determination atomic oxygen fluence, which is dependent on atmospheric density values used in model atmospheres, has its own uncertainty. However, for LDEF, the atomic oxygen fluences are based on one model. The wide range of values of erosion yield for each row is mainly due to the lack of precise knowledge of the initial thickness of each specimen. The best power fit through the mean values gives a power 0.32 of the cos of angle from ram and a value of 0.365×10^{-24} cm³ per oxygen atom for the erosion yield at ram. The power curve 0.5 of the cos of angle from ram, previously reported by Bruce Banks of NASA LeRC, is plotted for comparison.

Erosion Yield
FEP Specimens from Rows 7-11

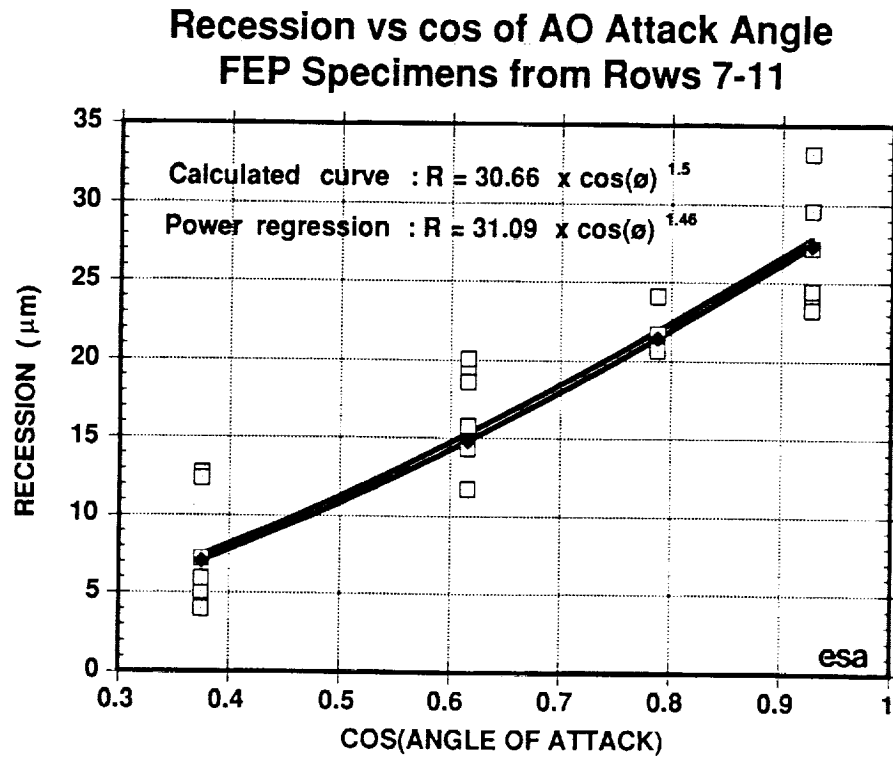


The recession for specimens from rows 7, 8, 10, and 11 on which the erosion yields are based plotted against the angle from ram. The calculated curve is based on an erosion yield of 0.365×10^{-24} cm³ per oxygen atom and the power 1.5 of cos of angle from ram.

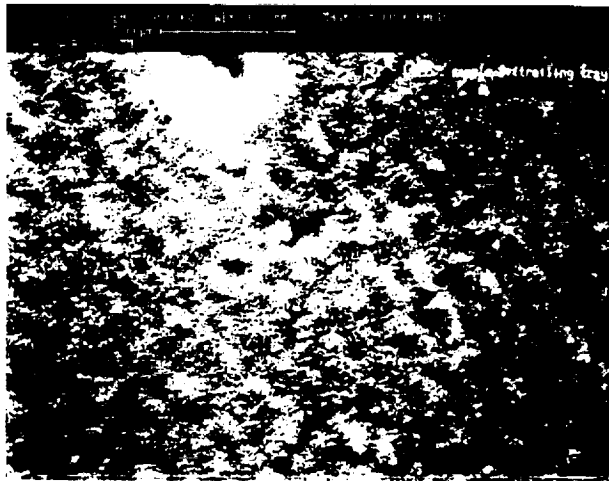
Recession vs Angle of Attack FEP Specimens from Rows 7-11



The recession of the FEP layer as a function of cos of angle from ram is plotted. The curves plotted predict about 31 microns recession in the ram direction. One of the cos factors is essentially from the nearly cosine dependence of the atomic oxygen fluence.



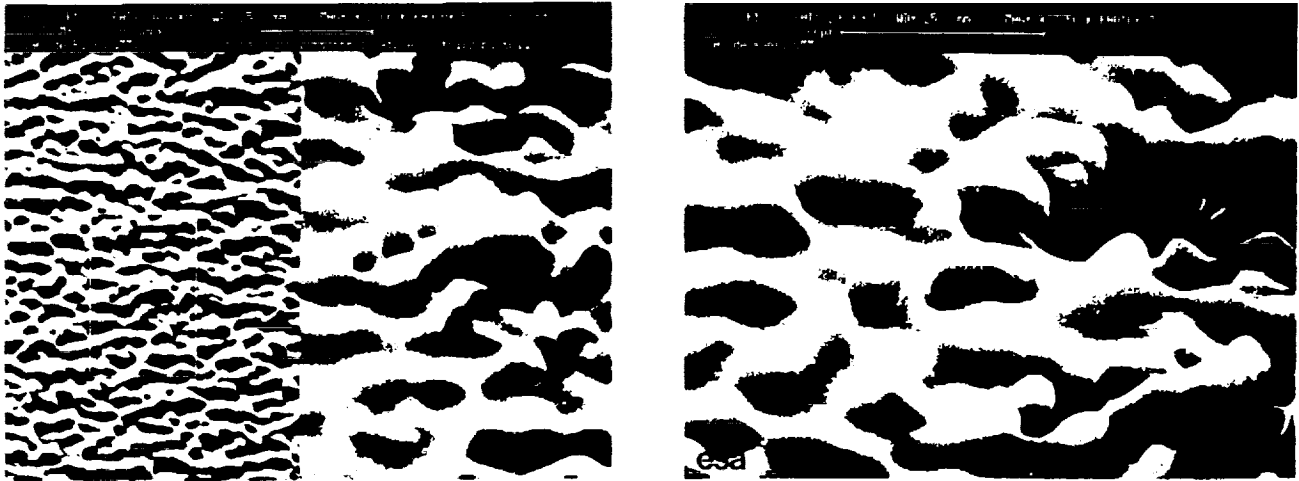
This SEM image of FEP from an exposed region of blanket E02 is representative of large areas of all the blankets exposed only to UV. The surface is smooth and apparently not affected.



**SEM of FEP
Trailing Edge E02**

(Original photograph unavailable)

In contrast, some effects can be observed visually on a sample of blanket F04. The following SEM images, showing the same area under increasing magnification, clearly show a textured area due to unexplained phenomena. Furthermore this effect seems to be directional.



**SEM of FEP
Trailing Edge F04**

(Original photograph unavailable)

The mass loss and mechanical properties data obtained at Boeing is presented in this table.

BOEING DATA

Blanket Nr	Mass Unexp (g)	Mass Exp (g)	Thick Unexp (μm)	Thick Exp (μm)	Elong Unexp (%)	Elong Exp (%)	Load Unexp (N)	Load Exp (N)	Tensile Unexp (N/mm2)	Tensile Exp (N/mm2)
D1	0.10052(2)	0.09775(3)	134.74	131.02	310(2)	241(2)	12.32	6.76	20.23	11.41
A2	0.09636(2)	0.09815(3)	129.16	131.56	300(1)	240(2)	10.63	8.54	18.21	14.36
E2	0.09627(3)	0.09288(3)	129.04	124.50	328(2)	213(2)	13.08	8.05	22.42	14.30
F2		0.09640(6)		129.21		239(4)		8.54		14.62
A4	0.09230(3)	0.09241(6)	123.72	123.87	283(2)	267(6)	11.70	10.01	20.92	17.87
F4	0.09886(3)	0.08949(4)	132.51	119.95	306(3)	190(5)	13.17	7.56	21.98	13.94
B5	0.09541(2)	0.09173(2)	127.89	122.95	340(2)	215(2)	13.21	7.78	22.85	14.00
C5	0.09636(2)	0.09754(3)	129.16	130.74	307(2)	198(2)	11.74	8.67	20.11	14.67
D5	0.09834(3)	0.09806(3)	131.81	131.44	327(2)	244(2)	12.41	8.63	20.82	14.52
C6	0.09142(3)	0.09042(3)	122.54	121.2	310(2)	245(2)	11.08	7.83	19.99	14.29
B7	0.09645(3)	0.09096(3)	129.28	121.92	293(2)	313(2)	12.63	10.41	21.61	18.88
D7		0.08773(3)		117.59	280(2)	315(2)	9.25	10.01		18.83
C8		0.07951(3)		106.57		262(4)		10.05		20.86
A10	0.09370(3)	0.07361(5)	125.59	98.67	350(2)	252(4)	12.68	8.81	22.33	19.74
E10	0.09378(3)	0.07568(2)	125.70	101.44	324(2)	322(2)	12.41	9.16	21.84	19.98
C11	0.09308(2)	0.08069(3)	124.76	108.16	315(2)	315(2)	10.63	9.92	18.85	20.29
D11	0.09764(1)	0.08043(3)	130.88	107.81	320(1)	270(1)	9.12	7.92	15.41	16.24

Average Mass, Thickness, % Elongation and Load for each Blanket Specimen (3.47 cm²)
(number in parentheses shows number of individual data points used to obtain average)

The thermo-optical data obtained at Boeing is presented in this table. The atomic oxygen fluence is from the original calculation made at Boeing in early 1990. Values determined using more precise orbit routines have lead to an increase in the calculated values of between about three and five percent, depending on location. These slight corrections do not change the essential conclusions in any way.

BOEING DATA

Blanket Nr	UV (ESH)	AO (at/cm ³)	Alpha Exp	Eps Exp	Alpha Unexp	Eps Unexp
D1	7500	1.22E+17	0.062	0.804	0.063	0.804
A2	9600	1.37E+09	0.073	0.805		
E2	9600	1.37E+09	0.067	0.800		
F2	9600	1.37E+09	0.062	0.803		
A4	10400	2.99E+05	0.087	0.803		
F4	10400	2.99E+05	0.064	0.791		
B5	8200	1.09E+13	0.062	0.804		
C5	8200	1.09E+13	0.065	0.807		
D5	8200	1.09E+13	0.062	0.804	0.064	0.799
C6	6500	4.93E+19	0.061	0.799		
B7	7200	3.16E+21	0.059	0.789		
D7	7200	3.16E+21	0.060	0.793		
C8	9400	6.63E+21	0.062	0.777		
A10	10700	7.78E+21	0.070	0.776	0.061	0.803
E10	10700	7.78E+21	0.072	0.779		
C11	8600	5.16E+21	0.066	0.786		
D11	8600	5.16E+21	0.064	0.799		

Thermo-optical Data
(Each value is the average of three measurements)

Mass and thickness data for the FEP layer of the thermal control blankets obtained at ESTEC are shown in this chart.

ESTEC DATA

Blanket Nr	Mass Exposed (g)	Thickness (μm)	Blanket Nr	Mass Exposed (g)	Thickness (μm)	Blanket Nr	Mass Exposed (g)	Thickness (μm)
D01 MB	0.136646	132.39	C05 MB	0.132608	128.48	A10 MB	0.102977	99.77
D01 MM	0.130383	126.33	C05 MM	0.136600	132.35	A10 MM	0.106467	103.15
D01 MT	0.123777	119.93	C05 MT	0.129454	125.43	A10 MT	0.096813	93.80
A02 MB	0.133275	129.13	D05 MB	0.128098	124.11	E10 MB	0.105835	102.54
A02 MM	0.130525	126.46	D05 MM	0.133538	129.38	E10 MM	0.107047	103.72
A02 MT	0.123354	119.52	D05 MT	0.134969	130.77	E10 MT	0.100538	97.41
E02 MB	0.134030	129.86	C06 MB	0.133128	128.99	C11 MB	0.110334	106.90
E02 MM	0.129889	125.85	C06 MM	0.129548	125.52	C11 MM	0.118949	115.25
E02 MT	0.123589	119.74	C06 MT	0.127089	123.13	C11 MT	0.110886	107.44
A04 MB	0.129243	125.22	B07 MB	0.118297	114.62	D11 MB	0.111878	108.40
A04 MM	0.129904	125.86	B07 MM	0.125845	121.93	D11 MM	0.114802	111.23
A04 MT	0.131158	127.08	B07 MT	0.124966	121.08	D11 MT	0.116304	112.69
F04 MB	0.127139	123.18	D07 MB	0.126953	123.00			
F04 MM	0.132623	128.50	D07 MM	0.123657	119.81			
F04 MT	0.134668	130.48	D07 MT	0.117955	114.28			
B05 MB	0.132259	128.14	C08 MB	0.109739	106.32			
B05 MM	0.132414	128.29	C08 MM	0.108617	105.24			
B05 MT	0.133841	129.68	C08 MT	0.106192	102.89			

**Mass and Thickness
for each Blanket Specimen (4.796 cm²)**

Thermo-optical data obtained at ESTEC for the silvered Teflon thermal control blankets are shown in this chart.

ESTEC DATA

Blanket Nr	Absorptance	Emittance	Blanket Nr	Absorptance	Emittance	Blanket Nr	Absorptance	Emittance
D01 M B		0.802	C05 M B		0.799	A10 M B		0.770
D01 M M	0.073	0.796	C05 M M	0.075	0.802	A10 M M	0.087	0.775
D01 M T		0.789	C05 M T		0.796	A10 M T		0.761
A02 M B		0.800	D05 M B		0.794	E10 M B		0.774
A02 M M	0.082	0.799	D05 M M	0.079	0.800	E10 M M		0.776
A02 M T		0.790	D05 M T		0.801	E10 M T	0.102	0.768
E02 M B		0.801	C06 M B		0.799	C11 M B		0.776
E02 M M	0.087	0.796	C06 M M	0.071	0.796	C11 M M	0.079	0.788
E02 M T		0.790	C06 M T		0.792	C11 M T		0.781
A04 M B		0.796	B07 M B		0.783	D11 M B		0.777
A04 M M	0.079	0.798	B07 M M	0.073	0.791	D11 M M	0.082	0.781
A04 M T		0.799	B07 M T		0.790	D11 M T		0.784
F04 M B		0.795	D07 M B		0.794	Spare	0.077	0.795
F04 M M	0.082	0.802	D07 M M	0.068	0.789			
F04 M T		0.803	D07 M T		0.782			
B05 M B		0.798	C08 M B		0.775			
B05 M M	0.068	0.799	C08 M M	0.084	0.774			
B05 M T		0.800	C08 M T		0.771			

Thermo-optical Data

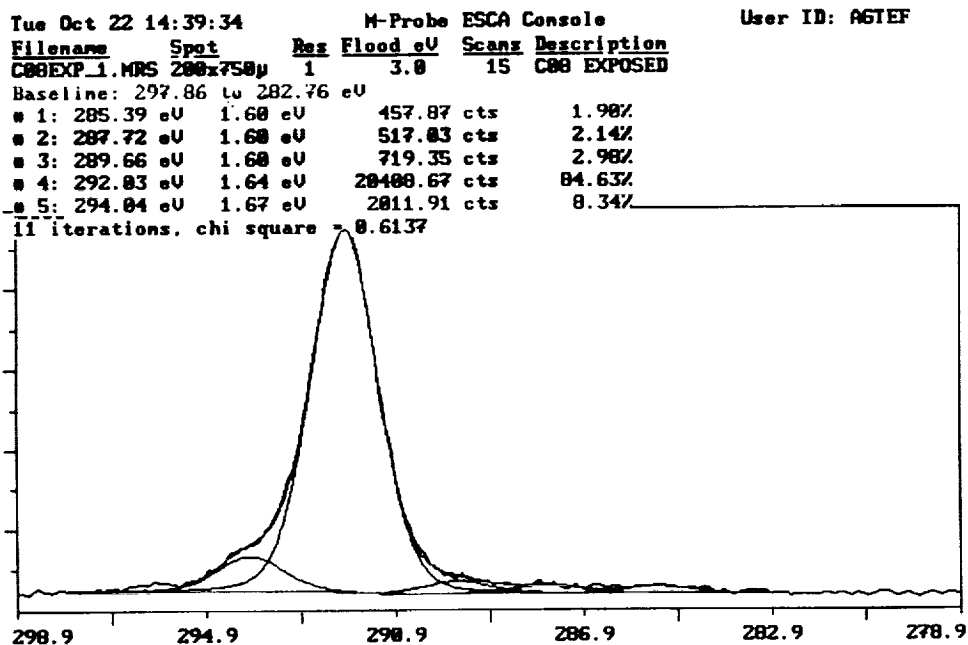
A comparison of total hemispherical and normal emittance is shown for a flight specimen from blanket E10, a ground control spare flight specimen, and a 1 mil silvered FEP Teflon sample. The increase in total hemispherical to normal emittance for the exposed specimen is due to a thickness decrease as confirmed by the 1mil sample. Slight changes in the total hemispherical and normal emittance for the flight specimen were observed after the specimen was polished.

ESTEC DATA

Sample	ϵ_H	ϵ_N	ϵ_H/ϵ_N
Spare	0.805	0.795	1.013
E10	0.795	0.770	1.033
E10 polished	0.792	0.763	1.038
1 mil FEP/Ag	0.547	0.487	1.128

Total Hemispherical Emittance

The ESCA spectrum for an exposed area on blanket C08 is essentially identical to a spectrum of unexposed FEP.

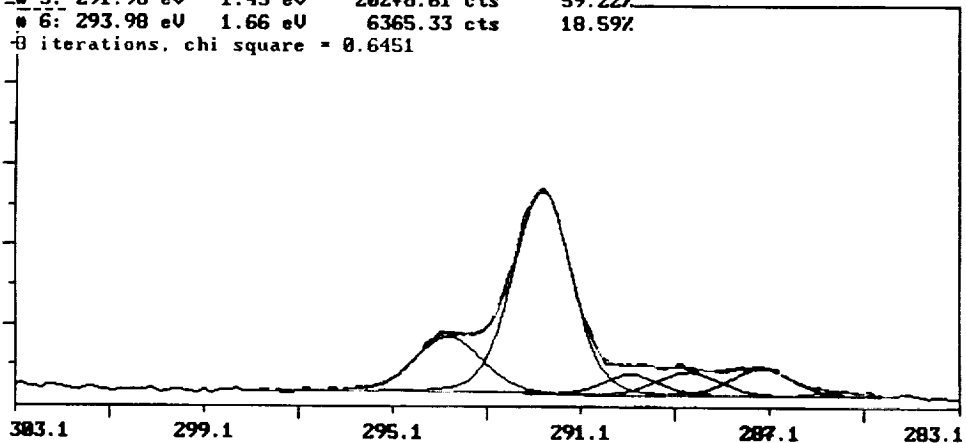


This spectrum for an exposed area from blanket C06 shows the competition between the effects of ultraviolet radiation and atomic oxygen exposure. As the UV breaks bonds and causes structural rearrangements, sites are created where the oxygen atoms can react and produce volatile products. The reactions with atomic oxygen occur on the surface but the UV damage extends into the material.

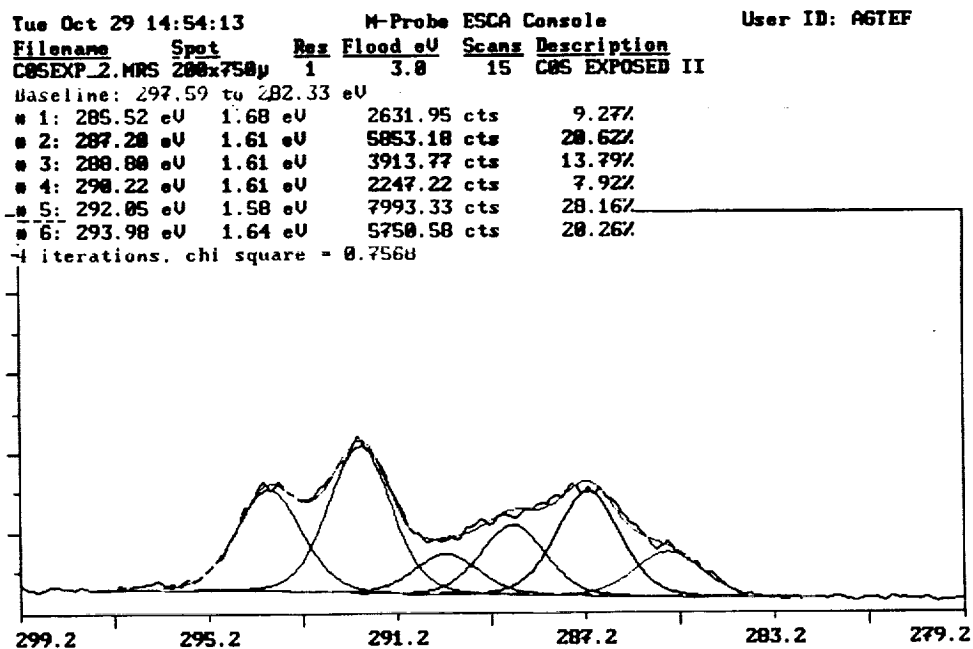
```

Tue Oct 22 14:46:55      M-Probe ESCA Console      User ID: AGTEF
Filename  Spot      Res Flood eV  Scans Description
C6EXP_1.MRS 200x750µ  1      5.0      15 C06 EXPOSED
Baseline: 297.96 to 284.55 eV
# 1: 285.67 eV  1.18 eV    381.79 cts    1.11%
# 2: 287.32 eV  1.48 eV    2854.24 cts   8.33%
# 3: 288.87 eV  1.51 eV    2422.08 cts   7.87%
# 4: 290.08 eV  1.37 eV    1941.98 cts   5.67%
# 5: 291.98 eV  1.45 eV    20278.61 cts  59.22%
# 6: 293.98 eV  1.66 eV    6365.33 cts  18.59%
0 iterations, chi square = 0.6451

```



This ESCA spectrum for an exposed area on blanket C05 shows evidence of significant changes in the chemical structure of the FEP. The changes in this spectrum relative to the spectrum from C08 are representative of UV induced bond breaking and subsequent cross-linking.



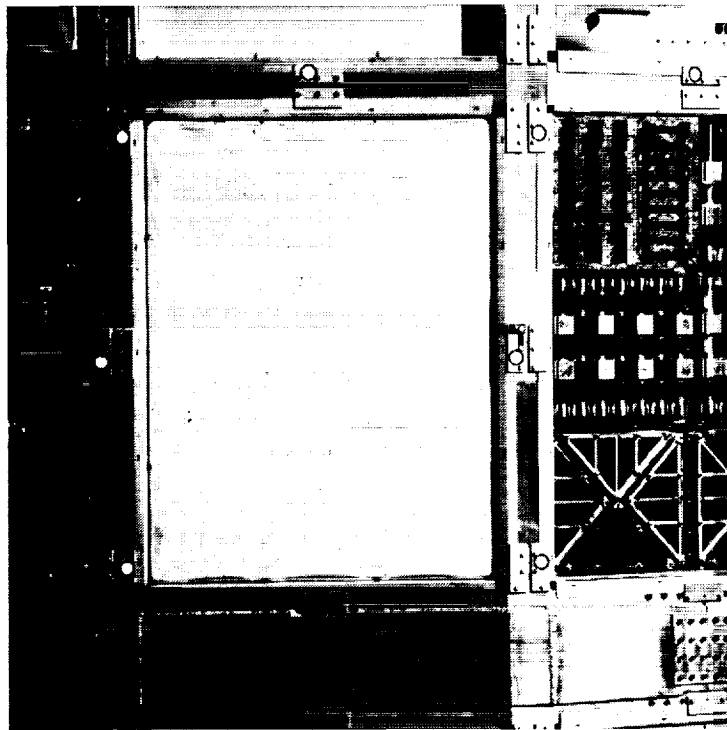
N93-12786

**RECESSION OF FEP SPECIMENS
FROM TRAYS D11 and B7**

**H. G. Pippin
Boeing Defense & Space Group**

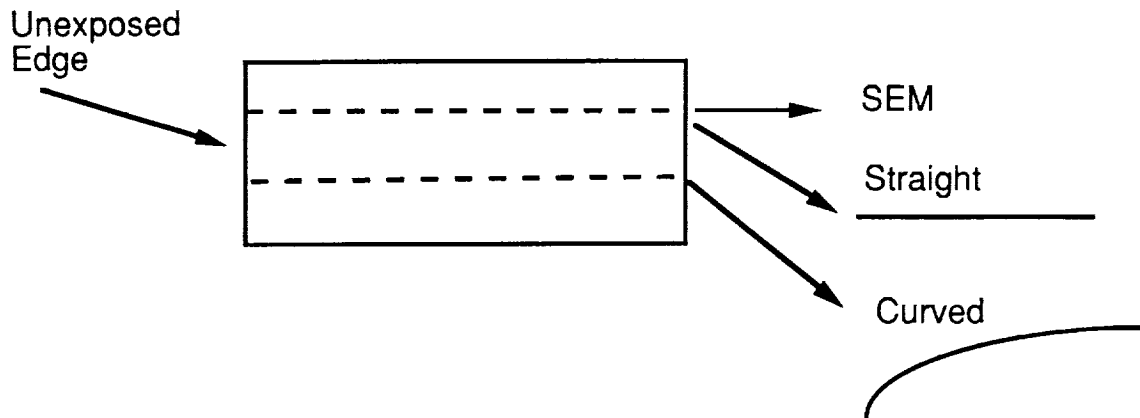
In this presentation we reported work done at Boeing Defense and Space Group on analysis of silvered teflon specimens taken from selected locations of the Long Duration Exposure Facility under support from a contract provided by NASA LaRC.

This photograph was taken on orbit during the retrieval of LDEF and shows blanket D11. The samples discussed in this presentation were taken from the unexposed side of D11 and extended through the folded area of this blanket into the exposed area. Two similar areas were cut from blanket B7, one from the edge of the blanket near row six and one from the edge of the blanket near row eight and within a few centimeters of the copper grounding strap for B7.



The specimens were each divided into three sections by cutting with a scapel. Two of the sections were mounted in a potting compound, which was cut and polished such that the cross-sectional thickness of each was exposed. One piece was mounted straight and the other was mounted in an attempt to configure the specimen such that it was bent with a radius of curvature similar to the on-orbit configuration. The third portion of each specimen was used for SEM images to help define the angle of exposure with respect to the ram at each location on the specimen.

FEP SPECIMENS FROM BLANKETS D11 and B7



Photomicrographs were taken in cross section from the edge of the blanket through the curved transition region into the exposed area of the blanket. The thickness of the Fluorinated Ethylene Propylene (FEP) layer was determined at known distances from the edge of the blanket. SEM images were obtained at known distances to help define the angle with respect to ram and therefore establish the atomic oxygen fluence on each location and correlate this exposure with thickness. Thickness measurements made within a two to three centimeter distance minimized the uncertainty arising from variations in the as-manufactured thickness of each blanket. The nominal angle from ram of the exposed portion of each blanket, and the fact that the unexposed edge portions are approximately at right angles to the exposed portion were also used to help define the angles.

Thickness measurements were taken at specified locations. An average thickness for the unexposed portion of the blanket was determined. Changes in thickness were then determined by difference.

Orientation of Individual Specimens



- **Obtained photomicrographs from edge of blanket, through transition region, into exposed area**
 - **Obtained thickness vs. distance from edge of blanket**
 - **Obtained Sem Images at known distances from edge of blankets to verify angle from RAM at specific locations**

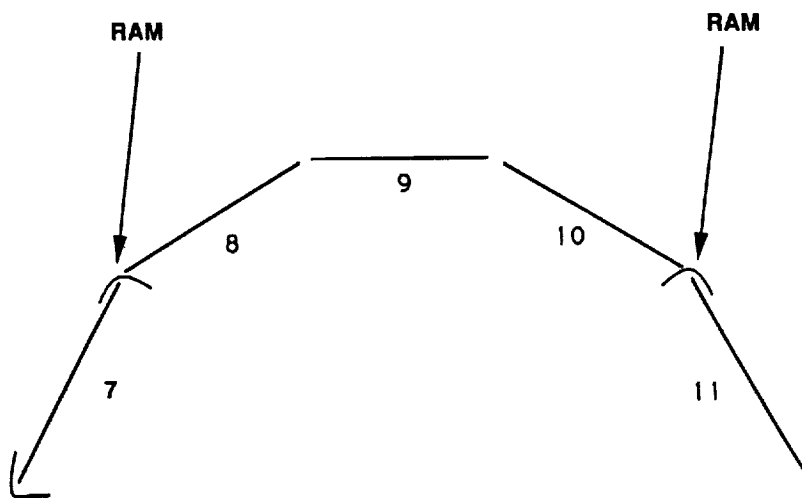
RESULTS

THICKNESS vs LOCATION

CHANGES IN THICKNESS vs LOCATION

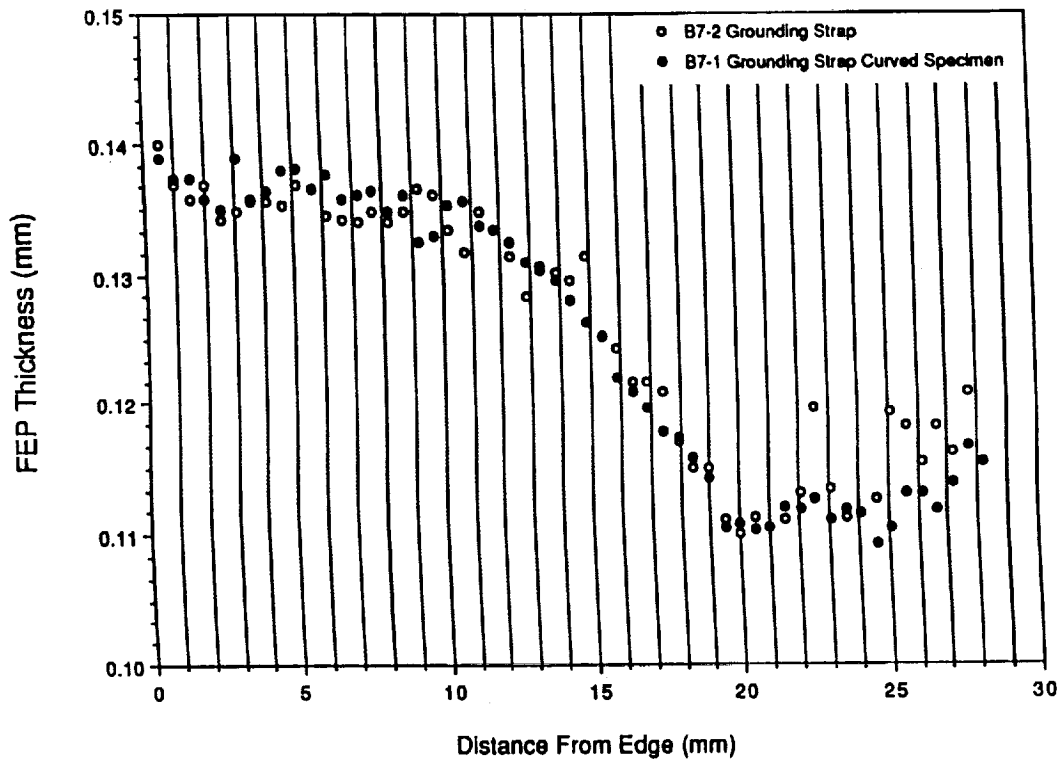
The details of the locations of the three specimens are shown in this diagram. The specimen from D11 was the most "open" to the ram direction; that is, its orientation was such that the least complication from secondary scattering was likely for this specimen. For the specimen from B7 near the copper grounding strap (on the row eight side) there is some possibility that some oxygen atoms may be blocked by the edge of the tray and longer on toward row eight. The slightly raised side of the tray and longeron immediately behind the B7 specimen near row six is a source of secondary scattering and enhanced dosage of atomic oxygen for the surface of the specimen which approaches ninety degrees from ram. SEM photos of locations show surface roughening consistent with atoms scattered from this surface.

ORIENTATION OF FEP SPECIMENS

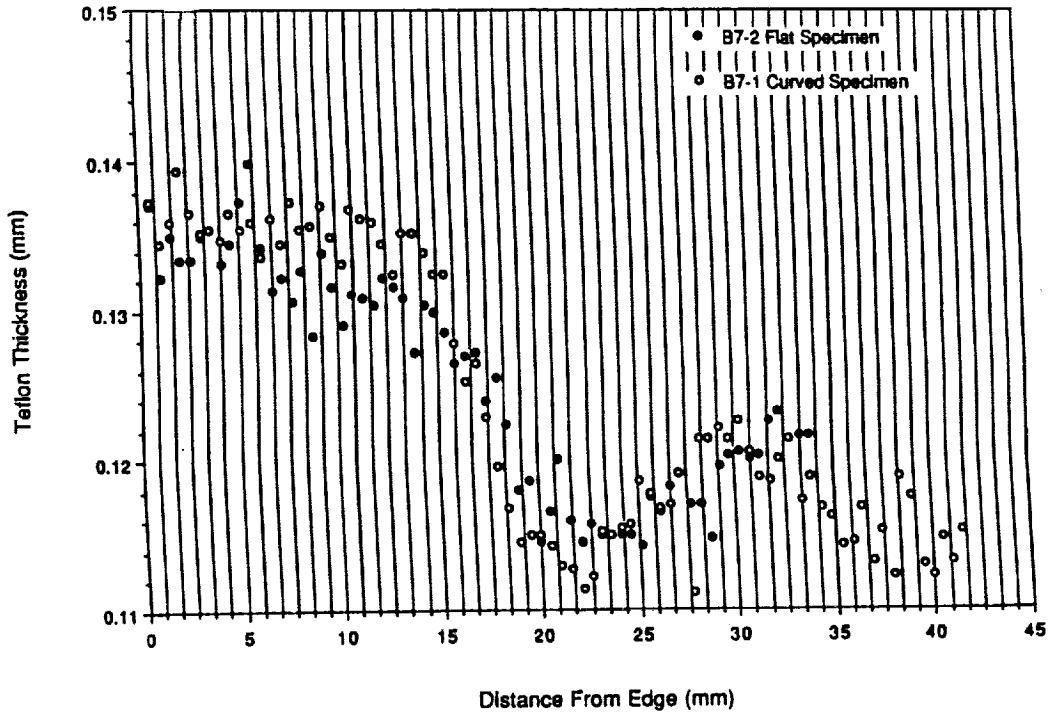


The next three charts show the results of the thickness measurements. There was essentially no difference in the measured thickness of the curved specimens under tension and the straight specimens at each location. Based on thickness variations measured by ESSA/ESTEC over the entire length of a blanket, one can expect a thickness variation of 1-2 micros over the length of material examined in each of these specimens. This thickness variation is also borne out by the slight thickness differences of the unexposed portions of the various specimens.

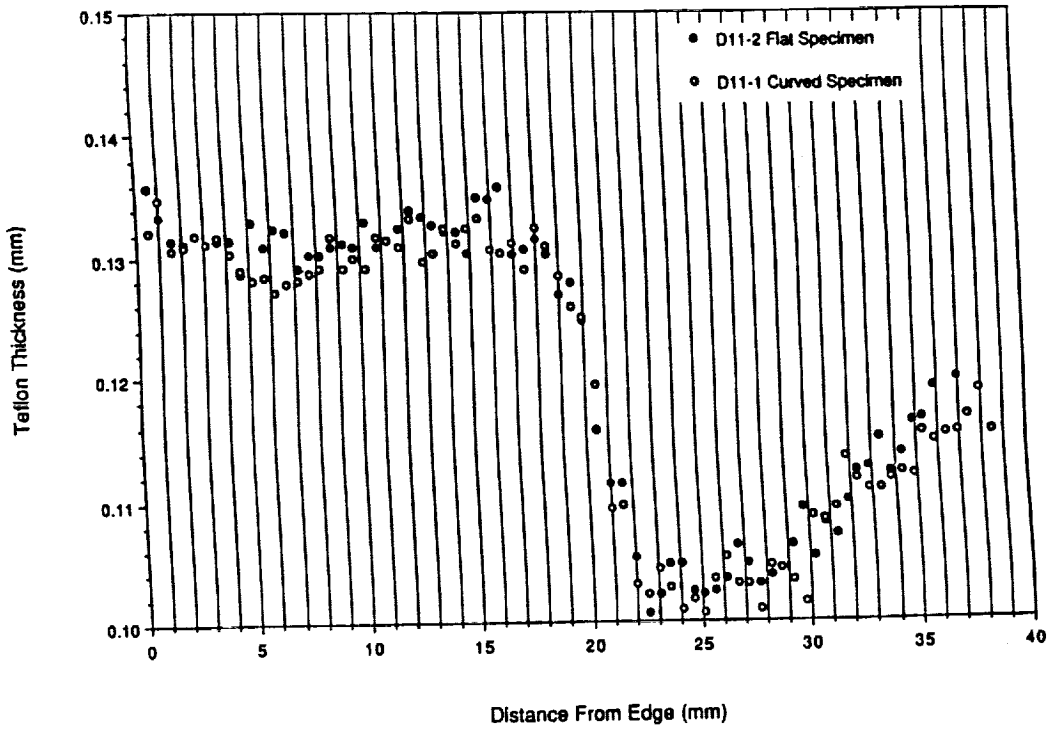
Atomic Oxygen Erosion of Thermal Control Blankets



Atomic Oxygen Erosion of Thermal Control Blankets

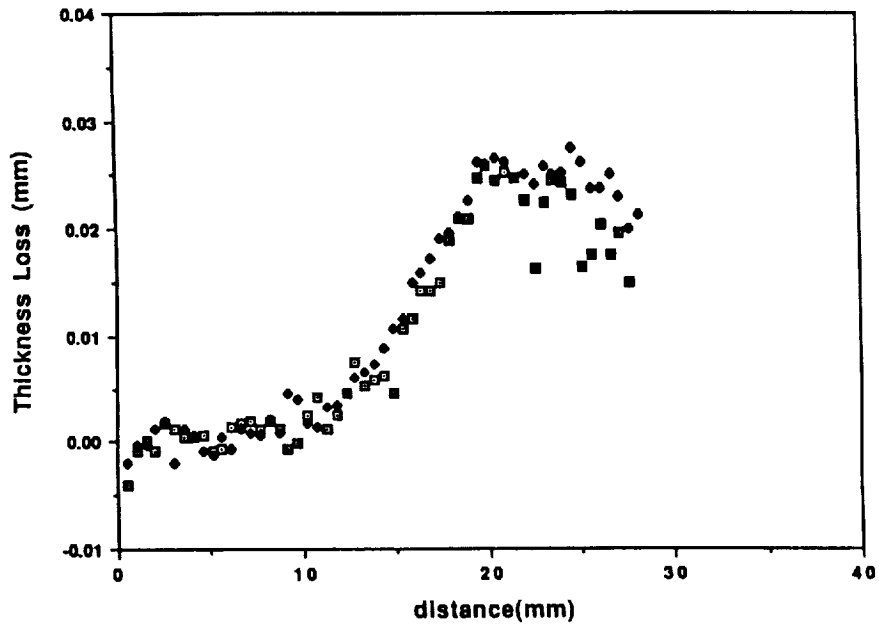


Atomic Oxygen Erosion of Thermal Control Blankets

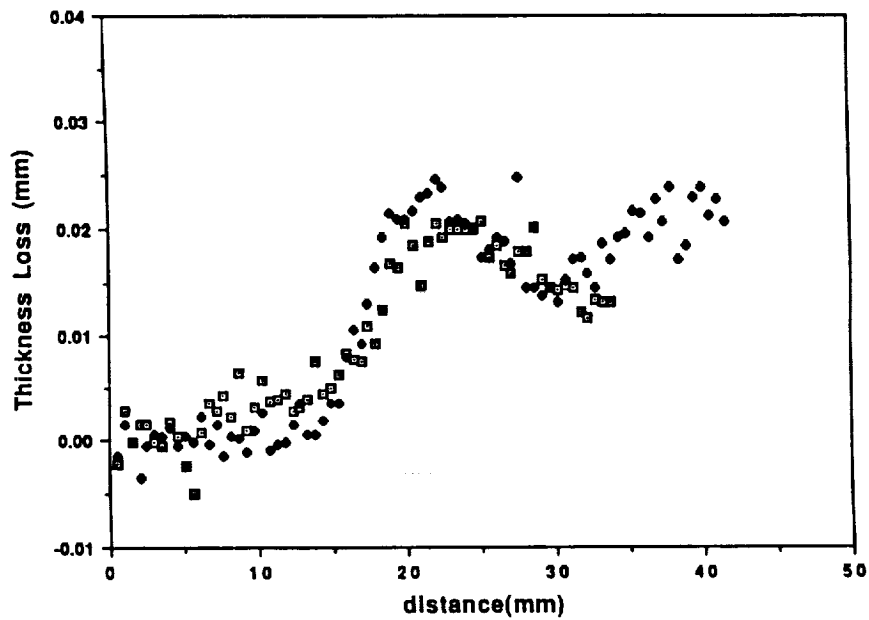


The next three charts show the thickness loss for each specimen as a function of distance from the edge of the blanket. The values essentially correct for initial thickness differences in the various specimens. The shape of the thickness loss curve from the B7 blanket specimen from the row six side is due to curvature in this blanket, clearly visible in the on-orbit photos. Data are shown for two specimens from each blanket.

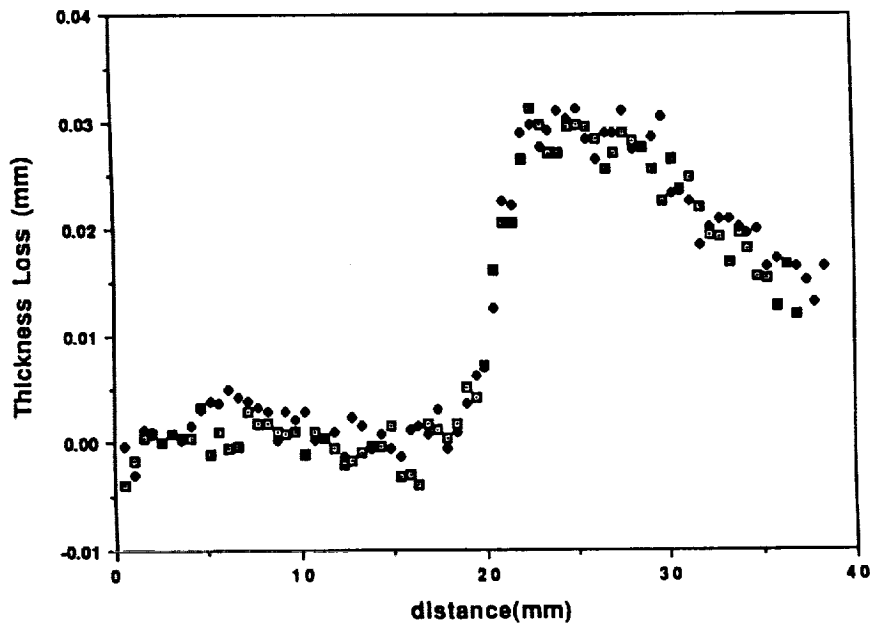
Thickness Loss B7 near Grounding Strap



Thickness Loss from B7 FEP



Thickness Loss from d11 FEP



FITS TO DATA

ANGLE DETERMINATION

SEM-SEMI QUANTITATIVE

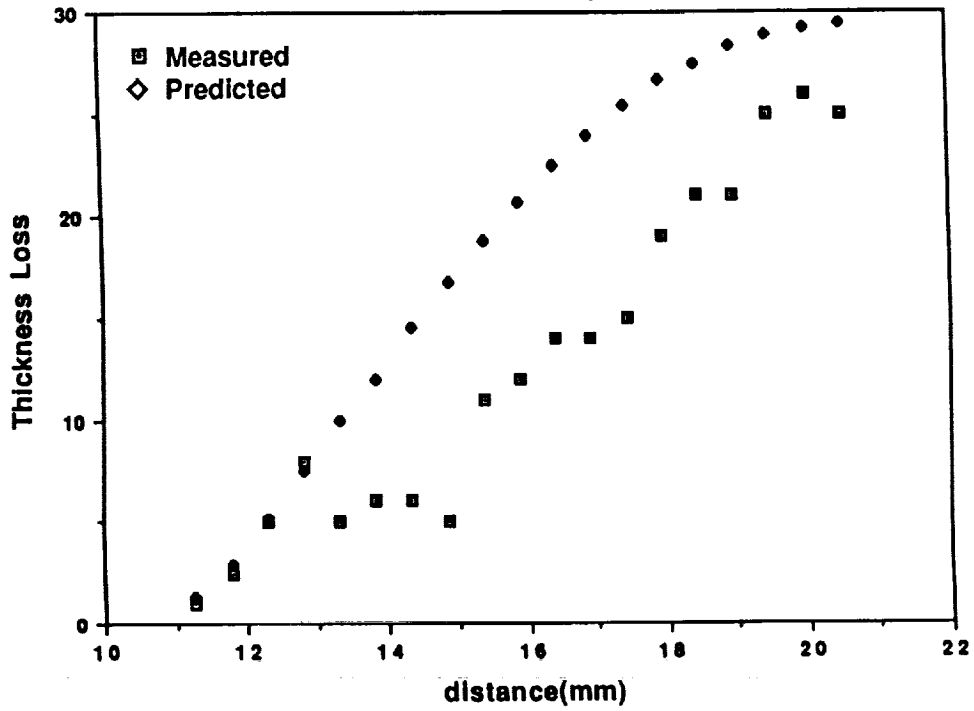
RADIUS OF CURVATURE CHANGES

To complete this determination of the recession vs angle, it was necessary to define the angle with respect to ram. The use of SEM images to determine the orientation of the textured peaks with respect to the ram direction was only semi-quantitative and established the angle from ram only within a few degrees in each case. However, these measurements did allow definition of the ram direction exposure location to within a millimeter along the length of the specimen for two of the three specimens. Due to the apparent indirect scattering from adjacent aluminum surfaces, the angles for the B7 specimen were not clear from the SEM images. A second consideration in trying to determine the angle from ram is that the radius of curvature was not necessarily constant throughout the transition region from unexposed to exposed blanket surfaces, and therefore the angle change per fixed distance is not constant. With these caveats as reminders, we estimated the angles by assuming a constant radius of curvature as a first approximation and compared the results to recession rates determined from measurements of the exposed areas of the blankets from rows 7, 8, 10, and 11. The results of this exercise are shown in the next few charts.

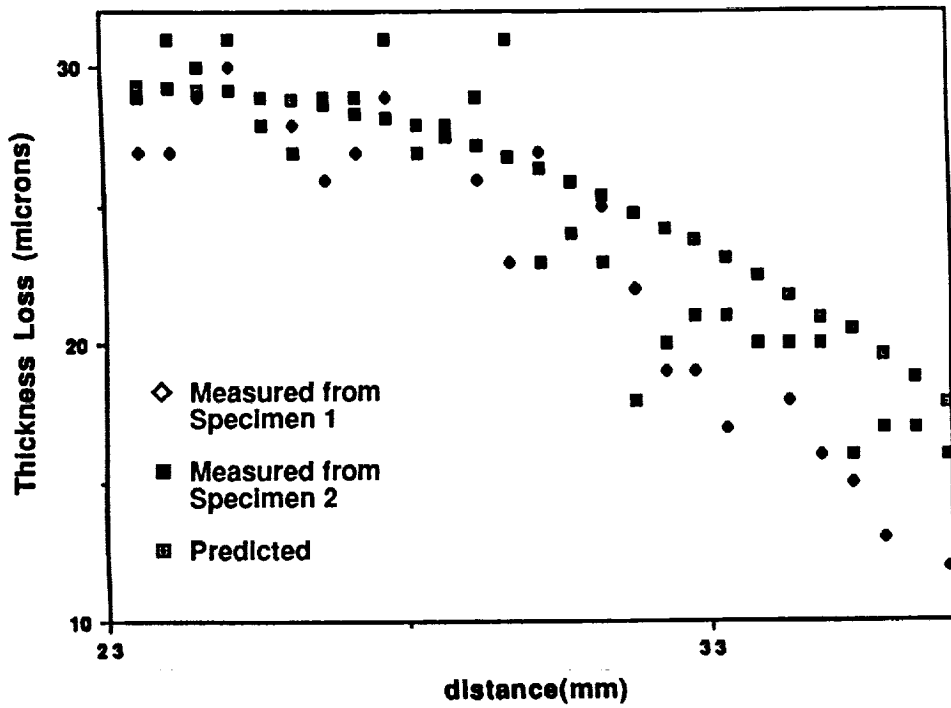
From the calculated atomic oxygen fluences, it can be shown that 90 degrees from the ram produces a thickness loss of less than 1 micron. For each specimen the distance along the blanket where the thickness loss reaches less than one micron is assumed to be 90 degrees. The location of the ram direction is well enough defined from the SEM images. A calculation of thickness loss is made from the end-of-mission atomic oxygen fluences as a function of angle. The angle change is assumed to be linear with distance between the 90 from ram and ram locations. The results of this fit are shown for the B7 specimens taken from near the grounding strap. The predicted recession of 29.4 microns is about 15% higher than the value taken from these measurements.

The next two charts show a comparison of thickness loss calculated from recession rates with the measured recession rates for two regions of the specimens from blanket D11. For this blanket the fit is good, indicating that our assumption of constant rate of angle change with linear distance was valid for this specimen. For distances greater than 30 mm from the edge of the blanket the calculated values appear to be slightly high, indicating our assumption of 52 degrees at the end of the specimen farthest from the unexposed edge is slightly off.

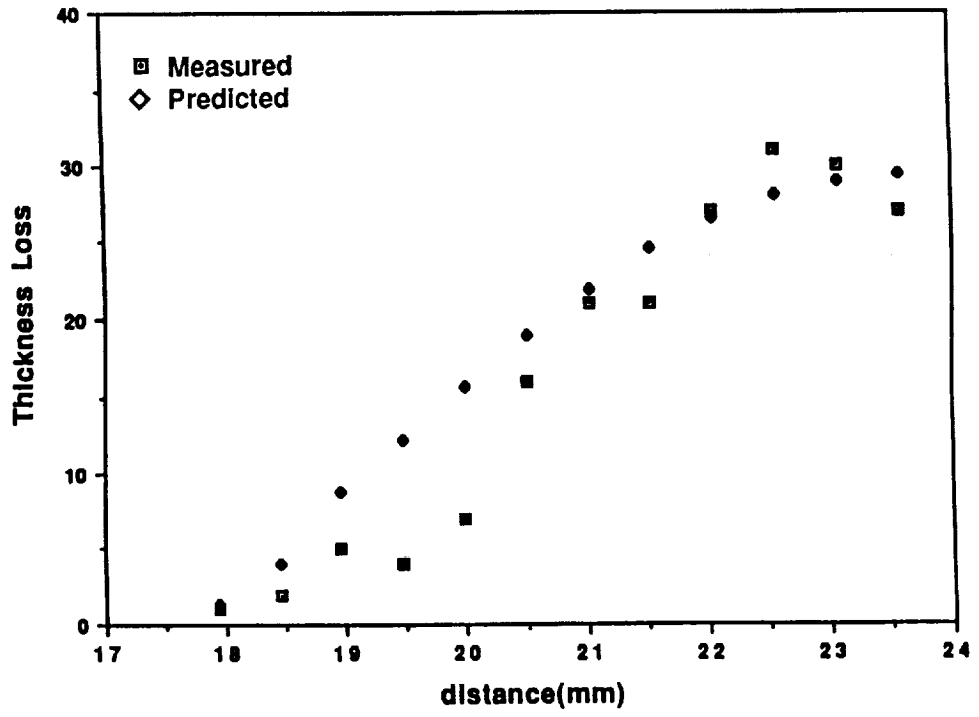
**Measured and Predicted Thickness Loss
FEP from B7 near strap**



**Predicted and Measured Thickness Loss
FEP from D-11 Blanket**

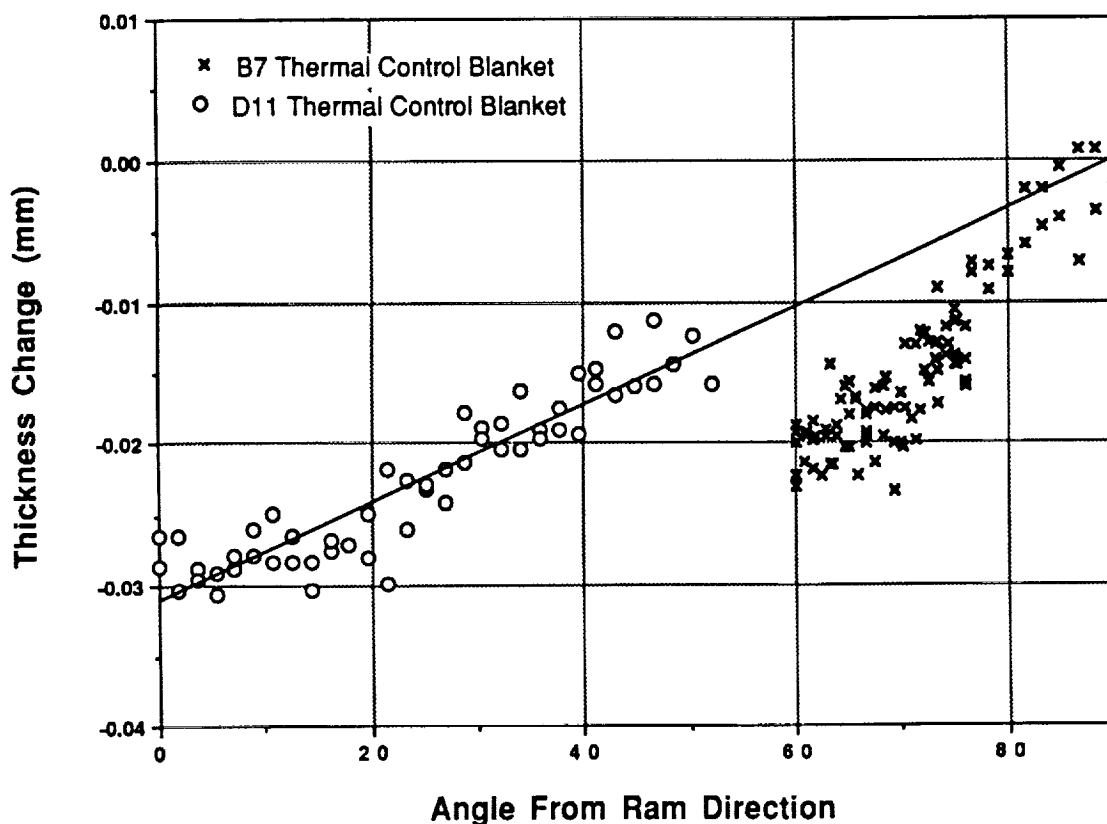


Measured and Predicted Thickness Loss FEP from D-11



Fits of mass loss vs apparent angle show the data from D11 is consistent with our fluence determinations and our recession measurements from the exposed areas of the blanket surfaces. The fact that the B7 results do not lie along this line indicates that the actual angles for these specimens are not so well defined. However, these results can be improved from repeat measurements using specimens from both edges of blankets from rows 11, 10, 8, and 7, and possibly from material from the edge of row six nearest row seven. Adhesive backed FEP tape on brackets from the McDonnell-Douglas experiment on row nine offer well defined angles since the tape is mounted to aluminum. Tape from areas on the space end of LDEF and on portions of the A0069 experiment on row nine also provide FEP exposures through well defined ranges of angles with respect to ram.

Mass Loss vs. Apparent Angle



CHARACTERIZATION OF SELECTED LDEF - EXPOSED POLYMER FILMS AND RESINS

Philip R. Young and Wayne S. Slemp
NASA Langley Research Center
Hampton, VA 23665-5225

INTRODUCTION

The National Aeronautics and Space Administration's Long Duration Exposure Facility (LDEF) provided a unique environmental exposure of a wide variety of materials (1,2.) The effects of 5 years and 10 months of Low-Earth Orbit (LEO) exposure of these materials to atomic oxygen, ultraviolet and particulate radiation, meteoroid and debris, vacuum, contamination, and thermal cycling is providing a data base unparalleled in the history of space environment research. Working through the Environmental Effects on Materials Special Investigation Group (MSIG), a number of polymeric materials in various processed forms have been assembled from LDEF investigators for analysis at the NASA Langley Research Center. This paper reports the status of on-going chemical characterization of these materials.

CHARACTERIZATION OF SELECTED LDEF-EXPOSED POLYMER FILMS AND RESINS

The longer missions being envisioned for the U.S. Space Program are placing increased demands on materials, particularly non-metallic materials. The objective of the current work is to assess the response of selected polymeric materials to the extended LEO environment provided by LDEF. The approach has been to characterize molecular level effects in addition to more obvious visual, physical and mechanical effects. This approach should provide fundamental information for use in developing new and improved materials for long-term LEO missions.

- PROBLEM:** Inadequate knowledge of space environmental effects on materials for long duration application.
- OBJECTIVE:** Assess the response of selected polymeric materials to extended exposure to the low earth orbit.
- APPROACH:** Characterize the molecular level effects of long term exposure to space as well as visual, physical and mechanical effects.
- BENEFIT:** Fundamental information for use in developing new and improved materials for LEO missions.

OUTLINE

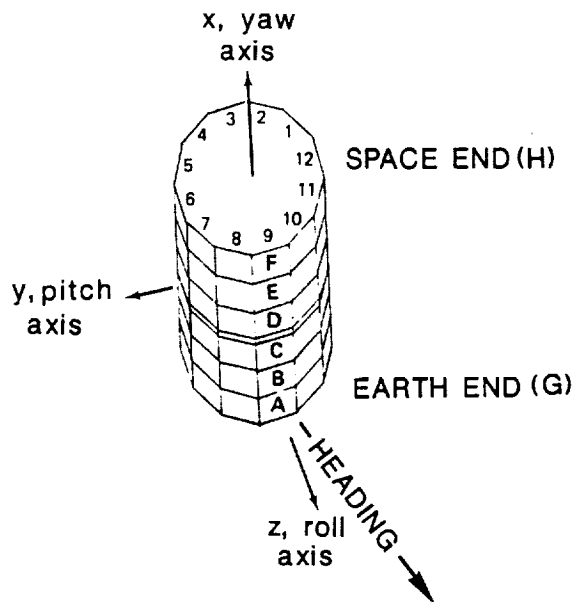
This presentation discusses several types of polymers that have either been examined, are currently being examined, or are awaiting examination. It focuses on reporting recent experimental results. For the first time, initial results from the characterization of specimens which flew inside a Row 9 Environmental Exposure Control Canister (EECC) and received only 10 months of exposure are discussed. The potential effects of the ubiquitous LDEF contamination on the performance of selected polymeric materials is presented. Finally, the possibility that some specimens may continue to change or exhibit post exposure effects is proposed.

- **Polymeric Materials**
- **Recent Experimental Results**
- **Contamination Effects on Materials**
- **Post-Exposure Effects**

LDEF SKETCH AND ORBITAL ORIENTATION

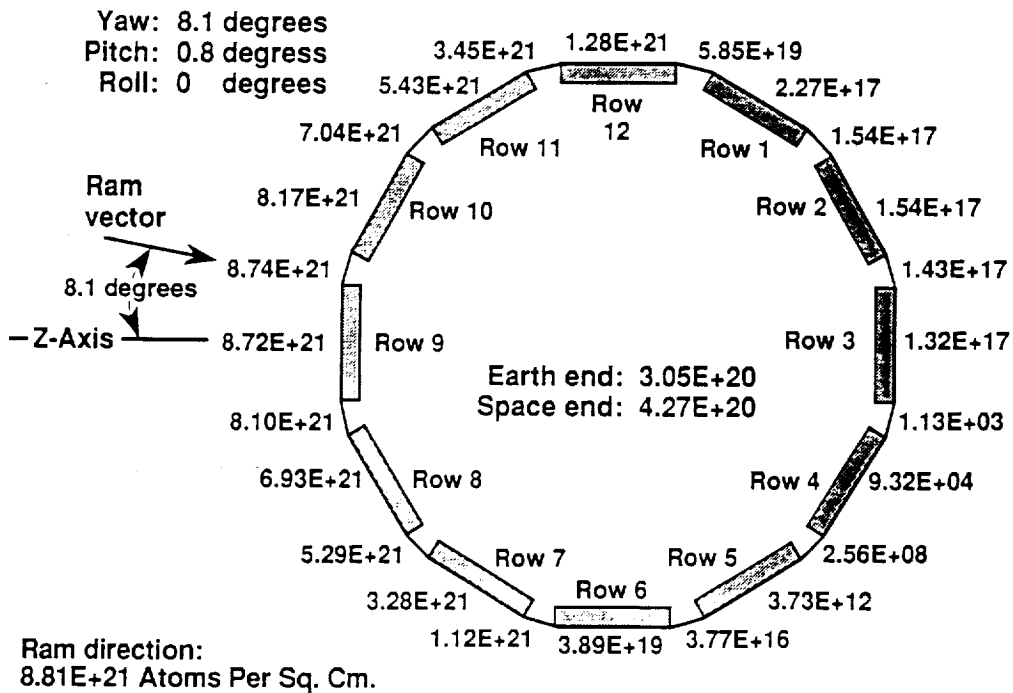
A sketch of the LDEF structure and orbital orientation is depicted in the figure. As described in Reference 1, the spacecraft was 30 feet long, 14 feet in diameter, and had 12 sides or rows with 6 experiment trays per row. One end of the gravity gradient stabilized vehicle faced space and one end faced Earth. Additional experiment trays were mounted on the space and earth ends.

Rows are numbered 1 through 12 in the figure and trays are lettered A through F. Thus, the location of specimens discussed in this report should follow from this tray and row notation scheme. For example, B9 denotes the location of specimens on Tray B at Row 9. The orbital orientation of the satellite was such that Row 9 nominally faced the RAM direction and Row 3 faced the WAKE direction. Recent LDEF supporting data analysis have determined that the actual RAM direction was 8° of yaw from the perpendicular to Row 9, in the direction of Row 10.



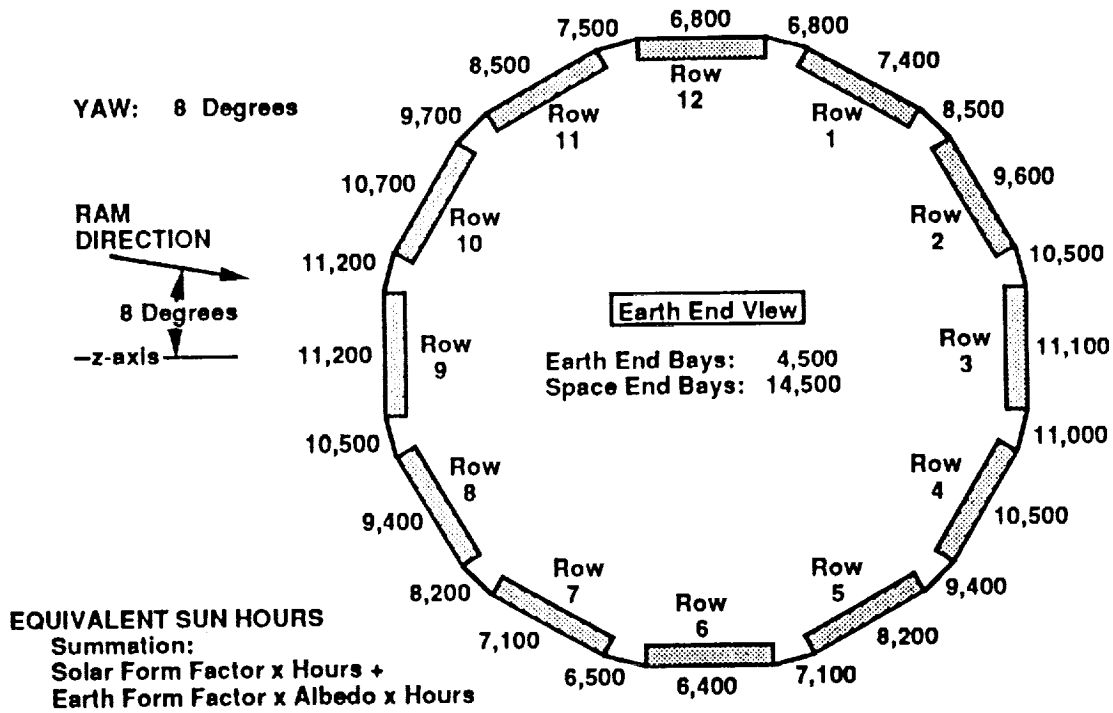
ATOMIC OXYGEN FLUENCE AT EACH LDEF TRAY

LDEF provided a very stable platform for LEO exposure of materials. The environment a specimen experienced depended on its location on the vehicle. Two significant environmental effects of concern for polymeric materials are atomic oxygen (AO) and ultraviolet (UV) radiation. The total AO fluence and equivalent UV sun hours for each LDEF row and tray have been determined by MSIG under NASA Contracts NAS1-18224 and NAS1-19247 entitled "LDEF Materials Analysis" with Boeing Defense and Space Group, Seattle, WA. The figure gives the AO fluence at end of mission for all row, longeron, and end bay locations, including the fluence received during the retrieval attitude excursion.



CUMULATIVE EQUIVALENT SUN HOURS AT END OF MISSION

Cumulative equivalent sun hours for all row, longeron, and end bay locations are given in the figure. The materials discussed in this report were exposed to additional space environmental effects. The particulate radiation (p^+ , e^- , cosmic), micrometeoroid and debris, and thermal cycling environments experienced by LDEF during approximately 34,000 orbits may be found in Reference 3. A discussion of various contamination issues may also be found in Reference 3.



POLYMERIC MATERIALS

Materials included in this study are listed in the figure. They were assembled from a number of LDEF locations. Many came from Langley's materials experiment located at B9 (4). Several LDEF Principal Investigators have unselfishly and generously made specimens from their experiments available to the authors.

The characterization of materials listed at the top of the figure is essentially complete. Results of this characterization have been summarized in a number of reports (5-9.) These reports contain experimental information describing how specimens were analyzed. The examination of materials at the bottom of the figure is in progress or is pending.

At first glance, only about one-fourth of this study appears to be complete. However, knowledge gained during the characterization of the initial specimens is useful as an aid in expediting the analysis of remaining specimens, thus, reducing the time required to complete that task. Where possible, future work will emphasize various solution property measurements of molecular weight and molecular weight distribution.

Characterization Complete or In-Progress

Silvered FEP Teflon
FEP Teflon
P1700 polysulfone
PMR-15
5208/934 Epoxy
Kapton
Polyimide-Polysiloxane Copolymer

Source: LDEF MSIG (various LDEF locations) and Expts. A0134/S0010
(W. Slemp)

Characterization Pending

Polystyrene
Polyvinyl toluene
Polytetrafluoroethylene
Polymethylmethacrylate
Nylon
Polyethylene terephthalate
Kapton

Source: J. Gregory, P.I.
Expt: A0114 (C9/C3)

Polyethylene terephthalate
Polyurethane
Various silicones
Kevlar
Teflon

Kapton

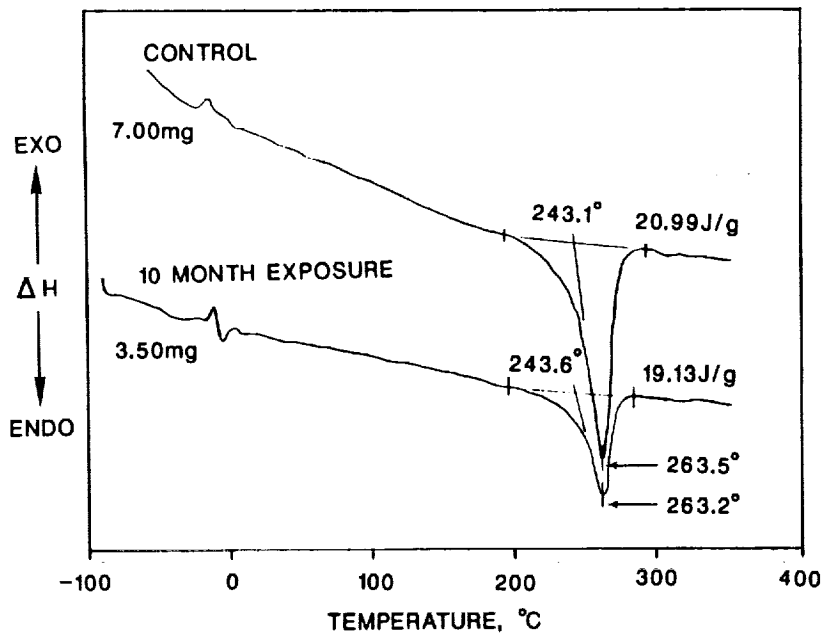
Source: A. Whitaker, P.I.
A0171 (A8)

BTDA-ODA
6F-DDSO₂
6F-BDAF
PMDA-DAF
FEP Teflon
Kynar
Kapton

Source: W. Slemp, P.I.
S0010 (B9)

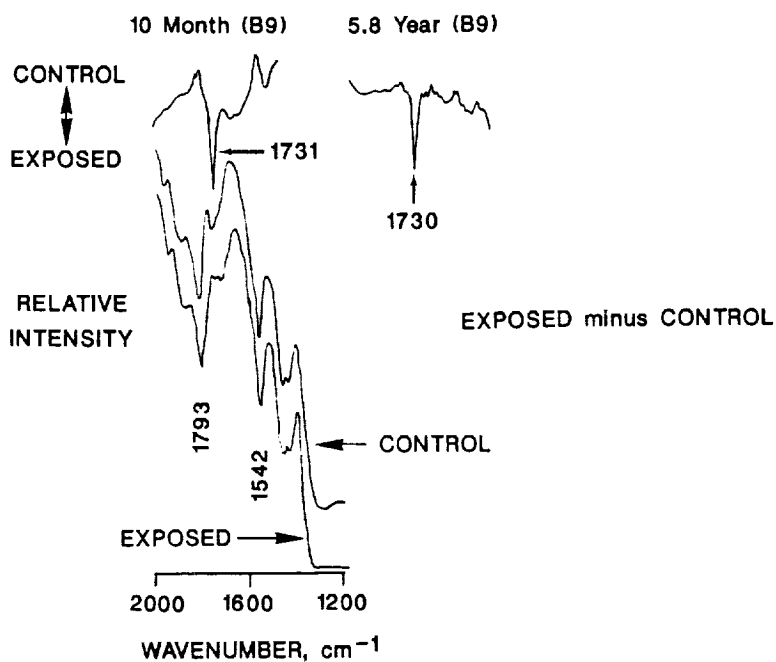
DSC THERMOGRAMS OF FEP TEFLON SPECIMENS

The 5.8-year exposure of silvered FEP Teflon thermal blankets on LDEF has been the subject of considerable research (3,8,10.) We have examined FEP specimens which received only the 10-month exposure provided by the EECC. The approximate AO fluence and equivalent sun hours experienced by these 10-month B9 specimens are 2.6×10^{20} atoms/cm² and 2,300 hours, respectively. Differential Scanning Calorimetry (DSC) thermograms of 10-month specimens are virtually superimposable over thermograms of control specimens. No significant differences were noted in low-temperature transitions, the melt point, or the heat of fusion associated with that melt. This was essentially the same conclusion derived from DSC analysis of 5.8-year FEP specimens.



DR-FTIR SPECTRA OF LDEF-EXPOSED FEP TEFLON

Standard transmission and diffuse reflectance spectra of exposed 10-month and 5.8-year FEP specimens do not exhibit interpretable differences when compared with control spectra. This suggests there are no gross differences in molecular structure of the FEP polymer backbone as a result of exposure. However, subtractive techniques reveal a weak new band around 1730 cm^{-1} in the spectrum of exposed film. This band is most likely due to the formation of carbonyl as a result of exposure to AO. It may be associated with UV-induced crosslinking of the FEP surface documented in another publication (10). The 1730 cm^{-1} carbonyl band, found in several LDEF FEP specimens, is considered to be primarily a surface phenomenon.



XPS ANALYSIS OF FEP TEFLON FILMS

X-ray photoelectron spectroscopic (XPS) analyses of two control FEP Teflon films, two 10-month specimens, and a 5.8-year specimen located at B9 are summarized below. The carbon 1s photopeaks for all samples were virtually superimposable. Multiple carbon 1s peaks associated with a crosslinked FEP surface were absent. Thus, we conclude that VUV exposure of these films was either insufficient to crosslink the surface, or that atomic oxygen had eroded the crosslinked surface away. A decrease in the CF₃:CF₂:CF ratio from 1:5:1 for control FEP to 1:4:1 after 5.8 years of exposure was noted (11).

The small amount of oxygen detected in samples after exposure probably correlates with the carbonyl discussed in the previous figure. No silicon was detected in these particular specimens. Thus, the observed oxygen was not likely associated with contamination.

PHOTOPEAK	CONTROL		10-MONTH EXPOSURE		5.8 YEAR
	SAMPLE 1	SAMPLE 2	SAMPLE 1	SAMPLE 2	
C 1s B.E. ^a (eV)	291.7	290.9	291.8	290.9	290.2
	A.C. ^b (%)	32.0	31.3	32.9	30.8
F 1s B.E. (eV)	689.1	688.6	689.3	688.4	688.6
	A.C. (%)	67.7	68.7	66.7	68.7
O 1s B.E. (eV)	--	--	--	532.5	532.2
	A.C. (%)	NSP ^c	NSP	NSP	0.5
Si 2p B.E. (eV)		--		--	--
	A.C. (%)		NSP	NSP	NSP

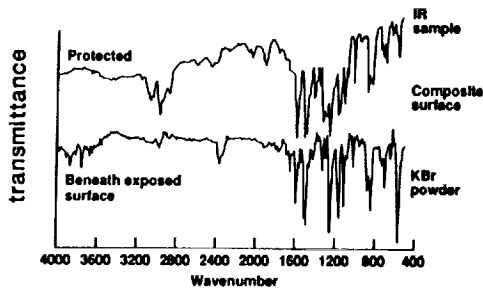
- ^a Binding Energy.
- ^b Atomic Concentration.
- ^c No Significant Peak.

LDEF - EXPOSED COMPOSITE MATERIALS

Considerable effort went into characterizing various graphite fiber reinforced polymer matrix composite materials which received 5.8 years of exposure on a Row 9 experiment (4). Since several reports have focused on these composites (5-7), only results pertinent to the present study are summarized here.

The figure gives infrared spectra, glass transition temperature, and molecular weight distribution results obtained on a series of polysulfone matrix composites. No significant differences were noted at the molecular level in these materials as a result of exposure, a general finding that also applied to epoxy matrix composites. However, the loss of about one 5 mil ply of the 4 ply composites, attributable to AO erosion, was noted. This apparently was a major contributor to the decrease in selected mechanical properties observed with exposure.

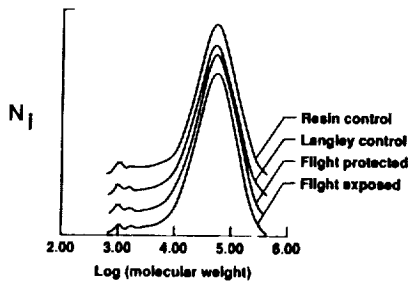
INFRARED SPECTRA



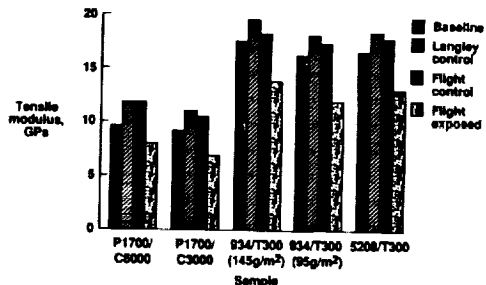
GLASS TRANSITION TEMPERATURE

Sample	Tg (°C)	Contacted Side
Langley Control	167°	Random
	167°	
	170°	
	166°	
Flight Protected	164°	Side A
	166°	Side B
Flight Exposed	170°	Exposed side
	171°	
	169°	Nonexposed side
	171°	

MOLECULAR WEIGHT DISTRIBUTION



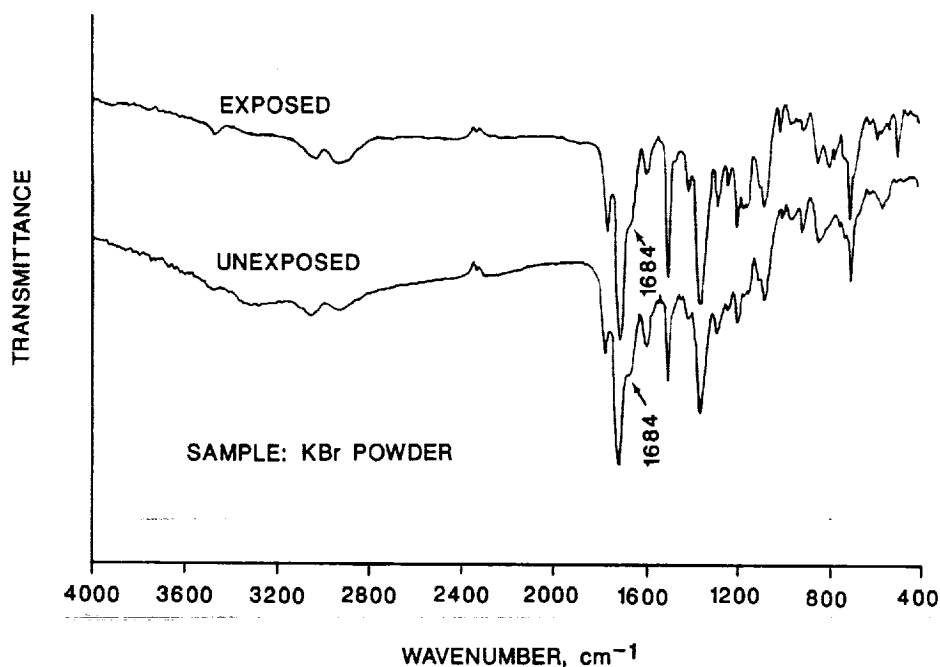
MECHANICAL PROPERTIES



DF-FTIR SPECTRA OF PMR-15/C6000 LDEF COMPOSITES

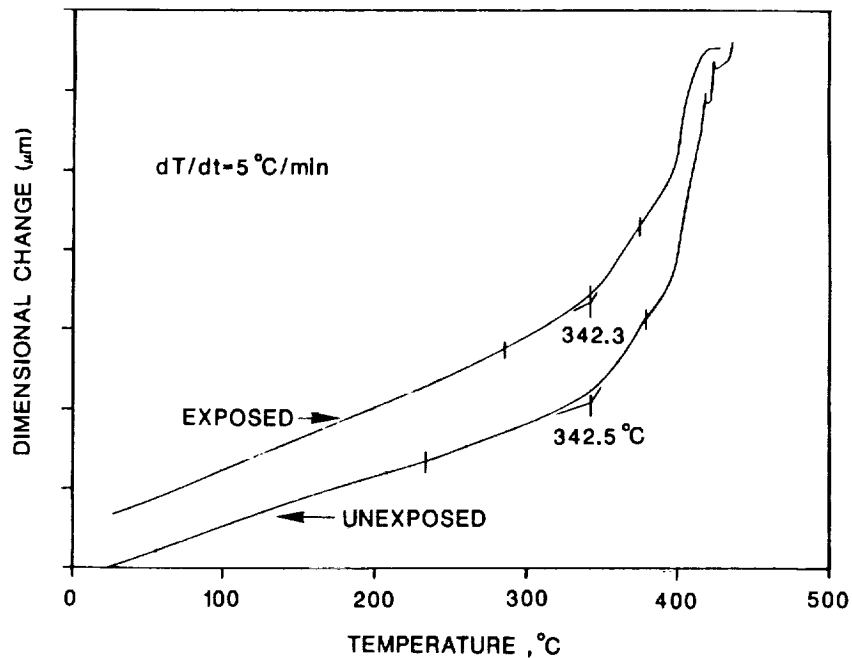
A PMR-15/C6000 composite specimen which flew on an LDEF Row 7 experiment was provided for analysis by Richard F. Vyhna, Rockwell International, Tulsa, OK. AO and UV exposure parameters for this sample can be derived from previous figures. Diffuse reflectance - FTIR spectra of exposed and protected areas of this composite are shown in the figure. The spectra are virtually identical.

A new band at 1667cm^{-1} had been anticipated in the spectrum of the exposed surface. The presence of that band would have meant that methylene groups in the amine portion of the addition end-capped polyimide resin had oxidized to carbonyl (12). The 1667cm^{-1} band is missing. The shoulder at 1684cm^{-1} is associated with the dianhydride carbonyl portion of the polymer backbone.



TMA OF PMR - 15/C6000 LDEF COMPOSITES

The PMR - 15/C6000 composite specimen from Row 7 was also examined by Thermal Mechanical Analysis (TMA) in the expansion mode. For the analysis, a probe is placed in contact with the composite surface. The temperature of the specimen is then increased, and any displacement in the probe is carefully noted. The inflection at 342°C in the curves for unexposed and exposed samples is indicative of the glass transition temperature (T_g) of the matrix resin. Since 342°C is an acceptable T_g for properly cured PMR - 15 (13), we conclude that the T_g of this material was not affected by 5.8 years of exposure. However, AO induced resin loss was noted with this specimen.

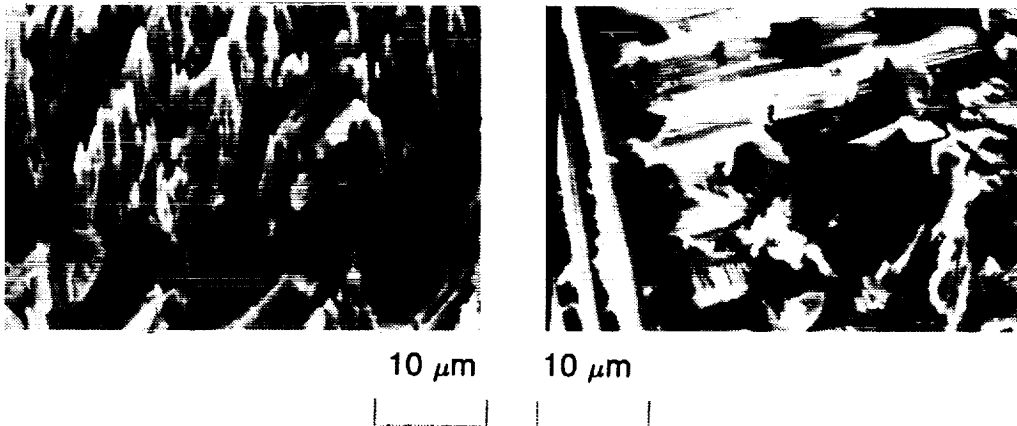


C-5

SEM OF LDEF - EXPOSED 5208/T300 COMPOSITE

As previously discussed, we have found no significant differences in matrix resin chemistry in composites which survived 5.8 years of exposure. Any molecular level changes resulting from exposure must have been lost in the layer of materials eroded away by atomic oxygen. The scanning electron microscope (SEM) analysis of a Row 9 5208/T300 epoxy specimen is shown in the figure. The loss of both resin and fiber are apparent in the figure, as are cracks in fibers. Resin/fiber content measurements show greater than 10% resin loss in Row 9 composites. Microscopic analysis shows that the top ply of 4-ply specimens has been severely eroded. The SEM in this figure is typical of the behavior observed for other examined Row 9 composite specimens.

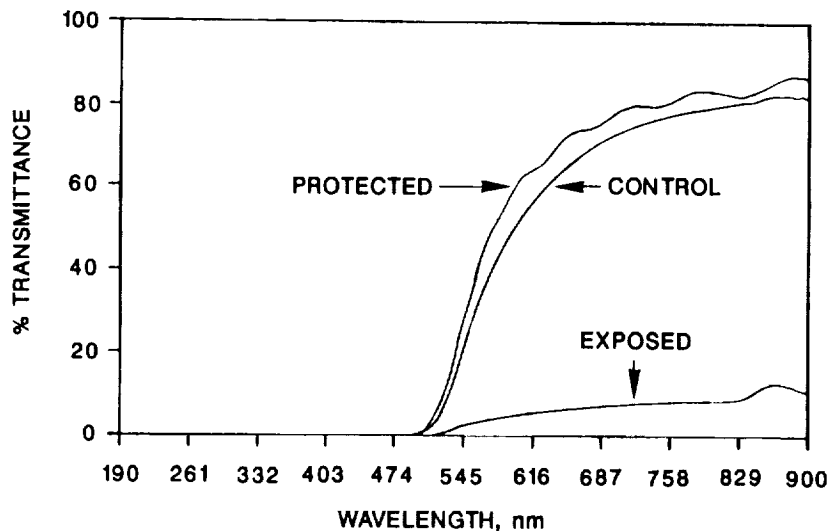
[±45]_s



UV - VIS SPECTRA OF LDEF - EXPOSED KAPTON FILM

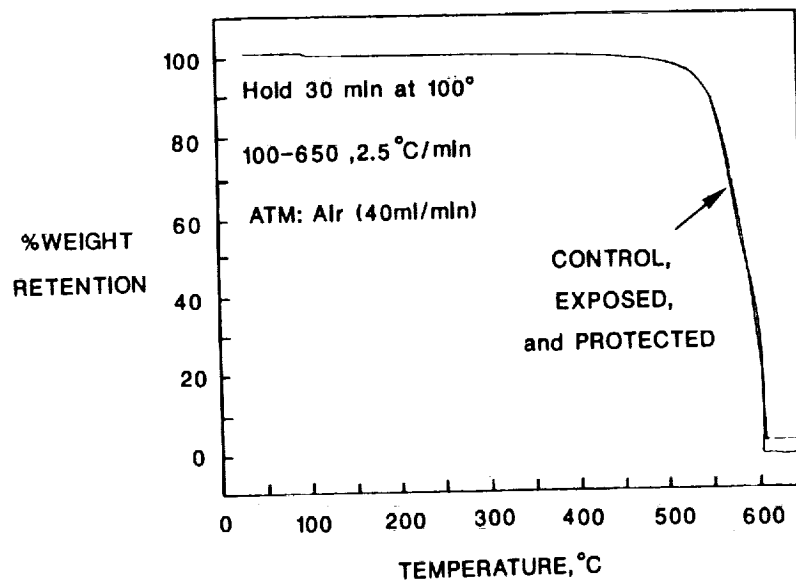
Several 5-mil Kapton film specimens which flew on the space end (H7) of LDEF and received 5.8 years of exposure were provided by James B. Whiteside, Grumman Aerospace Corporation, Bethpage, N.Y. AO and UV exposure for this location can be derived from previous figures. Due to their orientation in the experiment tray, AO exposure was perpendicular to the edge of the film and parallel to its surface. These specimens were of particular interest because of their unique AO and VUV exposure. They have been extensively studied by a variety of characterization techniques.

The figure shows UV-VIS transmission spectra of exposed film, film which flew protected from direct exposure, and a control film. No explanation is offered for slightly less transmission observed for the control specimen compared to the protected specimen. The significant decrease noted for the exposed specimen is attributed to UV degradation and AO-induced roughening of the surface. That surface exhibited a diffuse appearance.



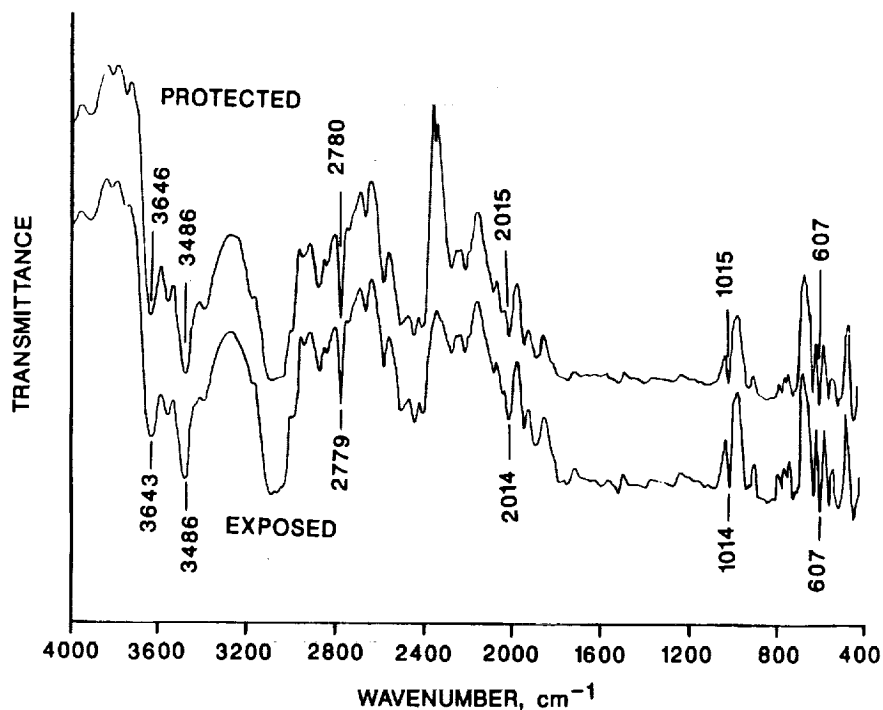
TGA OF LDEF - EXPOSED KAPTON FILM

Thermal gravimetric analysis (TGA) failed to differentiate between control, flight protected, and flight Kapton films exposed on the space end of LDEF. Weight loss curves for the three specimens were virtually superimposable. Perhaps isothermal TGA weight loss measurements, currently being performed, will detect a difference between the films.



DR - FTIR SPECTRA OF LDEF - EXPOSED KAPTON FILM

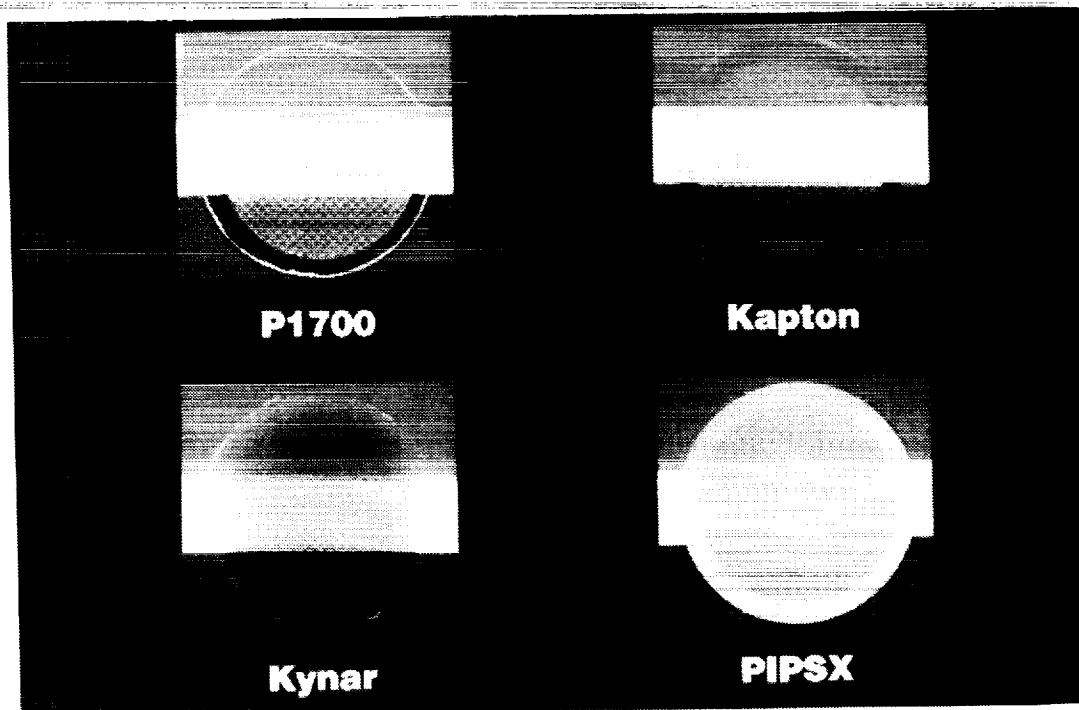
The 5-mil Kapton films from the space end of LDEF were too thick to be analyzed by standard transmission infrared techniques. Analysis by diffuse reflectance resulted in poor quality spectra. However, careful comparison of spectra in the figure reveal that no new peaks are formed as the result of exposure, no peaks are missing, and that there were no significant shifts in frequency of various bands. Thus, we conclude that the overall molecular chemistry of this polyimide has not changed as the result of exposure.



EFFECT OF 10 - MONTH LDEF EXPOSURE ON FOUR POLYMER FILMS

An analysis is in progress on several films which flew inside an EECC and received 10 months of exposure at LDEF location B9. This exposure occurred early in the LDEF flight when AO fluence was at a minimum. A photograph of four of these films is shown in the figure. Approximately 1-inch diameter films were held in place by an aluminum template with machined 0.81 inch diameter holes.

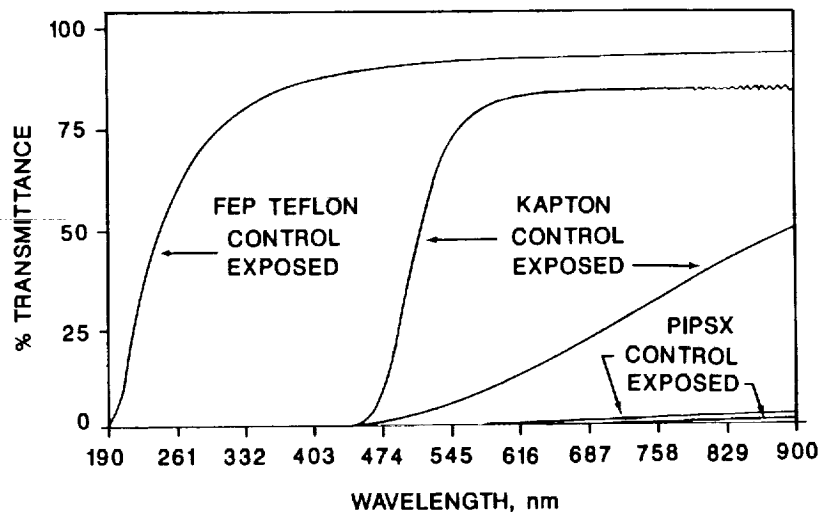
Exposed and template - protected areas are apparent in the photograph. P1700, Kapton, and Kynar are commercially available polysulfone, polyimide, and poly (vinylidene fluoride) materials. PIPSX is an experimental polyimide-polysulfone copolymer synthesized under NASA Grant NAG-1-343 with Virginia Tech.



UV-VIS SPECTRA OF 10-MONTH EXPOSED FILMS

UV-VIS spectra of three of the 10-month exposed B9 films are shown in the figure. No change was noted for the FEP Teflon film; spectra for control and exposed specimens were superimposable. The transmission of the Kapton film decreased significantly after exposure. This behavior was observed previously with Kapton from the space end of LDEF. The transmission of the opaque PIPSX film was minimal below 900 nm for both control and exposed specimens.

Research in progress on canister films is revealing molecular level effects not apparent in similar materials after 5.8 years of exposure. For example, subtractive DR-FTIR techniques show new bands in the spectrum of polysulfone film indicative of chain scission. Solution property measurements also suggest a change in selected molecular weight parameters as a result of exposure. Complete results of this research will be reported at a future date.



SEM OF POLYIMIDE - POLYSILIXANE COPOLYMER

The evidence emerging from the investigation of most polymeric materials which flew on LDEF suggests that there are no gross changes in chemistry as a result of exposure. This conclusion is based on various infrared, thermal, XPS, and solution property measurements. The subtle differences which are observed are primarily surface effects. However, substantial changes are often noted in physical and mechanical properties.

At least one material, an experimental polyimide-polysiloxane copolymer, which flew on a B9 experiment, did exhibit a significant change in chemistry after only 10 months of exposure. The figure shows SEM photomicrographs of unexposed and exposed film. A two-phase morphology is apparent. Regions that were light in appearance before exposure became dark after exposure, and dark areas became light. These two phases may have contained different amounts of the two copolymer segments which responded differently to AO exposure.

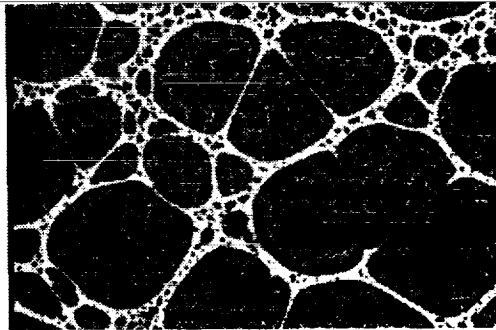
10 months of exposure

200 μm



Unexposed

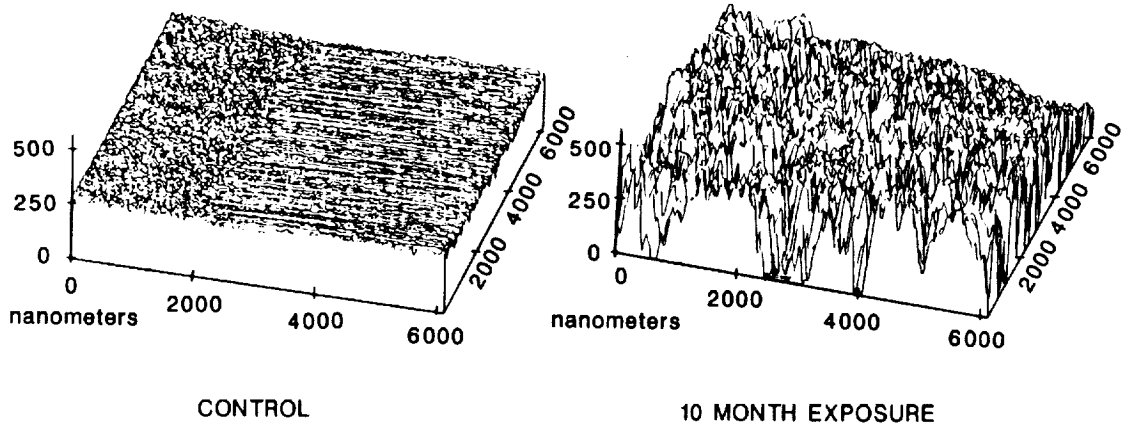
200 μm



Exposed

STM ANALYSIS OF POLYIMIDE-POLYSILOXANE COPOLYMER

Scanning tunneling microscopy (STM) analysis of control and exposed copolymer films shows considerable roughening of the surface after 10 months of flight time. Much of this roughening is assumed to be due to attack by atomic oxygen. The STM analysis of FEP teflon and Kapton film exposed for 10 months did not exhibit this type of behavior.



XPS ANALYSIS OF POLYIMIDE-POLYSILOXANE COPOLYMER

XPS analysis gave anticipated results for this copolymer. The figure summarizes data for control and exposed specimens. A 21.6% atomic concentration of silicon is noted for the control. The 102.2 electron volt binding for that sample suggests that the silicon is present as an organic silicone, as it should be. After 10 months of exposure, the surface concentration of silicon had risen to 30.8%. The 103.4eV binding energy is that of an inorganic silicate.

Atomic oxygen appears to have eroded the surface of this material to expose silicon atoms, which were then oxidized to a silica/silicate-like structure. AO has been shown to oxidize silicones to silicates (14). Further, silicates are known to be effective barriers to AO erosion (5,14,15). The behavior exhibited by this material suggests the possibility of designing AO protection into the molecular structure of selected polymers. Two additional polyimide-polysiloxane copolymers which received exposure on LDEF are currently undergoing analysis.

PHOTOPEAK	CONTROL	EXPOSED ^a
C 1s B.E. ^b (eV)	284.7	284.6
A.C. ^c (%)	54.4	16.8
O 1s B.E. (eV)	532.5	533.0
A.C. (%)	23.7	52.4
N 1s B.E. (eV)	--	--
A.C. (%)	NSP ^d	NSP
Si 2p B.E. (eV)	102.2	103.4
A.C. (%)	21.6	30.8

- ^a 10-Month Exposure.
- ^b Binding Energy.
- ^c Atomic Concentration.
- ^d No Significant Peak.

XPS ANALYSIS OF LDEF-EXPOSED 934/T300 COMPOSITES

Silicon has been detected as a component in the ubiquitous contamination found on LDEF (3, 5, 8). While not found on all LDEF specimens, this occurrence probably complicates the interpretation of some materials results.

The XPS analysis of two side-by-side 5.8-year exposed epoxy composites located on a B9 experiment is given in the figure. One specimen had been intentionally coated with 1000Å of nickel followed by 600Å of silicon dioxide. The other specimen was uncoated. Note that almost as much silicon was detected on the sample that was not supposed to contain silicon as was found on the sample that was supposed to contain it. The silicon on the uncoated composite undoubtedly affected the manner in which the surface was attacked by atomic oxygen.

PHOTOPEAK	600Å SiO ₂ /1000Å Ni/COMPOSITE		UNCOATED	
	COVERED	EXPOSED ^a	COVERED	EXPOSED ^a
C 1s	65.1 ^b	28.9	62.8	54.3
O 1s	29.7	47.6	24.8	33.0
N 1s	—	—	3.4	5.2
Ni 2p	4.6	11.7	—	—
Si 2p	2.4	11.8	3.4	7.5
F 1s	—	—	2.0	—
S 2p	—	—	2.0	—
Na 1s	—	—	1.7	—

^a 5.8 year exposure.

^b Atomic Concentration, %.

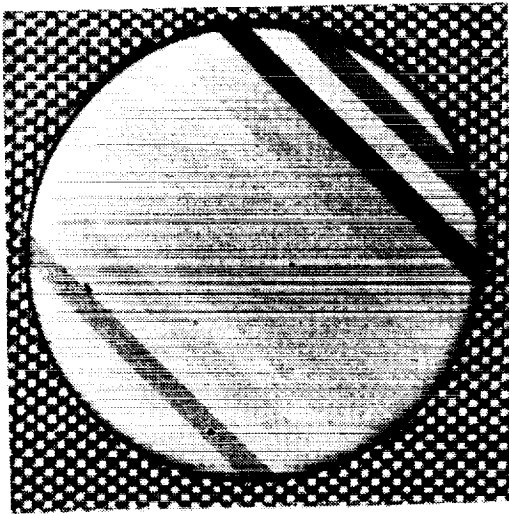
LDEF-EXPOSED 934/T300 EPOXY COMPOSITES

Photographs of the two B9 934/T300 composite specimens described in the preceding discussion are shown below. The thin SiO_2/Ni coating on the composite on the right appears to have been effective in protecting the surface from attack by atomic oxygen. The eroded area in the uncoated composite is apparent.

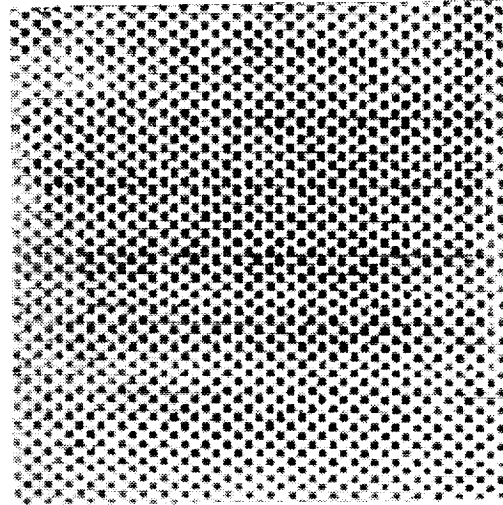
As previously noted, a small amount of silicon, presumably from contamination, was detected on the uncoated composite. This silicon probably provided some protection from atomic oxygen erosion. Thus, this specimen likely behaved differently than it would have behaved had it not been contaminated. The silicon-containing contamination no doubt caused some LDEF polymeric materials to erode less than would have been the case without contamination.

$(\pm 45)_s$, 5mil per ply

UNCOATED



600Å SiO_2 /1000Å Ni/COMPOSITE

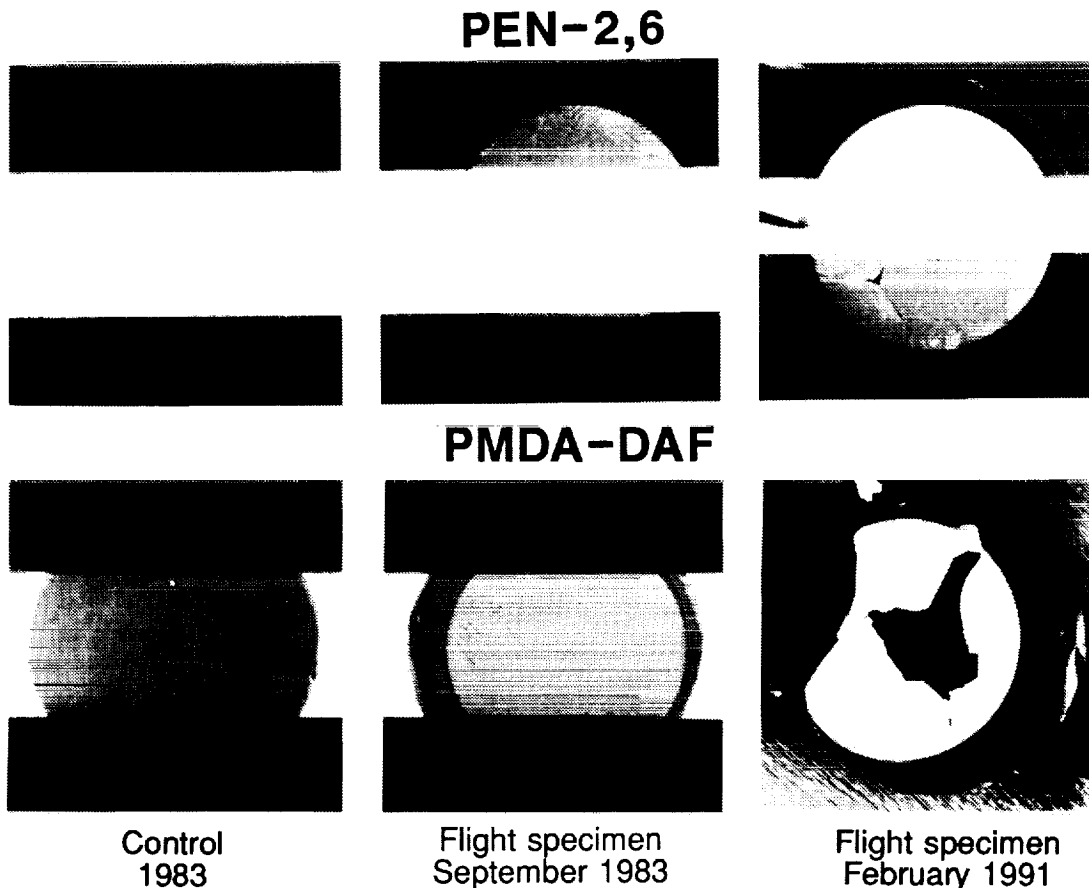


STS-8 EXPOSED POLYMER FILMS

The possibility that some polymeric materials which received exposure on LDEF may continue to degrade cannot be ignored. Environmentally exposed films and coatings have been qualitatively observed in this laboratory to change with time. An appreciation of this phenomenon may be necessary in order to analyze LDEF specimens in an efficient manner.

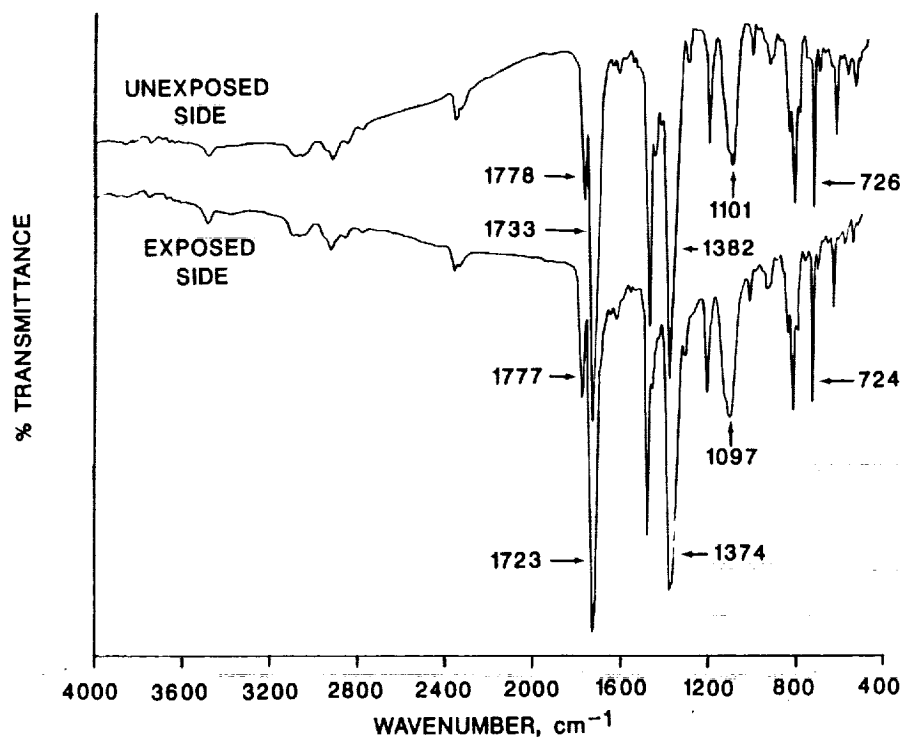
A series of thin films in a Langley experiment received 40 hours of LEO exposure in 1983 on-board STS-8 Challenger. Those films were photographed and characterized upon their return to Langley. In February 1991, the specimens were removed from a desiccator where they had been stored in tin containers. Two of four films had changed dramatically.

The figure shows photographs of control and flight specimens taken in 1983 and repeat photographs taken in 1991. PEN-2,6 shown at the top of the figure, is a state-of-the-art polyester designed to exhibit improved radiation stability (16). The film had cracked and turned opaque during storage. PMDA-DAF, shown at the bottom, is an experimental polyimide expected to exhibit unusual stability (17). That film turned opaque and lost much of its structural integrity.



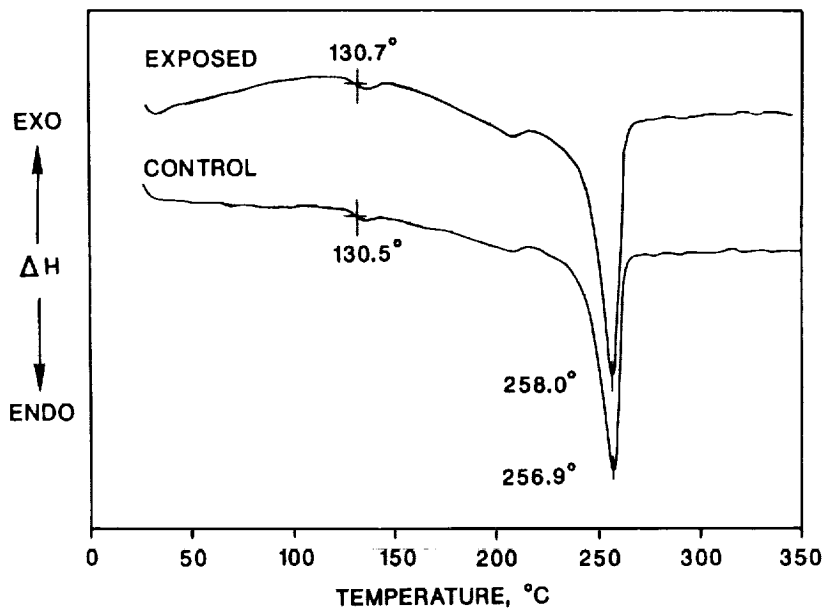
DR-FTIR SPECTRA OF STS-8 PMDA-DAF FILMS

While the physical appearance and mechanical properties of the two films had clearly deteriorated, chemical analyses to date have shown little difference between exposed and control specimens. The figure gives DR-FTIR spectra for the PMDA-DAF film. The spectra of both sides are essentially the same except for slight shifts in the absorption of five imide-related bands noted in the figure. These frequency shifts have not been interpreted but similar shifts in imide-related bands have been observed in this laboratory for polyimides that were not exposed to space.



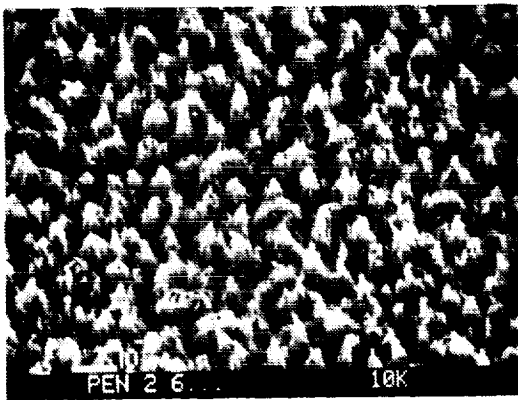
DSC THERMOGRAMS OF STS-8 PEN-2,6 FILM

DSC thermograms of exposed and control PEN-2,6 polyester film are shown below. No real differences are noted in the T_g , T_m , or the heat of fusion associated with the melt. X-ray diffraction also failed to detect a change in crystallinity in the exposed film. Thus, the increased opaqueness with age was not likely due to crystallinity effects. FTIR spectra failed to show differences in these specimens.



SEM OF STS-8 EXPOSED PEN-2,6 FILM

The figure shows the 1983 SEM analysis of the exposed polyester film, and a repeat SEM analysis conducted in November 1991. The two photomicrographs are surprisingly similar. A detailed SEM study of both the PEN-2,6 and PMDA-DAF films failed to explain the appearance of aged flight specimens. XPS analyses to date have also been inconclusive. Hopefully, pending solution property measurements on the polyester film will show differences in molecular weight and molecular weight distribution. Such an result would help explain why the films cracked. The observations made on STS-8 films keynote the urgent need to analyze non-metallic LDEF materials in an expedient manner.



1983 ANALYSIS

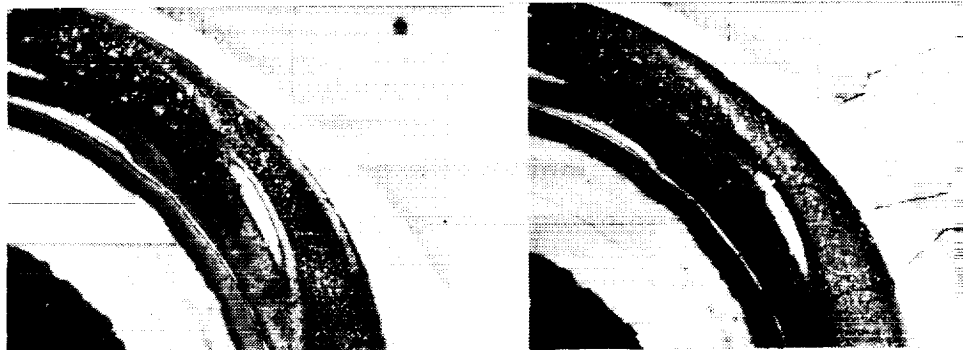


1991 ANALYSIS

MICROMETEOROID IMPACT ON Ag/FEP TEFLON THERMAL BLANKET

Selected LDEF specimens may be changing in appearance with time. A micrometeoroid impact on a Row 11 thermal blanket was photographed under magnification in April 1990, shortly after the analysis of LDEF materials began. That photograph is shown below on the left. The same area was photographed again under the same magnification in November 1991. The photograph on the right shows that cracks in the vapor deposited silver have continued to form on the silvered side of the thermal blanket material. Cracks that were present in 1990 appear to have intensified with age. The overall appearance tends to be duller.

(X100)



April 1990

November 1991

POST EXPOSURE EFFECTS FRONT COVER-LDEF THERMAL CONTROL SURFACES EXPERIMENT

J. M. Zwiener of the Marshall Space Flight Center provided two photographs taken one year apart of the front cover of the Row 9 Thermal Control Surfaces Experiment (S0069). The photographs were taken under similar lighting, angle, and distance considerations. The silvered FEP Teflon covered panel had changed in visual appearance during the year in which it was stored under prudent laboratory conditions. The diffraction patterns visible in the upper left-hand corner of the 1990 photo are real. They are not present in the 1991 photo. Brownish streaks in the coating had also intensified with age.

(S0069)



March 10, 1990

March 14, 1991

Source: J. M. Zwiener
NASA-MSFC

POSSIBLE ORIGIN OF POST-EXPOSURE EFFECTS

These distressing observations, combined with others that have been orally reported within the LDEF community, highlight the urgent need to analyze polymeric LDEF materials in an expedient manner. Otherwise, valuable information may be obscured and, in some instances, incorrect or biased interpretations may result.

Among the possible origins of these effects are residual free radicals, embrittled surfaces due to crosslinking, and unbalanced stress due to AO erosion of one film surface and not the other. Increased sensitivity to oxidation, hydrolysis, or light may be difficult to quantify. A decrease in molecular weight is considered to be a major factor contribution to the loss of structural integrity of the STS-8 films. The general area of post-exposure effects is being pursued under NASA Research Grant NAGW-2495 with the University of Queensland, Queensland, Australia.

- **Residual Free Radicals**
- **Decrease in Molecular Weight**
- **Crosslinking Embrittleness**
- **Increased Sensitivity to Oxidation and/or Hydrolysis**
- **Increased Sensitivity to Light**
- **Unbalanced Stress (Due to Surface Erosion)**

SUMMARY

The LDEF is providing a wealth of information on extended LEO exposure of selected polymeric materials. While dramatic visual effects and AO-induced resin loss have been observed, no significant change at the molecular level in many surviving polymers has been found. Due to minimum AO fluence, 10-month canister samples may exhibit surface effects not present in 5.8-year exposed samples. Potential molecular level effects with 5.8-year samples attributable to exposure have probably been eroded away by atomic oxygen .

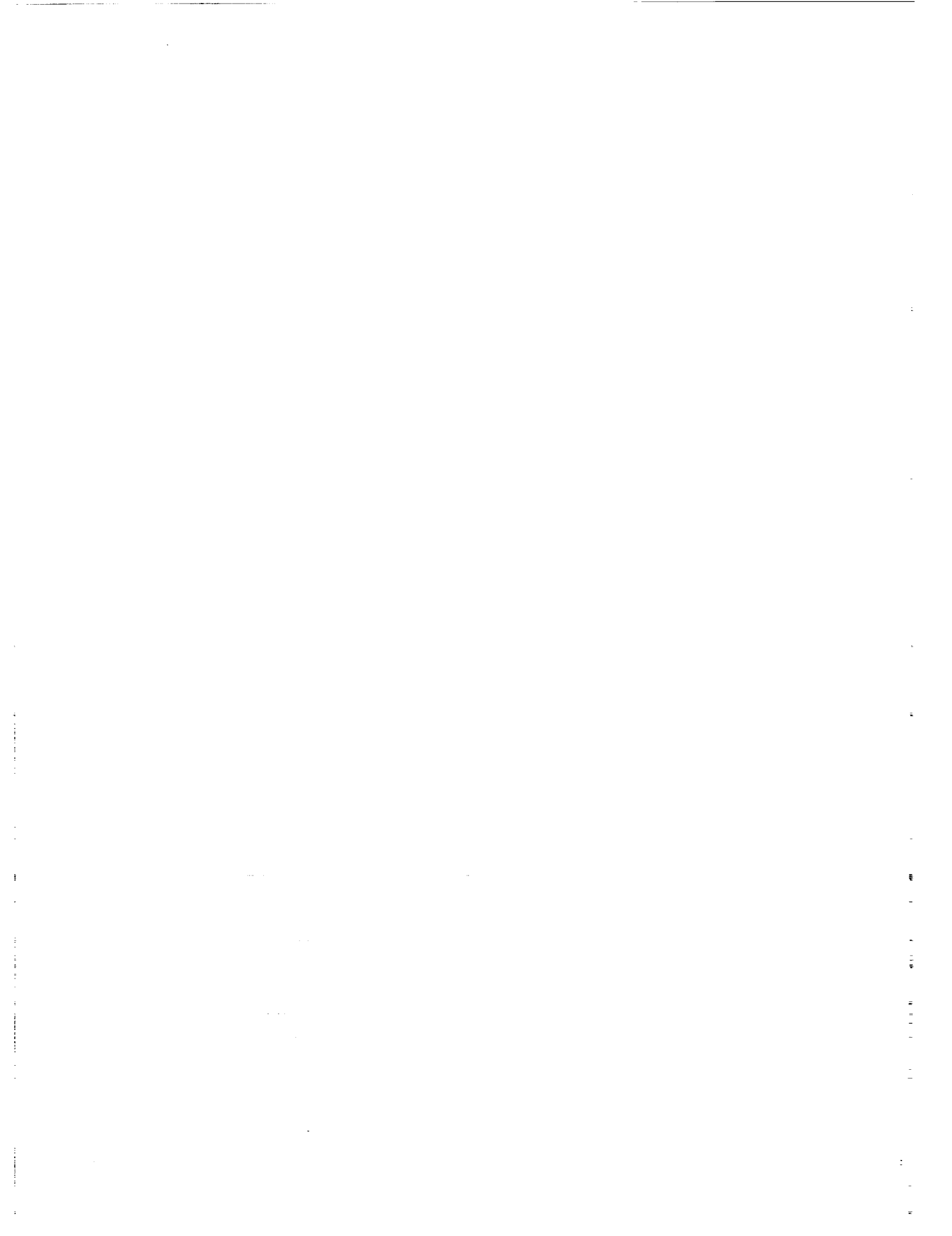
The role that silicon in the molecular contamination can play on AO erosion rate needs to be quantified. Further, the possibility that selected specimens may continue to degrade must be appreciated. The ultimate benefit of continued LDEF-related materials research will be analytical information leading to the synthesis and development of new materials with long-term durability in the LEO environment.

LDEF is providing a wealth of information on extended LEO exposure of polymeric materials.

- **Dramatic visual effects and AO-induced resin loss.**
- **No significant change at the molecular level in many surviving polymers.**
- **Molecular contamination may bias environmental exposure results.**
- **Some specimens may continue to degrade.**

REFERENCES

1. L. G. Clark, W. H. Kinard, D. J. Carter, and J. L. Jones, ed.; The Long Duration Exposure Facility (LDEF). NASA SP-473, 1984.
2. B. A. Stein and P. R. Young, compilers; LDEF Materials Data Analysis Workshop. NASA CP-10046, 1990.
3. LDEF-69 Months in Space First Post Retrieval Symposium. NASA CP 3134 (1991).
4. W. S. Slemp, NASA SP-43, 1984, pp. 24-26.
5. P. R. Young, W. S. Slemp, W. G. Witte, and J. Y. Shen; SAMPE Intl. Symp., **36(1)**, 403(1991).
6. P. R. Young and W. S. Slemp; in "LDEF-69 Months in Space First Post Retrieval Symposium," NASA-CP 3134, XXXX (1991).
7. W. S. Slemp, P. R. Young, W. G. Witte, and J. Y. Shen; *Ibid.*
8. P. R. Young and W. S. Slemp; NASA TM 104096, December 1991.
9. P. R. Young, W. S. Slemp, and C. R. Gautreaux; SAMPE Intl. Symp., **37**, 159, (1992).
10. A. E. Stiegman, D. E. Brinza, M. S. Anderson, T. K. Minton, E. G. Lave, and R. H. Liang; JPL Publication 91-10, May 1991.
11. NASA Grant NAG-1-1186, Interim Report V, Virginia Polytechnic Institute and State University, Blacksburg, VA.
12. P. R. Young and A. C. Chang; SAMPE Intl. Symp., **23**, 538(1988).
13. R. H. Pater; SAMPE Journal, Nov./Dec., 17 (1981).
14. M. J. Meshishnek, W. K. Stuckey, J. S. Evangelsides, L. A. Feldman, R. V. Peterson, G. S. Arnold, and D. R. Peplinski; Section 5-1 to 5-33, NASA TM 100459, Vol. II, 1988.
15. W. S. Slemp, B. Santos-Mason, G. F. Sykes, Jr., and W. G. Witte; Section 5-1 to 5-15, NASA TM 100459, Vol. I, 1988.
16. V. L. Bell and G. F. Pezdirtz; J. Sci. Polym. Chem. Ed., **21**, 3083(1983).
17. V. L. Bell; J. Polym. Sci. Polym. Chem. Ed., **14**, 225(1976).



**EFFECTS OF ORBITAL EXPOSURE ON HALAR
DURING THE LDEF MISSION**

William E. Brower, Jr., Harish Holla, and Robert A. Bauer
Department of Mechanical and Industrial Engineering
Marquette University
1515 W. Wisconsin Avenue
Milwaukee, Wisconsin 53233

ABSTRACT

Thermomechanical Analysis (TMA), Differential Scanning Calorimetry (DSC), and Thermogravimetric Analysis (TGA) were performed on samples of Halar exposed on the LDEF Mission for 6 years in orbit and unexposed Halar control samples. Sections 10-100 microns thick were removed from the exposed surface down to a depth of 1,000 microns through the 3 mm thick samples. The TMA and DSC results, which arise from the entire slice and not just its surface, showed no differences between the LDEF and the control samples. TMA scans were run from ambient to 300 C; results were compared by a tabulation of the glass transition temperatures. DSC scans were run from ambient to 700 C; the enthalpy of melting was compared for the samples as a function of section depth within the sample. The TGA results, which arise from the surface of the sample initially, showed a sharp increase in the topmost 50 micron section (the exposed, discolored side) in the weight loss of 170 C in oxygen. This weight loss dropped to bulk values in the range of depth of 50-200 microns. The control sample showed only a slight increase in weight loss as the top surface was approached. The LDEF Halar sample appears to be mechanically undamaged, with a surface layer which oxidizes faster as a result of orbital exposure.

INTRODUCTION

The first reports of the effects of prolonged orbital exposure by Whitaker (1) showed some weight loss data for a range of solar array materials. Tennyson et al (2) reported dimensional changes and changes in thermal expansion coefficients for a range of composite samples. B. J. Dunbar (3) reported on the general effects encountered by the LDEF samples - atomic oxygen, particle strikes, and UV exposure. Some of the Mylar 5 mil coatings were completely gone; this result gives added interest to the Halar and RTV studies of this investigation. Steckel and Le (4) were the first to report degradation as a function of depth in the sample, although their results were calculated from bulk weight loss data. The thrust of this investigation was to determine the depth profile of the damage to the Halar and RTV LDEF samples. Results for the Halar samples are reported here. Thermomechanical Analysis (TMA), Thermogravimetric Analysis (TGA), and Differential Scanning Calorimetry (DSC) were employed to assess the effects of orbital exposure during the LDEF Mission.

EXPERIMENTAL PROCEDURE

The procedure for preparing samples from the piece of LDEF exposed Halar and the Halar control is shown schematically in Figure 1. First, 1 cm x 1/4 cm pieces were cut from the full Halar pieces. These pieces were best suited for sectioning in the Edmund Model DK-10 microtome. Although the nominal minimum section thickness was 10 microns for the micrometer, the typical section was 50 microns thick. Wide variations in section thicknesses between sections and within a section occurred as shown in Tables 3-8,* due to bending of the microtome blade, play in the micrometer drive, and the inherent toughness of the Halar. Table 1 shows the dimensions of the samples that were cut from the fully exposed and control samples of Halar. The density, calculated from the measured volume and the measured weight of the cut samples, did not appear to vary between the exposed and the control. Piece

*Tables 1 through 8 are cited in text.

7 (exposed) did have a significantly lower density than the rest of the exposed sample and the control samples. It is hard to imagine such a sharp variation of density within the exposed sample of Halar. The test conditions during the various thermal analyses are given in Table 2. The heating rates were all the same, whereas the temperature range varied with the technique. TGA and DSC could be performed well above the glass transition temperature, but TMA could not. The TGA atmosphere was oxygen to assess oxidation rates.

RESULTS AND DISCUSSION

The results are presented for each technique by showing some thermograms, the output of the thermal analysis run. Tables of peak temperatures, peak integrals, or baseline shift amounts (weight changes, penetrations) have been compiled from all the thermograms. All the thermograms used to obtain the data in Tables 3-8 are given in Appendices A, B, and C. These temperatures, integrals, or shifts are then plotted versus section depth for the three techniques employed; TMA, TGA, and DSC. Since the section thicknesses varied within the section itself, each section was weighed, and its depth is given in the tables as the calculated average depth from the weight of the section and the density of the Halar from Table 1.

The penetration versus temperature TMA thermogram is shown in Figure 2 for the top section of the LDEF Halar sample. Although visible discoloration was present in this top section, the glass transition temperature, 253 C in Figure 2, was essentially the same as the control, 254 C, as shown in Figure 3. The glass transition temperatures for all the sections analyzed in the TMA are given in Table 3 for the LDEF exposed Halar sample, and in Table 4 for the control Halar sample. The temperatures were determined by the inflection points of the plots within the transition. Figure 4 is a plot of the transition temperatures as a function of section depth in the sample. All the temperatures are within ± 2 C. There is no trend with depth, and the control is essentially the same as the LDEF exposed sample.

Figure 5 is the TGA thermogram for weight gain or loss while heating in oxygen for the topmost LDEF exposed sample. Significant weight losses occurred at 170 C and in the range 300-500 C. As can be seen in Figure 6, the weight loss at 170 C is far less for the topmost control sample than for the exposed Halar sample, while the weight loss at the higher temperature range is similar for both samples. TGA weight losses at 170 C, 290 C, and 420 C are given in Table 5 for all the LDEF exposed Halar sections and in Table 6 for all the Halar control sections. The plot of weight loss at 170 C versus section depth is shown in Figure 7. The LDEF exposed Halar shows a dramatic increase in weight loss as compared to the control samples for the first two sections from the top. Discoloration was evident in both of the top two TGA sections of the exposed sample. Apparently the oxidation rate differs from the control for the LDEF exposed Halar only to a depth of about 50 microns.

The DSC thermogram is shown in Figure 8 for the topmost LDEF exposed sample. A noisy melting endotherm is evident at 235 C, and a strong exotherm at 446 C. The topmost control sample, Figure 9, showed a weak melting endotherm at 234 C. The second section of the control sample, Figure 10, showed an endotherm at 235 C very similar to the LDEF sample. Plots of melting temperature versus section depth and melting enthalpy (the integral of the melting endotherm) versus depth are shown in Figures 11 and 12. In both cases, there appears to be no difference between the LDEF and the control samples. No significant variation with section depth is evident for either melting temperature or for enthalpy of melting.

The TMA and DSC techniques measure the response of the whole sample section which is placed in the analyzer. Near surface effects that are truncated in several atom layers would not be resolvable in the roughly 50 micron thick sections. The TGA, however, measures the oxidation rate at the surface of the section placed in the analyzer. The topmost section had as its top surface the actual top surface given the orbital exposure. The

other side of the section was produced by the microtome. Thus, the TGA is the most surface sensitive of the three techniques employed, and it is the only technique to sense damage from orbital exposure. This 50 micron damage depth is in rough agreement with the observation of severe damage to 125 micron thick Mylar (3).

CONCLUSIONS

The orbital exposure during the LDEF Mission did not appear to mechanically damage the Halar sample. To a surface section resolution of about 50 microns, no thermodynamic damage was detectible via differential thermal analysis. The top 50 microns of the LDEF exposed sample did exhibit a higher oxidation rate than the control samples, which correlates to the depth of the discoloration.

References

- (1) A. F. Whitaker, "Coatings Could Protect Composites From Hostile Space Environments," *Adv. Materials & Processes*, 4 (1991), 30-32.
- (2) R. C. Tennyson, G. E. Mabson, W. D. Morison, and J. Kleinman, "LDEF Mission Update: Composites in Space," *Adv. Materials & Processes*, 5 (1991), 33-36.
- (3) B. J. Dunbar, "A Materials Scientist in Space," *MRS Bulletin*, May (1991), 36-41.
- (4) G. L. Steckel and T. D. Le, "LDEF Mission Update: Composites Survive Space Exposure," *Adv. Materials & Processes*, 8 (1991), 35-38.

**Table 1 Thickness and Density Measurements for Cut Halar LDEF and Control
Samples Before Sectioning**

Dimensional Characteristics of Halar Samples

Measured Thickness

Pc#1 Control (inches)	Pc#2 Control (inches)	Pc#3 Control (inches)	Pc#4 Exposed (inches)	Pc#5 Exposed (inches)	Pc#6 Control (inches)	Pc#7 Exposed (inches)
0.1209	0.1220	0.1257	0.1215	0.1224	0.1256	0.1180
	0.1218	0.1256	0.1202	0.1218	0.1241	0.1202
	0.1218	0.1254	0.1196	0.1198	0.1252	0.1202

Calculated Density

Pc#1 Control (gr/cc)	Pc#2 Control (gr/cc)	Pc#3 Control (gr/cc)	Pc#4 Exposed (gr/cc)	Pc#5 Exposed (gr/cc)	Pc#6 Control (gr/cc)	Pc#7 Exposed (gr/cc)
1.651	1.549	1.558	1.515	1.568	1.573	1.205

Table 2 Test Conditions for LDEF Samples for Thermal Analysis

Technique	Test Atmosphere	Heating Rate, C/min	Temp Range, C
TMA	flowing Ar	10	25-300
TGA	flowing O2	10	25-700
DSC	flowing Ar	10	25-600

Table 3 Glass Transition Temperatures as Determined by Thermomechanical Analysis
for Halar LDEF Samples

Halar in TMA Transition temp. determined by inflection pt

Exposed
Piece #4

Area= 0.248 cm²
Density= 1.515 gr/cm³

Sample ID	Wt (gr)	Thick (um)	Depth (um)	Temp C
H4C1	0.0027	71.9	36.0	253.3
H4C1A	0.0027	71.9	36.0	251.0
H4C2	0.0047	125.1	134.4	254.1
H4C3	0.0013	34.6	214.3	252.2
H4C4	0.0030	79.8	271.5	251.1
H4C5	0.0038	101.1	362.0	252.0
H4C6	0.0045	119.8	472.4	252.0
H4C7	0.0044	117.1	590.9	
H4C8	0.0014	37.3	668.1	
H4C9	0.0080	212.9	793.1	
H4C10	0.0028	74.5	936.9	
H4C11	0.0051	135.7	1042.0	
H4C12	0.0019	50.6	1135.2	
H4C13	0.0053	141.1	1231.0	
H4C14	0.0039	103.8	1353.4	
H4C15	0.0050	133.1	1471.8	
H4C16	0.0019	50.6	1563.7	
H4C17	0.0078	207.6	1692.7	
cutoff	0.0486	1293.5		
total	0.1161	3161.9		
original	0.1148	3053.0		

Table 4 Glass Transition Temperatures as Determined by Thermomechanical Analysis
for Halar Control Samples

Halar in TMA Transition temp. determined by inflection pt

Control
Piece #3

Area= 0.3035 cm²
Density= 1.558 gr/cm³

Sample ID	Wt (gr)	Thick (um)	Depth (um)	Temp C
H3C1	0.0016	33.8	16.9	253.7
H3C2	0.0010	21.1	44.4	254.1
H3C3	0.0050	105.7	107.8	253.4
H3C4	0.0007	14.8	168.0	252.7
H3C5	0.0182	384.9	367.8	253.2
H3C6	0.0011	23.3	572.0	
H3C7	0.0001	2.1	584.7	
H3C8	0.0095	200.9	686.2	252.7
H3C9	0.0007	14.8	794.0	
H3C10	0.0090	190.3	896.6	252.7
H3C11	0.0052	110.0	1046.7	
H3C12	0.0006	12.7	1108.0	
H3C13	0.0084	177.6	1203.2	
H3C14	0.0003	6.3	1295.2	
H3C15	0.0100	211.5	1404.0	
H3C16	0.0016	33.8	1526.7	
cutoff	0.0734	1552.3		
total	0.1464	3096.1		
original	0.1508	3190.0		

Table 5 Weight Losses at Various Temperature Ranges as Determined by Thermogravimetric Analysis for Halar LDEF Samples

Halar in TGA Weight changes occur after onset temperatures

Exposed
Piece #7

Area= 0.270 cm²
Density= 1.205 gr/cm³

Sample ID	Wt(gr)	thick (um)	mean depth	170 C d %wt	290 C d %wt	420 C d %wt
H7C1	0.0004	12.3	6.2	23.0	61.6	14.3
H7C2	0.0029	89.1	56.9	3.9	68.7	27.3
H7C3	0.0003	9.2	106.0	0.0	78.0	20.6
H7C4	0.0048	147.5	184.4	1.1	74.7	24.8
H7C5	0.0006	18.4	267.4	0.0	82.6	24.2
H7C6	0.0040	122.9	338.1	0.5	72.8	26.8
H7C7	0.0006	18.4	408.8	0.0	84.9	22.0
H7C8	0.0066	202.9	519.4	0.4	64.1	35.7
H7C9	0.0029	89.1	665.4	0.0	67.7	31.8
H7C10	0.0047	144.5	782.2	0.3	65.3	34.7
H7C11	0.0011	33.8	871.4	0.0	69.5	29.8
H7C12	0.0044	135.2	955.9	nd	68.5	31.3
H7C13	0.0037	113.7	1080.4			
H7C14	0.0039	119.9	1197.2			
H7C15	0.0007	21.5	1267.9			
H7C16	0.0057	175.2	1366.2			
H7C17	0.0008	24.6	1466.1			
cutoff	0.0509	1564.5				
total	0.0990	3042.9				
original	0.0994	3053				

Table 6 Weight Losses at Various Temperature Ranges as Determined by Thermogravimetric Analysis for Halar Control Samples

Halar in TGA Weight changes occur after onset temperatures

Control
Piece #6

Area= 0.2639 cm²
Density= 1.573 gr/cm³

Sample ID	Wt(gr)	thick (um)	mean depth	170 C d %wt	290 C d %wt	420 C d %wt
H6C1	0.0046	110.8	55.4	1.3	66.2	32.5
H6C2	0.0040	96.4	159.0	0.8	72.5	27.1
H6C3	0.0049	118.0	266.2	0.2	68.0	31.8
H6C4	0.0030	72.3	361.3	0.0	66.7	32.8
H6C5	0.0008	19.3	407.1	0.0	74.9	25.1
H6C6	0.0047	113.2	473.4	0.0	67.4	32.2
H6C7	0.0006	14.5	537.2			
H6C8	0.0040	96.4	592.6	0.0	65.9	34.0
H6C9	0.0033	79.5	680.5			
H6C10	0.0030	72.3	756.4	0.0	68.6	31.4
H6C11	0.0007	16.9	801.0			
H6C12	0.0039	93.9	856.4	0.0	69.3	30.7
H6C13	0.0005	12.0	909.4			
H6C14	0.0041	98.8	964.8	0.1	66.5	33.5
H6C15	0.0007	16.9	1022.6			
H6C16	0.0043	103.6	1082.8	0.0	67.4	33.7
H6C17	0.0022	53.0	1161.1			
H6C18	0.0059	142.1	1258.7	0.3	65.0	34.6
cutoff	0.0803	1934.4				
total	0.1355	3264.2				
original	0.1320	3180				

Table 7 Transition Temperatures and Enthalpy of Melting as Determined by
Differential Scanning Calorimetry for Halar LDEF Samples

Halar in DSC		Temperatures determined by peaks				
Exposed Piece #5						
Area=	0.1281 cm ²					
Density=	1.568 gr/cm ³					
Sample ID	Wt (gr)	Thick (um)	Depth (um)	temp C	temp C	H
H5C1	0.0042	209.1	104.6	445.6	235.1	
H5C2	0.0018	89.6	253.9	449.7	237.5	6.26
H5C3	0.0039	194.2	395.8	445.4	235.9	4.35
H5C4	0.0021	104.6	545.2	435.6	237.7	3.24
H5C5	0.0048	239.0	716.9	441.0	235.6	5.80
H5C6	0.0019	94.6	883.7	449.3	236.2	2.49
H5C7	0.0034	169.3	1015.6			
H5C8	0.0032	159.3	1179.9			
H5C9	0.0022	109.5	1314.3			
H5C10	0.0070	348.5	1543.4			
H5C11	0.0016	79.7	1757.4			
H5C12	0.0034	169.3	1881.9			
H5C13	0.0038	189.2	2061.1			
H5C14	0.0013	64.7	2188.1			
H5C15	0.0076	378.4	2409.6			
H5C16	0.0010	49.8	2623.7			
H5C17	0.0027	134.4	2715.8			
cutoff	0.0388	1931.7				
total	0.0947	4714.7				
original	0.0883	3094.0				

Table 8 Transition Temperatures and Enthalpy of Melting as Determined by
Differential Scanning Calorimetry for Halar Control Samples

Halar in DSC		Temperatures determined by peaks				
Control						
Piece #2						
Area=	0.265 cm ²					
Density=	1.549 gr/cm ³					
Sample ID	Wt (gr)	Thick (um)	Depth (um)	temp C	temp C	H
H2C1	0.0012	29.2	14.6	448.8	234.7	3.02
H2C2	0.0058	141.3	99.8	452.0	235.1	6.78
H2C3	0.0006	14.6	177.8			
H2C4	0.0053	129.1	249.6	448.0	238.0	
H2C5	0.0003	7.3	317.8			
H2C6	0.0053	129.1	386.0	447.7	236.0	3.60
H2C7	0.0067	163.2	532.2			
H2C8	0.0048	116.9	672.2	450.2	235.5	3.32
H2C9	0.0023	56.0	758.7			
H2C10	0.0042	102.3	837.8	449.5	236.7	2.23
H2C11	0.0066	160.8	969.4			
H2C12	0.0005	12.2	1055.9			
H2C13	0.0059	143.7	1133.8			
H2C14	0.0024	58.5	1235.0			
H2C15	0.0025	60.9	1294.7			
H2C16	0.0020	48.7	1349.4			
H2C17	0.0023	56.0	1401.8			
H2C18	0.0027	65.8	1462.7			
cutoff	0.0463	1127.9				
total	0.1077	2623.7				
original	0.1207	3094.0				

LDEF or CONTROL Sample

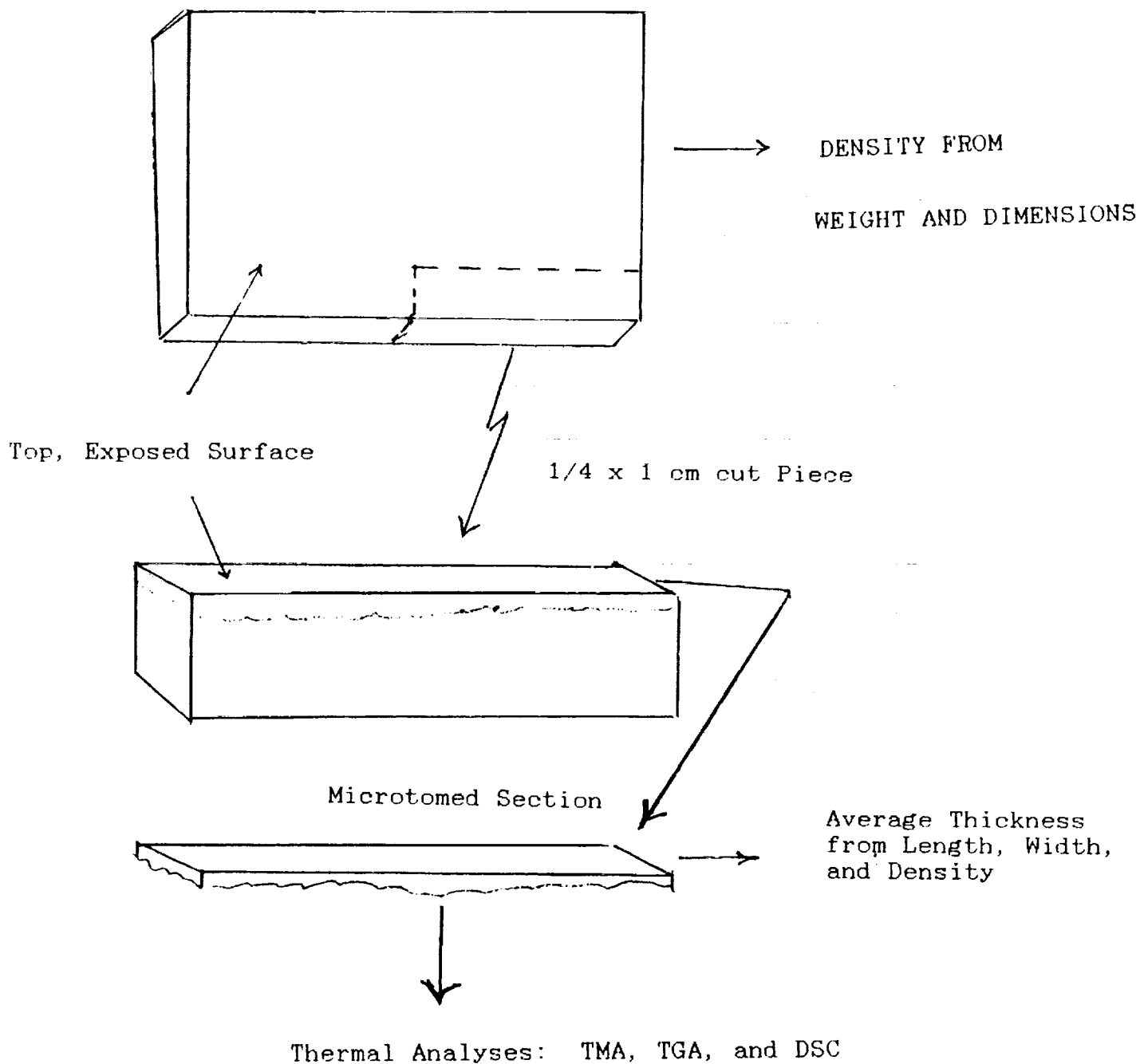


Figure 1 Schematic Diagram of LDEF Sample Sectioning Procedure

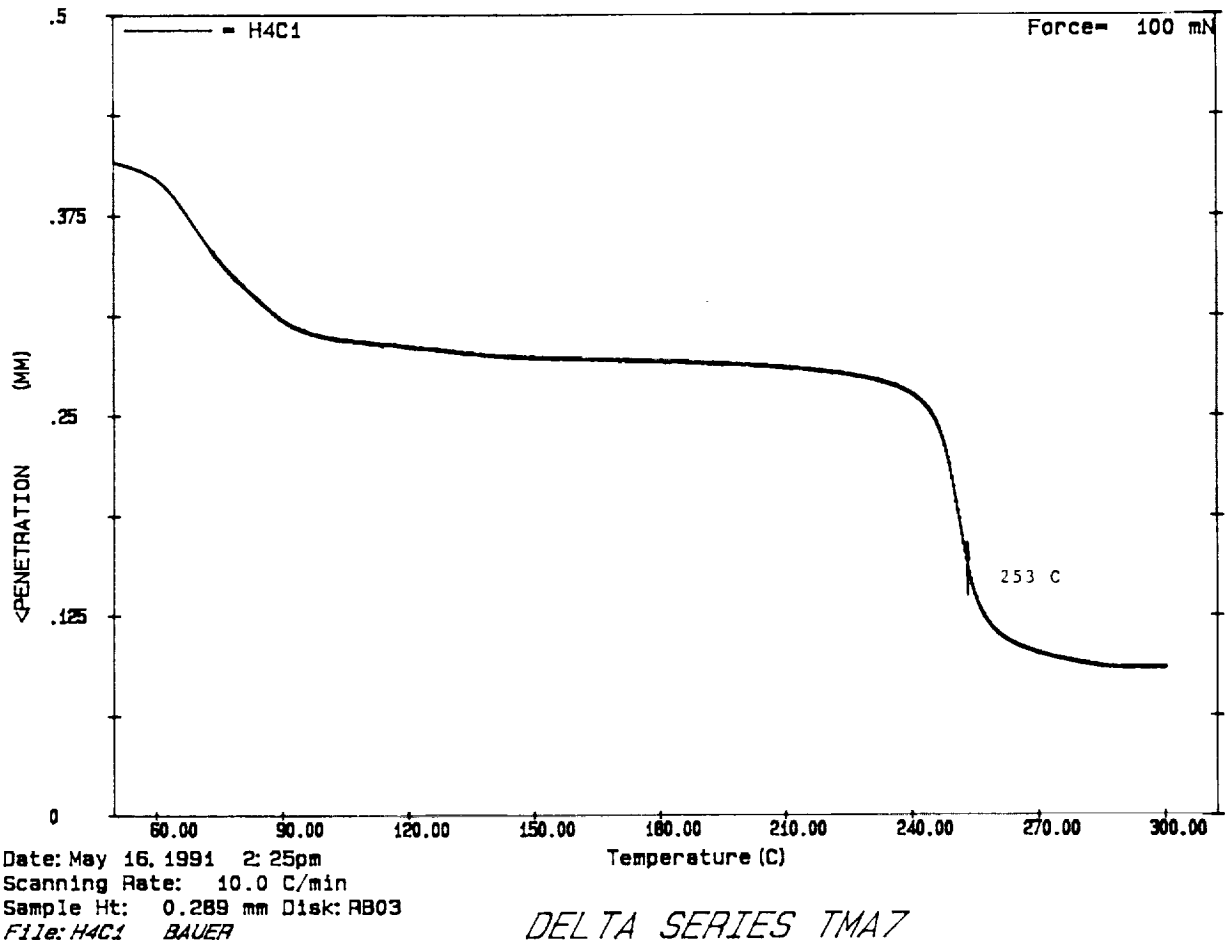
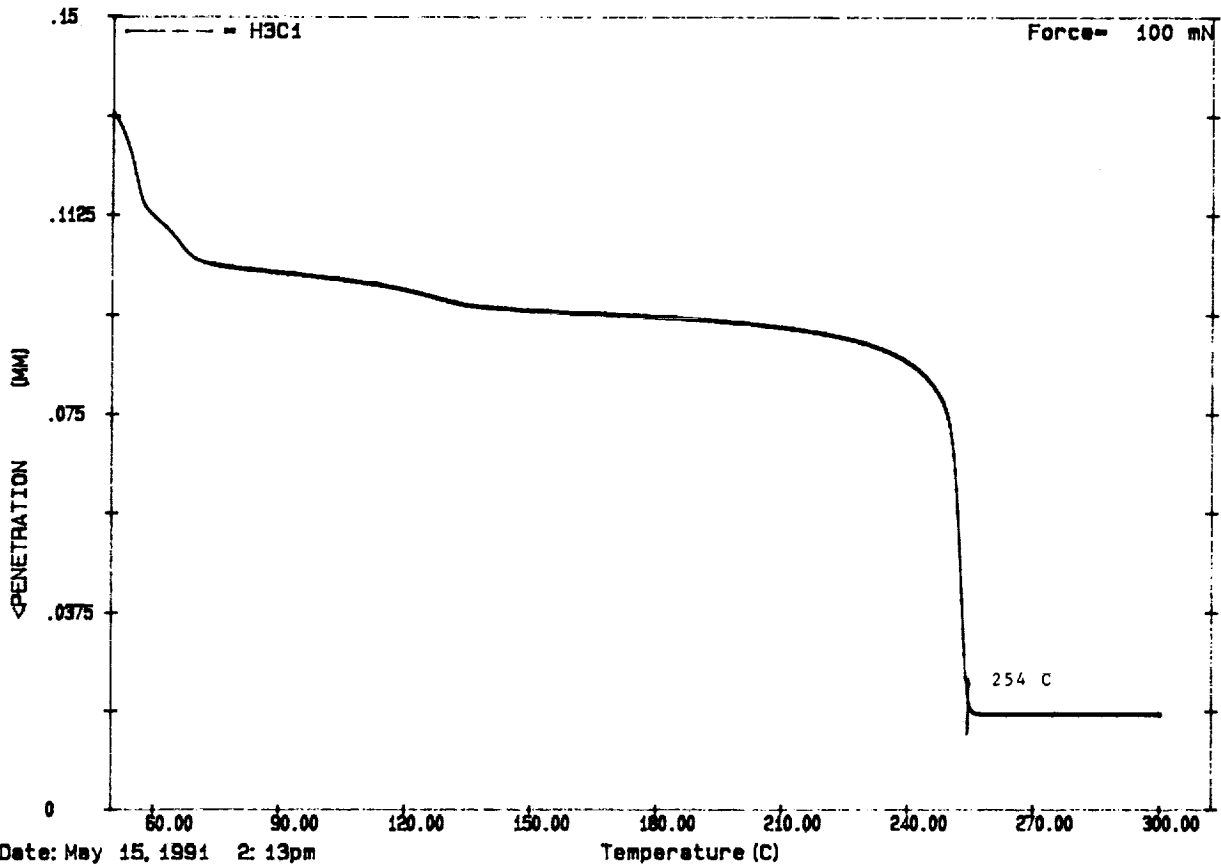


Figure 2 TMA Plot for the Top Section of the Halar, LDEF Sample Which Showed Visible Discoloration



Date: May 15, 1991 2:13pm
 Scanning Rate: 10.0 C/min
 Sample Ht: 0.128 mm Disk: RB03
 File: H3C1 BAUER

DELTA SERIES TMA7

Figure 3 TMA Plot for the Top Section of the Halar Control Sample

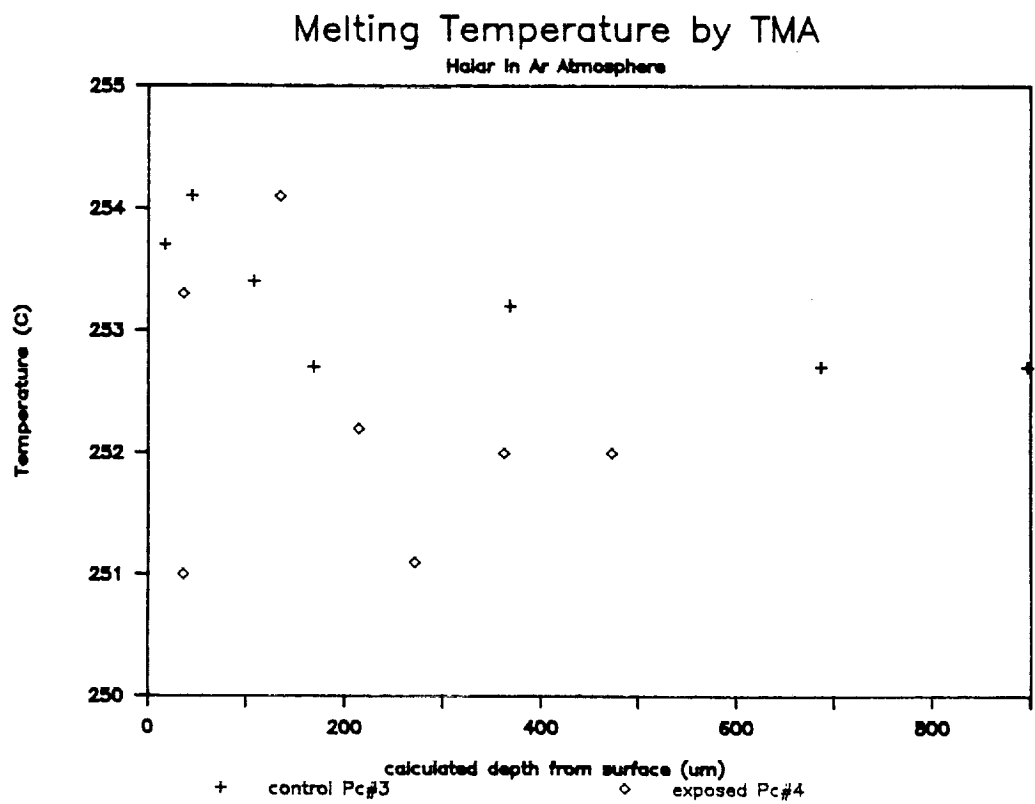


Figure 4 TMA Glass Transition Temperature as a Function of Section Depth for Halar LDEF and Control Samples

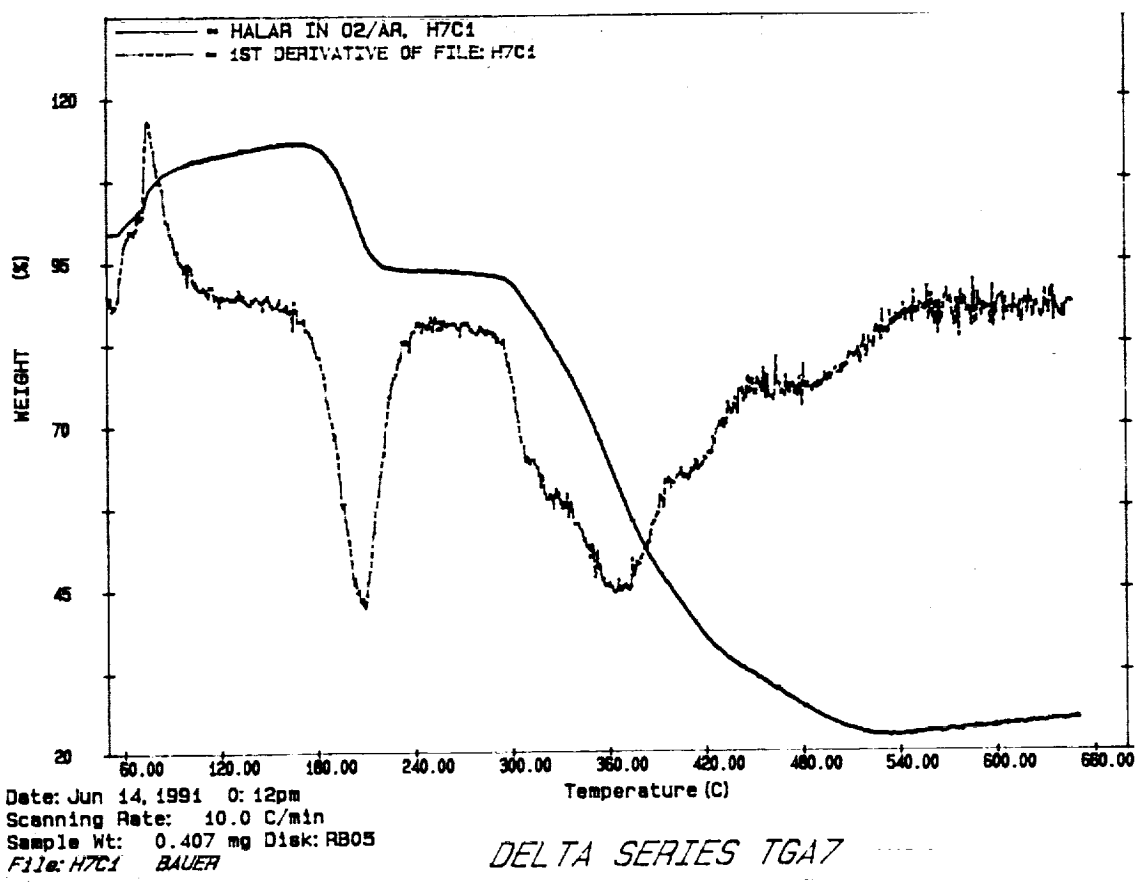


Figure 5 TGA Plot for the Top Section of the Halar LDEF Sample Showing a Large Weight Loss at 170° C

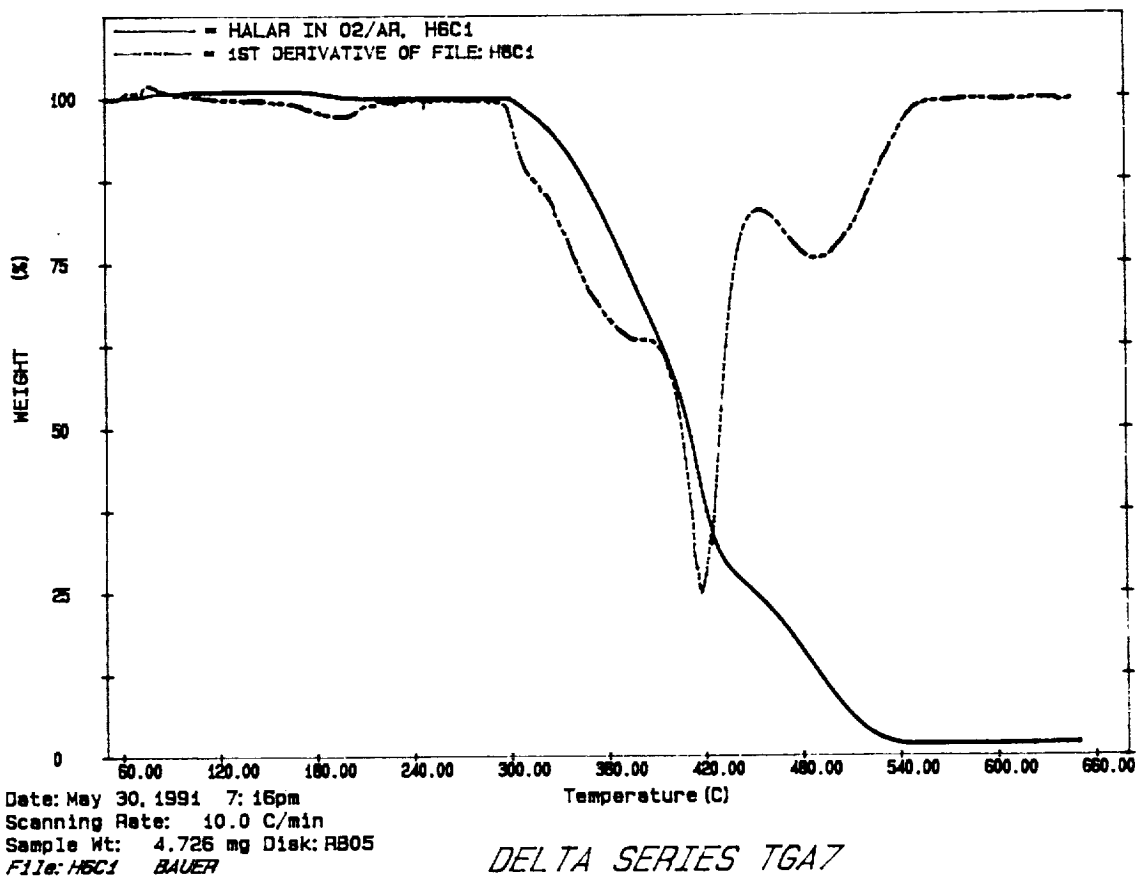


Figure 6 TGA Plot for the Top Section of the Halar Control Sample

Percent Weight Loss in TGA

Halar In O₂/Ar Atmosphere, Onset 170C

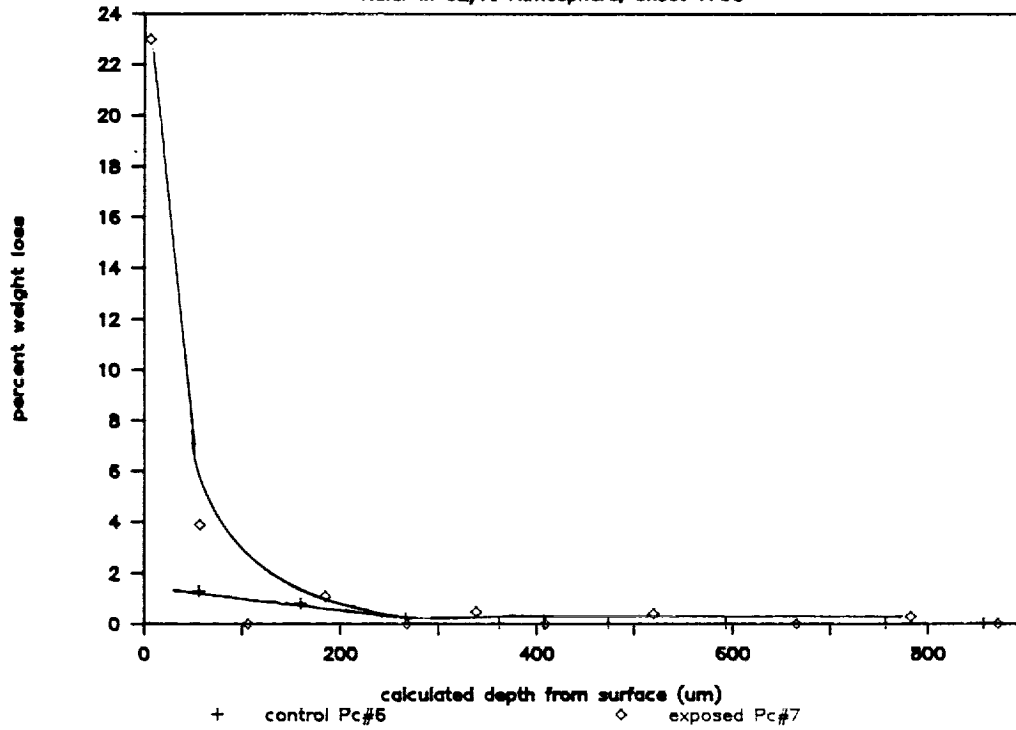
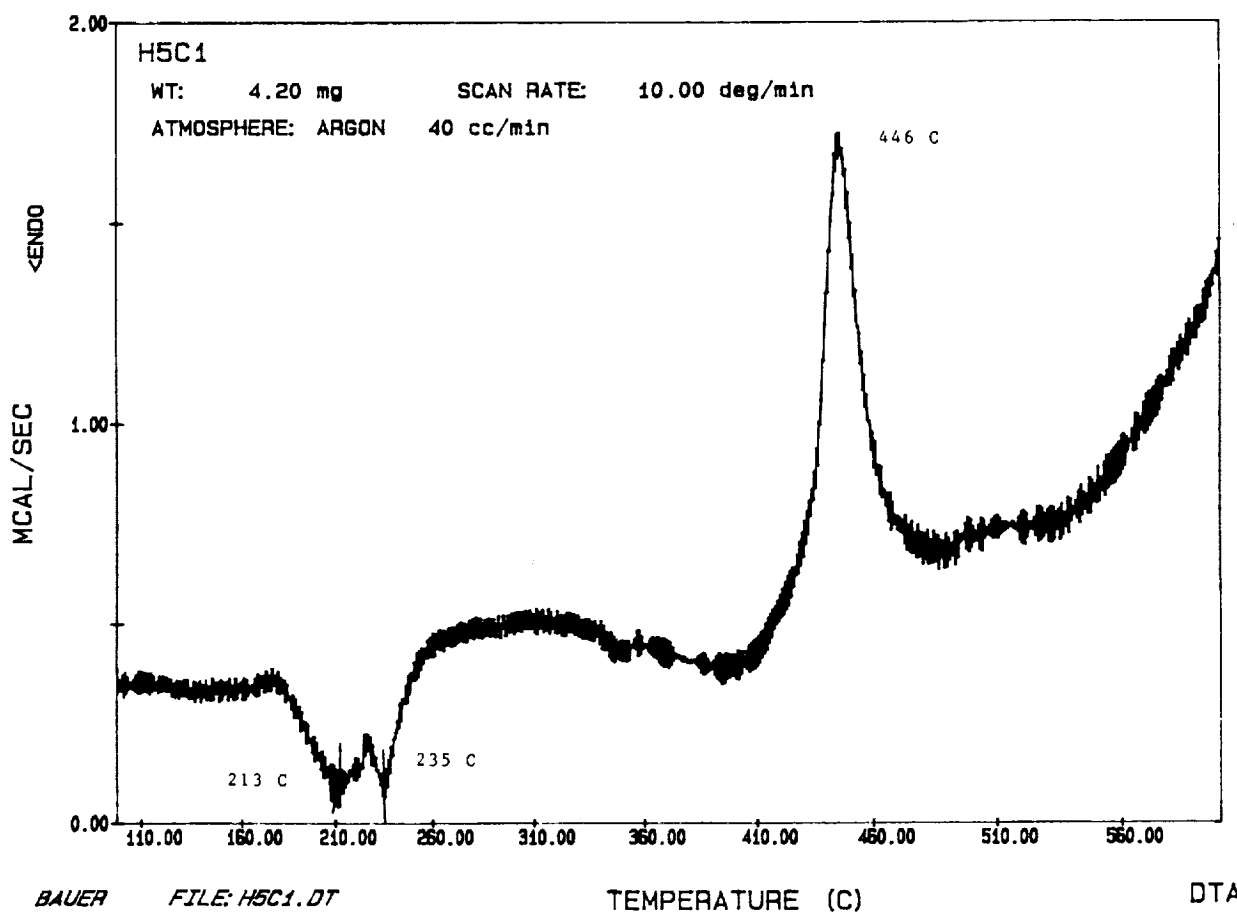


Figure 7 TGA Weight Loss at 170° C as a Function of Sectioning Depth for Halar, LDEF and Control Samples



BAUER FILE: H5C1.DT
 DATE: 91/05/23 TIME: 16:20

Figure 8 DSC Plot for the Top Section of the Halar LDEF Sample Showing an Endotherm at 235° C and an Exotherm at 446° C

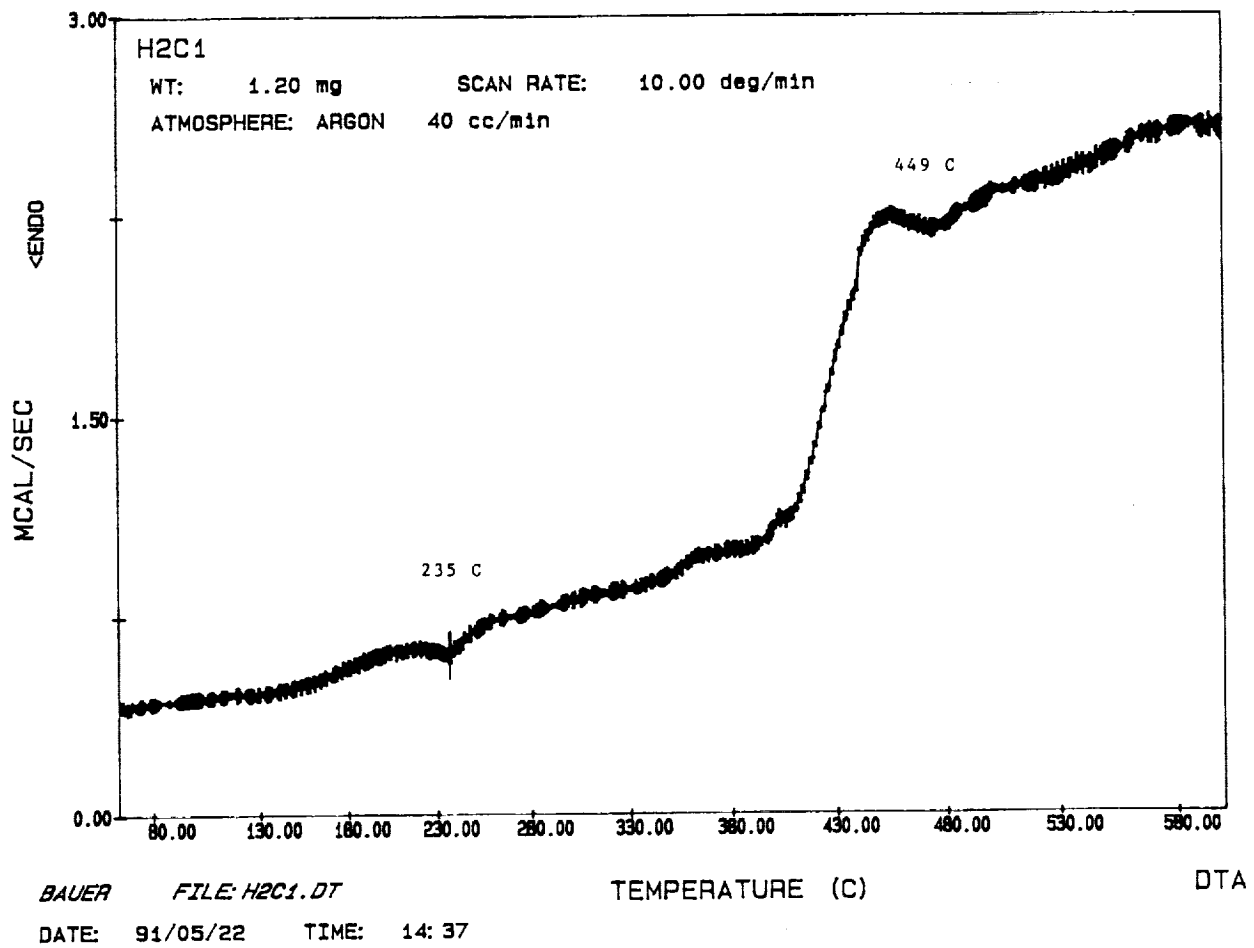


Figure 9 DSC Plot for the Top Section of the Halar Control Sample Showing a Weak Endotherm at 234° C and a Weak Exotherm at 449° C

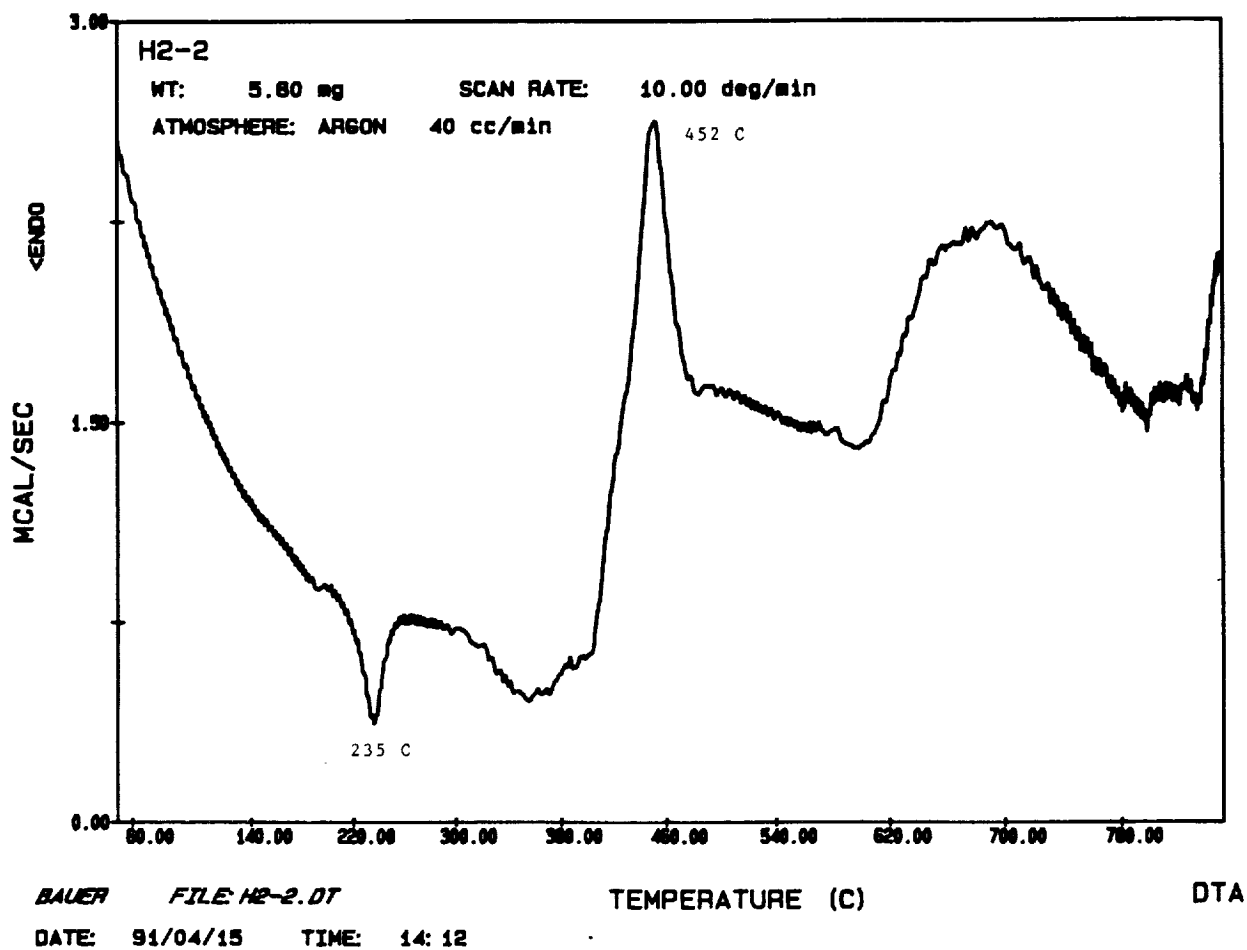


Figure 10 DSC Plot for the Second Section of the Halar Control Sample Showing a Strong Endotherm at 235° C and a Strong Exotherm at 452° C

Melting Temperature by DSC

Halar In Ar Atmosphere

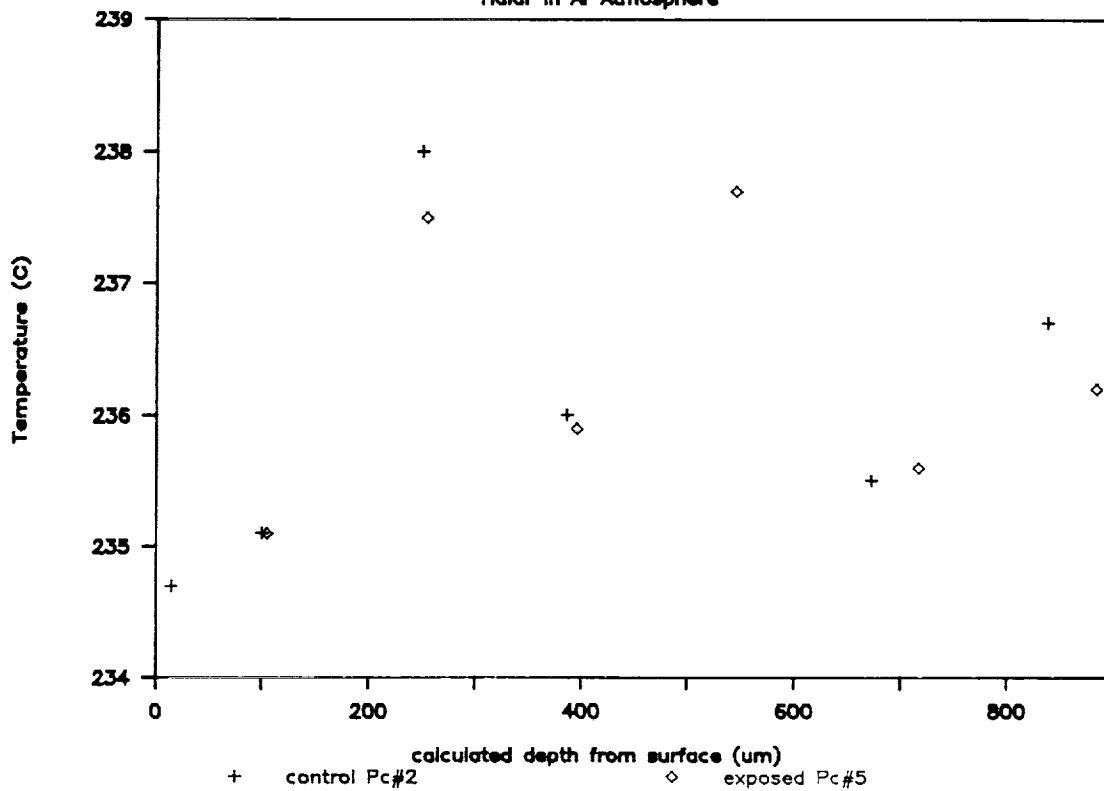


Figure 11 DSC Melting Endotherm Temperature as a Function of Section Depth for Halar LDEF and Control Samples

Melting Enthalpy by DSC

Halar in Ar Atmosphere

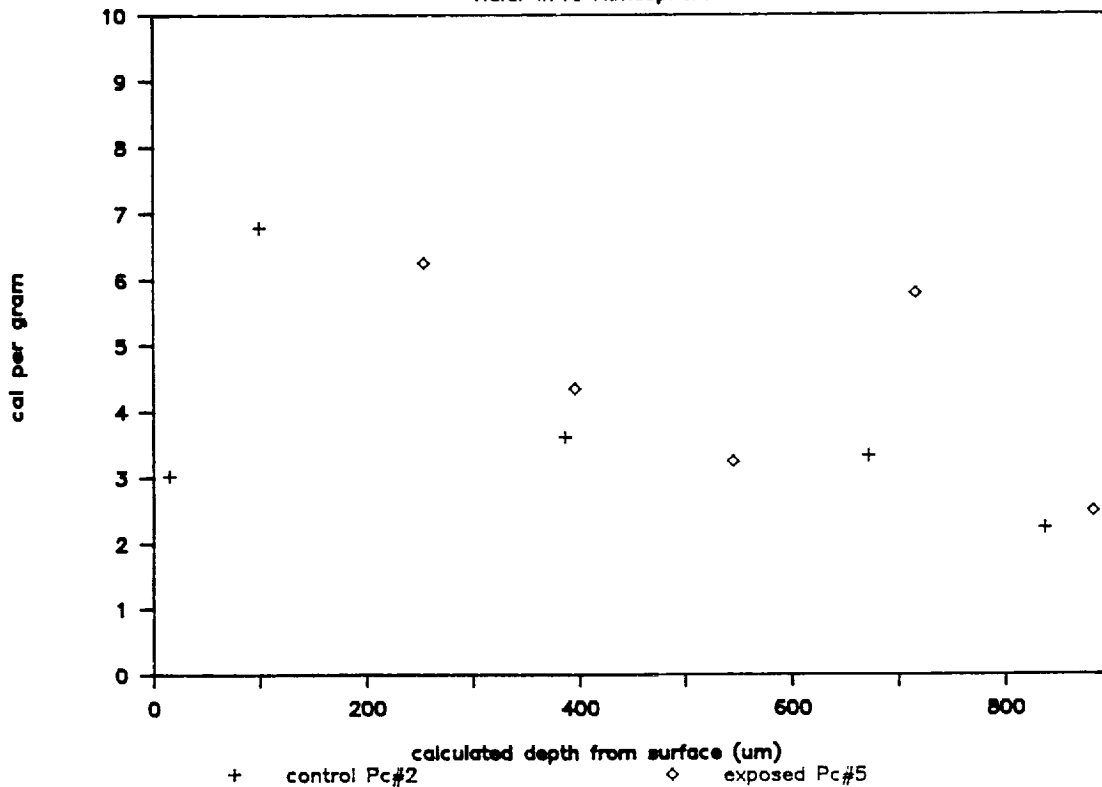


Figure 12 DSC Melting Enthalpy as a Function of Section Depth for Halar LDEF and Control Samples

LONG DURATION EXPOSURE FACILITY
M0003-5
RECENT RESULTS ON POLYMERIC FILMS

Charles J. Hurley
University of Dayton Research Institute
Dayton, OH

Michele Jones
USAF Wright Laboratories
Wright-Patterson AFB, OH

INTRODUCTION

The M0003-5 polymeric film specimens orbited on the LDEF M0003 Space Environment Effects on Spacecraft Materials were a part of a Wright Laboratories Materials Directorate larger thermal control materials experiment. They were selected from new materials which emerged from development programs during the 1978-1982 time frame. Included were materials described in the technical literature which were being considered or had been applied to satellites. Materials that had been exposed on previous satellite materials experiments were also included to provide data correlation with earlier space flight experiments. The objective was to determine the effects of the LDEF environment on the physical and optical properties of polymeric thin film thermal control materials, the interaction of the LDEF environment with silvered spacecraft surfaces and the performance of low outgassing adhesives. Sixteen combinations of various polymeric films, metallized and unmetallized, adhesively bonded and unbonded films were orbited on LDEF in the M0003-5 experiment. The films were exposed in two separate locations on the vehicle. One set was exposed on the direct leading edge of the satellite. The other set was exposed on the direct trailing edge of the vehicle.

The purpose of the experiment was to understand the changes in the properties of materials before and after exposure to the space environment and to compare the changes with predictions based on laboratory experiments. The basic approach was to measure the optical and physical properties of materials before and after long-term exposure to a low earth orbital environment comprised of UV, VUV, electrons, protons, atomic oxygen, thermal cycling, vacuum, debris and micrometeoroids. Due to the unanticipated extended orbital flight of LDEF, the polymeric film materials were exposed for a full five years and ten months to the space environment.

LDEF M0003 SUB-EXPERIMENTS

The individual experiments listed below were supplied by the organization named and integrated into the flight hardware trays by Aerospace Corporation. Deintegration was accomplished by the same organization.

#	NAME	ORGANIZATION
1	RADAR CAMOUFLAGE MATERIALS & EO SIGNATURE COATINGS	AVIONICS LAB
2	LASER OPTICS	WEAPONS LAB
3	STRUCTURAL MATERIALS	WEAPONS LAB
4	SOLAR POWER COMPONENTS	PROPULSION LAB
5	THERMAL CONTROL MATERIALS	MATERIALS LAB
6	LASER COMMUNICATION COMPONENTS	SPACE DIVISION/ McD-D ASTRONAUTICS
7	LASER MIRROR COATING	NAVAL WEAPONS CTR
8	COMPOSITE MATERIALS, ELECTRONIC PIECE PARTS, FIBER OPTICS	BOEING AEROSPACE
9	THERMAL CONTROL, ANTENNA, COMPOSITE MATERIALS, COLD WELDING	LOCKHEED MISSILE & SPACE CORP.
10	ADVANCED COMPOSITE MATERIALS	FLIGHT DYNAMICS LAB AEROSPACE CORP.
11	CONTAMINATION MONITORING	AEROSPACE CORP.
12	RADIATION DOSIMETRY	AEROSPACE CORP.
13	LASER HARDENED MATERIALS	McD-D ASTRONAUTICS
14	QUARTZ CRYSTAL MICROBALANCE	BERKLEY INDUSTRY
15	THERMAL CONTROL MATERIALS	AEROSPACE CORP.
16	ADVANCED COMPOSITE MATERIALS	AEROSPACE CORP.
17	RADIATION DOSIMETRY	AEROSPACE CORP.
18	THERMAL CONTROL COATINGS	AEROSPACE CORP.
19	ELECTRONIC DEVICES	AEROSPACE CORP.

**LDEF/WL/ML EXPERIMENT
THERMAL CONTROL MATERIALS
M0003-5**

THERMAL CONTROL MATERIALS

A Series

Pigmented Coatings	44
Metallized Polymer Films	28
Quartz Fabrics	8

B Series

Optical Solar Reflectors (second surface)	8
Gold Mirrors (first surface)	4
Silver Mirrors (first surface)	6
Aluminum Mirrors (first surface)	4

C Series

Metallized Polymeric Films	8
Metallized Bonded Films	14
Clear Films	10
Total	134

LDEF IN THE ORBITER PROCESSING FACILITY

Fifty seven experiments were placed in a low earth orbit aboard LDEF on April 7, 1984 for a planned one year mission. The LDEF vehicle was recovered on January 12, 1990 from a degrading orbit by the Space Shuttle Columbia. After a landing at Edwards Air Force Base, California, the Space Shuttle, with LDEF still contained inside, was transported to Kennedy Space Center, Florida. LDEF was removed from the shuttle bay in the Orbiter Processing Facility (OPF) in late January 1990.

The photograph shown in figure 1 shows the extensive damage done to some experiments on the leading edge side and the space end of the vehicle. The M0003 experiment is located near the center of the vehicle at the scuff plate.

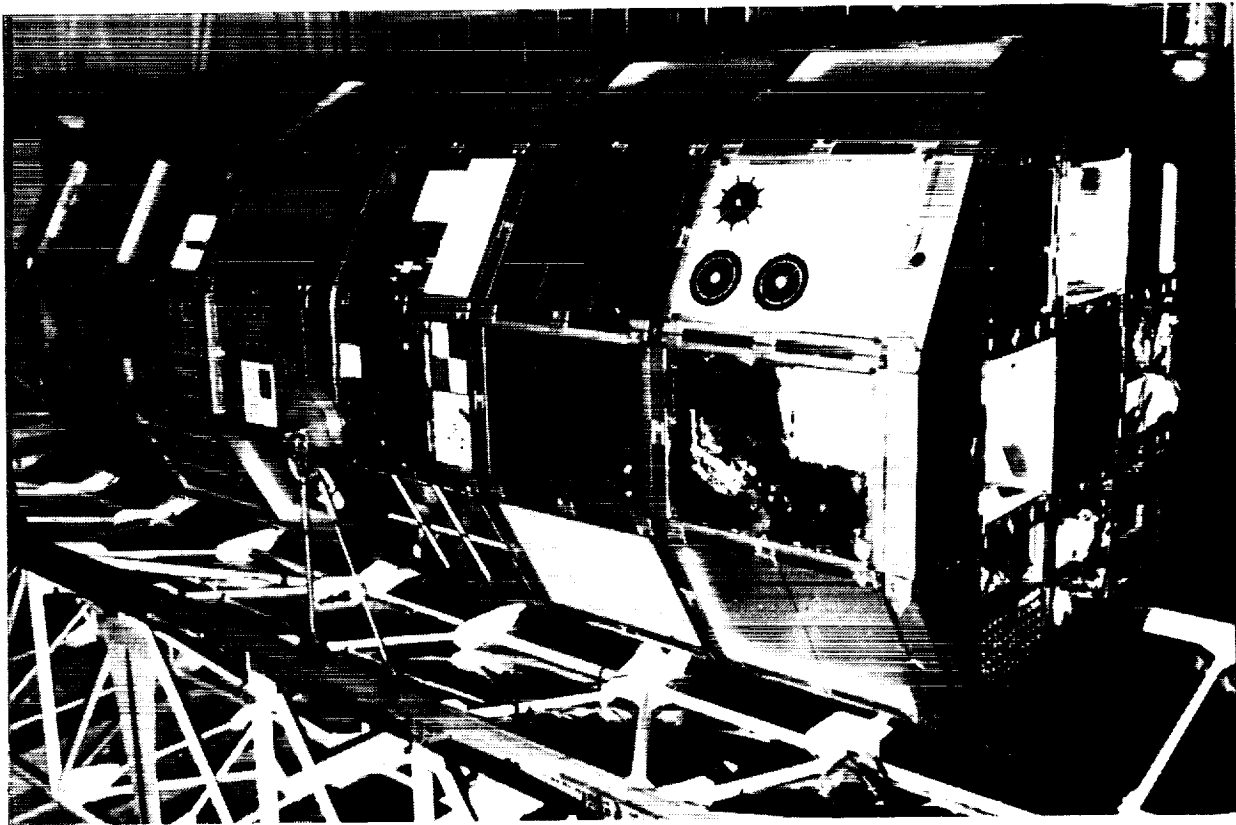


Figure 1. LDEF in Orbiter Processing Facility

LDEF in SAEF II

After completion of activities in the Orbiter Processing Facility, LDEF was transported to the Spacecraft Assembly and Experiment Facility II (SAEFII). This facility provided a controlled, clean working environment for the principal investigators and other observers to examine the various experiments. The photograph shown in figure 2 shows only a portion of the leading edge side of LDEF. The M0003 experiment is located to the far left of the photograph near the scuff plate.



Figure 2. LDEF in SAEF II

M0003-5 LEADING EDGE EXPERIMENT

The M0003-5 experiment was located in a 3 " deep leading edge tray designated as D9. It contained a variety of thermal control pigmented coatings, metallized polymer films, clear films and mirrors. The photograph in figure 3 shows the preflight layout of the materials. The polymer films are the horizontal strips shown in the upper left portion of the mounting hardware.

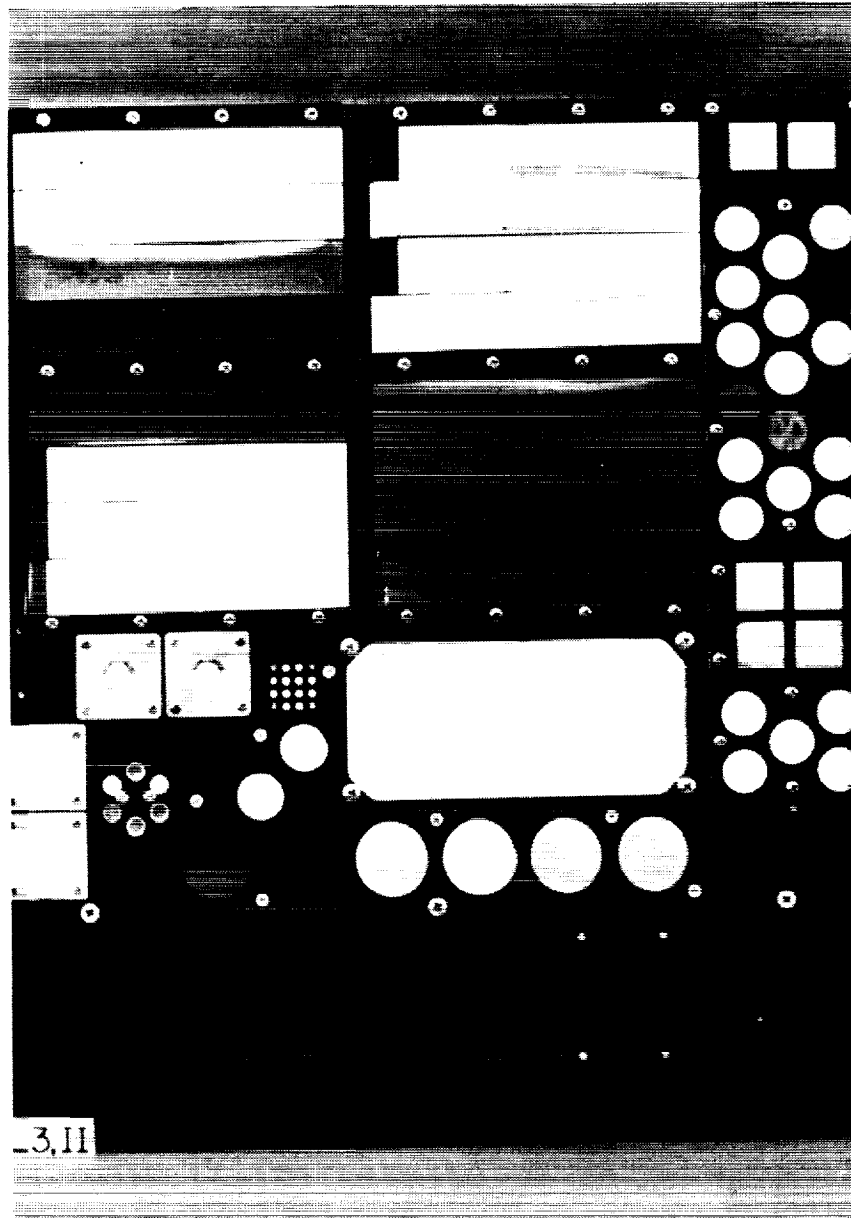


Figure 3. M0003-5 Pre flight Leading Edge Tray Experiment

RECOVERED LEADING EDGE M0003 TRAY

A photograph of the recovered M0003 leading edge tray originally located in the D9 position is shown in figure 4. Among the various areas of visible damage, note the condition of the polymeric films portion of the M0003-5 experiment located in the lower left quadrant of the tray. Physical damage, discoloration and bonding separation and tearing has occurred. Atomic oxygen probably caused the physical damage, radiation caused the discoloration and the debonding probably occurred as a result of thermal cycling.

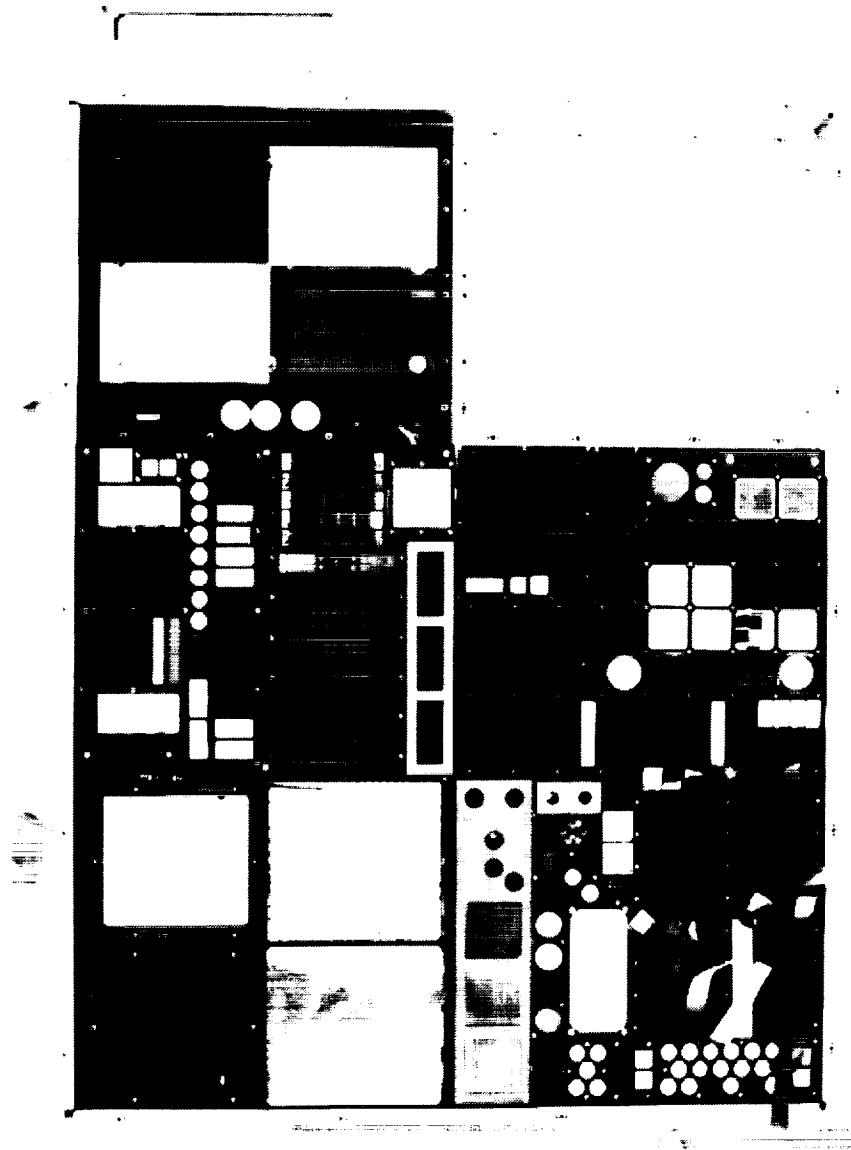


Figure 4. M0003 Post Flight Leading Edge Tray

LDEF/M0003 IN SAEF II

The photograph in figure 5 shows the M0003 experiment and the surrounding trays on LDEF in SAEF II. Note the extensive damage to the experiment located in tray D10 immediately above the D9 M0003 experiment tray. Also observe the serious damage that occurred to the M0003-1 experiment located in the lower right quadrant of the M0003 tray. Damage is also evident to the M0003-5 polymer film materials.

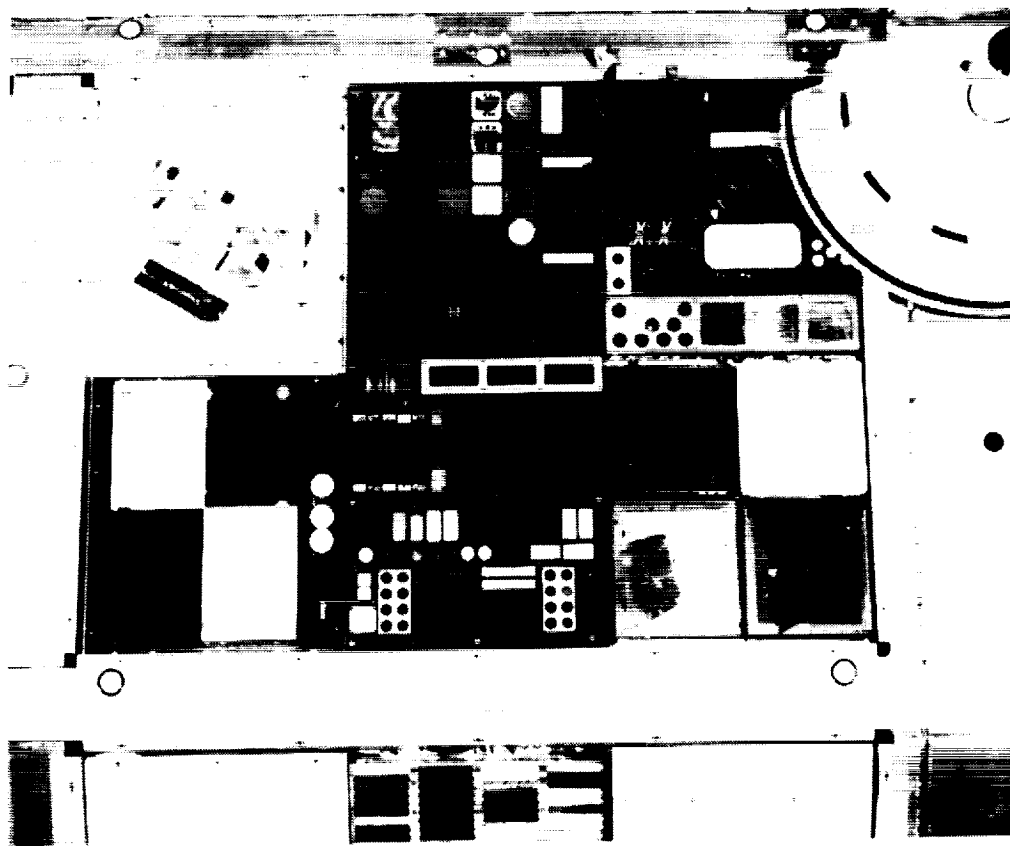


Figure 5. LDEF/M0003 IN SAEF II

ORIGINAL PAGE
BLACK AND WHITE PHOTOGRAPH

M0003-5 POST FLIGHT LEADING EDGE TRAY CLOSEUP

The photograph in figure 6 below shows a closeup of the M0003-5 experiment materials. Note the extensive damage to the polymeric film strips. There is obvious physical damage, discoloration and debonding and tearing of the polymer film materials. There is apparent scarring due to probable AO impingement deflected from the scuff plate. Most of the intact films on the leading edge were partially covered by the scuff plate.

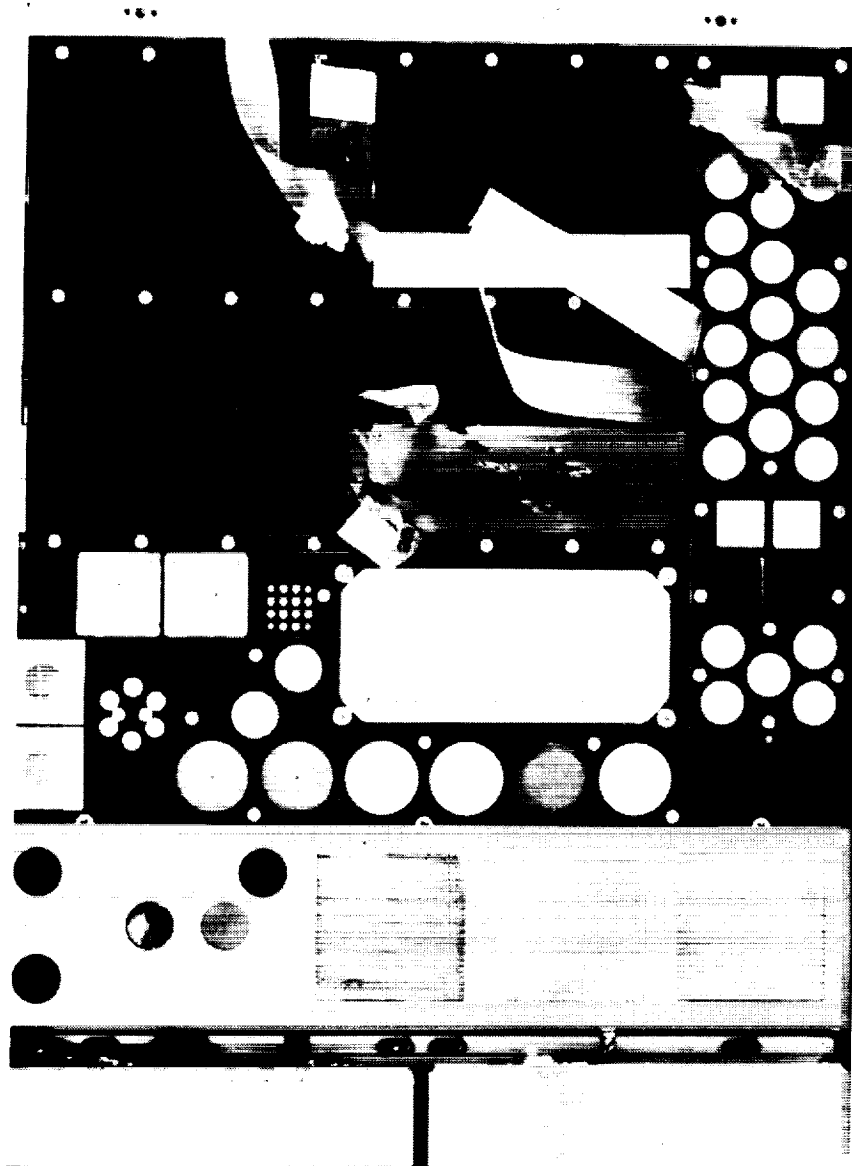


Figure 6. M0003-5 Post Flight Leading Edge Tray Closeup

M0003-5 PREFLIGHT TRAILING EDGE EXPERIMENT

The photograph in figure 7 shows the preflight polymeric film materials in the trailing edge tray. The polymer films are the horizontal strips shown in the upper and lower left portion of the mounting hardware.

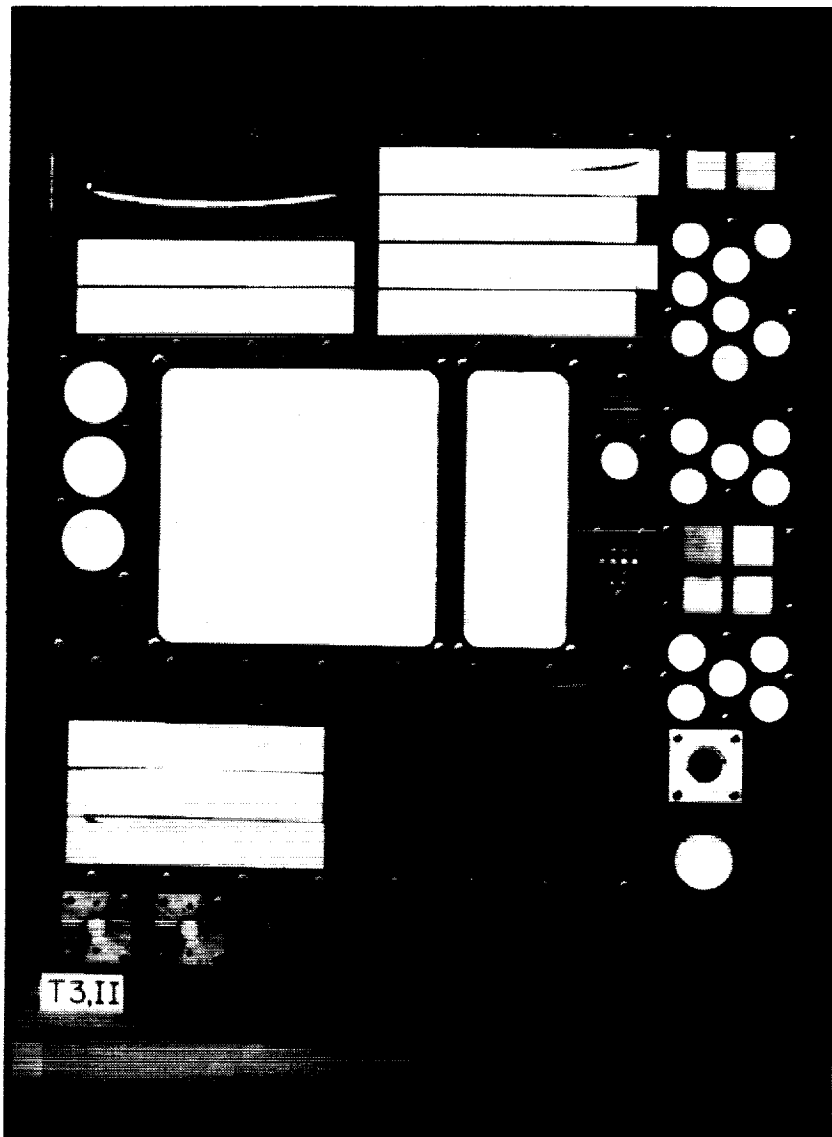


Figure 7. M0003-5 Preflight Trailing Edge Experiment

RECOVERED POST FLIGHT TRAILING EDGE M0003 TRAY

The photograph in figure 8 shows the post flight materials in the recovered trailing edge tray. Among the various areas of visible damage, note the condition of the M0003-5 polymeric film strips located in the upper right quadrant of the tray. The damage is primarily due to contamination, radiation and debonding and tearing of the polymeric films.

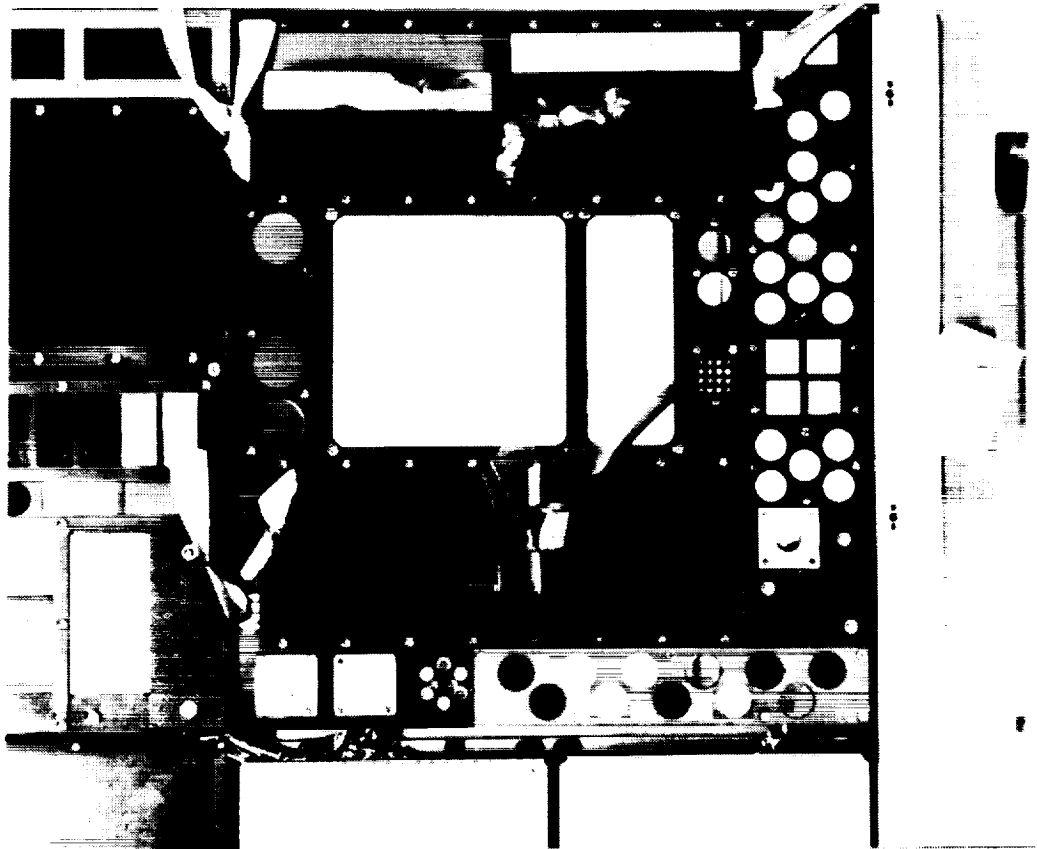


Figure 8. M0003 Post Flight Trailing Edge Tray

M0003-5 POST FLIGHT TRAILING EDGE TRAY CLOSEUP

The photograph in figure 9 below shows a closeup of the M0003-5 experiment materials. Note the extensive damage to the polymeric film strips. There are obvious physical changes, radiation damage, contamination, and debonding and tearing of the polymeric film materials.

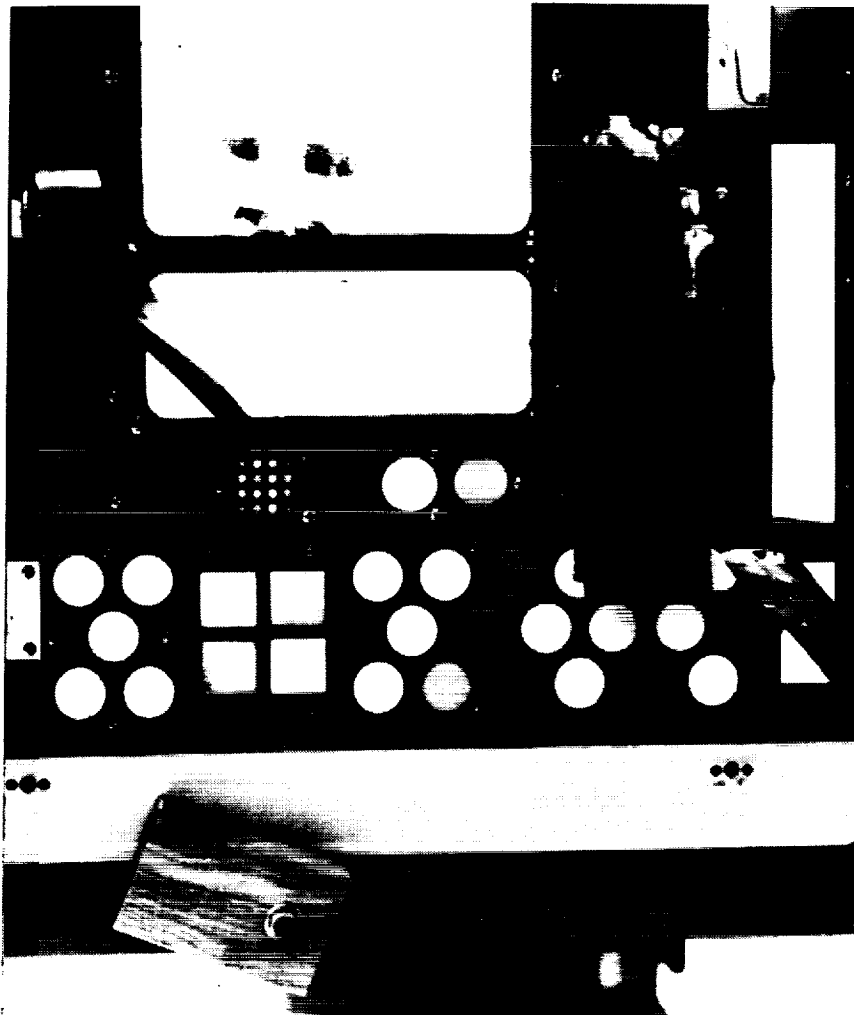


Figure 9. M0003-5 Post Flight Trailing Edge Tray Closeup

KAPTON/Al 1mil

Control C1-C3 (Laboratory Specimen)

The specimen top surface has surface scratches and dust. A weave pattern from the protective cloth used during storage is visible on the surface. There was no apparent change in the metallic surface.

C3-L3 (Leading Edge Specimen)

Fifty percent of the metallized Kapton strip is missing. It is golden yellow and has circular surface stains, vertical lines in the film and cracks through the film. The edge of the exposed strip is torn and ragged. The unexposed Al metallized surface is bright, shiny, and reflective.

C3-T3 (Trailing Edge Specimen)

The exposed Kapton surface is bright, shiny, reflective and apparently undamaged. Some debris is present on the surface. The Kapton surface is wrinkled and bunched near the left side of the film. The unexposed metallized layer is bright, shiny, reflective and apparently undamaged.

A comparison photograph of the specimens is illustrated in figure 10 and figure 11 compares the UV-Vis-NIR reflectance changes in the materials.

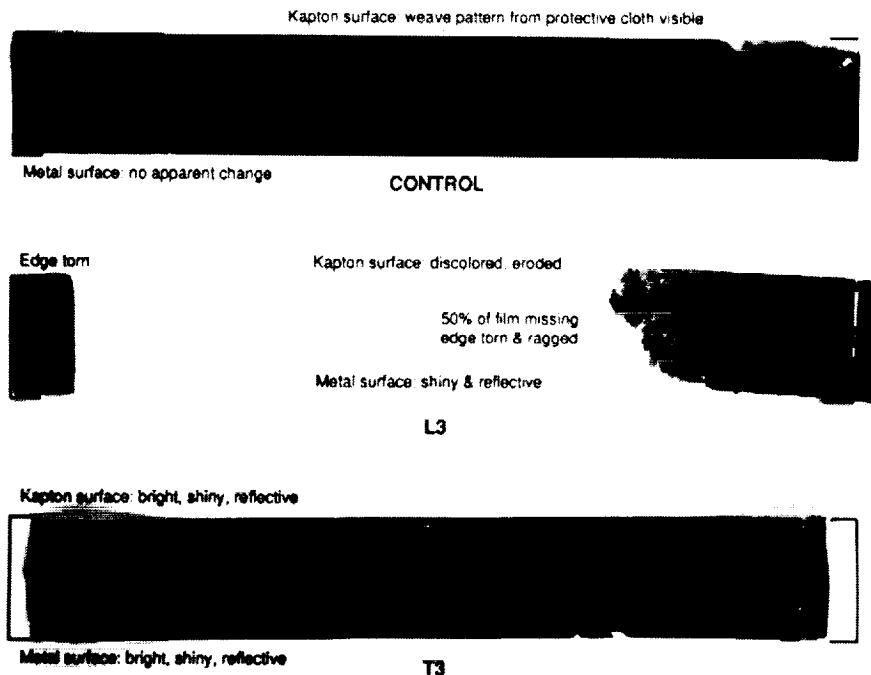


Figure 10. Comparison of Kapton/Al 1 mil Specimens

KAPTON/Al 1mil

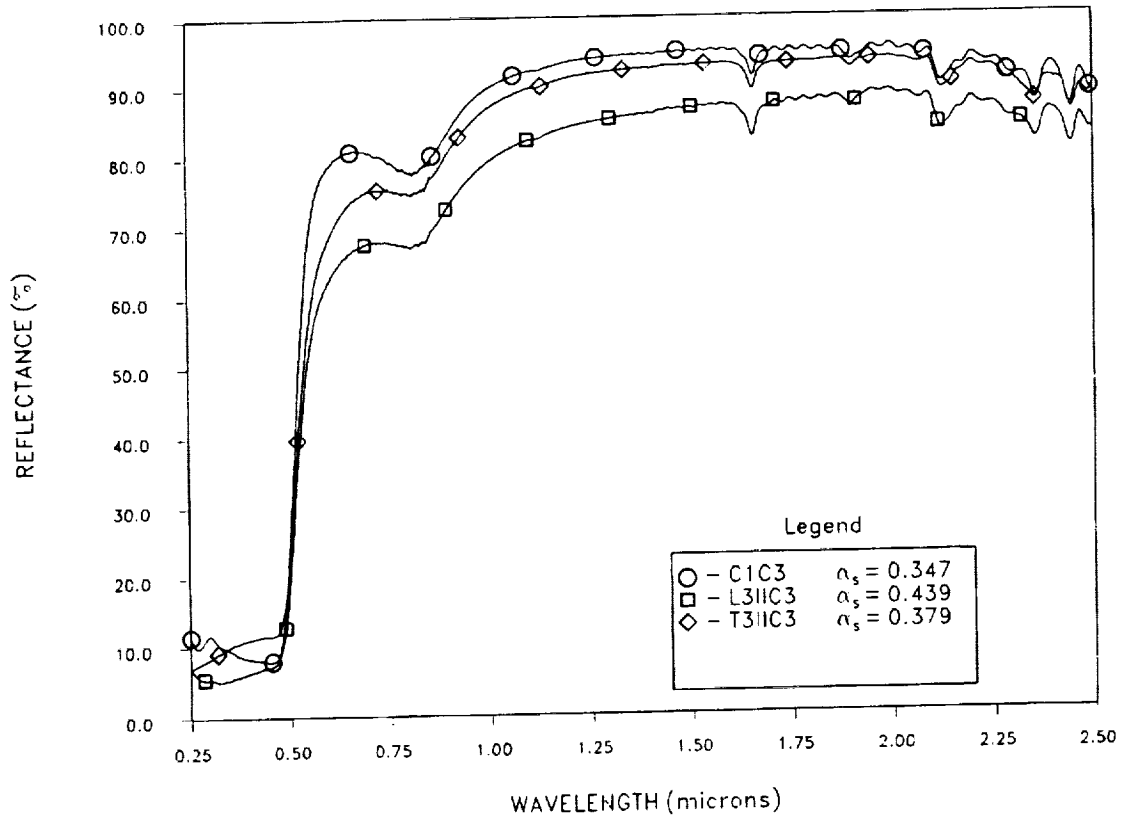


Figure 11 Comparison Reflectance Curves of Kapton/Al 1mil Specimens

FTIR SPECTRA UNAVAILABLE

KAPTON/Al 5 mil

Control C1-C4 (Laboratory Specimen)

A weave pattern from the protective cloth used during storage is visible on the surface. The metallized surface has scratches and dust and pinholes present.

C4-L3 (Leading Edge Specimen)

The metallized Kapton strip is severely discolored. The Kapton surface has large, dark, non-reflective and abraded areas. Some areas remain shiny and reflective. The surface has longitudinal lines. There are multiple probable impact sites. The separated end of the strip appears eroded. The unexposed Al metallized Kapton surface is bright, shiny and reflective. There are two small sites where the aluminum delaminated from the Kapton film.

C4-T3 (Trailing Edge Specimen)

The Kapton surface is shiny, reflective and appears undamaged. There is debris present on the surface. The metallized layer is bright, shiny, reflective and appears undamaged.

A comparison photograph of the specimens is illustrated in figure 12 and figure 13 compares the UV-Vis-NIR reflectance changes in the materials.

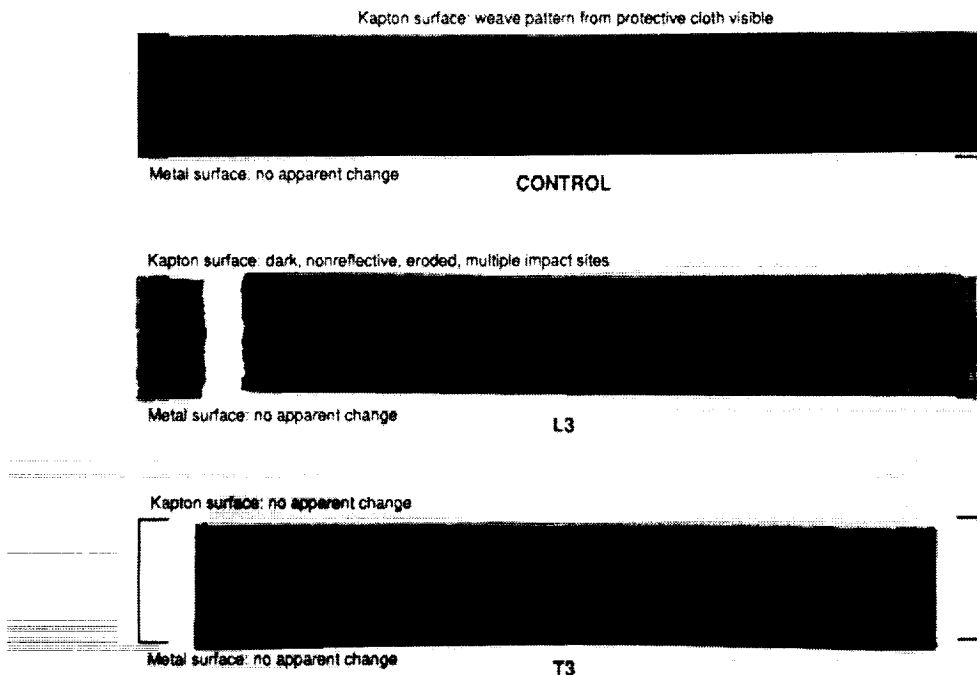


Figure 12. Comparison of Kapton/Al 5 mil Specimens

KAPTON/Al 5 mil

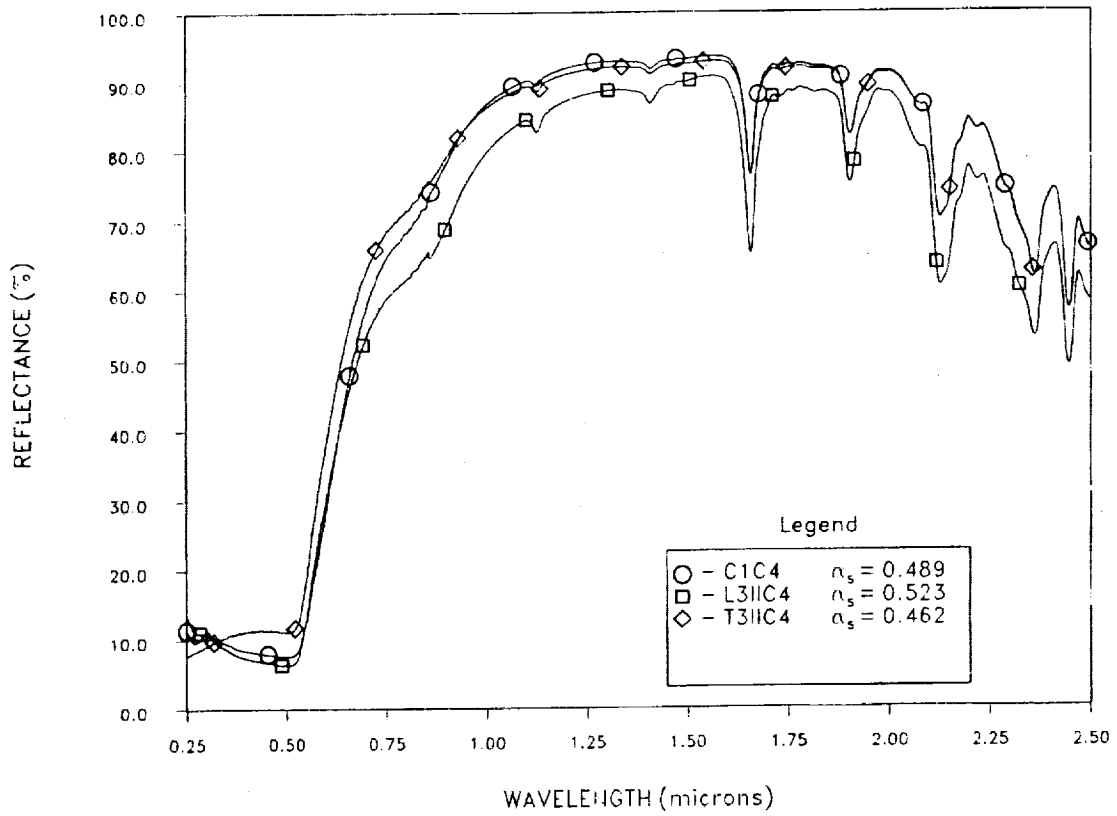


Figure 13. Comparison Reflectance Curves of Kapton/Al 5 mil Specimens

FTIR SPECTRA UNAVAILABLE

POLYPHENYLSULFONE R-5000 10 mil

Control C1-C16 (Laboratory Specimen)
Specimen is in good condition.

C16-L3

The polyphenylsulfone film surface has a deep yellow color with longitudinal lines or cracks. In the center of the film, there are three large irregularly shaped whitish areas with surrounding diagonal scratches. One irregular shaped hole is present. There are several probable impact sites with circular white rings surrounding them. There are also several dark stains or smears on the surface. The unexposed surface of the strip is shiny and reflective.

C16-T3

The polyphenylsulfone is discolored a dark brown, but is transparent. Debris is present on the surface. Other than discoloration, no apparent damage is visible.

A comparison photograph of the specimens is illustrated in figure 14 and figure 15 compares the UV-Vis-NIR reflectance changes in the materials

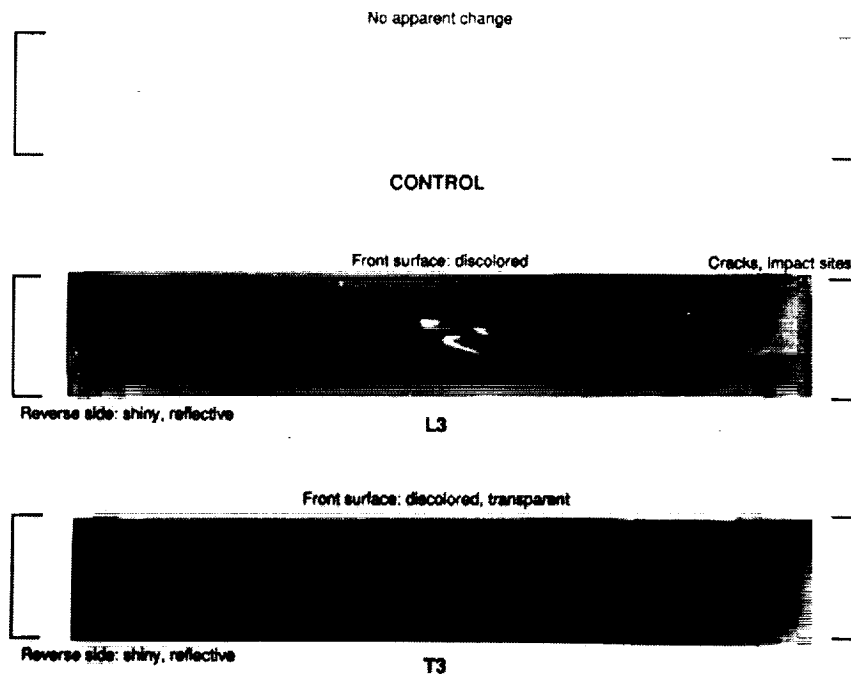


Figure 14. Comparison of Polyphenylsulfone 10 mil Specimens

POLYPHENYSULFONE R-5000 10 MIL

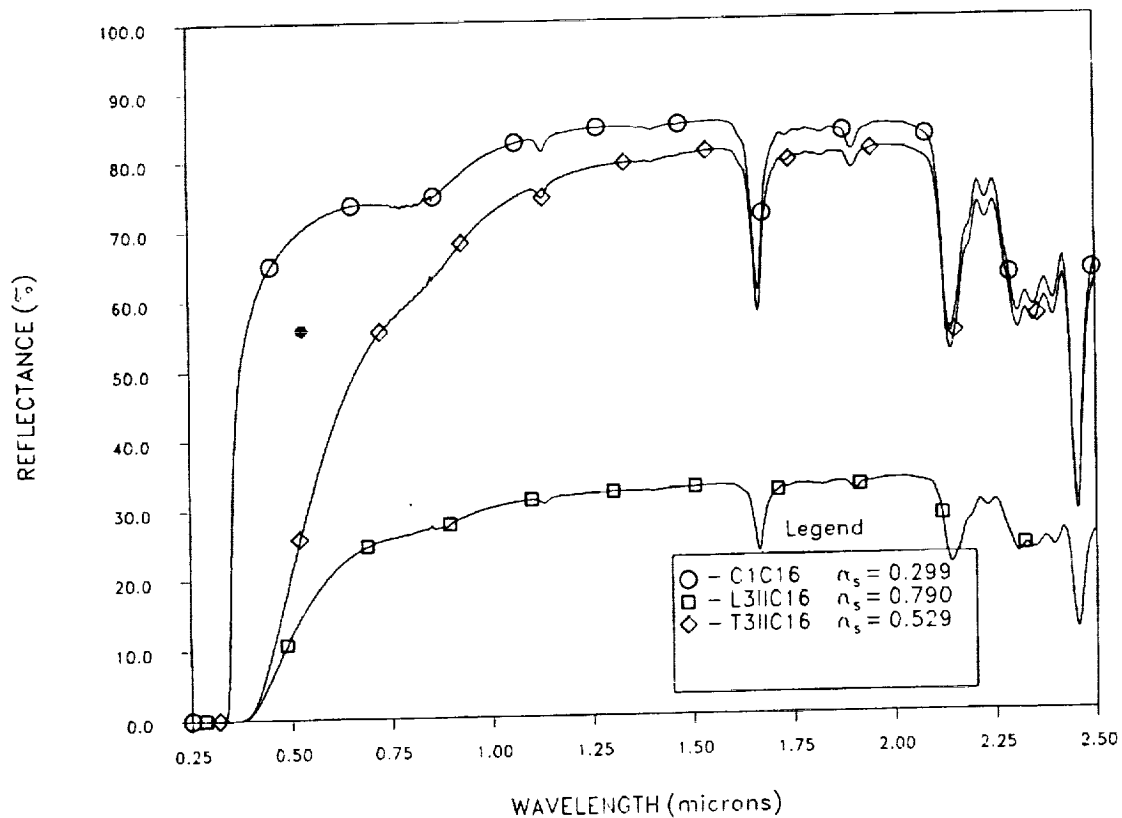


Figure 15. Comparison Reflectance Curves of Polyphenylsulfone 10 mil Specimens

FTIR SPECTRA UNAVAILABLE

FEP/Ag/INCONEL 5 mil

Control C1-C2 (Laboratory Specimen)

The specimen has surface scratches, dust and pinholes in the metallized coating.

C2-L3 (Leading Edge Specimen)

The metallized FEP strip is torn, coiled, wrinkled and discolored. The FEP surface is shiny, reflective and semitransparent with a surface haze. The metallized surface of the FEP is crazed, flaked and has a black powdery appearance. Some metallization remains in the coiled area.

C2-T3 (Trailing Edge Specimen)

The exposed surface of the FEP film is torn, stained and slightly discolored, with a probable slight haze. The metallized surface of the FEP is cracked, crazed and peeling. A substantial amount of the metallized layer has flaked away, and the area is essentially transparent. The ends of the strip show some discoloration, but little flaking or peeling.

A comparison photograph of the specimens is illustrated in figure 16 and figure 17 compares the UV-Vis-NIR reflectance changes in the materials.

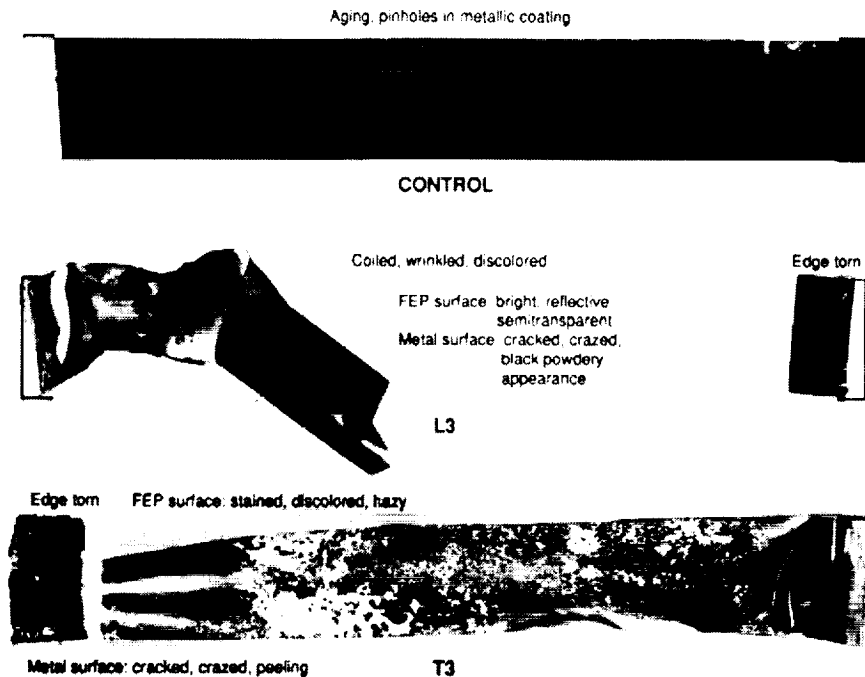


Figure 16. Comparison of FEP/Ag/Inconel 5 mil Specimens

FEP/Ag/INCONEL 5 mil

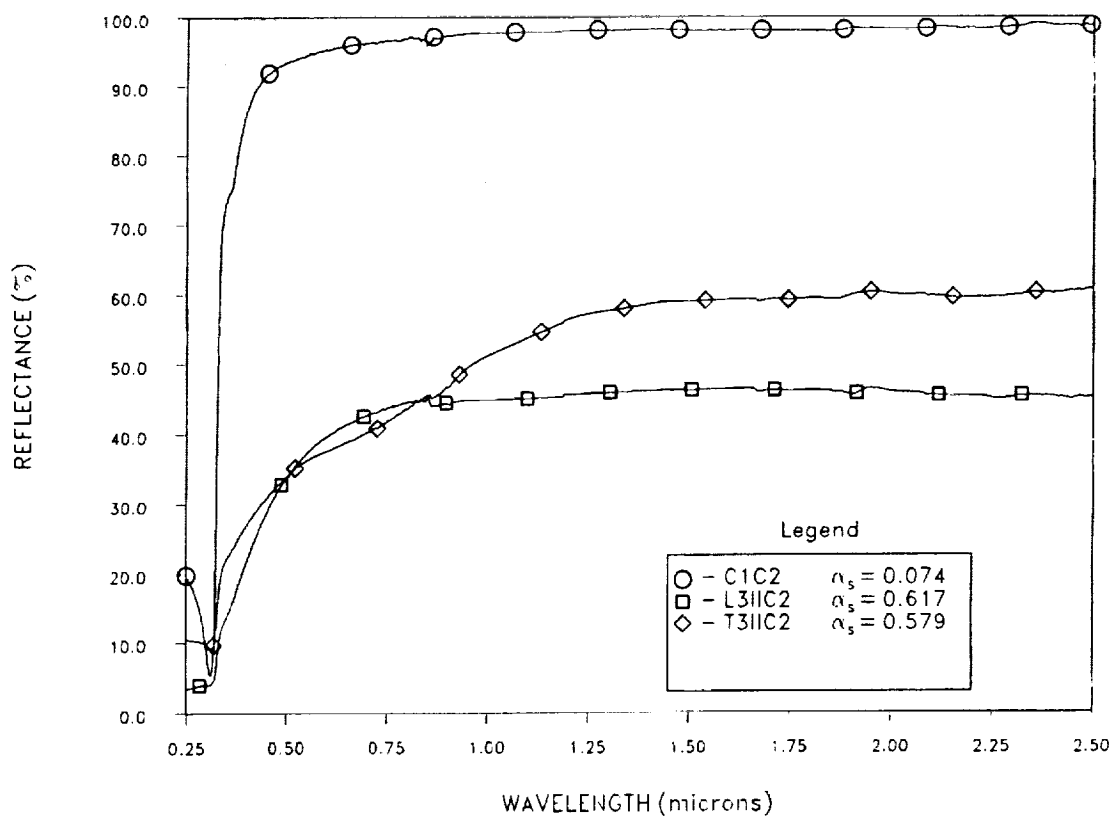


Figure 17. Comparison Reflectance Curves of FEP/Ag/Inconel 5 mil Specimens

FTIR SPECTRA UNAVAILABLE

LEADING EDGE POLYMERIC FILMS MOUNTING

The photograph shown in figure 18 illustrates the front surface of the leading edge polymer film mounting plate prior to removal of the polymer films. It should be noted that in many cases the lapped adhesive bonds failed or the polymer film was separated from one side of the mounting plate by tearing. The debonding and tearing of the films was probably due to thermal cycling effects. Scarring due to probable AO impingement deflected from the scuff plate is evident. The RTV 560 + 12% graphite adhesive failed in all cases.

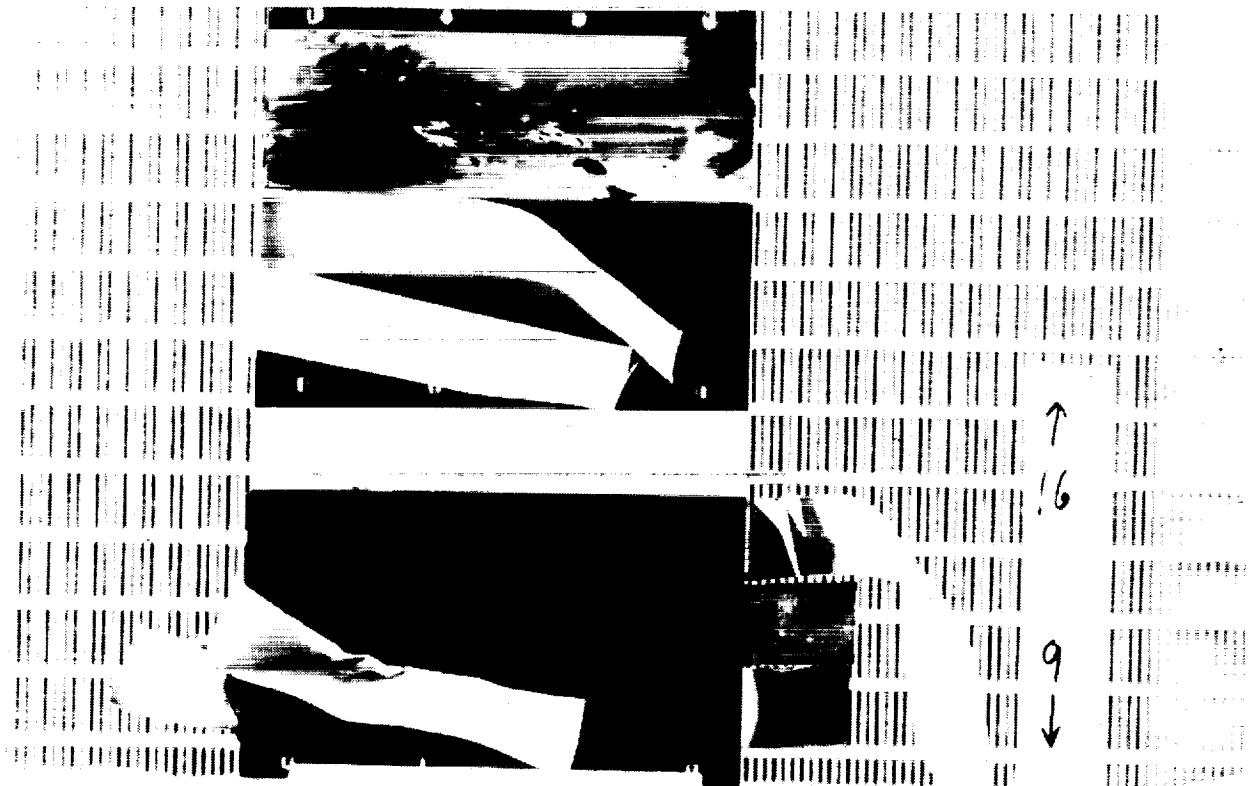


Figure 18. Polymer Film Leading Edge Front Surface Plate

LEADING EDGE POLYMERIC FILMS MOUNTING

The photograph shown in figure 19 illustrates the rear face of one of the leading edge polymer films mounting plates prior to removal of the polymer films. It should be noted that the original adhesive bonding of the films to the mounting plate has not been visibly affected.

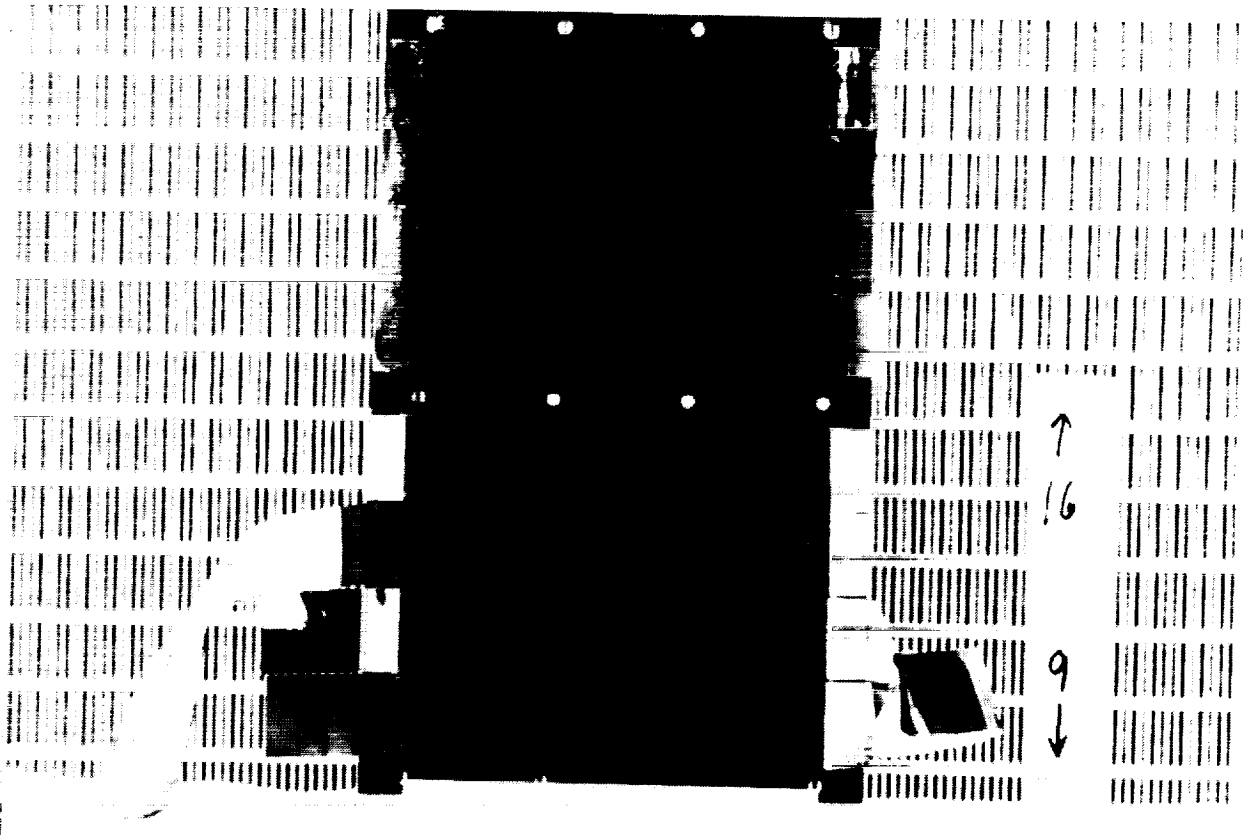


Figure 19. Polymer Film Leading Edge Rear Surface Plate

TRAILING EDGE POLYMERIC FILMS MOUNTING

The photograph shown in figure 20 illustrates the front surface of one of the trailing edge polymer film mounting plates prior to the removal of the polymer films. It should be observed that two of the lapped adhesive bonds failed and one film was separated from one side of the mounting due to tearing. The debonding and tearing were probably caused by thermal cycling effects. The RTV 560 + 12% graphite adhesive failed in all cases.

ORIGINAL PAGE
BLACK AND WHITE PHOTOGRAPH

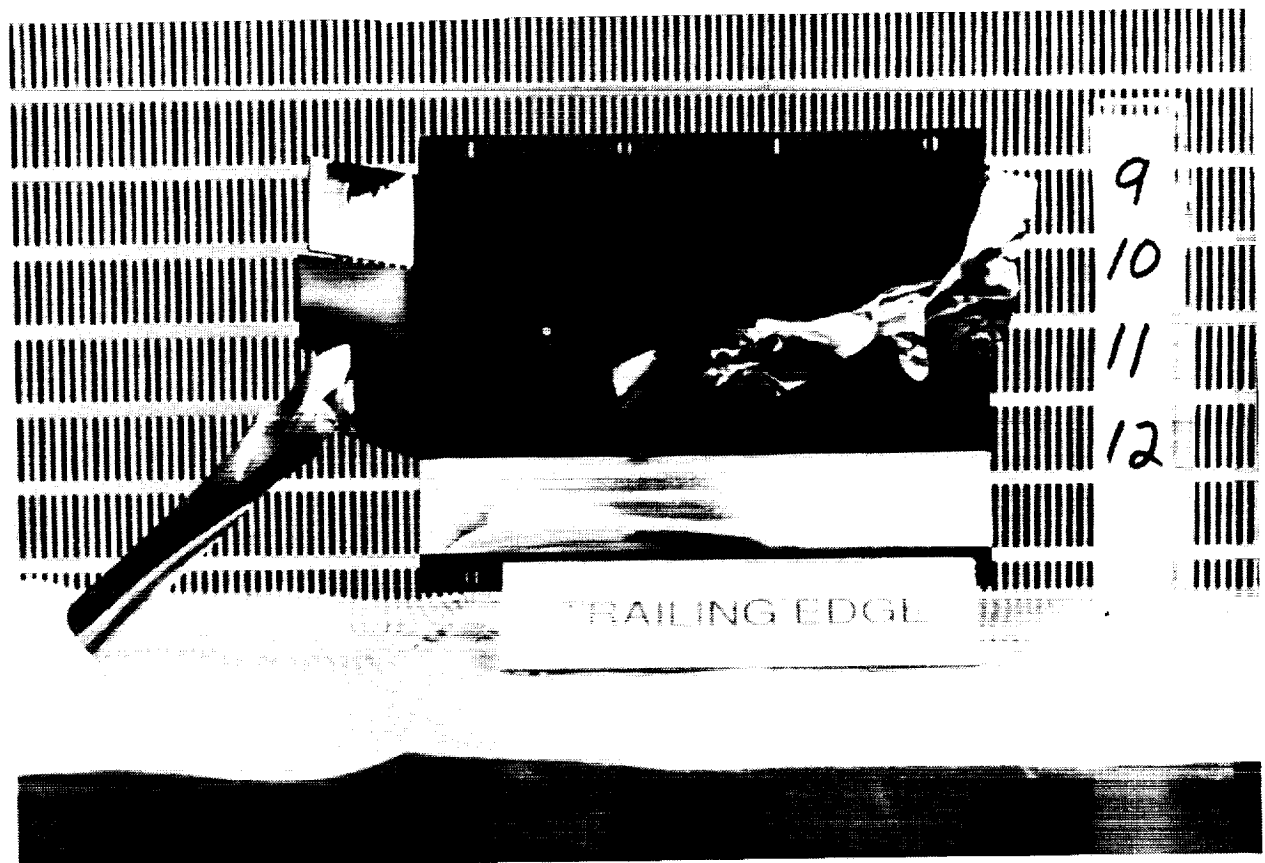


Figure 20. Polymer Film Trailing Edge Front Surface Plate

TRAILING EDGE POLYMERIC FILMS MOUNTING

The photograph shown in figure 21 illustrates the rear face of one of the trailing edge mounting plates prior to removal of the polymer films. It should be noted that the original adhesive bonding of the films to the mounting plate has not been visibly affected.

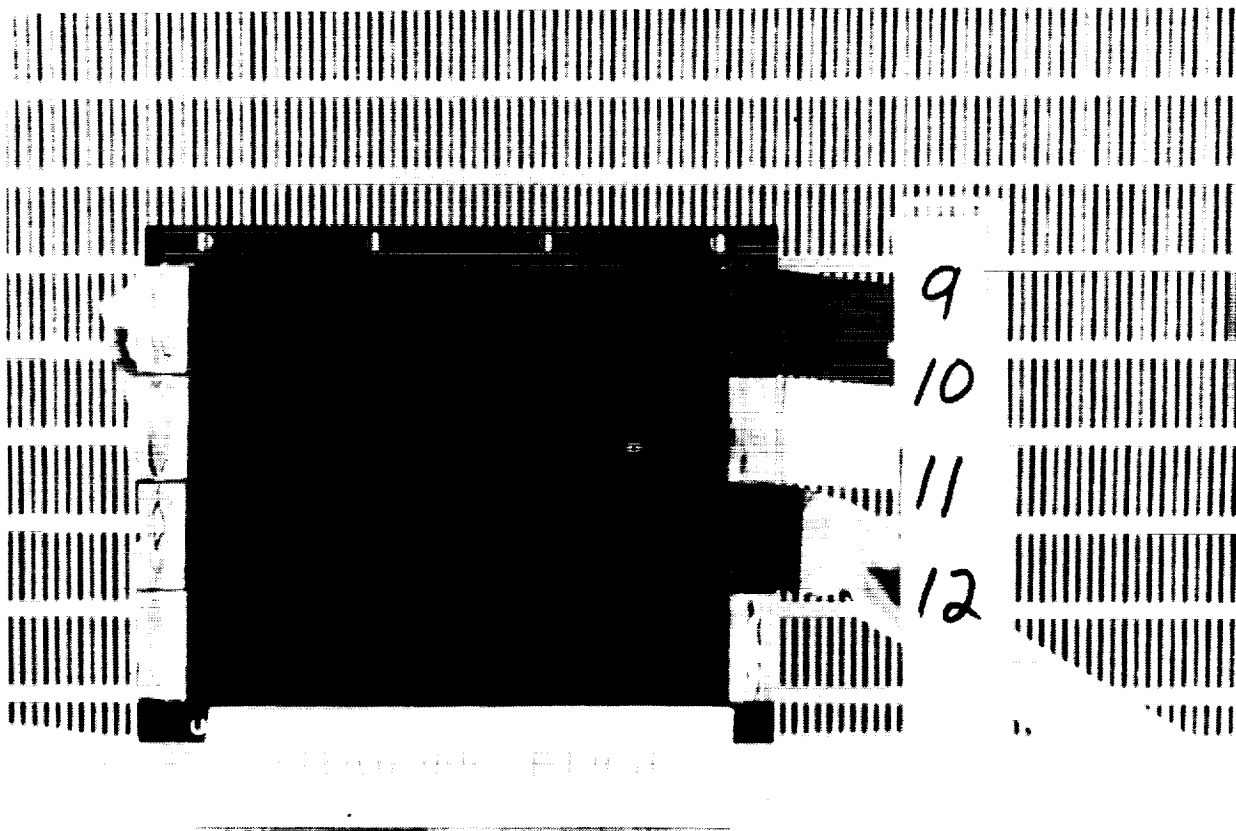


Figure 21. Polymer Film Trailing Edge Rear Surface Plate

FEP/Ag/INCONEL/RTV 560 + GRAPHITE/KAPTON 5 mil

Control C1-C9 (Laboratory Specimen)

Specimen has surface scratches. There are small areas of yellow discoloration near the bond area. The metallized coating has pinholes. Some pinholes have tarnish rings surrounding the pinhole site.

C9-L3

The metallized FEP strip is curled, coiled and discolored. The FEP exposed surface in the unbonded area is shiny, reflective and semitransparent. The FEP surface over the bonded area does not differ from the rest of the strip. The exposed Kapton surface is apparently undamaged. The RTV 560 adhesive bond between the FEP/Ag/Inconel and the Kapton/Al failed completely. The RTV 560 remained adhered to the Kapton surface. There is no visual evidence of an adhesive residue on the Inconel surface of the FEP. The metallized surface of the FEP is crazed, flaked and has a black powdery appearance. The metallized face of the Kapton is bright, reflective and appears undamaged.

C9-T3

The FEP is wrinkled, curled and distorted. The FEP surface is shiny and reflective with a milky haze. The adhesive bond between the FEP/Ag/ Inconel and the Kapton Al failed completely. The RTV 560 + 12% graphite adhesive remained adhered to the Kapton/Al tab, and is intact . The metallized layer of the FEP is reflective, but darker in color. The exposed Kapton is bright, shiny and reflective.

A comparison photograph of the specimens is illustrated in figure 22 and figure 23 compares the UV-Vis-NIR reflectance changes in the materials.

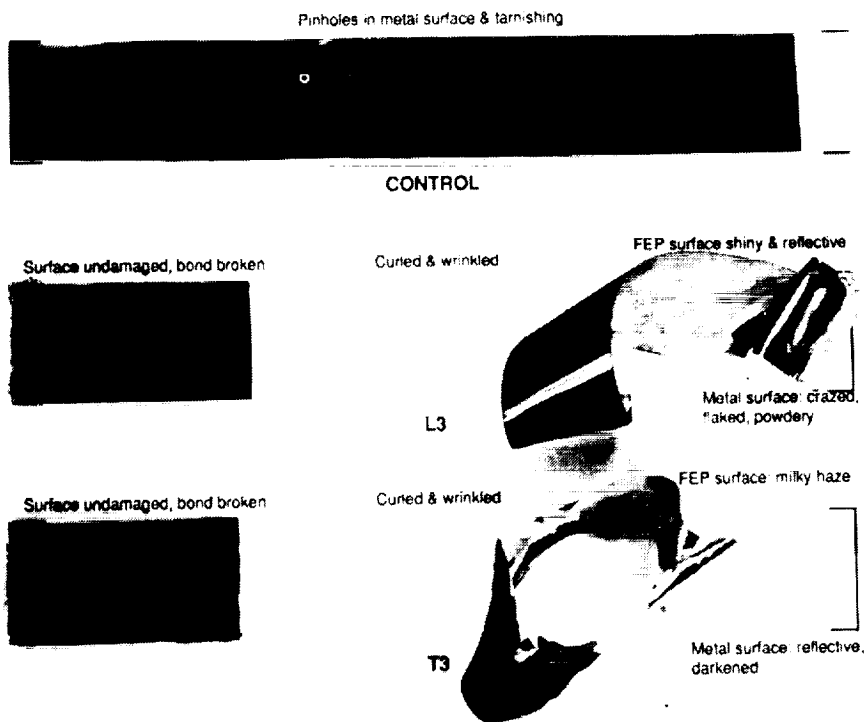


Figure 22. Comparison of FEP/Ag/Inconel/RTV 560 + Graphite/Kapton 5 mil

FEP/Ag/INCONEL/RTV 560 + GRAPHITE/KAPTON 5 MIL

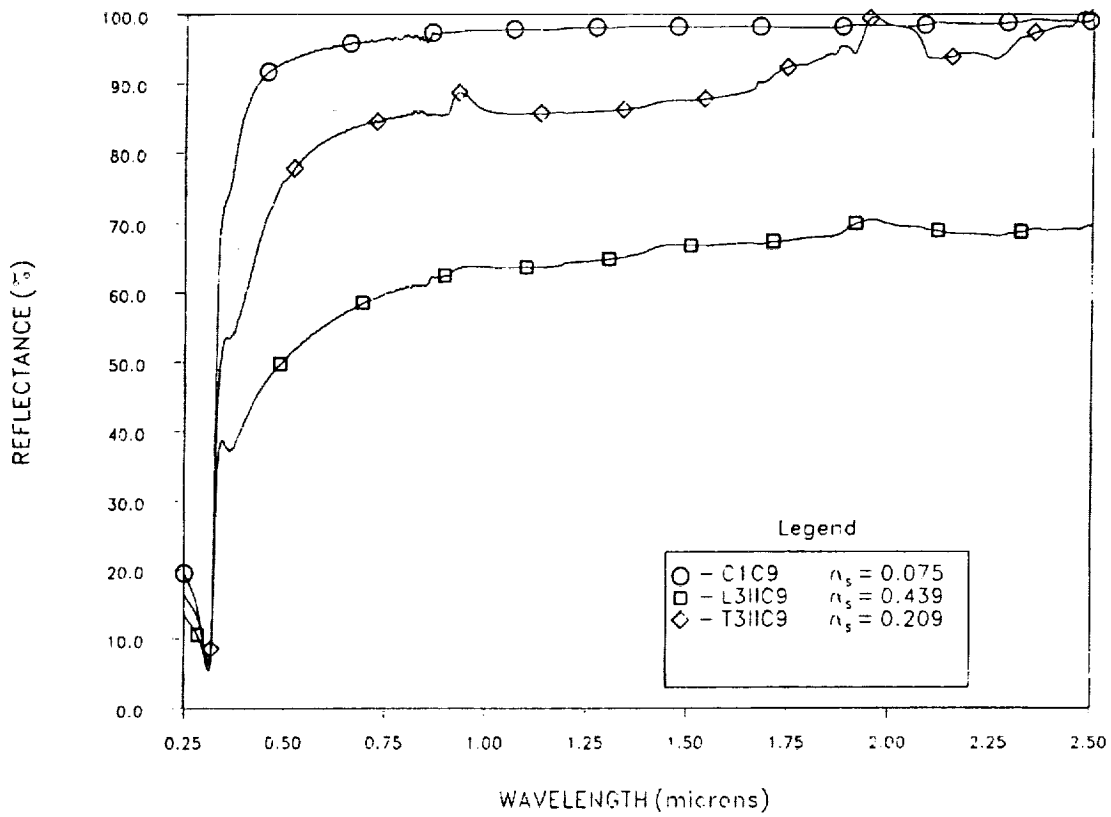


Figure 23. Comparison Reflectance Curves of FEP/Ag/Inconel/RTV 560 + 12% Graphite/Kapton/Al 5 mil Specimens

FTIR SPECTRA UNAVAILABLE

FEP/Ag/INCONEL/EC57C/KAPTON/Al 5 mil

Control C1-C6 (Laboratory Specimen)

Specimen has scratches and dust. Severe scratches in bonded area. Pinholes are present in the metallized coating.

C6-L3 (Leading Edge Specimen)

The metallized FEP strip is torn, coiled and discolored. The FEP exposed surface in the unbonded area is shiny, reflective and semitransparent. The FEP exposed surface over the bonded area has a milky appearance with possible surface erosion and yellow brown surface stains. The exposed Kapton surface is discolored and eroded. The EC57C adhesive bond between the FEP/Ag/Inconel and the Kapton/Al is intact. The metallized face of the FEP is crazed and flaked and has a black powdery appearance. The metallized face of the FEP in the bond area is intact. The Al metallized face of the Kapton is bright, reflective and appears undamaged.

C6-T3 (Trailing Edge Specimen)

The film strip is torn and curled. The FEP surface appears hazy and milky. The metallized side of the FEP film is darkened and hazy. There are some areas of black powdery smears. The adhesive bond is intact. The FEP surface over the bond area has a slight yellow discoloration. The Kapton tab is shiny, reflective and appears undamaged. The metallized side of the Kapton is also bright, shiny and appears undamaged.

A comparison photograph of the specimens is illustrated in figure 24 and figure 25 compares the UV-Vis-NIR reflectance changes in the materials.

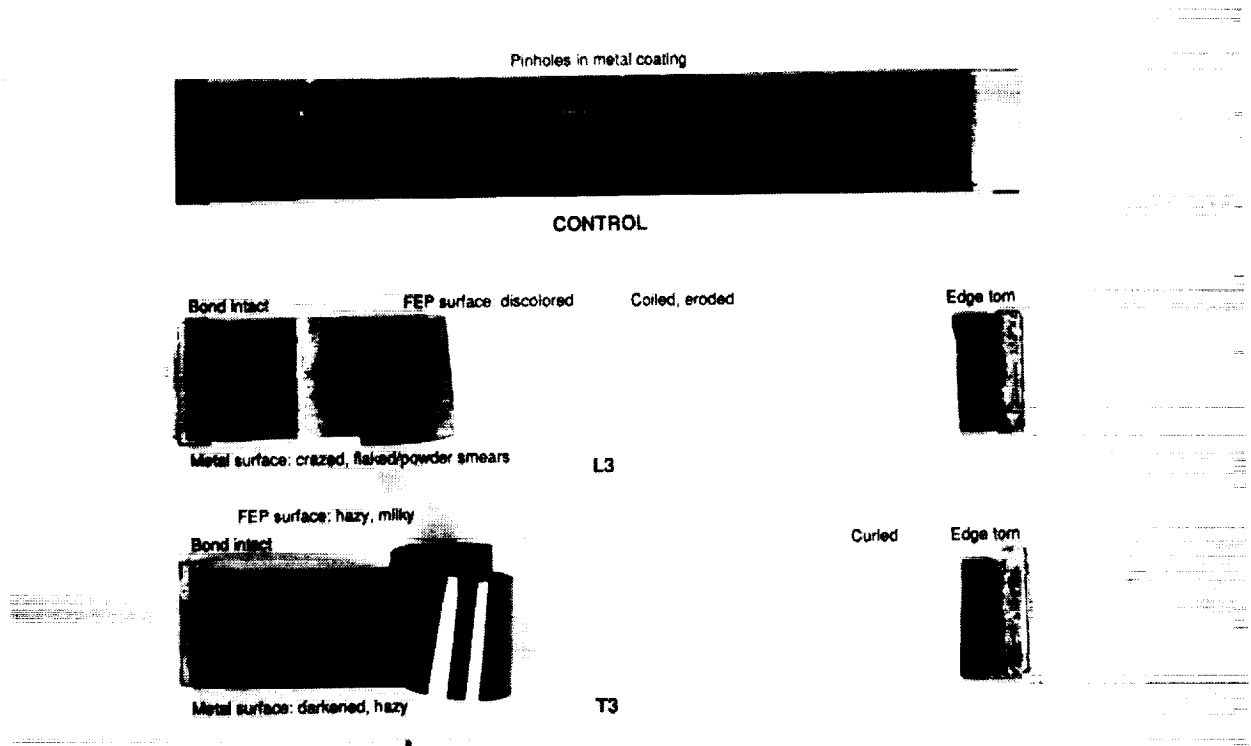


Figure 24. Comparison of FEP/Ag/Inconel/EC57C/Kapton/Al 5 mil

FEP/Ag/INCONEL/EC57C/KAPTON/Al 5 mil

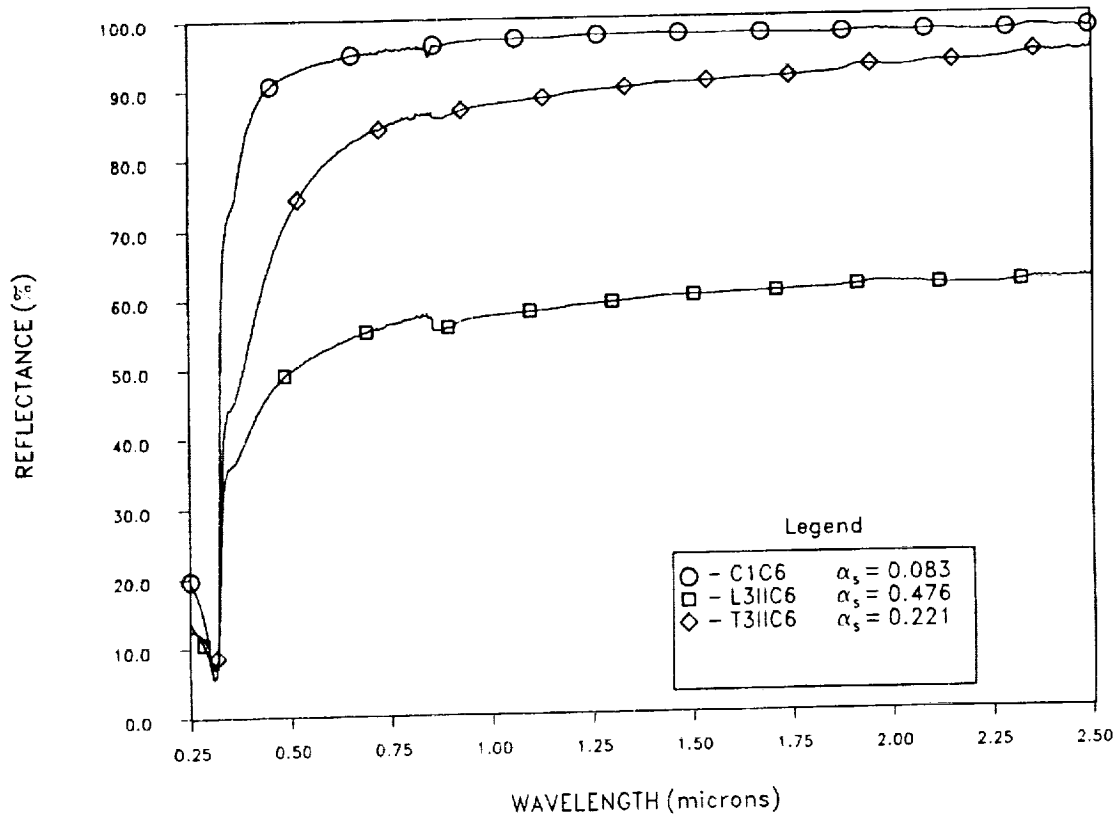


Figure 25. Comparison Reflectance Curves of FEP/Ag/Inconel/EC57C/Kapton/Al 5 mil Specimens

FTIR SPECTRA UNAVAILABLE

FEP/Ag/INCONEL/Y966/KAPTON 5 mil

Control C1-C11 (Laboratory Specimen)

Specimen has surface scratches. Pinholes are present in the metallized layer.

C11-L3

The metallized FEP strip is torn, curled and discolored. The FEP surface is shiny, reflective and semi-transparent. The FEP surface over the bonded area has a milky appearance and whitish smears. The exposed Kapton surface is dull, discolored and possibly eroded. The Y966 adhesive bond between the FEP/Ag/Inconel and the Kapton/Al is intact. The metallized surface of the FEP is crazed, flaked and has a black powdery appearance. The metallized face of the FEP in the bond is intact. The Al metallized surface of the Kapton is bright, reflective and apparently undamaged.

C11-T3

The FEP film is torn, shiny, reflective and may have a slight haze. The FEP film is wrinkled and distorted near the bond site. The adhesive bond between the FEP/Ag/Inconel and the Kapton/Al is intact. The metallized surface of the FEP is shiny, but may have darkened. The Kapton surface is bright, shiny and undamaged. The aluminized surface of the Kapton is shiny and reflective.

A comparison photograph of the specimens is illustrated in figure 26 and figure 27 compares the UV-Vis-NIR reflectance changes in the materials.

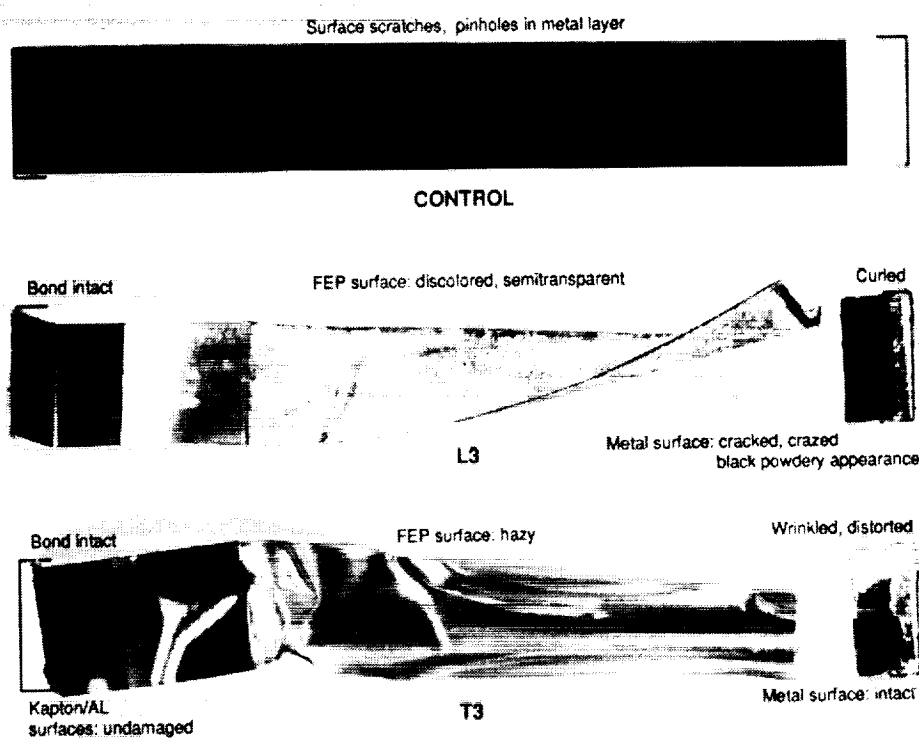


Figure 26. Comparison of FEP/Ag/Inconel /Y966/Kapton/5 mil

FEP/Ag/INCONEL/Y966/KAPTAN 5 mil

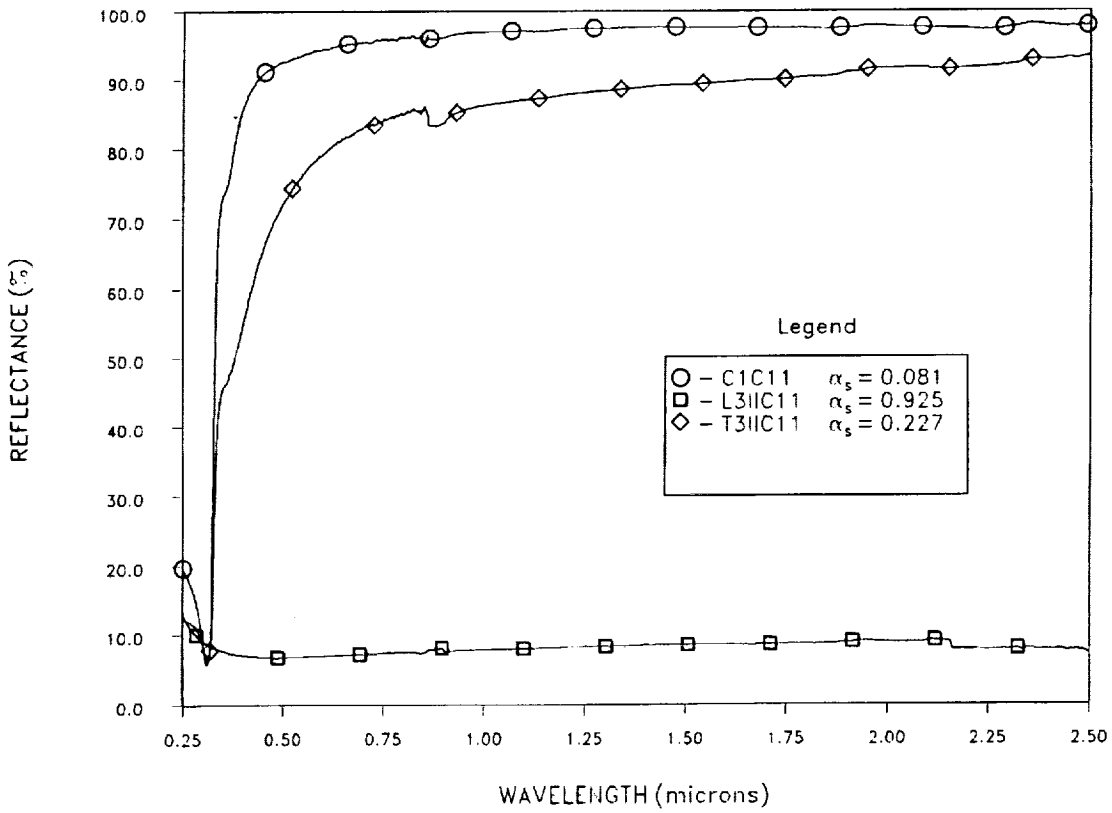


Figure 27. Comparison Reflectance Curves of FEP/Ag/Inconel/Y966/Kapton 5 mil Specimens

FTIR SPECTRA UNAVAILABLE

OBSERVATIONS

1. 14 out of 32 polymer film strips exhibited adhesive bond separation or tearing due probably to thermal cycling.
2. The EC57C and Y966 adhesive bonds remained intact.
3. Kapton/Al materials exhibited probable AO erosion.
4. RTV 560 + 12% graphite adhesive bonds failed in all cases.
5. The most significant changes in reflectance occurred in the leading edge polymer films.



LDEF MATERIALS WORKSHOP '91 AGENDA

NASA Langley Research Center
H. J. E. Reid Conference Center
14 Ames Road Building 1222
Hampton, Virginia 23665-5225
November 19 - 22, 1991

Tuesday, November 19, 1991

8:30 a.m. Introductions

William H. Kinard, LDEF Chief Scientist
Bland A. Stein, Workshop Coordinator
Philip R. Young, Workshop Coordinator

9:00 a.m. Technical Session

- LDEF Materials, Environmental Parameters, and Data Bases (Plenary Session)

Cochairman: Bruce Banks, NASA - Lewis Research Center
Cochairman: Mike Meshishnek, The Aerospace Corporation
Recorder: Roger Bourassa, Boeing Defense & Space Group

LDEF Atomic Oxygen Fluence Update Roger Bourassa
Boeing Defense & Space Group

LDEF Yaw and Pitch Angle Estimates Bruce Banks

LDEF Experiment M0003 Meteoroid and Debris Survey Mike Meshishnek
The Aerospace Corporation

Atomic Oxygen Erosion Yields of LDEF Materials Bruce Banks, LeRC for John Gregory
University of Alabama in Huntsville

The LDEF M0003 Experiment Deintegration Observation Data Base Sandy Gyetvay
The Aerospace Corporation

Overview of Flight Data from LDEF M0003 Experiment Power and Data System John Coggi
The Aerospace Corporation

12:00 Noon Lunch

Tuesday, November 19, 1991 continued

1:00 p.m. Technical Session

- LDEF Contamination (Plenary Session)

Cochairman: Steve Koontz, NASA Johnson Space Center
Cochairman: Wayne Stuckey, The Aerospace Corporation
Recorder: Russell Crutcher, Boeing Defense & Space Group

Introduction	Wayne Stuckey The Aerospace Corporation
Materials SIG Quantification and Characterization of Surface Contaminants	Russell Crutcher Boeing Defense & Space Group
Z-306 Molecular Contamination Ad-Hoc Committee Results	John Golden Boeing Defense & Space Group
LDEF Contamination Modelling	Tim Gordon Applied Science Technology and Ray Rantanen ROR Enterprises
M0003 Contamination Results	Wayne Stuckey and Carol Hemminger The Aerospace Corporation
Organic Contamination on LDEF	Gale Harvey NASA Langley Research Center
5:00 p.m. End Session	

Wednesday, November 20, 1991

8:00 a.m. Technical Session

- **Thermal Control Coatings, Protective Coatings and Surface Treatments (Plenary Session)**

Cochairman: Ann Whitaker, NASA Marshall Space Flight Center
 Cochairman: Wayne Slemp, NASA Langley Research Center
 Recorder: John Golden, Boeing Defense & Space Group

Thermal Control Materials on Thermal Control Surfaces (TCSE) Experiment	James Zwiener, NASA MSFC for Don Wilkes AZ Technology
Vacuum Deposited Coatings	Wayne Slemp NASA Langley Research Center
Anodized Aluminum on LDEF	John Golden Boeing Defense & Space Group
Thermal Control Tape	Rachel Kamenetsky NASA Marshall Space Flight Center
Fluorescence in Thermal Control Coatings	James Zwiener NASA Marshall Space Flight Center
Thermal Control Coatings on DoD Flight Experiment	William Lehn, Nichols Research Corp. for Charles Hurley Univ. of Dayton Research Institute and Michele Jones U.S.A.F Wright Laboratories
Next Generation LDEF: Retrieval Payload Carrier	Arthur Perry American Space Technologies, Inc.

Optical Transmission and Reflection Measurements
of Thin Metal Films Exposed on LDEF

Roger Linton, NASA MSFC for John Gregory
University of Alabama in Huntsville and

Oxidation of Black Chromium Coatings on LDEF

John Golden
Boeing Defense & Space Group

LANL Results from Space-and Ground-based Atomic
Oxygen Exposures of Metals and Inorganic Materials

Jon Cross
Los Alamos National Laboratory (LANL)

AXAF Optical Materials and Issues

James Bilbro, NASA MSFC for Alan Shapiro
NASA Marshall Space Flight Center

Effects of Space Exposure on Pyroelectric
Infrared Detectors

James Robertson
NASA Langley Research Center

Status and Results of LDEF Optical Systems
SSIG Data Base

Gail Bohnhoff-Hlavacek
Boeing Defense & Space Group

5:00 p.m. **End Session**

Thursday, November 21, 1991

8:00 a.m. Technical Session

• Polymer-Matrix Composites (Concurrent Session)

Cochairman: Rod Tennyson, University of Toronto
Cochairman: Gary Steckel, The Aerospace Corporation
Recorder: Pete George, Boeing Defense & Space Group

M0003 and Other Polymer-Matrix Composites

Gary Steckel
The Aerospace Corporation

A0134: Polymer Matrix Composites

Wayne Slemp
NASA Langley Research Center

Space Environmental Effects on LDEF Low-Earth
Orbit (LEO) Exposed Graphite-Reinforced
Polymer-Matrix Composites

Pete George
Boeing Defense & Space Group

Long-Term Environmental Effects on
Carbon-and Glass-Fiber Composites

Ann Whitaker
NASA Marshall Space Flight Center

Evaluation of Long-Duration Exposure to the
Natural Space Environment on Graphite-Polyimide
and Graphite-Epoxy Mechanical Properties

Richard Vyhna
Rockwell International

Proposed Test Program and Data Base
for LDEF Polymer-Matrix Composites

Pete George
Boeing Defense & Space Group and
Rod Tennyson
University of Toronto

12:00 Noon **Lunch**

Thursday, November 21, 1991

8:00 a.m. Technical Session

- **Lubricants, Adhesives, Seals, Fasteners, Solar Cells, and Batteries (Concurrent Session)**

Cochairman: James Mason, NASA Goddard Space Flight Center
Cochairman: Joel Edelman, LDEF Consultant
Recorder: Harry Dursch, Boeing Defense & Space Group

Identification and Evaluation of Lubricants, Adhesives, and Seals Used on LDEF	Bruce Keough Boeing Defense & Space Group
Results from the Testing and Analysis of LDEF Batteries	Steve Spear Boeing Defense & Space Group
Effects of Long-Term Exposure on Fastener Assemblies	Steve Spear Boeing Defense & Space Group
Results from the Testing and Analysis of Solar Cells Flown on LDEF	Harry Dursch Boeing Defense & Space Group
System Related Testing and Analysis of FRECOPA	Christian Durin Centre National D'etudes Spatiales

12:00 Noon **Lunch**

1:00 p.m.

- Working meetings of **Theme Panels** to prepare charts for Workshop Summary Session and begin draft of panel report. **(Concurrent Session)**

5:00 p.m. **End Session**

Friday, November 22, 1991

8:00 a.m. Technical Session

- **LDEF Materials Workshop '91 - Summary (Plenary Session)**
 - 20-minute presentations by panel chairmen followed by question/answer periods
 - Final general discussion period moderated by workshop coordinators

12:00 Noon **End Workshop**

 **LDEF
MSIG
MATERIALS
SPECIAL INVESTIGATION GROUP**



ATTENDEE LIST

S. Carl Ahmed
POBox 03-4075
Technology Transfer Specialists, Inc.
Indialantic FL 32903-0975
407/777-0019

Ruth Amundsen
Mail Stop 431
NASA Langley Research Center
Hampton VA 23665-5225
804/864-7044
804/864-7202

J. I. Applin
Mail Stop 431
NASA Langley Research Center
Hampton VA 23665-5225
804/864-7082

D. F. Auvil
Mail Stop 424
NASA Langley Research Center
Hampton VA 23665-5225
804/864-5631

Robert D. Averill
Mail Stop 433
NASA Langley Research Ctr.
Hampton VA 23665-5225
804/864-7088
804/864-7009

C. D. Bailey
Mail Stop 424
NASA Langley Research Center
Hampton VA 23665-5225
804/864-5634

Bruce A. Banks
NASA LeRC M/S 302-1
21000 Brookpark Rd
Cleveland OH 44135
216/433-2308 (FTS 297-2308)
216/433-6106

W. M. Berrios
Mail Stop 434
NASA Langley Research Center
Hampton VA 23665-5225
804/864-7183

Charles F. Bersch
Institute for Defense Analyses
1801 N. Beauregard St.
Alexandria VA 22311
703/578-2863
703/578-2877

Anthony Beverina
Kaman Sciences Corp./Suite 200
2560 Huntington Ave.
Alexandria VA 22303
703/329-7167
703/329-7197

John Bianchi
202 Ross Hall/Dept. of Mech. Engrg
Auburn University
Auburn University AL 36899
205/844-3345
205/844-3307

James W. Bilbro
Mail Code EB23
NASA Marshall Space Flight Ctr.
Huntsville AL 35812
205/544-3467
205/544-2659

Brian Blakkolb
TRW Space & Defense
One Space Park M/S R4-2173
Redondo Beach CA 90278
213/813-8960
213/812-8768

Charles Blatchley
Spire Corporation
One Patriots Park
Bedford MA 01730
617/275-6000
617/275-7470

Dr. Jeffrey Blezius
MPB Technologies
151 Hymus Blvd.
Pointe-Claire, Quebec CANADA H9
91 514/694-8751
91 514/695-7492

M. D. Blue
GTRI/Baker Bldg. 323
Georgia Tech.
Atlanta GA 30332
404/894-3646
404/894-6285

Gail Bohnhoff-Hlavacek
Boeing M/S 8H-01
PO Box 3999
Seattle WA 98124
206/773-6892
206/773-4946

Roger J. Bourassa
Boeing Defense & Space Group-M/S
PO Box 3999
Seattle WA 98124-2499
206/773-8437
206/773-4946

David E. Bowles
Mail Stop 191
NASA Langley Research Ctr.
Hampton VA 23556-5225
804/864-3095
804/864-7729

F. L. Boyer
Mail Stop 424
NASA Langley Research Center
Hampton VA 23665-5225
804/864-5666

David Brinza
JPL Mail Stop 67-201
4800 Oak Grove Dr.
Pasadena CA 91109
818/354-6836
818/393-6869

W. Brower
Marquette University

Milwaukee WI 53233
414/288-7081
414/288-7082

Richard W. Cahill
Lockheed Missiles & Space Co. 0/77-60, B/
Box 3504
Sunnyvale CA 94088
408/743-2739
408/742-2423

George Caledonia
Physical Sciences, Inc.
20 New England Business Center
Andover MA 01810
508/689-0003

*** Where there are two phone numbers given, the second one is the **FAX** number.

Robert L. Calloway
LDEF Science Office M/S 404
NASA Langley Research Ctr.
Hampton VA 23665-5225
804/864-2960
804/864-8094

Mark A. Carlson
McDonnell Douglas Space Systems Co
5301 Bolsa Ave. M/S 15-1/103
Huntington Beach CA 92647
714/896-3311 x 70083
714/869-2937

Soo-Kong Chang
Spar Aerospace Ltd
1700 Ormond Dr.
Weston, Ontario CANADA M9L 2W
416/745-9696 X 4351
416/745-4172

Robert J Christie
Rockwell International
22021 Brookpark Rd
Cleveland OH 44126
216/734-2550
216/734-9129

Carroll H. Clatterbuck
Mail Code 313.2
NASA Goddard Space Flight Ctr.
Greenbelt MD 20771
301/286-67991
301/286-2717

Craig Cleckner
Mail Stop 431
NASA Langley Research Center
Hampton VA 23665-5225
804/864-7048
804/864-7202

Jean Clough
Mail Stop 115
NASA Langley Research Center
Hampton VA 23665-5225
804/864-6122

John M. Coggi
The Aerospace Corp.
PO Box 92957
Los Angeles CA 90009-2957
213/336-6922
213/336-1636

Capt. Cady Coleman
WL/MLBP
Wright Laboratory/USAF
Wright-Patterson AFB OH 45433-6
513/255-9163
513/255-9019

Thomas Cookson
General Dynamics Space Systems
POBox 85990
San Diego CA 92186-5990
619/547-5081
619/974-4000

John E. Cooney
Space Systems/Loral
3825 Fabian Way, M/S G-97
Palo Alto CA 94303
415/852-4703
415/852-4267

Jonathan D. Coopersmith
Mail Code 732.5; Bldg. 7, Rm. 011
NASA Goddard Space Flight Ctr.
Greenbelt MD 20771
301/286-7969
301/286-6916

Diane Cotten
Martin Marietta--M/S 8048
POBox 179
Denver CO 80227
303/977-8385
303/977-1907

Joan Cranmer
JHU/APL
Johns Hopkins Rd
Laurel MD 20833
301/953-5000 X3810
301/953-6119

Dr. Jon B. Cross
CLS-2/MS G738
Los Alamos National Laboratory
Los Alamos NM 87545
505/667-0511
505/665-4631

E. Russ Crutcher
Boeing Defense & Space Group-M/S 88-23
POBox 3999
Seattle WA 98124-2499
206/773-7002
206/773-4946

John M. Davis
NASA
Marshall Space Flight Ctr.
Huntsville AL 35812
205/544-2494
205/544-5786

Judith R. J. Davis
M/S 226
NASA Langley Research Ctr
Hampton VA 23665-5225
804/864-4255
804/864-8312

Dr. A. de Rooij
ESA/ESTEC
PO Box 299, 2200 AG
Noordwijk NETHERLANDS
9011 31 0 1719 83716
9011 31 0 2523 76722

Don D. Dees
Boeing Defense & Space Group-M/S JM-95
PO Box 240002,499 Boeing
Huntsville AL 35824
205/461-5839
205/461-2286

Linda L. DeHainaut
LITC
Phillips Laboratory (AFSC)
Kirtland AFB NM 87117-6008
505/846-9877
505/846-0473

Michael D. DePiero
C. S. Draper Lab, M/S 63
555 Technology Sq
Cambridge MA 02139
617/258-2775
617/258-1131

John M. Dispennette
202 Ross Hall/Dept. of Mech. Engrg
Auburn University
Auburn University AL 36899
205/844-3345
205/844-3307

Tom Dragone
Orbital Sciences Corp
14119-A Sullyfield Cr/POBox 10840
Chantilly VA 22021
703/802-8107
703/802-8245

Christian Durin
CNES-Space Center of Toulouse
18 Avenue Edouard Belin
Toulouse Cedex FRANCE 31055
9011 33 61 28 14 39
9011 33 61 27 47 32

Harry W. Dursch
Boeing M/S 82-32
PO Box 3999
Seattle WA 98124
206/773-0527
206/773-4946

Capt. Deidra Dykeman
RL/OCPC
Griffiss AFB
Griffiss AFB NY 13441-5700
315/330-3145
315/330-7901

Joel Edelman
LDEF Corporation
14636 Silverstone Dr.
Silver Spring MD 20905
301/236-9311

Curt Eiche
Martin Marietta M/S B4383
PO Box 179
Denver CO 80201
303/971-1762
303/971-9768

Phyllis Ellingboe
Sheldahl, Inc.
1150 Sheldahl Rd, POBox 170
Northfield MN 55057
507/663-8000 x276
507/663-8470

John Emond
Ofc. of Commercial Programs Code CC
NASA Headquarters
Washington DC 20546
703/557-4599

W. W. Fernald
Mail Stop 433
NASA Langley Research Center
Hampton VA 23665-5225
804/864-7081

Robert H. Flowers
Martin Marietta M/S 8041
POBox 179
Denver CO 80201
303/977-6832
303/977-1907

Thad Frederickson
ILC Dover, Inc.
PO Box 266, Road 35
Frederica DE 19946
302/335-3911
302/335-0762

Al Freeland
Sheldahl, Inc.
1150 Sheldahl Rd., PO Box 170
Northfield MN 55057
507/663-8000 x502
507/663-8470

Joe Froechtenigt
Martin Marietta Astronautics Group
PO Box 179
Denver CO 80201
303/971-9258
303/971-9141

Joan G. Funk
Mail Stop 188B
NASA Langley Research Center
Hampton VA 23665-5225
804/864-3092
804/864-7893

Carol R. Gautreaux
Mail Stop 226
NASA Langley Research Ctr
Hampton VA 23665-5225
804/864-4280
804/864-3800

Dr. Raymond B. Gavert
NASA Space Sta. Prgm MSS-2
10701 Parkridge Blvd., Rm. 2372
Reston VA 22091
703/487-7336
703/487-7994

Pete George
Boeing Defense & Space Group-M/S 73-09
POBox 3999
Seattle WA 98124-2499
206/234-2679
206/237-0052

Michael B. Glasgow
College of William & Mary/Chem. Dept.
PO Box 8795
Williamsburg VA 23787-8795
804/221-2540

Johnny L. Golden
Boeing Defense & Space Group-M/S
POBox 3999
Seattle WA 98124-2499
206/773-2055
206/773-4946

Tim Gordon
Applied Science Technologies
4801 S. Holland Way
Littleton CO
303/973-7708

Dana Gould
Mail Stop 431
NASA Langley Research Center
Hampton VA 23665-5225
804/864-7747
804/864-7202

Dr. Raj Gounder
Boeing Aerospace Operations, Inc.
2101 Executive Dr., Tower Bx 74
Hampton VA 23666
804/838-2741
804/838-2780

Brian Gries
McDonnell Douglas
16055 Space Center Blvd.
Houston TX 77062-6208

Doris K. Grigsby
NASA/AESP, Oklahoma State Univ
300 North Cordell
Stillwater OK 74078
405/744-7015
405/744-7785

Frederick C. Gross
Mail Code 313
NASA Goddard Space Flight Ctr.
Greenbelt MD 20771
301/286-8349
301/286-4661

Koorosh Guidanean
L'Garde Incorporated
15181 Woodlawn Ave.
Tustin CA 92680
714/259-0771
714/259-7822

Sandra R. Gyetvay
The Aerospace Corp.-M/S M2/241
PO Box 92957
Los Angeles CA 90009-2957
213/336-8339
213/336-1636

Yoshiro Harada
IIT Research Institute
10 West 35th St.
Chicago IL 60616
312/567-4432
312/567-4386

Gale Harvey
Mail Stop 401A
NASA Langley Research Ctr.
Hampton VA 23665-5225
804/864-6742
804/864-7790

Dr. James A. Harvey
Univ. of Dayton Research Inst.
OLAC PL/STSC Bldg. 8424
Edwards AFB CA 93523-5000
805/275-5976
805/275-5041

Yoshihiro Hashimoto
Thermal Control & Structure Group/Tech De
IHI 229, Tonogaya, Mizuho-Machi,
Nishitama-Gun, Tokyo JAPAN 190-
9011 81 0425-56-7184
9011 81 0425-56-7575

Dr. Carol Hemminger
The Aerospace Corp. M2/250
PO Box 92957
Los Angeles CA 90009-2957
213/336-7666
213/336-1636

Sylvester G. Hill
Boeing Defense & Space Group-M/S 82-32
PO Box 3999
Seattle WA 98124-2499
206/773-2767
206/773-4946

S. E. Holloway III
Mail Stop 433
NASA Langley Research Center
Hampton VA 23665-5225
804/864-7090

Jerry L. Hunter
Analytical Instrumentation Facility
North Carolina State Univ - Box 7916
Raleigh NC 27695
919/515-7659
919/515-2463

Charles Hurley
University of Dayton/Research Inst.
300 College Park
Dayton OH 45469-0137
513/255-3220
513/258-8075

Takashi Ishii
Nissan Research & Development Inc
750 17th St., NW #902
Washington DC 20006
202/466-5284
202/457-0851

C. E. Jenkins, Jr.
Mail Stop 433
NASA Langley Research Center
Hampton VA 23665-5225
804/864-7080

Roger N. Johnson
Westinghouse Hanford Co/LG-39
PO Box 1970
Richland WA 99352
509/376-3582 (FTS 444)
509/376-4945 (FTS 444)

James L. Jones
Mail Stop 404
NASA LaRC
Hampton VA 23665-5225
804/864-3795
804/864-8094

H. C. Jones
Mail Stop 424
NASA Langley Research Center
Hampton VA 23665-5225
804/864-5651

Michele D. Jones
MLBT
Wright Laboratory
Wright-Patterson AFB OH 45433-6533
513/255-8097
513/255-9019

Michael P. Joseph
7421 Orangewood Ave., PO Box 311
OCA Applied Optics
Garden Grove CA 92642
714/895-1667
714/4356

Lester Jung
G. E. Aerospace
PO Box 800 M/S 410-1D
Princeton NJ 08543
609/490-6321
609/490-3962 (63)

Rachel R. Kamenetzky
Mail Code EH12
NASA MSFC
MSFC AL 35812
205/544-2510
205/544-0212

Mike Kangilaski
G. E. Space Nuclear Engrg & Tech.
P. O. Box 530954/6835 Via Del Oro
San Jose CA 95153-5354
408/365-6351

Lonny Kauder
Mail Code 732.5
NASA Goddard Space Flight Ctr.
Greenbelt MD 20771
301/286-5309
301/286-6916

John M. Kazaroff
NASA-Lewis Research Ctr M/S SPTD-2
21000 Brookpark Rd
Cleveland OH 44135
216/977-7513
216/977-7500

William T. Kemp
PL/STET
Kirtland AFB
Albuquerque NM 87117-6008
505/846-4439
505/846-6098

Dr. John R. Kenemuth
LITC
Phillips Laboratory (AFSC)
Kirtland AFB NM 87117-6008
505/846-4270
505/846-0473

James T. Kenny
Jet Propulsion Laboratory
4800 Oak Grove Dr. M/S 125-112
Pasadena CA 91109
818/354-3719
818/393-5011

Bruce Keough
Boeing Defense & Space Group-M/S
POBox 3999
Seattle WA 98124-2499
206/773-8438
206/773-4946

Hamed Khozaim
SSD/CNT
14800 Aviation Blvd.
Hawthorn CA 90250
213/363-8641
213/363-8725

Richard Kiefer
College of William & Mary/Chem. Dept.
PO Box 8795
Williamsburg VA 23787-8795
804/221-2553

Brian Killough
Mail Stop 431
NASA Langley Research Center
Hampton VA 23665-5225
804/864-7047

Thomas D. Kim
OLAC PL/STSC
Phillips Laboratory
Edwards AFB CA 93523-5000
805/275-5304
805/275-5041

Myung-Hee Kim
College of William & Mary/Chem. Dept.
PO Box 8795
Williamsburg VA 23787-8795
804/221-2540

William H. Kinard
LDEF Science Office M/S 404
NASA Langley Research Ctr.
Hampton VA 23665-5225
804/864-3796
804/864-8094

Thomas J. Kosic
Hughes Aircraft Co., EDSG
P O Box 902
El Segundo CA 90245
310/616-9819
310/616-5987

James L. Koury
OLAC-PL/STSC
Phillips Lab
Edwards AFB CA 93523-5000
805/275-5646
805/275-5041

Thomas Kuelker
EDO Canada Ltd
1940 Centre Ave., NE
Calgary, Alberta CANADA 52E 0A7
91 403/569-5400
91 403 569-5499

Dr. Kaplesh Kumar
C. S. Draper Laboratory, Inc. M/S 37
555 Technology Square
Cambridge MA 02139
617/258-1131

Richard Kutyn
Orbital Sciences Corp
PO Box 10840
Chantilly VA 22021
703/802-8098
704/802-8045

T. J. Lash
Mail Stop 424
NASA Langley Research Center
Hampton VA 23665-5225
804/864-5644

Chong Le
SSD/CNSE, Los Angeles AFB
PO Box 92960
Los Angeles CA 90009-2960
213/363-6867
213/363-6882

William T. Lee
Rocketdyne/Div of Rockwell Intl
6633 Canoga Ave LB25
Canoga Park CA 91303
818/700-3272
818/700-4313

Chia-Shih Lee
SSD/CNSE, Los Angeles AFB
PO Box 92960
Los Angeles CA 90009-2960
213/363-6867
213/363-6882

T. H. Leffel
Mail Stop 424
NASA Langley Research Center
Hampton VA 23665-5225
804/864-5647

Dr. William L. Lehn
Nichols Research Corp./Suite 157
4141 Col. Glenn Hwy
Dayton OH 45431
513/724-1173
513/427-1508

Dr. Alan Letton
Dept. of Mech Engrg/ M/S 3123
Texas A & M
College Station TX 77843-3123
409/845-1534
409/845-3081

François Levadou
ESA/ESTEC
POBox 299
2200 AG Noordwijk NETHERLANDS
31/1719-83915
31/1719-84992

Arlene S. Levine
LDEF Science Ofc-M/S 404
NASA Langley Research Center
Hampton VA 23665-5225
804/864-3318
804/864-8094

Roger Linton
Mail Stop EH12
NASA Marshall Space Flight Ctr
Huntsville AL 35812
205/544-2526
205/544-0212

Scott Lissit
W. J. Schafer Associates, Inc./Suite 800
1901 N. Fort Myer Dr.
Arlington VA 22209
703/558-7900
703/525-2691

John Loria
CODE RX
NASA Headquarters
Washington DC 20546
FTS 453-2838
426-0608

M. H. Lucy
Mail Stop 433
NASA Langley Research Center
Hampton VA 23665-5225
804/864-7069

David H. Ma
Lockheed Missiles & Space Co
POBox 3504
Sunnyvale CA 94089-3504
408/742-1074
408/742-1071

Howard G. Maahs
Mail Stop 188B
NASA LaRC
Hampton VA 23665-5225
804/864-3498
804/864-7893

Diane J. Martin
W. J. Schafer Assoc, Inc./Suite 800
1901 N. Fort Myer Dr.
Arlington VA 22209
703/558-7900
703/525-2691

Glenna D. Martin
LDEF Science Project Ofc. M/S 404
NASA Langley Research Ctr.
Hampton VA 23665-5225
804/864-3773
804/864-8094

J. B. Mason
NASA
Goddard Space Flight Ctr.
Greenbelt MD 20771
301/286-6555
301/286-4653

Eugene McKannan
Boeing JR-03
499 Boeing Blvd. PO Box 240002
Huntsville AL 35824
205/461-3586
205/461-3800

Tom McKay
LORAL Infrared & Imaging Systems
2 Forbes Road M/S 345
Lexington MA 02173
617/863-4067
617/863-3496

Joe McKenzie
Grumman--SSEIC
12000 Aerospace Dr.
Houston TX 77546
713/929-7467
713/929-7333

Richard Mell
Mail Code EH-34, Bldg. 4612
NASA/MSFC
Huntsville AL 35812
205/544-7329

Bob Mercer
6337 N. Camino Los Mochis
Tucson AZ 85718-3528
602/293-1667 or 299-8530
602/293-7601

Celia Merzbacher
CODE 6505
Naval Research Lab
Washington DC 20375
202/404-7987
202/404-7085

Michael J. Meshishnek
The Aerospace Corp.
PO Box 92957
Los Angeles CA 90009-2957
213/336-8760
213/336-1636

Charles J. Miglionico
PLWSMD
Kirtland AFB
Albuquerque NM 87117
505/846-4798
505/846-1724

Kristina M. Montt
MDSSC/Mail Code 732.5
NASA Goddard Space Flight Ctr.
Greenbelt MD 20771
301/286-4986
301/286-6916

Nigel Morris
Rutherford Appleton Laboratory
Chilton
Didcot, Oxon England OX11 0QX
9011 44 235 445210
9011 44 235 445848

W. H. Morrow
Resonance Ltd.
171 Dufferin St., So.; Unit # 7
Alliston, Ontario CANADA L0M 1A0
705/435-2577
705/435-2585

Thomas Morton
NASA Lewis Research Ctr.-M/S 301-3
21000 Brookpark Rd.
Cleveland OH 44135
216/433-6287
297-8311

James B. Moss
Martin Marietta M/S B4383
PO Box 179
Denver CO 80201
303/971-1554
303/971-9768

Henry Nahra
NASA Lewis Research Ctr
21000 Brookpark Rd
Cleveland OH 44135
216/433-5385 (FTS 297)
216/433-8050

Oscar Nespoli
Canadian Space Agency
POBox 11490, Station H
Ottawa, Ontario CANADA K2H 8S2
613/998-2187
613/998-2817

Walter F. Nicaise
L6-39
Westinghouse Hanford Co.
Richland WA 99352
509/376-0522
509/376-4945

Robert L. O'Neal
LDEF Science Ofc. M/S 404
NASA Langley Research Ctr.
Hampton VA 23665-5225
804/864-3792
804/864-8094

Evelyne Orndoff
Johnson Space Center
NASA JSC
Houston TX 77058
713/483-9117
713/483-9167

Robert Orwoll
College of William & Mary/Chem. Dep
PO Box 8795
Williamsburg VA 23787-8795
804/221-2549

Richard Osiecki
Lockheed Research Lab/Orgn 92-40, B-205
3251 Hanover St.
Palo Alto CA 94304-1191
415/424-2389
415/354-5415

V. A. Overbay
Mail Stop 424
NASA Langley Research Center
Hampton VA 23665-5225
804/864-5636

G. Owsley
Mail Stop 433
NASA Langley Research Center
Hampton VA 23665-5225
804/864-7070

Norbert Pailer
Dornier GmbH/Space Division
PO Box 1420
D-7990 Friedrichshafen 1 GERMANY
9011 07545 83430
9011 07545/84411

Alain Paillous
ONERA-CERT/DERTS
2 Ave. E. Belin
31055 Toulouse-Cedex FRANCE
9011 33 61 55 71 19
9011 33 61 55 71 72

George M. Parsons III
USArmy Strategic Defense Cmnd CS
POBox 1500
Huntsville AL 35807-3801
205/955-1667
205/955-5722

Arthur T. Perry
American Space Technology, Inc. Suite 35
2800 28th St.
Santa Monica CA 90405
213/450-7515
213/450-7304

Wanda C. Peters
McDonnell Douglas Space Systems Co.
7404 Executive Pl./Suite 200
Seabrook MD 20706
301/286-7969
301/464-7413

Ron Peterson
Hughes Aircraft

310/616-9048
310/616-5987

Brian C. Petrie
Lockheed Missiles & Space Co.
PO Box 3504, B-564, Dept. 78-30
Sunnyvale CA 94089-3504
408/742-8244
408/742-7743

J. R. Phillips
Mail Stop 433
NASA Langley Research Center
Hampton VA 23665-5225
804/864-7075

Ross Phillips
Mail Stop 433
NASA Langley Research Ctr.
Hampton VA 23665-5225
804/864-7075
804/864-7009

H. Gary Pippin
Boeing Defense & Space Group-M/S 82-32
POBox 3999
Seattle WA 98124-2499
206/773-2846
206/773-4946

Bob Poley
Ball Aerospace
PO Box 1062
Boulder CO 80306
303/939-4460
303/442-4812

Professor R. Prabhakaran
Old Dominion University
Dept. of Mechanical Engineering
Norfolk VA 23529

William H. Prosser
Mail Stop 231
NASA Langley Research Ctr.
Hampton VA 23665-5225
804/864-4960
804/864-4914

J. R. Rawls
Mail Stop 424
NASA Langley Research Center
Hampton VA 23665-5225
804/864-4093

Gary D. Rea
Martin Marietta M/S 8041
POBox 179
Denver CO 80201
303/977-6831
303/977-1907

Douglas L. Reeder
General Research Corp.
5383 Hollister Ave.,
Santa Barbara CA 93111
805/964-7724
805/967-7094

Brian Remington
ILC Dover, Inc.
PO Box 266, Road 35
Frederica DE 19946
302/335-3911
302/335-0762

G. Paul Richter
NASA-Lewis Research Ctr M/S SPT
21000 Brookpark Rd
Cleveland OH 44135
216/977-8538
216/977-7500

James B. Robertson
Mail Stop 152E
NASA Langley Research Ctr.
Hampton VA 23665-5225
804/864-6643
804/864-7793

William R. Robertson
Dynamics Research Corp.
1755 Jefferson Davis Hwy/ Suite 802
Arlington VA 22202
703/521-3812 X 6046
703/550-4123

Michael Rodriguez
MDSSC Mail Code 732.4
NASA Goddard Space Flight Ctr.
Greenbelt MD 20771
301/286-9296
888-6919

William A. Roettker
Mail Stop 431
NASA Langley Research Center
Hampton VA 23665-5225
804/864-7046
804/864-7202

Frank Rose
Auburn Univ/Space Power Inst.
231 Leach Ctr.
Auburn University AL 36849
205/844-5894
205/844-5900

Gilbert L. Roth
Code QP
NASA Headquarters
Washington DC 20546
202/453-1877
202/472-4841

Dr. H. R. Ruge
The Aerospace Corp. M2-264
PO Box 92957
Los Angeles CA 90009
213/336-7085
213/336-6136

T. S. Sampair
Mail Stop 904
Lockheed Engineering & Sciences Corp.
Hampton VA 23666
804/766-9600

Matthew Schor
W. J. Schafer Assoc., Inc./Suite 800
1901 N. Fort Myer Dr
Arlington VA 22209
703/558-7900
703/525-2691

John R. Schuster
General Dynamics Space Sys. M/Z C1-8900
POB 85990
San Diego CA 92186-5990
619-547-7120
619-547-7162

Dr. David Schwam
Case Western Reserve University
Cleveland OH 44106
216/368-3864
216/368-3209

Dr. Helmut Schulle
Dornier of North America, Inc.
1350 I Street, NW/Suite 800
Washington DC 20005
202/408-1110
202/408-4892

Martha Scott
Grumman Space Sta. Prgm
620 Discovery Dr.
Huntsville AL 35806
205/971-6012
205/971-6019

David Shular
Mail Code ED 64
NASA Marshall Space Flight Ctr.
Huntsville AL 35812
205/544-8734
205/544-5874

D. D. Shuster
Mail Stop 459
NASA Langley Research Center
Hampton VA 23665-5225
804/864-3336

Charles Simon
ISST/M&D SIG
1810 NW 6th St.
Gainesville FL 32609
904/371-4778
904/372-5042

Wayne S. Slemp
Mail Stop 183
NASA Langley Research Ctr.
Hampton VA 23665-5225
804/864-1334
804/864-3800

Fred A. Smidt
Code 4670
Naval Research Laboratory
Washington DC 20375-5000
202/767-4800
202/767-5301

Bryan K. Smith
NASA Lewis Research Ctr. M/S 500-222
21000 Brookpark Rd.
Cleveland OH 44135
216/433-6703 (FTS 297)
216/433-8050

Charles A. Smith
McDonnell Douglas
5201 Bolsa, M/S T-50
Huntington Beach CA 92647-2048
714/896-4015
714/896-3311 X 69339

Richard E. Snyder
Mail Stop 114
NASA Langley Research Ctr.
Hampton VA 23665-5225
804/864-6016

Steve Spear
Boeing M/S 73-09
PO Box 3999
Seattle WA 98124
206/234-2667
206/237-1750

Gary L. Steckel
The Aerospace Corp. M/S M2/321
PO Box 92957
Los Angeles CA 90009
310/336-7116
310/336-7055

Bland A. Stein
Mail Stop 188M
NASA Langley Research Ctr.
Hampton VA 23665-5225
804/864-3492
804/864-7729

Dr. Charles Stein
Phillips Lab/WSMD
Kirtland AFB
Albuquerque NM 87117
505/846-4822
505/846-1724

Dr. Thomas Strganac
Dept. of Aerospace Engrg M/S 3141
Texas A & M
College Station TX 77843-3123
409/845-1694
409/845-6051

John W. Strickland
BAMSI, Inc.
150 West Park Loop, Suite 107
Huntsville AL 35806
205/772-9072
205/722-9287

Dr. Wayne K. Stuckey
The Aerospace Corp. M2/250
PO Box 92957
Los Angeles CA 90009-2957
213/336-7389
213/336-1636

Dr. Richard D. Sudduth
Boeing Defense & Space Group-M/S JY-34
PO Box 240002,499 Boeing
Huntsville AL 35824

Louis A. Teichman
Mail Stop 191
NASA Langley Research Ctr.
Hampton VA 23665-5225
804/864-3510
804/864-7729

Stephen S. Tompkins
Materials Div. M/S 188B
NASA Langley Research Ctr.
Hampton VA 23665-5225
804/864-3096
804/864-7793

Bob Turner
W. J. Schafer
1901 N. Fort Myer Dr.
Arlington VA 22094
703/558-7900
703/525-2691

June Tveekrem
Mail Code 732
NASA Goddard Space Flight Ctr
Greenbelt MD 20771
301-286-2832
301/286-2477

Richard F. Vyhna
Rockwell International
POBox 582808
Tulsa OK 74158
918/835-3111 X2252
918/834-7722

Donald A. Wallace
QCM Research
2825 Laguna Canyon Rd/PO Box 277
Laguna Beach CA 92652
714/497-5748
714/497-7331

Scott A. Wallace
QCM Research
2825 Laguna Canyon Rd/PO Box 27
Laguna Beach CA 92652
714/497-5748
714/497-7331

Dr. Tom Ward
U.S. Dept. of Energy GA-155, SC-1
1000 Independence Ave., S. W.
Washington DC 20585
202/586-4612 FTS 896-4612
896-9386

Dr. Ann F. Whitaker
Mail Code EH, 11
NASA Marshall Space Flight Ctr.
MSFC AL 35812
205/544-2510
205/544-0212

Ken Whiteacre
Martin Marietta
PO Box 179, M/S 8048
Denver CO 80201
303/977-8373
303/977-1921

Dr. James B. Whiteside
Grumman Corporate Research Ctr.
Mail Stop A08-35
Bethpage NY 11714-3580
516/575-2354
516/575-7716

Donald R. Wilkes
AZ Technology
3322 Memorial Pky., SW Suite 93
Huntsville AL 35801
205/880-7481
205/880-7483

Kevin Duane Williams
Dept. of Mechanical Engrg. M/S 312
Texas A & M
College Station TX 77843-3123
409/847-9233
409/845-3081

Brenda K. Wilson
W. J. Schafer Associates
525 School St., SW/Suite 301
Washington DC 20024
202/863-9159
202/863-9292

B. B. Wolff
Mail Stop 424
Lockheed Engineering & Sciences Corp.
Hampton VA 23666
804/766-9604

Philip R. Young
Mail Stop 226
NASA Langley Research Ctr.
Hampton VA 23665-5225
804/864-4265 FTS 928-4265
804/864-8312

Ainslie T. Young, Jr.
Los Alamos National Lab/MST-DO, MS-G75
POBox 1663
Los Alamos NM 87545
505/667-4553 fts 843
505/665-3748

Naser Zargar
McDonnell Douglas Space Systems Co.
5301 Bolsa Ave. M/S 17-7
Huntington Beach CA 92647
714/896-3311 X70337
714/896-5034

Dr. D. G. Zimcik
Canadian Space Agency
POBox 11490, Station H
Ottawa, Ontario CANADA K2H 8S2
613/998-2187
613/998-2817



REPORT DOCUMENTATION PAGE			Form Approved OMB No. 0704-0188	
Public reporting burden for this collection of information is estimated to average 1 hour per response, including the time for reviewing instructions, searching existing data sources, gathering and maintaining the data needed, and completing and reviewing the collection of information. Send comments regarding this burden estimate or any other aspect of this collection of information, including suggestions for reducing this burden, to Washington Headquarters Services, Directorate for Information Operations and Reports, 1215 Jefferson Davis Highway, Suite 1204, Arlington, VA 22202-4302, and to the Office of Management and Budget, Paperwork Reduction Project (0704-0188), Washington, DC 20503.				
1. AGENCY USE ONLY (Leave blank)	2. REPORT DATE September 1992	3. REPORT TYPE AND DATES COVERED Conference Publication		
4. TITLE AND SUBTITLE LDEF Materials Workshop '91			5. FUNDING NUMBERS 506-48-91-08	
6. AUTHOR(S) Bland A. Stein and Philip R. Young, Compilers				
7. PERFORMING ORGANIZATION NAME(S) AND ADDRESS(ES) NASA Langley Research Center Hampton, VA 23681-0001			8. PERFORMING ORGANIZATION REPORT NUMBER L-17135	
9. SPONSORING/MONITORING AGENCY NAME(S) AND ADDRESS(ES) National Aeronautics and Space Administration Washington, DC 20546-0001			10. SPONSORING/MONITORING AGENCY REPORT NUMBER NASA CP-3162, Part 1	
11. SUPPLEMENTARY NOTES				
12a. DISTRIBUTION/AVAILABILITY STATEMENT Unclassified-Unlimited Subject Category 27			12b. DISTRIBUTION CODE	
13. ABSTRACT (Maximum 200 words) The LDEF Materials Workshop '91 was a follow-on to the Materials Sessions at the First LDEF Post-Retrieval Symposium held in Kissimmee, Florida, June 1991. The workshop comprised a series of technical sessions on materials themes, followed by theme panel meetings. Themes included Materials, Environmental Parameters, and Data Bases; Contamination; Thermal Control and Protective Coatings and Surface Treatments; Polymers and Films; Polymer Matrix Composites; Metals, Ceramics, and Optical Materials; Lubricants Adhesives, Seals, Fasteners, Solar Cells, and Batteries. This report contains most of the papers presented at the Technical sessions. It also contains theme panel reports and visual aids. This document continues the LDEF Space Environmental Effects on Materials Special Investigation Group (MSIG) pursuit of its charter to investigate the effects of LEO exposure on materials which were not originally planned to be test specimens and to integrate this information with data generated by Principal Investigators into an LDEF Materials Data Base.				
14. SUBJECT TERMS Long Duration Exposure Facility (LDEF); Space environmental effects on materials; Space exposure of materials			15. NUMBER OF PAGES 473	
			16. PRICE CODE A20	
17. SECURITY CLASSIFICATION OF REPORT Unclassified	18. SECURITY CLASSIFICATION OF THIS PAGE Unclassified	19. SECURITY CLASSIFICATION OF ABSTRACT Unclassified	20. LIMITATION OF ABSTRACT	